Short-distance constraints on the hadronic light-by-light contribution to the muon g-2

Inaugural dissertation
of the Faculty of Science,
University of Bern

presented by

Laetitia Laub

from Riddes/VS

Supervisor of the doctoral thesis:

Prof. Dr. Gilberto Colangelo

Institute for Theoretical Physics
Albert Einstein Center for Fundamental Physics
University of Bern

Short-distance constraints on the hadronic light-by-light contribution to the muon g-2

Inaugural dissertation
of the Faculty of Science,
University of Bern

presented by

Laetitia Laub

from Riddes/VS

Supervisor of the doctoral thesis:

Prof. Dr. Gilberto Colangelo

Institute for Theoretical Physics
Albert Einstein Center for Fundamental Physics
University of Bern

Accepted by the Faculty of Science.

Bern, 18.06.2021

The Dean

Prof. Dr. Zoltán Balogh

Abstract

The aim of this work is to investigate the information available from perturbative QCD to constrain the hadronic light-by-light contribution to $(g-2)_\mu$ and to implement it in a way that is compatible with the dispersive description.

The first regime of interest is the one where three photon virtualities are large. Because the external photon is soft in the $g-2$ kinematics, an operator product expansion in presence of an external electromagnetic field needs to be used. The leading order in this expansion corresponds to the usual massless quark loop. [1] In this work, it is shown that the non-perturbative corrections are small and that the α_s-correction is negative and amounts to about 10% of the quark loop. The second interesting regime is the one where two photon virtualities are much larger than the third. This leads to the so-called Melnikov-Vainshtein constraint. [2]

A way to satisfy the short-distance constraints using heavy pseudoscalars is then presented. This is done using a large-N_c inspired Regge model for the transition form factors of the radially excited pseudoscalars. The contribution of the heavy pseudoscalars is then matched to the quark loop and its first gluonic correction in order to reduce the model-dependence of our estimation.

With the recent results from Fermilab [3], the discrepancy between the experimental and theoretical determinations of the anomalous magnetic moment of the muon has been pushed to 4.2σ. In order to reach the 5σ-threshold, the experimental and theoretical uncertainties need to be reduced further.

Acknowledgments

First and foremost, I would like to thank my advisor, Gilberto Colangelo, for giving me the opportunity to work on these projects and to discover the world of research. His expertise and guidance were always greatly appreciated!

I would also like to give very special thanks to Franziska Hagelstein and Nils Hermansson-Truedsson with whom I have collaborated on a daily basis and who were always very helpful and patient. Franziska was very supportive in every step of the PhD and her advice and suggestions taught me a lot. Working with Nils was a pleasure too and he was always there to help, despite a global pandemics. Many thanks to Nils for proofreading this thesis as well.

I would also like to thank my other collaborators, Johan Bijnens, Martin Hoferichter, Antonio Rodríguez-Sánchez and Peter Stoffer, for many interesting discussions and for always taking the time to answer my sometimes naive questions. I am grateful to Massimiliano Procura and Jan Lüdtke too, for interesting meetings on the occasion of their visits to Bern. Thanks also go to Marc Knecht for agreeing to be the external referee and to Uwe-Jens Wiese for chairing the defense.

I am also grateful to my fellow PhD students (Marcel Balsiger, Samuel Favrod, Monika Hager, Manes Hornung, Greg Jackson, Joachim Monnard, Simona Procacci, Philipp Schicho and Francesco Saturnino) for making the PhD life more pleasant.

Finally, many thanks to Clara Laub and Thomas Moner-Banet for their support in this and everything else!

Contents

Chapter 1

Introduction

> The important thing is to never stop questioning.
>
> Albert Einstein

There is a long-standing 3-4σ discrepancy between the experimental and theoretical determination of the anomalous magnetic moment of the muon, which could indicate physics beyond the Standard Model. [3, 4] In order to reach the 5σ-threshold for scientific discovery, both the experimental and theoretical uncertainties must be reduced further, which has resulted in a lot of activity surrounding this topic in recent years.

On the experimental side, the long-awaited result from the first run of the E989 experiment at Fermilab [3] has recently confirmed the previous result from the Brookhaven National Laboratory (BNL) [5]. The largest part of the error is statistical and further data collection will therefore result in a better precision, with the goal to ultimately reduce the uncertainty by a factor of 4 compared to the BNL result [6].

The theoretical uncertainty must reach the same accuracy goal. The largest source of uncertainties in the Standard Model prediction stems from hadronic contributions: the hadronic vacuum polarization (HVP) and the hadronic light-by-light (HLbL). The HVP contribution can be accurately described from data for the electron-positron to hadrons cross-section, through a dispersion relation. [7–13] In addition, the determinations from lattice QCD are becoming more precise. [14–23] The HLbL contribution is smaller, but is very relevant for the current accuracy goal. [4] It can be calculated on the lattice [24, 25], or using a dispersive description, despite the fact that it is less straight-forward than for HVP. [1, 2, 26–36] Moreover, perturbative QCD becomes applicable at high-energy, which leads to some short-distance constraints on the dispersive contributions. Analyzing these constraints and implementing them in a way that is compatible with the dispersive description for HLbL is the main topic of this thesis.

The first problem addressed in this work is the following. The quark loop has been used for a long time in the literature to describe the high-energy behavior of the HLbL tensor [2] and while there is no doubt that this should be a good description in the case where all four photons are highly virtual, this situation does not correspond to the $g-2$ kinematics where the external photon is real. [1] That the quark loop is a good description of HLbL even for the latter case

has only been proven recently thanks to an operator product expansion (OPE) in presence of an external electromagnetic field. It is shown that the leading contribution in this OPE corresponds to the massless quark loop. [1] In addition, it can be shown that the non-perturbative corrections are small. [37] The gluonic correction has also been computed and amounts to around 10% of the leading quark loop. [38]

Another interesting constraint is the so-called Melnikov-Vainshtein constraint and concerns the regime where two of the photon virtualities are much larger than the third. [2] There is no doubt on the validity of this constraint, but reconciling it with the dispersive description for the HLbL in the $g-2$ kinematics is far from obvious. [2, 30, 39–43] This is the second problem addressed in this work: a model for the transition form factors of radially excited pseudoscalars is built and used to saturate the short-distance constraints described above.

The thesis is organized as follows. In chapter 2, the status of the determination of the muon $g-2$ is presented. In the next chapter, QCD renormalization is reviewed as a basis for introducing the operator product expansion which is a powerful tool that is used in many different forms in this work. In particular, an OPE in presence of an external electromagnetic field is presented, which will be useful to show that the massless quark-loop is a good description of the HLbL tensor in the regime where all the photons are highly virtual, except for the soft external photon. This is the object of chapter 4. Finally, in chapter 5, a hadronic model for the transition form factor of radially excited pseudoscalars is presented as a solution to reconcile the aforementioned short-distance constraints with the dispersive description of HLbL.

Chapter 2

Magnetic moments

> That tiny shift, so elusive and hard to measure, would clarify in a fundamental way our thinking about particles and fields.
>
> Freeman Dyson, on the Lamb shift

Magnetic moments describe the response of an object to an external magnetic field. Classically, they can be generated by moving charges: a current will create a magnetic moment proportional to the angular momentum of the system. The system can then be seen as a tiny magnet on which a torque is applied by the external magnetic field. Some elementary particles - such as the electron or the muon - have an intrinsic angular momentum - the spin - which will in turn generate an intrinsic magnetic moment. As elementary particles are believed to be point-like, the spin (and its associated magnetic moment) cannot depend on internal motion: it is an inherent property.

These intrinsic magnetic moments are of great interest in particle physics, because they can be measured very precisely and computed unambiguously from the theory side. For this reason, they have been important in the historical development of quantum physics. They played a central role in the discovery of spin, the development of quantum electrodynamics as the fundamental theory of electromagnetism and the advent of quantum field theory (QFT) in general. The *Standard Model* (SM) of elementary particles can describe the results of most collider experiments very accurately.

The anomalous magnetic moment of the muon is still an active area of research, because it is one of the rare observable for which there is a discrepancy between theory and experiment. This discrepancy is currently at 4.2σ [3] and could be a hint of physics beyond the Standard Model. A tremendous amount of effort has been made to investigate this discrepancy, both from the theory and experimental sides. This work is part of this initiative.

In this chapter, I start by presenting the history of magnetic moments in particle physics. I then discuss the current determination of the anomalous magnetic moment of the muon, both experimentally and theoretically.

2.1 Historical overview: from the discovery of spin to new physics

The aim of this short review is not to give an exhaustive overview of the development of quantum physics, but rather to focus on magnetic moments and see how this single quantity has played a key role in that development. This should allow us to better understand magnetic moments and hopefully will give us some insights as to why it is, to this day, a very active area of research.

At the beginning of the twentieth century, several experiments exhibited unexpected behavior, suggesting that, on microscopic scales, light could behave both as a wave and as a particle. Those experiments would lead to the birth of quantum mechanics. In particular, the study of atomic spectra has resulted in significant steps forward in experimental techniques, but also in the development of mathematical tools to describe particles. It also led to the discovery of spin. We will therefore start our discussion with the study of the spectrum of the hydrogen atom.

After classical theory failed, Niels Bohr developed (in 1913) a model for the hydrogen atom based on the assumption that the angular momentum is quantized and that the electron moves in a Coulomb potential created by the nucleus, without radiating energy as it is orbiting. This leads to[1]:

$$E_n = -\frac{m_e \alpha^2 Z^2}{2n^2}\,, \tag{2.1}$$

where m_e is the electron mass, α the fine-structure constant, Z the atomic number (which accounts for the fact that the above formula is also valid for hydrogen-like atoms[2]) and n is a natural number called the principal quantum number. By making the orbit of the electron elliptic, Arnold Sommerfeld introduced two additional quantum numbers: the orbital momentum $l = 0, ..., n-1$ and the magnetic quantum number $m = -l, ..., l$. This explains some of the splitting of the energy levels given in (2.1) when an external magnetic field is applied[3]. [44, 45] In that case, a term must be added to the Hamiltonian:

$$H = -\vec{\mu} \cdot \vec{B}\,, \tag{2.2}$$

where $\vec{\mu} = \mu_0 \vec{L}$ is the angular momentum and $\mu_0 = \frac{e}{2m_e}$ is the Bohr magneton[4].

The formalism described above can be used to study the atomic spectra of other atoms than the hydrogen (or hydrogen-like atoms). The reason is that many spectral lines correspond to excitations of a single electron in the outermost orbital: the *radiant electron*. The latter evolves in a Coulomb potential created by the nucleus and the other electrons, also called *core electrons*. This for instance allows for a better understanding of the spectra of alkali atoms. [44]

In 1916, Sommerfeld introduced some relativistic effects to the Bohr model. He noticed that this results in some splitting between levels with the same n but different l [44, 46]

$$\Delta E_{\text{rel}} := E_{n,l+1} - E_{n,l} = \frac{m_e \alpha^4 Z^4}{2n^3 l(l+1)}\,. \tag{2.3}$$

In order to use (2.3) for alkali atoms, the factor Z^4 should be replaced by $(Z-s)^4$, where s is determined experimentally and accounts for the screening of the nucleus charges by the core electrons. [44]

[1] Natural units ($\hbar = \epsilon_0 = c = 1$) are used throughout this work.

[2] I.e. atoms with a single electron, like He^+ or Li^{++}.

[3] This is the Zeeman effect which was first observed already in 1896.

[4] In this work, e represents the elementary charge and the charge of an electron is therefore $-e$.

These considerations led to significant improvements in the understanding of atomic spectra. However, (2.1) and (2.3) are still not sufficient to explain all the experimental observations. For example, the S-levels (corresponding to $l = 0$) of sodium (Na) atoms split in two in presence of an external magnetic field, which cannot be explained with the three quantum numbers considered so far. This was referred to as the *anomalous Zeeman effect*. But even when no external magnetic field is present (which implies that m cannot play any role in the splitting of spectral lines), it was observed that the Na (and other alkalis) levels corresponding to $l > 0$ have a doublet structure: one spectral line is made of two energy levels close together. [44]

Alfred Landé found that (2.3) could also be used as an empirical formula to describe the splitting observed between levels with the same n and l (such as the doublet structure described above)

$$\Delta E_{\text{alkali}} = \frac{m_e \alpha^4 (Z-s)^4}{2n^3 l(l+1)} \,. \tag{2.4}$$

He then tried to explain this based on the assumption that these splittings were due to magnetic interactions between the radiant and core electrons, but concluded in 1924 that this hypothesis should be abandoned. [44] This led Wolfgang Pauli to postulate that the alkali multiplets were due to a characteristic of the electron itself. In 1925, he wrote his paper on the famous Pauli's exclusion principle where he introduces a fourth quantum number to explain the spectrum structures that he described as a "classically indescribable two-valuedness" [44, 47].

After learning about this, Ralph Kronig postulated the existence of spin: if the electron was similar to a small sphere rotating on itself, its rotation axis could point in two different directions, thereby explaining Pauli's two-valuedness. [48] A consequence of this rotation is that the electron has an intrinsic angular momentum $\vec{S}$, the spin. In turn, this implies that the electron has an intrinsic magnetic moment:

$$\vec{\mu}_s = g\mu_0 \vec{S} \,, \tag{2.5}$$

which could explain the anomalous Zeeman effect. [48] The constant g can be extracted from the value of the splitting of the $l = 0$ energy level in presence of an external magnetic field. The result of this procedure leads to the puzzling conclusion that $g = 2$ and not 1, implying that spin is twice as effective as the orbital angular momentum in creating a magnetic moment. Kronig then tried to reproduce (2.4) by computing the spin-orbit interactions. However, the result he obtained was off by a factor of 2. This lead Pauli to reject the idea of spin[5] and Kronig ended up giving up on it. [48]

A few months later, Samuel Goudsmit enters the picture by writing a paper suggesting a different choice for Pauli's fourth quantum number, which made the Pauli's principle more transparent: this choice corresponds to the present convention of using $m_s = \pm 1/2$ and $m_l = -l, ..., l$. [49] When he explained this to George Uhlenbeck as they were collaborating, the latter immediately realized that this implied that the electron had another degree of freedom, that he was rotating. In one afternoon, they independently reinvented Kronig's spin. Paul Ehrenfest gave the idea a better reception than Pauli and the Goudsmit-Uhlenbeck duo published a small article about spin in Nature. It is worth mentioning that they didn't compute the spin-orbit interaction at the time and were unaware of the factor two issue. [50]

[5] He also pointed out that if an electron has a radius of $\frac{e^2}{m_e}$, which was believed at the time, then the surface velocity of the rotating electron would exceed the speed of light. [48]

In 1926, Llewellyn Thomas realized that relativity implies a correction to the spin-orbit effect described above. This solved the factor 2 issue and even Pauli retracted his objections to the concept of spin. [48]

A few questions remained unanswered: why was $g = 2$ and how could one quantize Thomas' classical computation? [44] Both questions were answered two years later when Paul Dirac devised his famous relativistic wave equation for the electron:

$$(i\gamma^\mu \partial_\mu - m_e)\psi(x) = 0\,, \tag{2.6}$$

where, ψ is the spinor wave function of the electron allowing $|\psi|^2$ to be interpreted as a probability density and γ^μ stands for a set of four 4×4 matrices obeying the following anti-commutation relation:

$$\{\gamma^\mu, \gamma^\nu\} = 2g^{\mu\nu}\mathbb{1}_4\,, \tag{2.7}$$

where $g^{\mu\nu}$ is the Minkowski metric. [46] An external electromagnetic field can be added to the picture with the prescription

$$i\partial_\mu \to i\partial_\mu - eA_\mu \iff \partial_\mu \to \partial_\mu + ieA_\mu, \tag{2.8}$$

where $A^\mu = (\Phi, \vec{A})$ is the electromagnetic four-vector. It can then be shown that the electron has an intrinsic angular momentum of $\hbar/2$ and that its magnetic moment corresponds to what was found out from Goudsmit and Uhlenbeck's work. Charles G. Darwin and Walter Gordon later derived the exact hydrogen spectra from Dirac's equation

$$E = m_e^2 \left(1 + \frac{\alpha^2}{\left(n - j - 1/2 + \sqrt{(j+1/2)^2 - \alpha^2} \right)^2} \right)^{-1/2}. \tag{2.9}$$

When expanded in α and upon the identification $j = l + 1/2$, accounting for spin, this result reproduces (2.4) [46]. Dirac's equation[6] therefore closed the chapter opened by Sommerfeld twelve years prior. But as we will see, the story of magnetic moments was not over and the $g-$factor would later be found to slightly deviate from 2.

In parallel to the breakthroughs in the study of atomic spectra, other aspects of quantum field theories were developed. In 1926, Max Born, Werner Heisenberg and Pascual Jordan found a method to quantize the free radiation field in terms of raising and lowering operators as well as their canonical commutation relation. This formalism was for example used to understand the black body radiation better. In 1928, Eugene Wigner and Jordan realized that Pauli's exclusion principle required anti-commutation relations instead of the commutation relations used to quantize the radiation field. [46]

Despite these successes, scientists soon began to doubt QFT. One of the reason was that more and more particles were being discovered and at that time, QFT only contained electrons, positrons and photons. [46] In 1933, Enrico Fermi proposed a theory of interactions between neutrons, protons, electrons and neutrinos which was successful in describing β-decays, but the overall context and how everything hung together was far from being obvious.

[6] Dirac's equation was inspired by the work of other physicists: Erwin Schrödinger, Oskar Klein and Gordon's work on wave mechanics on the one hand and Pauli's attempt at describing spin with matrices on the other.

Another issue was that infinities were encountered in various calculations, such as the electron self-energy. In modern terms, this problem can be easily understood with Feynman diagrams[7]. Within the context of QED, the interactions of a particle (e.g. the electron) with the cloud of virtual particles surrounding it must be taken into account. In Feynman's diagrammatic representation, the electron self-energy then looks as follows

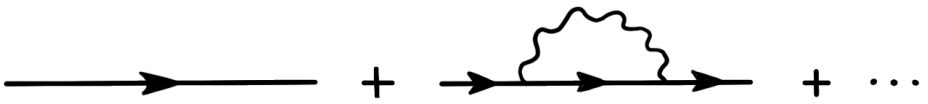

The first diagram represents an electron propagating without interactions and the second shows an electron propagating, emitting a virtual photon and later reabsorbing it. It is also possible for the electron to emit more than one photon and that's what the three dots stand for. At each vertex, energy and momentum must be conserved, but as soon as the diagram contains a closed loop, there must be an integral over all the possible momenta flowing there. This leads to the aforementioned infinities because of the high-energy tail of the integrals. These UV-divergences made it impossible to obtain results from QED when calculating radiative corrections.

On the experimental side, Isidor Rabi invented magnetic resonance in 1937, which would allow for more precise measurements on the atomic spectra. In particular, he and two of his students -John Nafe, Edward Nelson- were able to measure the hyperfine structure of the ground state of the hydrogen atom in 1946. [48] Surprisingly, they found a result slightly different than what would be obtained from a calculation based on Dirac's result. [48] This was the first hint, that the magnetic moment of the electron was not exactly equal to 2, that there was a deviation from this value: the *anomalous magnetic moment*, defined as

$$a_e := \frac{(g-2)_e}{2}\,, \tag{2.10}$$

where the subscript e stands for electron.

A subsequent experiment by Willis Lamb and Robert Retherford measured the splitting between the $2S_{1/2}$ and $2P_{1/2}$ levels of the hydrogen, which should be degenerate according to Dirac's theory. This was a definite proof that the Coulomb law needed some corrections.

Inspired by these results, Polykarp Kusch and Henry Foley designed an experiment relying on atomic beam magnetic resonance to measure the Zeeman effect of the $2P_{1/2}$ and $2P_{3/2}$ states of gallium atoms. From this, they were able to measure the magnetic moment of the electron very precisely [51–53]

$$g = 2.00244 \pm 0.00006 \iff a_e = 0.00122 \pm 0.00003\,. \tag{2.11}$$

These results sparked a lot of activity on the theory side because of the suspicion that this result could be related the UV-divergences in QED. [45, 48]

Greatly motivated by Lamb's experiment, Hans Bethe managed to bypass some of the problematic infinities and essentially developed a non-relativistic theory of the Lamb shift. [48]

[7]Which were introduced by Richard Feynman in 1948.

Later in 1947, Julian Schwinger was able to compute the first correction to the anomalous magnetic moment of the electron in QED [54]

$$a_e = \frac{\alpha}{2\pi} \approx 0.00116\,,$$

which was in remarkable agreement with (2.11). This result was a huge success for QED and contributed to put quantum field theories on a firmer basis.

Subsequent to this result, Schwinger published two articles on how to deal with the infinities arising in QED. [55, 56] The trick was to reabsorb them in a redefinition of the parameters of the theory. Since then, a lot of progress has been made and what appeared at first as a suspicious sleight of hands, is today understood as a fundamental property of quantum field theories, simply expressing the limitations of the energy range described by these theories.

Experimental techniques were greatly improved in the following years. During the 1960-1970, the Michigan experiment was developed by Horace Richard Crane, Arthur Rich and their coworkers [48]. The basic idea is that the difference between the spin precession angular frequency ω_s and the cyclotron angular velocity ω_c of an electron moving in a magnetic field is proportional to the anomalous magnetic moment[8] [48]

$$\vec{\omega}_a := \vec{\omega}_s - \vec{\omega}_c = -a_e \frac{e}{m_e} \vec{B}\,. \tag{2.12}$$

In 1980, higher precision was achieved thanks to the Penning trap technique, where an electron is trapped in a magnetic field for month and repeated measurements of ω_a are performed. [48]

On the theory side - because the infinities were under control - it was possible to include more corrections and make the predictions of a_e even more precise. The theory was therefore able to follow the experimental progress in measuring the anomalous magnetic moment of the electron. Up until recently, the matching of the theoretical value of the electron $g-2$ with its measured value in Penning trap experiment was used to determine the value of the fine-structure constant α. In 2018, the fine-structure constant was determined more precisely via cesium recoil measurements. This led to the theoretical determination of the electron $g-2$ standing $2.4\,\sigma$ above the experimental one. [57]. Two years later, an even more precise determination of the fine-structure constant was realized based on rubidium recoil measurement. [58] Surprisingly, this result is more that 5σ away from the cesium measurement. This also has an impact on the electron $g-2$ and based on the rubidium experiment, the theoretical prediction becomes smaller: it now stands $1.6\,\sigma$ *below* the experimental one. [58] Hopefully, future measurements will be able to clarify the situation.

Since QED, much progress has been made in quantum field theory: weak and strong interactions were better understood and modelled, leading to the famous Standard Model of elementary particles[9].

While the anomalous magnetic moment of the electron is mostly sensitive to QED, the situation is different for the muon. Because of its larger mass, all the sectors of the SM are required to match the current level of experimental accuracy. Even more intriguing is the fact that there is

[8] This fact is still used in nowadays muon $g-2$ experiments. Details on that topic are postponed to section 2.2.

[9] The fourth force, gravity, is not included in this Theory.

currently a discrepancy of 4.2σ between the theoretical and experimental determinations, which might indicate some New Physics [1–5, 7–9, 11–13, 24, 26–30, 57, 59–63]

$$\begin{aligned} a_\mu^{\text{exp}} &= 116\,592\,061(41) \times 10^{-11}\,, \\ a_\mu^{\text{th}} &= 116\,591\,810(43) \times 10^{-11}\,, \\ \Delta a_\mu &:= a_\mu^{\text{exp}} - a_\mu^{\text{th}} = 251(59) \times 10^{-11}\,. \end{aligned} \tag{2.13}$$

We have seen in this section that magnetic moments have driven our understanding of particles forward. Time and time again, deviations from the accepted theory have been observed, and have subsequently lead to significant developments. With the current state of the $(g-2)_\mu$ determination, we are now very close to confirming the discrepancy which could indicate a limitation of our current theories. Physics beyond the SM has been of great interest for years, and given the history of magnetic moments, it would seem fitting that the $(g-2)_\mu$ becomes the first confirmed discovery of New Physics.

It explains the amount of research about the muon anomalous magnetic moment, as physicists are trying to push this discrepancy to the 5σ threshold. It is however not an easy task, for several reasons. The experimental determination of the anomalous magnetic moment of the muon is more difficult than that of the electron, mostly because of the difference in lifetime of the two leptons. As the muon has a life time of $2 \cdot 10^{-6}$s [64], the Penning trap technique cannot be used. The measurement of the muon anomalous magnetic moment is the subject of the next section. On the theory side, the uncertainty is difficult to reduce because a_μ is dominated by low energies, where the strong interaction becomes non-perturbative. The status of the theoretical determination of this quantity is postponed to section 2.3.

2.2 Experiment principle

Almost twenty years ago, the Brookhaven E821 experiment measured the muon anomalous magnetic moment at a 0.54 part per million (ppm) accuracy. This result is 3.7σ higher than the current SM prediction. The running E989 experiment at Fermilab is aiming at confirming this result and reducing its uncertainty by a factor of 4. [4, 5]

The aim of this section is to shortly review the principles of the measurements of the $(g-2)_\mu$ experiment. For practical purposes, we focus on the ongoing E989 experiment at Fermilab. However, technical details about the apparatus involved and error control go beyond the scope of this introduction[10]. This review is mostly based on Aaron T. Fienberg's PhD thesis [65] as well as Fred Jegerlehner's book [33].

The measurement focuses on studying the motion of muons inside a magnetic field. Due to the Lorentz force, the particle will follow a circular path with an angular frequency called cyclotron frequency ω_c [65]

$$\vec{\omega}_c = -\frac{e\vec{B}}{m_\mu \gamma}\,, \tag{2.14}$$

where $\gamma = \left(1 - v^2\right)^{-1/2}$, with v the muon velocity (in units of c). The external magnetic field also affects the spin. The time-independent Hamiltonian describing the spin behavior (when the

[10]The interested reader can refer to [6] for more information.

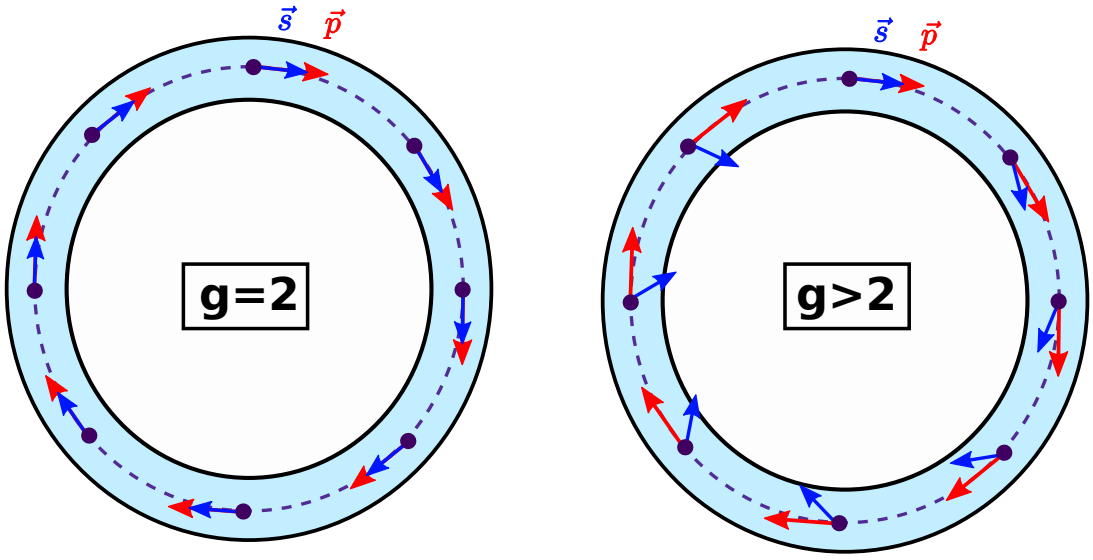

Figure 2.1: Evolution of the momentum and spin of a particle in a uniform magnetic field. When $g = 2$ (left), the two vectors rotate with the same frequency, but not when $g > 2$ (right). This figure is inspired from [66].

particle is at rest) is given by [65]

$$H = -g\mu_0 \vec{S} \cdot \vec{B} \,. \tag{2.15}$$

If we choose our coordinate systems such that the magnetic field points toward the z-direction, the time evolution of the system reads [65]

$$\mathcal{U}(t, t_0) = \exp[ig\mu_0 S_z B(t - t_0)] \,. \tag{2.16}$$

This equation has the same form as the operator that generates rotation about the z-axis. It means that the spin rotates about the external magnetic field with a precession angular frequency given by (in the laboratory frame) [65]

$$\vec{\omega}_s = -\frac{ge\vec{B}}{2m_\mu} - (1-\gamma)\frac{e\vec{B}}{m_\mu \gamma} \,, \tag{2.17}$$

where the first term can easily be read in (2.16) and the second term is the famous Thomas' precession, already mentioned in the historical review. It is a relativistic correction which accounts for the frequency difference between the particle rest frame and the laboratory frame. The situation is illustrated on Fig. 2.1: since g is slightly different from 2, the momentum and spin of the particle rotate at a different pace. The difference between the cyclotron frequency (2.14) and the spin precession frequency (2.17) is directly proportional to a_μ [65]

$$\vec{\omega}_a := \vec{\omega}_s - \vec{\omega}_c = -a_\mu \frac{e}{m_\mu} \vec{B} \,. \tag{2.18}$$

Therefore, if one can measure ω_a and the magnetic field precisely, a_μ follows.

The setup of the E989 experiment at Fermilab is represented on Fig. 2.2. The first step is to understand how muons are created[11]. We begin by focusing a proton beam onto an Inconel[12]

[11] The experiment actually studies anti-muon, but the anomalous magnetic moment is the same for a particle and its anti-particle, assuming that the underlying theory is CPT invariant. [6]

[12] a type of nickel-chromium superalloy

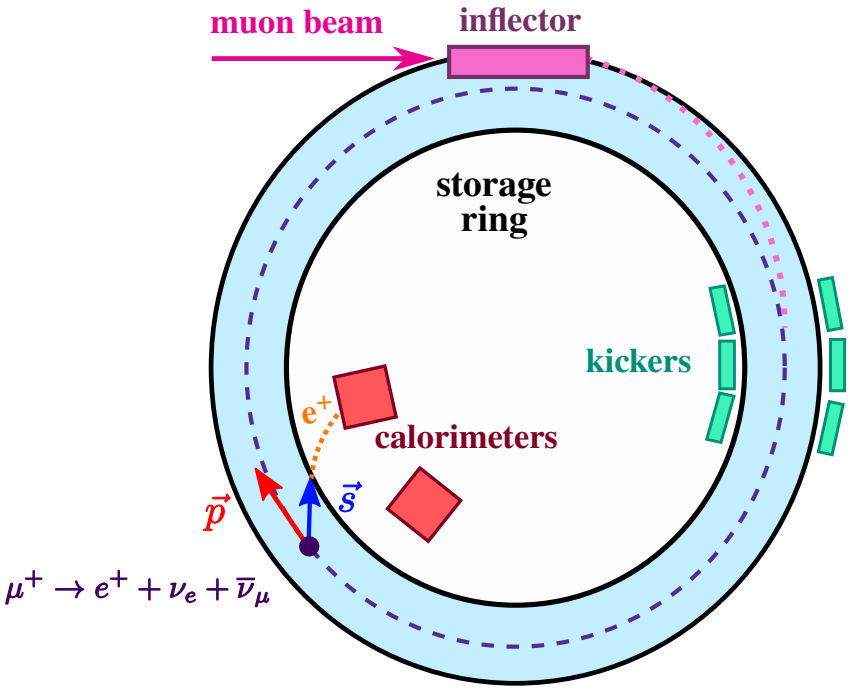

Figure 2.2: E989 at Fermilab. This figure is inspired from [67].

target, thereby creating positive pions. These pions then decay through weak interactions into a anti-muon (thereafter muon for simplicity) and a neutrino:

$$\pi^+ \longrightarrow W^+ \longrightarrow \mu^+ \nu_\mu \,.$$

The produced neutrino is left-handed, due to the maximal parity violation of the weak interactions (only left-handed neutrino interact with W bosons). Since the pion is spinless, angular momentum conservation implies that the created μ^+ is also left-handed. [33]

A magnetic inflector injects the muons in the storage ring close to their ideal trajectory, without modifying the magnetic field inside the chamber. This is an important feature as a uniform magnetic field is a necessary condition for (2.18) to hold. [68] During the first circulation of the muons in the storage ring, some kicker plates set the muons on the correct trajectory. [33]

The uniform magnetic field focalizes the muon beam in the radial direction, but not in the vertical direction. For that reason, a quadrupole electric field must be added in the storage chamber. It modifies the equation for the anomalous angular frequency (2.18) according to

$$\vec{\omega}_a = -\frac{e}{m}\left[a_\mu \vec{B} - \left(a_\mu - \frac{1}{\gamma^2 - 1}\right)\vec{\beta} \times \vec{E}\right] . \tag{2.19}$$

From the above equation, we see that for a special choice of γ, the effect of the electric field vanishes. This so-called magic $\gamma \approx 29.3$ corresponds to a momentum of 3.094 GeV/c.[13]

A precise determination of the anomalous angular frequency and of the magnetic field are therefore enough for an accurate determination of a_μ. The magnetic field is measured in the storage chamber using nuclear magnetic resonance probes: it can be extracted from the proton

[13] It is impossible for all the muons in the storage ring to be exactly at the magic momentum and this results in a lower observed frequency. This effect is accounted for in the analysis. [6]

Larmor frequency ω_p in the storage ring [65]

$$B = \frac{\omega_p}{2\mu_p}\,, \tag{2.20}$$

where μ_p is the magnetic dipole moment of the proton. In addition, the elementary charge is expressed as

$$e = \frac{4m_e\mu_e}{g_e}\,, \tag{2.21}$$

where m_e is the mass of the electron, g_e its g-factor and μ_e its magnetic dipole moment.

Finally, the value for the anomalous magnetic moment of the muon reads [65]

$$a_\mu = \frac{g_e}{2}\frac{\omega_a}{\tilde{\omega}_p}\frac{m_\mu}{m_e}\frac{\mu_p}{\mu_e}\,, \tag{2.22}$$

As mentioned before, the magnetic field in the storage ring is very uniform, but taking small fluctuations into account is necessary at the accuracy level aimed for in this experiment. For this reason, the Larmor frequency ω_p has been replaced by its value weighted by the muon distribution and averaged over the running time $\tilde{\omega}_p$ [6]. The g-factor of the electron g_e has been measured with sufficient precision from cyclotron spectroscopy [69]. In addition, recommended values from CODATA [70] are used for the ratios of masses m_μ/m_e and of the magnetic moments μ_p/μ_e, which are based on muonium spectroscopy [71]. [72]

The only thing left to discuss is the measurement of ω_a. The muons rapidly decay through weak interactions:

$$\mu^+ \to W^+ + \overline{\nu}_\mu \to \overline{\nu}_\mu + e^+ + \nu_e\,.$$

The direction of the muon spin and that of the positron momentum are correlated. The positron emission probability density in the muon rest frame reads [65]

$$\frac{\mathrm{d}^2P}{\mathrm{d}E\,\mathrm{d}\cos\theta} = N_r(E)\,(1 + A_r(E)\cos\theta)\,, \tag{2.23}$$

where θ is the angle between the muon spin and the positron momentum, N_r is the particle density and A_r is called asymmetry factor. The subscript r indicates that all these quantities are in the muon rest frame. N_r increases with the energy and A_r tends to 1 as the energy of the positron tends to the muon mass energy, which means that positrons are preferentially emitted along the muon spin. The density distribution (2.23) has to be boosted to the lab frame. This introduces a dependence in the angle between the muon momentum and spin, so that in the end, the density distribution is modulated by the cosine of the anomalous angular frequency [65]

$$\frac{\mathrm{d}^2P}{\mathrm{d}E\,\mathrm{d}t} \propto e^{-t/(\gamma\tau_\mu)}N_l(E)\,(1 + A_l(E)\cos(\omega_a t + \phi))\,. \tag{2.24}$$

The asymmetry factor A_l and the density N_l in the laboratory frame are different from the quantity A_r and N_r in the muon rest frame. Twenty-four calorimeters are placed around the muon storage ring and collect the emitted positrons. Their energy is measured as a function of time and the density (2.24) can be reconstructed and fitted to finally extract ω_a. [65] The principle of the Fermilab experiment is similar to the previous muon $g-2$ experiment held at Brookhaven twenty years prior. In particular, the muon storage ring has actually been transported between the two facilities. Thanks to improvements in technologies and higher statistics, the Fermilab experiment

aims at reducing the uncertainty by a factor of 4 compared to the previous experiment, reaching an unprecedented 0.14 ppm precision. [6]

The results of the first run of the E989 experiment have recently been released: see Fig. 2.3. [3] This result is compatible with the previous Brookhaven National Laboratory (BNL) result

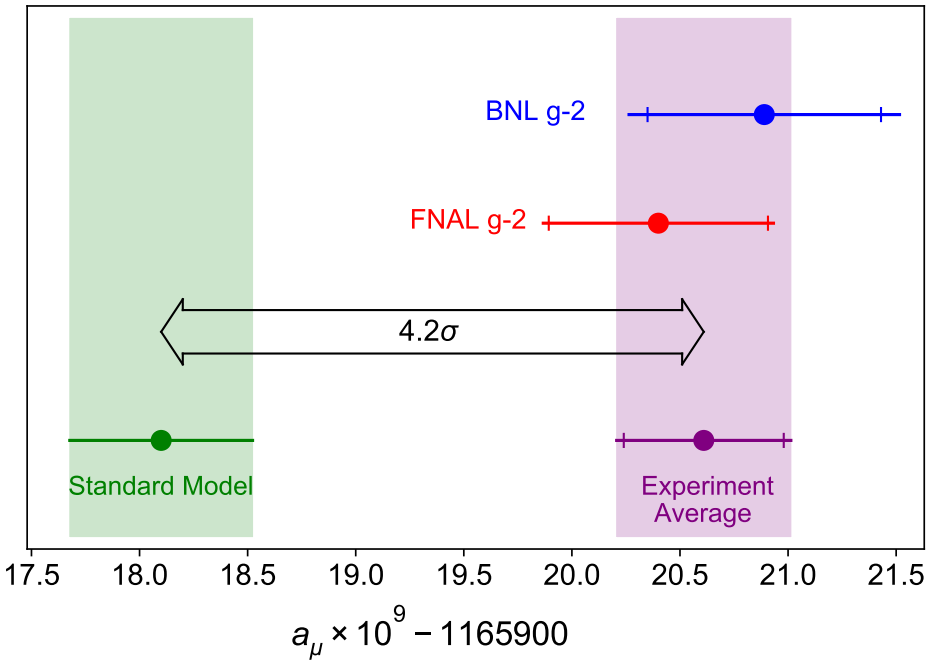

Figure 2.3: Result from the first run of the E989 experiment at Fermilab. The inner ticks on the experimental error bars indicate the statistical uncertainties. This figure is reproduced from Ref. [3].

and stands 3.3σ higher than the SM prediction. Since the uncertainty is mostly dominated by statistical effects[14], this result can be combined with the BNL result, leading to a total 4.2σ discrepancy. [3]

In addition, the upcoming J-PARC experiment (which uses less energetic muons and a smaller magnet [72]) will provide an important and independent crosscheck.

The experimental improvements described above are combined with a theoretical effort so that the uncertainty can be reduced on both sides, with the aim of reaching a conclusion on the possible discovery of physics beyond the Standard Model. The discussion of the theoretical determination of $(g-2)_\mu$ is the focus of the next section.

2.3 Theoretical determination

The aim of this section is to review the current status of the SM determination of a_μ. This discussion is mainly based on the recent white paper from the Muon $g-2$ Theory Initiative [4]. We begin with the QED contributions.

[14]The statistical part of the uncertainties is indicated by the inner ticks on the error bar.

2.3.1 QED contributions

The interaction of a lepton with an external magnetic field is embedded in the following class of diagrams

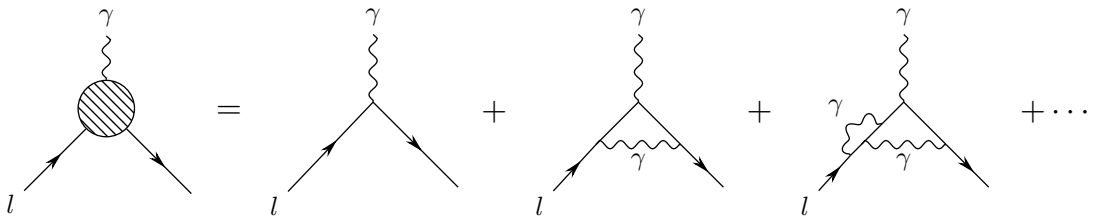

Figure 2.4: QED contributions to the anomalous magnetic moment of a lepton l.

The QED coupling constant is small, which leads to a well-defined ordering of the Feynman diagrams as shown in the figure above: diagrams with more loops are more difficult to compute but contribute less. Because of the external photon, this class of diagram has one Lorentz index and can be decomposed into

$$\Gamma^\mu = \gamma^\mu F_1(q^2) + \frac{i\sigma^{\mu\nu}q_\nu}{2m} F_2(q^2)\,, \tag{2.25}$$

where all the physical information is encapsulated in the two scalar functions F_1 and F_2. The former is called Dirac form factor and is related to the charge renormalization. The latter is called the Pauli form factor and is related to the anomalous magnetic moment in the static limit [73]

$$\lim_{q^2\to 0} F_2(q^2) = a\,. \tag{2.26}$$

The tree level diagram does not contribute to (2.26): the first contribution is the one-loop correction, which was calculated by Julian Schwinger in 1947 (see section 2.1). This contribution does not depend on the nature of the lepton: it is therefore the same for the electron and the muon. This is no longer the case for the two-loop contributions where the mass of the leptons explicitly appears. However, since a_μ is a dimensionless quantity, only lepton mass ratios can appear [4]

$$\begin{aligned} a_\mu^{\text{QED}} &= A_1 + A_2\left(\frac{m_\mu}{m_e}\right) + A_2\left(\frac{m_\mu}{m_\tau}\right) + A_3\left(\frac{m_\mu}{m_e}, \frac{m_\mu}{m_\tau}\right)\,, \\ A_i &= A_i^{(2)}\left(\frac{\alpha}{\pi}\right) + A_i^{(4)}\left(\frac{\alpha}{\pi}\right)^4 + A_i^{(6)}\left(\frac{\alpha}{\pi}\right)^3 + \cdots \end{aligned} \tag{2.27}$$

The functions $A_i^{(n)}$ can be calculated from the direct evaluation of Feynman diagrams: they can therefore be written as a series in the fine-structure α. Nowadays, the coefficients $A_i^{(2n)}$ for $i = 1, 2, 3$ and $n = 1, \ldots, 5$ are known, which corresponds to a full five-loop computation [15]. This leads to [4, 57, 59]

$$a_\mu^{\text{QED}} = 116\,584\,718.931(104) \times 10^{-11}\,, \tag{2.28}$$

where the error stems from the truncation of the series and of the uncertainty on the tau mass m_τ. The above value was evaluated using the fine-structure constant determination from cesium recoil measurements [74]. The QED contribution is by far the largest contribution to the muon anomalous magnetic moment and its error is well under control.

[15] Involving over 15,000 diagrams! [33]

2.3.2 Electroweak contributions

Electroweak contributions are those that contain at least one electroweak gauge boson: $W^{\pm}$, Z or the Higgs boson. Compared to the pure QED contributions described above, these contributions have more types of particles appearing in the loops. In addition, electroweak interactions violate parity. It will influence the Lorentz decomposition (2.25) as there is another building block available, the γ_5 matrix [75]

$$\Gamma^{\mu} = \gamma^{\mu} F_1(q^2) + \frac{i\sigma^{\mu\nu} q_{\nu}}{2m} F_2(q^2) + \frac{\sigma^{\mu\nu} q_{\nu}}{2m} \gamma_5 F_3(q^2) + \left(\gamma^{\mu} - \frac{2mq^{\mu}}{q^2}\right) \gamma_5 F_4(q^2) \,. \tag{2.29}$$

The interpretation of the first two terms remains unchanged: the anomalous magnetic moment is still given by (2.26). The new terms correspond to the dipole moment:

$$F_3(q^2) = -2md$$

and F_4 is called anapole. [75]

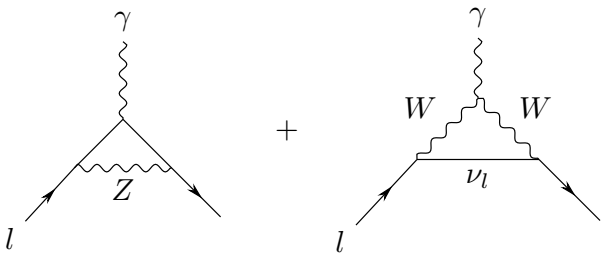

Figure 2.5: Examples of EW contributions to a_{μ}

Examples of electroweak contributions are shown in Fig. 2.5. One of their key features is that they are strongly suppressed by the boson masses. [4] For this reason, at the current accuracy goal, it is enough to consider a two-loop computation. Estimates of the leading logarithms beyond that have also been included, leading to [4, 60, 61]

$$a_{\mu}^{\mathrm{EW}} = 153.6(1.0) \times 10^{-11} \,. \tag{2.30}$$

2.3.3 Hadronic contributions

Hadronic contributions are very challenging because of the non-perturbative nature of the strong interaction at the muon mass scale. They currently largely dominate the theoretical uncertainty of the SM prediction for a_{μ}. There are two ways to deal with these contributions while still having control over the uncertainties. The first method is to use lattice QCD and the second is a data-driven approach. In the latter case, unitarity and analiticity properties of Green functions are used to relate the hadronic content of the $(g-2)_{\mu}$ contributions to other experimental quantities whose experimental error is under control. Below, we discuss how this can be done for the two main contributions: the Hadronic Vacuum Polarization (HVP) and the Hadronic Light-by-Light (HLbL) (see Figs. 2.6a and 2.6b respectively).

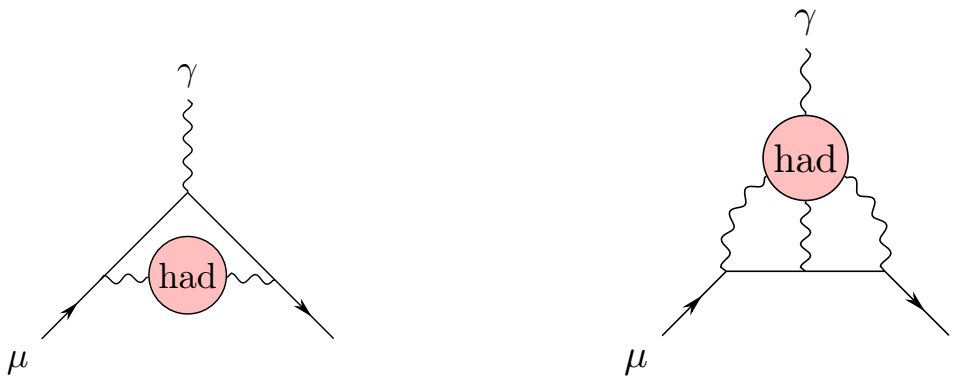

(a) Hadronic vacuum polarization (b) Hadronic light-by-light

Figure 2.6: Hadronic contributions to $(g-2)_\mu$. The pink blobs symbolize hadronic intermediate states.

2.3.3.1 Hadronic vacuum polarization

We consider the leading-order hadronic vacuum polarization contribution to $(g-2)_\mu$ represented in Fig. 2.6a. All the hadronic content is contained in the photon self-energy

$$\Pi^{\mu\nu}(q) := ie^2 \int \mathrm{d}x^4 e^{iq\cdot x} \langle 0|T\{j^\mu_{\mathrm{em}}(x) j^\nu_{\mathrm{em}}(0)\}|0\rangle = (q^2 g^{\mu\nu} - q^\mu q^\nu)\Pi(q^2)\,, \tag{2.31}$$

which has to be transverse due to the Ward identity $q_\mu \Pi^{\mu\nu}(q^2) = 0$. The above Green function is analytic in the $s := q^2$ plane and the Cauchy theorem therefore relates the full function and its imaginary part according to

$$\Pi(s) - \Pi(0) = \frac{s}{\pi} \int_{4m_\pi^2}^{\infty} \mathrm{d}s' \frac{\mathrm{Im}(\Pi(s'))}{s'(s'-s)}\,. \tag{2.32}$$

Expressing the function this way is advantageous because the imaginary part can then be written in terms of the total hadronic e^+e^- cross section thanks to the optical theorem. Neglecting the electron mass, this relation reads

$$\frac{3}{\alpha}\mathrm{Im}\left(\Pi(s)\right) = \frac{3s}{4\pi\alpha^2}\sigma(e^+e^- \to \text{hadrons}) =: R_{\mathrm{had}}(s)\,, \tag{2.33}$$

where the function R_{had} is called the R-ratio. These considerations lead to the following expression for the muon $g-2$ contribution [76]

$$a_\mu = \left(\frac{\alpha m_\mu}{3\pi}\right)^2 \int_{4m_\pi^2}^{\infty} \mathrm{d}s \frac{\hat{K}(s) R_{\mathrm{had}}(s)}{s^2}\,, \tag{2.34}$$

where $\hat{K}$ is a known kernel function that grows from 0.63 at the hadron production threshold $4m_\pi^2$ and tends to 1 at high s. Because of the $1/s^2$ factor, low-energy contributions to the hadronic R-ratio R_{had} dominate the $(g-2)_\mu$ integral.

Below 2 GeV, the total cross section is obtained by summing over all possible final states. There exists data for over 35 exclusive channels in that region: see Fig. 2.7. The dominating channel is the two-pion channel, which accounts for about 70% of the total a_μ^{HVP}. [4]

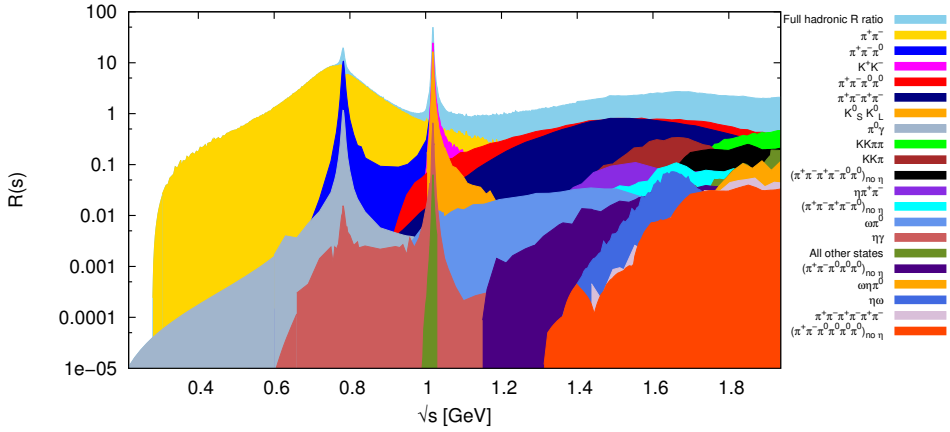

Figure 2.7: Exclusive channels contribution to the hadronic R-ratio. This figure is reproduced from Ref. [8].

Above 2 GeV, considering exclusive channels becomes impossible for two reasons: measurements on exclusive channels usually do not reach such energies and the number of high multiplicity states that need to be included increases. Instead, one has to either consider inclusive measurements or perturbative QCD[16].

The main difficulty in the determination of $a_\mu^{\rm HVP}$ is deciding how to combine the different data. In particular, the range where pQCD is more reliable than inclusive data is debated and different groups use different prescriptions. [4]

In addition to the diagram displayed in Fig. 2.6a and discussed so far, the current accuracy goal requires the consideration of NLO and NNLO HVP contribution: see Fig 2.8.

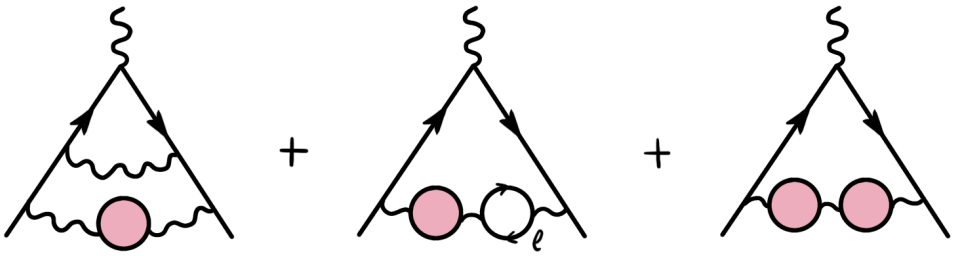

Figure 2.8: Higher order HVP contributions. This figure is based on Ref. [13].

This finally leads to [4, 7–13]

$$a_\mu^{\rm HVP} = 6845(40) \times 10^{-11}\,, \tag{2.35}$$

where the uncertainty is one order of magnitude larger than that of the QED and EW sectors and stems mostly from the experimental error on the data used in the analysis. The white paper lattice result for that quantity [4, 14–22] ,

$$a_\mu^{\rm HVP,\ lattice} = 7116(184) \times 10^{-11}\,, \tag{2.36}$$

[16]The perturbative contribution to (2.31) from QCD as well as non-perturbative corrections can be computed with a framework called the operator product expansion (OPE). This will be discussed in the next chapter.

has a larger error: this result is both compatible with the dispersive estimation and the "no new physics scenario". This result was not included in the final SM estimation of a_μ because of the large error. [4] Since the completion of the white paper [4], a new lattice result has been released [23]. Their result

$$a_\mu^{\mathrm{HVP}} = 7075(55) \times 10^{-11}\,, \tag{2.37}$$

has a much smaller uncertainty and seems to tend toward a no new physics interpretation. However, this result should be replicated by other studies before any firm conclusion can be drawn. [23]

2.3.3.2 Hadronic light-by-light contribution

We now discuss the hadronic light-by-light contribution to a_μ^{SM}: see Fig. 2.6b. It is suppressed by an extra power of α compared to the HVP. It is therefore smaller, but it is also a more complicated calculation and the uncertainty is non-negligible at the desired accuracy level.

The hadronic content of this contribution is contained in the light-by-light tensor, evaluated in pure QCD (i.e. with the electromagnetic coupling constant set to 0) [77]

$$\Pi^{\mu\nu\lambda\sigma}(q_1,q_2,q_3) \equiv -i \int \mathrm{d}^4x \mathrm{d}^4y \mathrm{d}^4z e^{-i(q_1\cdot x+q_2\cdot y+q_3\cdot z)} \langle 0|T\left\{j^\mu_{\mathrm{em}}(x) j^\nu_{\mathrm{em}}(y) j^\lambda_{\mathrm{em}}(z) j^\sigma_{\mathrm{em}}(0)\right\}|0\rangle\,, \tag{2.38}$$

where $j^\mu_{\mathrm{em}}(x) = \frac{2}{3}\overline{u}(x)\gamma^\mu u(x) - \frac{1}{3}\overline{d}(x)\gamma^\mu d(x) - \frac{1}{3}\overline{s}(x)\gamma^\mu s(x)$ is the light quark electromagnetic current: see Fig. 2.9.

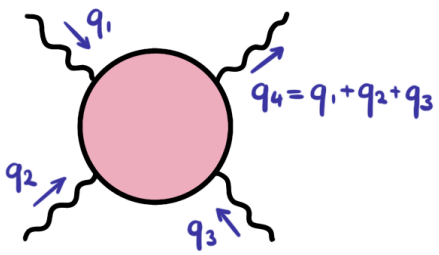

Figure 2.9: Hadronic light-by-light tensor.

A data-driven approach for the hadronic light-by-light tensor is not as evident as for the case of HVP because the unitary relation for the four-point function (2.38) is significantly more complicated and does not involve a single experimental quantity.

The first difficulty is that, contrary to HVP, the HLbL tensor has four Lorentz indices. One can therefore write 138 different Lorentz structures from the four-momenta and the metric tensor [77]

$$\Pi^{\mu\nu\lambda\sigma} = \sum_{i=1}^{138} L_i^{\mu\nu\lambda\sigma} \Xi_i\,. \tag{2.39}$$

However, because of gauge invariance, these structures are not independent. Following the BTT procedure[17], it is possible to write a decomposition involving 54 scalar functions that are free of

[17] After Bardeen and Tung [78] and Tarrach [79].

kinematic zeros and singularities and are therefore amenable to a dispersive treatment [77]

$$\Pi^{\mu\nu\lambda\sigma} = \sum_{i=1}^{54} T_i^{\mu\nu\lambda\sigma} \Pi_i \,. \tag{2.40}$$

Once the scalar functions are known, the $(g-2)_\mu$ contribution can be computed thanks to the master integral (once the appropriate limit $q_4 \to 0$ has been considered)

$$a_\mu^{\mathrm{HLbL}} = \frac{2\alpha^3}{3\pi^2} \int_0^\infty \mathrm{d}Q_1 \int_0^\infty \mathrm{d}Q_2 \int_{-1}^1 \mathrm{d}\tau \sqrt{1-\tau^2} Q_1^3 Q_2^3 \sum_{i=1}^{12} T_i(Q_1, Q_2, \tau) \overline{\Pi}_i(Q_1, Q_2, \tau) \,, \tag{2.41}$$

where $Q_i^2 = -q_i^2$, $Q_3^2 = Q_1^2 + Q_2^2 + 2\tau Q_1 Q_2$, the T_i are known kernel functions[18] and the functions $\overline{\Pi}_i$ are combinations of the scalar functions Π_j that appear in (2.40)[19].

In a data-driven approach, dispersion relations are used to relate the scalar functions appearing in (2.41) to other quantities that can be measured/for which there exist experimental results. In the context of $(g-2)_\mu$, the external photon is soft and this a priori leads to two different dispersive methods for describing the HLbL tensor and its contribution to $(g-2)_\mu$[20] [30].

- **Method 1:** The first method (m1) consists of describing the HLbL tensor for general kinematics (i.e. with $q_4 \neq 0$). In that case, six independent kinematic variables are required. Those can be chosen to be two of the Mandelstam variables and the four photon virtualities:

$$\begin{aligned} &s := (q_1 + q_2)^2 \,, \\ &t := (q_1 + q_3)^2 \,, \\ &q_i^2, \ \text{for } i = 1, 2, 3, 4 \,. \end{aligned} \tag{2.42}$$

  It is then possible to write a Mandelstam representation for the scalar functions Π_i, by considering fixed virtualities[21] and cuts in the s, t and u-channels [77].

  The optical theorem can then be used to relate the discontinuities of the scalar functions to subprocesses that are unambiguously defined by the on-shell intermediate states appearing in the cuts: see Fig. 2.10.

  In addition, thanks to the kernel functions T_i, processes with lighter intermediate states are expected to contribute more. The dominant contribution is therefore the one with a single on-shell pion. Other one-particle intermediate states include different pseudoscalars, such as the η and η', scalar, tensor and axial resonances. The dominant two-particle intermediate states is that with a two-pion cut. The latter can be further decomposed through a secondary cut in the cross-channel. The contribution with a pion pole in the secondary cut is called the pion box. Other states, such as multi-pion states or heavier

[18] Expressions can be found in Ref. [27].

[19] The relations between the $\overline{\Pi}$ and Π can also be found in Ref. [27].

[20] Other methods for the computation of a_μ^{HLbL} rely on the dispersive description of the Pauli form factor [80,81] or the Schwinger sum rule [82], but will not be discussed here.

[21] The virtuality of the external photon q_4^2 can be set to 0 from the beginning.

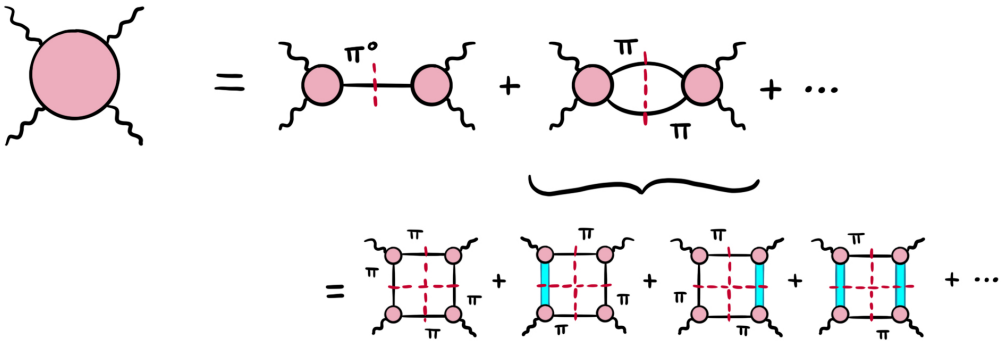

Figure 2.10: Dispersive contributions for the HLbL tensor with general kinematics. The pink blobs represent hadronic interaction, the red cuts indicate that the intermediary states are on-shell and the thick cyan lines indicate states heavier than pions. This picture is based on Ref. [27].

resonances can also show up in the secondary cut. [4, 27, 77] The limit $q_4 \to 0$ is only considered afterwards and can be expressed as

$$s \to q_3^2\,,$$
$$t \to q_2^2\,.$$

The hadronic content in the contribution listed above can then be related to data and their contribution to $(g-2)_\mu$ evaluated. This was the method developed in Bern in Refs. [27,77] and which is currently used in the white paper [4].

- **Method 2:** The second method (m2) would consist of directly setting $q_4 = 0$ in the HLbL tensor and of writing a dispersion relation directly in that limit. [30] In that case, there are three independent variables and the Mandelstam variables would be directly related to the photon virtualities

$$s = q_3^2\,,$$
$$t = q_2^2\,,$$
$$u = q_1^2\,.$$

Such a dispersion relation would look complicated and involve cuts in the HLbL amplitudes (see Fig. 2.11a) as well as cuts separating one electromagnetic current from the rest (see Fig. 2.11b). [30]

The two methods described above to construct a dispersive description of the HLbL are equally valid, and must lead to the same results once all the intermediary states are taken into account. However, single contributions cannot be directly compared[22].

Regardless of which method is chosen, as the energy increases, intermediate states with more particles need to be included in the cuts and the computational difficulty escalates. But, similarly to the HVP case, it is expected that perturbative QCD becomes relevant at sufficiently high energy. However, the situation is again more complicated for HLbL because there is more than one scale at play: two regimes are relevant, leading to two **short-distance constraints**

[22]This point will be addressed further below.

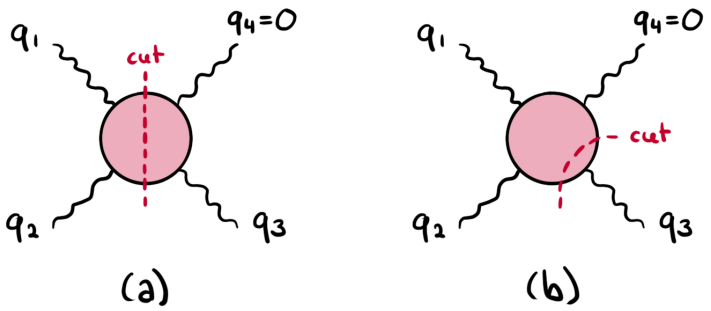

Figure 2.11: Possible cuts appearing in a dispersive description of the HLbL tensor in the $g-2$ kinematics: (a) Cuts in the HLbL amplitudes, (b) Cuts generated by states coupling to one electromagnetic current.

(SDCs)[23]. The first regime of interest is the one where all three photon virtualities are large: $Q_1 \approx Q_2 \approx Q_3 \gg \Lambda_{\text{QCD}}$. In that case, the HLbL tensor is well described by the perturbative quark loop. This has been suspected for a while, but it is a priori not obvious why this should be true for the $g-2$ kinematics. It was only proven recently, using an operator product expansion in presence of an external photon. [1,37,38] This framework will be introduced in the next chapter and the aforementioned proof is the main topic of chapter 4. The other regime of interest is when two photon virtualities are much larger than the third. In that case, it is possible to use an OPE on two of the four electromagnetic currents in (2.38), leading to the so-called Melnikov-Vainshtein constraint on the HLbL tensor [2]

$$\Pi_{\mu\nu\lambda\sigma}(q_1,q_2,q_3) \overset{Q_1^2\approx Q_2^2\gg Q_3^2}{\longrightarrow} 2i\frac{q^\alpha}{q^2}\epsilon_{\mu\nu\alpha\beta}\int \mathrm{d}^4x\,\mathrm{d}^4y e^{-i(q_1+q_2)\cdot x}e^{-iq_3\cdot y}\,\langle 0|T\{j_5^\beta(w)j_\lambda^{\text{em}}(z)j_\sigma^{\text{em}}(0)\}|0\rangle\,, \tag{2.43}$$

where $q \equiv \frac{q_1+q_2}{2} \approx q_1 \approx -q_2$ and $j_5^\mu(x) = \overline{\psi}(x)\mathcal{Q}^2\gamma^\mu\gamma^5\psi(x)$ is the axial current with $\psi = (u,\,d,\,s)^T$, $\mathcal{Q} = \text{diag}(2/3,-1/3,-1/3)$ and $\gamma^5 = i\gamma^0\gamma^1\gamma^2\gamma^3$. The convention $\epsilon^{0123} = +1$ is used for the epsilon tensor. This has led to a controversy, because the way to reconcile this constraint with the dispersive treatment for HLbL described here was not obvious. [2,30,39–42,83]

To understand the debate better, we now focus on the pion-pole contribution. Its definition depends on the dispersion relation used for HLbL and it only contributes to the first scalar function $\hat{\Pi}_1$ (and the crossed versions). [27,77] In the first dispersive method (m1), the pion pole arises from [30,43,77]

$$\hat{\Pi}_1^{\pi^0,\text{m1}} = \lim_{s\to q_3^2}\frac{F_{\pi^0\gamma^*\gamma^*}(q_1^2,q_2^2)F_{\pi^0\gamma^*\gamma^*}(q_3^2,q_4^2)}{s-m_\pi^2}\bigg|_{q_4^2=0} = \frac{F_{\pi^0\gamma^*\gamma^*}(q_1^2,q_2^2)F_{\pi^0\gamma^*\gamma^*}(q_3^2,0)}{q_3^2-m_\pi^2} \tag{2.44}$$

where $F_{\pi^0\gamma^*\gamma^*}$ is the pion transition form factor (TFF), defined through

$$i\int \mathrm{d}^4x\, e^{iq_1\cdot x}\left\langle 0\middle|T\left\{j_\mu^{\text{em}}(x)j_\nu^{\text{em}}(0)\right\}\middle|\pi^0(q_1+q_2)\right\rangle =: \epsilon_{\mu\nu\alpha\beta}q_1^\alpha q_2^\beta F_{\pi^0\gamma^*\gamma^*}(q_1^2,q_2^2)\,. \tag{2.45}$$

In the second dispersive method, the pion pole would arise from [43]

$$\hat{\Pi}_1^{\pi^0,\text{m2}} = \lim_{q_4\to 0}\frac{F_{\pi^0\gamma^*\gamma^*}(q_1^2,q_2^2)F_{\pi^0\gamma^*\gamma^*}(q_3^2,q_4^2)}{(q_3+q_4)^2-m_\pi^2} = \frac{F_{\pi^0\gamma^*\gamma^*}(q_1^2,q_2^2)F_{\pi^0\gamma^*\gamma^*}(m_\pi^2,0)}{q_3^2-m_\pi^2}\,. \tag{2.46}$$

[23]Note that we are now looking at SDCs from pQCD on the hadronic light-by-light tensor and not on the contributions from a dispersive description. We can therefore simply work with $q_4 = 0$ directly.

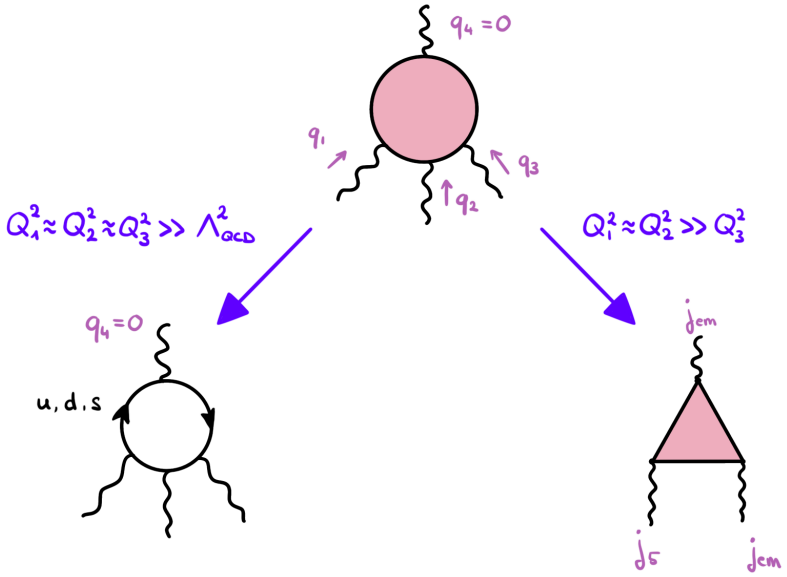

Figure 2.12: High-energy domains for the HLbL tensor. When the three photon virtualities are large, the tensor is well described by the quark loop. When two virtualities are much larger than the third, the HLbL tensor is related to the three point function of two electromagnetic and one axial current.

It needs to be stressed that these two pion poles are not equivalent and are contributions from different dispersive descriptions. [30, 43] However, it can be noticed that [30]

$$\hat{\Pi}_1^{\pi^0,m1} = \hat{\Pi}_1^{\pi^0,m2} + \frac{F_{\pi^0\gamma^*\gamma^*}(q_1^2,q_2^2)\left(F_{\pi^0\gamma^*\gamma^*}(q_3^2,0) - F_{\pi^0\gamma^*\gamma^*}(m_\pi^2,0)\right)}{q_3^2 - m_\pi^2}\,, \tag{2.47}$$

where the second term on the right-hand side does not have a pole at $q_3^2 = m_\pi^2$ and is generated from a cut through the singly-virtual TFF. [30] We therefore see that going from one description to the other simply corresponds to a reshuffling of the contributions from different cuts. [30] The Melnikov-Vainshtein constraint can be translated into the BTT language, leading to the following expression for the third isospin component of the first scalar function in the chiral limit[24]

$$\hat{\Pi}_1^{(3)}(q,q,q_3) \overset{-q^2\gg -q_3^2}{\to} -\frac{1}{6\pi^2 q^2 q_3^2}\,. \tag{2.48}$$

In that limit, the pion-pole contribution from method 2 (2.46) has exactly the right behavior because the pion TFF satisfies [25]

$$F_{\pi^0\gamma^*\gamma^*}(0,0) = \frac{1}{4\pi^2 F_\pi} \tag{2.49}$$

$$\lim_{-q^2\to\infty} q^2 F_{\pi^0\gamma^*\gamma,^*}(q^2,q^2) = \frac{2F_\pi}{3}\,. \tag{2.50}$$

The authors of Refs. [2, 83] have therefore suggested that

$$\hat{\Pi}_1^{\mathrm{MV}}(q_1,q_2,q_3) = \frac{F_{\pi^0\gamma^*\gamma^*}(q_1^2,q_2^2)F_{\pi^0\gamma^*\gamma^*}(0,0)}{q_3^2 - m_\pi^2}\,, \tag{2.51}$$

[24] This is explained in details in Ref. [30] or chapter 5 of this work.

[25] The second equation below results from the operator product expansion of two electromagnetic currents and will be discussed in section 3.4.

would be an accurate description of the full $\hat{\Pi}_1^{(3)}$. However, there is no reason why this should be the case for small virtualities q_1^2 and q_2^2. Instead, if one wants to use the pion pole (2.46), a dispersion relation for method 2 needs to be worked out so that other contributions can be included in a consistent manner and so that the low-energy which dominates the $g-2$ integral can be accurately described. In chapter 5 [30], we will instead see how the SDC can be reconciled with method 1.

The pion pole from method 1 (2.44) does not fulfil the constraint (2.48) on its own. This is not a problem *per se*, as pointed out also in Ref. [43][26]. Other states couple to the axial current $j_5^{\mu,(3)}(x)$ and must be responsible for the behaviour of the full scalar function in that regime.

The dispersive determination of the HLbL contribution (method 1), which is based on all the considerations described above, leads to [1, 2, 4, 26–36]

$$a_\mu^{\text{HLbL,LO}} = 92(19) \times 10^{-11}\,. \tag{2.52}$$

where the error is dominated by the short-distance description.

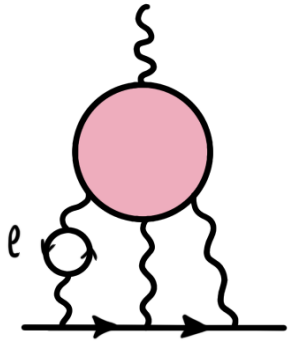

Figure 2.13: NLO HLbL contributions. A lepton loop is included on one of the intermediate photon propagators.

NLO contributions to HLbL (see Fig. 2.13) have also been estimated, leading to [4, 63]

$$a_\mu^{\text{HLbL,NLO}} = 2(1) \times 10^{-11}\,. \tag{2.53}$$

The lattice result for the HLbL contribution is [4, 24]

$$a_\mu^{\text{HLbL, lattice}} = 78.7(30.6)_{\text{stat}}(17.7)_{\text{syst}} \times 10^{-11}\,, \tag{2.54}$$

with an uncertainty comparable to one obtained with dispersive methods. The final white paper value for the HLbL contribution therefore combines the two results, leading to [4]

$$a_\mu^{\text{HLbL}} = 92(18) \times 10^{-11}\,. \tag{2.55}$$

Since the publication of the white paper, a new lattice result has been obtained [25]

$$a_\mu^{\text{HLbL}} = 106.8(14.7) \times 10^{-11}\,. \tag{2.56}$$

It is more precise than the previous lattice result from Ref. [24] and consistent with the white paper value for HLbL.

[26] The connection between the two methods m1 and m2 for the pseudoscalar poles and the consequences of the constraint (2.43) for these individual contributions have been worked out and discussed in details in Ref. [43].

2.3.4 Standard Model prediction

By combining all the sectors, one finally finds the Standard Model prediction [1, 2, 4, 7–9, 11–13, 24, 26–30, 57, 59–63]

$$a_\mu^{\mathrm{SM}} = a_\mu^{\mathrm{QED}} + a_\mu^{\mathrm{EW}} + a_\mu^{\mathrm{HVP}} + a_\mu^{\mathrm{HLbL}} = 116\,591\,810(43) \times 10^{-11}\,. \tag{2.57}$$

In the future, the theoretical uncertainty should be reduced further in order to match the accuracy goal of Fermilab. Further improvements will rely on more precise data for the hadronic contributions as well as progress in lattice QCD.

Chapter 3

Operator product expansion

> If you think you understand quantum mechanics, you don't understand quantum mechanics.
>
> Richard Feynman

In this chapter, the Operator Product Expansion (OPE) is introduced. It is a central tool in QFT and can be used to deal with some non-perturbative aspects of quantum chromodynamics (QCD). We begin with a short review of the renormalization of QCD and the $\overline{\text{MS}}$-scheme in section 3.1. This will allow us to fix notations and to introduce some concepts - such as the scale dependence of renormalized coupling constants - which will be central for the OPE in QCD. The latter is formally introduced in the subsequent section 3.2. Technical aspects of the OPE (in a vacuum) are treated in section 3.3, by means of an explicit example: the derivation of the high-energy behavior the HVP contribution to $(g-2)_\mu$. This knowledge will also be useful to understand the derivation of the Melnikov-Vainshtein constraint on the HLbL tensor, discussed in section 5.2.3.2. Finally, we look at what changes when the OPE is performed in presence of an external photon in section 3.4. This less common OPE is necessary to derive one of the SDC of HLbL in the $(g-2)$ kinematics. This specific point will be expanded upon in the next chapter.

3.1 Renormalization in QCD

QCD is a non-abelian gauge theory associated with the symmetry group $SU(3)$ and describes the strong interactions in the SM. Its Lagrangian reads [73]:

$$\begin{aligned}\mathcal{L}_{\text{QCD}} = &-\frac{1}{4}(\partial_\mu G^a_{0,\nu} - \partial_\nu G^a_{0,\mu})^2 + \overline{q}_0(i\not{\partial} - m_{q,0})q_0 - \overline{c}^a_0\partial^2 c^a_0 \\ &- \frac{1}{2\xi_0}(\partial^\mu G^a_{0,\mu})^2 + g_{s,0}G^a_{0,\mu}\overline{q}_0\gamma^\mu t^a q_0 - g_{s,0}f^{abc}(\partial_\mu G^a_{0,\nu}G^{b,\mu}_0 G^{c\nu}_0) \\ &- \frac{1}{4}g_{s,0}(f^{eab}G^a_{0,\mu}G^b_{0,\nu})(f^{ecd}G^{c\mu}_0 G^{d\nu}_0) - g_{s,0}\overline{c}^a_0 f^{abc}\partial^\mu G^b_{0,\mu}c^c_0\,, \end{aligned} \tag{3.1}$$

where q_0 is the quark color triplet of flavor q ($q = u, d, s, c, b, t$), $G^a_{0,\mu}$ the gluon field and c^a_0 the ghost field. Finally, ξ is the gauge-fixing parameter, $g_{s,0}$ is the strong coupling and $m_{q,0}$ the

quark mass. The subscripts 0 stand for bare quantities. The non-abelian structure manifests itself in the group structure: the t_a are the group generators satisfying

$$[t^a, t^b] = if^{abc}t_c\,, \tag{3.2}$$

which leads to gluon self-interaction vertices. In addition, ghost particles must appear in loops to preserve unitarity.

When the above Lagrangian is used to compute diagrams that contain loops, infinities often arise. This is due to the fact that loops correspond to integrals over all possible momenta and that the integrands often diverge at high-energies. There is in principle an infinite number of such problematic diagrams, which a priori renders the perturbative expansion meaningless. This issue has been a huge setback in the development of QFT (see section 2.1). However, the plethora of divergences showing up in QCD can be reduced to seven problematic amplitudes, displayed in Fig. 3.1. The latter can be made finite order by order in perturbation theory through a redefinition of the Lagrangian fields and parameters. It can then be shown that all the physical amplitudes will be finite as well (at the considered order in perturbation theory). [84,85] The first

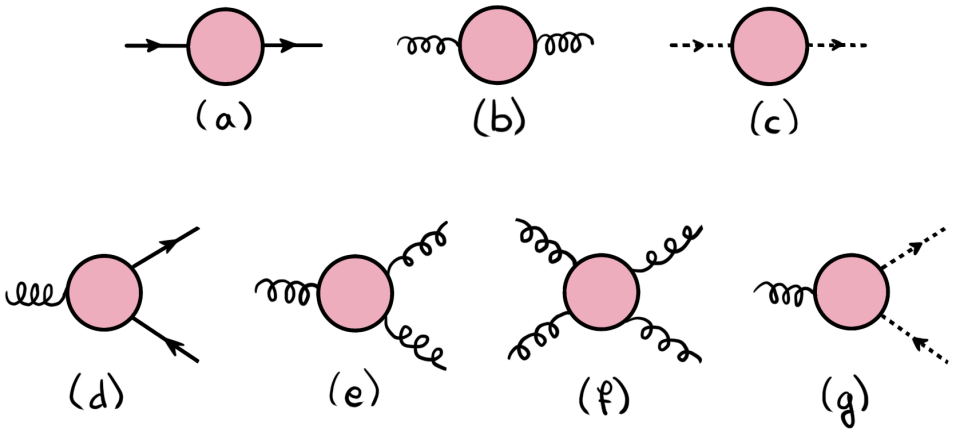

Figure 3.1: Superficially divergent amplitudes in QCD.

step, called regularization, is to parametrize the divergences. It is customary to use *dimensional regularization* in QCD. The idea is to consider the theory in d spacetime dimensions instead of four. The symmetries are preserved by this choice and the problematic integrals become d-dimensional as well. This introduces a new parameter $\epsilon := \frac{4-d}{2}$ which has to be taken to zero in order to recover the original theory at the end of the calculation. The problematic divergences in 4-dimensions simply become poles in $1/\epsilon$. [73, 84, 85]

Consider now the following rescaling of the d-dimensional fields

$$\begin{aligned} q_0 &= Z_2^{1/2} q_r\,, \\ G^a_{\mu,0} &= Z_3^{1/2} G^a_{\mu,r}\,, \\ c^a_0 &= Z_{2c}^{1/2} c^a\,, \end{aligned} \tag{3.3}$$

the subscript r stands for renormalized quantities and the different Z are renormalization factors

to be determined. The strong coupling constant should also be rescaled[1]

$$Z_2 Z_3^{1/2} g_{s,0} = \mu^\epsilon Z_1 g_{s,r}\,, \tag{3.4}$$

$$Z_2 m_{q,0} = Z_m m_{q,r}\,, \tag{3.5}$$

$$\xi_0 = Z_3 \xi_r\,. \tag{3.6}$$

Notice the factor μ^ϵ appearing in (3.4): μ is an arbitrary scale introduced to make the renormalized coupling constant dimensionless in d-dimensions. The original Lagrangian can then be rewritten as follows [73]

$$\begin{aligned}
\mathcal{L}_{\rm QCD} = \quad & -\tfrac{1}{4}(\partial_\mu G^a_{r,\nu} - \partial_\nu G^a_{r,\mu})^2 + \overline{q}_r(i\partial\!\!\!/ - m_{q,r})q_r - \overline{c}^a_r \partial^2 c^a_r \\
& -\tfrac{1}{2\xi_r}(\partial^\mu G^a_{r,\mu})^2 + g_{s,r} G^a_{r,\mu}\overline{q}_r\gamma^\mu t^a q_r - g_{s,r} f^{abc}(\partial_\mu G^a_{r,\nu} G^{b,\mu}_r G^{c\nu}_r) \\
& -\tfrac{1}{4} g_{s,r}(f^{eab} G^a_{r,\mu} G^b_{r,\nu})(f^{ecd} G^{c\mu}_r G^{d\nu}_r) - g_{s,r}\overline{c}^a_r f^{abc}\partial^\mu G^b_{r,\mu} c^c_r \\
& -\delta_3 \tfrac{1}{4}(\partial_\mu G^a_{r,\nu} - \partial_\nu G^a_{r,\mu})^2 + \overline{q}_r(i\delta_2\partial\!\!\!/ - \delta_m m_{q,r})q_r - \delta_{2c}\overline{c}^a_r\partial^2 c^a_r \\
& +\delta_1 g_{s,r} G^a_{r,\mu}\overline{q}_r\gamma^\mu t^a q_r - \delta_1^{3g} g_{s,r} f^{abc}(\partial_\mu G^a_{r,\nu} G^{b,\mu}_r G^{c\nu}_r) \\
& -\delta_1^{4g}\tfrac{1}{4} g_{s,r}(f^{eab} G^a_{r,\mu} G^b_{r,\nu})(f^{ecd} G^{c\mu}_r G^{d\nu}_r) - \delta_1^c g_{s,r}\overline{c}^a_r f^{abc}\partial^\mu G^b_{r,\mu} c^c_r\,,
\end{aligned} \tag{3.7}$$

(first group: same as the original Lagrangian (3.1) with renormalized instead of bare quantities; second group: counterterms)

where

$$\begin{aligned}
&\delta_2 = Z_2 - 1\,, \quad && \delta_3 = Z_3 - 1\,, && \delta_{2c} = Z_{2c} - 1\,, && \delta_m = (Z_m - 1)\,, \\
&\delta_1 = \mu^\epsilon Z_1 - 1\,, && \delta_1^{3g} = \mu^\epsilon Z_1 Z_2^{-1} Z_3 - 1\,, && \delta_1^{4g} = \mu^\epsilon (Z_1 Z_2^{-1})^2 - 1\,, && \delta_1^c = \mu^\epsilon Z_1 Z_2^{-1} Z_{2c}\,.
\end{aligned} \tag{3.8}$$

The counterterms can then be adjusted to cancel the aforementioned divergences. To illustrate the procedure, we are going to explicitly consider the calculation δ_2 at one loop order. The relevant amplitude is the quark propagator: see Fig. 3.1a. It can be fully expressed in terms of the *quark self-energy*, a *one-particle irreducible* (1PI) diagram, as shown in Fig. 3.2. 1PI diagrams are connected diagrams which cannot be separated into two diagrams by cutting a single internal line.

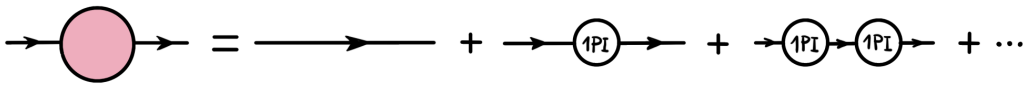

Figure 3.2: Full quark propagator as a function of the quark self-energy.

The quark self-energy can be Lorentz decomposed as follows [85]

$$\Sigma(\not{p})^{(2)} = \Sigma_1^{(2)}(p^2) + (\not{p} - m)\Sigma_2^{(2)}(p^2)\,, \tag{3.9}$$

where the upper index (2) indicates that the quantity is considered up to second order in the strong coupling constant $g_{s,r}$ (or equivalently at one-loop order). At one-loop order, when expressing the amplitude in terms of renormalized quantities, there is only one diagram that contributes to the quark self-energy and the associated counterterm (which we are trying to determine): see Fig. 3.3. [85] Using dimensional regularization, the corresponding amplitudes

[1] Gauge invariance imposes some relations between the rescaling of the different interactions vertices, reducing the number of required renormalization parameters.

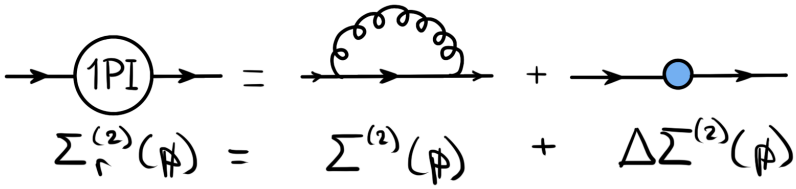

Figure 3.3: Quark self-energy at one loop order.

read [84, 85]

$$\Sigma_1^{(2)}(p^2) = -3m_{r,q}\mu^{2\epsilon}\frac{\alpha_{s,R}}{4\pi}C_F\left(\frac{1}{\hat{\epsilon}} + \text{finite terms}\right),$$
$$\Sigma_2^{(2)}(p^2) = \xi\mu^{2\epsilon}\frac{\alpha_{s,R}}{4\pi}C_F\left(\frac{1}{\hat{\epsilon}} + \text{finite terms}\right), \tag{3.10}$$

where we have defined $\alpha_{s,r} = \frac{g_{s,r}^2}{4\pi}$, $\frac{1}{\hat{\epsilon}} := \frac{1}{\epsilon} - \gamma + \log 4\pi$, γ is the Euler-Mascheroni constant and $C_F = \frac{N_c^2-1}{2N_c} = \frac{4}{3}$ is a group theory factor involving the number of colors $N_c = 3$. The counterterm simply reads (the appropriate Feynman rules can be read out off the Lagrangian (3.7)) [84]

$$\Delta\Sigma^{(2)}(\not{p}) = (\delta_2\not{p} - \delta_m m_q)\,. \tag{3.11}$$

Combining (3.10) and (3.11) leads to:

$$\Sigma_r^{(2)} = (\not{p} - m_{q,r})\left[\Sigma_2^{(2)} + \delta_2\right] + \left[\Sigma_1^{(2)} - m_{q,r}(\delta_m - \delta_2)\right]. \tag{3.12}$$

The values of the counterterms can now be fixed to make the amplitude $\Sigma_r^{(2)}$ finite. There is a freedom in the choice which can be reduced to how much of the finite terms are included in the counterterms. Different choices correspond to different renormalization schemes. Some choices will make some calculation easier than others, but physical quantities will not depend on this choice. In this work, we will use the modified minimal renormalization scheme or $\overline{\text{MS}}$-scheme, where only the poles $\frac{1}{\hat{\epsilon}}$ are included in the counterterms:

$$Z_2 = 1 + \delta_2 = 1 - \frac{\alpha_{s,r}}{4\pi\hat{\epsilon}}C_F\xi + \mathcal{O}(\alpha_{s,r}^2)\,, \tag{3.13}$$
$$Z_m = 1 + \delta_m = 1 - \frac{\alpha_{s,r}}{4\pi\hat{\epsilon}}C_F(3+\xi) + \mathcal{O}(\alpha_{s,r}^2)\,. \tag{3.14}$$

Note that the above counterterms depend on the gauge-parameter ξ. This dependence will always vanish for physical amplitudes.

Other counterterms can be computed in a similar fashion. Considering the gluon self-energy permits the calculation of δ_3 (and Z_3). The relevant diagrams are represented on Fig. 3.4 and lead to [84]

$$Z_3 = 1 + \delta_3 = 1 + \frac{\alpha_{s,r}}{4\pi\hat{\epsilon}}\left[\left(\left(\frac{13}{6} - \frac{\xi}{2}\right)C_A - \frac{4}{3}T_F n_q\right) + \mathcal{O}(\alpha_{s,r}^2)\right], \tag{3.15}$$

where $C_A = N_c = 3$ and $T_F = \frac{1}{2}$ are group theory factors. Similarly, the counterterm Z_c can be determined from the ghost self-energy.

The parameter Z_1 can be computed from the quark-gluon amplitude. The relevant diagrams are shown in Fig. 3.5. This leads to:

$$Z_1 = 1 - \frac{\alpha_{s,r}}{4\pi\hat{\epsilon}}\left(\xi C_F + \frac{3+\xi}{4}C_A\right) + \mathcal{O}(\alpha_{s,r}^2)\,. \tag{3.16}$$

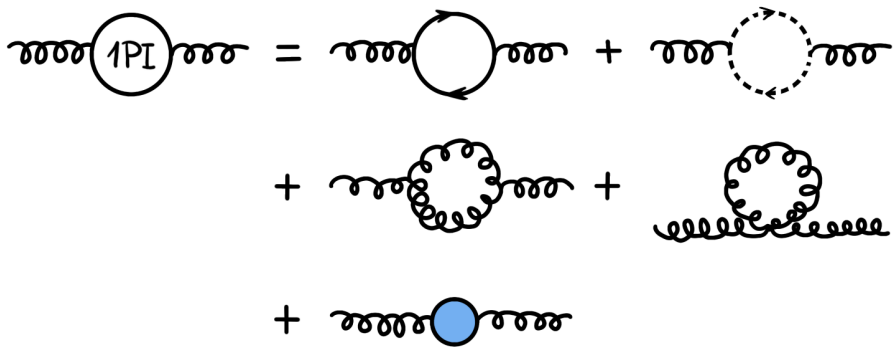

Figure 3.4: Gluon self-energy at one-loop order.

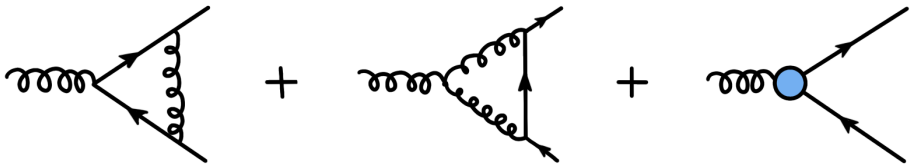

Figure 3.5: Quark-gluon vertex renormalization.

The parameter Z_1 could also be determined from the three or four gluon amplitudes. This would lead to the same result thanks to the Slavnov-Taylor identities, which are the non-abelian generalization of the Ward-Takahashi identity for QED. [85]

Combining (3.4), (3.13), (3.15) and (3.16), we find that the relation between the bare and renormalized coupling constants read [84]

$$\alpha_{s,0} = \mu^{2\epsilon} Z_\alpha \alpha_{s,r} \,, \tag{3.17}$$

$$Z_\alpha := Z_1^2 Z_2^{-2} Z_3^{-1} = 1 - \frac{\alpha_{s,r}}{4\pi\hat{\epsilon}} \Bigg(\underbrace{\frac{11}{3} C_A - \frac{4}{3} T_F n_q}_{:=\beta_0} \Bigg) + \mathcal{O}(\alpha_{s,r}^2) \,. \tag{3.18}$$

Z_α is a function of the renormalized coupling constant $\alpha_{s,r}$, but the gauge-parameter dependence has cancelled. Notice also the scale μ in (3.17): as mentioned before, it was introduced to make the renormalized coupling constant dimensionless in d dimensions. The bare coupling α_0 is a dimensionless constant from the original Lagrangian (3.1) and therefore cannot depend on this scale. This results in a dependence on μ for the renormalized coupling which remains even when the limit $\hat{\epsilon} \to 0$ is considered to return to the 4 dimensional theory (after reabsorbing the divergences in the appropriate counterterms). This μ dependence, also referred to as the *running of the coupling*, is an intrinsic property of the $\overline{\text{MS}}$-scheme.[2] It must cancel in the final result of the calculation of a physical observable , but it is very relevant for intermediate steps and this dependence will therefore be discussed here. In fact, it is so important that it has its own function called the β-function and defined as:

$$\beta\left(\alpha_{s,r}(\mu)\right) := \mu \frac{d\alpha_{s,r}}{d\mu} \,. \tag{3.19}$$

The β-function is directly related to the residue of the simple pole in ϵ of Z_α [84] and in the

[2] Refer e.g. to Refs. [84, 85] for a more detailed discussion of this topic.

one-loop approximation, we have:

$$\beta(\alpha_{s,r}) = -2\beta_0 \frac{\alpha_{s,r}^2}{4\pi} = \mu \frac{\mathrm{d}\alpha_{s,r}}{\mathrm{d}\mu} \,. \tag{3.20}$$

Solving the differential equation leads to an explicit expression for the running of the coupling:

$$\alpha_{s,r}(\mu) = \frac{\alpha_{s,r}(Q)}{1 + \alpha_{s,r}(Q)\frac{\beta_0}{4\pi} \ln \frac{\mu}{Q^2}} \,, \tag{3.21}$$

where Q is a reference scale, for which the value of $\alpha_{s,r}$ is known experimentally. The running of the coupling is shown on Fig 3.6. It is obvious from (3.21) that the strong coupling is small at high-energy or short-distance. However, at low energy, the coupling constant explodes: QCD becomes non-perturbative. An important consequence of the non-perturbative nature of the strong interaction at low energy is that quarks and gluons form color singlet bound states and can never be isolated.

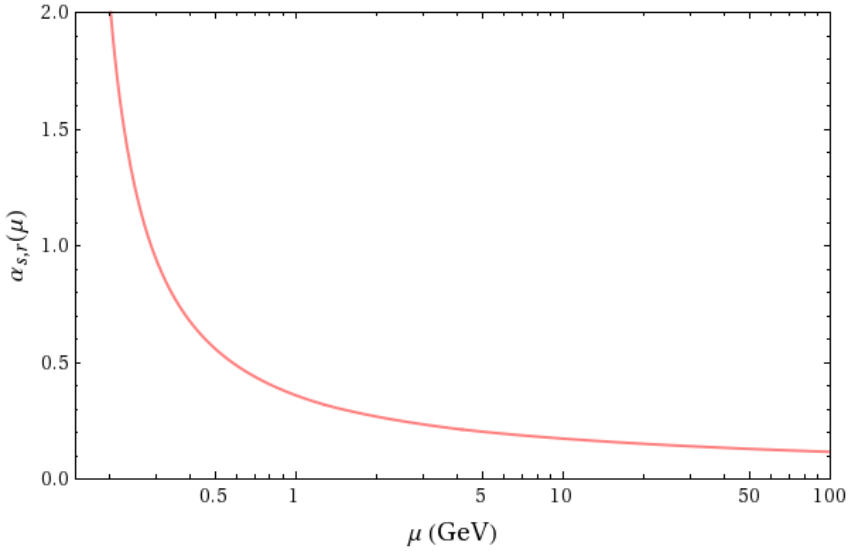

Figure 3.6: Running of the renormalized strong coupling constant $\alpha_{s,r}(\mu)$ at one loop in the $\overline{\text{MS}}$-scheme: see (3.21). At high energy (or equivalently on short-distances), QCD is perturbative. At low-energy, quarks and gluons hadronize and the theory becomes non-perturbative. Non-perturbative tools such as lattice QCD need to be used.

3.2 OPE - generalities

As we have seen at the end of the previous section, the strong coupling constant becomes large at low energy and non-perturbative effects such as quark confinement appear. As a consequence, the degrees of freedom of the theory change: at low-energy we observe hadrons, bound together by strong interactions. This often leads us to study singlet composite operators (i.e. operators made out of several quark and gluon fields at the same point). For example, the axial current has the same quantum numbers as pseudoscalar mesons (e.g. π, η and η') and much information on the latter can be obtained from the study of the former.

As a result we are often interested in studying Green functions of composite operators rather than the usual S-matrix elements and Green functions of fields. We have already seen such

functions in the previous chapter: the HLbL contribution to the muon $g-2$ is related to the correlation function of four electromagnetic currents.

A very useful tool in the study of composite operators is the Operator Product Expansion (OPE). Consider the product of two composite operators $A(x)B(0)$. When $x \to 0$, the product can be written as a series of local operators O_n

$$A(x)B(0) \overset{x\to 0}{\sim} \sum_n c_n(x) O_n(0)\,, \tag{3.22}$$

where all the x-dependence is contained in the coefficients c_n, called Wilson coefficients[3]. [86] The operators O_n, appearing on the RHS of (3.22) must have the same symmetry properties as the initial product of operators. The OPE can appear in various contexts. It can for example be used to derive the effective Lagrangian of the Fermi-theory of the electroweak interactions. [87] In this chapter, we only focus on the applications for QCD in the deep Euclidean domain.

Before explaining the procedure to determine which operators appear in the series (3.22) and compute the Wilson coefficients, we need to discuss operator renormalization. Consider for example an operator of the form $Q_s(x) = \overline{q}_0 q_0 \overline{q}_0 q_0(x)$, where the subscript s stands for tree level operator. As we push computations to higher order in perturbation theory, by inserting the operators in the Dyson series, the operators become dressed: see Fig. 3.7.

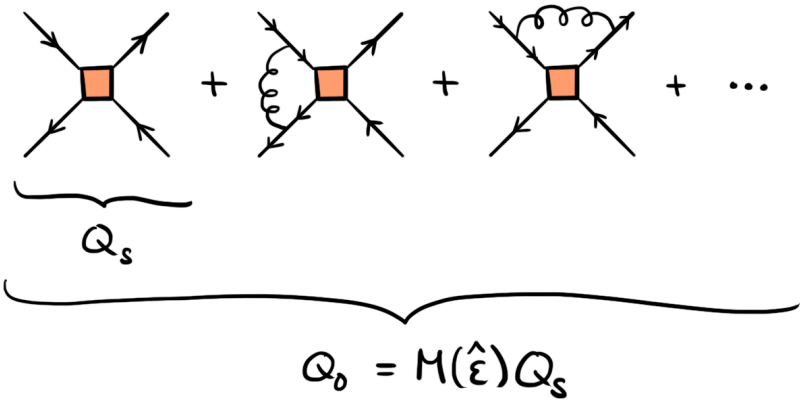

Figure 3.7: Dressed operators, resulting from inserting tree level operators in the Dyson series. The orange squares represent operator insertions.

Just as with regular Feynman diagrams, the dressing procedure leads to divergences. We can use dimensional regularization to express the divergences as poles in $1/\hat{\epsilon}$ just as in standard perturbation theory [37, 87]

$$Q_0(x) = M(\hat{\epsilon}) Q_s(x)\,, \tag{3.25}$$

[3]Similar expansions can be written for time-ordered products

$$T\{A(x)B(0)\} \overset{x\to 0}{\sim} \sum_n c_n(x) O_n(0)\,, \tag{3.23}$$

or matrix elements thereof, for example:

$$\langle 0|T\{A(x)B(0)\}|0\rangle \overset{x\to 0}{\sim} \sum_n c_n(x)\, \langle 0|O_n(0)|0\rangle\ . \tag{3.24}$$

where dressed operators are indicated with the subscript 0. Expressing the operator in terms of renormalized fields instead of bare fields does not suffice to remove all the divergences: new counterterms need to be added. In analogy with field renormalization, we define renormalized operators as

$$Q_0(x) = Z_Q(\mu) Q_r(x;\mu)\,. \tag{3.26}$$

The Z_Q can then be adjusted to cancel the divergences, in a similar fashion to what was presented in section 3.1. With the $\overline{\text{MS}}$-prescription, only the poles in $\hat{\epsilon}$ are included in the counterterms. Notice also that this procedure introduces an arbitrary scale μ as we have seen before.

Before looking at the implications of operator renormalization for the OPE, operator mixing should at least be mentioned. As we have seen in (3.3), each bare field and its renormalized counterpart are in a one-to-one correspondence. The reason is that all the fields appearing in the Lagrangian have different quantum numbers. The situation is slightly different for operators: different operators can have the same quantum number and therefore mix under renormalization. [85] The way to deal with this, is to include all the operators with the same quantum numbers, $Q_{i,s}$ for $i = 1, \ldots, p$, in vectors: $\vec{Q}_s = (Q_{1,s}, \ldots, Q_{p,s})^T$ and similarly for the dressed and renormalized operators. The Z factor in (3.26) then becomes a matrix, which can have non-diagonal entries. An explicit example of such mixing is worked out in the next chapter: see section 4.1.3. [37]

The operator product expansion can finally be written in terms of renormalized operators (we focus for now on vacuum expectation values):

$$\langle 0|T\{A(x)B(0)\}|0\rangle \overset{x\to 0}{\sim} \sum_n c_{s,n}(x)\,\langle 0|O_{s,n}(0)|0\rangle = \sum_n c_{r,n}(x;\mu)\,\langle 0|O_{r,n}(0;\mu)|0\rangle\ . \tag{3.27}$$

The OPE is a way to separate the scales: the Wilson coefficients $c_{r,n}$ contain the short-distance contributions and the matrix elements $\langle O_{r,n}(0;\mu)\rangle := \langle 0|O_{r,n}(0;\mu)|0\rangle$ contain all the non-perturbative long-distance contributions. Therefore, perturbation theory can be used to calculate the Wilson coefficients, whereas the matrix elements have to be evaluated on the lattice, or determined with other non-perturbative methods. The scale μ acts as a separation scale between short and long-distance effects: variations of μ shuffle the physics around. Neglecting operator mixing, the μ dependence of an operator O_n is given by [84, 88, 89]:

$$O_n(\mu) \sim \left(\frac{\ln(Q/\Lambda_{\text{QCD}})}{\ln(\mu/\Lambda_{\text{QCD}})}\right)^{\frac{\gamma_{n,0}}{2\beta_0}} O_n(Q)\,, \tag{3.28}$$

where Λ_{QCD} is the scale at which quarks hadronize[4]. The coefficients β_0 and $\gamma_{n,0}$ are the one-loop coefficients of the β-function defined in (3.19) and of the anomalous dimension of the operator O_n respectively. The latter can be extracted from the renormalization factor Z in (3.26).

The Wilson coefficients depend on μ in such a way as to cancel the scale-dependence [5] of the

[4] In order to guarantee that Wilson coefficients can be computed in pQCD, the separation scale μ should be chosen such that $\mu \gg \Lambda_{\text{QCD}}$

[5] Taking mixing into account, the scale-dependence of the Wilson coefficients can be expressed as [84]

$$\vec{C}(\mu) = T_{\alpha_s}\left\{\exp\left[\int_{\alpha_s(M)}^{\alpha_s(\mu)} \mathrm{d}\alpha_s \frac{\gamma^T(\alpha_s)}{\beta(\alpha_s)}\right]\right\}\vec{C}(M)\,, \tag{3.29}$$

where T_{α_s} implies an ordering of the matrix exponential according to the value of α_s. The sum of the terms in the OPE must be μ-independent, but when mixing is taken into account, it is no longer true for a single term in the sum.

overall products. In addition, they scale with x according to [73, 88]

$$C_{r,n} \sim \left(\frac{1}{|x|}\right)^{d_A^*+d_B^*-d_n^*}, \tag{3.30}$$

where $d_j^* = d_j + \gamma_j$ is the sum of the canonical dimension of an operator and of its anomalous dimension[6]. This is based on dimensional analysis as well as the fact that in the deep Euclidean region, where the OPE is valid, the light quark masses can be ignored. This relation gives an ordering of the operators showing up in the series (3.27): operators of low dimensions contribute more and the series can be truncated.

3.3 OPE in vacuum - the case of HVP

In this section, we use the QCD correlator of two electromagnetic currents

$$\Pi^{\mu\nu}(q) := ie^2 \int \mathrm{d}x^4 e^{iq\cdot x} \langle 0|T\{j^\mu_{\mathrm{em}}(x) j^\nu_{\mathrm{em}}(0)\}|0\rangle = (q^2 g^{\mu\nu} - q^\mu q^\nu)\Pi(q^2)\,, \tag{3.31}$$

as a laboratory to study OPE techniques, where $j^\mu_{\mathrm{em}}(x) = \frac{2}{3} : \overline{u}(x)\gamma^\mu u(x) : -\frac{1}{3} : \overline{d}(x)\gamma^\mu d(x) : -\frac{1}{3} : \overline{s}(x)\gamma^\mu s(x) :$ is the light-quark current[7]. This discussion closely follows the analysis of Ref. [85], *mutatis mutandis*. The Green function (3.31) is relevant for the determination of the HVP contribution to $(g-2)_\mu$: see section 2.3.3. We will therefore also shortly comment on the implications of the results we will obtain in that context.

From here on, we work in d dimensions. By contracting (3.31) with the metric tensor, we find:

$$\Pi(q^2) = \frac{ie^2}{q^2(d-1)} \int \mathrm{d}^d x\, e^{iq\cdot x}\, \langle 0|T\{j^\mu_{\mathrm{em}}(x) j_{\mu,\mathrm{em}}(0)\}|0\rangle\ . \tag{3.32}$$

For all the contributions considered in this work, the description can be simplified by considering each flavor component separately [90]

$$\Pi(q^2) = e^2 \sum_{A=1}^{n_f} e_A^2 \Pi_A(q^2)\,, \tag{3.33}$$

where Π_A is the QCD correlator of the vector currents containing only quarks of flavor q_A (and charge e_A) $J^\mu_A(x) \equiv : \overline{q}_A \gamma^\mu q_A(x) :$[8]. For convenience, the factor e^2 has also been taken out of the single-flavor correlators.

The correlation function is a Fourier transform of a product of local operators. If Euclidean momenta are considered, the limit $x^\mu \to 0$ in (3.27) becomes a condition over the virtuality: $Q^2 \to \infty$ [85] and

$$\begin{aligned}\Pi_A(q^2) &= \frac{i}{q^2(d-1)} \int \mathrm{d}^d x e^{iq\cdot x}\, \langle 0|T\{J^\mu_A(x) J_{A,\mu}(0)\}|0\rangle \\ &\overset{Q^2\to\infty}{\sim} -\frac{i}{(d-1)} \sum_n \langle 0|O_n(0)|0\rangle \underbrace{\frac{1}{Q^2} \int \mathrm{d}^d x\, e^{iq\cdot x} c_n(x)}_{:=\tilde{c}_n(Q^2)}\ .\end{aligned} \tag{3.34}$$

[6] Equation (3.30) is valid modulo factors of $\log|x|$. [73]

[7] We define currents as the normal-ordered product so that tadpole contributions to the Green functions are absent. [33]

[8] Equation (3.33) is no longer valid beyond the NLO in perturbation theory, but this goes beyond the scope of this discussion.

From dimensional analysis, the scaling of Fourier transformed coefficients can be derived $c_n \sim \left(Q^2\right)^{-(d(O_n)+2-d)/2}$. If we want to include terms up to $(Q^2)^N$ in the description, we have to consider operators of dimensions up to

$$d(O_n) = d - 4 + 2N\,. \tag{3.35}$$

Let us now consider the operators O_n. We know that they must be singlets (otherwise their vacuum expectation value would vanish) and that they can be sorted according to their dimensions.

The most obvious singlet operator is the unit operator. It is dimensionless and will therefore be the leading contribution in the OPE. The corresponding Wilson coefficient simply corresponds to standard perturbation theory, with fully contracted Feynman diagrams. The other operators with non-zero vacuum expectation values correspond to non-perturbative effects.

The non-trivial, colorless, Lorentz and flavor singlets of lowest dimension is the quark-antiquark pair, leading to the following matrix element or *vacuum condensate*

$$\langle 0|\overline{q}_A q_A|0\rangle\ . \tag{3.36}$$

This matrix element would vanish in perturbation theory, but confinement impacts the vacuum properties of QCD and as a result, it is non-zero. The condensates go beyond perturbation theory and parametrize non-perturbative effects; they express long-range physics and have to be determined using either phenomenology or lattice QCD. As we will see below, there are still many unknowns regarding these quantities, which limit the precision at which they can be calculated. [89, 91]

In the chiral limit, the QCD Lagrangian is symmetric under $SU(3)_L \times SU(3)_R$, but this symmetry is spontaneously broken by the vacuum state. [92] The fact that the quark condensate is non-vanishing is therefore a direct consequence of this spontaneous symmetry breaking and we say that this condensate is an order parameter of chiral symmetry breaking. [89] In addition, still in the chiral limit, all the light quark condensates are equal [92]

$$\langle 0|\overline{u}u|0\rangle = \langle 0|\overline{d}d|0\rangle = \langle 0|\overline{s}s|0\rangle\ , \tag{3.37}$$

and can be related to physical quantities unambiguously, for example through the Gell-Mann, Oakes, Renner relation [92, 93]

$$\lim_{m_{\text{quark}}\to 0} \frac{m_\pi^2}{m_u + m_d} = -\frac{1}{2F_\pi^2}\,\langle 0|\overline{u}u + \overline{d}d|0\rangle\ , \tag{3.38}$$

where $F_\pi \approx 92$ MeV is the pion decay constant and m_π the pion mass. The condensate can therefore be evaluated on the lattice (in the $\overline{\text{MS}}$-scheme and for $\mu = 2$ GeV) [94]

$$\frac{1}{2}\left(\langle 0|\overline{u}u|0\rangle + \langle 0|\overline{d}d|0\rangle\right) = -\left[272(5)\text{MeV}\right]^3\ . \tag{3.39}$$

Away from the chiral limit, the situation is more complicated, because the perturbative and non-perturbative contributions mix and the definition of the condensates becomes ambiguous. [92,93]

The next condensate is the 4-dimensional gluon condensate

$$\langle 0|\frac{\alpha_s}{\pi} G^a_{\mu\nu} G_a^{\mu\nu}|0\rangle\ . \tag{3.40}$$

The scale-dependence of α_s compensates that of the operator G^2. By including the strong coupling constant directly in (3.40), we ensure that the condensate is renormalization group-invariant. [89] But, contrary to the quark condensates, it is difficult to evaluate on the lattice and the best evaluation that we currently have comes from charmonium sum rules [89, 91, 95], leading to:

$$\langle 0|\frac{\alpha_s}{\pi}G_a^{\mu\nu}G^a_{\mu\nu}|0\rangle = (0.012 \pm 0.004)\ \text{GeV}^4\,. \tag{3.41}$$

Going to higher dimensions leads to even more condensates. For example, in dimension six, we can write [89]

$$\langle 0|\overline{q}\Gamma q\overline{q}\Gamma q|0\rangle\ \text{, with } \Gamma \in \{\gamma^\mu, \gamma^5, \gamma^\mu\gamma^5, \sigma^{\mu\nu}, \mathbb{1}\}\,, \tag{3.42}$$

$$\langle 0|\overline{q}\Gamma t^a q\overline{q}\Gamma t_a q|0\rangle\,\text{, where } t_a \text{ acts in color space}\,, \tag{3.43}$$

$$\langle 0|\overline{q}t_a\sigma_{\mu\nu}qF^{a,\mu\nu}|0\rangle\ , \tag{3.44}$$

$$\langle 0|f_{abc}G^{a,\mu\nu}G^b_{\nu\rho}G^{c,\rho}_{\mu}|0\rangle\ . \tag{3.45}$$

We could in principle keep going and build more condensates of arbitrarily high dimensions. However, it is expected that in addition to introducing non-zero vacuum condensates, non-perturbative effects will break the operator expansion (3.34) itself for a critical dimension d_{crit}. In Ref. [91], non-vanishing condensates are argued to be the effect of large-size instantons while the OPE breakdown results from short-size instantons[9]. They also evaluate $d_{\text{crit}} \approx 11$. [91]

Now that we have listed the kinds of operators that can appear in (3.34), we need to see how the Wilson coefficients can be evaluated. We begin by computing the Wilson coefficient $\tilde{c}_{\mathbb{1}}(q^2)$ corresponding to perturbation theory. We start by the leading order in α_s and since only light quarks are considered, we can neglect m_A^2-corrections and higher. The corresponding diagram is shown in Fig. 3.8. Under the Wick's theorem, it is obtained by contracting all the quark fields [85]

$$\begin{aligned}
\Pi_A^{\text{pert,LO}}(q^2) =& \frac{i}{q^2(d-1)}\int \mathrm{d}^d x e^{iq\cdot x}\,\langle 0|\overline{q}_A(x)\gamma^\mu \overbrace{q_A(x)\overline{q}_A}(0)\gamma_\mu q_A(0)|0\rangle \\
=& -\frac{1}{q^2(d-1)}\int \mathrm{d}^d x e^{iq\cdot x}\,\langle 0|(\gamma^\mu)_{ij}(\gamma^\mu)_{kl}\overbrace{q^{\overline{b}}_{A,l}(0)\overline{q}^{\overline{a}}_{A,i}}(x)\overbrace{q^{\overline{a}}_{A,j}(x)\overline{q}^{\overline{b}}_{A,k}}(0)|0\rangle \\
=& \frac{iN_c}{4q^2(d-1)}\int \frac{d^d p}{(2\pi)^d}\,\mathrm{Tr}\left[\gamma^\mu S(p)\gamma_\mu S(p)\right]\,,
\end{aligned} \tag{3.46}$$

where we have used [85]

$$\overbrace{q^{\overline{a}}_{A,i}(x)\overline{q}^{\overline{b}}_{A,j}}(y) = i\delta^{\overline{a}\overline{b}}S_{ij}(x-y) = i\int \frac{\mathrm{d}^d p}{(2\pi)^d}e^{-ip\cdot(x-y)}\underbrace{\frac{\not{p}+m_A}{p^2-m_A^2+i0}}_{:=S(p)}\,, \tag{3.47}$$

and the simple Roman indices stand for Dirac indices, while $\overline{a}$ and $\overline{b}$ live in color-space.

Neglecting terms of order $\mathcal{O}(m_A^2)$ and using standard Feynman integral techniques leads to [85]

$$\Pi_A^{\text{pert,LO}}(q^2) = \frac{1}{4\pi^2}\left(\frac{1}{\hat{\epsilon}} + \log\left(-q^2\right) + \frac{5}{3}\right)\,. \tag{3.48}$$

[9] Instantons are finite-action solutions of the classical field equations of motion in Euclidean space. [96] They correspond to non-perturbative gauge-field configurations. [97]

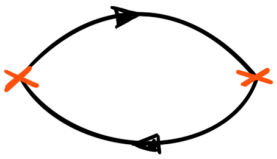

Figure 3.8: Operator product expansion for HVP: perturbative contribution, leading order. The orange crosses represent the current insertions.

Note that (3.31) is singular when $\hat{\epsilon} \to 0$. This has nothing to do with operator renormalization, but is a common feature of Green functions of multiple operators. It can be removed by fixing the value of the Green function at a chosen euclidean point. [85,98] In fact, this specific Green function and the associated divergence appears in QED renormalization. It is removed by reabsorbing the divergent $\Pi(0)$ in the photon wave function renormalization factor. [33] However, our aim is to analyze the HVP contribution to $(g-2)_\mu$, which only involves the imaginary part of the divergent Green function (see (2.33) and (2.34)). The only relevant term for us in (3.48) is therefore the logarithmic term and we do not need to worry about UV divergences.

To include α_s corrections to the result (3.48), the NLO term in the Dyson series must be considered:

$$\Pi_A^{\text{NLO}} = -\frac{i}{q^2(d-1)}\frac{i^2}{2!}\int \mathrm{d}^d x\, \mathrm{d}^d y\, \mathrm{d}^d z\, e^{iq\cdot x}\, \langle 0|T\{:\overline{q}_A(x)\gamma^\mu q_A(x) :: \overline{q}_A(0)\gamma_\mu q_A(0) : \mathcal{L}_{\text{int}}^{\text{qgq}}(y)\mathcal{L}_{\text{int}}^{\text{qgq}}(z)\}|0\rangle \ ,$$

where $\mathcal{L}_{\text{int}}^{\text{qgq}}$ is the gluon-quark interaction Lagrangian

$$\mathcal{L}_{\text{int}}^{\text{qgq}}(z) = g_s : G_\mu^a(z)\overline{q}_A(z)\gamma^\mu t_a q_A(z) : \ . \tag{3.49}$$

The perturbative contribution is then obtained by fully contracting the fields in all possible ways. The topologies are shown in Fig. 3.9.

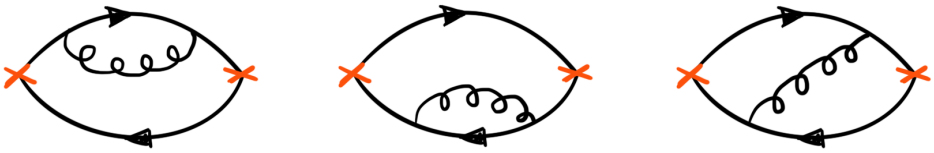

Figure 3.9: Operator product expansion for HVP: perturbative contribution, next-to-leading order. The orange crosses represent the current insertions.

Working in the Feynamn gauge $\xi = 1$, the gluon propagator becomes [85]

$$D_{\mu\nu} = -\frac{g_{\mu\nu}}{k^2 + i0} \tag{3.50}$$

and we find [85]

$$\Pi_A^{\text{pt,NLO}} = \frac{\alpha_s}{4\pi^3}\log(-q^2) + \text{const}\,, \tag{3.51}$$

where only the logarithmic term has been written explicitly as it is the only one that contributes to the R-ratio.

Before looking at the result for the R-ratio, a comment on the validity of using these results in the physical regions $q^2 > 0$ is in order. The OPE and perturbation theory are valid in the

deep Eucliden-region, where strong interactions can be described in terms of quarks and gluons. In the physical region, quarks and gluons form colorless bound states and cannot be isolated. This is a purely non-perturbative effect which is translated into the appearance of resonances in the spectrum. The degrees of freedom are completely different. However, as the energy increases and q^2 becomes large, the resonances become wider and the spectrum looks very similar to that obtained using perturbation QCD in terms of quarks and gluons. This is known as the local *quark-hadron duality*[10]. [89]

For high $s = q^2$, we can therefore select the imaginary part of (3.48) and (3.51) and combine the different quark flavors according to (3.33) to find [90]

$$R(s) = 3 \sum_{A=1}^{n_f} e_A^2 \left(1 + \frac{\alpha_s}{\pi} + \cdots\right) , \tag{3.52}$$

where n_f is the number of flavors active at the energy $\sqrt{s}$, i.e. with $4m_A^2 < s$. Equation (3.52) can be pushed to higher orders in perturbation theory. However, the region where pQCD becomes more reliable than inclusive data is currently not agreed upon and different groups use different prescriptions. [4]

The next step is to describe the non-perturbative contributions to (3.34), parametrized by the non-zero vacuum condensates discussed above. The method to compute the associated Wilson coefficients is similar to what is done in regular perturbation theory, but some fields are left uncontracted. They then need to be Taylor expanded around 0 to generate local vacuum condensates. In some cases, Dirac algebra and color decomposition need to be used to reduce the number of condensates.

We begin by computing the coefficient $c_{\langle\overline{q}q\rangle}(Q^2)$. To do this, we consider the leading order in the Dyson series, but contrary to what was done in (3.46), a quark-antiquark pair is left uncontracted [85]

$$\begin{aligned}\Pi_A^{\overline{q}q}(q^2) =& \frac{i}{q^2(d-1)} \int \mathrm{d}^d x e^{iq\cdot x} (\gamma^\mu)_{ij} (\gamma_\mu)_{kl} \overbrace{q_{A,l}^{\overline{b}}(0) \overline{q}_{A,i}^{\overline{a}}}(x) \langle 0| {:}\, \overline{q}_{A,k}^{\overline{b}}(0) q_{A,j}^{\overline{a}}(x) \,{:}|0\rangle \\ &+ \frac{i}{q^2(d-1)} \int \mathrm{d}^d x e^{iq\cdot x} (\gamma^\mu)_{ij} (\gamma_\mu)_{kl} \overbrace{q_{A,j}^{\overline{a}}(x) \overline{q}_{A,k}^{\overline{b}}}(0) \langle 0| {:}\, \overline{q}_{A,i}^{\overline{a}}(x) q_{A,l}^{\overline{b}}(0) \,{:}|0\rangle \ . \end{aligned} \tag{3.53}$$

The corresponding diagrams are shown in Fig. 3.10. The uncontracted fields are represented by a dot. As explained above, in perturbation theory, these contributions would vanish. Their contribution stems from non-perturbative effects.

The next step is to Taylor-expand the quark fields that appear in the vacuum expectation values around 0. It is customary to work with the Fock-Schwinger gauge for the non-perturbative part of the OPE. It is expressed as

$$x_\mu G_a^\mu(x) t^a = 0 \, . \tag{3.54}$$

With this choice of gauge, it can be shown[11] that the fields can be Taylor expanded in terms of

[10] Global quark-hadron duality claims that despite the resonances, the physical spectrum and the one described by perturbative QCD are equivalent on average. [89]

[11] See Ref. [85] for a proof.

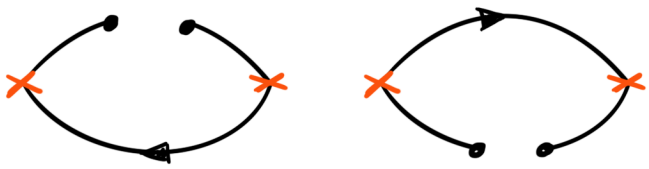

Figure 3.10: Operator product expansion for HVP: non-perturbative contribution due to the quark condensate (represented by two dots). The orange crosses represent the current insertions.

the covariant derivatives

$$G^a_\mu(x) = \sum_{n=0}^{\infty} \frac{1}{n!(n+2)} x^\omega x^{\omega_1} ... x^{\omega_n} [D_{\omega_1}(0), \dots, [D_{\omega_n}(0), G^a_{\omega\mu}(0)] \dots] \,, \tag{3.55}$$

$$q_A(x) = \sum_{n=0}^{\infty} \frac{1}{n!} x^{\omega_1} \dots x^{\omega_n} D_{\omega_1}(0) \dots D_{\omega_n}(0) q_A(0) \,, \tag{3.56}$$

$$\overline{q}_A(x) = \sum_{n=0}^{\infty} \frac{1}{n!} x^{\omega_1} \dots x^{\omega_n} \overline{q}_A(0) D^\dagger_{\omega_1}(0) \dots D^\dagger_{\omega_n}(0) \,, \tag{3.57}$$

where $\overline{q}(0)\partial^\dagger_\mu \equiv \partial_\mu \overline{q}(0)$, the covariant derivative is given by $D^\mu \equiv \partial^\mu - i g_s G^a_\mu t^a$ and the field strength tensor by $G^a_{\mu\nu} := \partial_\mu G^a_\nu - \partial_\nu G^a_\mu$ [85]. The matrix element in (3.53) can therefore be expressed as

$$\langle 0| \colon \overline{q}^{\overline{a}}_{A,i}(x) q^{\overline{b}}_{A,l}(0) \colon |0\rangle = \langle 0| \colon \overline{q}^{\overline{a}}_{A,i}(0) q^{\overline{b}}_{A,l}(0) \colon |0\rangle + x^\rho \langle 0| \colon \left(\overline{q}_{A,i} D^\dagger_\rho\right)^{\overline{a}} (0) q^{\overline{b}}_{A,l}(0) \colon |0\rangle + \dots \tag{3.58}$$

Furthermore, only singlets can contribute to the matrix elements, leading to

$$\langle 0| \colon \overline{q}^{\overline{a}}_{A,i}(x) q^{\overline{b}}_{A,l}(0) \colon |0\rangle = \frac{\delta_{li}\delta_{\overline{a}\overline{b}}}{4N_c} \langle 0|\overline{q}_A q_A|0\rangle \,. \tag{3.59}$$

The first order term in the expansion (3.58) also contributes to $\Pi^{\overline{q}q}_A(q^2)$. The reduction of that condensate relies on the fact that the covariant derivative has the same parity transformation property as the Dirac matrix γ^ρ. Therefore

$$\langle 0| \colon \left(\overline{q}_{A,i} D^\dagger_\rho\right)^{\overline{a}} (0) q^{\overline{b}}_{A,l}(0) \colon |0\rangle = C \delta_{\overline{a}\overline{b}} (\gamma_\rho)_{li} \,. \tag{3.60}$$

To find the proportionality factor C, one should contract (3.60) with $(\gamma^\rho)_{il}\delta_{\overline{b}\overline{a}}$ and use the equations of motion $\overline{q}_A(x)(i\not{D}^\dagger + m_A) = 0$ [85]

$$C N_c d = \langle 0| \colon \left(\overline{q}_A \not{D}^\dagger\right)^{\overline{a}}_l (0) q^{\overline{a}}_{A,l}(0) \colon |0\rangle = i m_A \langle 0|\overline{q}_A q_A|0\rangle \,, \tag{3.61}$$

so that finally

$$\langle 0| \colon \left(\overline{q}_{A,i} D^\dagger_\rho\right)^{\overline{a}} (0) q^{\overline{b}}_{A,l}(0) \colon |0\rangle = i m_A \frac{\delta_{\overline{a}\overline{b}} (\gamma_\rho)_{li}}{4 d N_c} \langle 0|\overline{q}_A q_A|0\rangle \,. \tag{3.62}$$

With the above considerations, (3.58) becomes

$$\langle 0| \colon \overline{q}^{\overline{a}}_{A,i}(x) q^{\overline{b}}_{A,l}(0) \colon |0\rangle = \frac{\delta_{\overline{a}\overline{b}}}{4N_c} \langle 0|\overline{q}_A q_A|0\rangle \left(\delta_{li} + i m_A x^\rho \frac{(\gamma_\rho)_{li}}{d}\right) \,. \tag{3.63}$$

Taking that into consideration, the second term of (3.53) can be written as

$$\begin{aligned}
&\frac{i}{q^2(d-1)}\int \mathrm{d}^d x e^{iq\cdot x}(\gamma^\mu)_{ij}(\gamma_\mu)_{kl}\overbrace{q^{\bar{a}}_{A,j}(x)\overline{q}^{\bar{b}}_{A,k}}(0)\,\langle 0|{:}\,\overline{q}^{\bar{a}}_{A,i}(x)q^{\bar{b}}_{A,l}(0)\,{:}|0\rangle \\
&= \frac{i\,\langle 0|\overline{q}_A q_A|0\rangle}{4q^2(d-1)}\int \mathrm{d}^d x\int\frac{\mathrm{d}^d p}{(2\pi)^d}e^{i(q+p)\cdot x}\,\mathrm{Tr}\left[\gamma^\mu S(p)\gamma_\mu\right] \\
&- \frac{m_A\,\langle 0|\overline{q}_A q_A|0\rangle}{4q^2 d(d-1)}\int \mathrm{d}^d x\int\frac{\mathrm{d}^d p}{(2\pi)^d}e^{i(q+p)\cdot x}x^\rho\,\mathrm{Tr}\left[\gamma^\mu S(p)\gamma_\mu\gamma_\rho\right]\,. \qquad (3.64)
\end{aligned}$$

The first term of the above equation can be calculated using standard methods. The second term is more difficult, because of the appearance of the factor x^ρ. This apparent translation-invariance breaking is a consequence of using the Fock-Schwinger gauge. The final result cannot depend on the choice of gauge and the translation-invariance breaking will disappear, but it must be dealt with in intermediate steps. [85] To do this, we use the following method. Express the x^ρ as a derivative

$$e^{ix\cdot(p-q)}x^\rho = \frac{\partial}{\partial p_\rho}e^{ix\cdot(p-q)}\,, \qquad (3.65)$$

and partially integrate the expression so that the derivative acts on the Dirac trace. The derivative of a propagator has a very simple form [85]

$$-\frac{\partial}{\partial p_\rho}S(p) = S(p)\gamma^\rho S(p)\,. \qquad (3.66)$$

After these steps, the translation-breaking term can also be dealt with using standard methods. [85] Note that the trace of an odd number of γ-matrices vanishes. Therefore, (neglecting $\mathcal{O}(m_A^2)$ terms) only the part linear in m_A of the propagator appearing in the translation invariant term of (3.64) gives a contribution and the overall result is proportional to m_A. This could have been expected because the μ-dependence of the mass and of the condensate must cancel each other. [88] The quark condensate is therefore effectively a dimension 4 operator and the final result reads [85, 91]

$$\Pi_A^{\bar{q}q} = \frac{2m_A}{q^4}\,\langle 0|\overline{q}_A q_A|0\rangle\,. \qquad (3.67)$$

The next step is to consider the contribution of the other dimension 4 condensate: the gluon $\langle 0|\frac{\alpha_s}{\pi}G^2|0\rangle$. To do that, we must start from the NLO in the Dyson series (3.49), contract all the quark fields and leave the gluon fields uncontracted. The corresponding topologies are shown in Fig. 3.11.

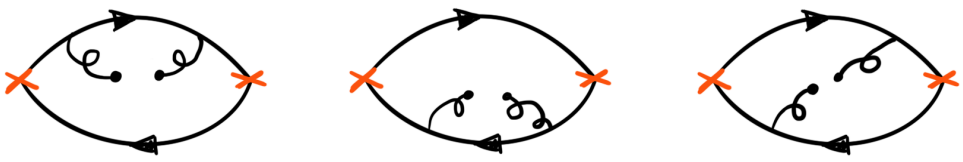

Figure 3.11: Operator product expansion for HVP: non-perturbative contribution due to the gluon condensate. The orange crosses represent the current insertions.

We here only explain how to deal with the condensate reduction. In the Fock-Schwinger gauge, the LO term of the Taylor expansion of the gluon field reads (see (3.55))

$$G^a_\mu(x) = \frac{1}{2}x^\omega G^a_{\omega\mu}(0)\,. \qquad (3.68)$$

Using this and Lorentz invariance leads to [85]

$$\begin{aligned}\langle 0|\colon G^a_\lambda(y)G^a_\sigma(z)\colon|0\rangle &= \frac{1}{4}y^\alpha z^\beta \langle 0|\colon F^a_{\alpha\lambda}(0)F^a_{\beta\sigma}(0)\colon|0\rangle \\ &= \frac{y^\alpha z^\beta}{4d(d-1)}(g_{\alpha\beta}g_{\lambda\sigma}-g_{\alpha\sigma}g_{\beta\lambda})\langle 0|\colon F^a_{\mu\nu}(0)F^{\mu\nu}_a(0)\colon|0\rangle\ , \end{aligned} \tag{3.69}$$

The y and z-factors can be dealt with the partial derivative trick described above in the case of the quark condensate contribution. This leads to [85, 91]

$$\Pi^{GG}_A(q^2) = \frac{1}{12q^4}\langle 0|\frac{\alpha_s}{\pi}G^2|0\rangle\ . \tag{3.70}$$

The different flavor chanels can finally be combined and we get

$$\frac{9Q^4}{2e^2}\Pi^{\text{N.P.}}_{D=4}(Q^2) = 4m_u\langle 0|\overline{u}u|0\rangle + m_d\langle 0|\overline{d}d|0\rangle + m_s\langle 0|\overline{s}s|0\rangle + \frac{1}{4}\langle 0|\frac{\alpha_s}{\pi}G^2|0\rangle\ . \tag{3.71}$$

The computation can be extended with similar techniques to higher dimensional operators or to higher orders in α_s.

We shortly comment on the non-perturbative corrections to $R(s)$. The parametrization of non-perturbative effects in terms of vacuum condensates built out of quarks and gluons only makes sense in the deep Euclidean domain. In the physical region, quarks and gluons hadronize and the degrees of freedom are different. It is unclear how to compute non-perturbative effects in that region from first principles. Instead of comparing the OPE prediction and the data in the physical region, we can instead use a dispersion relation to express the Green function $\Pi(Q^2)$ in the Euclidean region as a function of the experimental data and compare that to OPE result.

This is the approach of Ref. [99] and is most conveniently done using an auxiliary function called the Adler function $D(q^2)$, defined from the derivative of the Green function $\Pi(q^2)$. The OPE for the Adler function can therefore directly be derived from the OPE for $\Pi(q^2)$ calculated above [12] [99]

$$D^{\text{OPE}}(-q^2) := -12\pi^2 q^2\frac{\mathrm{d}\Pi^{\text{OPE}}(q^2)}{\mathrm{d}q^2}\,. \tag{3.72}$$

On the other hand, the Adler function in the Euclidean domain can also be reconstructed from the data [99]

$$D(Q^2) = Q^2\int_{4m_\pi^2}^\infty \frac{R^{\text{data}}(s)}{(s+Q^2)^2}\mathrm{d}s\,. \tag{3.73}$$

By comparing (3.72) and (3.73) up to order α_s^3, the authors of Ref. [99] showed that including the non-perturbative corrections of the OPE does not improve the description of the data: the non-perturbative corrections to HVP can be ignored.

3.4 Beyond the OPE in vacuum - the case of HLbL

The method presented in the previous section is not limited to the study of the vacuum expectation value of the product of two local operators. We could for example consider the product

[12] In Ref. [99], the calculation of the Wilson coefficients is pushed to higher order in α_s compared to (3.48), (3.51) and (3.71).

of two electromagnetic fields in presence of an external pion:

$$\Pi_{\pi^0}(q^2) = i\int \mathrm{d}^4x\, e^{iq_1\cdot x}\left\langle 0\middle|T\left\{j_\mu^{\mathrm{em}}(x)j_\nu^{\mathrm{em}}(0)\right\}\middle|\pi^0(q_1+q_2)\right\rangle . \tag{3.74}$$

The pion transition form factor (TFF) $F_{\pi^0\gamma^*\gamma^*}(q_1^2,q_2^2)$ can be defined from the above correlator,

$$\Pi_{\pi^0}(q^2) = \epsilon_{\mu\nu\alpha\beta}q_1^\alpha q_2^\beta F_{\pi^0\gamma^*\gamma^*}(q_1^2,q_2^2)\,, \tag{3.75}$$

and is of great interest for $(g-2)_\mu$ because it contains all the hadronic content of the pion pole, which is the leading contribution for HLbL in the dispersive approach (more details can be found in sections 2.3.3 and 5.2.2).

The pion has different quantum numbers than the vacuum: it can be interpolated by the third isospin component of the axial current $A_\mu(x) = \sum_A e_A^2\overline{q}_A\gamma_5\gamma_\mu q_A(x)$

$$\left\langle 0\middle|A_\mu^a(0)\middle|\pi^0(p)\right\rangle = i\delta_{a,3}F_\pi p_\mu\,, \tag{3.76}$$

where $F_\pi = 92.28$ MeV is the pion decay constant [100].

In the previous section, we computed the OPE for two electromagnetic currents in the vacuum. When we considered the LO term in the Dyson series and left a pair of quark-antiquark fields uncontracted, we only kept the contribution proportional to the singlet: it was the only part that would have a non-vanishing vacuum expectation value. If we consider (3.74) instead, the non-vanishing contribution arising from the uncontracted quark-antiquark pair is proportional to the axial vector current (see for example Ref. [33]):

$$\begin{aligned}
&\sum_A e_A^2\left\langle 0\middle|:\overline{q_A(x)\gamma_\mu q_A(x)\overline{q}_A(0)\gamma_\nu q_A}(0):\middle|\pi^0(q_1+q_2)\right\rangle\\
&= -\epsilon_{\mu\nu\alpha\beta}\sum_A e_A^2\int\frac{\mathrm{d}^4p}{(2\pi)^4}\frac{e^{-ip(y-x)}}{p^2}\,p^\alpha\left\langle 0\middle|:\overline{q}_A(0)\gamma_5\gamma^\beta q_A(x):\middle|\pi^0(q_1+q_2)\right\rangle\\
&\overset{x\to 0}{=} -\epsilon_{\mu\nu\alpha\beta}\sum_A e_A^2\int\frac{\mathrm{d}^4p}{(2\pi)^4}\frac{e^{-ip(y-x)}}{p^2}\,p^\alpha\left\langle 0\middle|:\overline{q}_A\gamma_5\gamma^\beta q_A(0):\middle|\pi^0(q_1+q_2)\right\rangle ,
\end{aligned} \tag{3.77}$$

where the convention $\epsilon^{0123} = +1$ is used. This leads to (considering the case where $Q_1^2 \approx Q_2^2 \gg \Lambda_{\mathrm{QCD}}^2$ and defining $q = q_1 \approx -q_2$)

$$\begin{aligned}
\Pi_{\pi^0}^{\mathrm{LO}}(q^2) &= -2i\epsilon_{\mu\nu\alpha\beta}\int\frac{\mathrm{d}^4p}{(2\pi)^4}\int\mathrm{d}^4x e^{i(q_1+p)\cdot x}\frac{p^\alpha}{p^2}\left\langle\Omega\middle|j_5^\beta(0)\middle|\pi^0(q_1+q_2)\right\rangle\\
&= \frac{2F_\pi}{3q^2}\epsilon_{\mu\nu\alpha\beta}q_1^\alpha q_2^\beta\,,
\end{aligned} \tag{3.78}$$

which can be used to extract the high-energy behavior of the pion TFF by identification with the definition (3.75) [101]

$$F_{\pi^0\gamma^*\gamma^*}(Q^2,Q^2) \sim -\frac{2F_\pi}{3Q^2}\,. \tag{3.79}$$

We now turn to the study of the HLbL tensor, which will be the main focus of the rest of this work,

$$\Pi^{\mu\nu\lambda\sigma}(q_1,q_2,q_3) = -i\int\mathrm{d}^4x\mathrm{d}^4y\mathrm{d}^4z e^{-i(q_1\cdot x+q_2\cdot y+q_3\cdot z)}\left\langle 0|T\left\{j_{\mathrm{em}}^\mu(x)j_{\mathrm{em}}^\nu(y)j_{\mathrm{em}}^\lambda(z)j_{\mathrm{em}}^\sigma(0)\right\}|0\right\rangle . \tag{3.80}$$

In the $g-2$ kinematics, one of the photon is soft $q_4 = q_1 + q_2 + q_3 \to 0$ and there are three different scales at play, corresponding to the three photon virtualities $Q_i^2 = -q_i^2$. The situation is therefore more complicated than for the study of HVP, which involved only one energy scale. For HLbL, there are two different short-distance regimes of interest for OPE studies. One of them corresponds to the situation where two photon virtualities are much larger than the third: $Q_1^2 \approx Q_2^2 \gg Q_3^2$. In that case, one can do an OPE for two of the four electromagnetic currents. Similarly to the case of the pion TFF, the relevant operator resulting from the OPE is the axial current. This leads to the Melnikov-Vainshtein constraint [2]

$$\Pi_{\mu\nu\lambda\sigma}(q_1, q_2, q_3) \approx -2i\frac{q^\alpha}{q^2}\epsilon_{\mu\nu\alpha\beta}\int \mathrm{d}^4w\,\mathrm{d}^4z\,\langle 0|T\{j_5^\beta(w)j_\lambda^{\mathrm{em}}(z)j_\sigma^{\mathrm{em}}(0)\}|0\rangle\ . \tag{3.81}$$

This is useful because the three-point function appearing on the RHS of (3.81) is related to the Adler-Bell-Jackiw triangle anomaly and its properties are well known (see for example Ref. [2, 102, 103]). More details about this computation, its implications, as well as the method to translate this constraint in a $g-2$ language can be found in chapter 5.

The other interesting regime for an OPE is the configuration where all three virtualities are large: $Q_1^2 \approx Q_2^2 \approx Q_3^2 \gg \Lambda_{\mathrm{QCD}}$. The method to deal with this configuration is not obvious, because the external photon is soft. If we deviate from the $g-2$ kinematics and instead consider all the four virualities to be large, we can apply the exact same method as the one described in the previous section and write a series of vacuum condensates for the correlator (3.80). [1]

Two of the terms that would appear in this OPE are shown in Fig. 3.12. The first fully contracted diagram corresponds to the leading perturbative contribution (Fig. 3.12a). The second involves a quark condensate (Fig. 3.12b).

However, in the $g-2$ kinematics, the topologies illustrated in Fig. 3.12b become problematic: no momentum runs in the loop and one of the propagators is therefore divergent when $q_4 \to 0$. [1] Unless some subtle cancellations occur, this causes the expansion to break down. Despite this issue, the quark loop was still used in the literature as a description of the HLbL tensor in the $g-2$ kinematics, when three virtualities were large.

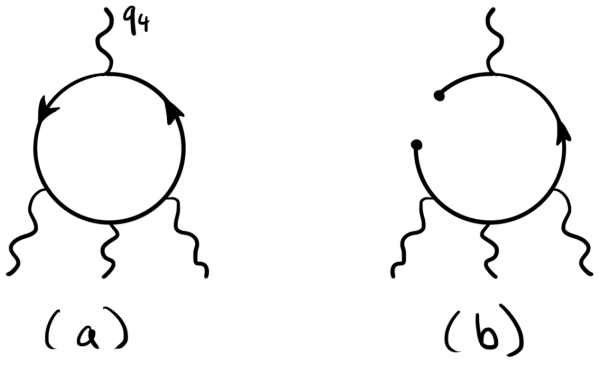

Figure 3.12: Operator product expansion for HLbL away from the $g-2$ kinematics: (a) leading perturbative contribution, (b) quark-condensate contribution. This figure is adapted from Ref. [1].

A way to construct a systematic expansion for HLbL in the $g-2$ kinematics was found in Ref. [1]. The solution is to use an OPE in presence of an external electromagnetic background

field. In this approach, no singularities appear in the limit $q_4 \to 0$.

Consider the following three-point correlator

$$\Pi^{\mu\nu\lambda}(q_1,q_2) = \int \mathrm{d}^4x \int \mathrm{d}^4y\, e^{-i(q_1\cdot x+q_2\cdot y)} \langle 0|T\left\{j^\mu_{\mathrm{em}}(x) j^\nu_{\mathrm{em}}(y) j^\lambda_{\mathrm{em}}(0)\right\}|\gamma(q_4)\rangle \ . \tag{3.82}$$

In the static limit $q_4 \to 0$, the soft photon can be factored out, thereby defining a new five-point correlation function [1]

$$\Pi^{\mu\nu\lambda}(q_1,q_2) \equiv \Pi_F^{\mu\nu\lambda\rho\sigma}(q_1,q_2)\, \langle 0|F_{\rho\sigma}|\gamma\rangle \ . \tag{3.83}$$

The tensor $\Pi_F^{\mu\nu\lambda\rho\sigma}$ is directly related to the derivative of the HLbL tensor in the static limit

$$-i\Pi_F^{\mu\nu\lambda[\rho\sigma]} = \lim_{q_4\to 0} \frac{\partial \Pi^{\mu\nu\lambda\rho}}{\partial q_{4\sigma}} = \sum_{i=1}^{54} \frac{\partial T_i^{\mu\nu\lambda\rho}}{\partial q_{4\sigma}} \Pi_i(q_1,q_2,q_3)\,, \tag{3.84}$$

where $[\rho\sigma]$ indicates an antisymmetrization with respect to the last two indices. It is therefore possible to define some projectors which return the scalar functions Π_i when acting on the tensor $\Pi_F^{\mu\nu\lambda[\rho\sigma]}$. More details on the projectors can be found in section 4.2.2. [1]

This gives us a well defined procedure to study the HLbL tensor when one of the photon is soft and the other are highly virtual: derive an OPE for the tensor (3.82) in the static limit, then extract the field strength tensor $F_{\rho\sigma}$ to get the tensor $\Pi_F^{\mu\nu\lambda\sigma\rho}$ and finally apply a set of projectors to obtain the scalar function Π_i which contain all the dynamical information of the HLbL tensor.

Compared to the OPE in the vacuum presented in the previous section, what are the differences in presence of an external magnetic field? The soft photon can either be produced from a hard fermion line (meaning that the fermion line scatters off the external background field), or it can be produced by a soft degree of freedom, via expectation values of operators that have the same quantum numbers as $F_{\mu\nu}$. This gives rise to new condensates. [1] A list of such operators as well as a renormalization program to deal with operator mixing is detailed in section 4.1.3. In this section, we instead focus on hard emission of the soft photon which are relevant for the leading term of the OPE for (3.82).

Our aim here is to compute the leading order ($\alpha_s = 0$) perturbative contribution from the three-point correlator (3.82) in the static limit $q_4 \to 0$. If we fully contract all the quark fields, we obtain a contribution proportional to the unit operator and the matrix element $\langle 0|\mathbb{1}|\gamma\rangle$ vanishes. To get a non-zero contribution, we must include an electromagnetic vertex from the Dyson series:

$$\Pi^{\mu\nu\lambda}_{\mathrm{LO,pt}}(q_1,q_2) \propto \int \mathrm{d}^4x\mathrm{d}^4y\, e^{-i(q_1\cdot x+q_2\cdot y)} \langle 0|T\{j^\mu_{\mathrm{em}}(x) j^\nu_{\mathrm{em}}(y) j^\lambda_{\mathrm{em}}(0) \underbrace{\int \mathrm{d}^4z j^\rho_{\mathrm{em}}(z) A_\rho(z)\}}_{\text{from Dyson series}}|\gamma\rangle \ , \tag{3.85}$$

where all the quark fields must be contracted in all possible ways. Contracting the quarks fields coming from the vertex insertion of the Dyson series will lead to the following kind of structures

$$\begin{aligned} & iee_A \int \mathrm{d}z\, \langle 0|\cdots \overline{q}_A(y)\gamma^\nu \overbrace{q_A(y)\overline{q}_A(0)\gamma^\lambda q_A(0)\overline{q}_A(z)}\gamma^\rho q_A(z) A_\rho(z)|\gamma\rangle \\ & = \langle 0|\cdots \underbrace{iee_A \int \mathrm{d}z\, S(y-z) A_\rho(z)\gamma^\rho S(z)}\, |\gamma\rangle\,. \end{aligned}$$

This is an example of hard production of the soft photon. Contracting all the quark fields in (3.85) leads to six different topologies shown in Fig. 3.13. By using the Schwinger gauge, the

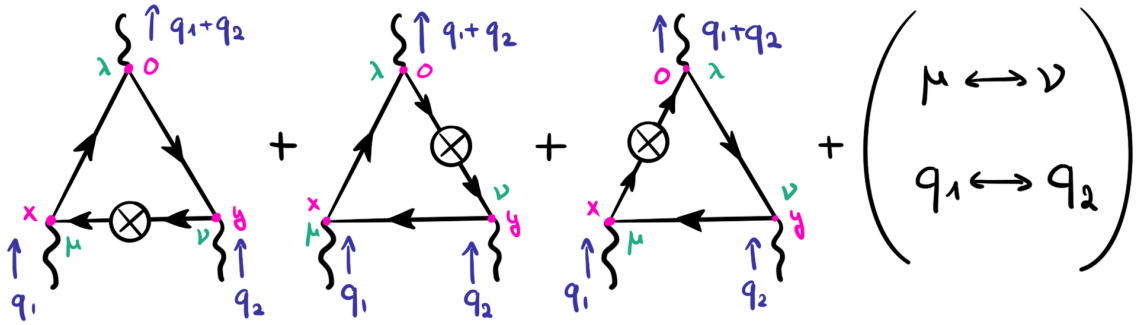

Figure 3.13: Leading contributions to the OPE for the three-point correlator $\Pi^{\mu\nu\lambda}$.

photon field can be expressed as $A^\rho(z) = \frac{1}{2} z^\sigma F_{\sigma\rho}(0)$ and the matrix element $\langle 0|F_{\rho\sigma}|\gamma\rangle$ appearing in (3.83) can directly be isolated to extract the tensor $\Pi_F^{\mu\nu\lambda\rho\sigma}$. The Π_i can then be obtained by applying some projectors on the antisymmetrized $\Pi_F^{\mu\nu\lambda[\rho\sigma]}$. The result of this procedure (in the massless case) is exactly the same as what would be obtained from the usual quark loop (c.f. Fig. 3.12a). [1]

This is the first step in proving that the quark loop is a good description of the HLbL tensor in the case where one photon is soft and the other have large virtualities. The next step is to show that the α_s correction and the non-perturbative contributions to the OPE described above are small in comparison. This is the objective of the next chapter.

Chapter 4

Operator product expansion for HLbL

> It does not matter how slowly you go, so long as you do not stop.
>
> Confucius

In the following articles, a formal OPE for the HLbL amplitude is built, which is valid for the $(g-2)_\mu$ kinematics where one of the photon is real. In the first article, non-perturbative corrections are considered and the second article analyses the two-loop perturbative corrections. They both build upon Ref. [1] which covers the LO contribution (which is reviewed in section 3.4 of this work), as well as the first non-zero power correction which is also addressed in the first article below.

4.1 Short-distances HLbL contributions to the muon anomalous magnetic moment beyond perturbation theory

This section is a copy of Ref. [37], published in the Journal of High-Energy Physics (JHEP) on October 30, 2020

Authors: Johan Bijnens, Nils Hermansson–Truedsson, Laetitia Laub, Antonio Rodríguez–Sánchez

---

Abstract: The hadronic light-by-light contribution to the muon anomalous magnetic moment depends on an integration over three off-shell momenta squared (Q_i^2) of the correlator of four electromagnetic currents and the fourth leg at zero momentum. We derive the short-distance expansion of this correlator in the limit where all three Q_i^2 are large and in the Euclidean domain in QCD. This is done via a systematic operator product expansion (OPE) in a background field which we construct. The leading order term in the expansion is the massless quark loop. We also compute the non-perturbative part of the next-to-leading contribution, which is suppressed by quark masses, and the chiral limit part of the next-to-next-to leading contributions to the OPE. We build a renormalisation program for the OPE. The numerical role of the higher-order contributions is estimated and found to be small.

4.1.1 Introduction

The Standard Model (SM) is the theoretical framework developed to describe particle physics at its most fundamental level, and is able to predict the anomalous magnetic moments of the leptons with a high number of significant digits. At the current level of precision, all the building blocks of the SM leave sizable numerical imprints for the muon anomalous magnetic moment, or, $a_\mu = (g-2)_\mu/2$. Summing all the contributions, one finds [4]

$$a_\mu^{\rm SM} = 116\,591\,810(43) \times 10^{-11}\,, \tag{4.1}$$

showing a 3.7σ tension with the very precise experimental value [5, 100],

$$a_\mu^{\rm exp} = 116\,592\,091(63) \times 10^{-11}\,. \tag{4.2}$$

The experimental value is expected to be significantly improved [6, 104]. In case the discrepancy grows this could be a sign of new physics beyond the SM.

The current uncertainties in the theoretical prediction are dominated by contributions from the hadronic sector. Since the relevant energy scale, i.e. the muon mass, is far below the region of applicability of perturbative QCD, the assessment of these contributions resorts to the use of non-perturbative tools. Further improvements are needed in order to find a SM value at the level of precision competing with that of the future experimental one. Decreasing the errors on the hadronic contributions would therefore shed some light on whether or not the current tension is a hint of new physics. An overview and assessment of the current theoretical situation is the white-paper [4].

In this paper, we focus on the hadronic light-by-light (HLbL) scattering contribution, represented by the diagram in Fig. 4.1. The calculation of the $(g-2)_\mu$ requires the integration of the HLbL tensor over q_1, q_2 and q_3, with the fourth photon in the static limit, i.e. $q_4 \to 0$. Working with three Euclidean squared loop momenta $q_i^2 = -Q_i^2$, this means one has to consider different kinematic regions of Q_i^2. We consider the short-distance regime with photon virtualities $Q_1^2 \sim Q_2^2 \sim Q_3^2 \gg \Lambda_{\rm QCD}^2$, and derive so-called short-distance constraints by means of an operator product expansion (OPE). The second important regime is with mixed virtualities, namely $Q_3^2, \Lambda_{\rm QCD}^2 \ll Q_1^2 \sim Q_2^2$, and has been considered in Ref. [2]. There has been a lot of recent work in the latter regime Refs. [30, 39–43, 83, 105].

The first full calculations of the HLbL were made using models in Refs. [106–108]. More recently a dispersion theory based approach as in Refs. [27, 77] has allowed for better control of the low-energy region. In the latter approach one considers individual intermediate states, for which short-distance constraints such as those derived herein can be used, examples are Refs. [30, 39, 40, 105, 107, 109]. One should of course be careful in comparing at the correct kinematics.

The naive OPE in the vacuum for the HLbL tensor, which is valid for $Q_1^2 \sim Q_2^2 \sim Q_3^3 \sim Q_4^2 \gg \Lambda_{\rm QCD}^2$, has the perturbative quark loop as its first term. The quark loop has always been used as an estimate for the whole contribution, using constituent quarks and in various models see e.g. Ref. [110–115] and for the contributions from heavy quarks [116]. However, the naive OPE breaks down for the $(g-2)_\mu$ kinematics with $q_4 \to 0$ [1]. The OPE of the HLbL tensor in this kinematics must be performed by taking into account that the static photon needs

to be formulated as a soft degree of freedom. It was shown in Ref. [1] (see also Ref. [2]) how this could be done by factoring out the soft photon as a background field. The background field can originate either from the hard degrees of freedom (e.g. the massless quark loop) or the soft ones (e.g. the so-called di-quark magnetic susceptibility contribution). The resulting OPE, originally formulated for baryon magnetic moment sum rules in Refs. [117] and [118], and whose application to other hadronic $(g-2)_\mu$ contributions was introduced in Ref. [60], has the massless quark loop as the leading term and the di-quark magnetic susceptibility of the vacuum as the leading quark-mass suppressed contribution. In this work we extend the results of Ref. [1] by computing the leading non-perturbative corrections not suppressed by masses. We also provide some more details about the calculations of Ref. [1]. Our result should be useful to help reducing the error coming from the intermediate and short-distance regime [4].

In Sec. 4.1.2 we briefly recapitulate the definitions of the four-point function of four electromagnetic currents, its decomposition in scalar functions and how it can be used for the muon $g-2$ HLbL contribution. This follows the conventions of Refs. [27, 77]. It also gives the relation between the needed derivative of the four-point function and the three-point function in a constant field background that is used in the remainder of this paper.

In Sec. 4.1.3 we give a complete description of the OPE in a constant background field and compare it to the usual vacuum OPE [91] and the one used in flavour-breaking transitions. We in addition comment on the physical meaning of the obtained matrix elements and build a renormalisation program. The renormalisation program is needed to systematically separate short-distance and long-distance effects while cancelling divergences. Both infrared and ultraviolet divergences are addressed. We also estimate the values of the matrix elements. The content of this section can in the future be used to obtain predictions for other Green functions in different kinematic regions.

Details on the calculation of the different non-perturbative pieces are provided in Sec. 4.1.4, in particular we explain the different tools used, existing and newly developed, to obtain our analytic results and how the different infrared divergences systematically cancel. Finally, making use of the results of that section and the estimates of the matrix elements, in Sec. 4.1.5 we calculate the numerical contribution of the different pieces for the $(g-2)_\mu$. Final remarks and conclusions are made in Sec. 4.1.6. Several intermediate derivations are relegated to the appendices as well as the full formulae.

4.1.2 The HLbL tensor

As can be seen in Fig. 4.1, the HLbL process involves a four-point correlation function of electromagnetic quark currents, i.e.

$$\Pi^{\mu_1\mu_2\mu_3\mu_4}(q_1,q_2,q_3) \equiv -i\int \frac{d^4q_4}{(2\pi)^4}\left(\prod_{i=1}^{4}\int d^4x_i\, e^{-iq_ix_i}\right)\langle 0|T\left(\prod_{j=1}^{4} J^{\mu_j}(x_j)\right)|0\rangle\,. \tag{4.3}$$

The currents are given by $J^\mu(x) = \bar{q}\,Q_q\gamma^\mu q$ with the quark fields $q=(u,d,s)$ and charge matrix $Q_q = \mathrm{diag}(e_q) = \mathrm{diag}(2/3,-1/3,-1/3)$. The tensor in (4.3) is the same as $\Pi^{\mu\nu\lambda\sigma}$ in Ref. [1], but with the internal notation slightly changed in the definition in order to make manifest some of its symmetry properties. This will be systematically exploited in the following sections. Moreover,

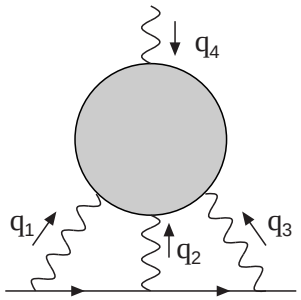

Figure 4.1: HLbL contribution to the $(g-2)_\mu$.

the integral over q_4 is introduced to remove the δ-function of conservation of momentum[1], i.e.

$$\sum_{i=1}^{4} q_i = 0\,. \tag{4.4}$$

This defines q_4 as the negative of that in Ref. [1], which again is a choice to maximise the number of explicit symmetries.

The conservation of the electromagnetic current implies that the HLbL tensor satisfies the following Ward identities,

$$q_{i,\,\mu_i}\,\Pi^{\mu_1\mu_2\mu_3\mu_4}(q_1,q_2,q_3) = 0,\ \forall i \in [1,4]\,, \tag{4.5}$$

where q_4 must be rewritten in terms of the other three momenta through (4.4). Note that the last Ward identity implies that all the information on the HLbL tensor is contained in its derivative [119],

$$\Pi^{\mu_1\mu_2\mu_3\mu_4}(q_1,q_2,q_3) = -q_{4,\,\nu_4}\frac{\partial\Pi^{\mu_1\mu_2\mu_3\nu_4}}{\partial q_{4,\,\mu_4}}(q_1,q_2,q_3)\,. \tag{4.6}$$

In the $(g-2)_\mu$ kinematics, the loop integral over the loop momenta q_1, q_2 and q_3 can be rewritten as an integral over the Euclidean momenta $Q_i^2 \equiv -q_i^2 > 0$. The fourth photon, i.e. with momentum q_4, is taken in the static limit. This corresponds to taking the $q_4 = -q_1 - q_2 - q_3 \longrightarrow 0$ limit after doing the derivative in (4.6). Notice how in this limit

$$\lim_{q_4\to 0}\frac{\partial\Pi^{\mu_1\mu_2\mu_3\nu_4}}{\partial q_{4,\,\mu_4}}(q_1,q_2,q_3) = -\lim_{q_4\to 0}\frac{\partial\Pi^{\mu_1\mu_2\mu_3\mu_4}}{\partial q_{4,\,\nu_4}}(q_1,q_2,q_3)\,, \tag{4.7}$$

i.e. it is anti-symmetric in the indices $\mu_4\nu_4$. This can be proven by multiplying both sides of (4.6) by $q_{4,\,\mu_4}$, then taking the derivative with respect to $q_{4,\alpha}$ and setting $\alpha = \nu_4$. The resulting linear and anti-symmetric structure of the HLbL tensor is directly related to the fact that $F_{\mu\nu} \equiv \partial_\mu A_\nu - \partial_\nu A_\mu$ is the lowest dimension gauge invariant photon operator.

Let us take advantage of the work of Refs. [27,77] to find general relations between the tensor $\frac{\partial\Pi^{\mu_1\mu_2\mu_3\nu_4}}{\partial q_{4,\,\mu_4}}$ and its explicit contribution to the $(g-2)_\mu$. Making use of the Ward identities above, one can rewrite in full generality the HLbL tensor as a linear combination of 54 scalar functions $\Pi_i(q_1,q_2,q_3)$ according to [27,77]

$$\Pi^{\mu_1\mu_2\mu_3\mu_4}(q_1,q_2,q_3) = \sum_{i=1}^{54} T_i^{\mu_1\mu_2\mu_3\mu_4}\Pi_i(q_1,q_2,q_3)\,. \tag{4.8}$$

[1]The integral could be performed instead in any other of the four momenta, leaving the HLbL tensor as a function of the other three.

Expressions for the $T_i^{\mu_1\mu_2\mu_3\mu_4}$ in terms of the Lorentz basis built with q_1, q_2, q_3 and the metric $g_{\mu\nu}$ can be found in Refs. [27, 77]. In particular, the $T_i^{\mu_1\mu_2\mu_3\mu_4}$ satisfy the same Ward identities as the HLbL tensor. As a consequence, in the static limit $q_4 \to 0$

$$\lim_{q_4\to 0} \frac{\partial \Pi^{\mu_1\mu_2\mu_3\nu_4}}{\partial q_4^{\mu_4}} = \sum_{i=1}^{54} \frac{\partial T_i^{\mu_1\mu_2\mu_3\nu_4}}{\partial q_4^{\mu_4}} \Pi_i(q_1, q_2, q_3)\,. \tag{4.9}$$

In the static limit $q_4 \to 0$, the remaining tensor can thus be written as a function of 19 linear combinations $\hat{\Pi}_i$ of the original $\Pi_i(q_1, q_2, q_3)$. Only 6 $\hat{\Pi}_i$ functions contribute to the $(g-2)_\mu$ and one finds

$$\begin{aligned} a_\mu^{\text{HLbL}} = \frac{2\alpha^3}{3\pi^2} \int_0^\infty dQ_1 \int_0^\infty dQ_2 \int_{-1}^1 d\tau\, \sqrt{1-\tau^2}\, Q_1^3 Q_2^3 \\ \times \sum_{i=1}^{12} T_i(Q_1, Q_2, \tau)\, \overline{\Pi}_i(Q_1, Q_2, \tau)\,, \end{aligned} \tag{4.10}$$

where the integration variable τ is defined via $Q_3^2 = Q_1^2 + Q_2^2 + 2\tau Q_1 Q_2$. The functions $T_i(Q_1, Q_2, \tau)$ can be found in Refs. [27, 77] and

$$\begin{aligned} &\overline{\Pi}_1 = \hat{\Pi}_1\,,\ \overline{\Pi}_2 = C_{23}\left[\hat{\Pi}_1\right]\,,\ \overline{\Pi}_3 = \hat{\Pi}_4\,,\ \overline{\Pi}_4 = C_{23}\left[\hat{\Pi}_4\right]\,, \\ &\overline{\Pi}_5 = \hat{\Pi}_7\,,\ \overline{\Pi}_6 = C_{12}\left[C_{13}\left[\hat{\Pi}_7\right]\right]\,,\ \overline{\Pi}_7 = C_{23}\left[\hat{\Pi}_7\right]\,, \\ &\overline{\Pi}_8 = C_{13}\left[\hat{\Pi}_{17}\right]\,,\ \overline{\Pi}_9 = \hat{\Pi}_{17}\,,\ \overline{\Pi}_{10} = \hat{\Pi}_{39}\,, \\ &\overline{\Pi}_{11} = -C_{23}\left[\hat{\Pi}_{54}\right]\,,\ \overline{\Pi}_{12} = \hat{\Pi}_{54}\,. \end{aligned} \tag{4.11}$$

The exact definition of the $\hat{\Pi}_i$ functions is given in Refs. [27, 77]. The C_{ij} in (4.11) represent interchanging q_i and q_j. In order to find general Lorentz projectors from the derivative of the tensor in the static limit, i.e.

$$\lim_{q_4\to 0} \frac{\partial \Pi^{\mu_1\mu_2\mu_3\nu_4}}{\partial q_4^{\mu_4}}\,, \tag{4.12}$$

to the $\hat{\Pi}_i$ functions, we start by taking 19 independent projectors in the $\{q_1, q_2, q_3, g\}$ basis. Any other projector can be related to that set through the Ward identities given above. Applying them to (4.9) returns a system of 19 equations dependent on the 19 $\hat{\Pi}_i$. A solution to that system of equations for the relevant $\hat{\Pi}_i$ is given in App. 4.1.A. In practice, this means that for any contribution to the HLbL tensor in any basis, one can compute the associated $(g-2)_\mu$ contribution by taking the derivative with respect to q_4, then taking the static limit $q_4 \to 0$, applying the 6 Lorentz projectors given in App. 4.1.A to find the associated $\hat{\Pi}_i$ and finally using them in the integral of (4.10).

As explained above, the integral of (4.10) requires the knowledge of the HLbL tensor with three Euclidean momenta Q_i at different kinematic regions and the fourth in the static limit $q_4 \to 0$. In this work, which extends the results of Ref. [1], we focus on the kinematic region where the three loop momenta are large. As was shown in Ref. [1], if one defines

$$\Pi^{\mu_1\mu_2\mu_3}(q_1, q_2) \equiv -\frac{1}{e} \int \frac{d^4q_3}{(2\pi)^4} \left(\prod_{i=1}^3 \int d^4x_i\, e^{-iq_i x_i}\right) \langle 0|T\left(\prod_{j=1}^3 J^{\mu_j}(x_j)\right)|\gamma(q_4)\rangle\,, \tag{4.13}$$

then in the static limit for the studied kinematic region, one can factor out the soft photon contributions according to

$$\Pi^{\mu_1\mu_2\mu_3}(q_1,q_2) = \Pi_F^{\mu_1\mu_2\mu_3\mu_4\nu_4}(q_1,q_2)\langle 0|e_q F_{\nu_4\mu_4}|\gamma(q_4)\rangle\,. \tag{4.14}$$

As mentioned in the introduction, the soft background field $F_{\mu\nu}$ can originate from the hard degrees of freedom or the soft ones. One then finally has [1]

$$\lim_{q_4\to 0}\frac{\partial\Pi^{\mu_1\mu_2\mu_3\mu_4}}{\partial q_4^{\nu_4}} = -i\,\Pi_F^{\mu_1\mu_2\mu_3[\mu_4\nu_4]}(q_1,q_2)\,. \tag{4.15}$$

For this OPE the massless quark loop is the leading term and the di-quark magnetic susceptibility of the vacuum is the leading, quark-mass suppressed, non-perturbative contribution. In this work we compute the leading non-perturbative (not mass-suppressed) corrections.

4.1.3 The operator product expansion: a theoretical description

In this section we describe the OPE and the associated renormalisation program. From this we systematically separate the long-distance effects from the short-distance ones. The general framework and operators involved are presented in Sec. 4.1.3.1 whereas the mixing of these operators is elaborated on in Sec. 4.1.3.2. Finally, the OPE developed as well as operators and corresponding matrix elements involved are discussed.

4.1.3.1 General framework

Perturbative calculations are known to provide a huge predictive power in the framework of Quantum Field Theory. However, when the calculation of a given observable involves the interplay of two (or more) very different scales, large logarithms between them slow down, if not spoil, the convergence of the series. These large logarithms can be avoided in many cases through the OPE [86, 120], which integrates out the heavy degrees of freedom leaving the low-energy (long-distance) dependence encoded in effective operators, in such a way that the contributions from higher-dimension operators become suppressed by extra powers of the high-energy scale [87, 121, 122]. There are cases in which this logarithmic re-summation is not enough, since one (or several) relevant couplings of the theory diverge when its running is performed. This is the case for QCD, where a low-energy description in terms of approximately free quarks and gluons does not hold and the matrix elements between initial and final states cannot be computed within perturbative QCD. The contributions from the operators whose quantum numbers are compatible with the transition must be fitted to data, computed with effective field theories or other non-perturbative methods, such as lattice QCD, dispersion relations or model estimates.

In the OPE of two-point correlation functions [91], all the local operators with the same quantum numbers as the QCD vacuum, such as the identity or $\bar{q}q$, can give a contribution to the Green functions[2]. In the OPE used in flavour-breaking transitions (e.g. see Ref. [87]) all the local operators with quantum numbers compatible with the studied transition among hadrons can give a contribution. In the OPE we are working with [117, 118], applied to (4.13), any local

[2]The words n-point function, correlation function and Green function are all used but have the same meaning.

operator with the same quantum numbers as $F_{\mu\nu}$ can absorb the remaining soft static photon and, as a consequence, give a contribution [1, 60]. Higher-dimensional operators are suppressed by extra powers of $\left(\frac{\Lambda_{\rm QCD}}{Q_i}\right)^d$, providing a hierarchy of contributions with a systematic counting. Up to dimension 6 and order α_s a basis of those operators is[3]

$$S_{1,\,\mu\nu} \equiv e\, e_q F_{\mu\nu}\ , \tag{4.16}$$

$$S_{2,\,\mu\nu} \equiv \bar{q}\sigma_{\mu\nu} q\ , \tag{4.17}$$

$$S_{3,\,\mu\nu} \equiv i\ \bar{q} G_{\mu\nu} q\ , \tag{4.18}$$

$$S_{4,\,\mu\nu} \equiv i\,\bar{q}\bar{G}_{\mu\nu}\gamma_5 q\ , \tag{4.19}$$

$$S_{5,\,\mu\nu} \equiv \bar{q} q\ e\, e_q F_{\mu\nu}\ , \tag{4.20}$$

$$S_{6,\,\mu\nu} \equiv \frac{\alpha_s}{\pi}\, G_a^{\alpha\beta} G^a_{\alpha\beta}\ e\, e_q F_{\mu\nu}\ , \tag{4.21}$$

$$S_{7,\,\mu\nu} \equiv \bar{q}(G_{\mu\lambda} D_\nu + D_\nu G_{\mu\lambda})\gamma^\lambda q - (\mu \leftrightarrow \nu)\ , \tag{4.22}$$

$$S_{\{8\},\,\mu\nu} \equiv \alpha_s\,(\bar{q}\,\Gamma\, q\ \bar{q}\Gamma q)_{\mu\nu}\ . \tag{4.23}$$

We use here the notation of Ref. [85]. In particular, $G_{\mu\nu} = i g_S \lambda^a G^a_{\mu\nu}$, $\bar{G}^{\mu\nu} \equiv \frac{i}{2}\epsilon^{\mu\nu\lambda\rho} G_{\lambda\rho}$, covariant derivatives act on all objects to their right and $\mathrm{tr}\left(\gamma_5\gamma^\mu\gamma^\nu\gamma^\alpha\gamma^\beta\right) = -4i\varepsilon^{\mu\nu\alpha\beta}$. For $S_{1\ldots7,\mu\nu}$ the quark field q refers to a given flavour and there are in principle different operators for different flavours q. Notice, however, that taking into account that the (massless) QCD vacuum preserves $SU(3)_{\rm V}$, the contributions of the operators to the studied transition depend, in the chiral limit ($m_u = m_d = m_s = 0$), on a common constant multiplied by the corresponding quark electric charge. Note that with the conventions of Ref. [85], $G^{\mu\nu}$ is order g_s.[4] The four-quark operators are only indicated generically in (4.23). A decomposition valid in the chiral limit into twelve operators is given in App. 4.1.B. In fact, only two combinations of four-quark operators contribute as discussed in Sec. 4.1.4. The adopted notation is analogous to the one in Ref. [87].

In order to perform the OPE of the tensor in (4.13), one applies Wick's theorem with any number of needed (suppressed) extra (QCD or QED) vertices coming from the Dyson series. The uncontracted operators must then be Taylor expanded (e.g. see Ref. [85]), so that the resulting expression is of the form[5]

$$\Pi^{\mu_1\mu_2\mu_3}(q_1,q_2) = \frac{1}{e}\vec{C}^{T,\mu_1\mu_2\mu_3\mu_4\nu_4}(q_1,q_2)\langle\vec{S}_{\mu_4\nu_4}\rangle = \vec{C}^{T,\mu_1\mu_2\mu_3\mu_4\nu_4}(q_1,q_2)\,\vec{X}_S\,\langle e_q F_{\mu_4\nu_4}\rangle\,, \tag{4.24}$$

where $\vec{X}_S$ contains the magnetic susceptibilities of the operators,[6] $\langle S_{i,\mu\nu}\rangle = e e_q X^i_S \langle F_{\mu\nu}\rangle$.

Even when this was a first step to achieve the separation between short-distance and long-distance effects, such a separation is not yet complete. Let us illustrate this with the simplest

[3] Notice how the order in α_s depends on the short-distance structure of the studied Green function. For example in baryon sum rules, the four-quark operators $S_{\{8\}}$ do not enter α_s-suppressed. In our calculation, at order g_s^3 one may have a contribution from a three-gluon operator [117], but it enters suppressed by g_s, loops and flavour (in the $SU(3)_V$ limit its contribution vanishes, since it transforms as a singlet and the photon field transforms as an octet).

[4] In fact, the gluon tensor is named $F^{\mu\nu}$ in that reference. We rename it as $G^{\mu\nu}$ to avoid ambiguity with the electromagnetic field strength $F_{\mu\nu}$. Similar renamings should be obvious.

[5] Further technical details on the computation of the different pieces are given in Sec. 4.1.4.

[6] We will define the susceptibilities more precisely later.

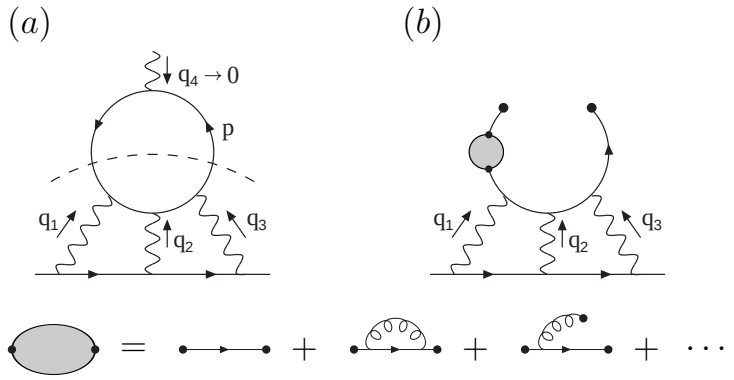

Figure 4.2: Example of contributions of HLbL in the studied kinematic region. (a) The quark loop. (b) The di-quark magnetic susceptibility. A complete separation between short-distance and long-distance effects should subtract possible divergent low-momenta contributions from the quark loop and possible divergent perturbative series arising from soft lines.

contributions: the quark loop and the (di-quark) magnetic susceptibility, represented in Fig. 4.2. In Fig. 4.2b one has short-distance contributions that arise from expanding the Dyson series and introducing vertices in the soft lines, represented by a blob. Since there is no momentum flowing, the resulting series, $\sum c_n \alpha_s^n(0)$, is manifestly divergent. This kind of effects must be subtracted, since they belong to the non-perturbative domain. A slightly different problem arises with Fig. 4.2a. The quark loop runs over all possible momenta. If the low-momenta contributions do not vanish, they must somehow be subtracted and reabsorbed into the long distance matrix elements. This is the case for the $\mathcal{O}(m_q^2)$ mass corrections, whose (not regulated) Wilson coefficient, $C_{m_q^2}$, leads to divergent series $\sum_n c_n\, \alpha_s^n(Q^2) \log^n\left(Q^2/m_q^2\right)$, i.e. the coefficients are not well defined in the chiral limit. The m_q^2 dependence in the coefficients originates from the low-energy domain and must be included in the operator expectation values as well.

The way of achieving these subtractions is by dressing and renormalising the $\vec{S}^{\mu\nu}$ operators (normal-ordered operators in the notation of Ref. [123], tree-level operators in the notation of Ref. [87]). Following a notation close to the one in Ref. [87], the dressed operators $\vec{Q}_0^{\mu\nu}$ in terms of the tree-level ones $\vec{S}^{\mu\nu}$ are obtained by reinserting them into the Dyson series, leading to a result of the form

$$\vec{Q}_0^{\mu\nu} = \hat{M}(\epsilon)\vec{S}^{\mu\nu}\,, \tag{4.25}$$

where the $\epsilon = -\frac{d-4}{2}$ dependence appears in dimensional regularization as a consequence of ultraviolet divergences in the loop diagrams. The infrared divergences that can appear are regularised using the quark mass. The resulting redefinition of the matrix elements[7] involves two steps, calculating the relevant contributions leading to an expression at one-loop order of the form

$$\hat{M}(\epsilon) = \mathbb{I} + \frac{m_q^{-2a\hat{\epsilon}}}{\hat{\epsilon}}\hat{M}_{\hat{\epsilon}} + \hat{M}_{\rm rem}\,, \tag{4.26}$$

where $\hat{M}_{\hat{\epsilon}}$ and $\hat{M}_{\rm rem}$ are perturbations either in e, in g_s or in powers of $\frac{m_q}{\Lambda_{\rm QCD}}$ and $\frac{1}{\hat{\epsilon}} = \frac{1}{\epsilon} - \gamma_E + \log(4\pi)$. a depends on the dimension of the operators when $d \neq 4$. The ultraviolet divergences are unphysical, and are removed via renormalisation. A convenient and simple renormalisation

[7] We need here the condensates induced by the external field. We refer to those as matrix elements to distinguish them from the usual (vacuum) condensates.

scheme is by performing the operator renormalisation in the $\overline{MS}$ scheme, which basically removes the $\frac{1}{\hat{\epsilon}}$ factors and takes out from the bare operators the non-canonical part of their dimension, proportional to $2a\epsilon$:

$$\vec{Q}_0^{\mu\nu} = \hat{Z}_{\overline{MS}}(\mu,\epsilon)\,\vec{Q}_{\overline{MS}}^{\mu\nu}(\mu)\,, \tag{4.27}$$

$$\hat{Z}_{\overline{MS}}(\mu,\epsilon) = \mathbb{I} + \frac{\hat{M}_{\hat{\epsilon}}\,\mu^{2a\epsilon}}{\hat{\epsilon}}\,, \tag{4.28}$$

$$\vec{Q}_{\overline{MS}}^{\mu\nu}(\mu) = \hat{U}_{\overline{MS}}(\mu)\,\vec{S}^{\mu\nu} = \left(\mathbb{I} - a\log\left(\frac{m_q^2}{\mu^2}\right)\hat{M}_{\hat{\epsilon}} + \hat{M}_{\text{rem}}\right)\vec{S}^{\mu\nu}\,. \tag{4.29}$$

Putting this back into (4.24) one finds

$$\begin{aligned}\Pi^{\mu_1\mu_2\mu_3}(q_1,q_2) &= \frac{1}{e}\vec{C}^{T,\mu_1\mu_2\mu_3\mu_4\nu_4}(q_1,q_2)\hat{U}^{-1}_{\overline{MS}}(\mu)\langle\vec{Q}_{\overline{MS},\mu_4\nu_4}(\mu)\rangle \\ &\equiv \frac{1}{e}\vec{C}^{T,\mu_1\mu_2\mu_3\mu_4\nu_4}_{\overline{MS}}(q_1,q_2)\langle\vec{Q}_{\overline{MS},\mu_4\nu_4}(\mu)\rangle\,.\end{aligned} \tag{4.30}$$

This equation defines the regularized and renormalised Wilson coefficients. The renormalised Wilson coefficients,

$$\vec{C}^{\mu_1\mu_2\mu_3\mu_4\nu_4}_{\overline{MS}}(q_1,q_2,\mu) = \hat{U}^{-1\,T}_{\overline{MS}}(\mu)\vec{C}^{\mu_1\mu_2\mu_3\mu_4\nu_4}(q_1,q_2)\,, \tag{4.31}$$

become free from long-distance effects and infrared divergences, completing the desired separation. For the matrix elements we define the magnetic susceptibilities $\vec{X} = (X_1,\ldots)$.[8]

$$\langle\vec{Q}_{\overline{MS},\mu\nu}(\mu)\rangle = e\vec{X}\langle e_q F_{\mu\nu}\rangle \tag{4.32}$$

The contributions we calculate explicitly in Sec. 4.1.4 are: The leading contribution stems from $Q_1^{\mu\nu}$ at $d=2$ and corresponds to the massless quark loop. This operator receives mass corrections suppressed by powers of $\frac{m_q^2}{\Lambda^2}$. The first correction from a different operator comes from the $d=3$ di-quark operator, $Q_2^{\mu\nu}$, which happens to enter suppressed by one power of the quark mass becoming effectively $d=4$. This contribution using the mixing as defined in (4.26–4.29) removes the $m_q^2\log\left(m_q^2\right)$ part of the quark loop and together with that forms the $d=4$ contribution. The $d=5$ contributions from $Q_{3-5}^{\mu\nu}$ are also suppressed by one power of the quark mass. $Q_{6-8}^{\mu\nu}$ give the first contributions that are not suppressed by the quark masses. The mixing here again removes contributions proportional to $\log\left(m_q^2\right)$ and other infrared divergences. We therefore calculate with respect to the massless quark loop the corrections of orders $g_s\,\frac{\Lambda^4_{\text{QCD}}}{Q^4}$, $\frac{m_q^2}{Q^2}$, $g_s^2\,\frac{\Lambda^4_{\text{QCD}}}{Q^4}$, $m_q\frac{\Lambda_{\text{QCD}}}{Q^2}$,$m_q\frac{\Lambda^3_{\text{QCD}}}{Q^4}$, $m_q^3\frac{\Lambda_{\text{QCD}}}{Q^4}$. The computation of the last three is needed, since they give contributions to the $g_s^2\,\frac{\Lambda^4_{\text{QCD}}}{Q^4}$ through operator mixing as defined above and calculated in Sec. 4.1.3.2. This is analogous to the mixing between bi-linear quark condensate and gluon condensate in the usual vacuum OPE [124–126].

4.1.3.2 The operator mixing

In this section we calculate the mixing matrix $\hat{U}_{\overline{MS}}$. However, there are some parts that can be ignored. These we discuss first. The original Wilson coefficients contain in principle infrared

[8] The four-quark operators have a slightly different definition of the susceptibilities to get the charge behaviour correctly, see Sec. 4.1.3.3. X_2 is often referred to as the (di-quark) magnetic susceptibility.

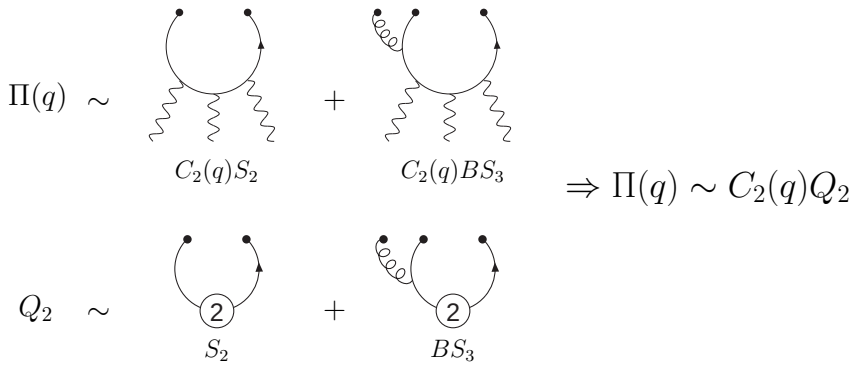

Figure 4.3: An example of a cancellation for contributions arising from attaching extra vertices to soft, at zero momentum, lines. The circle with "2" inside refers to the S_2 operator defined in (4.17), B indicates the extra factor compared to the left diagrams. All Lorentz indices have been suppressed for clarity.

divergent parts that arise from attaching extra vertices to the soft zero-momentum lines. These long-distance contributions, explicitly independent of momenta, systematically cancel with analogous terms in the dressing procedure, which in addition are independent of the studied physical process, so we simply ignore them in both sides of the calculation. An example of this is sketched in Fig. 4.3. The top graphs show the contribution from $S_{2,\mu\nu}$ to the correlator we calculate and the bottom line contributions to the mixing matrix. The contribution from the top right is via the diagram in the bottom right absorbed into the definition of the operator $Q_{2,\mu\nu}$.

As a consequence, only mixing terms with loops need to be considered for the calculation of $\hat{U}_{\overline{MS}}$. This limits the type of terms that can show up. Then, at this stage, we have two possibilities. 1) If no more (QCD or QED) vertices are added, the original operator can only mix with lower dimensional ones, since loops imply connecting the fields of both operators with propagators. The only remaining scale to compensate dimensions is m_q and as a consequence $\hat{M}(\epsilon)$ becomes a m_q^n perturbation, with n positive. The calculation for $\hat{U}^{21}_{\overline{MS}}$ is of this type. 2) Alternatively, one can have mixing terms with operators with equal or higher dimensions that show up by adding fields through introducing extra vertices. However, these new vertices come with an extra cost (g_s or e), and then they can also be regarded as perturbations, an example of this type is $\hat{U}^{76}_{\overline{MS}}$. Finally, when studying the mixing of lower dimensional operators with higher dimensional ones, one finds terms that go as m_q^{-n}. A well-known case of this in the usual vacuum OPE is the gluon condensate mixing with the quark condensate

$$\langle \bar{q}q \rangle = -\frac{1}{12m_q} \left\langle \frac{\alpha_S}{\pi} G^a_{\mu\nu} G^{a\mu\nu} \right\rangle + \cdots . \tag{4.33}$$

However this kind of mixing is simply absorbing in the renormalised operator unphysical (infrared) divergences contained in the perturbative Wilson coefficients. The quark mass is used as an infrared regulator as well as for calculating genuine quark mass corrections.[9]

The first step is thus the dressing of the tree level operators and the computation of the associated matrix $\hat{M}(\epsilon)$. All the diagrams involved are shown in Fig. 4.4. The first diagram for each operator always corresponds to identity term in (4.26). The procedure should be done,

[9]The procedure is equivalent to what is used in the usual vacuum OPE [123–127].

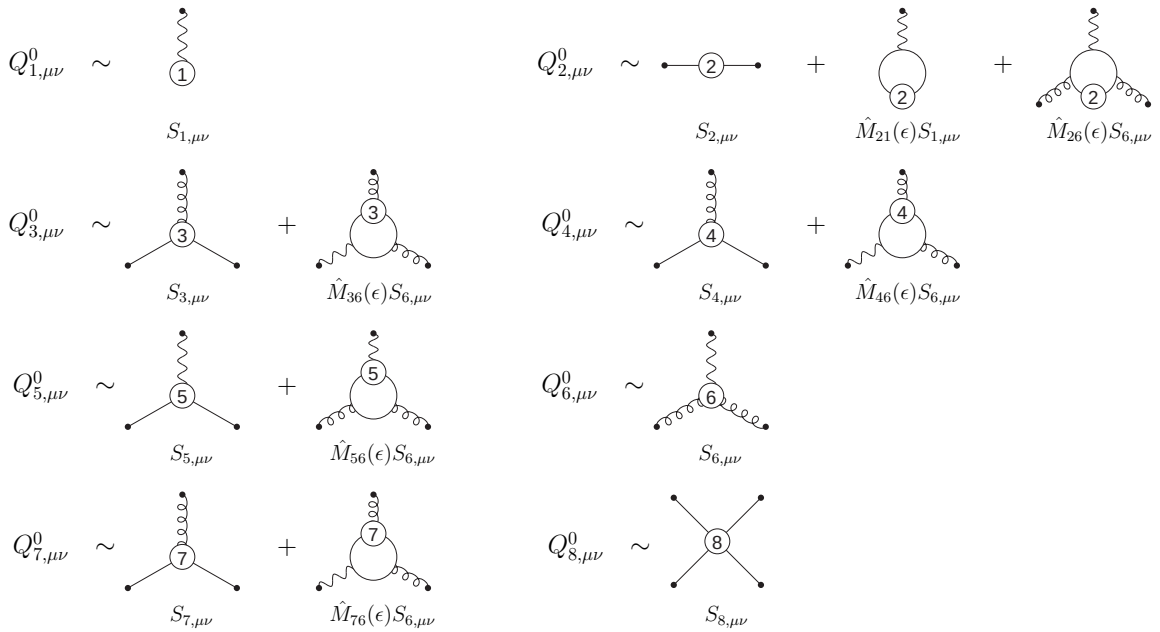

Figure 4.4: Topologies involved in the computation of the matrix $\hat{M}(\epsilon)$. All the possible permutations of the bosonic lines attached to the fermion loops must be considered. The numbered circles refer to the operators defined in (4.16)-(4.23). The "outside" black dots form the operators that mix in.

as is also the case for the usual vacuum OPE, only including operators up to the dimension considered.

The only way $Q_1^{\mu\nu}$ mixes with other operators is by introducing extra electromagnetic vertices. Since $Q_1^{\mu\nu}$ is already $\mathcal{O}(e)$, the resulting corrections are $\mathcal{O}(e^2)$, and thus do not need to be considered. The first non-trivial case is that of the operator $Q_2^{\mu\nu}$. The non-zero element of $\hat{M}(\varepsilon)$ and thus $\hat{U}_{\overline{MS}}$ are calculated in the next subsubsections. As in Sec. 4.1.4 the calculations in this section benefit very much from using the radial gauge.

$Q_2^{\mu\nu}$ The mixing with $Q_1^{\mu\nu} = ee_q F^{\mu\nu}$ requires an extra electromagnetic vertex and closing the quark lines. This corresponds to the second Q_2-diagram in Fig. 4.4. Let us sketch it in some detail to illustrate the procedure:

$$\begin{aligned} Q^0_{2,\mu\nu} = \bar{q}\sigma_{\mu\nu}q_0 = \bar{q}\sigma_{\mu\nu}q\, e^{iS} &= \bar{q}\sigma_{\mu\nu}q\left(1 + ie\int d^dx\, e_q\,\bar{q}(x)\gamma^{\nu_1}A_{\nu_1}(x)q(x) + \dots\right) \\ &= \bar{q}\sigma_{\mu\nu}q\left(1 + ie\, e_q\frac{iF_{\mu_1\nu_1}}{2}\lim_{p_1\to 0}\partial^{\mu_1}_{p_1}\int d^dx\, e^{-ip_1x}\bar{q}(x)\gamma^{\nu_1}q(x) + \cdots\right) \\ &= S_{2,\,\mu\nu} + S_{1,\,\mu\nu}\frac{N_c\, m_q}{4\pi^2}\left(-\frac{1}{\hat{\epsilon}} + \log\!\left(m_q^2\right)\right) + \cdots\,, \end{aligned} \tag{4.34}$$

where we have used that we are working in the radial gauge, $A_\mu(x) = \frac{1}{2}x^\nu F_{\nu\mu}$ [85,124].[10] Taking into account (4.26) and (4.29), one finds

$$\hat{U}^{21}_{\overline{MS}}(\mu) = \frac{N_c m_q}{4\pi^2}\log\left(\frac{m_q^2}{\mu^2}\right)\,. \tag{4.35}$$

[10]The results are of course gauge-independent.

Through the $\overline{MS}$ renormalisation we have introduced a subtraction point, μ, which is the scale of separation between long-distance and short-distance effects. In particular this mixing term, when plugged into (4.31), removes the (infrared divergent) long-distance parts from the loops associated to the perturbative $\mathcal{O}(m_q^2)$ corrections by effectively replacing $\log Q_i^2/m_q^2 \to \log Q_i^2/\mu^2$.[11] Notice how, in contrast with the usual vacuum OPE, where these divergences can only start at $\mathcal{O}(m_q^4)$ (and be regulated by the quark condensate), the divergences in this OPE with respect to the quark loop start at $\mathcal{O}(m_q^2)$. They become regulated by $Q_2^{\mu\nu}$.

At the order we are working with, $Q_2^{\mu\nu}$ also mixes with $Q_6^{\mu\nu}$ through the third Q_2-diagram in Fig. 4.4, leading to

$$\hat{U}^{26}_{\overline{MS}}(\mu) = -\frac{1}{72 m_q^3}\,. \tag{4.36}$$

The Wilson coefficient proportional to $\frac{S_2^{\mu\nu}}{m_q^2}$ combined with this matrix element cancels the power divergence of the (unregulated) Wilson coefficient associated to $S_6^{\mu\nu}$, while the mass correction to the Wilson coefficient associated to $S_1^{\mu\nu}$ gives a finite contribution that needs to be included. Once again, this interplay is analogous to the corresponding one in the vacuum OPE [123–126].

$Q_{3-6}^{\mu\nu}$ Since $Q_3^{\mu\nu}$ and $Q_4^{\mu\nu}$ are already $\mathcal{O}(g_s)$ and two lines need to be closed to form a loop to give a non-zero contribution, they only mix with the gluon matrix element at the order we are working with (see Fig. 4.4), giving a finite contribution to its associated regulated Wilson coefficient. One finds,

$$U^{36}_{\overline{MS}}(\mu) = \frac{1}{36 m_q}\,, \tag{4.37}$$

$$U^{46}_{\overline{MS}}(\mu) = \frac{1}{24 m_q}\,. \tag{4.38}$$

Since $Q_5^{\mu\nu}$ is already order e, it can only mix with $Q_1^{\mu\nu}$ and $Q_6^{\mu\nu}$ at the order we are working with. Dimensional analysis shows that the mixing with $Q_1^{\mu\nu}$ only modifies the very tiny and safely neglected $\mathcal{O}(m_q^4)$ contribution. The mixing with $Q_6^{\mu\nu}$ is the same as the mixing of the quark condensate with the gluon condensate, as in (4.33), since at the order in e we are working with the photon does not see strong interactions [91, 123–126],

$$U^{56}_{\overline{MS}}(\mu) = -\frac{1}{12 m_q}\,. \tag{4.39}$$

$Q_7^{\mu\nu}$ The last operator to treat is $Q_7^{\mu\nu}$ which through the topologies shown in Fig. 4.4 only mixes with $Q_6^{\mu\nu}$. One has

$$U^{76}_{\overline{MS}}(\mu) = -\frac{1}{12}\left(1 - 2\log\frac{m_q^2}{\mu^2}\right)\,. \tag{4.40}$$

[11] In Ref. [1] this replacement was not done for the m_q^2 quark loop numerics.

Full matrix $\hat{U}_{\overline{MS}}(\mu)$ Putting all the elements together one finds for $N_c = 3$

$$\hat{U}_{\overline{MS}}(\mu) = \begin{pmatrix} 1 & 0 & 0 & 0 & 0 & 0 & 0 & 0 \\ \frac{3\,m_q}{4\pi^2}\log\frac{m_q^2}{\mu^2} & 1 & 0 & 0 & 0 & -\frac{1}{72m_q^3} & 0 & 0 \\ 0 & 0 & 1 & 0 & 0 & \frac{1}{36m_q} & 0 & 0 \\ 0 & 0 & 0 & 1 & 0 & \frac{1}{24m_q} & 0 & 0 \\ 0 & 0 & 0 & 0 & 1 & -\frac{1}{12m_q} & 0 & 0 \\ 0 & 0 & 0 & 0 & 0 & 1 & 0 & 0 \\ 0 & 0 & 0 & 0 & 0 & \frac{1}{6}\left(\log\frac{m_q^2}{\mu^2} - \frac{1}{2}\right) & 1 & 0 \\ 0 & 0 & 0 & 0 & 0 & 0 & 0 & 1 \end{pmatrix}. \tag{4.41}$$

4.1.3.3 Values of the matrix elements

Apart from providing model-independent information on the kinematic dependence of the non-perturbative corrections for the short-distance HLbL, in principle this OPE can be used to study different Green functions with all its (Euclidean) momenta large except for one soft photon. This might also allow to obtain more information on the expectation values (or the susceptibilities). However in absence of the latter we need to determine the values in a different way. We can find values for all of them with a number of assumptions that should at least give the correct order of magnitude.

$Q_5^{\mu\nu}$ and $Q_6^{\mu\nu}$ The matrix elements associated to $Q_5^{\mu\nu}$ and $Q_6^{\mu\nu}$ are directly related to the quark and the gluon condensates, respectively. The former one is well-known, since it is the order parameter of the spontaneous chiral symmetry breaking of QCD, both from chiral perturbation theory and the lattice. Updated lattice values can be found in Ref. [94]. The gluon condensate is not so well-known, since separating its effect from those of the perturbative series is non-trivial. However its order of magnitude is known, namely $X_6 \sim 0.02\,\text{GeV}^4$ [91].

$Q_2^{\mu\nu}$, $Q_3^{\mu\nu}$ and $Q_4^{\mu\nu}$ The matrix elements $\langle 0|Q_i^{\mu\nu}|\gamma(q_4)\rangle = X_i\langle 0|e\,e_q F^{\mu\nu}|\gamma(q_4)\rangle$ are directly related to the values of QCD two-point functions at zero momentum, $\Pi_{VQ_i}(q^2)$. In order to see that, let us take a generic dressed operator $Q_{i,0}^{\mu\nu}$. Its contribution to a matrix element with a final static photon can only arise through an extra electromagnetic vertex. Then, in the static limit,

$$\langle 0|Q_{i,0}^{\mu\nu}|\gamma(q_4)\rangle = \langle 0|Q_{i,0(\text{QCD})}^{\mu\nu} ie\int d^4x\, e_q\, A_\beta(x) J^\beta(x)|\gamma(q_4)\rangle = -\langle 0|e\,e_q\,F^{\mu\nu}|\gamma(q_4)\rangle\,\Pi_{JQ_i}^{\text{QCD}}(0)\,, \tag{4.42}$$

where

$$\Pi_{JQ_i}^{\text{QCD},\alpha\mu\nu}(q) = \int d^4x\, e^{-iqx}\, T(J^\alpha(x) Q_{i,0(\text{QCD})}^{\mu\nu}(0)) = (q^\mu g^{\alpha\nu} - q^\nu g^{\alpha\mu})\Pi_{JQ_i}^{\text{QCD}}(q^2)\,. \tag{4.43}$$

These two-point functions can be computed at large Euclidean momenta through the OPE in the vacuum [91].

One could compute these matrix elements in chiral perturbation theory. In fact, promoting the global $SU(3)_\text{V}$ symmetries to local ones lead to trivial transformations for the operators

$Q_2^{\mu\nu}, Q_3^{\mu\nu}, Q_4^{\mu\nu}$ and $Q_8^{\mu\nu}$. The resulting effective low-energy Lagrangians are given in Ref. [128].[12] At the lowest order the $X_i^{\overline{MS}}(\mu)$ are directly proportional to the low-energy constants $\Lambda_1^{i,\overline{MS}}(\mu)$. However, this gives no extra information by itself in the $SU(3)_V$ limit, since the $\Lambda_1^{i,\overline{MS}}(\mu)$ are not known.

For X_2, X_3 and X_4 we obtain an educated guess by making use of (4.42) and extrapolating the argument for X_2 from Ref. [129–132]. First of all, in the large-N_c limit the QCD spectrum is made of an infinite number of free, stable meson states [133–135]. The two-point functions in that limit are then saturated by the exchange of resonances. Owing to the quantum numbers of the studied two-point functions, the corresponding resonances must be vector mesons [136]. The low-energy part of the $N_c = 3$ QCD spectrum is actually close to the sum of narrow width resonances predicted by the large-N_c limit, while at higher energies a transition towards the flat perturbative QCD spectrum is observed. Taking all this into account, and that in the chiral limit the VT two-point function vanishes in the perturbative regime, it is reasonable to assume that the physical spectrum is saturated by the contribution of the lowest vector meson, i.e. the ρ meson. Using the formalism developed in Ref. [137] and adding a tensor source [128, 132], one can write the two-point functions of (4.43) on the form

$$\Pi_{JQ_i}(q^2) = \frac{C_{Ti}}{q^2 - M_\rho^2}\,. \tag{4.44}$$

Here, the C_{T_i} are constants. It then follows that

$$X_i = \frac{C_{T_i}}{M_\rho^2}\,. \tag{4.45}$$

In order to estimate the C_{T_i}, we can match the ansatz of (4.44) with the short-distance OPE of (4.43). This is sometimes referred to as a vector-meson-dominance (VMD) estimate. We find

$$\Pi_{JQ_2}(q^2) = \frac{2\langle\bar{q}q\rangle}{q^2}\,, \tag{4.46}$$

$$\Pi_{JQ_3}(q^2) = -\frac{\langle\bar{q}G_a^{\mu\nu}\frac{\lambda^a}{2}\sigma_{\mu\nu}q\rangle}{6q^2} \equiv -m_0^2\frac{\langle\bar{q}q\rangle}{6q^2}, \tag{4.47}$$

$$\Pi_{JQ_4}(q^2) = -\frac{\langle\bar{q}G_a^{\mu\nu}\frac{\lambda^a}{2}\sigma_{\mu\nu}q\rangle}{6q^2} \equiv -m_0^2\frac{\langle\bar{q}q\rangle}{6q^2}. \tag{4.48}$$

This leads to

$$X_2 = \frac{2}{M_\rho^2}\langle\bar{q}q\rangle, \tag{4.49}$$

$$X_3 = -\frac{m_0^2}{6M_\rho^2}\langle\bar{q}q\rangle\,, \tag{4.50}$$

$$X_4 = -\frac{m_0^2}{6M_\rho^2}\langle\bar{q}q\rangle\,. \tag{4.51}$$

The obtained value for X_2 is, in fact, in very good agreement with a precise lattice determination [138, 139].[13] No precise modern evaluation of m_0^2 can be found in the literature. However,

[12] Since the symmetry transformation of $Q_3^{\mu\nu}, Q_4^{\mu\nu}$ and $Q_8^{\mu\nu}$ are identical, their Lagrangians are functionally equivalent and only the low-energy couplings are different.

[13] The sign differs from the one quoted there, presumably because of a number of non-trivial convention differences. They give the VMD estimate also with the opposite sign.

once again, some numerical estimates are available [140]. The estimates of X_3 and X_4 are new to the best of our knowledge.

Notice how, once again, the mass correction to (4.46) leads to an infrared divergent term which is regularised by the mixing of the tensor current with $F_{\mu\nu}$ of (4.35),

$$\langle 0|Q^{\mu\nu}_{2,0}|\gamma(q)\rangle = iee_q\epsilon_\alpha\Pi^{\alpha\mu\nu,0}_{\rm QCD}(q) = iee_q\left(q^\mu\epsilon^\nu - q^\nu\epsilon^\mu\right)\frac{m_qN_c}{2\pi^2}\left[1+\frac{1}{2\hat\epsilon}-\frac{1}{2}\log\left(\frac{-q^2}{m_q^2}\right)-\frac{1}{2}\log m_q^2\right]$$

$$= \hat Z_{\overline{MS}}(\mu)\,\langle 0|Q^{\mu\nu}_{2,R}(\mu)|\gamma(q)\rangle = i\,e\,e_q\epsilon_\alpha\Pi^{\alpha\mu\nu}_{R,\overline{MS}}(q,\mu) - \frac{N_c\mu^{2\epsilon}m_q}{4\pi^2\hat\epsilon}ee_q(-i(q^\mu\epsilon^\nu - q^\nu\epsilon^\mu))\,, \tag{4.52}$$

with

$$\Pi_{R,\overline{MS}}(q^2,\mu) = \frac{m_qN_c}{2\pi^2}\left(1-\frac{1}{2}\log\frac{-q^2}{\mu^2}\right). \tag{4.53}$$

$Q_7^{\mu\nu}$ Our largest uncertainty comes from Q_7, where we simply perform a dimensional guess inspired in its mixing with the gluon matrix element. One has

$$|X_7| \sim \frac{1}{6}\left\langle\frac{\alpha_s}{\pi}GG\right\rangle. \tag{4.54}$$

Notice how the derivative term of this operator makes non-trivial its low-energy effective realization when trying to promote invariance under the global symmetry to a local one.

$Q_{8,1}^{\mu\nu}$ and $Q_{8,2}^{\mu\nu}$ For the four-quark operators there are only two combinations that contribute. These are

$$S^{\mu\nu}_{8,1} = -\frac{g_s^2}{2}\epsilon^{\mu\nu\lambda\sigma}\sum_{A,B}\bar q_A\gamma_\lambda\frac{\lambda_a}{2}q_Ae^3_{q_B}\bar q_B\gamma_\sigma\gamma_5\frac{\lambda_a}{2}q_B\,, \tag{4.55}$$

$$S^{\mu\nu}_{8,2} = -\frac{g_s^2}{2}\epsilon^{\mu\nu\lambda\sigma}\sum_{A,B}e^2_{q_A}\bar q_A\frac{\lambda_a}{2}\gamma_\lambda q_Ae_{q_B}\bar q_B\frac{\lambda_a}{2}\gamma_\sigma\gamma^5q_B\,. \tag{4.56}$$

These do not mix with other operators at the order we work so the $Q^{\mu\nu}_{8,i}$ are the same. Note that the two operators only differ in the way the quark charges appear.

For both operators we define a generalised magnetic susceptibility

$$\left\langle Q^{\mu\nu}_{8,i}\right\rangle = e\overline{X}_{8,i}F^{\mu\nu}\,. \tag{4.57}$$

In the massless limit we can also use

$$\left\langle Q^{\mu\nu}_{8,1}\right\rangle = eX_{8,1}F^{\mu\nu}\sum_B e_q^4\,, \tag{4.58}$$

which is a definition more similar to (4.32). This is not possible for $Q^{\mu\nu}_{8,2}$.

The operators $Q^{\mu\nu}_{8,1}$ and $Q^{\mu\nu}_{8,2}$ can be decomposed in a basis of 12 four-quark operators containing different flavour and Dirac matrices (see App. 4.1.B for details on the reduction). However, in the large-N_c limit not all of these survive. In particular, one finds that only two are non-vanishing due to the factorisation of two colour singlet currents in this limit. These are

$$\langle 0|\bar q\sigma_{\mu\nu}\lambda_8q\,\bar qq \pm \bar q\sigma_{\mu\nu}q\,\bar q\lambda_8q|\gamma(q)\rangle_{N_c\to\infty} = 3\,\langle 0|\bar q\sigma_{\mu\nu}\lambda_8q|\gamma(q)\rangle\langle\bar qq\rangle = 3\sum_i\lambda_{8,ii}X_2\langle\bar qq\rangle e_{q,i}F_{\mu\nu}\,. \tag{4.59}$$

In the first equality we have performed the sum over flavour indices for the quark condensate. In the second step we have projected out the flavour matrix λ_8 which is traced with the quark charge matrix. Here one sees why only these two matrix elements can survive. First of all, the quark charge matrix is a linear combination of λ_3 and λ_8, so the relation $\mathrm{Tr}(\lambda_a\lambda_b) = 2\,\delta_{ab}$ implies that only matrix elements with λ_3 or λ_8 are non-zero. In addition, the only non-vanishing two-quark condensates are $\langle\bar{q}q\rangle$ and the di-quark matrix element $\bar{q}\sigma_{\mu\nu}q$. To leading order in N_c, one therefore finds

$$\overline{X}_{8,1}^{N_c\to\infty} = \overline{X}_{8,2}^{N_c\to\infty} = -2\frac{\pi\alpha_s}{9}X_2\langle\bar{q}q\rangle\,. \tag{4.60}$$

Alternatively one can directly evaluate the large-N_c limit of the two matrix elements needed by using $\lambda_{a\alpha\beta}\lambda_{a\gamma\delta} = 2\delta_{\alpha\delta}\delta_{\gamma\beta}$. Then use Fierzing and the charge matrix equivalent of (4.59). The result agrees with (4.60). This way one sees also directly that $q_A = q_B$ in the non-zero part of the matrix elements at large N_c. The entire contribution to HLbL is then proportional to $\sum_A e_{q_A}^4$.

4.1.4 Calculation of the HLbL contributions

In this section we consider the analytic calculations of the various contributions in the OPE discussed above. They are the fully connected quark loop, diagram topologies with one quark line non-contracted (related to two-quark operator matrix elements), diagram topologies with two quark lines non-contracted (giving rise to four-quark operator matrix elements) as well as the gluon matrix contribution. One check we have performed on all contributions is that

$$q_{1\mu_1}\Pi^{\mu_1\mu_2\mu_3} = q_{2\mu_2}\Pi^{\mu_1\mu_2\mu_3} = q_{3\mu_3}\Pi^{\mu_1\mu_2\mu_3} = 0\,, \tag{4.61}$$

where $\Pi^{\mu_1\mu_2\mu_3}$ is defined in (4.13).

This work relied heavily on FORM [141,142]. The Feynman integral reduction for the quark loop and the gluon matrix element contributions was done with Reduze 2 [143] and Kira [144]. In the supplementary material we provide the analytic results as FORM output in the file results.txt.

4.1.4.1 The quark loop

The quark loop contribution arises from allowing for a soft emission from one hard vertex, which is equivalent to modifying a quark propagator by an external background field [117, 124], as shown explicitly in Ref. [1]. Starting from (4.13), the needed background field, $F_{\nu_4\mu_4}$, is simply obtained by Taylor expanding the photon field appearing in the Dyson series. In the static limit in the radial gauge one has

$$A^{\mu_4}(x_4) = \frac{1}{2}x^{\nu_4}F_{\nu_4\mu_4} = \lim_{q_4\to 0}\frac{i}{2}\,\partial^{\nu_4}\,e^{-iq_4x}F_{\nu_4\mu_4}\,. \tag{4.62}$$

Define the quark propagator for a quark of mass m_q as

$$S(p) = \frac{\not{p} + m_q}{p^2 - m_q^2 + i\varepsilon}\,. \tag{4.63}$$

One may then write $\Pi_F^{\mu_1\mu_2\mu_3\mu_4\nu_4}$ in a very compact way. After having contracted all the quark fields in the definition of the tensor in question one finds

$$\Pi_F^{\mu_1\mu_2\mu_3\mu_4\nu_4}(q_1,q_2) = \int \frac{d^4p}{(2\pi)^d} \\ -\frac{N_c e_q^4}{2} \lim_{q_4\to 0} \frac{\partial}{\partial q_4^{\nu_4}} \left[\sum_{\sigma(1,2,4)} \mathrm{Tr}\Big(\gamma^{\mu_3} S(p+q_1+q_2+q_4)\gamma^{\mu_4} S(p+q_1+q_2)\gamma^{\mu_1} S(p+q_2)\gamma^{\mu_2} S(p)\Big)\right], \tag{4.64}$$

where $\sigma(i,j,k)$ denotes a member of the permutation group acting on the set $\{i,j,k\} = \{(q_\ell,\mu_\ell)\}_{\ell\in\{i,j,k\}}$. In other words, $\sigma(i,j,k)$ simply states that we sum over all permutations of momentum and Lorentz index pairs. Using iteratively the relation

$$\frac{\partial}{\partial q_4^{\nu_4}} S(p+q_4) = -S(p+q_4)\gamma^{\nu_4} S(p+q_4)\,, \tag{4.65}$$

allows for a systematic computation of the quark loop. Applying the projectors given in App. 4.1.A and reducing the (ultraviolet finite) integrals, the result is left in terms of scalar tadpole, self-energy and triangle integrals. Expanding these in the masses,[14] one finds

$$\hat{\Pi}_{i,S}(Q_1^2,Q_2^2,Q_3^2) = \hat{\Pi}^0_{i,S}(Q_1^2,Q_2^2,Q_3^2) + m_q^2\,\hat{\Pi}^{m_q^2}_{i,S}(Q_1^2,Q_2^2,Q_3^2,m_q^2) + \mathcal{O}(m_q^4)\,, \tag{4.66}$$

where

$$\hat{\Pi}^0_{m,S} = \frac{N_c\, e_q^4}{\pi^2} \sum_{i,j,k,n} \left[c^{(m,n)}_{i,j,k} + f^{(m,n)}_{i,j,k} F + g^{(m,n)}_{i,j,k} \log\left(\frac{Q_2^2}{Q_3^2}\right) + h^{(m,n)}_{i,j,k} \log\left(\frac{Q_1^2}{Q_2^2}\right)\right] \lambda^{-n}\, Q_1^{2i}\, Q_2^{2j}\, Q_3^{2k}\,, \tag{4.67}$$

$$\hat{\Pi}^{m_q^2}_{m,S} = \frac{N_c\, e_q^4}{\pi^2} \sum_{i,j,k,n} \lambda^{-n}\, Q_1^{2i}\, Q_2^{2j}\, Q_3^{2k} \\ \times \left[d^{(m,n)}_{i,j,k} + p^{(m,n)}_{i,j,k} F + q^{(m,n)}_{i,j,k} \log\left(\frac{Q_2^2}{Q_3^2}\right) + r^{(m,n)}_{i,j,k} \log\left(\frac{Q_1^2}{Q_2^2}\right) + s^{(m,n)}_{i,j,k} \log\left(\frac{Q_3^2}{m_q^2}\right)\right]. \tag{4.68}$$

Here, $\lambda = \lambda(q_1^2,q_2^2,q_3^2)$ is the Källén function defined through

$$\lambda(q_1^2,q_2^2,q_3^2) = q_1^4 + q_2^4 + q_3^4 - 2q_1^2q_2^2 - 2q_1^2q_3^2 - 2q_2^2q_3^2\,, \tag{4.69}$$

and $F = F(Q_1^2,Q_2^2,Q_3^2)$ the massless triangle integral

$$F(Q_1^2,Q_2^2,Q_3^2) \equiv (4\pi)^2 i \int \frac{d^4k}{(2\pi)^4} \frac{1}{k^2(k-q_1)^2(k-q_1-q_2)^2}\,. \tag{4.70}$$

The different coefficients (c,d,f,g,h,p,q,r,s) can be found in App. 4.1.C. Explicit analytic formulas for $F(Q_1^2,Q_2^2,Q_3^2)$ in terms of Clausen, Glaisher and L functions can be found in Ref. [145]. Spurious singularities in the $\lambda\to 0$ limit cancel against the zeros of the triangle function F for the different $\hat{\Pi}_i$.

[14] Taking into account that the mass dependence goes as $\sim A + B\,m_q^2\log(m_q^2) + C\,m_q^2 + \mathcal{O}(m_q^4)$, one needs to be careful in order to obtain the correct coefficients as the naive Taylor expansion does not hold.

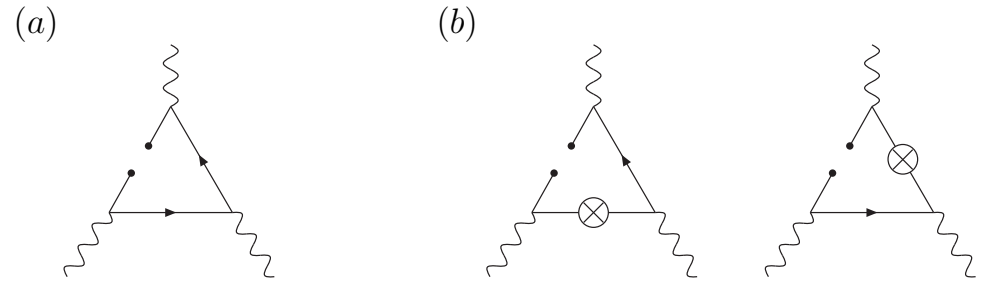

Figure 4.5: Diagrams with one cut quark line without gauge boson (a), and with gauge boson (b). The crossed vertices represent a gauge boson insertion on a propagator.

As explained above, one finds logarithmic infrared divergences for $\hat{\Pi}^{m_q^2}_{i,S}(Q_1^2,Q_2^2,Q_3^2)$. Rearranging the logarithms, they can be expressed on the form $\log\frac{Q_3^2}{m_q^2}$. Once the operator renormalisation is performed through (4.31), all the infrared divergences exactly cancel. This yields the finite result

$$\hat{\Pi}_i^{\overline{MS}}(Q_1^2,Q_2^2,Q_3^2,\mu^2)=\hat{\Pi}^0_{i,S}(Q_1^2,Q_2^2,Q_3^2)+m_q^2\,\hat{\Pi}^{m_q^2}_{i,\overline{MS}}(Q_1^2,Q_2^2,Q_3^2,\mu^2)+\mathcal{O}(m_q^4)\,. \tag{4.71}$$

As a consequence, while the massless quark loop corresponds to the leading term in the short-distance regime, the naive mass correction does not. Infrared divergent logarithms must be substracted first.

4.1.4.2 Contributions from diagrams with one cut quark line

Several kinds of contributions need to be taken into account up to the computed order from topologies in which, starting from (4.13), one quark line is left uncontracted: see Fig. 4.5. There are several expansions involved. First, the uncontracted quark fields must be Taylor expanded. Working in the radial gauge both for the gluon and for the photon, the Taylor expansion [85,124] of the quark bilinears can be written as:

$$\bar{q}_a(x_i)q_b(x_j)=\sum_{m,n}\frac{(-1)^n}{n!m!}x_{i,\mu_1}\cdots x_{i,\mu_n}\,x_{j,\nu_1}\cdots x_{j,\nu_m}\,\bar{q}_a(0)D^{\mu_1}\cdots D^{\mu_n}D^{\nu_1}\cdots D^{\nu_m}q_b(0)\,. \tag{4.72}$$

Since our computation goes up to dimension $D=6$, we need to expand up to three derivatives. A lower number of derivatives in that expansion can give contributions (apart from the di-quark magnetic susceptibility, which, as shown in Ref. [1], gives a contribution already at $D=4$ when combined with masses) when combined with mass terms from the hard propagators or from soft gluons or photons coming from hard propagators. A first simplification consists in realizing that one can put the gluons and photons together with covariant derivative terms. Extending the results of Refs. [85, 124], one finds

$$\bar{q}(x_i)\Big(B^\epsilon(u)+ie_qA^\epsilon(u)\Big)q(x_j)=\sum_{p=1}^{\infty}\frac{1}{(p-1)!(p+1)}u^{\omega_1}\cdots u^{\omega_p}\,\bar{q}(x_i)\Big[D^{\omega_1},\Big[D^{\omega_2},\ldots,[D^{\omega_p},D^\epsilon]\Big]\Big]q(x_j)\,. \tag{4.73}$$

In fact, it can be shown that for a given flavour the sum of all the contributions that enter into our computation can be reduced to a compact form. Define Γ^A to be an element in the set of

Clifford matrices according to

$$\Gamma^A \in \left\{ \mathbb{1}, \gamma^5, \gamma^\mu, \gamma^\mu\gamma_5, \sigma^{\mu\nu} \equiv \frac{i}{2}[\gamma^\mu, \gamma^\nu] \right\}. \tag{4.74}$$

The compact expression for $\Pi^{\mu_1\mu_2\mu_3}$ is then

$$\begin{aligned}\Pi^{\mu_1\mu_2\mu_3}(q_1,q_2) = -e_q^3 \lim_{q_3\to -q_1-q_2} \sum_{A,p,n,\sigma(1,2,3)} (-1)^n \langle 0|\bar{q} D_{\nu_1}\dots D_{\nu_n} c_A \Gamma^A q|\gamma(q_4)\rangle \\ \times \mathrm{Tr}\left\{\gamma^{\mu_3}\Gamma^A\gamma^{\mu_1} iS(-q_1)\gamma^{\nu_1} iS(-q_1)\dots\gamma^{\nu_p} iS(-q_1)\gamma^{\mu_2} iS(q_3)\gamma^{\nu_{p+1}} iS(q_3)\dots\gamma^{\nu_n} iS(q_3)\right\},\end{aligned} \tag{4.75}$$

where $\sigma(1,2,3)$ again denotes a pairwise permutation over q_i and μ_i. The coefficients c_A are defined as

$$c_A = \left[\mathrm{Tr}\Big(\Gamma^A\Gamma^A\Big)\right]^{-1}, \tag{4.76}$$

such that one in a standard fashion can decompose in a spinor basis according to

$$\bar{q}_i q_j = \sum_A c_A \Gamma^A_{ji}\, \bar{q}\,\Gamma^A q\,. \tag{4.77}$$

Here, all dependence on the other quantum numbers such as colour or flavour has been suppressed.

The proof of (4.75) up to the order that we need, i.e. up to $p = 3$, can be found in App. 4.1.D. Note that already for $p \le 3$ the proof involves a very large cancellation of contributions, and the compact form allows for a much simplified calculation of the diagram topologies with one cut quark line.

The reduction of the matrix elements $\langle 0|\bar{q} D_{\nu_1}\dots D_{\nu_n}\Gamma^A q|\gamma(q_4)\rangle$ into the matrix elements of Sec. 4.1.3 is rather involved. One needs to recursively exploit spinor algebra relations, symmetry transformations under Lorentz, parity and charge conjugation as well as the equations of motion of the quarks and the gluons. The resulting non-zero matrix elements are of eight types. With zero derivatives we have

$$\frac{1}{ee_q}\langle\bar{q}\sigma^{\alpha_1\alpha_2} q\rangle = X_S^2 \langle F^{\alpha_1\alpha_2}\rangle\,. \tag{4.78}$$

With one derivative one has

$$\frac{1}{ee_q}\langle\bar{q} D^{\nu_1}\gamma^{\alpha_1}\gamma_5 q\rangle = -\frac{im_q}{4} X_S^2 \epsilon^{\nu_1\alpha_1\alpha\beta}\langle F_{\alpha\beta}\rangle\,, \tag{4.79}$$

and with two they are

$$\frac{1}{ee_q}\langle\bar{q} D^{\nu_1} D^{\nu_2} q\rangle = -\frac{i}{2}\langle F^{\nu_1\nu_2}\rangle\left(X_S^5 - X_S^3\right), \tag{4.80}$$

$$\frac{1}{ee_q}\langle\bar{q} D^{\nu_1} D^{\nu_2}\gamma^5 q\rangle = -\frac{1}{4} X_S^4 \epsilon^{\nu_1\nu_2\alpha\beta}\langle F_{\alpha\beta}\rangle\,, \tag{4.81}$$

$$\frac{1}{ee_q}\langle\bar{q} D^{\nu_1} D^{\nu_2}\sigma^{\alpha_1\alpha_2} q\rangle = A_1 g^{\nu_1\nu_2}\langle F^{\alpha_1\alpha_2}\rangle + A_2\Big(g^{\nu_1\alpha_1}\langle F^{\nu_2\alpha_2}\rangle + g^{\nu_2\alpha_1}\langle F^{\nu_1\alpha_2}\rangle - g^{\nu_1\alpha_2}\langle F^{\nu_2\alpha_1}\rangle - g^{\nu_2\alpha_2}\langle F^{\nu_1\alpha_1}\rangle\Big). \tag{4.82}$$

Here, we have defined the linear combinations

$$A_1 = \frac{-\left(m_q^2 X_S^2 + X_S^4\right) + \frac{X_S^5 - X_S^3}{2}}{3}\,, \tag{4.83}$$

$$A_2 = \frac{\left(m_q^2 X_S^2 + X_S^4\right) + X_S^5 - X_S^3}{12}\,. \tag{4.84}$$

For three derivatives there are two contributions. These are

$$\begin{aligned}\frac{1}{ee_q}\langle\bar{q}D^{\nu_1}D^{\nu_2}D^{\nu_3}\gamma^{\nu_4}q\rangle &= A_3\Big(g^{\nu_1\nu_2}\langle F^{\nu_3\nu_4}\rangle - g^{\nu_2\nu_3}\langle F^{\nu_1\nu_4}\rangle\Big)\\ &\quad + A_4\Big(g^{\nu_1\nu_4}\langle F^{\nu_2\nu_3}\rangle + g^{\nu_3\nu_4}\langle F^{\nu_1\nu_2}\rangle\Big)\\ &\quad + A_5\, g^{\nu_2\nu_4}\langle F^{\nu_1\nu_3}\rangle\,, \end{aligned}\tag{4.85}$$

$$\begin{aligned}\frac{1}{ee_q}\langle\bar{q}D^{\nu_1}D^{\nu_2}D^{\nu_3}\gamma^{\nu_4}\gamma_5 q\rangle &= A_6\, g^{\nu_1\nu_3}\langle\bar{F}^{\nu_2\nu_4}\rangle\\ &\quad + A_7\Big(g^{\nu_1\nu_2}\langle\bar{F}^{\nu_3\nu_4}\rangle + g^{\nu_2\nu_3}\langle\bar{F}^{\nu_1\nu_4}\rangle\Big)\\ &\quad + A_8\Big(g^{\nu_1\nu_4}\langle\bar{F}^{\nu_2\nu_3}\rangle - g^{\nu_3\nu_4}\langle\bar{F}^{\nu_1\nu_2}\rangle\Big)\,. \end{aligned}\tag{4.86}$$

Here, $\bar{F}^{\mu\nu} \equiv \frac{i}{2}\epsilon^{\mu\nu\alpha\beta}F^{\alpha\beta}$ and the A_i are given by

$$A_3 = \frac{1}{24}\Big(-5X_S^{8,1} + 2X_S^7 - 5m_q X_S^4 + 2m_q X_S^3\Big)\,, \tag{4.87}$$

$$A_4 = \frac{1}{24}\Big(-X_S^{8,1} + X_S^7 - 3m_q X_S^5 - m_q X_S^4 + 4m_q X_S^3\Big)\,, \tag{4.88}$$

$$A_5 = \frac{1}{24}\Big(-2X_S^{8,1} - X_S^7 - 3m_q X_S^5 - 2m_q X_S^4 + 2m_q X_S^3\Big)\,, \tag{4.89}$$

$$A_6 = \frac{1}{24}\Big(-6X_S^{8,1} + X_S^7 - m_q X_S^5 - 2m_q X_S^4 + 2m_q X_S^3 + 2m_q^3 X_S^2\Big)\,, \tag{4.90}$$

$$A_7 = \frac{1}{24}\Big(-X_S^{8,1} + X_S^7 - m_q X_S^5 + m_q X_S^4 + 2m_q X_S^3 + 2m_q^3 X_S^2\Big)\,, \tag{4.91}$$

$$A_8 = \frac{1}{24}\Big(X_S^{8,1} + 3m_q X_S^4\Big)\,. \tag{4.92}$$

The operator

$$S_{q8,1}^{\mu\nu} \equiv -\frac{g_s^2}{2}\epsilon^{\mu\nu\lambda\sigma}\sum_A \bar{q}_A\gamma_\lambda\frac{\lambda_a}{2}q_A\bar{q}\gamma_\sigma\gamma_5\frac{\lambda_a}{2}q \tag{4.93}$$

enters from using the gluon equation of motion. Its susceptibility is defined as

$$\langle S_{q8,1}^{\mu\nu}\rangle = e_q X_S^{8,1}\langle F^{\mu\nu}\rangle\,. \tag{4.94}$$

Using the above decompositions in (4.75) and rewriting the $S_i^{\mu\nu}$ into the $Q_i^{\mu\nu}$ and replacing the X_S^i with the corresponding X_i, one finds

$$\hat{\Pi}_m = e_q^4 \sum_{i,j,k,n,p} c_{i,j,k}^{m,n,p}\, m_q^n\, X_p\, Q_1^{-2i}Q_2^{-2j}Q_3^{-2k}\,. \tag{4.95}$$

The numerical coefficients $c_{i,j,k}^{m,n,p}$ can be found in App. 4.1.C.

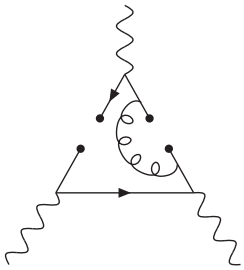

Figure 4.6: Contributions from four-quark operators obtained cutting two quark lines. All possible ways to connect the gluon to the quark lines must be considered.

4.1.4.3 Contributions from four-quark operators

The four-quark operator contributions arise from cutting two quark lines.[15] The resulting diagrams become split in two parts and, as a consequence, introduce flavour mixing. An extra gluon propagator needs to be included from the Dyson series expansion to connect the quark lines. The resulting contribution, up to permutations of $\sigma(1,2,3)$, is shown in Fig. 4.6 where the gluon can be connected in three different positions in the quark line above and in two different positions in the one below. These diagram contributions can be compactly written as

$$\begin{aligned}\Pi^{\mu_1\mu_2\mu_3}(q_1,q_2) = &-\frac{1}{16}\sum_{A,B}\left\langle e_{q_A}^2\,\bar{q}_A\frac{\lambda_a}{2}\Gamma^{\omega_1 P}q_A\,e_{q_B}\bar{q}_B\frac{\lambda_a}{2}\Gamma^{\omega_2 Q}q_B\right\rangle\\ &\times\lim_{q_3\to -q_1-q_2}\sum_{\sigma(1,2,3)}\frac{1}{q_3^2}\mathrm{Tr}\left[\Gamma_{Q\omega_2}\left(\gamma^{\mu_3}S(-q_3)\gamma^{\epsilon}+\gamma^{\epsilon}S(q_3)\gamma^{\mu_3}\right)\right]\\ &\times\mathrm{Tr}\left[-\Gamma_{P,\omega_1}\left(\gamma^{\mu_1}S(-q_1)\gamma^{\mu_2}S(q_3)\gamma^{\epsilon}+\gamma^{\epsilon}S(-q_3)\gamma^{\mu_1}S(q_2)\gamma^{\mu_2}+\gamma^{\mu_1}S(-q_1)\gamma^{\epsilon}S(q_2)\gamma^{\mu_2}\right)\right],\end{aligned} \tag{4.96}$$

where $\Gamma^{\omega P}\in\{\gamma^{\omega},\gamma^{\omega}\gamma_5\}$ and $\Gamma^{\omega}_{P}\in\{\gamma^{\omega},-\gamma^{\omega}\gamma_5\}$. In fact charge conjugation requires that A and B must be different to get a non-zero matrix element and one of the remaining two possible contributions vanishes when taking the traces. Recalling the definition of $\overline{X}_{8,2}$ in (4.57) we find

$$\hat{\Pi}_1=\hat{\Pi}_4=8\overline{X}_{8,2}\frac{Q_1^2+Q_2^2}{Q_1^4Q_2^4Q_3^2}\,, \tag{4.97}$$

$$\hat{\Pi}_{54}=8\overline{X}_{8,2}\frac{Q_2^4-Q_1^4}{Q_1^6Q_2^6Q_3^2}\,, \tag{4.98}$$

$$\hat{\Pi}_7=\hat{\Pi}_{17}=\hat{\Pi}_{39}=0\,. \tag{4.99}$$

A reduction of all possible four-quark matrix elements into a basis of 12 independent ones is given in App. 4.1.B for the chiral limit, i.e. $m_u=m_d=m_s=0$.

4.1.4.4 The gluon matrix element

The gluon matrix element contribution arises from all the possible combinations in which, starting from (4.13), one extra QED and two extra QCD vertices are added (see Fig. 4.7). The gauge

[15] Afterwards one needs to add the one coming from the one cut line and the gluon equation of motion.

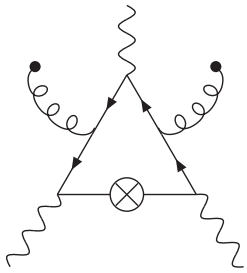

Figure 4.7: An example of a topology of the gluon matrix element contributions.

boson fields $F_{\mu\nu}$, $G^a_{\mu\nu}$ and $G^b_{\mu\nu}$ are then Taylor expanded according to (4.62). Since all the quark fields are connected, the colour chain always leads to the same colour trace, namely

$$\mathrm{Tr}\left(\frac{\lambda^a}{2}\frac{\lambda^b}{2}\right) = \frac{\delta^{ab}}{2}\,. \tag{4.100}$$

Once the colour and the space-time terms from the Taylor expansions have been factored out, the remaining six-point function is fully symmetric under the exchange of indices. Taking advantage of this symmetry, one can rewrite the whole contribution as a sum of permutations according to

$$\begin{aligned}\Pi^{\mu_1\mu_2\mu_3}_{GG}(q_1,q_2) = e_q^4 F_{\nu_4\mu_4}\frac{4\pi^2\langle\alpha_s G^{\mu\nu}_a G^a_{\mu\nu}\rangle}{32d(d-1)}\left(g_{\nu_5\nu_6}g_{\mu_5\mu_6} - g_{\mu_5\nu_6}g_{\nu_5\mu_6}\right)\left(\prod_{i=4}^{6}\lim_{q_i\to 0}\frac{\partial}{\partial q_i^{\nu_i}}\right)\int\frac{d^4p}{(2\pi)^d}\\ \times\sum_{\sigma(1,2,4,5,6)}\mathrm{Tr}\Big(\gamma^{\mu_3}S(p+q_1+q_2+q_4+q_5+q_6)\gamma^{\mu_1}S(p+q_2+q_4+q_5+q_6)\\ \times\gamma^{\mu_2}S(p+q_4+q_5+q_6)\gamma^{\mu_4}S(p+q_5+q_6)\gamma^{\mu_5}S(p+q_6)\gamma^{\mu_6}S(p)\Big)\,.\end{aligned} \tag{4.101}$$

Here, $\sigma(1,2,4,5,6)$ is the set of pairwise permutations of μ_i and q_i for $i = 1, 2, 3, 5, 6$. Also, the equation has been written in terms of $d = 4 - 2\epsilon$ for renormalisation purposes. Using (4.64) iteratively in the above equation, then taking the momentum limits, calculating the Dirac trace and projecting the results into the $\hat{\Pi}_i$, one finds the results in terms of ultraviolet finite integrals. We do this by reducing the loop integrals to combinations of triangle, self-energy and tadpole integrals with the help of the package `KIRA`, all the time carefully performing both the expansions in ϵ and in the quark masses. Without including operator mixing the result takes the form

$$\hat{\Pi}_{GGm,S} = X_{6,S}\, e_q^4 \sum_{i,j,k}\left[c^{(m)}_{i,j,k} + f^{(m)}_{i,j,k}\, m_q^{-2} + g^{(m)}_{i,j,k}\log\left(\frac{Q_1^2}{Q_2^2}\right) + h^{(m)}_{i,j,k}\log\left(\frac{Q_3^2}{m_q^2}\right)\right] Q_1^{-2i}\, Q_2^{-2j}\, Q_3^{-2k}\,, \tag{4.102}$$

where c, f, g and h are numerical coefficients given in App. 4.1.C.

When operator mixing is taken into account, the found divergences, which scale as $\frac{1}{m_q^2}$ and $\log\frac{Q^2}{m_q^2}$, exactly cancel respectively with the X_1 and X_7 contributions. The dependence on the triangle integral also cancels, leading to a fully analytic gluon matrix element contribution. One should note that the final expressions for this contribution are very simple, even compared to the quark loop, and there are substantial cancellations along the way that lead to this simple form.

4.1.5 Numerical results

In this section we present numerical results for the full $a_\mu^{\rm HLbL}$ integral in (4.10). Using the relations in (4.11) between the set of functions $\bar{\Pi}_i$ and the $\hat{\Pi}_i$ given in the appendices as well as Sec. 4.1.4.3, we evaluate $a_\mu^{\rm HLbL}$ for the matrix element as well as loop contributions. We use the matrix elements as estimated in Sec. 4.1.3.3. For this purpose, we use the CUBA library [146], in particular the `Vegas` integrator building on Monte Carlo sampling the three-dimensional integral. The results have been checked as well with an adaptive deterministic integrator implemented by us. Care has to be taken in the numerics since λ can vanish or get very small and appears with rather high negative powers in some expressions. Those areas in the integration have to be treated by expanding the loop functions around the $\lambda = 0$ points analytically, some of these limits are given explicitly in App. 4.1.C.2.

We investigate the various contributions first at two benchmark values of the lower momentum cut-off, i.e. $Q_{1,2,3} > Q_{\rm min} \in \{1, 2\}$ GeV. Then we proceed to investigate how the different pieces scale with $Q_{\rm min}$ and compare the respective sizes. For notational convenience, we refer to the contributions with respect to the corresponding X_i.

At the sought precision level it is sufficient to assess the order of magnitude of these corrections. Therefore, in want of precise input we resort to simplified input as discussed in the previous section. For this purpose, we use

$$m_u = m_d = 5\,\text{MeV}\,, \qquad m_s = 100\,\text{MeV}\,, \qquad \mu = Q_{\rm min}\,, \qquad \alpha_s = 0.33\,. \tag{4.103}$$

Given the smallness of the matrix element and quark mass correction contributions we did not take into account the running with μ of the various inputs but kept them fixed. The benchmark points for $Q_{\rm min} \in \{1, 2\}$ GeV are presented in Table 4.1. Since the contributions from the matrix element X_2 come in both suppressed at order m_q and at order m_q^3, we here present the respective contributions, labelled $X_{2,m}$ and X_{2,m^3}, of these. The table shows that power correction are suppressed by at least two orders of magnitude with respect to the quark loop. This is also visible in Figs. 4.8–4.10 where we consider the scaling with $Q_{\rm min}$. The $T_i\,(Q_1, Q_2, \tau)$ in (4.10), when expanded for large Q_i, are of order m_μ^2, except for T_1 which is m_μ^4. The variation with $Q_{\rm min}$ from dimensions is thus $1/Q_{\rm min}^2$ for the massless quark loop, $1/Q_{\rm min}^4$ for the $d = 4$ contributions and $1/Q_{\rm min}^6$ for the $d = 6$ contributions. The scaling is found to agree with naive dimensional counting.

The power corrections not suppressed by quark masses, i.e. X_6, X_7, $X_{8,1}$ and $X_{8,2}$, are found to be numerically suppressed. This is partially explained by their extra suppression in powers of $\Lambda_{\rm QCD}$. Their numerical impact is similar to the one of the di-quark magnetic susceptibility, X_2, and clearly more important than the perturbative mass contributions. We find that even at 1 GeV, all these power corrections are suppressed by at least two orders of magnitude with respect to the massless quark loop. Even though this result motivates studying whether the smallness of the corrections pinpoint a trend also for the purely perturbative ones, no strong conclusions should be derived from it.

Contribution	Inputs (GeV units)	$Q_{\min} = 1\,\text{GeV}$	$Q_{\min} = 2\,\text{GeV}$
$X_{1,0}$		$1.73 \cdot 10^{-10}$	$4.35 \cdot 10^{-11}$
X_{1,m^2}		$-5.7 \cdot 10^{-14}$	$-3.6 \cdot 10^{-15}$
$X_{2,m}$	$X_2 = -4 \cdot 10^{-2}$	$-1.2 \cdot 10^{-12}$	$-7.3 \cdot 10^{-14}$
X_{2,m^3}	$X_2 = -4 \cdot 10^{-2}$	$6.4 \cdot 10^{-15}$	$1.0 \cdot 10^{-16}$
X_3	$X_3 = 3.51 \cdot 10^{-3}$	$-3.0 \cdot 10^{-14}$	$-4.7 \cdot 10^{-16}$
X_4	$X_4 = 3.51 \cdot 10^{-3}$	$3.3 \cdot 10^{-14}$	$5.3 \cdot 10^{-16}$
X_5	$X_5 = -1.56 \cdot 10^{-2}$	$-1.8 \cdot 10^{-13}$	$-2.8 \cdot 10^{-15}$
X_6	$X_6 = 2 \cdot 10^{-2}$	$1.3 \cdot 10^{-13}$	$2.0 \cdot 10^{-15}$
X_7	$X_7 = 3.33 \cdot 10^{-3}$	$9.2 \cdot 10^{-13}$	$1.5 \cdot 10^{-14}$
$X_{8,1}$	$\overline{X}_{8,1} = -1.44 \cdot 10^{-4}$	$3.0 \cdot 10^{-13}$	$4.7 \cdot 10^{-15}$
$X_{8,2}$	$\overline{X}_{8,2} = -1.44 \cdot 10^{-4}$	$-1.3 \cdot 10^{-13}$	$-2.0 \cdot 10^{-15}$

Table 4.1: Numerical results for a_μ^{HLbL} for the indicated inputs.

4.1.6 Conclusions and prospects

The leading asymptotic behaviour of the HLbL for the $(g-2)_\mu$ kinematics has been confirmed to be given by the massless quark loop contribution. Although this had been commonly assumed previously, this is by no means obvious due to the static limit associated to the $(g-2)_\mu$ definition with the external photon leg at zero momentum. The main result of this work and of Ref. [1] is to show how a proper short-distance expansion can be done in the limit of $Q_1^2 \sim Q_2^2 \sim Q_3^2 \gg \Lambda_{QCD}^2$.

In order to show that the quark loop is the first order of a well-defined expansion, the soft photon has been formulated as a long-distance, or, background, degree of freedom, following previous works of Refs. [117, 118]. We stress that using the vacuum OPE valid for HLbL when all the four Euclidean momenta are large, one would for the $(g-2)_\mu$ kinematics have obtained a divergent expansion [1].

A comprehensive description of the resulting OPE has been provided, including a detailed explanation on how to achieve a complete and systematic separation of short and long distance effects while cancelling internal divergences. The physical meaning of some of the resulting matrix elements is also given, and we have used those to present estimates of all of them. The obtained results could in the future be used to analyse other Green functions and their phenomenological applications.

The resulting OPE is applied to the HLbL in the $(g-2)_\mu$ kinematics for $Q_1, Q_2, Q_3 \gg \Lambda_{\text{QCD}}$. As a consequence of setting one of the momenta to zero, the long distance effects become functionally more important. The quark loop is still found to be the dominant contribution, but the first non-perturbative correction becomes suppressed by just one power of Λ_{QCD} (plus one power of m_q), in contrast with the Λ_{QCD}^3 $(\bar{q}q)$ suppression in the OPE applicable when all the Euclidean momenta are large.

However, no operators allowed by the symmetries are found to enter without quark mass suppression below Λ_{QCD}^4 with respect to the quark loop contribution. These Λ_{QCD}^4 contributions are computed and their role for the $(g-2)_\mu$ is estimated. They are found to be very small.

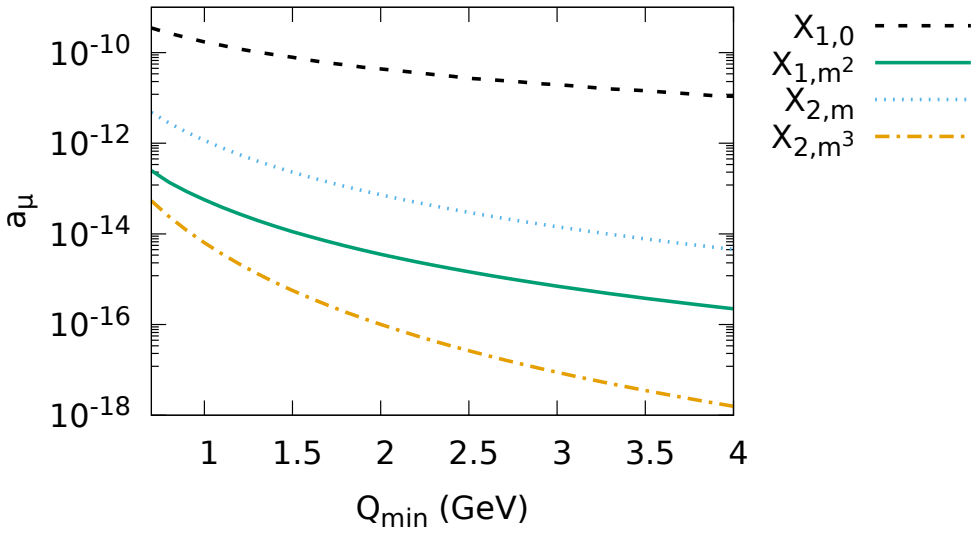

Figure 4.8: Numerical contributions from the X_1 and X_2 pieces in absolute value using the inputs from Table 4.1. As expected, the quark loop fully dominates.

Whether or not this may be indicating that the quark loop gives a precise description of the HLbL at relatively low momenta (i.e. $Q_i \sim 1\,\text{GeV}$) will only be known once the two-loop perturbative corrections have been computed. This calculation is already under way and will be presented in a future publication.

Acknowledgments

N. H.–T. and L.L. are funded by the Albert Einstein Center for Fundamental Physics at Universität Bern and the Swiss National Science Foundation respectively. J. B. and A. R.–S. are supported in part by the Swedish Research Council grants contract numbers 2016-05996 and 2019-03779, and by the European Research Council (ERC) under the European Union's Horizon 2020 research and innovation programme under grant agreement No 668679.

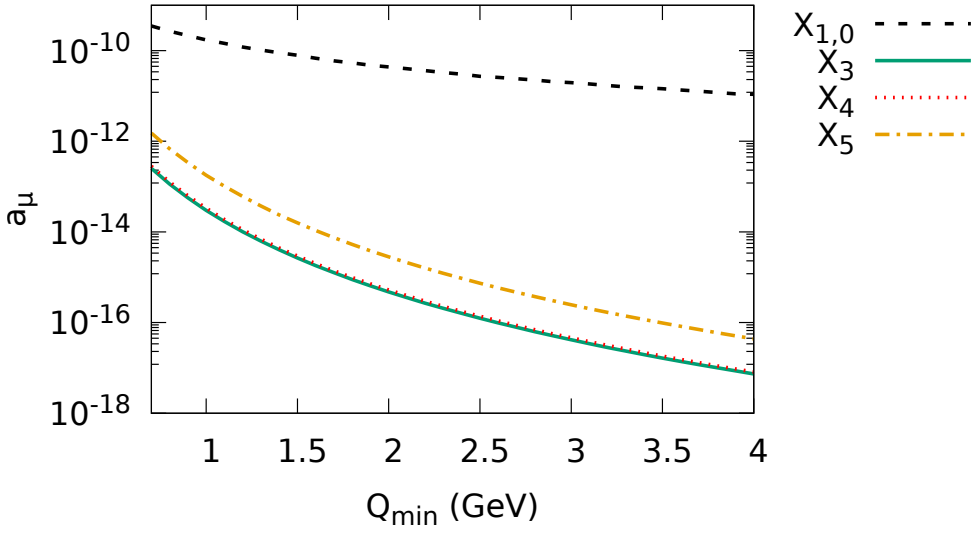

Figure 4.9: Numerical contributions from the X_{3-5} pieces in absolute value using the inputs from Table 4.1. The massless quark loop is shown for comparison.

4.1.A A set of Lorentz projectors for the $\hat{\Pi}_i$

In this appendix we present a set of projectors useful for projecting to the set of $\hat{\Pi}_i$. Note that due to gauge invariance this set is not unique. We have derived and used a second set of projectors. Obtaining the same results with both projectors is one of the checks we did. Below we only present one of the sets of projectors.

$$\begin{aligned} P^{\mu\nu\lambda\rho\sigma}_{\hat{\Pi}_1}(q_1,q_2,q_3) = &-8\lambda^{-2}q_1^\nu q_1^\sigma q_2^\lambda q_2^\rho q_3^\mu + 2\lambda^{-1}g^{\mu\sigma}g^{\nu\rho}q_2^\lambda \\ &-8\lambda^{-2}q_2^2 g^{\mu\sigma}q_1^\nu q_2^\lambda q_3^\rho - 4\lambda^{-2}\left(q_3^2+q_2^2-q_1^2\right)g^{\mu\sigma}q_1^\lambda q_2^\rho q_3^\nu \\ &-8\lambda^{-2}q_1^2 g^{\nu\sigma}q_1^\lambda q_2^\mu q_3^\rho - 4\lambda^{-2}\left(q_3^2-q_2^2+q_1^2\right)g^{\nu\sigma}q_1^\rho q_2^\lambda q_3^\mu\,, \end{aligned} \tag{4.104}$$

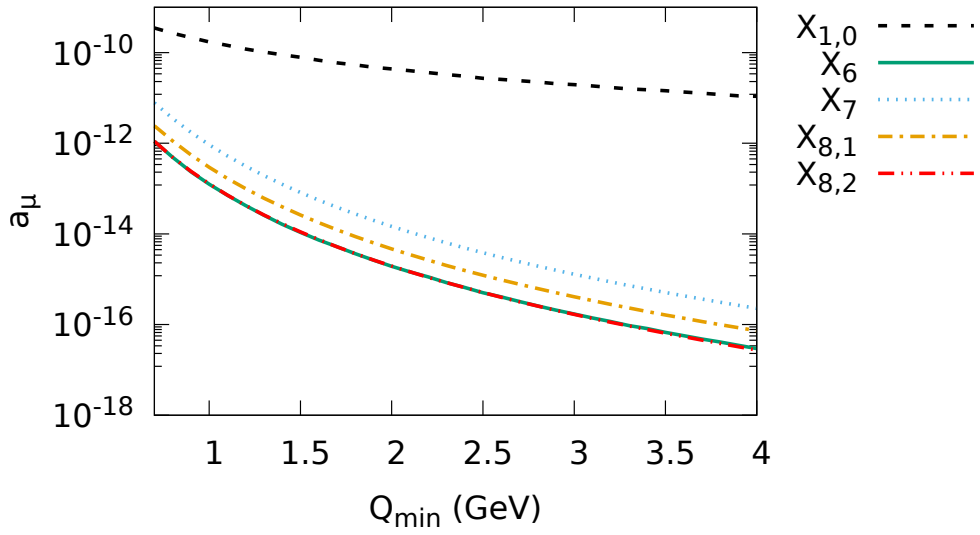

Figure 4.10: Numerical contributions from the X_{6-8} pieces in absolute value using the inputs from Table 4.1. Even when they are not suppressed by the quark mass size, they are found to be small compared with the massless quark loop contribution.

$$
\begin{aligned}
P^{\mu\nu\lambda\rho\sigma}_{\hat{\Pi}_4}(q_1,q_2,q_3) = {} & 8\lambda^{-4}\left(6q_3^8+11q_2^2q_3^6-29q_2^4q_3^4+q_2^6q_3^2+11q_2^8+11q_1^2q_3^6+14q_1^2q_2^2q_3^4\right.\\
& \left.-q_1^2q_2^4q_3^2-44q_1^2q_2^6-29q_1^4q_3^4-q_1^4q_2^2q_3^2+66q_1^4q_2^4+q_1^6q_3^2-44q_1^6q_2^2+11q_1^8\right)q_1^\nu q_1^\sigma q_2^\lambda q_2^\rho q_3^\mu\\
& +\lambda^{-2}\left(q_3^4-6q_2^2q_3^2-q_2^4+2q_1^2q_2^2-q_1^4\right)g^{\mu\nu}g^{\lambda\sigma}q_1^\rho+\lambda^{-2}\left(q_3^4-q_2^4-6q_1^2q_3^2+2q_1^2q_2^2-q_1^4\right)g^{\mu\nu}g^{\lambda\sigma}q_2^\rho\\
& -4\lambda^{-3}\left(q_3^6+3q_2^2q_3^4-4q_2^4q_3^2+3q_1^2q_3^4+8q_1^2q_2^2q_3^2-4q_1^4q_3^2\right)g^{\mu\nu}q_1^\lambda q_1^\sigma q_2^\rho\\
& +2\lambda^{-2}\left(q_2^2q_3^2-q_1^2q_3^2\right)g^{\mu\lambda}g^{\nu\sigma}q_1^\rho+\lambda^{-2}\left(q_3^4-q_2^4-2q_1^2q_3^2+2q_1^2q_2^2-q_1^4\right)g^{\mu\lambda}g^{\nu\sigma}q_3^\rho\\
& +2\lambda^{-3}\left(3q_3^6+q_2^2q_3^4-q_2^4q_3^2-3q_2^6-3q_1^2q_3^4+4q_1^2q_2^2q_3^2+9q_1^2q_2^4-3q_1^4q_3^2-9q_1^4q_2^2+3q_1^6\right)g^{\mu\lambda}q_1^\rho q_3^\nu q_3^\sigma\\
& +2\lambda^{-2}\left(q_3^4-4q_2^2q_3^2-q_2^4+2q_1^2q_2^2-q_1^4\right)g^{\mu\rho}g^{\lambda\sigma}q_1^\nu\\
& -2\lambda^{-2}\left(q_2^2q_3^2-q_1^2q_3^2\right)g^{\mu\sigma}g^{\nu\lambda}q_2^\rho+\lambda^{-2}\left(q_3^4-2q_2^2q_3^2-q_2^4+2q_1^2q_2^2-q_1^4\right)g^{\mu\sigma}g^{\nu\lambda}q_3^\rho\\
& -10\lambda^{-3}\left(q_3^6-q_2^2q_3^4-3q_2^4q_3^2-q_2^6-q_1^2q_3^4+4q_1^2q_2^2q_3^2+3q_1^2q_2^4-q_1^4q_3^2-3q_1^4q_2^2+q_1^6\right)g^{\mu\sigma}q_1^\nu q_2^\lambda q_3^\rho\\
& -4\lambda^{-3}\left(2q_3^6-9q_2^2q_3^4-3q_2^4q_3^2+q_1^2q_3^4+6q_1^2q_2^2q_3^2-3q_1^4q_2^2\right)g^{\mu\sigma}q_1^\lambda q_2^\rho q_3^\nu\\
& +2\lambda^{-3}\left(3q_3^6-3q_2^2q_3^4-3q_2^4q_3^2+3q_2^6+q_1^2q_3^4+4q_1^2q_2^2q_3^2-9q_1^2q_2^4-q_1^4q_3^2+9q_1^4q_2^2-3q_1^6\right)g^{\nu\lambda}q_2^\mu q_2^\sigma q_3^\rho\\
& +2\lambda^{-2}\left(q_3^4-q_2^4-4q_1^2q_3^2+2q_1^2q_2^2-q_1^4\right)g^{\nu\sigma}g^{\lambda\rho}q_3^\mu\\
& -10\lambda^{-3}\left(q_3^6-q_2^2q_3^4-q_2^4q_3^2+q_2^6-q_1^2q_3^4+4q_1^2q_2^2q_3^2-3q_1^2q_2^4-3q_1^4q_3^2+3q_1^4q_2^2-q_1^6\right)g^{\nu\sigma}q_1^\lambda q_2^\mu q_3^\rho\\
& -4\lambda^{-3}\left(2q_3^6+q_2^2q_3^4-3q_2^4q_3^2-9q_1^2q_3^4+6q_1^2q_2^2q_3^2-3q_1^4q_2^2\right)g^{\nu\sigma}q_1^\rho q_2^\lambda q_3^\mu\\
& +\lambda^{-3}\left(6q_3^6-6q_2^2q_3^4-6q_2^4q_3^2+6q_2^6-50q_1^2q_3^4+72q_1^2q_2^2q_3^2+10q_1^2q_2^4+22q_1^4q_3^2\right.\\
& \left.-38q_1^4q_2^2+22q_1^6\right)g^{\lambda\sigma}q_1^\nu q_2^\rho q_3^\mu \qquad +\lambda^{-3}\left(6q_3^6-50q_2^2q_3^4+22q_2^4q_3^2+22q_2^6-6q_1^2q_3^4\right.\\
& \left.+72q_1^2q_2^2q_3^2-38q_1^2q_2^4-6q_1^4q_3^2+10q_1^4q_2^2+6q_1^6\right)g^{\lambda\sigma}q_1^\rho q_2^\mu q_3^\nu\,, \qquad (4.105)
\end{aligned}
$$

$$
\begin{aligned}
&P^{\mu\nu\lambda\rho\sigma}_{\hat{\Pi}_7}(q_1,q_2,q_3) = 80\lambda^{-4}\left(-2q_3^6 - q_2^2q_3^4 + q_2^4q_3^2 + 2q_2^6 + 2q_1^2q_3^4 - 3q_1^2q_2^2q_3^2 - 6q_1^2q_2^4 + 2q_1^4q_3^2\right.\\
&\left.+6q_1^4q_2^2 - 2q_1^6\right) q_1^\nu q_1^\sigma q_2^\lambda q_2^\rho q_3^\mu - 2\lambda^{-2}\left(q_3^2 + q_2^2 - q_1^2\right) g^{\mu\nu}g^{\lambda\sigma}q_1^\rho + 2\lambda^{-2}\left(2q_3^2 - q_2^2 + q_1^2\right) g^{\mu\nu}g^{\lambda\sigma}q_2^\rho\\
&+ 20\lambda^{-3}\left(q_3^4 + q_2^2q_3^2 - q_1^2q_3^2\right) g^{\mu\nu}q_1^\lambda q_1^\sigma q_2^\rho + 2\lambda^{-2}q_3^2 g^{\mu\lambda}g^{\nu\sigma}q_1^\rho\\
&- 2\lambda^{-2}\left(q_2^2 - q_1^2\right) g^{\mu\lambda}g^{\nu\sigma}q_3^\rho - 4\lambda^{-3}\left(3q_3^4 + 4q_2^2q_3^2 + 3q_2^4 - 6q_1^2q_3^2 - 6q_1^2q_2^2 + 3q_1^4\right) g^{\mu\lambda}q_1^\rho q_3^\nu q_3^\sigma\\
&- 4\lambda^{-2}\left(q_3^2 + q_2^2 - q_1^2\right) g^{\mu\rho}g^{\lambda\sigma}q_1^\nu - 2\lambda^{-2}q_3^2 g^{\mu\sigma}g^{\nu\lambda}q_2^\rho - 2\lambda^{-2}\left(q_3^2 + q_2^2 - q_1^2\right) g^{\mu\sigma}g^{\nu\lambda}q_3^\rho\\
&+ 20\lambda^{-3}\left(q_3^4 + 2q_2^2q_3^2 + q_2^4 - 2q_1^2q_3^2 - 2q_1^2q_2^2 + q_1^4\right) g^{\mu\sigma}q_1^\nu q_2^\lambda q_3^\rho + 20\lambda^{-3}\left(q_3^4 + q_2^2q_3^2 - q_1^2q_3^2\right) g^{\mu\sigma}q_1^\lambda q_2^\rho q_3^\nu\\
&- 4\lambda^{-3}\left(2q_3^4 + q_2^2q_3^2 - 3q_2^4 + q_1^2q_3^2 + 6q_1^2q_2^2 - 3q_1^4\right) g^{\nu\lambda}q_2^\mu q_2^\sigma q_3^\rho + 4\lambda^{-2}\left(q_3^2 - q_2^2 + q_1^2\right) g^{\nu\sigma}g^{\lambda\rho}q_3^\mu\\
&+ 20\lambda^{-3}\left(q_2^2q_3^2 - q_2^4 - q_1^2q_3^2 + 2q_1^2q_2^2 - q_1^4\right) g^{\nu\sigma}q_1^\lambda q_2^\mu q_3^\rho - 20\lambda^{-3}\left(q_3^4 - q_2^2q_3^2 + q_1^2q_3^2\right) g^{\nu\sigma}q_1^\rho q_2^\lambda q_3^\mu\\
&+ 4\lambda^{-3}\left(6q_3^4 - 7q_2^2q_3^2 + q_2^4 + 3q_1^2q_3^2 + 8q_1^2q_2^2 - 9q_1^4\right) g^{\lambda\sigma}q_1^\nu q_2^\rho q_3^\mu\\
&- 4\lambda^{-3}\left(3q_3^4 + 4q_2^2q_3^2 - 7q_2^4 - 6q_1^2q_3^2 + 4q_1^2q_2^2 + 3q_1^4\right) g^{\lambda\sigma}q_1^\rho q_2^\mu q_3^\nu\,, \qquad (4.106)
\end{aligned}
$$

$$
\begin{aligned}
&P^{\mu\nu\lambda\rho\sigma}_{\hat{\Pi}_{17}}(q_1,q_2,q_3) = 80\lambda^{-3}\left(q_3^2 - q_2^2 - q_1^2\right) q_1^\nu q_1^\sigma q_2^\lambda q_2^\rho q_3^\mu - 2\lambda^{-2}\left(q_3^2 - 3q_2^2 - q_1^2\right) g^{\mu\nu}g^{\lambda\sigma}q_1^\rho\\
&- 2\lambda^{-2}\left(q_3^2 - q_2^2 - 3q_1^2\right) g^{\mu\nu}g^{\lambda\sigma}q_2^\rho - 8\lambda^{-2}g^{\mu\nu}q_1^\lambda q_1^\sigma q_2^\rho\\
&- 2\lambda^{-2}\left(q_3^2 + q_2^2 - q_1^2\right) g^{\mu\lambda}g^{\nu\sigma}q_1^\rho - 2\lambda^{-2}\left(q_3^2 - q_2^2 - q_1^2\right) g^{\mu\lambda}g^{\nu\sigma}q_3^\rho\\
&- 4\lambda^{-2}\left(q_3^2 - 2q_2^2 - q_1^2\right) g^{\mu\rho}g^{\lambda\sigma}q_1^\nu - 2\lambda^{-2}\left(q_3^2 - q_2^2 + q_1^2\right) g^{\mu\sigma}g^{\nu\lambda}q_2^\rho\\
&- 2\lambda^{-2}\left(q_3^2 - q_2^2 - q_1^2\right) g^{\mu\sigma}g^{\nu\lambda}q_3^\rho - 4\lambda^{-2}q_3^2 g^{\mu\sigma}g^{\nu\rho}q_2^\lambda\\
&+ 8\lambda^{-3}\left(2q_3^4 + q_2^2q_3^2 - 3q_2^4 - 4q_1^2q_3^2 + q_1^2q_2^2 + 2q_1^4\right) g^{\mu\sigma}q_1^\nu q_2^\lambda q_3^\rho\\
&+ 8\lambda^{-3}\left(4q_3^4 - 3q_2^2q_3^2 - q_2^4 - 3q_1^2q_3^2 + 2q_1^2q_2^2 - q_1^4\right) g^{\mu\sigma}q_1^\lambda q_2^\rho q_3^\nu - 4\lambda^{-2}\left(q_3^2 - q_2^2 - 2q_1^2\right) g^{\nu\sigma}g^{\lambda\rho}q_3^\mu\\
&+ 8\lambda^{-3}\left(2q_3^4 - 4q_2^2q_3^2 + 2q_2^4 + q_1^2q_3^2 + q_1^2q_2^2 - 3q_1^4\right) g^{\nu\sigma}q_1^\lambda q_2^\mu q_3^\rho\\
&+ 8\lambda^{-3}\left(4q_3^4 - 3q_2^2q_3^2 - q_2^4 - 3q_1^2q_3^2 + 2q_1^2q_2^2 - q_1^4\right) g^{\nu\sigma}q_1^\rho q_2^\lambda q_3^\mu\\
&- 8\lambda^{-3}\left(2q_3^4 - 4q_2^2q_3^2 + 2q_2^4 - 9q_1^2q_3^2 + 11q_1^2q_2^2 + 7q_1^4\right) g^{\lambda\sigma}q_1^\nu q_2^\rho q_3^\mu\\
&- 8\lambda^{-3}\left(2q_3^4 - 9q_2^2q_3^2 + 7q_2^4 - 4q_1^2q_3^2 + 11q_1^2q_2^2 + 2q_1^4\right) g^{\lambda\sigma}q_1^\rho q_2^\mu q_3^\nu\,, \qquad (4.107)
\end{aligned}
$$

$$
\begin{aligned}
P^{\mu\nu\lambda\rho\sigma}_{\hat{\Pi}_{39}}(q_1,q_2,q_3) &= 160\lambda^{-4}\left(q_3^6-q_2^2q_3^4-q_2^4q_3^2+q_2^6-q_1^2q_3^4+q_1^2q_2^2q_3^2-q_1^2q_2^4-q_1^4q_3^2\right.\\
&\left.-q_1^4q_2^2+q_1^6\right)q_1^\nu q_1^\sigma q_2^\lambda q_2^\rho q_3^\mu-2\lambda^{-2}q_2^2g^{\mu\nu}g^{\lambda\sigma}q_1^\rho-2\lambda^{-2}q_1^2g^{\mu\nu}g^{\lambda\sigma}q_2^\rho\\
&-4\lambda^{-3}\left(2q_3^4+q_2^2q_3^2-3q_2^4+q_1^2q_3^2+6q_1^2q_2^2-3q_1^4\right)g^{\mu\nu}q_1^\lambda q_1^\sigma q_2^\rho-2\lambda^{-2}q_3^2g^{\mu\lambda}g^{\nu\sigma}q_1^\rho\\
&-2\lambda^{-2}q_1^2g^{\mu\lambda}g^{\nu\sigma}q_3^\rho+4\lambda^{-3}\left(3q_3^4-q_2^2q_3^2-2q_2^4-6q_1^2q_3^2-q_1^2q_2^2+3q_1^4\right)g^{\mu\lambda}q_1^\rho q_3^\nu q_3^\sigma\\
&-4\lambda^{-2}q_2^2g^{\mu\rho}g^{\lambda\sigma}q_1^\nu-2\lambda^{-2}q_3^2g^{\mu\sigma}g^{\nu\lambda}q_2^\rho-2\lambda^{-2}q_2^2g^{\mu\sigma}g^{\nu\lambda}q_3^\rho\\
&-4\lambda^{-2}q_3^2g^{\mu\sigma}g^{\nu\rho}q_2^\lambda-4\lambda^{-3}\left(q_3^4-7q_2^2q_3^2-4q_2^4-2q_1^2q_3^2+3q_1^2q_2^2+q_1^4\right)g^{\mu\sigma}q_1^\nu q_2^\lambda q_3^\rho\\
&+4\lambda^{-3}\left(4q_3^4+7q_2^2q_3^2-q_2^4-3q_1^2q_3^2+2q_1^2q_2^2-q_1^4\right)g^{\mu\sigma}q_1^\lambda q_2^\rho q_3^\nu\\
&+4\lambda^{-3}\left(3q_3^4-6q_2^2q_3^2+3q_2^4-q_1^2q_3^2-q_1^2q_2^2-2q_1^4\right)g^{\nu\lambda}q_2^\mu q_2^\sigma q_3^\rho-4\lambda^{-2}q_1^2g^{\nu\sigma}g^{\lambda\rho}q_3^\mu\\
&-4\lambda^{-3}\left(q_3^4-2q_2^2q_3^2+q_2^4-7q_1^2q_3^2+3q_1^2q_2^2-4q_1^4\right)g^{\nu\sigma}q_1^\lambda q_2^\mu q_3^\rho\\
&+4\lambda^{-3}\left(4q_3^4-3q_2^2q_3^2-q_2^4+7q_1^2q_3^2+2q_1^2q_2^2-q_1^4\right)g^{\nu\sigma}q_1^\rho q_2^\lambda q_3^\mu\\
&-4\lambda^{-3}\left(q_3^4-2q_2^2q_3^2+q_2^4+3q_1^2q_3^2-7q_1^2q_2^2-4q_1^4\right)g^{\lambda\sigma}q_1^\nu q_2^\rho q_3^\mu\\
&-4\lambda^{-3}\left(q_3^4+3q_2^2q_3^2-4q_2^4-2q_1^2q_3^2-7q_1^2q_2^2+q_1^4\right)g^{\lambda\sigma}q_1^\rho q_2^\mu q_3^\nu\,,
\end{aligned}
\tag{4.108}
$$

$$
\begin{aligned}
P^{\mu\nu\lambda\rho\sigma}_{\hat{\Pi}_{54}}(q_1,q_2,q_3) &= -40\lambda^{-3}\left(q_2^2-q_1^2\right)q_1^\nu q_1^\sigma q_2^\lambda q_2^\rho q_3^\mu+\lambda^{-2}\left(q_3^2+q_2^2-q_1^2\right)g^{\mu\nu}g^{\lambda\sigma}q_1^\rho\\
&-\lambda^{-2}\left(q_3^2-q_2^2+q_1^2\right)g^{\mu\nu}g^{\lambda\sigma}q_2^\rho+2\lambda^{-2}\left(q_2^2-q_1^2\right)g^{\mu\lambda}g^{\nu\sigma}q_1^\rho+\lambda^{-2}\left(q_3^2-q_2^2-3q_1^2\right)g^{\mu\lambda}g^{\nu\sigma}q_3^\rho\\
&+2\lambda^{-2}g^{\mu\lambda}q_1^\rho q_3^\nu q_3^\sigma+4\lambda^{-2}q_2^2g^{\mu\rho}g^{\lambda\sigma}q_1^\nu+2\lambda^{-2}\left(q_2^2-q_1^2\right)g^{\mu\sigma}g^{\nu\lambda}q_2^\rho\\
&-\lambda^{-2}\left(q_3^2-3q_2^2-q_1^2\right)g^{\mu\sigma}g^{\nu\lambda}q_3^\rho+4\lambda^{-2}\left(q_2^2-q_1^2\right)g^{\mu\sigma}g^{\nu\rho}q_2^\lambda\\
&+2\lambda^{-3}\left(3q_3^4-6q_2^2q_3^2-17q_2^4-6q_1^2q_3^2+14q_1^2q_2^2+3q_1^4\right)g^{\mu\sigma}q_1^\nu q_2^\lambda q_3^\rho\\
&+2\lambda^{-3}\left(2q_3^4-14q_2^2q_3^2-8q_2^4+6q_1^2q_3^2+16q_1^2q_2^2-8q_1^4\right)g^{\mu\sigma}q_1^\lambda q_2^\rho q_3^\nu-2\lambda^{-2}g^{\nu\lambda}q_2^\mu q_2^\sigma q_3^\rho\\
&-4\lambda^{-2}q_1^2g^{\nu\sigma}g^{\lambda\rho}q_3^\mu-2\lambda^{-3}\left(3q_3^4-6q_2^2q_3^2+3q_2^4-6q_1^2q_3^2+14q_1^2q_2^2-17q_1^4\right)g^{\nu\sigma}q_1^\lambda q_2^\mu q_3^\rho\\
&-2\lambda^{-3}\left(2q_3^4+6q_2^2q_3^2-8q_2^4-14q_1^2q_3^2+16q_1^2q_2^2-8q_1^4\right)g^{\nu\sigma}q_1^\rho q_2^\lambda q_3^\mu\\
&-2\lambda^{-3}\left(3q_3^4-6q_2^2q_3^2+3q_2^4+4q_1^2q_3^2+4q_1^2q_2^2-7q_1^4\right)g^{\lambda\sigma}q_1^\nu q_2^\rho q_3^\mu\\
&+2\lambda^{-3}\left(3q_3^4+4q_2^2q_3^2-7q_2^4-6q_1^2q_3^2+4q_1^2q_2^2+3q_1^4\right)g^{\lambda\sigma}q_1^\rho q_2^\mu q_3^\nu\,,
\end{aligned}
\tag{4.109}
$$

where $\lambda=\lambda(q_1^2,q_2^2,q_3^2)$ is the Källén function defined through

$$
\lambda(q_1^2,q_2^2,q_3^2)=q_1^4+q_2^4+q_3^4-2q_1^2q_2^2-2q_1^2q_3^2-2q_2^2q_3^2\,. \tag{4.110}
$$

4.1.B Four-quark reduction

In this section we reduce the number of four-quark matrix elements from the basis $\bar{q}_{iA\bar{\alpha}}q_{jB\bar{\beta}}\bar{q}_{kC\bar{\gamma}}q_{lD\bar{\delta}}$, where the barred Greek indices denote colour, the capital ones flavour and the latin ones spinor, into one with only twelve non-zero elements.

First of all, due to confinement only colour singlet operators can give contributions. From

this one has

$$\bar{q}_{iA\bar{\alpha}}q_{jB\bar{\beta}}\bar{q}_{kC\bar{\gamma}}q_{lD\bar{\delta}} = \frac{1}{N_c^2-1}\bar{q}_{i'A'}q_{j'B'}\bar{q}_{k'C'}q_{l'D'}\Big[\delta_{\bar{\alpha}\bar{\beta}}\delta_{\bar{\gamma}\bar{\delta}}\left(\delta_{iA}^{i'A'}\delta_{jB}^{j'B'}\delta_{kC}^{k'C'}\delta_{lD}^{l'D'} + \frac{1}{N_c}\delta_{iA}^{i'A'}\delta_{kC}^{k'C'}\delta_{jB}^{l'D'}\delta_{lD}^{j'B'}\right) - \delta_{\bar{\alpha}\bar{\delta}}\delta_{\bar{\beta}\bar{\gamma}}\left(\frac{1}{N_c}\delta_{iA}^{i'A'}\delta_{jB}^{j'B'}\delta_{kC}^{k'C'}\delta_{lD}^{l'D'} + \delta_{iA}^{i'A'}\delta_{kC}^{k'C'}\delta_{jB}^{l'D'}\delta_{lD}^{j'B'}\right)\Big]. \tag{4.111}$$

Next, taking into account that the QCD vacuum preserves $SU(3)_{\mathrm{V}}$ in the flavour sector up to small quark mass corrections, the contributing four-quark operators must break $SU(3)_{\mathrm{V}}$ in the same direction as the octet charge operator. There are therefore four independent flavour structures which contribute and can be taken to be

$$O_1 = Q_{AB}\delta_{CD}\bar{q}_{iA}q_{jB}\bar{q}_{kC}q_{lD}\,, \tag{4.112}$$
$$O_2 = Q_{CD}\delta_{AB}\bar{q}_{iA}q_{jB}\bar{q}_{kC}q_{lD}\,, \tag{4.113}$$
$$O_3 = Q_{AD}\delta_{BC}\bar{q}_{iA}q_{jB}\bar{q}_{kC}q_{lD}\,, \tag{4.114}$$
$$O_4 = Q_{BC}\delta_{AD}\bar{q}_{iA}q_{jB}\bar{q}_{kC}q_{lD}\,. \tag{4.115}$$

The charge operator can be expressed with Gell-Mann matrices through

$$Q = \frac{\lambda^3}{2} + \frac{\lambda^8}{2\sqrt{3}}\,, \tag{4.116}$$

and the third and fourth operators O_3 and O_4 can be rewritten using a Fierzlike identity:

$$O_{3,4} = \Bigg(\frac{\delta_{AB}}{3}Q_{CD} + Q_{AB}\frac{\delta_{CD}}{3} \pm \frac{i}{4}\left(\lambda^1_{AB}\lambda^2_{CD} - \lambda^2_{AB}\lambda^1_{CD} + \lambda^4_{AB}\lambda^5_{CD} - \lambda^5_{AB}\lambda^4_{CD}\right) + \frac{1}{12}\sum_{i=1}^{5}\lambda^i_{AB}\lambda^i_{CD} - \frac{1}{6}\sum_{i=6}^{7}\lambda^i_{AB}\lambda^i_{CD} + \frac{1}{4\sqrt{3}}\left(\lambda^3_{AB}\lambda^8_{CD} + \lambda^8_{AB}\lambda^3_{CD}\right) - \frac{1}{12}\lambda^8_{AB}\lambda^8_{CD}\Bigg)\bar{q}_{iA}q_{jB}\bar{q}_{kC}q_{lD}\,. \tag{4.117}$$

Orthogonal operators $\tilde{O}_i$ satisfying

$$\begin{aligned}&\tilde{O}_n = P^n_{ABCD}\,\bar{q}_{iA}q_{jB}\bar{q}_{kC}q_{lD}\,,\\ &\text{with } P^n_{ABCD}P^m_{BADC} = \delta^{mn}\,,\end{aligned} \tag{4.118}$$

can be obtained from linear combinations of the operators O_i $(i = 1,\ldots,4)$ as

$$\tilde{O}_1 = \frac{1}{2}\left(O_1 + O_2\right)\,, \tag{4.119}$$
$$\tilde{O}_2 = \frac{1}{2}\left(O_1 - O_2\right)\,, \tag{4.120}$$
$$\tilde{O}_3 = \frac{-i}{2}\left(O_3 - O_4\right) = \frac{1}{4}\left(\lambda^1_{AB}\lambda^2_{CD} - \lambda^2_{AB}\lambda^1_{CD} + \lambda^4_{AB}\lambda^5_{CD} - \lambda^5_{AB}\lambda^4_{CD}\right)\bar{q}_{iA}q_{jB}\bar{q}_{kC}q_{lD}\,, \tag{4.121}$$
$$\tilde{O}_4 = \frac{3}{2\sqrt{5}}\left(O_3 + O_4 - \frac{2}{3}\left(O_1 + O_2\right)\right) = \frac{3}{\sqrt{5}}\Bigg(\frac{1}{12}\sum_{i=1}^{5}\lambda^i_{AB}\lambda^i_{CD} - \frac{1}{6}\sum_{i=6}^{7}\lambda^i_{AB}\lambda^i_{CD} + \frac{1}{4\sqrt{3}}\left(\lambda^3_{AB}\lambda^8_{CD} + \lambda^8_{AB}\lambda^3_{CD}\right) - \frac{1}{12}\lambda^8_{AB}\lambda^8_{CD}\Bigg)\bar{q}_{iA}q_{jB}\bar{q}_{kC}q_{lD}\,. \tag{4.122}$$

This leads to

$$\bar{q}_{iA}q_{jB}\bar{q}_{kC}q_{lD} = \sum_n P^n_{BADC}\tilde{O}_n. \tag{4.123}$$

Finally, the fact that the vacuum expectation values of the operators must be proportional to Q implies

$$\langle\bar{q}_i q_j \bar{q}_k \lambda^3 q_l\rangle = \sqrt{3}\langle\bar{q}_i q_j \bar{q}_k \lambda^8 q_l\rangle\,, \tag{4.124}$$
$$\langle\bar{q}_i \lambda^3 q_j \bar{q}_k q_l\rangle = \sqrt{3}\langle\bar{q}_i \lambda^8 q_j \bar{q}_k q_l\rangle\,, \tag{4.125}$$
$$\langle\bar{q}_i \lambda^1 q_j \bar{q}_k \lambda^2 q_l\rangle - \langle\bar{q}_i \lambda^2 q_j \bar{q}_k \lambda^1 q_l\rangle = \langle\bar{q}_i \lambda^5 q_j \bar{q}_k \lambda^4 q_l\rangle - \langle\bar{q}_i \lambda^4 q_j \bar{q}_k \lambda^5 q_l\rangle\,, \tag{4.126}$$
$$\langle\bar{q}_i \lambda^1 q_j \bar{q}_k \lambda^1 q_l\rangle = -\langle\bar{q}_i \lambda^8 q_j \bar{q}_k \lambda^8 q_l\rangle = \langle\bar{q}_i \lambda^n q_j \bar{q}_k \lambda^n q_l\rangle\,, \quad \text{for } n = 2,\ldots,5\,, \tag{4.127}$$
$$\langle\bar{q}_i \lambda^1 q_j \bar{q}_k \lambda^1 q_l\rangle = -\frac{1}{2}\langle\bar{q}_i \lambda^n q_j \bar{q}_k \lambda^n q_l\rangle\,, \quad \text{for } n = 6,7\,, \tag{4.128}$$
$$\langle\bar{q}_i \lambda^1 q_j \bar{q}_k \lambda^1 q_l\rangle = \frac{1}{2\sqrt{3}}\left(\langle\bar{q}_i \lambda^3 q_j \bar{q}_k \lambda^8 q_l\rangle + \langle\bar{q}_i \lambda^8 q_j \bar{q}_k \lambda^3 q_l\rangle\right)\,, \tag{4.129}$$

and the final flavour decomposition reads

$$\begin{aligned}
\bar{q}_{iA}q_{jB}\bar{q}_{kC}q_{lD} &= \frac{1}{2}(\bar{q}_i\lambda_1 q_j\bar{q}_k\lambda_2 q_l - \bar{q}_i\lambda_2 q_j\bar{q}_k\lambda_1 q_l)\left(\frac{\lambda^1_{BA}}{2}\frac{\lambda^2_{DC}}{2} - \frac{\lambda^2_{BA}}{2}\frac{\lambda^1_{DC}}{2} + \frac{\lambda^4_{BA}}{2}\frac{\lambda^5_{DC}}{2} - \frac{\lambda^5_{BA}}{2}\frac{\lambda^4_{DC}}{2}\right)\\
&+ \bar{q}_i\lambda_1 q_j\bar{q}_k\lambda_1 q_l\left(\sum_{i=1}^{5}\frac{\lambda^i_{BA}}{2}\frac{\lambda^i_{DC}}{2} - 2\sum_{i=6}^{7}\frac{\lambda^i_{BA}}{2}\frac{\lambda^i_{DC}}{2} - \frac{\lambda^8_{BA}}{2}\frac{\lambda^8_{DC}}{2} + \sqrt{3}\left(\frac{\lambda^3_{BA}}{2}\frac{\lambda^8_{DC}}{2} + \frac{\lambda^8_{BA}}{2}\frac{\lambda^3_{DC}}{2}\right)\right)\\
&+ \frac{1}{2}(\bar{q}_i\lambda_8 q_j\bar{q}_k q_l + \bar{q}_i q_j\bar{q}_k\lambda_8 q_l)\left(\frac{\lambda^8_{BA}+\sqrt{3}\lambda^3_{BA}}{2}\frac{\delta_{DC}}{3} + \frac{\delta_{BA}}{3}\frac{\lambda^8_{DC}+\sqrt{3}\lambda^3_{DC}}{2}\right)\\
&+ \frac{1}{2}(\bar{q}_i\lambda_8 q_j\bar{q}_k q_l - \bar{q}_i q_j\bar{q}_k\lambda_8 q_l)\left(\frac{\lambda^8_{BA}+\sqrt{3}\lambda^3_{BA}}{2}\frac{\delta_{DC}}{3} - \frac{\delta_{BA}}{3}\frac{\lambda^8_{DC}+\sqrt{3}\lambda^3_{DC}}{2}\right)\,.
\end{aligned} \tag{4.130}$$

Only the spinor reduction remains. As usual, one can decompose each operator above according to

$$\hat{O}_{i'j'k'l'} = \sum_{A,B} c_A c_B \hat{O}_{ijkl}\Gamma^{ijA}\Gamma^{klB}\ \ \Gamma^A_{i'j'}\Gamma^B_{k'l'}\,, \tag{4.131}$$

where Γ^A is an element in the spinor basis of (4.74) and c_A the corresponding normalisation defined in (4.76). However, many restrictions apply. Proportionality with $F_{\mu\nu}$ leaves a small number of independent Lorentz structures possible. Moreover, since $\hat{O}_{ijkl}$ are by construction either symmetric or anti-symmetric under the exchange $(ij) \leftrightarrow (kl)$, the reduced matrix element $\hat{O}_{ijkl}\Gamma^{ijB}\Gamma^{klA}$ is trivially related to $\hat{O}_{ijkl}\Gamma^{ijA}\Gamma^{klB}$. Taking advantage of this and requiring that the reduced matrix elements should be odd under charge conjugation one finds

$$\begin{aligned}
\frac{1}{2}(\bar{q}_i\lambda_1 q_j\bar{q}_k\lambda_2 q_l - \bar{q}_i\lambda_2 q_j\bar{q}_k\lambda_1 q_l) &= \frac{1}{64}\Big(\gamma^\mu_{ji}\gamma^\nu_{lk} - \gamma^\nu_{ji}\gamma^\mu_{lk}\Big)\Big[\bar{q}\lambda_1\gamma_\mu q\bar{q}\lambda_2\gamma_\nu q - \bar{q}\lambda_2\gamma_\mu q\bar{q}\lambda_1\gamma_\nu q\Big]\\
&+ \frac{1}{64}\Big((\gamma^\mu\gamma_5)_{ji}(\gamma^\nu\gamma_5)_{lk} - (\gamma^\nu\gamma_5)_{ji}(\gamma^\mu\gamma_5)_{lk}\Big)\Big[\bar{q}\lambda_1\gamma_\mu\gamma_5 q\bar{q}\lambda_2\gamma_\nu\gamma_5 q - \bar{q}\lambda_2\gamma_\mu\gamma_5 q\bar{q}\lambda_1\gamma_\nu\gamma_5 q\Big]\\
&+ \frac{1}{64}g_{\lambda\alpha}\Big(\sigma^{\mu\lambda}_{ji}\sigma^{\alpha\nu}_{lk} - \sigma^{\nu\lambda}_{ji}\sigma^{\alpha\mu}_{lk}\Big)\times\frac{1}{2}g^{\rho\beta}\Big[\bar{q}\sigma_{\mu\rho}\lambda_1 q\,\bar{q}\sigma_{\beta\nu}\lambda_2 q - \bar{q}\sigma_{\mu\rho}\lambda_2 q\,\bar{q}\sigma_{\beta\nu}\lambda_1 q\Big]
\end{aligned} \tag{4.132}$$

$$\begin{aligned}\bar{q}_i\lambda_1 q_j\bar{q}_k\lambda_1 q_l &= \frac{1}{32}\Big(\sigma^{\mu\nu}_{ji}\delta_{lk}+\delta_{ji}\sigma^{\mu\nu}_{lk}\Big)\Big[\bar{q}\lambda_1 q\bar{q}\lambda_1\sigma_{\mu\nu}q\Big]\\ &+\frac{1}{64}\epsilon^{\mu\nu\mu_1\nu_1}\epsilon_{\mu_1\nu_1\mu_2\nu_2}\Big((\gamma_\mu\gamma_5)_{ji}(\gamma_\nu)_{lk}-(\gamma_\mu)_{ji}(\gamma_\nu\gamma_5)_{lk}\Big)\Big[\bar{q}\lambda_1\gamma^{\mu_2}\gamma_5 q\bar{q}\lambda_1\gamma^{\nu_2}q\Big]\\ &+\frac{1}{32}\Big(\sigma^{\mu\nu}_{ji}\gamma_{5\,lk}+\gamma_{5\,ji}\sigma^{\mu\nu}_{lk}\Big)\Big[\bar{q}\lambda_1\sigma_{\mu\nu}q\,\bar{q}\lambda_1\gamma_5 q\Big]\,,\end{aligned} \tag{4.133}$$

$$\begin{aligned}\bar{q}_i\lambda_8 q_j\bar{q}_k q_l \pm \bar{q}_i q_j\bar{q}_k\lambda_8 q_l &= \frac{1}{32}\Big(\sigma^{\mu\nu}_{ji}\,\delta_{lk}\pm\delta_{ji}\sigma^{\mu\nu}_{lk}\Big)\Big[\bar{q}\sigma_{\mu\nu}\lambda_8 q\,\bar{q}q\pm\bar{q}\sigma_{\mu\nu}q\,\bar{q}\lambda_8 q\Big]\\ &+\frac{1}{64}\epsilon^{\mu\nu\mu_1\nu_1}\epsilon_{\mu_1\nu_1\mu_2\nu_2}\Big((\gamma_\mu\gamma_5)_{ji}(\gamma_\nu)_{lk}\mp(\gamma_\mu)_{ji}(\gamma_\nu\gamma_5)_{lk}\Big)\\ &\times\Big[\bar{q}\lambda_8\gamma^{\mu_2}\gamma_5 q\,\bar{q}\gamma^{\nu_2}q\pm\bar{q}\gamma^{\mu_2}\gamma_5 q\,\bar{q}\lambda_8\gamma^{\nu_2}q\Big]\\ &+\frac{1}{32}\Big(\sigma^{\mu\nu}_{ji}\gamma_{5\,lk}\pm\gamma_{5\,ji}\sigma^{\mu\nu}_{lk}\Big)\Big[\bar{q}\sigma^{\mu\nu}\lambda_8 q\,\bar{q}\gamma_5 q\pm\bar{q}\sigma^{\mu\nu}q\,\bar{q}\lambda_8\gamma_5 q\Big]\,.\end{aligned} \tag{4.134}$$

This reduces the original set of 1679616 matrix elements to a basis of 12 non-zero ones.

4.1.C Explicit expressions for the $\hat{\Pi}_i$

In this appendix, we seperately list the form factors $\hat{\Pi}_i$ for the contributions from the quark loop, one cut quark line topologies and the gluon matrix element. Note that those for the two-cut quark line topologies were given in Sec. 4.1.4.3.

4.1.C.1 The quark loop

Recall (4.71)

$$\hat{\Pi}^{\overline{MS}}_m = \hat{\Pi}^0_{m,S} + m_q^2\,\hat{\Pi}^{m_q^2}_{m,\overline{MS}} + \mathcal{O}(m_q^4)\,. \tag{4.135}$$

The two terms above are given by

$$\hat{\Pi}^0_{m,S} = \frac{N_c\,e_q^4}{\pi^2}\sum_{i,j,k,n}\left[c^{(m,n)}_{i,j,k}+f^{(m,n)}_{i,j,k}F+g^{(m,n)}_{i,j,k}\log\left(\frac{Q_2^2}{Q_3^2}\right)+h^{(m,n)}_{i,j,k}\log\left(\frac{Q_1^2}{Q_2^2}\right)\right]\lambda^{-n}\,Q_1^{2i}\,Q_2^{2j}\,Q_3^{2k}\,, \tag{4.136}$$

$$\begin{aligned}\hat{\Pi}^{m_q^2}_{m,\overline{MS}} &= \frac{N_c\,e_q^4}{\pi^2}\sum_{i,j,k,n}\lambda^{-n}\,Q_1^{2i}\,Q_2^{2j}\,Q_3^{2k}\\ &\cdot\left[d^{(m,n)}_{i,j,k}+p^{(m,n)}_{i,j,k}F+q^{(m,n)}_{i,j,k}\log\left(\frac{Q_2^2}{Q_3^2}\right)+r^{(m,n)}_{i,j,k}\log\left(\frac{Q_1^2}{Q_2^2}\right)+s^{(m,n)}_{i,j,k}\log\left(\frac{Q_3^2}{\mu^2}\right)\right]\,,\end{aligned} \tag{4.137}$$

where the non-zero coefficients are

$$c^{(1,1)}_{0,0,0} = 2\,, \tag{4.138}$$

$$\begin{aligned}&f^{(1,2)}_{0,1,2}=2\,,\ f^{(1,2)}_{0,2,1}=-4\,,\ f^{(1,2)}_{0,3,0}=2\,,\ f^{(1,2)}_{1,0,2}=2\,,\ f^{(1,2)}_{1,1,1}=4\,,\ f^{(1,2)}_{1,2,0}=-2\,,\ f^{(1,2)}_{2,0,1}=-4,\\ &f^{(1,2)}_{2,1,0}=-2\,,\ f^{(1,2)}_{3,0,0}=2,\end{aligned} \tag{4.139}$$

$$g^{(1,2)}_{0,0,2} = 2\,,\ g^{(1,2)}_{0,1,1} = 2\,,\ g^{(1,2)}_{0,2,0} = -4\,,\ g^{(1,2)}_{1,0,1} = 2\,,\ g^{(1,2)}_{1,1,0} = 8\,,\ g^{(1,2)}_{2,0,0} = -4, \tag{4.140}$$

$$\begin{aligned}&h^{(1,2)}_{0,0,2} = 1\,,\ h^{(1,2)}_{0,1,1} = -1\,,\ h^{(1,2)}_{0,2,0} = -1\,,\ h^{(1,2)}_{0,3,-1} = 1\,,\ h^{(1,2)}_{1,0,1} = 3\,,\ h^{(1,2)}_{1,1,0} = 4\,,\ h^{(1,2)}_{1,2,-1} = -3,\\ &h^{(1,2)}_{2,0,0} = -3\,,\ h^{(1,2)}_{2,1,-1} = 3\,,\ h^{(1,2)}_{3,0,-1} = -1,\end{aligned} \tag{4.141}$$

$$\begin{aligned}&c^{(4,3)}_{-1,0,5} = 2\,,\ c^{(4,3)}_{-1,1,4} = -6\,,\ c^{(4,3)}_{-1,2,3} = 4\,,\ c^{(4,3)}_{-1,3,2} = 4\,,\ c^{(4,3)}_{-1,4,1} = -6\,,\ c^{(4,3)}_{-1,5,0} = 2\,,\ c^{(4,3)}_{0,-1,5} = 2,\\ &c^{(4,3)}_{0,0,4} = 36\,,\ c^{(4,3)}_{0,1,3} = -20\,,\ c^{(4,3)}_{0,2,2} = -64\,,\ c^{(4,3)}_{0,3,1} = 34\,,\ c^{(4,3)}_{0,4,0} = 12\,,\ c^{(4,3)}_{1,-1,4} = -6\,,\ c^{(4,3)}_{1,0,3} = -20,\\ &c^{(4,3)}_{1,1,2} = 168\,,\ c^{(4,3)}_{1,2,1} = -28\,,\ c^{(4,3)}_{1,3,0} = -66\,,\ c^{(4,3)}_{2,-1,3} = 4\,,\ c^{(4,3)}_{2,0,2} = -64\,,\ c^{(4,3)}_{2,1,1} = -28\,,\ c^{(4,3)}_{2,2,0} = 104,\\ &c^{(4,3)}_{3,-1,2} = 4\,,\ c^{(4,3)}_{3,0,1} = 34\,,\ c^{(4,3)}_{3,1,0} = -66\,,\ c^{(4,3)}_{4,-1,1} = -6\,,\ c^{(4,3)}_{4,0,0} = 12\,,\ c^{(4,3)}_{5,-1,0} = 2,\end{aligned} \tag{4.142}$$

$$\begin{aligned}&f^{(4,4)}_{0,0,7} = 12\,,\ f^{(4,4)}_{0,1,6} = -6\,,\ f^{(4,4)}_{0,2,5} = -60\,,\ f^{(4,4)}_{0,3,4} = 66\,,\ f^{(4,4)}_{0,4,3} = 36\,,\ f^{(4,4)}_{0,5,2} = -66\,,\ f^{(4,4)}_{0,6,1} = 12,\\ &f^{(4,4)}_{0,7,0} = 6\,,\ f^{(4,4)}_{1,0,6} = -6\,,\ f^{(4,4)}_{1,1,5} = 216\,,\ f^{(4,4)}_{1,2,4} = -138\,,\ f^{(4,4)}_{1,3,3} = -360\,,\ f^{(4,4)}_{1,4,2} = 270\,,\ f^{(4,4)}_{1,5,1} = 48,\\ &f^{(4,4)}_{1,6,0} = -30\,,\ f^{(4,4)}_{2,0,5} = -60\,,\ f^{(4,4)}_{2,1,4} = -138\,,\ f^{(4,4)}_{2,2,3} = 744\,,\ f^{(4,4)}_{2,3,2} = -204\,,\ f^{(4,4)}_{2,4,1} = -300,\\ &f^{(4,4)}_{2,5,0} = 54\,,\ f^{(4,4)}_{3,0,4} = 66\,,\ f^{(4,4)}_{3,1,3} = -360\,,\ f^{(4,4)}_{3,2,2} = -204\,,\ f^{(4,4)}_{3,3,1} = 480\,,\ f^{(4,4)}_{3,4,0} = -30\,,\ f^{(4,4)}_{4,0,3} = 36,\\ &f^{(4,4)}_{4,1,2} = 270\,,\ f^{(4,4)}_{4,2,1} = -300\,,\ f^{(4,4)}_{4,3,0} = -30\,,\ f^{(4,4)}_{5,0,2} = -66\,,\ f^{(4,4)}_{5,1,1} = 48\,,\ f^{(4,4)}_{5,2,0} = 54\,,\ f^{(4,4)}_{6,0,1} = 12,\\ &f^{(4,4)}_{6,1,0} = -30\,,\ f^{(4,4)}_{7,0,0} = 6,\end{aligned} \tag{4.143}$$

$$\begin{aligned}&g^{(4,4)}_{-1,0,7} = 1\,,\ g^{(4,4)}_{-1,1,6} = -3\,,\ g^{(4,4)}_{-1,2,5} = 1\,,\ g^{(4,4)}_{-1,3,4} = 5\,,\ g^{(4,4)}_{-1,4,3} = -5\,,\ g^{(4,4)}_{-1,5,2} = -1\,,\ g^{(4,4)}_{-1,6,1} = 3,\\ &g^{(4,4)}_{-1,7,0} = -1\,,\ g^{(4,4)}_{0,-1,7} = 1\,,\ g^{(4,4)}_{0,0,6} = 50\,,\ g^{(4,4)}_{0,1,5} = -13\,,\ g^{(4,4)}_{0,2,4} = -184\,,\ g^{(4,4)}_{0,3,3} = 119\,,\ g^{(4,4)}_{0,4,2} = 106,\\ &g^{(4,4)}_{0,5,1} = -75\,,\ g^{(4,4)}_{0,6,0} = -4\,,\ g^{(4,4)}_{1,-1,6} = -3\,,\ g^{(4,4)}_{1,0,5} = -13\,,\ g^{(4,4)}_{1,1,4} = 486\,,\ g^{(4,4)}_{1,2,3} = -162\,,\ g^{(4,4)}_{1,3,2} = -559,\\ &g^{(4,4)}_{1,4,1} = 207\,,\ g^{(4,4)}_{1,5,0} = 44\,,\ g^{(4,4)}_{2,-1,5} = 1\,,\ g^{(4,4)}_{2,0,4} = -184\,,\ g^{(4,4)}_{2,1,3} = -162\,,\ g^{(4,4)}_{2,2,2} = 908\,,\ g^{(4,4)}_{2,3,1} = -135,\\ &g^{(4,4)}_{2,4,0} = -124\,,\ g^{(4,4)}_{3,-1,4} = 5\,,\ g^{(4,4)}_{3,0,3} = 119\,,\ g^{(4,4)}_{3,1,2} = -559\,,\ g^{(4,4)}_{3,2,1} = -135\,,\ g^{(4,4)}_{3,3,0} = 170\,,\ g^{(4,4)}_{4,-1,3} = -5,\\ &g^{(4,4)}_{4,0,2} = 106\,,\ g^{(4,4)}_{4,1,1} = 207\,,\ g^{(4,4)}_{4,2,0} = -124\,,\ g^{(4,4)}_{5,-1,2} = -1\,,\ g^{(4,4)}_{5,0,1} = -75\,,\ g^{(4,4)}_{5,1,0} = 44\,,\ g^{(4,4)}_{6,-1,1} = 3,\\ &g^{(4,4)}_{6,0,0} = -4\,,\ g^{(4,4)}_{7,-1,0} = -1,\end{aligned} \tag{4.144}$$

$$\begin{aligned}&h^{(4,4)}_{0,-1,7} = 1\,,\ h^{(4,4)}_{0,0,6} = 25\,,\ h^{(4,4)}_{0,1,5} = -63\,,\ h^{(4,4)}_{0,2,4} = 1\,,\ h^{(4,4)}_{0,3,3} = 91\,,\ h^{(4,4)}_{0,4,2} = -45\,,\ h^{(4,4)}_{0,5,1} = -29,\\ &h^{(4,4)}_{0,6,0} = 19\,,\ h^{(4,4)}_{1,-1,6} = -3\,,\ h^{(4,4)}_{1,0,5} = 50\,,\ h^{(4,4)}_{1,1,4} = 243\,,\ h^{(4,4)}_{1,2,3} = -500\,,\ h^{(4,4)}_{1,3,2} = 19\,,\ h^{(4,4)}_{1,4,1} = 258,\\ &h^{(4,4)}_{1,5,0} = -67\,,\ h^{(4,4)}_{2,-1,5} = 1\,,\ h^{(4,4)}_{2,0,4} = -185\,,\ h^{(4,4)}_{2,1,3} = 338\,,\ h^{(4,4)}_{2,2,2} = 454\,,\ h^{(4,4)}_{2,3,1} = -563\,,\ h^{(4,4)}_{2,4,0} = 51,\\ &h^{(4,4)}_{3,-1,4} = 5\,,\ h^{(4,4)}_{3,0,3} = 28\,,\ h^{(4,4)}_{3,1,2} = -578\,,\ h^{(4,4)}_{3,2,1} = 428\,,\ h^{(4,4)}_{3,3,0} = 85\,,\ h^{(4,4)}_{4,-1,3} = -5\,,\ h^{(4,4)}_{4,0,2} = 151,\\ &h^{(4,4)}_{4,1,1} = -51\,,\ h^{(4,4)}_{4,2,0} = -175\,,\ h^{(4,4)}_{5,-1,2} = -1\,,\ h^{(4,4)}_{5,0,1} = -46\,,\ h^{(4,4)}_{5,1,0} = 111\,,\ h^{(4,4)}_{6,-1,1} = 3\,,\ h^{(4,4)}_{6,0,0} = -23,\\ &h^{(4,4)}_{7,-1,0} = -1.\end{aligned} \tag{4.145}$$

$$c^{(7,3)}_{-1,0,4} = 6\,,\ c^{(7,3)}_{-1,1,3} = -12\,,\ c^{(7,3)}_{-1,3,1} = 12\,,\ c^{(7,3)}_{-1,4,0} = -6\,,\ c^{(7,3)}_{0,-1,4} = 4\,,\ c^{(7,3)}_{0,0,3} = 64\,,\ c^{(7,3)}_{0,1,2} = 68,$$
$$c^{(7,3)}_{0,2,1} = -112\,,\ c^{(7,3)}_{0,3,0} = -24\,,\ c^{(7,3)}_{1,-1,3} = -16\,,\ c^{(7,3)}_{1,0,2} = -116\,,\ c^{(7,3)}_{1,1,1} = 100\,,\ c^{(7,3)}_{1,2,0} = 104\,,\ c^{(7,3)}_{2,-1,2} = 24,$$
$$c^{(7,3)}_{2,0,1} = 16\,,\ c^{(7,3)}_{2,1,0} = -108\,,\ c^{(7,3)}_{3,-1,1} = -16\,,\ c^{(7,3)}_{3,0,0} = 30\,,\ c^{(7,3)}_{4,-1,0} = 4,$$
(4.146)

$$f^{(7,4)}_{0,0,6} = 24\,,\ f^{(7,4)}_{0,1,5} = 36\,,\ f^{(7,4)}_{0,2,4} = -156\,,\ f^{(7,4)}_{0,3,3} = 24\,,\ f^{(7,4)}_{0,4,2} = 144\,,\ f^{(7,4)}_{0,5,1} = -60\,,\ f^{(7,4)}_{0,6,0} = -12,$$
$$f^{(7,4)}_{1,0,5} = -36\,,\ f^{(7,4)}_{1,1,4} = 288\,,\ f^{(7,4)}_{1,2,3} = 312\,,\ f^{(7,4)}_{1,3,2} = -576\,,\ f^{(7,4)}_{1,4,1} = -36\,,\ f^{(7,4)}_{1,5,0} = 48\,,\ f^{(7,4)}_{2,0,4} = -84,$$
$$f^{(7,4)}_{2,1,3} = -600\,,\ f^{(7,4)}_{2,2,2} = 432\,,\ f^{(7,4)}_{2,3,1} = 456\,,\ f^{(7,4)}_{2,4,0} = -60\,,\ f^{(7,4)}_{3,0,3} = 216\,,\ f^{(7,4)}_{3,1,2} = 144,$$
$$f^{(7,4)}_{3,2,1} = -552\,,\ f^{(7,4)}_{4,0,2} = -144\,,\ f^{(7,4)}_{4,1,1} = 180\,,\ f^{(7,4)}_{4,2,0} = 60\,,\ f^{(7,4)}_{5,0,1} = 12\,,\ f^{(7,4)}_{5,1,0} = -48\,,\ f^{(7,4)}_{6,0,0} = 12,$$
(4.147)

$$g^{(7,4)}_{-1,0,6} = 2\,,\ g^{(7,4)}_{-1,2,4} = -18\,,\ g^{(7,4)}_{-1,3,3} = 32\,,\ g^{(7,4)}_{-1,4,2} = -18\,,\ g^{(7,4)}_{-1,6,0} = 2\,,\ g^{(7,4)}_{0,-1,6} = 2\,,\ g^{(7,4)}_{0,0,5} = 104,$$
$$g^{(7,4)}_{0,1,4} = 126\,,\ g^{(7,4)}_{0,2,3} = -368\,,\ g^{(7,4)}_{0,3,2} = -58\,,\ g^{(7,4)}_{0,4,1} = 184\,,\ g^{(7,4)}_{0,5,0} = 10\,,\ g^{(7,4)}_{1,-1,5} = -8\,,\ g^{(7,4)}_{1,0,4} = -158,$$
$$g^{(7,4)}_{1,1,3} = 544\,,\ g^{(7,4)}_{1,2,2} = 652\,,\ g^{(7,4)}_{1,3,1} = -440\,,\ g^{(7,4)}_{1,4,0} = -78\,,\ g^{(7,4)}_{2,-1,4} = 10\,,\ g^{(7,4)}_{2,0,3} = -160,$$
$$g^{(7,4)}_{2,1,2} = -924\,,\ g^{(7,4)}_{2,2,1} = 208\,,\ g^{(7,4)}_{2,3,0} = 170\,,\ g^{(7,4)}_{3,0,2} = 358\,,\ g^{(7,4)}_{3,1,1} = 176\,,\ g^{(7,4)}_{3,2,0} = -170$$
$$g^{(7,4)}_{4,-1,2} = -10\,,\ g^{(7,4)}_{4,0,1} = -136\,,\ g^{(7,4)}_{4,1,0} = 78\,,\ g^{(7,4)}_{5,-1,1} = 8\,,\ g^{(7,4)}_{5,0,0} = -10\,,\ g^{(7,4)}_{6,-1,0} = -2,$$
(4.148)

$$h^{(7,4)}_{0,-1,6} = 2\,,\ h^{(7,4)}_{0,0,5} = 56\,,\ h^{(7,4)}_{0,1,4} = -46\,,\ h^{(7,4)}_{0,2,3} = -176\,,\ h^{(7,4)}_{0,3,2} = 214\,,\ h^{(7,4)}_{0,4,1} = -8\,,\ h^{(7,4)}_{0,5,0} = -42,$$
$$h^{(7,4)}_{1,-1,5} = -8\,,\ h^{(7,4)}_{1,0,4} = 16\,,\ h^{(7,4)}_{1,1,3} = 536\,,\ h^{(7,4)}_{1,2,2} = -256\,,\ h^{(7,4)}_{1,3,1} = -400\,,\ h^{(7,4)}_{1,4,0} = 112\,,\ h^{(7,4)}_{2,-1,4} = 10,$$
$$h^{(7,4)}_{2,0,3} = -336\,,\ h^{(7,4)}_{2,1,2} = -300\,,\ h^{(7,4)}_{2,2,1} = 800\,,\ h^{(7,4)}_{2,3,0} = -30\,,\ h^{(7,4)}_{3,0,2} = 352\,,\ h^{(7,4)}_{3,1,1} = -360,$$
$$h^{(7,4)}_{3,2,0} = -160\,,\ h^{(7,4)}_{4,-1,2} = -10\,,\ h^{(7,4)}_{4,0,1} = -40\,,\ h^{(7,4)}_{4,1,0} = 170\,,\ h^{(7,4)}_{5,-1,1} = 8\,,\ h^{(7,4)}_{5,0,0} = -48,$$
$$h^{(7,4)}_{6,-1,0} = -2,$$
(4.149)

$$c^{(17,2)}_{0,0,1} = 16\,,\ c^{(17,2)}_{0,1,0} = -12\,,\ c^{(17,2)}_{0,2,-1} = -4\,,\ c^{(17,2)}_{1,0,0} = -12\,,\ c^{(17,2)}_{1,1,-1} = 8\,,\ c^{(17,2)}_{2,0,-1} = -4, \quad (4.150)$$

$$f^{(17,3)}_{0,0,4} = 4\,,\ f^{(17,3)}_{0,1,3} = -4\,,\ f^{(17,3)}_{0,2,2} = -12\,,\ f^{(17,3)}_{0,3,1} = 20\,,\ f^{(17,3)}_{0,4,0} = -8\,,\ f^{(17,3)}_{1,0,3} = -4\,,\ f^{(17,3)}_{1,1,2} = 64,$$
$$f^{(17,3)}_{1,2,1} = -44\,,\ f^{(17,3)}_{1,3,0} = -16\,,\ f^{(17,3)}_{2,0,2} = -12\,,\ f^{(17,3)}_{2,1,1} = -44\,,\ f^{(17,3)}_{2,2,0} = 48\,,\ f^{(17,3)}_{3,0,1} = 20,$$
$$f^{(17,3)}_{3,1,0} = -16\,,\ f^{(17,3)}_{4,0,0} = -8,$$
(4.151)

$$g^{(17,3)}_{0,0,3} = 20\,,\ g^{(17,3)}_{0,1,2} = -16\,,\ g^{(17,3)}_{0,2,1} = -28\,,\ g^{(17,3)}_{0,3,0} = 24\,,\ g^{(17,3)}_{1,0,2} = -16\,,\ g^{(17,3)}_{1,1,1} = 104,$$
$$g^{(17,3)}_{1,2,0} = -24\,,\ g^{(17,3)}_{2,0,1} = -28\,,\ g^{(17,3)}_{2,1,0} = -24\,,\ g^{(17,3)}_{3,0,0} = 24,$$
(4.152)

$$h^{(17,3)}_{0,0,3} = 10\,,\ h^{(17,3)}_{0,1,2} = -28\,,\ h^{(17,3)}_{0,2,1} = 24\,,\ h^{(17,3)}_{0,3,0} = -4\,,\ h^{(17,3)}_{0,4,-1} = -2\,,\ h^{(17,3)}_{1,0,2} = 12\,,\ h^{(17,3)}_{1,1,1} = 52,$$
$$h^{(17,3)}_{1,2,0} = -68\,,\ h^{(17,3)}_{1,3,-1} = 4\,,\ h^{(17,3)}_{2,0,1} = -52\,,\ h^{(17,3)}_{2,1,0} = 44\,,\ h^{(17,3)}_{3,0,0} = 28\,,\ h^{(17,3)}_{3,1,-1} = -4\,,\ h^{(17,3)}_{4,0,-1} = 2,$$
(4.153)

$$c^{(39,3)}_{-1,0,4} = -4\,,\ c^{(39,3)}_{-1,1,3} = 16\,,\ c^{(39,3)}_{-1,2,2} = -24\,,\ c^{(39,3)}_{-1,3,1} = 16\,,\ c^{(39,3)}_{-1,4,0} = -4\,,\ c^{(39,3)}_{0,-1,4} = -4\,,\ c^{(39,3)}_{0,0,3} = -44,$$
$$c^{(39,3)}_{0,1,2} = 48\,,\ c^{(39,3)}_{0,2,1} = 48\,,\ c^{(39,3)}_{0,3,0} = -44\,,\ c^{(39,3)}_{0,4,-1} = -4\,,\ c^{(39,3)}_{1,-1,3} = 16\,,\ c^{(39,3)}_{1,0,2} = 48\,,\ c^{(39,3)}_{1,1,1} = -176,$$
$$c^{(39,3)}_{1,2,0} = 48\,,\ c^{(39,3)}_{1,3,-1} = 16\,,\ c^{(39,3)}_{2,-1,2} = -24\,,\ c^{(39,3)}_{2,0,1} = 48\,,\ c^{(39,3)}_{2,1,0} = 48\,,\ c^{(39,3)}_{2,2,-1} = -24\,,\ c^{(39,3)}_{3,-1,1} = 16,$$
$$c^{(39,3)}_{3,0,0} = -44\,,\ c^{(39,3)}_{3,1,-1} = 16\,,\ c^{(39,3)}_{4,-1,0} = -4\,,\ c^{(39,3)}_{4,0,-1} = -4,$$
(4.154)

$$f^{(39,4)}_{0,0,6} = -20\,,\ f^{(39,4)}_{0,1,5} = 24\,,\ f^{(39,4)}_{0,2,4} = 84\,,\ f^{(39,4)}_{0,3,3} = -176\,,\ f^{(39,4)}_{0,4,2} = 84\,,\ f^{(39,4)}_{0,5,1} = 24,$$
$$f^{(39,4)}_{0,6,0} = -20\,,\ f^{(39,4)}_{1,0,5} = 24\,,\ f^{(39,4)}_{1,1,4} = -288\,,\ f^{(39,4)}_{1,2,3} = 264\,,\ f^{(39,4)}_{1,3,2} = 264\,,\ f^{(39,4)}_{1,4,1} = -288,$$
$$f^{(39,4)}_{1,5,0} = 24\,,\ f^{(39,4)}_{2,0,4} = 84\,,\ f^{(39,4)}_{2,1,3} = 264\,,\ f^{(39,4)}_{2,2,2} = -792\,,\ f^{(39,4)}_{2,3,1} = 264\,,\ f^{(39,4)}_{2,4,0} = 84,$$
$$f^{(39,4)}_{3,0,3} = -176\,,\ f^{(39,4)}_{3,1,2} = 264\,,\ f^{(39,4)}_{3,2,1} = 264\,,\ f^{(39,4)}_{3,3,0} = -176\,,\ f^{(39,4)}_{4,0,2} = 84\,,\ f^{(39,4)}_{4,1,1} = -288,$$
$$f^{(39,4)}_{4,2,0} = 84\,,\ f^{(39,4)}_{5,0,1} = 24\,,\ f^{(39,4)}_{5,1,0} = 24\,,\ f^{(39,4)}_{6,0,0} = -20,$$
(4.155)

$$g^{(39,4)}_{-1,0,6} = -2\,,\ g^{(39,4)}_{-1,1,5} = 8\,,\ g^{(39,4)}_{-1,2,4} = -10\,,\ g^{(39,4)}_{-1,4,2} = 10\,,\ g^{(39,4)}_{-1,5,1} = -8\,,\ g^{(39,4)}_{-1,6,0} = 2\,,\ g^{(39,4)}_{0,-1,6} = -2,$$
$$g^{(39,4)}_{0,0,5} = -76\,,\ g^{(39,4)}_{0,1,4} = 74, g^{(39,4)}_{0,2,3} = 216\,,\ g^{(39,4)}_{0,3,2} = -302\,,\ g^{(39,4)}_{0,4,1} = 52\,,\ g^{(39,4)}_{0,5,0} = 38,$$
$$g^{(39,4)}_{1,-1,5} = 8\,,\ g^{(39,4)}_{1,0,4} = 74\,,\ g^{(39,4)}_{1,1,3} = -592\,,\ g^{(39,4)}_{1,2,2} = 340\,,\ g^{(39,4)}_{1,3,1} = 296\,,\ g^{(39,4)}_{1,4,0} = -126,$$
$$g^{(39,4)}_{2,-1,4} = -10\,,\ g^{(39,4)}_{2,0,3} = 216,$$
$$g^{(39,4)}_{2,1,2} = 340\,,\ g^{(39,4)}_{2,2,1} = -680\,,\ g^{(39,4)}_{2,3,0} = 86\,,\ g^{(39,4)}_{3,0,2} = -302\,,\ g^{(39,4)}_{3,1,1} = 296\,,\ g^{(39,4)}_{3,2,0} = 86,$$
$$g^{(39,4)}_{4,-1,2} = 10\,,\ g^{(39,4)}_{4,0,1} = 52\,,\ g^{(39,4)}_{4,1,0} = -126\,,\ g^{(39,4)}_{5,-1,1} = -8\,,\ g^{(39,4)}_{5,0,0} = 38\,,\ g^{(39,4)}_{6,-1,0} = 2,$$
(4.156)

$$h^{(39,4)}_{0,-1,6} = -2\,,\ h^{(39,4)}_{0,0,5} = -38\,,\ h^{(39,4)}_{0,1,4} = 126\,,\ h^{(39,4)}_{0,2,3} = -86\,,\ h^{(39,4)}_{0,3,2} = -86\,,\ h^{(39,4)}_{0,4,1} = 126,$$
$$h^{(39,4)}_{0,5,0} = -38\,,\ h^{(39,4)}_{0,6,-1} = -2\,,\ h^{(39,4)}_{1,-1,5} = 8\,,\ h^{(39,4)}_{1,0,4} = -52\,,\ h^{(39,4)}_{1,1,3} = -296\,,\ h^{(39,4)}_{1,2,2} = 680,$$
$$h^{(39,4)}_{1,3,1} = -296\,,\ h^{(39,4)}_{1,4,0} = -52\,,\ h^{(39,4)}_{1,5,-1} = 8\,,\ h^{(39,4)}_{2,-1,4} = -10\,,\ h^{(39,4)}_{2,0,3} = 302\,,\ h^{(39,4)}_{2,1,2} = -340,$$
$$h^{(39,4)}_{2,2,1} = -340\,,\ h^{(39,4)}_{2,3,0} = 302\,,\ h^{(39,4)}_{2,4,-1} = -10\,,\ h^{(39,4)}_{3,0,2} = -216\,,\ h^{(39,4)}_{3,1,1} = 592\,,\ h^{(39,4)}_{3,2,0} = -216,$$
$$h^{(39,4)}_{4,-1,2} = 10\,,\ h^{(39,4)}_{4,0,1} = -74\,,\ h^{(39,4)}_{4,1,0} = -74\,,\ h^{(39,4)}_{4,2,-1} = 10\,,\ h^{(39,4)}_{5,-1,1} = -8\,,\ h^{(39,4)}_{5,0,0} = 76,$$
$$h^{(39,4)}_{5,1,-1} = -8\,,\ h^{(39,4)}_{6,-1,0} = 2\,,\ h^{(39,4)}_{6,0,-1} = 2,$$
(4.157)

$$c^{(54,2)}_{-1,0,2} = -2\,,\ c^{(54,2)}_{-1,1,1} = 4\,,\ c^{(54,2)}_{-1,2,0} = -2\,,\ c^{(54,2)}_{0,-1,2} = 2\,,\ c^{(54,2)}_{0,1,0} = -14\,,\ c^{(54,2)}_{1,-1,1} = -4\,,\ c^{(54,2)}_{1,0,0} = 14,$$
$$c^{(54,2)}_{2,-1,0} = 2,$$
(4.158)

$$f^{(54,3)}_{0,1,3} = -18\,,\ f^{(54,3)}_{0,2,2} = 30\,,\ f^{(54,3)}_{0,3,1} = -6\,,\ f^{(54,3)}_{0,4,0} = -6\,,\ f^{(54,3)}_{1,0,3} = 18\,,\ f^{(54,3)}_{1,2,1} = -54\,,\ f^{(54,3)}_{1,3,0} = 12,$$
$$f^{(54,3)}_{2,0,2} = -30\,,\ f^{(54,3)}_{2,1,1} = 54\,,\ f^{(54,3)}_{3,0,1} = 6\,,\ f^{(54,3)}_{3,1,0} = -12\,,\ f^{(54,3)}_{4,0,0} = 6, \tag{4.159}$$

$$g^{(54,3)}_{-1,0,4} = -1\,,\ g^{(54,3)}_{-1,1,3} = 2\,,\ g^{(54,3)}_{-1,3,1} = -2\,,\ g^{(54,3)}_{-1,4,0} = 1\,,\ g^{(54,3)}_{0,-1,4} = 1\,,\ g^{(54,3)}_{0,1,2} = -48\,,\ g^{(54,3)}_{0,2,1} = 40,$$
$$g^{(54,3)}_{0,3,0} = 7\,,\ g^{(54,3)}_{1,-1,3} = -2\,,\ g^{(54,3)}_{1,0,2} = 48\,,\ g^{(54,3)}_{1,2,0} = -26\,,\ g^{(54,3)}_{2,0,1} = -40\,,\ g^{(54,3)}_{2,1,0} = 26\,,\ g^{(54,3)}_{3,-1,1} = 2,$$
$$g^{(54,3)}_{3,0,0} = -7\,,\ g^{(54,3)}_{4,-1,0} = -1, \tag{4.160}$$

$$h^{(54,3)}_{0,-1,4} = 1\,,\ h^{(54,3)}_{0,0,3} = -10\,,\ h^{(54,3)}_{0,2,1} = 26\,,\ h^{(54,3)}_{0,3,0} = -17\,,\ h^{(54,3)}_{1,-1,3} = -2\,,\ h^{(54,3)}_{1,0,2} = 48\,,\ h^{(54,3)}_{1,1,1} = -78,$$
$$h^{(54,3)}_{1,2,0} = 8\,,\ h^{(54,3)}_{2,0,1} = -14\,,\ h^{(54,3)}_{2,1,0} = 34\,,\ h^{(54,3)}_{3,-1,1} = 2\,,\ h^{(54,3)}_{3,0,0} = -24\,,\ h^{(54,3)}_{4,-1,0} = -1, \tag{4.161}$$

and

$$p^{(1,1)}_{0,0,0} = -4\,, \tag{4.162}$$

$$q^{(1,3)}_{-1,-1,1} = -2\,,\ q^{(1,3)}_{-1,0,0} = 2\,,\ q^{(1,3)}_{0,-1,0} = 2, \tag{4.163}$$

$$r^{(1,1)}_{-1,-1,1} = -1\,,\ r^{(1,1)}_{-1,0,0} = 3\,,\ r^{(1,1)}_{-1,1,-1} = -3\,,\ r^{(1,1)}_{-1,2,-2} = 1\,,\ r^{(1,1)}_{0,-1,0} = -1\,,\ r^{(1,1)}_{0,1,-2} = -3\,,\ r^{(1,1)}_{1,-1,-1} = 3,$$
$$r^{(1,1)}_{1,0,-2} = 3\,,\ r^{(1,1)}_{2,-1,-2} = -1, \tag{4.164}$$

$$s^{(1,0)}_{-1,-1,-1} = -1\,,\ s^{(1,0)}_{-1,0,-2} = 1\,,\ s^{(1,0)}_{0,-1,-2} = 1, \tag{4.165}$$

$$d^{(4,2)}_{-2,-1,4} = 1\,,\ d^{(4,2)}_{-2,0,3} = -3\,,\ d^{(4,2)}_{-2,1,2} = 2\,,\ d^{(4,2)}_{-2,2,1} = 2\,,\ d^{(4,2)}_{-2,3,0} = -3\,,\ d^{(4,2)}_{-2,4,-1} = 1\,,\ d^{(4,2)}_{-1,-2,4} = 1,$$
$$d^{(4,2)}_{-1,-1,3} = -10\,,\ d^{(4,2)}_{-1,0,2} = 6\,,\ d^{(4,2)}_{-1,1,1} = 8\,,\ d^{(4,2)}_{-1,2,0} = 1\,,\ d^{(4,2)}_{-1,3,-1} = -6\,,\ d^{(4,2)}_{0,-2,3} = -3\,,\ d^{(4,2)}_{0,-1,2} = 6,$$
$$d^{(4,2)}_{0,0,1} = -36\,,\ d^{(4,2)}_{0,1,0} = 2\,,\ d^{(4,2)}_{0,2,-1} = 15\,,\ d^{(4,2)}_{1,-2,2} = 2\,,\ d^{(4,2)}_{1,-1,1} = 8\,,\ d^{(4,2)}_{1,0,0} = 2\,,\ d^{(4,2)}_{1,1,-1} = -20,$$
$$d^{(4,2)}_{2,-2,1} = 2\,,\ d^{(4,2)}_{2,-1,0} = 1\,,\ d^{(4,2)}_{2,0,-1} = 15\,,\ d^{(4,2)}_{3,-2,0} = -3\,,\ d^{(4,2)}_{3,-1,-1} = -6\,,\ d^{(4,2)}_{4,-2,-1} = 1, \tag{4.166}$$

$$p^{(4,3)}_{0,0,4} = -40\,,\ p^{(4,3)}_{0,1,3} = 40\,,\ p^{(4,3)}_{0,2,2} = 24\,,\ p^{(4,3)}_{0,3,1} = -8\,,\ p^{(4,3)}_{0,4,0} = -16\,,\ p^{(4,3)}_{1,0,3} = 40\,,\ p^{(4,3)}_{1,1,2} = -208,$$
$$p^{(4,3)}_{1,2,1} = 8\,,\ p^{(4,3)}_{1,3,0} = 64\,,\ p^{(4,3)}_{2,0,2} = 24\,,\ p^{(4,3)}_{2,1,1} = 8\,,\ p^{(4,3)}_{2,2,0} = -96\,,\ p^{(4,3)}_{3,0,1} = -8\,,\ p^{(4,3)}_{3,1,0} = 64,$$
$$p^{(4,3)}_{4,0,0} = -16, \tag{4.167}$$

$$q^{(4,3)}_{-1,-1,5} = -4\,,\ q^{(4,3)}_{-1,0,4} = 16\,,\ q^{(4,3)}_{-1,1,3} = -32\,,\ q^{(4,3)}_{-1,2,2} = 40\,,\ q^{(4,3)}_{-1,3,1} = -28\,,\ q^{(4,3)}_{-1,4,0} = 8\,,\ q^{(4,3)}_{0,-1,4} = 16,$$
$$q^{(4,3)}_{0,0,3} = -160\,,\ q^{(4,3)}_{0,1,2} = 40\,,\ q^{(4,3)}_{0,2,1} = 128\,,\ q^{(4,3)}_{0,3,0} = -24\,,\ q^{(4,3)}_{1,-1,3} = -32\,,\ q^{(4,3)}_{1,0,2} = 40\,,\ q^{(4,3)}_{1,1,1} = -200,$$
$$q^{(4,3)}_{1,2,0} = 16\,,\ q^{(4,3)}_{2,-1,2} = 40\,,\ q^{(4,3)}_{2,0,1} = 128\,,\ q^{(4,3)}_{2,1,0} = 16\,,\ q^{(4,3)}_{3,-1,1} = -28\,,\ q^{(4,3)}_{3,0,0} = -24\,,\ q^{(4,3)}_{4,-1,0} = 8,$$
(4.168)

$$r^{(4,3)}_{-1,-1,5} = -2\,,\ r^{(4,3)}_{-1,0,4} = 12\,,\ r^{(4,3)}_{-1,1,3} = -30\,,\ r^{(4,3)}_{-1,2,2} = 40\,,\ r^{(4,3)}_{-1,3,1} = -30\,,\ r^{(4,3)}_{-1,4,0} = 12,$$
$$r^{(4,3)}_{-1,5,-1} = -2\,,\ r^{(4,3)}_{0,-1,4} = 4\,,\ r^{(4,3)}_{0,0,3} = -80\,,\ r^{(4,3)}_{0,1,2} = 112\,,\ r^{(4,3)}_{0,2,1} = 8\,,\ r^{(4,3)}_{0,3,0} = -52\,,\ r^{(4,3)}_{0,4,-1} = 8,$$
$$r^{(4,3)}_{1,-1,3} = -2\,,\ r^{(4,3)}_{1,0,2} = -72\,,\ r^{(4,3)}_{1,1,1} = -100\,,\ r^{(4,3)}_{1,2,0} = 88\,,\ r^{(4,3)}_{1,3,-1} = -10\,,\ r^{(4,3)}_{2,0,1} = 120\,,\ r^{(4,3)}_{2,1,0} = -72,$$
$$r^{(4,3)}_{3,-1,1} = 2\,,\ r^{(4,3)}_{3,0,0} = 28\,,\ r^{(4,3)}_{3,1,-1} = 10\,,\ r^{(4,3)}_{4,-1,0} = -4\,,\ r^{(4,3)}_{4,0,-1} = -8\,,\ r^{(4,3)}_{5,-1,-1} = 2,$$
(4.169)

$$s^{(4,0)}_{-1,-1,-1} = -2,$$ (4.170)

$$d^{(7,2)}_{-2,-1,3} = 2\,,\ d^{(7,2)}_{-2,0,2} = -4\,,\ d^{(7,2)}_{-2,2,0} = 4\,,\ d^{(7,2)}_{-2,3,-1} = -2\,,\ d^{(7,2)}_{-1,-2,3} = 2\,,\ d^{(7,2)}_{-1,-1,2} = -20,$$
$$d^{(7,2)}_{-1,0,1} = -12\,,\ d^{(7,2)}_{-1,1,0} = 20\,,\ d^{(7,2)}_{-1,2,-1} = 10\,,\ d^{(7,2)}_{0,-2,2} = -8\,,\ d^{(7,2)}_{0,-1,1} = 24\,,\ d^{(7,2)}_{0,0,0} = -20,$$
$$d^{(7,2)}_{0,1,-1} = -20\,,\ d^{(7,2)}_{1,-2,1} = 12\,,\ d^{(7,2)}_{1,-1,0} = 4\,,\ d^{(7,2)}_{1,0,-1} = 20\,,\ d^{(7,2)}_{2,-2,0} = -8\,,\ d^{(7,2)}_{2,-1,-1} = -10,$$
$$d^{(7,2)}_{3,-2,-1} = 2,$$
(4.171)

$$p^{(7,3)}_{0,0,3} = -72\,,\ p^{(7,3)}_{0,1,2} = -72\,,\ p^{(7,3)}_{0,2,1} = 120\,,\ p^{(7,3)}_{0,3,0} = 24\,,\ p^{(7,3)}_{1,0,2} = 120\,,\ p^{(7,3)}_{1,1,1} = -96\,,\ p^{(7,3)}_{1,2,0} = -72,$$
$$p^{(7,3)}_{2,0,1} = -24\,,\ p^{(7,3)}_{2,1,0} = 72\,,\ p^{(7,3)}_{3,0,0} = -24,$$
(4.172)

$$q^{(7,3)}_{-2,0,4} = 4\,,\ q^{(7,3)}_{-2,1,3} = -16\,,\ q^{(7,3)}_{-2,2,2} = 24\,,\ q^{(7,3)}_{-2,3,1} = -16\,,\ q^{(7,3)}_{-2,4,0} = 4\,,\ q^{(7,3)}_{-1,0,3} = -40\,,\ q^{(7,3)}_{-1,1,2} = 48,$$
$$q^{(7,3)}_{-1,2,1} = 24\,,\ q^{(7,3)}_{-1,3,0} = -32\,,\ q^{(7,3)}_{0,-1,3} = -8\,,\ q^{(7,3)}_{0,0,2} = -144\,,\ q^{(7,3)}_{0,1,1} = -168\,,\ q^{(7,3)}_{0,2,0} = 64\,,\ q^{(7,3)}_{1,-1,2} = 24,$$
$$q^{(7,3)}_{1,0,1} = 184\,,\ q^{(7,3)}_{1,1,0} = -40\,,\ q^{(7,3)}_{2,-1,1} = -24\,,\ q^{(7,3)}_{2,0,0} = -4\,,\ q^{(7,3)}_{3,-1,0} = 8,$$
(4.173)

$$r^{(7,3)}_{0,-1,3} = -8\,,\ r^{(7,3)}_{0,0,2} = -144\,,\ r^{(7,3)}_{0,1,1} = 72\,,\ r^{(7,3)}_{0,2,0} = 80\,,\ r^{(7,3)}_{1,-1,2} = 24\,,\ r^{(7,3)}_{1,0,1} = 80\,,\ r^{(7,3)}_{1,1,0} = -152,$$
$$r^{(7,3)}_{2,-1,1} = -24\,,\ r^{(7,3)}_{2,0,0} = 64\,,\ r^{(7,3)}_{3,-1,0} = 8,$$
(4.174)

$$d^{(17,1)}_{-1,-1,0} = -4\,,\ d^{(17,1)}_{-1,0,-1} = 4\,,\ d^{(17,1)}_{0,-1,-1} = 4,$$ (4.175)

$$p^{(17,2)}_{0,0,1} = -24\,,\ p^{(17,2)}_{0,1,0} = 24\,,\ p^{(17,2)}_{1,0,0} = 24,$$ (4.176)

$$q^{(17,2)}_{-1,-1,2} = -4\,,\ q^{(17,2)}_{-1,0,1} = 8\,,\ q^{(17,2)}_{-1,1,0} = -4\,,\ q^{(17,2)}_{0,-1,1} = 8\,,\ q^{(17,2)}_{0,0,0} = -40\,,\ q^{(17,2)}_{1,-1,0} = -4,$$ (4.177)

$$r^{(17,2)}_{-1,-1,2} = -2\,,\ r^{(17,2)}_{-1,0,1} = 8\,,\ r^{(17,2)}_{-1,1,0} = -12\,,\ r^{(17,2)}_{-1,2,-1} = 8\,,\ r^{(17,2)}_{-1,3,-2} = -2\,,\ r^{(17,2)}_{0,0,0} = -20,$$
$$r^{(17,2)}_{0,1,-1} = 16\,,\ r^{(17,2)}_{0,2,-2} = 4\,,\ r^{(17,2)}_{1,-1,0} = 8\,,\ r^{(17,2)}_{1,0,-1} = -16\,,\ r^{(17,2)}_{2,-1,-1} = -8\,,\ r^{(17,2)}_{2,0,-2} = -4\,,\ r^{(17,2)}_{3,-1,-2} = 2, \tag{4.178}$$

$$s^{(17,0)}_{-1,-1,-2} = -2, \tag{4.179}$$

$$d^{(39,2)}_{-2,-1,3} = -2\,,\ d^{(39,2)}_{-2,0,2} = 8\,,\ d^{(39,2)}_{-2,1,1} = -12\,,\ d^{(39,2)}_{-2,2,0} = 8\,,\ d^{(39,2)}_{-2,3,-1} = -2\,,\ d^{(39,2)}_{-1,-2,3} = -2,$$
$$d^{(39,2)}_{-1,-1,2} = 18\,,\ d^{(39,2)}_{-1,0,1} = -16\,,\ d^{(39,2)}_{-1,1,0} = -16\,,\ d^{(39,2)}_{-1,2,-1} = 18\,,\ d^{(39,2)}_{-1,3,-2} = -2\,,\ d^{(39,2)}_{0,-2,2} = 8,$$
$$d^{(39,2)}_{0,-1,1} = -16\,,\ d^{(39,2)}_{0,0,0} = 32\,,\ d^{(39,2)}_{0,1,-1} = -16\,,\ d^{(39,2)}_{0,2,-2} = 8\,,\ d^{(39,2)}_{1,-2,1} = -12\,,\ d^{(39,2)}_{1,-1,0} = -16,$$
$$d^{(39,2)}_{1,0,-1} = -16\,,\ d^{(39,2)}_{1,1,-2} = -12\,,\ d^{(39,2)}_{2,-2,0} = 8\,,\ d^{(39,2)}_{2,-1,-1} = 18\,,\ d^{(39,2)}_{2,0,-2} = 8\,,\ d^{(39,2)}_{3,-2,-1} = -2,$$
$$d^{(39,2)}_{3,-1,-2} = -2, \tag{4.180}$$

$$p^{(39,3)}_{0,0,3} = 48\,,\ p^{(39,3)}_{0,1,2} = -48\,,\ p^{(39,3)}_{0,2,1} = -48\,,\ p^{(39,3)}_{0,3,0} = 48\,,\ p^{(39,3)}_{1,0,2} = -48\,,\ p^{(39,3)}_{1,1,1} = 192,$$
$$p^{(39,3)}_{1,2,0} = -48\,,\ p^{(39,3)}_{2,0,1} = -48\,,\ p^{(39,3)}_{2,1,0} = -48\,,\ p^{(39,3)}_{3,0,0} = 48, \tag{4.181}$$

$$q^{(39,3)}_{-1,0,3} = 8\,,\ q^{(39,3)}_{-1,1,2} = -24\,,\ q^{(39,3)}_{-1,2,1} = 24\,,\ q^{(39,3)}_{-1,3,0} = -8\,,\ q^{(39,3)}_{0,-1,3} = 8\,,\ q^{(39,3)}_{0,0,2} = 128\,,\ q^{(39,3)}_{0,1,1} = -72,$$
$$q^{(39,3)}_{0,2,0} = -64\,,\ q^{(39,3)}_{1,-1,2} = -24\,,\ q^{(39,3)}_{1,0,1} = -72\,,\ q^{(39,3)}_{1,1,0} = 144\,,\ q^{(39,3)}_{2,-1,1} = 24\,,\ q^{(39,3)}_{2,0,0} = -64,$$
$$q^{(39,3)}_{3,-1,0} = -8, \tag{4.182}$$

$$r^{(39,3)}_{0,-1,3} = 8\,,\ r^{(39,3)}_{0,0,2} = 64\,,\ r^{(39,3)}_{0,1,1} = -144\,,\ r^{(39,3)}_{0,2,0} = 64\,,\ r^{(39,3)}_{0,3,-1} = 8\,,\ r^{(39,3)}_{1,-1,2} = -24\,,\ r^{(39,3)}_{1,0,1} = 72,$$
$$r^{(39,3)}_{1,1,0} = 72\,,\ r^{(39,3)}_{1,2,-1} = -24\,,\ r^{(39,3)}_{2,-1,1} = 24\,,\ r^{(39,3)}_{2,0,0} = -128\,,\ r^{(39,3)}_{2,1,-1} = 24\,,\ r^{(39,3)}_{3,-1,0} = -8,$$
$$r^{(39,3)}_{3,0,-1} = -8, \tag{4.183}$$

$$d^{(54,1)}_{-1,0,-1} = 4\,,\ d^{(54,1)}_{0,-1,-1} = -4, \tag{4.184}$$

$$p^{(54,2)}_{0,1,0} = 24\,,\ p^{(54,2)}_{1,0,0} = -24, \tag{4.185}$$

$$q^{(54,2)}_{-2,-1,3} = -2\,,\ q^{(54,2)}_{-2,0,2} = 6\,,\ q^{(54,2)}_{-2,1,1} = -6\,,\ q^{(54,2)}_{-2,2,0} = 2\,,\ q^{(54,2)}_{-1,-2,3} = 2\,,\ q^{(54,2)}_{-1,0,1} = 14\,,\ q^{(54,2)}_{-1,1,0} = -16,$$
$$q^{(54,2)}_{0,-2,2} = -6\,,\ q^{(54,2)}_{0,-1,1} = -14\,,\ q^{(54,2)}_{1,-2,1} = 6\,,\ q^{(54,2)}_{1,-1,0} = 16\,,\ q^{(54,2)}_{2,-2,0} = -2, \tag{4.186}$$

$$r^{(54,2)}_{-2,-1,3}=-1\,,\ r^{(54,2)}_{-2,0,2}=4\,,\ r^{(54,2)}_{-2,1,1}=-6\,,\ r^{(54,2)}_{-2,2,0}=4\,,\ r^{(54,2)}_{-2,3,-1}=-1\,,\ r^{(54,2)}_{-1,-2,3}=1\,,\ r^{(54,2)}_{-1,0,1}=2,$$
$$r^{(54,2)}_{-1,1,0}=-8\,,\ r^{(54,2)}_{-1,2,-1}=5\,,\ r^{(54,2)}_{0,-2,2}=-2\,,\ r^{(54,2)}_{0,-1,1}=-12\,,\ r^{(54,2)}_{0,0,0}=26\,,\ r^{(54,2)}_{0,1,-1}=-4\,,\ r^{(54,2)}_{1,-1,0}=8,$$
$$r^{(54,2)}_{1,0,-1}=-4\,,\ r^{(54,2)}_{2,-2,0}=2\,,\ r^{(54,2)}_{2,-1,-1}=5\,,\ r^{(54,2)}_{3,-2,-1}=-1, \tag{4.187}$$

$$s^{(54,0)}_{-2,-1,-1}=-1\,,\ s^{(54,0)}_{-1,-2,-1}=1\,. \tag{4.188}$$

4.1.C.2 Some massless quark loop limits

Here we give the explicit limits for the massless quark loop in the regimes where two momenta become much larger than the other, this is a subset of the regions where λ becomes small. In order to find them, we change the variables to one of the large momenta, the small one and the angle between them. We then expand in the small over the large momentum. All negative powers of λ cancel and the leading contribution in the ratio of small over large momentum is always independent of the angle and is given below. The choice of third variable is not unique, however the results to the order given are always the same.

$Q_1 \sim Q_3 \gg Q_2$

$$\frac{\pi^2\hat{\Pi}_1}{e_q^4 N_c} = -\frac{1}{9Q_1^4}\left[3\log\left(\frac{Q_1^2}{Q_2^2}\right)+5\right], \tag{4.189}$$
$$\frac{\pi^2\hat{\Pi}_4}{e_q^4 N_c} = -\frac{1}{3Q_2^2Q_1^2}, \tag{4.190}$$
$$\frac{\pi^2\hat{\Pi}_7}{e_q^4 N_c} = -\frac{1}{3Q_2^2Q_1^4}, \tag{4.191}$$
$$\frac{\pi^2\hat{\Pi}_{17}}{e_q^4 N_c} = \frac{1}{18Q_1^6}\left[6\log\left(\frac{Q_1^2}{Q_2^2}\right)-5\right], \tag{4.192}$$
$$\frac{\pi^2\hat{\Pi}_{39}}{e_q^4 N_c} = \frac{1}{3Q_2^2Q_1^4}, \tag{4.193}$$
$$\frac{\pi^2\hat{\Pi}_{54}}{e_q^4 N_c} = -\frac{1}{6Q_2^2Q_1^4}. \tag{4.194}$$

$Q_1 \sim Q_2 \gg Q_3$

$$\frac{\pi^2\hat{\Pi}_1}{e_q^4 N_c} = -\frac{1}{Q_3^2 Q_2^2}\,, \tag{4.195}$$

$$\frac{\pi^2\hat{\Pi}_4}{e_q^4 N_c} = -\frac{1}{3Q_2^4}\,, \tag{4.196}$$

$$\frac{\pi^2\hat{\Pi}_7}{e_q^4 N_c} = -\frac{1}{3Q_2^6}\,, \tag{4.197}$$

$$\frac{\pi^2\hat{\Pi}_{17}}{e_q^4 N_c} = \frac{1}{3Q_3^2 Q_2^4}\,, \tag{4.198}$$

$$\frac{\pi^2\hat{\Pi}_{39}}{e_q^4 N_c} = \frac{1}{3Q_3^2 Q_2^4}\,, \tag{4.199}$$

$$\frac{\pi^2\hat{\Pi}_{54}}{e_q^4 N_c} = \mathcal{O}(Q_2^{-7})\,. \tag{4.200}$$

$Q_2 \sim Q_3 \gg Q_1$

$$\frac{\pi^2\hat{\Pi}_1}{e_q^4 N_c} = -\frac{1}{9Q_3^4}\left[3\log\left(\frac{Q_3^2}{Q_1^2}\right)+5\right]\,, \tag{4.201}$$

$$\frac{\pi^2\hat{\Pi}_4}{e_q^4 N_c} = -\frac{1}{3Q_1^2 Q_3^2}\,, \tag{4.202}$$

$$\frac{\pi^2\hat{\Pi}_7}{e_q^4 N_c} = \mathcal{O}(Q_3^{-5})\,, \tag{4.203}$$

$$\frac{\pi^2\hat{\Pi}_{17}}{e_q^4 N_c} = \frac{1}{18Q_3^6}\left[6\log\left(\frac{Q_3^2}{Q_1^2}\right)-5\right]\,, \tag{4.204}$$

$$\frac{\pi^2\hat{\Pi}_{39}}{e_q^4 N_c} = \frac{1}{3Q_1^2 Q_3^4}\,, \tag{4.205}$$

$$\frac{\pi^2\hat{\Pi}_{54}}{e_q^4 N_c} = \frac{1}{6Q_1^2 Q_3^4}\,. \tag{4.206}$$

4.1.C.3 Contributions from diagrams with one-cut quark lines

The explicit expressions of the $\hat{\Pi}_i$ for the one-cut quark line diagrams can be written as

$$\hat{\Pi}_m = e_q^4 \sum_{i,j,k,n,p} c_{i,j,k}^{m,n,p}\, m_q^n\, X_p\; Q_1^{-2i} Q_2^{-2j} Q_3^{-2k}\,, \tag{4.207}$$

where the non-zero coefficients are

$$c_{-1,2,3}^{1,0,8} = 4\,,\; c_{0,1,3}^{1,0,8} = -4\,,\; c_{0,2,2}^{1,0,8} = -\frac{8}{3}\,,\; c_{1,0,3}^{1,0,8} = -4\,,\; c_{1,2,1}^{1,0,8} = -\frac{16}{3}\,,\; c_{2,-1,3}^{1,0,8} = 4\,,\; c_{2,0,2}^{1,0,8} = -\frac{8}{3},$$
$$c_{2,1,1}^{1,0,8} = -\frac{16}{3}, \tag{4.208}$$

$$c_{-1,2,3}^{1,0,7} = -\frac{4}{3}\,,\; c_{0,1,3}^{1,0,7} = \frac{4}{3}\,,\; c_{1,0,3}^{1,0,7} = \frac{4}{3}\,,\; c_{2,-1,3}^{1,0,7} = -\frac{4}{3}, \tag{4.209}$$

$$c^{1,1,5}_{-1,2,3} = \frac{4}{3}\,,\ c^{1,1,5}_{0,1,3} = -4\,,\ c^{1,1,5}_{1,0,3} = -4\,,\ c^{1,1,5}_{1,2,1} = -8\,,\ c^{1,1,5}_{2,-1,3} = \frac{4}{3}\,,\ c^{1,1,5}_{2,1,1} = -8\,,\ c^{1,1,5}_{2,2,0} = -\frac{4}{3}, \tag{4.210}$$

$$c^{1,1,4}_{-1,2,3} = -\frac{4}{3}\,,\ c^{1,1,4}_{0,1,3} = -\frac{4}{3}\,,\ c^{1,1,4}_{1,0,3} = -\frac{4}{3}\,,\ c^{1,1,4}_{1,2,1} = -8\,,\ c^{1,1,4}_{2,-1,3} = -\frac{4}{3}\,,\ c^{1,1,4}_{2,1,1} = -8\,,\ c^{1,1,4}_{2,2,0} = \frac{20}{3}, \tag{4.211}$$

$$c^{1,1,3}_{-1,2,3} = -\frac{8}{3}\,,\ c^{1,1,3}_{0,1,3} = \frac{16}{3}\,,\ c^{1,1,3}_{1,0,3} = \frac{16}{3}\,,\ c^{1,1,3}_{1,2,1} = 8\,,\ c^{1,1,3}_{2,-1,3} = -\frac{8}{3}\,,\ c^{1,1,3}_{2,1,1} = 8\,,\ c^{1,1,3}_{2,2,0} = \frac{4}{3}, \tag{4.212}$$

$$c^{1,1,2}_{0,1,2} = -4\,,\ c^{1,1,2}_{1,0,2} = -4\,,\ c^{1,1,2}_{1,1,1} = 4 \tag{4.213}$$

$$\begin{aligned} &c^{1,3,2}_{-1,2,3} = -\frac{8}{3}\,,\ c^{1,3,2}_{0,1,3} = 8\,,\ c^{1,3,2}_{0,2,2} = 8\,,\ c^{1,3,2}_{1,0,3} = 8\,,\ c^{1,3,2}_{1,2,1} = -8\,,\ c^{1,3,2}_{2,-1,3} = -\frac{8}{3}\,,\ c^{1,3,2}_{2,0,2} = 8, \\ &c^{1,3,2}_{2,1,1} = -8\,,\ c^{1,3,2}_{2,2,0} = \frac{8}{3}, \end{aligned} \tag{4.214}$$

$$\begin{aligned} &c^{4,0,8}_{-1,3,2} = -\frac{4}{3}\,,\ c^{4,0,8}_{0,2,2} = -\frac{8}{3}\,,\ c^{4,0,8}_{0,3,1} = -\frac{4}{3}\,,\ c^{4,0,8}_{1,1,2} = -\frac{32}{3}\,,\ c^{4,0,8}_{1,2,1} = -\frac{16}{3}\,,\ c^{4,0,8}_{1,3,0} = -\frac{8}{3}\,,\ c^{4,0,8}_{2,0,2} = -\frac{8}{3}, \\ &c^{4,0,8}_{2,1,1} = -\frac{16}{3}\,,\ c^{4,0,8}_{2,2,0} = -\frac{8}{3}\,,\ c^{4,0,8}_{2,3,-1} = -\frac{8}{3}\,,\ c^{4,0,8}_{3,-1,2} = -\frac{4}{3}\,,\ c^{4,0,8}_{3,0,1} = -\frac{4}{3}\,,\ c^{4,0,8}_{3,1,0} = -\frac{8}{3}\,,\ c^{4,0,8}_{3,2,-1} = -\frac{8}{3}, \end{aligned} \tag{4.215}$$

$$c^{4,0,7}_{0,2,2} = \frac{4}{3}\,,\ c^{4,0,7}_{2,0,2} = \frac{4}{3}, \tag{4.216}$$

$$\begin{aligned} &c^{4,1,5}_{-1,3,2} = -4\,,\ c^{4,1,5}_{0,2,2} = \frac{4}{3}\,,\ c^{4,1,5}_{0,3,1} = -4\,,\ c^{4,1,5}_{1,1,2} = -16\,,\ c^{4,1,5}_{1,2,1} = -8\,,\ c^{4,1,5}_{1,3,0} = -4\,,\ c^{4,1,5}_{2,0,2} = \frac{4}{3}, \\ &c^{4,1,5}_{2,1,1} = -8\,,\ c^{4,1,5}_{2,3,-1} = -4\,,\ c^{4,1,5}_{3,-1,2} = -4\,,\ c^{4,1,5}_{3,0,1} = -4\,,\ c^{4,1,5}_{3,1,0} = -4\,,\ c^{4,1,5}_{3,2,-1} = -4, \end{aligned} \tag{4.217}$$

$$\begin{aligned} &c^{4,1,4}_{1,1,2} = -16\,,\ c^{4,1,4}_{1,2,1} = -8\,,\ c^{4,1,4}_{1,3,0} = -4\,,\ c^{4,1,4}_{2,1,1} = -8\,,\ c^{4,1,4}_{2,2,0} = 8\,,\ c^{4,1,4}_{2,3,-1} = -4\,,\ c^{4,1,4}_{3,1,0} = -4, \\ &c^{4,1,4}_{3,2,-1} = -4, \end{aligned} \tag{4.218}$$

$$\begin{aligned} &c^{4,1,3}_{-1,3,2} = 4\,,\ c^{4,1,3}_{0,3,1} = 4\,,\ c^{4,1,3}_{1,1,2} = 16\,,\ c^{4,1,3}_{1,2,1} = 8\,,\ c^{4,1,3}_{1,3,0} = 4\,,\ c^{4,1,3}_{2,1,1} = 8\,,\ c^{4,1,3}_{2,3,-1} = 4, \\ &c^{4,1,3}_{3,-1,2} = 4\,,\ c^{4,1,3}_{3,0,1} = 4\,,\ c^{4,1,3}_{3,1,0} = 4\,,\ c^{4,1,3}_{3,2,-1} = 4, \end{aligned} \tag{4.219}$$

$$c^{4,1,2}_{1,1,1} = 8, \tag{4.220}$$

$$c^{4,3,2}_{0,2,2} = \frac{16}{3}\,,\ c^{4,3,2}_{1,1,2} = -16\,,\ c^{4,3,2}_{1,2,1} = -8\,,\ c^{4,3,2}_{2,0,2} = \frac{16}{3}\,,\ c^{4,3,2}_{2,1,1} = -8\,,\ c^{4,3,2}_{2,2,0} = 8, \tag{4.221}$$

$$c^{7,0,8}_{0,3,2} = -\frac{8}{3}\,,\ c^{7,0,8}_{2,3,0} = -\frac{16}{3}\,,\ c^{7,0,8}_{3,0,2} = \frac{8}{3}\,,\ c^{7,0,8}_{3,2,0} = -\frac{8}{3}, \tag{4.222}$$

$$c^{7,1,5}_{0,3,2} = -8\,,\ c^{7,1,5}_{2,3,0} = -8\,,\ c^{7,1,5}_{3,0,2} = 8\,,\ c^{7,1,5}_{3,2,0} = -8, \tag{4.223}$$

$$c^{7,1,4}_{2,3,0} = -8, \tag{4.224}$$

$$c^{7,1,3}_{0,3,2} = 8\,,\ c^{7,1,3}_{2,3,0} = 8\,,\ c^{7,1,3}_{3,0,2} = -8\,,\ c^{7,1,3}_{3,2,0} = 8, \tag{4.225}$$

$$\begin{aligned} &c^{17,0,8}_{0,2,3} = -\frac{28}{3}\,,\ c^{17,0,8}_{0,3,2} = \frac{4}{3}\,,\ c^{17,0,8}_{1,1,3} = -\frac{32}{3}\,,\ c^{17,0,8}_{1,2,2} = -\frac{16}{3}\,,\ c^{17,0,8}_{2,0,3} = -\frac{28}{3}\,,\ c^{17,0,8}_{2,1,2} = -\frac{16}{3}, \\ &c^{17,0,8}_{2,2,1} = \frac{16}{3}\,,\ c^{17,0,8}_{2,3,0} = -\frac{4}{3}\,,\ c^{17,0,8}_{3,0,2} = \frac{4}{3}\,,\ c^{17,0,8}_{3,2,0} = -\frac{4}{3}, \end{aligned} \tag{4.226}$$

$$c^{17,0,7}_{0,2,3} = \frac{8}{3}\,,\ c^{17,0,7}_{2,0,3} = \frac{8}{3}, \tag{4.227}$$

$$c^{17,1,5}_{0,2,3} = -\frac{8}{3}\,,\ c^{17,1,5}_{1,1,3} = -16\,,\ c^{17,1,5}_{1,2,2} = -8\,,\ c^{17,1,5}_{2,0,3} = -\frac{8}{3}\,,\ c^{17,1,5}_{2,1,2} = -8\,,\ c^{17,1,5}_{2,2,1} = 8, \tag{4.228}$$

$$\begin{aligned} &c^{17,1,4}_{0,2,3} = -\frac{4}{3}\,,\ c^{17,1,4}_{0,3,2} = 4\,,\ c^{17,1,4}_{1,1,3} = -16\,,\ c^{17,1,4}_{1,2,2} = -8\,,\ c^{17,1,4}_{2,0,3} = -\frac{4}{3}\,,\ c^{17,1,4}_{2,1,2} = -8, \\ &c^{17,1,4}_{2,2,1} = 8\,,\ c^{17,1,4}_{2,3,0} = -4\,,\ c^{17,1,4}_{3,0,2} = 4\,,\ c^{17,1,4}_{3,2,0} = -4, \end{aligned} \tag{4.229}$$

$$c^{17,1,3}_{0,2,3} = \frac{16}{3}\,,\ c^{17,1,3}_{1,1,3} = 16\,,\ c^{17,1,3}_{1,2,2} = 8\,,\ c^{17,1,3}_{2,0,3} = \frac{16}{3}\,,\ c^{17,1,3}_{2,1,2} = 8\,,\ c^{17,1,3}_{2,2,1} = -8, \tag{4.230}$$

$$c^{17,1,2}_{1,1,2} = 8, \tag{4.231}$$

$$c_{0,2,3}^{17,3,2}=\frac{16}{3}\,,\ c_{1,1,3}^{17,3,2}=-16\,,\ c_{1,2,2}^{17,3,2}=-8\,,\ c_{2,0,3}^{17,3,2}=\frac{16}{3}\,,\ c_{2,1,2}^{17,3,2}=-8\,,\ c_{2,2,1}^{17,3,2}=8, \tag{4.232}$$

$$c_{0,2,3}^{39,0,8}=4\,,\ c_{0,3,2}^{39,0,8}=4\,,\ c_{2,0,3}^{39,0,8}=4\,,\ c_{2,3,0}^{39,0,8}=4\,,\ c_{3,0,2}^{39,0,8}=4\,,\ c_{3,2,0}^{39,0,8}=4, \tag{4.233}$$

$$c_{0,2,3}^{39,1,5}=8\,,\ c_{0,3,2}^{39,1,5}=8\,,\ c_{2,0,3}^{39,1,5}=8\,,\ c_{2,3,0}^{39,1,5}=8\,,\ c_{3,0,2}^{39,1,5}=8\,,\ c_{3,2,0}^{39,1,5}=8, \tag{4.234}$$

$$c_{0,2,3}^{39,1,4}=8\,,\ c_{0,3,2}^{39,1,4}=8\,,\ c_{2,0,3}^{39,1,4}=8\,,\ c_{2,3,0}^{39,1,4}=8\,,\ c_{3,0,2}^{39,1,4}=8\,,\ c_{3,2,0}^{39,1,4}=8, \tag{4.235}$$

$$c_{0,2,3}^{39,1,3}=-8\,,\ c_{0,3,2}^{39,1,3}=-8\,,\ c_{2,0,3}^{39,1,3}=-8\,,\ c_{2,3,0}^{39,1,3}=-8\,,\ c_{3,0,2}^{39,1,3}=-8\,,\ c_{3,2,0}^{39,1,3}=-8, \tag{4.236}$$

$$\begin{aligned}&c_{0,2,3}^{54,0,8}=-\frac{4}{3}\,,\ c_{0,3,2}^{54,0,8}=\frac{4}{3}\,,\ c_{1,2,2}^{54,0,8}=\frac{16}{3}\,,\ c_{1,3,1}^{54,0,8}=\frac{16}{3}\,,\ c_{2,0,3}^{54,0,8}=\frac{4}{3}\,,\ c_{2,1,2}^{54,0,8}=-\frac{16}{3},\\&c_{2,3,0}^{54,0,8}=\frac{4}{3}\,,\ c_{3,0,2}^{54,0,8}=-\frac{4}{3}\,,\ c_{3,1,1}^{54,0,8}=-\frac{16}{3}\,,\ c_{3,2,0}^{54,0,8}=-\frac{4}{3},\end{aligned} \tag{4.237}$$

$$\begin{aligned}&c_{0,3,2}^{54,1,5}=\frac{4}{3}\,,\ c_{1,2,2}^{54,1,5}=8\,,\ c_{1,3,1}^{54,1,5}=8\,,\ c_{2,1,2}^{54,1,5}=-8\,,\ c_{2,3,0}^{54,1,5}=\frac{4}{3}\,,\ c_{3,0,2}^{54,1,5}=-\frac{4}{3},\\&c_{3,1,1}^{54,1,5}=-8\,,\ c_{3,2,0}^{54,1,5}=-\frac{4}{3},\end{aligned} \tag{4.238}$$

$$\begin{aligned}&c_{0,2,3}^{54,1,4}=-4\,,\ c_{0,3,2}^{54,1,4}=-\frac{8}{3}\,,\ c_{1,2,2}^{54,1,4}=8\,,\ c_{1,3,1}^{54,1,4}=8\,,\ c_{2,0,3}^{54,1,4}=4\,,\ c_{2,1,2}^{54,1,4}=-8,\\&c_{2,3,0}^{54,1,4}=-\frac{8}{3}\,,\ c_{3,0,2}^{54,1,4}=\frac{8}{3}\,,\ c_{3,1,1}^{54,1,4}=-8\,,\ c_{3,2,0}^{54,1,4}=\frac{8}{3},\end{aligned} \tag{4.239}$$

$$\begin{aligned}&c_{0,3,2}^{54,1,3}=-\frac{4}{3}\,,\ c_{1,2,2}^{54,1,3}=-8\,,\ c_{1,3,1}^{54,1,3}=-8\,,\ c_{2,1,2}^{54,1,3}=8\,,\ c_{2,3,0}^{54,1,3}=-\frac{4}{3}\,,\ c_{3,0,2}^{54,1,3}=\frac{4}{3},\\&c_{3,1,1}^{54,1,3}=8\,,\ c_{3,2,0}^{54,1,3}=\frac{4}{3},\end{aligned} \tag{4.240}$$

$$c_{1,2,1}^{54,1,2}=-4\,,\ c_{2,1,1}^{54,1,2}=4 \tag{4.241}$$

$$\begin{aligned}&c_{0,3,2}^{54,3,2}=-\frac{8}{3}\,,\ c_{1,2,2}^{54,3,2}=8\,,\ c_{1,3,1}^{54,3,2}=8\,,\ c_{2,1,2}^{54,3,2}=-8\,,\ c_{2,3,0}^{54,3,2}=-\frac{8}{3}\,,\ c_{3,0,2}^{54,3,2}=\frac{8}{3},\\&c_{3,1,1}^{54,3,2}=-8\,,\ c_{3,2,0}^{54,3,2}=\frac{8}{3}\,.\end{aligned} \tag{4.242}$$

4.1.C.4 Gluon matrix element contributions

Before taking into account the contributions coming from the mixing with other operators, the contributions have the form

$$\hat{\Pi}_{GGm,S} = X_S^6\, e_q^4 \sum_{i,j,k} \left[c_{i,j,k}^{(m)} + f_{i,j,k}^{(m)}\, m_q^{-2} + g_{i,j,k}^{(m)} \log\left(\frac{Q_1^2}{Q_2^2}\right) + h_{i,j,k}^{(m)} \log\left(\frac{Q_3^2}{m_q^2}\right) \right] Q_1^{-2i}\, Q_2^{-2j}\, Q_3^{-2k}\,, \tag{4.243}$$

where

$$\begin{aligned} &c_{-1,2,3}^{(1)} = -\frac{5}{6}\,,\ c_{0,1,3}^{(1)} = \frac{17}{18}\,,\ c_{0,2,2}^{(1)} = \frac{4}{9}\,,\ c_{1,0,3}^{(1)} = \frac{17}{18}\,,\ c_{1,1,2}^{(1)} = \frac{2}{3}\,,\ c_{1,2,1}^{(1)} = \frac{7}{9}, \\ &c_{2,-1,3}^{(1)} = -\frac{5}{6}\,,\ c_{2,0,2}^{(1)} = \frac{4}{9}\,,\ c_{2,1,1}^{(1)} = \frac{7}{9}\,,\ c_{2,2,0}^{(1)} = \frac{7}{18}, \end{aligned} \tag{4.244}$$

$$f_{0,1,2}^{(1)} = \frac{1}{18}\,,\ f_{1,0,2}^{(1)} = \frac{1}{18}\,,\ f_{1,1,1}^{(1)} = -\frac{1}{18}, \tag{4.245}$$

$$g_{-1,2,3}^{(1)} = -\frac{2}{9}\,,\ g_{0,1,3}^{(1)} = \frac{2}{9}\,,\ g_{1,0,3}^{(1)} = -\frac{2}{9}\,,\ g_{2,-1,3}^{(1)} = \frac{2}{9}, \tag{4.246}$$

$$h_{-1,2,3}^{(1)} = \frac{2}{9}\,,\ h_{0,1,3}^{(1)} = -\frac{2}{9}\,,\ h_{1,0,3}^{(1)} = -\frac{2}{9}\,,\ h_{2,-1,3}^{(1)} = +\frac{2}{9}, \tag{4.247}$$

$$\begin{aligned} &c_{-1,3,2}^{(4)} = \frac{7}{18}\,,\ c_{0,2,2}^{(4)} = \frac{5}{6}\,,\ c_{0,3,1}^{(4)} = \frac{7}{18}\,,\ c_{1,1,2}^{(4)} = \frac{8}{9}\,,\ c_{1,2,1}^{(4)} = \frac{8}{9}\,,\ c_{1,3,0}^{(4)} = \frac{7}{18}, \\ &c_{2,0,2}^{(4)} = \frac{5}{6}\,,\ c_{2,1,1}^{(4)} = \frac{8}{9}\,,\ c_{2,2,0}^{(4)} = \frac{5}{9}\,,\ c_{2,3,-1}^{(4)} = \frac{7}{18}\,,\ c_{3,-1,2}^{(4)} = \frac{7}{18}\,,\ c_{3,0,1}^{(4)} = \frac{7}{18}, \\ &c_{3,1,0}^{(4)} = \frac{7}{18}\,,\ c_{3,2,-1}^{(4)} = \frac{7}{18}, \end{aligned} \tag{4.248}$$

$$f_{1,1,1}^{(4)} = -\frac{1}{9}, \tag{4.249}$$

$$g_{0,2,2}^{(4)} = \frac{2}{9}\,,\ g_{2,0,2}^{(4)} = -\frac{2}{9}, \tag{4.250}$$

$$h_{0,2,2}^{(4)} = -\frac{2}{9}\,,\ h_{2,0,2}^{(4)} = -\frac{2}{9}, \tag{4.251}$$

$$c_{0,3,2}^{(7)} = \frac{7}{9}\,,\ c_{2,3,0}^{(7)} = \frac{7}{9}\,,\ c_{3,0,2}^{(7)} = -\frac{7}{9}\,,\ c_{3,2,0}^{(7)} = \frac{7}{9}, \tag{4.252}$$

$$c^{(17)}_{0,2,3} = \frac{5}{3}\,,\ c^{(17)}_{1,1,3} = \frac{4}{3}\,,\ c^{(17)}_{1,2,2} = \frac{2}{3}\,,\ c^{(17)}_{2,0,3} = \frac{5}{3}\,,\ c^{(17)}_{2,1,2} = \frac{2}{3}\,,\ c^{(17)}_{2,2,1} = -\frac{4}{9}, \tag{4.253}$$

$$f^{(17)}_{1,1,2} = -\frac{1}{9}, \tag{4.254}$$

$$g^{(17)}_{0,2,3} = \frac{4}{9}\,,\ g^{(17)}_{2,0,3} = -\frac{4}{9}, \tag{4.255}$$

$$h^{(17)}_{0,2,3} = -\frac{4}{9}\,,\ h^{(17)}_{2,0,3} = -\frac{4}{9}, \tag{4.256}$$

$$\begin{aligned} &c^{(39)}_{0,2,3} = -\frac{7}{9}\,,\ c^{(39)}_{0,3,2} = -\frac{7}{9}\,,\ c^{(39)}_{1,2,2} = -\frac{4}{9}\,,\ c^{(39)}_{2,0,3} = -\frac{7}{9}\,,\ c^{(39)}_{2,1,2} = -\frac{4}{9}\,,\ c^{(39)}_{2,2,1} = -\frac{4}{9}, \\ &c^{(39)}_{2,3,0} = -\frac{7}{9}\,,\ c^{(39)}_{3,0,2} = -\frac{7}{9}\,,\ c^{(39)}_{3,2,0} = -\frac{7}{9}, \end{aligned} \tag{4.257}$$

$$\begin{aligned} &c^{(54)}_{0,3,2} = -\frac{5}{18}\,,\ c^{(54)}_{1,2,2} = -\frac{2}{3}\,,\ c^{(54)}_{1,3,1} = -\frac{2}{3}\,,\ c^{(54)}_{2,1,2} = \frac{2}{3}\,,\ c^{(54)}_{2,3,0} = -\frac{5}{18}\,,\ c^{(54)}_{3,0,2} = \frac{5}{18}, \\ &c^{(54)}_{3,1,1} = \frac{2}{3}\,,\ c^{(54)}_{3,2,0} = \frac{5}{18}, \end{aligned} \tag{4.258}$$

$$f^{(54)}_{1,2,1} = \frac{1}{18}\,,\ f^{(54)}_{2,1,1} = -\frac{1}{18}, \tag{4.259}$$

After including the mixing via (4.31), the divergences exactly cancel and the renormalised form factors can be expressed as

$$\hat{\Pi}^R_{GGm} = X_{6,R}\, e_q^4 \sum_{i,j,k} \left[c'^{(m)}_{i,j,k} + g^{(m)}_{i,j,k} \log\left(\frac{Q_1^2}{Q_2^2}\right) + h^{(m)}_{i,j,k} \log\left(\frac{Q_3^2}{\mu^2}\right) \right] Q_1^{-2i}\, Q_2^{-2j}\, Q_3^{-2k}\,, \tag{4.260}$$

where the associated coefficients $g^{(m)}_{i,j,k}$ and $h^{(m)}_{i,j,k}$ are the same as above and

$$\begin{aligned} &c'^{(1)}_{-1,2,3} = -\frac{20}{27}\,,\ c'^{(1)}_{0,1,3} = \frac{20}{27}\,,\ c'^{(1)}_{0,2,2} = \frac{5}{9}\,,\ c'^{(1)}_{1,0,3} = \frac{20}{27}\,,\ c'^{(1)}_{1,1,2} = \frac{2}{3}\,,\ c'^{(1)}_{1,2,1} = \frac{1}{9}, \\ &c'^{(1)}_{2,-1,3} = -\frac{20}{27}\,,\ c'^{(1)}_{2,0,2} = \frac{5}{9}\,,\ c'^{(1)}_{2,1,1} = \frac{1}{9}\,, \end{aligned} \tag{4.261}$$

$$\begin{aligned} &c'^{(4)}_{-1,3,2} = -\frac{1}{18}\,,\ c'^{(4)}_{0,2,2} = \frac{61}{54}\,,\ c'^{(4)}_{0,3,1} = -\frac{1}{18}\,,\ c'^{(4)}_{1,1,2} = -\frac{4}{9}\,,\ c'^{(4)}_{1,2,1} = \frac{2}{9}\,,\ c'^{(4)}_{1,3,0} = \frac{1}{9}, \\ &c'^{(4)}_{2,0,2} = \frac{61}{54}\,,\ c'^{(4)}_{2,1,1} = \frac{2}{9}\,,\ c'^{(4)}_{2,2,0} = \frac{1}{3}\,,\ c'^{(4)}_{2,3,-1} = \frac{1}{9}\,,\ c'^{(4)}_{3,-1,2} = -\frac{1}{18}\,,\ c'^{(4)}_{3,0,1} = -\frac{1}{18}, \\ &c'^{(4)}_{3,1,0} = \frac{1}{9}\,,\ c'^{(4)}_{3,2,-1} = \frac{1}{9}, \end{aligned} \tag{4.262}$$

$$c'^{(7)}_{0,3,2} = -\frac{1}{9}\,,\ c'^{(7)}_{2,3,0} = \frac{2}{9}\,,\ c'^{(7)}_{3,0,2} = \frac{1}{9}\,,\ c'^{(7)}_{3,2,0} = -\frac{1}{9}, \tag{4.263}$$

$$\begin{aligned} &c'^{(17)}_{0,2,3} = \frac{89}{54}\,,\ c'^{(17)}_{0,3,2} = -\frac{1}{6}\,,\ c'^{(17)}_{2,0,3} = \frac{89}{54}\,,\ c'^{(17)}_{2,2,1} = \frac{2}{9}, \\ &c'^{(17)}_{2,3,0} = \frac{1}{6}\,,\ c'^{(17)}_{3,0,2} = -\frac{1}{6}\,,\ c'^{(17)}_{3,2,0} = \frac{1}{6}, \end{aligned} \tag{4.264}$$

$$\begin{aligned} &c'^{(39)}_{0,2,3} = -\frac{1}{18}\,,\ c'^{(39)}_{0,3,2} = -\frac{1}{18}\,,\ c'^{(39)}_{1,2,2} = -\frac{4}{9}\,,\ c'^{(39)}_{2,0,3} = -\frac{1}{18}\,,\ c'^{(39)}_{2,1,2} = -\frac{4}{9}\,,\ c'^{(39)}_{2,2,1} = -\frac{4}{9}, \\ &c'^{(39)}_{2,3,0} = -\frac{1}{18}\,,\ c'^{(39)}_{3,0,2} = -\frac{1}{18}\,,\ c'^{(39)}_{3,2,0} = -\frac{1}{18}, \end{aligned} \tag{4.265}$$

$$c'^{(54)}_{0,2,3} = \frac{1}{6}\,,\ c'^{(54)}_{1,0,0} = -\frac{1}{18}\,,\ c'^{(54)}_{2,0,3} = -\frac{1}{6}\,,\ c'^{(54)}_{2,3,0} = -\frac{1}{18}\,,\ c'^{(54)}_{3,0,2} = \frac{1}{18}\,,\ c'^{(54)}_{3,2,0} = \frac{1}{18}\,. \tag{4.266}$$

4.1.D Derivation of (4.75) up to $n = 3$

Up to the order that we need, we have only contributions either without explicit gauge bosons or with one of them, which can be put together owing to (4.73). Let us start by writing down the expansion coming from the contributions without gauge bosons (see Fig. 4.5a). Starting from (4.13) and using the decomposition (4.77), one trivially finds (up to permutations of the set $P = \{1, 2, 3\}$):

$$\begin{aligned} \Pi^{\mu_1\mu_2\mu_3}_{\rm NB} =& -e_q^3 \sum_A \int \frac{d^4q_3}{(2\pi)^4} \left(\prod_{i=1}^{3} \int d^4x_i\, e^{-iq_i x_i} \right) \langle 0|\bar{q}(x_1) c_A \Gamma^A q(x_3)|\gamma(q_4)\rangle \\ &\times \mathrm{Tr}\Big[\gamma^{\mu_3}\Gamma^A \gamma^{\mu_1} iS(x_1 - x_2)\gamma^{\mu_2} iS(x_2 - x_3) \Big]. \end{aligned} \tag{4.267}$$

Taking Fourier transforms for the propagators, expanding the quark fields according to (4.72), rewriting the outcoming space time variables $x_{i,\mu}$ as $\lim_{p_{iA}\to 0} i\frac{\partial}{\partial p^\mu_{iA}} e^{-ip_{iA}x_i}$, integrating and taking derivatives iteratively using (4.64), one finds:

$$\begin{aligned} \Pi^{\mu_1\mu_2\mu_3}_{\rm NB} =& -e_q^3 \sum_A \sum_{m,n} (-1)^{n+m} \langle 0|\bar{q}\{D^{\nu_1}, \cdots, D^{\nu_n}\}\{D^{\nu'_1}, \cdots, D^{\nu'_m}\} c_A \Gamma^A q|\gamma(q_4)\rangle \\ &\times \mathrm{Tr}\Big[\gamma^{\mu_3}\Gamma^A \gamma^{\mu_1} iS(-q_1)\gamma^{\nu_1} iS(-q_1) \cdots \gamma^{\nu_n} iS(-q_1)\gamma^{\mu_2} iS(q_3)\gamma^{\nu'_1} iS(q_3) \cdots \gamma^{\nu'_m} iS(q_3) \Big], \end{aligned} \tag{4.268}$$

where $\{\}$ indicates symmetrization (normalized by the number of terms) and $q_3 = -q_1 - q_2$.

For the topologies with one gauge boson, the only change with respect to (4.268) is an extra vertex in the quark chain, which can be allocated in two different positions plus the boson field

itself (see Fig. 4.5b):

$$\begin{aligned}\Pi_{\rm B}^{\mu_1\mu_2\mu_3} =& -e_q^3\sum_A\int\frac{d^4q_3}{(2\pi)^4}\int d^4z\left(\prod_{i=1}^3\int d^4x_i\,e^{-iq_ix_i}\right)\langle 0|\bar q(x_1)c_A\Gamma^A(B_\epsilon(z)+ie_qA_\epsilon(z))q(x_3)|\gamma(q_4)\rangle\\ &\times\left(\mathrm{Tr}\Big[\gamma^{\mu_3}\Gamma^A\gamma^{\mu_1}iS(x_1-z)\gamma^\epsilon iS(z-x_2)\gamma^{\mu_2}iS(x_2-x_3)\Big]\right.\\ &\left.+\,\mathrm{Tr}\Big[\gamma^{\mu_3}\Gamma^A\gamma^{\mu_1}iS(x_1-x_2)\gamma^{\mu_2}iS(x_2-z)\gamma^\epsilon iS(z-x_3)\Big]\right).\end{aligned}\tag{4.269}$$

Using (4.73), the matrix element in (4.269) can be rewritten

$$\begin{aligned}\bar q(x_1)\Big(B_\epsilon(u)+ie_qA_\epsilon(u)\Big)q(x_3) =& \sum_{m,n}\frac{(-x_1)^{\nu_1}\cdots(-x_1)^{\nu_n}}{n!}\frac{x_3^{\nu_1'}\cdots x_3^{\nu_m'}}{m!}\\ &\times\sum_{p=1}^{p}\sum_{q=0}\frac{(-1)^{p-q+1}pu^{\omega_1}\cdots u^{\omega_p}}{(p+1)q!(p-q)!}\\ &\times\bar qD^{\nu_1}\cdots D^{\nu_n}D^{\omega_1}\cdots D^{\omega_q}D^\epsilon D^{\omega_{q+1}}\cdots D^{\omega_p}D^{\nu_1'}\cdots D^{\nu_m'}q,\end{aligned}\tag{4.270}$$

from which, following the same procedure as above, the contributions from one gauge boson can be re-expressed as

$$\begin{aligned}\Pi_{\rm B}^{\mu_1\mu_2\mu_3} =& -e_q^3\lim_{p_{1A}\to0}\lim_{p_{2A}\to0}\lim_{p_{3A}\to0}\sum_A\sum_{m,n}\frac{(i\partial_{p_{1A}})^{\nu_1}\cdots(i\partial_{p_{1A}})^{\nu_n}}{n!}\frac{(i\partial_{p_{3A}})^{\nu_1'}\cdots(i\partial_{p_{3A}})^{\nu_m'}}{m!}\\ &\times\sum_{p=1}^{p}\sum_{q=0}\frac{(i\partial_{p_{2A}})^{\omega_1}\cdots(i\partial_{p_{2A}})^{\omega_p}p(-1)^{p-q+1}}{(p+1)q!(p-q)!}\\ &\times\Big(\mathrm{Tr}[\gamma^{\mu_3}\Gamma^A\gamma^{\mu_1}iS(p_1^A-q_1)\gamma^\epsilon iS(p_1^A-p_2^A-q_1)\gamma^{\mu_2}iS(q_3+p_3^A)]\\ &+\mathrm{Tr}[\gamma^{\mu_3}\Gamma^A\gamma^{\mu_1}iS(p_1^A-q_1)\gamma^{\mu_2}iS(p_2^A+p_3^A+q_3)\gamma^\epsilon iS(q_3+p_3^A)]\Big)\\ &\times\langle 0|\bar qD^{\nu_1}\cdots D^{\nu_n}D^{\omega_1}\cdots D^{\omega_q}D^\epsilon D^{\omega_{q+1}}\cdots D^{\omega_p}D^{\nu_1'}\cdots D^{\nu_m'}c_A\Gamma^Aq|\gamma(q_4)\rangle\,.\end{aligned}\tag{4.271}$$

The next simplification consists in realizing that after taking the derivatives and the limits, all the traces start with $\gamma^{\mu_3}\Gamma^A\gamma^{\mu_1}$ and all the propagator on the left of γ^{μ_2} are of the form $S(-q_1)$ and all the propagators on the right are $S(q_3)$, which has a simple diagrammatic interpretation. On the other hand, we can always relabel the dummy Lorentz indices in such a way that the remaining quark current takes as indices $\bar qD^{\nu_1}\cdots D^{\nu_n}q$. Taking all this into account, any possible term in the sum can be uniquely codified as a pre-factor times a set of numbers separated by a "wall" term, v. For example, we define

$$\begin{aligned}3(31v2) \equiv& 3e_q^3\mathrm{Tr}[\gamma^{\mu_3}\Gamma^A\gamma^{\mu_1}iS(-q_1)\gamma^{\nu_3}iS(-q_1)\gamma^{\nu_1}iS(-q_1)\gamma^{\mu_2}iS(q_3)\gamma^{\nu_2}iS(q_3)]\\ &\times\langle 0|\bar qD_{\nu_1}\cdots D_{\nu_3}c_A\Gamma^Aq|\gamma(q_4)\rangle\,,\end{aligned}\tag{4.272}$$

where we have dropped the index A on the LHS since the Lorentz structure of the various traces does not depend on it. In this symbolic notation, one finds respectively, for $n=0$ ($D=3$) and

$n = 1$ ($D = 4$), using (4.268),

$$\Pi^{\mu_1\mu_2\mu_3}_{D=3} = -(v)\,, \tag{4.273}$$

$$\Pi^{\mu_1\mu_2\mu_3}_{D=4} = (1v) + (v1)\,. \tag{4.274}$$

From the same equation, the $n = 2$ ($D = 5$) piece coming from the topology without gauge bosons (NB) is

$$\Pi^{\mu_1\mu_2\mu_3}_{D=5,\mathrm{NB}} = -(1v2) - \frac{1}{2}[(v12) + (21v) + (v21) + (12v)]\,, \tag{4.275}$$

while the bosonic piece B leads, using (4.271), to

$$\Pi^{\mu_1\mu_2\mu_3}_{D=5,\mathrm{B}} = \frac{1}{2}[(21v) - (12v) + (v21) - (v12)]\,. \tag{4.276}$$

Summing, one finds

$$\Pi^{\mu_1\mu_2\mu_3}_{D=5} = -[(1v2) + (v12) + (12v)]\,. \tag{4.277}$$

Finally, for $n = 3$, using (4.268), one finds

$$\begin{aligned}\Pi^{\mu_1\mu_2\mu_3}_{D=6,\mathrm{NB}} = \frac{1}{6}[&(123v) + (132v) + (213v) + (231v) + (312v) + (321v)\\ &+ (v123) + (v132) + (v213) + (v231) + (v312) + (v321)]\\ &+ \frac{1}{2}[(12v3) + (21v3)] + \frac{1}{2}[(1v23) + (1v32)]\,.\end{aligned} \tag{4.278}$$

From (4.271), the contributions of the same order that come from $p = 2$ are

$$\begin{aligned}\Pi^{\mu_1\mu_2\mu_3}_{D=6,\mathrm{B1}} = \frac{1}{3}[&(123v) + (132v) + (213v) + (231v) + (312v) + (321v)\\ &+ (v123) + (v132) + (v213) + (v231) + (v312) + (v321)]\\ &- (213v) - (231v) - (v312) - (v132)\,,\end{aligned} \tag{4.279}$$

from $p = n = 1$

$$\Pi^{\mu_1\mu_2\mu_3}_{D=6\mathrm{B2}} = \frac{1}{2}[(123v) + (213v) + (231v) + (1v32) - (132v) - (312v) - (321v) - (1v23)]\,, \tag{4.280}$$

and from $p = m = 1$

$$\Pi^{\mu_1\mu_2\mu_3}_{D=6,\mathrm{B3}} = -\frac{1}{2}[(v213) + (v321) + (v231) - (v123) - (v321) - (v132) - (12v3) + (21v3)]\,. \tag{4.281}$$

Summing all of them

$$\Pi^{\mu_1\mu_2\mu_3}_{D=6} = \Pi^{\mu_1\mu_2\mu_3}_{D=6,\mathrm{NB+B1+B2+B3}} = [(123v) + (12v3) + (1v23) + (v123)]\,. \tag{4.282}$$

This simplification occurs for every Dirac structure Γ^A and therefore also for their sum. This completes the needed derivation. We conjecture that the duality holds at all dimensions[16] and that its trivial generalization holds for any number of external legs, greatly simplifying calculations for this kind of topology.

[16] We have explicitly checked that it holds for some specific (simpler to prove) higher-order coefficients ($1234v$, $12345v$, $123456v$ and $1234567v$) when two and three gauge bosons are incorporated.

4.2 The two-loop perturbative correction to the $(g-2)_\mu$ HLbL at short distances

This section is a copy of Ref. [38], published in the Journal of High-Energy Physics (JHEP) on April 26, 2021

Authors: Johan Bijnens, Nils Hermansson–Truedsson, Laetitia Laub, Antonio Rodríguez–Sánchez

---

Abstract: The short-distance behaviour of the hadronic light-by-light (HLbL) contribution to $(g-2)_\mu$ has recently been studied by means of an operator product expansion in a background electromagnetic field. The leading term in this expansion has been shown to be given by the massless quark loop, and the non-perturbative corrections are numerically very suppressed. Here, we calculate the perturbative QCD correction to the massless quark loop. The correction is found to be fairly small compared to the quark loop as far as we study energy scales where the perturbative running for the QCD coupling is well-defined, i.e. for scales $\mu \gtrsim 1\,\text{GeV}$. This should allow to reduce the large systematic uncertainty associated to high-multiplicity hadronic states.

4.2.1 Introduction

The muon anomalous magnetic moment is one of the most precise measurements in particle physics. The world average [4] for the anomaly $a_\mu = (g-2)/2$ is

$$a_\mu^{\text{exp}} = 116\ 592\ 089(54)(33) \times 10^{-11}\,. \tag{4.283}$$

The experimental accuracy is expected to improve with the now running experiment at Fermilab [6] and the planned experiment at J-PARC [104]. The Standard Model prediction [4] is

$$a_\mu^{\text{SM}} = 116\ 591\ 810(43) \times 10^{-11}\,. \tag{4.284}$$

The difference between this and the experimental value from Brookhaven National Laboratory [5] is

$$\Delta a_\mu \equiv a_\mu^{\text{exp}} - a_\mu^{\text{SM}} = 279(76) \times 10^{-11}\,, \tag{4.285}$$

or a 3.7σ discrepancy. In light of this discrepancy and the expected improved experimental accuracy it is important that the theoretical accuracy is checked as much as possible. The QED [57, 59] and the electroweak contribution [60, 61] are precise enough for the foreseeable future. The error is dominated by the hadronic contributions, the hadronic vacuum polarization [7–9, 11–13, 62] is at present the largest theory uncertainty but is steadily being improved. The remaining part, the hadronic light-by-light (HLbL) contribution is at present [4]

$$a_\mu^{\text{HLbL}} = 92(18) \times 10^{-11}. \tag{4.286}$$

This number contains the next-to-leading (NLO) HLbL contribution [63] and the average of the lattice [24] and phenomenological evaluation of the lowest-order HLbL. In the remainder we will use HLbL as a synonym for the LO part only, this contribution is depicted in Fig. 4.11. The

number in (4.286) is in good agreement with the older estimates [106–108,147,148] and the more recent Glasgow consensus [149] but with a smaller and much better understood error.

The phenomenological estimate of the HLbL [4],

$$a_\mu^{\text{HLbL-phen}} = 92(19) \times 10^{-11}, \tag{4.287}$$

uses the methods of Ref. [77] to separate different contributions. The pole contributions from π^0, η, η' [26,28,29] as well as the two-pion box and rescattering and two-kaon box contribution [27] are well-understood and together give

$$a_\mu^{\text{HLbL-1}} = 69.4(4.1) \times 10^{-11}\,. \tag{4.288}$$

The main uncertainty comes from the intermediate and short-distance domain. Heavier intermediate states have been considered in Refs. [31–36]. The heavy-quark contribution from charm is sufficiently well estimated from the quark loop and estimates of non-perturbative contributions and that of the bottom and top quarks are negligible [4,30,39,116]. The light-quark contribution can be estimated using the quark loop and/or higher resonance exchanges and leads to [4]

$$a_\mu^{\text{HLbL-SD1}} = 20(19) \times 10^{-11}. \tag{4.289}$$

The large error is due to the large uncertainty of which resonances to include and that their couplings to two off-shell photons are badly known [4]. In addition one needs to make sure that there is a proper matching with the short-distance QCD constraints.

Some short-distance constraints are used in determining the form-factors needed in the contributions from hadrons directly, see e.g. Ref. [109]. Here we discuss instead the short-distance constraints on the hadronic function defined in (4.290) and depicted as the shaded blob in Fig. 4.11. First attempts at matching the short-distance were using the quark loop and matching it on a long-distance contribution from the extended Nambu-Jona-Lasinio model [107]. The quark loop itself has a long history of being used in this context, see e.g. Ref. [110–115]. The first proper short-distance constraint was derived in Ref. [2]. It is valid in the regime where two of the internal photons have a virtuality much larger than the third one. Recent work in the latter regime includes Refs. [30, 39–43, 83, 105, 150].

This paper is concerned with the limit where all virtualities of the internal photon lines in Fig. 4.11 are large. The underlying problem here is that the external photon, corresponding to the magnetic field, has zero momentum, i.e. $q_4 \to 0$ in Fig. 4.11. The usual operator product expansion (OPE) in vacuum [91] corresponds to all four photon virtualities large and diverges when setting $q_4 \to 0$. The solution was found in Ref. [1]. One needs to use an alternative OPE in a background magnetic field as was done for the QCD sum rule calculations of nucleon magnetic moments [117, 118]. This method was earlier used in the context of the electroweak contribution to a_μ [60]. The first order term in this expansion corresponds to the massless quark loop [1], the next order is suppressed by quark masses and the small value of the magnetic susceptibility [1, 37]. For the non-perturbative part of this OPE the contribution suppressed by up to four powers of large momenta compared to the leading term have been evaluated in Ref. [37]. There are a number of subtleties involved and large number of expectation values in a magnetic field needed to be evaluated. The conclusion from [1, 37] is that the contribution

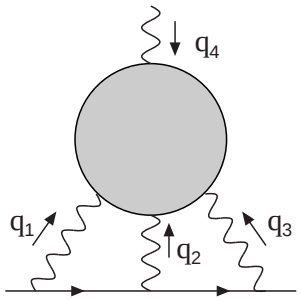

Figure 4.11: The HLbL contribution to the $(g-2)_\mu$.

from these higher orders in the non-perturbative part are small. The remaining uncertainty from this regime is the perturbative correction from gluon exchange to the massless quark loop. This paper performs that calculation. The putting together of this work with the other short-distance constraint [2] and the parts calculated using hadronic methods is deferred to future work.

In Sec. 4.2.2 we recall the main definitions needed for the calculation of the HLbL part of a_μ. We define here a set of intermediate quantities, the $\tilde{\Pi}_i$ that are both ultraviolet and infrared finite. From these we then determine the quantities $\hat{\Pi}_i$ that are needed to calculate a_μ. The main procedure of the calculation is described in Sec. 4.2.3. Sec. 4.2.4 gives the numerical results and discusses implications. We reiterate our main results in Sec. 4.2.5. A number of technical issues are relegated to the the appendices. The final result is too large to include in the manuscript but is included as supplementary material [151].

4.2.2 The HLbL tensor and $a_\mu^{\mathbf{HLbL}}$

The HLbL tensor $\Pi^{\mu_1\mu_2\mu_3\mu_4}$ is a 4-point correlation function of electromagnetic currents $J^\mu(x) = \bar{q}(x)\, Q_q \gamma^\mu q(x)$, where the quark fields are collected in $q = (u, d, s)$ and the corresponding charge matrix is $Q_q = \mathrm{diag}(e_q) = \mathrm{diag}(2/3, -1/3, -1/3)$. The correlator in question is defined via

$$\Pi^{\mu_1\mu_2\mu_3\mu_4} = -i \int \frac{d^4q_4}{(2\pi)^4} \left(\prod_{i=1}^{4} \int d^4x_i\, e^{-iq_ix_i} \right) \langle 0|T \left(\prod_{j=1}^{4} J^{\mu_j}(x_j) \right) |0\rangle \,, \tag{4.290}$$

where the q_i are the momenta of the external photon legs. This definition is slightly unconventional but allows to exploit more of the symmetries, as remarked in Ref. [37]. The contribution from the HLbL tensor to the $(g-2)_\mu$ is depicted in Fig. 4.11. It involves a loop integration over q_1, q_2 and q_3, whereas the fourth leg is in the static limit, i.e. $q_4 \to 0$.

The HLbL tensor satisfies the Ward identities $q_{i,\,\mu_i}\, \Pi^{\mu_1\mu_2\mu_3\mu_4} = 0$ for $i = 1, 2, 3, 4$, which implies [119]

$$\Pi^{\mu_1\mu_2\mu_3\mu_4} = -q_{4,\,\nu_4} \frac{\partial \Pi^{\mu_1\mu_2\mu_3\nu_4}}{\partial q_{4,\,\mu_4}} \,. \tag{4.291}$$

The whole information about the HLbL is then contained in its derivative. In fact, in the $(g-2)_\mu$ kinematics,

$$\lim_{q_4 \to 0} \frac{\partial \Pi^{\mu_1\mu_2\mu_3\nu_4}}{\partial q_4^{\mu_4}} \,, \tag{4.292}$$

there are only 19 independent Lorentz structures, which can be found by applying 19 independent

projectors $P^{\tilde{\Pi}_i}_{\mu_1\mu_2\mu_3\mu_4\nu_4}$, this according to

$$\tilde{\Pi}_i = P^{\tilde{\Pi}_i}_{\mu_1\mu_2\mu_3\mu_4\nu_4} \lim_{q_4\to 0} \frac{\partial \Pi^{\mu_1\mu_2\mu_3\nu_4}}{\partial q_4^{\mu_4}} \,. \tag{4.293}$$

A possible set of projectors is

$$P^{\tilde{\Pi}_1}_{\mu_1\mu_2\mu_3\mu_4\nu_4} = g_{\mu_1\mu_2}\, g_{\mu_3\nu_4}\, q_{1,\mu_4} \,, \tag{4.294}$$
$$P^{\tilde{\Pi}_2}_{\mu_1\mu_2\mu_3\mu_4\nu_4} = g_{\mu_2\mu_3}\, g_{\mu_1\nu_4}\, q_{2,\mu_4} \,, \tag{4.295}$$
$$P^{\tilde{\Pi}_3}_{\mu_1\mu_2\mu_3\mu_4\nu_4} = g_{\mu_3\mu_1}\, g_{\mu_2\nu_4}\, q_{3,\mu_4} \,, \tag{4.296}$$
$$P^{\tilde{\Pi}_4}_{\mu_1\mu_2\mu_3\mu_4\nu_4} = g_{\mu_2\mu_1}\, g_{\mu_3\nu_4}\, q_{2,\mu_4} \,, \tag{4.297}$$
$$P^{\tilde{\Pi}_5}_{\mu_1\mu_2\mu_3\mu_4\nu_4} = g_{\mu_3\mu_2}\, g_{\mu_1\nu_4}\, q_{3,\mu_4} \,, \tag{4.298}$$
$$P^{\tilde{\Pi}_6}_{\mu_1\mu_2\mu_3\mu_4\nu_4} = g_{\mu_1\mu_3}\, g_{\mu_2\nu_4}\, q_{1,\mu_4} \,, \tag{4.299}$$

$$P^{\tilde{\Pi}_7}_{\mu_1\mu_2\mu_3\mu_4\nu_4} = g_{\mu_1\nu_4}\, g_{\mu_2\mu_4}\, q_{2,\mu_3} \,, \tag{4.300}$$
$$P^{\tilde{\Pi}_8}_{\mu_1\mu_2\mu_3\mu_4\nu_4} = g_{\mu_2\nu_4}\, g_{\mu_3\mu_4}\, q_{3,\mu_1} \,, \tag{4.301}$$
$$P^{\tilde{\Pi}_9}_{\mu_1\mu_2\mu_3\mu_4\nu_4} = g_{\mu_3\nu_4}\, g_{\mu_1\mu_4}\, q_{1,\mu_2} \,, \tag{4.302}$$

$$P^{\tilde{\Pi}_{10}}_{\mu_1\mu_2\mu_3\mu_4\nu_4} = g_{\mu_1\mu_2}\, q_{1,\mu_3} q_{1,\nu_4}\, q_{2,\mu_4} \,, \tag{4.303}$$
$$P^{\tilde{\Pi}_{11}}_{\mu_1\mu_2\mu_3\mu_4\nu_4} = g_{\mu_2\mu_3}\, q_{2,\mu_1} q_{2,\nu_4}\, q_{3,\mu_4} \,, \tag{4.304}$$
$$P^{\tilde{\Pi}_{12}}_{\mu_1\mu_2\mu_3\mu_4\nu_4} = g_{\mu_3\mu_1}\, q_{3,\mu_2} q_{3,\nu_4}\, q_{1,\mu_4} \,, \tag{4.305}$$

$$P^{\tilde{\Pi}_{13}}_{\mu_1\mu_2\mu_3\mu_4\nu_4} = g_{\mu_1\nu_4}\, q_{1,\mu_2} q_{2,\mu_3}\, q_{3,\mu_4} \,, \tag{4.306}$$
$$P^{\tilde{\Pi}_{14}}_{\mu_1\mu_2\mu_3\mu_4\nu_4} = g_{\mu_2\nu_4}\, q_{2,\mu_3} q_{3,\mu_1}\, q_{1,\mu_4} \,, \tag{4.307}$$
$$P^{\tilde{\Pi}_{15}}_{\mu_1\mu_2\mu_3\mu_4\nu_4} = g_{\mu_3\nu_4}\, q_{3,\mu_1} q_{1,\mu_2}\, q_{2,\mu_4} \,, \tag{4.308}$$
$$P^{\tilde{\Pi}_{16}}_{\mu_1\mu_2\mu_3\mu_4\nu_4} = g_{\mu_2\nu_4}\, q_{2,\mu_1} q_{1,\mu_3}\, q_{3,\mu_4} \,, \tag{4.309}$$
$$P^{\tilde{\Pi}_{17}}_{\mu_1\mu_2\mu_3\mu_4\nu_4} = g_{\mu_3\nu_4}\, q_{3,\mu_2} q_{2,\mu_1}\, q_{1,\mu_4} \,, \tag{4.310}$$
$$P^{\tilde{\Pi}_{18}}_{\mu_1\mu_2\mu_3\mu_4\nu_4} = g_{\mu_1\nu_4}\, q_{1,\mu_3} q_{3,\mu_2}\, q_{2,\mu_4} \,, \tag{4.311}$$

$$P^{\tilde{\Pi}_{19}}_{\mu_1\mu_2\mu_3\mu_4\nu_4} = q_{3,\mu_1} q_{1,\mu_2}\, q_{2,\mu_3} q_{1,\nu_4}\, q_{2,\mu_4} \,, \tag{4.312}$$

which has been built in such a way that, combined with the crossing symmetries of the HLbL tensor, the $\tilde{\Pi}$ satisfy the following crossing symmetries

$$\begin{aligned}
&\tilde{\Pi}_1 = C_{12}[\tilde{\Pi}_4], \tilde{\Pi}_2 = C_{12}[\tilde{\Pi}_6], \tilde{\Pi}_3 = C_{12}[\tilde{\Pi}_5], \tilde{\Pi}_7 = C_{12}[\tilde{\Pi}_7], \tilde{\Pi}_8 = C_{12}[\tilde{\Pi}_9], \tilde{\Pi}_{10} = C_{12}[\tilde{\Pi}_{10}],\\
&\tilde{\Pi}_{11} = C_{12}[\tilde{\Pi}_{12}], \tilde{\Pi}_{13} = C_{12}[\tilde{\Pi}_{16}], \tilde{\Pi}_{14} = C_{12}[\tilde{\Pi}_{18}], \tilde{\Pi}_{15} = C_{12}[\tilde{\Pi}_{17}], \tilde{\Pi}_{19} = C_{12}[\tilde{\Pi}_{19}],\\
&\tilde{\Pi}_1 = C_{13}[\tilde{\Pi}_5], \tilde{\Pi}_2 = C_{13}[\tilde{\Pi}_4], \tilde{\Pi}_3 = C_{13}[\tilde{\Pi}_6], \tilde{\Pi}_7 = C_{13}[\tilde{\Pi}_8], \tilde{\Pi}_9 = C_{13}[\tilde{\Pi}_9], \tilde{\Pi}_{10} = C_{13}[\tilde{\Pi}_{11}],\\
&\tilde{\Pi}_{12} = C_{13}[\tilde{\Pi}_{12}], \tilde{\Pi}_{13} = C_{13}[\tilde{\Pi}_{17}], \tilde{\Pi}_{14} = C_{13}[\tilde{\Pi}_{16}], \tilde{\Pi}_{15} = C_{13}[\tilde{\Pi}_{18}], \tilde{\Pi}_{19} = C_{13}[\tilde{\Pi}_{19}].
\end{aligned} \tag{4.313}$$

The operator C_{ij} interchanges two momenta q_i and q_j. Notice how, from the knowledge of five of them, for example $\tilde{\Pi}_{1,7,10,13,19}$, one can easily infer the rest from these crossing symmetries.

These $\tilde{\Pi}_i$ are well-defined and are both ultraviolet and infrared finite to the order in α we are working. For our calculation we use two different sets of $\tilde{\Pi}_i$, related by gauge invariance, which thus provides a cross-check of our results.

An OPE is only valid for large Euclidean momenta [91]. As a consequence, it cannot be directly applied to the tensor in (4.290) for the $(g-2)_\mu$ kinematics, since by definition the external photon is soft, $q_4 \to 0$, even though the other Euclidean momenta are large, $-q_i^2 \equiv Q_i^2 \gg \Lambda^2_{\rm QCD}$ [1,37]. However, precisely the same fact allows one to connect the tensor in (4.290) to the OPE of the tensor operator with the background photon field

$$\Pi^{\mu_1\mu_2\mu_3}(q_1,q_2) = -\frac{1}{e}\int \frac{d^4q_3}{(2\pi)^4}\left(\prod_{i=1}^{3}\int d^4x_i\, e^{-iq_ix_i}\right)\langle 0|T\left(\prod_{j=1}^{3} J^{\mu_j}(x_j)\right)|\gamma(q_4)\rangle\,. \tag{4.314}$$

The OPE in question holds for large photon virtualities $Q_1^2 \sim Q_2^2 \sim Q_3^2 \gg \Lambda^2_{\rm QCD}$. In this expansion, any local operator with the same quantum numbers as $F_{\mu\nu}$, including $F_{\mu\nu}$ itself, can absorb the remaining soft static photon and, as a consequence, give a contribution [1, 37, 60]. Higher-dimensional operators are suppressed by extra powers ofeq:derq4bttTL $\left(\frac{\Lambda_{\rm QCD}}{Q_i}\right)^d$, providing a hierarchy of contributions with a systematic counting. A very detailed study of this OPE can be found in Ref. [37], where the different power corrections were computed and found to be small compared to the leading contribution[17]. The leading term comes from the $F_{\mu\nu}$ operator itself and is given by the massless quark loop at order α_s^0, and the leading mass effects are very small. In fact, this quark loop corresponds to the zero momentum limit of the derivative of the naive massless perturbative QCD tensor of (4.290), i.e.

$$\lim_{q_4\to 0}\frac{\partial\Pi^{\mu_1\mu_2\mu_3\nu_4}_{\rm pert}}{\partial q_4^{\mu_4}}\,. \tag{4.315}$$

In this work, we compute the leading α_s correction to the direct $F_{\mu\nu}$ contribution in the OPE of (4.314). This corresponds to a two-loop massless QCD calculation with three external legs off-shell.

Before discussing the gluonic correction to the quark loop in the next section, we first write down the quark loop result for the $\tilde{\Pi}_i$ basis. As will be remarked upon below, this basis was not

[17] Obviously, the results of this expansion cannot be applied to the whole integral domain of (4.323), but it can be used, apart from matching resonance models, for directly evaluating the significant contributions coming from the regions were the OPE is valid.

used in Ref. [37]. The whole solution for the quark loop can be simply written as

$$\begin{aligned}
\frac{\pi^2\tilde{\Pi}_1}{N_c e_q^4} &= C_{123}(0)\left(Q_3^2 - Q_1^2\right) - 1 + Q_2^{-2}\,Q_3^2 + 2\,Q_2^2\,Q_3^{-2} - Q_1^2\,Q_2^{-2} - 2\,Q_1^2\,Q_3^{-2} \\
&\quad + \log\frac{Q_2^2}{Q_3^2}\,\left(1 - Q_2^2\,Q_3^{-2} - Q_1^2\,Q_3^{-2}\right) \\
&\quad + \log\frac{Q_1^2}{Q_3^2}\,\left(-\frac{5}{2} + \frac{1}{2}\,Q_2^{-2}\,Q_3^2 + Q_2^2\,Q_3^{-2} + \frac{1}{2}\,Q_1^2\,Q_2^{-2} + Q_1^2\,Q_3^{-2}\right), \qquad (4.316) \\
\frac{\pi^2\tilde{\Pi}_7}{N_c e_q^4} &= C_{123}(0)\left(Q_3^2 - Q_2^2 - Q_1^2\right) \\
&\quad + \log\frac{Q_2^2}{Q_3^2}\,\left(-1 - Q_2^2\,Q_3^{-2} + Q_1^2\,Q_3^{-2}\right) + \log\frac{Q_1^2}{Q_3^2}\,\left(-1 + Q_2^2\,Q_3^{-2} - Q_1^2\,Q_3^{-2}\right), \qquad (4.317) \\
\frac{\pi^2\tilde{\Pi}_{10}}{N_c e_q^4} &= C_{123}(0)\left(\frac{1}{2}\,Q_3^4 - \frac{1}{2}\,Q_2^2\,Q_3^2 - \frac{1}{2}\,Q_1^2\,Q_3^2 + Q_1^2\,Q_2^2\right) \\
&\quad - \frac{1}{2}\,Q_3^2 + Q_2^2 - \frac{1}{2}\,Q_2^4\,Q_3^{-2} + Q_1^2 + Q_1^2\,Q_2^2\,Q_3^{-2} - \frac{1}{2}\,Q_1^4\,Q_3^{-2} \\
&\quad + \log\frac{Q_2^2}{Q_3^2}\,\left(-\frac{3}{4}\,Q_3^2 - \frac{1}{2}\,Q_2^2 + \frac{1}{4}\,Q_2^4\,Q_3^{-2} + Q_1^2 - \frac{1}{4}\,Q_1^4\,Q_3^{-2}\right) \\
&\quad + \log\frac{Q_1^2}{Q_3^2}\,\left(-\frac{3}{4}\,Q_3^2 + Q_2^2 - \frac{1}{4}\,Q_2^4\,Q_3^{-2} - \frac{1}{2}\,Q_1^2 + \frac{1}{4}\,Q_1^4\,Q_3^{-2}\right), \qquad (4.318) \\
\frac{\pi^2\tilde{\Pi}_{13}}{N_c e_q^4} &= C_{123}(0)\left(\frac{1}{2}\,Q_3^4 - \frac{1}{2}\,Q_2^4 - Q_1^2\,Q_3^2 + \frac{1}{2}\,Q_1^2\,Q_2^2\right) \\
&\quad + \frac{1}{4}\,Q_2^{-2}\,Q_3^4 - \frac{1}{2}\,Q_3^2 + \frac{1}{4}\,Q_2^2 - \frac{1}{2}\,Q_1^2\,Q_2^{-2}\,Q_3^2 - \frac{1}{2}\,Q_1^2 + \frac{1}{4}\,Q_1^4\,Q_2^{-2} \\
&\quad + \log\frac{Q_2^2}{Q_3^2}\,\left(-\frac{1}{4}\,Q_3^2 - \frac{7}{4}\,Q_2^2 + \frac{3}{4}\,Q_1^2\right) \\
&\quad + \log\frac{Q_1^2}{Q_3^2}\,\left(-Q_3^2 + Q_2^2 + \frac{1}{4}\,Q_1^2\,Q_2^{-2}\,Q_3^2 + \frac{1}{4}\,Q_1^2 - \frac{1}{4}\,Q_1^4\,Q_2^{-2}\right), \qquad (4.319) \\
\frac{\pi^2\tilde{\Pi}_{19}}{N_c e_q^4} &= C_{123}(0)\Big(-\frac{1}{4}\,Q_3^6 + \frac{1}{4}\,Q_2^2\,Q_3^4 + \frac{1}{4}\,Q_2^4\,Q_3^2 - \frac{1}{4}\,Q_2^6 + \frac{1}{4}\,Q_1^2\,Q_3^4 - \frac{3}{2}\,Q_1^2\,Q_2^2\,Q_3^2 + \frac{1}{4}\,Q_1^2\,Q_2^4 \\
&\quad + \frac{1}{4}\,Q_1^4\,Q_3^2 + \frac{1}{4}\,Q_1^4\,Q_2^2 - \frac{1}{4}\,Q_1^6\Big) \\
&\quad + \frac{1}{2}\,Q_3^4 - Q_2^2\,Q_3^2 + \frac{1}{2}\,Q_2^4 - Q_1^2\,Q_3^2 - Q_1^2\,Q_2^2 + \frac{1}{2}\,Q_1^4 \\
&\quad + \log\frac{Q_2^2}{Q_3^2}\,\left(\frac{1}{2}\,Q_3^4 + \frac{1}{2}\,Q_2^2\,Q_3^2 - Q_2^4 - Q_1^2\,Q_3^2 + \frac{1}{2}\,Q_1^2\,Q_2^2 + \frac{1}{2}\,Q_1^4\right) \\
&\quad + \log\frac{Q_1^2}{Q_3^2}\,\left(\frac{1}{2}\,Q_3^4 - Q_2^2\,Q_3^2 + \frac{1}{2}\,Q_2^4 + \frac{1}{2}\,Q_1^2\,Q_3^2 + \frac{1}{2}\,Q_1^2\,Q_2^2 - Q_1^4\right). \qquad (4.320)
\end{aligned}$$

Here N_c is the number of colours and $C_{123}(0)$ is a loop integral function that is defined in App. 4.2.A.

For the $(g-2)_\mu$ integration, it is convenient using the generic results of Refs. [27, 37, 77]. Following them, the HLbL tensor can be expanded in a basis of 54 scalar functions Π_i weighted with Lorentz structures $T_i^{\mu_1\mu_2\mu_3\mu_4}$,

$$\Pi^{\mu_1\mu_2\mu_3\mu_4} = \sum_{i=1}^{54} T_i^{\mu_1\mu_2\mu_3\mu_4}\Pi_i\,. \qquad (4.321)$$

Using

$$\lim_{q_4\to 0}\frac{\partial\Pi^{\mu_1\mu_2\mu_3\nu_4}}{\partial q_4^{\mu_4}} = \lim_{q_4\to 0}\sum_{i=1}^{54}\frac{\partial T_i^{\mu_1\mu_2\mu_3\nu_4}}{\partial q_4^{\mu_4}}\,\Pi_i\,, \tag{4.322}$$

the 19 $\tilde{\Pi}_i$ defined in (4.293) can be identified with the static $q_4 \to 0$ limit of certain linear combinations of the Π_i. Denoting these linear combinations $\hat{\Pi}_i$ it can further be shown that for a_μ^{HLbL} only six $\hat{\Pi}_i$ contribute, namely $\hat{\Pi}_{1,4,7,17,39,54}$.[18] In particular, the a_μ^{HLbL} may be written [27, 77]

$$a_\mu^{\mathrm{HLbL}} = \frac{2\alpha^3}{3\pi^2}\int_0^\infty dQ_1\int_0^\infty dQ_2\int_{-1}^1 d\tau\,\sqrt{1-\tau^2}\,Q_1^3Q_2^3\sum_{i=1}^{12}T_i(Q_1,Q_2,\tau)\,\overline{\Pi}_i(Q_1,Q_2,\tau)\,. \tag{4.323}$$

The integration variable τ is defined via $Q_3^2 = Q_1^2+Q_2^2+2\tau\,Q_1Q_2$, the $T_i(Q_1,Q_2,\tau)$ are functions and the $\overline{\Pi}_i$ are functions of the six $\hat{\Pi}_i$. The latter set of functions is related to the $\hat{\Pi}_i$ through

$$\begin{aligned}
&\overline{\Pi}_1 = \hat{\Pi}_1\,,\ \overline{\Pi}_2 = C_{23}\left[\hat{\Pi}_1\right]\,,\ \overline{\Pi}_3 = \hat{\Pi}_4\,,\ \overline{\Pi}_4 = C_{23}\left[\hat{\Pi}_4\right]\,,\\
&\overline{\Pi}_5 = \hat{\Pi}_7\,,\ \overline{\Pi}_6 = C_{12}\left[C_{13}\left[\hat{\Pi}_7\right]\right]\,,\ \overline{\Pi}_7 = C_{23}\left[\hat{\Pi}_7\right]\,,\\
&\overline{\Pi}_8 = C_{13}\left[\hat{\Pi}_{17}\right]\,,\ \overline{\Pi}_9 = \hat{\Pi}_{17}\,,\ \overline{\Pi}_{10} = \hat{\Pi}_{39}\,,\\
&\overline{\Pi}_{11} = -C_{23}\left[\hat{\Pi}_{54}\right]\,,\ \overline{\Pi}_{12} = \hat{\Pi}_{54}\,.
\end{aligned} \tag{4.324}$$

In summary, knowledge of $\hat{\Pi}_{1,4,7,17,39,54}$ is enough to determine a_μ^{HLbL} from (4.323). The $\hat{\Pi}_i$ can be obtained from the derivative of the HLbL tensor in the static limit with the projectors given in Ref. [37]. There we defined

$$\hat{\Pi}_i = P_{\hat{\Pi}_i\mu_1\mu_2\mu_3\mu_4\nu_4}\lim_{q_4\to 0}\frac{\partial\Pi^{\mu_1\mu_2\mu_3\nu_4}}{\partial q_{4,\mu_4}}\,. \tag{4.325}$$

with the projectors $P_{\hat{\Pi}_i\mu_1\mu_2\mu_3\mu_4\nu_4}$ given in App. A of [37]. Using the definitions of the $\tilde{\Pi}$ in (4.293) the relation between the $\hat{\Pi}$ and the $\tilde{\Pi}$ follows immediately. We have checked that this procedure reproduces the massless quark loop results as given in Ref. [37]. The $\tilde{\Pi}_i$ representation of the massless quark loop was given in (4.316)–(4.320), and it can be noted that it is much simpler than the expressions for the $\hat{\Pi}_i$ in Ref. [37].

4.2.3 The two-loop perturbative correction

In this section we present the calculation of the two-loop contribution. For the analytic calculation we use FORM [141]. The master integral reduction is done by means of Kira [144], which employs a Laporta algorithm to reach a minimal set of master integrals. Explicit analytic expressions of the master integrals can be found in the literature.

The gluonic corrections to the quark loop are obtained by including two quark-gluon vertices

[18] Using the set of projectors defined in Ref. [37], the identification of these $\hat{\Pi}_i$ as combinations of the $\tilde{\Pi}_i$ is straightforward.

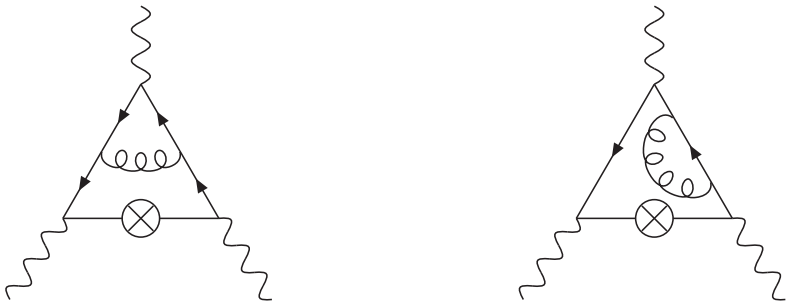

Figure 4.12: Two examples of the two-loop perturbative topologies. The external static photon has been indicated by a crossed vertex.

from the Dyson series expansion in (4.290), i.e.

$$\Pi^{\mu_1\mu_2\mu_3\mu_4} = -i\int \frac{d^4q_3}{(2\pi)^4}\left(\prod_{i=1}^{4}\int d^4x_i\, e^{-iq_ix_i}\right) \times \langle 0|T\left(\prod_{j=1}^{4} J^{\mu_j}(x_j)\frac{1}{2}\int d^4z_1\, d^4z_2\, i\mathcal{L}_{\rm int}^{\rm qgq}(z_1)\, i\mathcal{L}_{\rm int}^{\rm qgq}(z_2)\right)|0\rangle\,. \tag{4.326}$$

Denoting colour indices with bars, the interaction Lagrangians above are of the form

$$\mathcal{L}_{\rm int}^{\rm qgq}(z_i) = g_S\frac{\lambda^{a_i}_{\bar\gamma_i\bar\delta_i}}{2}B^{a_i}_{\nu_i}(z_i)\,\bar q^{\bar\gamma_i}(z_i)\gamma^{\nu_i}q^{\bar\delta_i}(z_i)\,, \tag{4.327}$$

where $B^{a_i}_{\nu_i}$ is the gluon field, g_S is the strong coupling and λ^{a_i} is an $SU(3)_c$ Gell-Mann matrix. The only nonzero topology at this order is obtained by connecting all the quarks to the same line. Two examples of the diagrams in question are shown in Fig. 4.12. As a consequence of the topology, both the quark electric charge e_q^4 and the colour factor, $\mathrm{Tr}(\lambda^a\lambda^b)\delta_{ab} = 2(N_c^2-1)$, can be factored out, allowing to re-express the total contribution as a sum of all possible hexagons where two of the external lines are to be contracted to form the second loop, i.e.,

$$\Pi^{\mu_1\mu_2\mu_3\mu_4} = \frac{(N_c^2-1)g_s^2e_q^4}{4}\int\frac{d^4q_5}{(2\pi)^4}\frac{g_{\mu_5\mu_6}}{q_5^2}\lim_{q_6\to -q_5}H^{\mu_1\mu_2\mu_3\mu_4\mu_5\mu_6}\,, \tag{4.328}$$

where

$$H^{\mu_1\mu_2\mu_3\mu_4\mu_5\mu_6} \equiv \int\frac{d^4p}{(2\pi)^4}\sum_{\sigma(1,2,4,5,6)}\mathrm{Tr}\Big(\gamma^{\mu_3}S(p+q_1+q_2+q_4+q_5+q_6)\gamma^{\mu_1}S(p+q_2+q_4+q_5+q_6) \times\gamma^{\mu_2}S(p+q_4+q_5+q_6)\gamma^{\mu_4}S(p+q_5+q_6)\gamma^{\mu_5}S(p+q_6)\gamma^{\mu_6}S(p)\Big)\,. \tag{4.329}$$

Here, $S(p) = \frac{\not p}{p^2}$ is the massless quark propagator and $\sigma(1,2,4,5,6)$ the set of pairwise permutations of μ_i and q_i for $i = 1,\ 2,\ 3,\ 5,\ 6$. The corresponding $\tilde\Pi_i$ for the two loops are

$$\begin{aligned}\tilde\Pi_i &= P^{\tilde\Pi_i}_{\mu_1\mu_2\mu_3\mu_4\nu_4}\lim_{q_4\to 0}\frac{\partial\Pi^{\mu_1\mu_2\mu_3\nu_4}}{\partial q_4^{\mu_4}}\\ &= -\frac{(N_c^2-1)g_s^2e_q^4}{4}\int\frac{d^4q_5}{(2\pi)^4}\frac{g_{\mu_5\mu_6}}{q_5^2}\lim_{\substack{q_4\to 0\\ q_6\to -q_5}}P^{\tilde\Pi_i}_{\mu_1\mu_2\mu_3\mu_4\nu_4}\frac{\partial}{\partial q_4^{\nu_4}}H^{\mu_1\mu_2\mu_3\mu_4\mu_5\mu_6}\,.\end{aligned} \tag{4.330}$$

$i_1, ..., i_7$	$M(i_1, ..., i_7)$
$1, 1, 0, 1, 1, 0, 0$	B_1^2
$1, 0, 1, 1, 0, 1, 0$	B_2^2
$0, 1, 1, 0, 1, 1, 0$	B_3^2
$1, 0, 1, 1, 1, 0, 0$	$B_1 B_2$
$0, 1, 1, 1, 1, 0, 0$	$B_1 B_3$
$0, 1, 1, 1, 0, 1, 0$	$B_2 B_3$
$1, 1, 1, 1, 1, 0, 0$	$B_1 C_{123}$
$1, 1, 1, 1, 0, 1, 0$	$B_2 C_{123}$
$1, 1, 1, 0, 1, 1, 0$	$B_3 C_{123}$
$0, 1, 0, 1, 0, 0, 1$	S_1
$0, 0, 1, 1, 0, 0, 1$	S_2
$0, 0, 1, 0, 1, 0, 1$	S_3
$0, 0, 1, 1, 1, 0, 1$	V_{123}
$0, 0, 1, 1, 1, 0, 2$	$\dot{V}_{123}$
$1, 0, 1, 0, 1, 0, 1$	V_{213}
$1, 0, 1, 0, 1, 0, 2$	$\dot{V}_{213}$
$0, 1, 1, 1, 0, 0, 1$	V_{312}
$0, 1, 1, 1, 0, 0, 2$	$\dot{V}_{312}$
$0, 1, 1, 1, 0, 1, 1$	W_{123}
$0, 1, 1, 1, 1, 0, 1$	W_{213}
$1, 0, 1, 1, 1, 0, 1$	W_{312}
$1, 1, 1, 1, 1, 1, 0$	C_{123}^2

Table 4.2: List of master integrals $M(i_1, ..., i_7)$ needed for the massless fully off-shell triangle at two-loop order. The last one is not needed at this order.

After taking the derivative, using

$$\frac{\partial}{\partial q_4^{\nu_4}} S(p+q_4) = -S(p+q_4)\gamma_{\nu_4} S(p+q_4)\,, \tag{4.331}$$

the limit $q_4 \to 0$ and the projectors, we have for every $\tilde{\Pi}_i$ a large set of scalar two-loop integrals depending on two external momenta, q_1, and q_2, which can be parametrized as

$$M(i_1, ..., i_7) = \frac{1}{i^2} \int \frac{d^d p_1}{(2\pi)^d} \int \frac{d^d p_2}{(2\pi)^d} \frac{1}{p_1^{2i_1}(p_1-q_1)^{2i_2}(p_1+q_2)^{2i_3} p_2^{2i_4}(p_2-q_1)^{2i_5}(p_2+q_2)^{2i_6}(p_1-p_2)^{2i_7}}\,. \tag{4.332}$$

Using KIRA [144] they can be reduced to the ones in Table 4.2, whose corresponding topologies are represented in Fig. 4.13. This reduction is done in $d = 4 - 2\epsilon \neq 4$ dimensions.

This is a good point to discuss how we handle renomalization and regularization. Both ultraviolet and infrared divergences are regulated using dimensional regularization. We work to the lowest order in α and to first order in α_S in the massless quark limit. There are no counterterms needed to this order and infrared divergences must vanish since the three photon

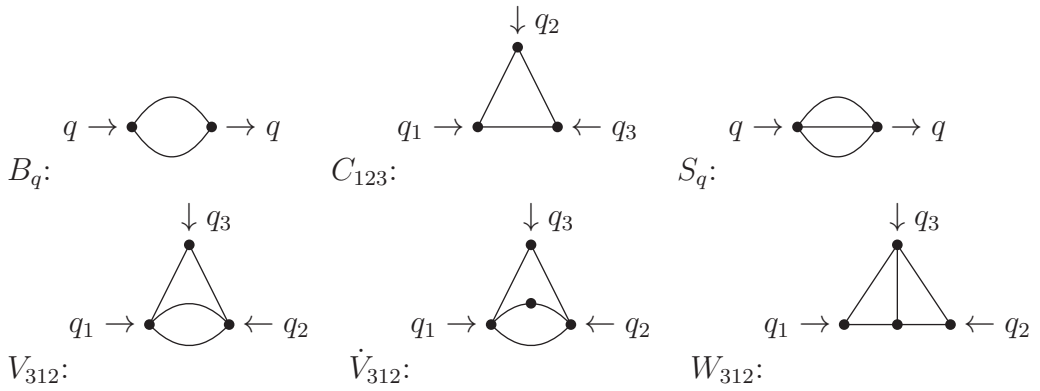

Figure 4.13: Master integrals appearing in the two-loop calculation. The dot on the propagator in $\dot{V}_{312}$ corresponds to a doubling of that propagator.

amplitude vanishes because of charge-conjugation. However, individual diagrams and master integral can be infrared and ultraviolet divergent. The quantities $\tilde{\Pi}_i$ are finite and the cancellation of all divergences, up to $1/\epsilon^3$ provides another good check on our calculations.

Strong efforts have been made to successfully obtain compact analytical expressions for all those two-loop integrals. All of the appearing master integrals can be found in terms of classical polylogarithms in Refs. [152, 153] up to the order that we need. They are collected together with their corresponding ϵ expansions in App. 4.2.A. Using these we find, as expected, that all the intermediate divergences exactly cancel, leading to a result of the following form

$$\begin{aligned}\tilde{\Pi}_m = {} & f^{pqr}_{m,ijk} F_{ijk}(2) Q_1^{2p} Q_2^{2q} Q_3^{2r} + w^{pqr}_{m,ijk} W_{ijk}(0) Q_1^{2p} Q_2^{2q} Q_3^{2r} + c^{pqr}_{m,ijk} C_{ijk}(0) Q_1^{2p} Q_2^{2q} Q_3^{2r} \\ & + n^{pqr}_{m,1} Q_1^{2p} Q_2^{2q} Q_3^{2r} \log \frac{Q_1^2}{Q_3^2} + n^{pqr}_{m,2} Q_1^{2p} Q_2^{2q} Q_3^{2r} C_{ijk}(0) \log \frac{Q_2^2}{Q_3^2} \\ & + l^{pqr}_{m,ijk1} Q_1^{2p} Q_2^{2q} Q_3^{2r} C_{ijk}(0) \log \frac{Q_1^2}{Q_3^2} + l_{m,ijk2} Q_1^{2p} Q_2^{2q} Q_3^{2r} C_{ijk}(0) \log \frac{Q_2^2}{Q_3^2} \,. \end{aligned} \tag{4.333}$$

The remaining loop functions, $C_{ijk}(0), W_{ijk}(0), F_{ijk}(2)$ can also be found in App. 4.2.A. The explicit numerical coefficients can be found in the file `pitildes.txt` of the supplementary material. In Table 4.3 we give numerical results for them in a benchmark point, $(Q_1^2, Q_2^2, Q_3^2) = (1, 1.3, 1.7)$ GeV^2, giving also the analogous quark loop ones for comparison. The loop corrections are found of the order of $\sim -\frac{\alpha_s}{\pi}$, i.e. they are found to be small as far as α_s is not large. The scale at which α_s should be set is similar to the scale Q^2 at which the $\tilde{\Pi}$ are evaluated. Otherwise, large logarithms $\ln \frac{\mu}{Q_i}$ appearing at higher orders would break the perturbative series. As a consequence, the series are found to be reliable as far as we do not go below $\sim 1\,$GeV.

Taking the linear combinations of the $\tilde{\Pi}_i$ which lead to the $\hat{\Pi}$, one finds analogous expressions for them, but with explicit negative powers of Källén functions $\lambda = (Q_1^2 + Q_2^2 - Q_3^2)^2 - 4Q_1^2 Q_2^2$. They introduce singularities which are, however, spurious. When expanding around them, they cancel against the zeros of the polylogarithms, as explicitly checked in different kinematic limits. Details on these expansions can be found in App. 4.2.A. Numerical values for the $\hat{\Pi}_i$ in the same benchmark point and comparison with the corresponding quark loop are given in Table 4.4. The analytical expressions are too long to be included here and are given in the file `resultsgluon.txt` of the supplementary material. The equivalent results for the massless quark loop are in the file

	$\tilde{\Pi}_1$	$\tilde{\Pi}_7$	$\tilde{\Pi}_{10}$	$\tilde{\Pi}_{13}$	$\tilde{\Pi}_{19}$
Quark loop	−0.0816	0.123	0.0363	0.0274	0.0263
Gluon corrections ($\times\pi/\alpha_s$)	0.0781	−0.136	−0.0376	−0.0398	−0.0411

Table 4.3: Values for the quark loop and gluonic correction contributions to the $\tilde{\Pi}$ in GeV units for a benchmark tuple $(Q_1^2, Q_2^2, Q_3^2) = (1, 1.3, 1.7)$ GeV^2. Sum over the three flavours has been made. The last line is in units of α_s/π.

	$\hat{\Pi}_1$	$\hat{\Pi}_4$	$\hat{\Pi}_7$	$\hat{\Pi}_{17}$	$\hat{\Pi}_{39}$	$\hat{\Pi}_{54}$
Quark loop	−0.0210	−0.0119	−0.00384	0.00386	0.0119	0.000422
Gluon corrections ($\times\pi/\alpha_s$)	0.0178	0.00560	0.00302	−0.00750	−0.0103	−0.000427

Table 4.4: Values for the quark loop and gluonic correction contributions to the $\hat{\Pi}$ in GeV units for a benchmark tuple $(Q_1^2, Q_2^2, Q_3^2) = (1, 1.3, 1.7)$ GeV^2. Sum over the three flavours has been made. The last line is in units of α_s/π.

`resultsquark.txt`. We have, however, included analytical expressions for both the quark loop and gluonic correction at the symmetric point $Q_1 = Q_2 = Q_3$ in App. 4.2.B.

A possible check on our result is taking the limit where one of the virtualities is much smaller than the other two, i.e. the limit of Ref. [2], where it is argued that the leading term should have no corrections. The consequences of this limit for the $\hat{\Pi}_i$ has been analyzed in Ref. [30], where it is shown that only for $\hat{\Pi}_1$ there is an unambiguous prediction. Taking into account the corrections to the OPE of two-photon currents to the axial current, i.e. the axial current gets an extra factor of $1 - \alpha_S/\pi$ [40, 154–156], we see that our result indeed satisfies the arguments of Ref. [2].

4.2.4 Results for the $(g-2)_\mu$ and phenomenological implications

Now that we have the needed gluonic corrections to the $\hat{\Pi}_i$, we can introduce them into (4.323) to calculate their corresponding contributions to $a_\mu^{\rm HLbL}$. Obviously, the identification of the $\hat{\Pi}_i$ with the ones obtained using the OPE only makes sense when such an expansion is valid, i.e., above some cut for the Euclidean momenta, $Q_{1,2,3} > Q_{\rm min}$. We restrict ourselves to those integration regions, keeping in mind that the (dominant) contributions from the remaining regions, necessarily computed with non-perturbative methods, must be added to the ones computed here.

The numerical integration has been done with the VEGAS implementation in the CUBA library, as well as our own implementation of two deterministic algorithms. We have checked that the results agree. The general expressions for the quark loop and the gluonic corrections have large negative powers of λ and become numerically unstable whenever λ is small. We therefore use, as in our previous work for the quark loop [37], expansions whenever that happens. There are six different expansions that need to be done. This is explained in more detail in App. 4.2.B. We have checked that the numerical results are not sensitive to changing the boundaries where we use the different expansions.

We perform the integrals of the $12\,\bar{\Pi}_i$ contributions at different $Q_{\rm min}$, both for the leading OPE

	Quark loop	Gluon corrections ($\frac{\alpha_s}{\pi}$ units)
$\bar{\Pi}_1$	0.0084	−0.0077
$\bar{\Pi}_2$	13.28	−12.30
$\bar{\Pi}_3$	0.78	−0.87
$\bar{\Pi}_4$	−2.25	0.62
$\bar{\Pi}_5$	0.00	0.20
$\bar{\Pi}_6$	2.34	−1.43
$\bar{\Pi}_7$	−0.097	0.056
$\bar{\Pi}_8$	0.035	0.41
$\bar{\Pi}_9$	0.623	−0.87
$\bar{\Pi}_{10}$	1.72	−1.61
$\bar{\Pi}_{11}$	0.696	−1.04
$\bar{\Pi}_{12}$	0.165	−0.16
Total	17.3	−17.0

Table 4.5: Leading contributions to the $(g-2)_\mu$ integration from $Q_{\min} = 1\,\text{GeV}$ in 10^{-11} units.

contribution, the quark loop, and the gluonic corrections. They are displayed for $Q_{\min} = 1$ GeV in Table 4.5.

Consistently with the size of the gluonic corrections found for the $\tilde{\Pi}_i$ in the previous section, we find that they are negative and of order $\frac{\alpha_s}{\pi}$. Given the power fall-off of the contributions of the $\hat{\Pi}$ with respect to the studied energies, the quantitative contribution above some energy cut $Q_{\min}$ is saturated by the regions nearby such a cut. As a consequence, a natural scale to effectively avoid large logarithms in the corresponding perturbative series is $\mu \sim Q_{\min}$, however the exact choice of it is ambiguous. In order to estimate perturbative uncertainties we will vary the scale dependence, a consequence of cutting the series at two-loops or at the first α_S correction, in the interval $\mu^2 \in (\frac{1}{2}, 2)Q^2_{\min}$. At the studied order, the whole scale dependence comes from $\alpha_s(\mu)$. Taking $\alpha_s^{N_f=5}(M_Z)$ from Ref. [94], we run it at five loops to $\alpha_s^{N_f=3}(m_\tau)$.[19] As a further conservative estimates of perturbative uncertainty, we add quadratically the difference obtained by taking the one obtained running from $\alpha_s^{N_f=3}(m_\tau)$ to $\alpha_s^{N_f=3}(Q_{\min})$ with the five loop running (which we take as our central result) with the one obtained keeping $\alpha_s^{N_f=3}$ with a fixed scale, $\mu = m_\tau$, which at the order we are working with is also a legitimate choice. Finally we also add quadratically the subleading uncertainty coming from $\alpha_s^{N_f=5}(M_Z)$.

The result, where we show the quark loop, the gluonic corrections and the obtained uncertainties is shown in Figure 4.14. While in general we consider our uncertainty estimates reliable, we notice that they may be slightly over-conservative in the region just below 1 GeV and over-optimistic just above it. This is a consequence of the sharp break down of the α_s running at $\mu \sim 0.7\,\text{GeV}$ which makes our uncertainty strongly dependent on the exact scale interval chosen to estimate them. In essence, we find that the correction is small and negative and that the series are well-behaved, having a gluonic correction of around -10% above the perturbative breakdown.

[19] We implement the running, in the conventional $\overline{\text{MS}}$ scheme, using RUNDEC [157].

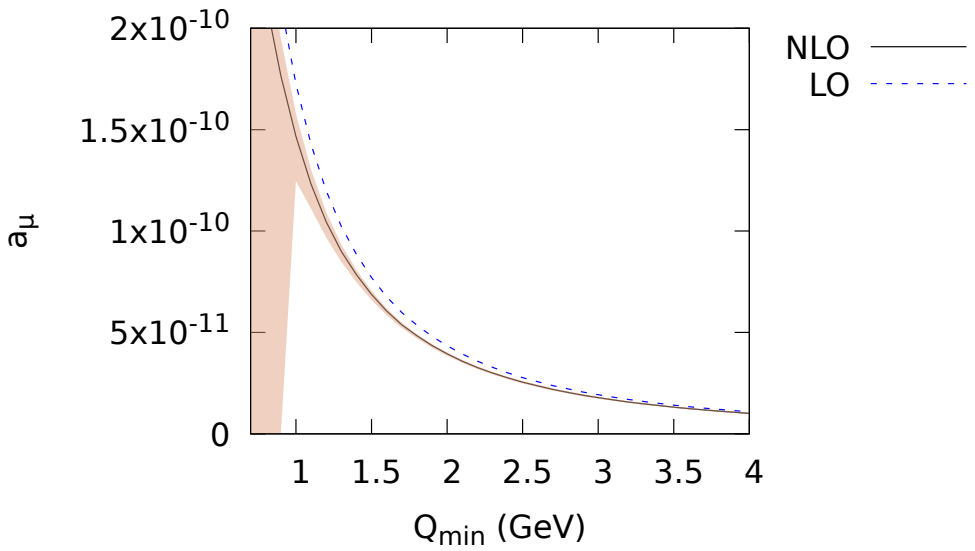

Figure 4.14: Numerical results for the hadronic HLbL $(g-2)_\mu$ in the $Q_i > Q_{\min}$ region, using the LO (massless quark loop) and NLO (gluonic corrections) contributions of its corresponding OPE. Uncertainties, apart from the one coming from the $\alpha_s(M_W)$ input, represented by shaded areas have being estimated attending to ambiguities when setting the α_s input (exact choice of scale and order of running for the β function) as a consequence of not including higher-orders.

4.2.5 Conclusions

One of the main sources of uncertainties entering in $(g-2)_\mu$ comes from the contributions of the short-distance regions of the HLbL tensor contributions. In this work, which can be regarded as a continuation of Refs. [1] and [37], we have culminated our task of giving a precise and systematic description of the contributions for three large loop momenta.

For years, it was assumed that some form of the quark loop, maybe with constituent quark masses, should be the leading order of some systematic expansion of the HLbL contribution tensor to the $(g-2)_\mu$ for large loop momenta. However, it was shown in Ref. [1] how applying an OPE directly to the HLbL tensor, where the massless quark loop is indeed the leading order, does not make sense for the $(g-2)_\mu$ kinematics. The correct expansion in this kinematic region was presented in that reference, where the massless quark loop was shown to be the leading order and the leading non-perturbative quark mass-suppressed correction was computed.

A very comprehensive analysis to study the role of both the quark mass-suppressed and not suppressed non-perturbative corrections to the expansion was made in Ref. [37], where many formal aspects and subtleties of the expansion were developed and presented in full detail, showing that it is well founded. The obtained results showed how above 1 GeV the non-perturbative corrections, even when functionally more important than in other expansions, are still typically below 1%.

In view of that, the most important corrections to the leading massless quark loop, and the one that ultimately allows to understand from where the expansion is valid, is the pure gluonic correction, which has been the subject of this work.

While in principle a multi-scale four-loop integral could be regarded as a formidable task, it has become feasible through combining existing tools developed for generic contributions of the HLbL tensor to the $(g-2)_\mu$, methods on finding compact expressions developed in Ref. [37], optimized software on reduction to master integrals, analytic reduction of those remaining master integrals and numerical integration routines.

Our final result brings good news. The size of the gluonic corrections are found small, typically of size -10% above the perturbative breakdown scale, and, as a consequence, the expansion is able to give a precise description of the $(g-2)_\mu$ contributions above it.

Taking all of this into account, we suggest as a legitimate method to compute the HLbL contribution to $(g-2)_\mu$ to use the results of this expansion from some point between $Q_{\min} = 1$ GeV and $Q_{\min} = 2$ GeV, which should give a more precise prediction than resonance models, and possible discontinuities in the matching should be incorporated as systematic model uncertainty.

Acknowledgments

We thank Martin Hoferichter for discussions. N. H.–T. and L.L. are funded by the Albert Einstein Center for Fundamental Physics at Universität Bern and the Swiss National Science Foundation, respectively. J. B. is supported in part by the Swedish Research Council grants contract numbers 2016-05996 and 2019-03779. A. R-.S- is partially supported by the Agence Nationale de la Recherche (ANR) under grant ANR-19- CE31-0012 (project MORA).

4.2.A Master integrals

The aim of this appendix is to list the expressions of the master integrals needed in Sec. 4.2.3 (see also Fig. 4.13). They can be found in Refs. [152, 153, 158] [20]. All n-loop master integrals contain the overall factor S_D^n, where

$$S_D = S_D(\epsilon) = \frac{(4\pi)^\epsilon}{16\pi^2}\frac{\Gamma(1+\epsilon)\Gamma^2(1-\epsilon)}{\Gamma(1-2\epsilon)}\,. \tag{4.334}$$

The functions C_{123} and W_{312} are finite in the limit $d \to 4$. Their ϵ-expansions can be written as follows

$$\begin{aligned} C_{123} &\equiv \int dp \frac{1}{p^{2\gamma}(p-q_1)^2(p+q_2)^2} \\ &= S_D C_{123}(0) + S_D C_{123}(1)\epsilon + C_{123}(2)\epsilon^2 + \mathcal{O}(\epsilon^3)\,, \end{aligned} \tag{4.335}$$

$$\begin{aligned} W_{312} &\equiv \int dp_1 dp_2 \frac{1}{p_1^2(p_1+q_2)^2 p_2^2(p_2-q_1)^2(p_1-p_2)^2} \\ &= S_D^2 W_{312}(0) + S_D^2 W_{312}(1)\epsilon + W_{312}(2)\epsilon^2 + \mathcal{O}(\epsilon^2)\,, \end{aligned} \tag{4.336}$$

[20] The formulas given in this appendix and those in Ref. [153] differ in a sign: an overall minus sign has been missed in (4.18) of Ref. [153]. This in turns leads to a minus instead of the plus sign in the second line of (4.24), which corresponds to our (4.340). We checked that our sign agrees with the corresponding formulas in Ref. [158], which is also cited in Ref. [153].

where $q_1 + q_2 + q_3 = 0$ and $d = 4 - 2\epsilon$. The integrations are defined as

$$\int dp = \frac{1}{i} \int \frac{d^d p}{(2\pi)^d} \,. \tag{4.337}$$

The remaining integrals appearing in the calculation contain some singularities which cancel out in the final amplitude. The ϵ-expansions of the integral B_q and S_q read

$$\begin{aligned} B_q &\equiv \int dp \frac{1}{p^2 (p-q)^2} \\ &= \frac{S_D}{\epsilon} + S_D \left[2 - \log\left(-q^2\right)\right] + S_D \left[4 - 2\log\left(-q^2\right) + \frac{1}{2}\log^2(-q^2)\right] \epsilon + \mathcal{O}(\epsilon^2) \,, \end{aligned} \tag{4.338}$$

and

$$\begin{aligned} S_q &\equiv \int dp_1 dp_2 \frac{1}{(p_1 - q)^2 p_2^2 (p_1 - p_2)^2} \\ &= - S_D^2 \frac{q^2}{4\epsilon} + S_D^2 \left[-\frac{13}{8} q^2 + \frac{1}{2}\log\left(-q^2\right) q^2\right] \\ &\quad + S_D^2 \left[-\frac{115}{16} q^2 + \frac{13}{4}\log\left(-q^2\right) q^2 - \frac{1}{2}\log^2(-q^2) q^2\right] \epsilon + \mathcal{O}(\epsilon^2) \,. \end{aligned} \tag{4.339}$$

The integrals V_{123} and $\dot{V}_{123}$ can be expressed as functions of the finite integrals C_{123} and W_{312}. Their ϵ-expansions can be written as

$$\begin{aligned} \dot{V}_{312} &\equiv \int dp_1 dp_2 \frac{1}{p_1^2 (p_1 - q_1)^2 (p_1 + q_2)^2 p_2^2 (p_1 - p_2)^2} \\ &= -S_D^2 \frac{C_{123}(0)}{\epsilon} + S_D^2 \left[\frac{1}{2} C_{123}(0) \left(\log\left(-q_1^2\right) + \log\left(-q_2^2\right)\right) - C_{123}(1)\right] \\ &\quad - \frac{S_D^2}{4} \left[C_{123}(0) \left(\log^2(-q_1^2) + \log^2(-q_2^2)\right) - 2 C_{123}(1) \left(\log\left(-q_1^2\right) + \log\left(-q_2^2\right)\right)\right. \\ &\qquad \left. + 4 (C_{123}(2) + W_{312}(0))\right] \epsilon + \mathcal{O}\left(\epsilon^2\right) \,, \end{aligned} \tag{4.340}$$

and

$$\begin{aligned} V_{312} &\equiv \int dp_1 dp_2 \frac{1}{(p_1 - q_1)^2 (p_1 + q_2)^2 p_2^2 (p_1 - p_2)^2} \\ &= \frac{S_D^2}{2\,\epsilon^2} + S_D^2 \left[\frac{5}{2} - \log\left(-q_3^2\right)\right] \frac{1}{\epsilon} + \frac{S_D^2}{2} \left[C_{123}(0)(-q_1^2 - q_2^2 + q_3^2)\right. \\ &\qquad \left. + \log\left(-q_1^2\right) \left(\log\left(-q_3^2\right) - \log\left(-q_2^2\right)\right) + \log\left(-q_2^2\right) \log\left(-q_3^2\right) + \log^2(-q_3^2) - 10\log\left(-q_3^2\right) + 19\right] \\ &\quad + S_D^2 \left[\frac{1}{2} (F_{312}(2) + 65) + \frac{1}{2} C_{123}(1)(-q_1^2 - q_2^2 + q_3^2)\right. \\ &\qquad + C_{123}(0) \left(-\frac{5}{2}(q_1^2 + q_2^2 - q_3^2) + \frac{1}{4}\log\left(-q_1^2\right)(q_1^2 + q_2^2 - q_3^2) + \frac{1}{4}\log\left(-q_2^2\right)(q_1^2 + q_2^2 - q_3^2)\right) \\ &\qquad + \log\left(-q_1^2\right) \left(\log\left(-q_2^2\right) \left(\log\left(-q_3^2\right) - \frac{5}{2}\right) - \log^2(-q_3^2) + \frac{5\log\left(-q_3^2\right)}{2}\right) \\ &\qquad \left. + \log\left(-q_2^2\right) \left(\frac{5\log\left(-q_3^2\right)}{2} - \log^2(-q_3^2)\right) + \frac{1}{3}\log^3(-q_3^2) + \frac{5}{2}\log^2(-q_3^2) - 19\log\left(-q_3^2\right)\right] \epsilon \\ &\quad + \mathcal{O}(\epsilon^2) \,, \end{aligned} \tag{4.341}$$

where $C_{123}(i)$ and $W_{312}(i)$ are the coefficients of the ϵ-expansion of their corresponding Master integral (c.f. (4.335) and (4.336)). Not all these coefficients survive in the gluonic corrections we are computing in section 4.2.3: $C_{123}(1)$, $C_{123}(2)$, $W_{312}(1)$ and $W_{312}(2)$ cancel in the final expression. The coefficients $C_{123}(0)$ and $W_{312}(0)$ that contribute, as well as the function $F_{312}(2)$ which appears in the expansion of V_{312}, are given below

$$C_{123}(0) = 2q_3^{-2}\frac{\mathcal{P}_2(z)}{z-\overline{z}}\,, \tag{4.342}$$

$$W_{312}(0) = 6q_3^{-2}\frac{\mathcal{P}_4(1-z^{-1})}{z-\overline{z}}\,, \tag{4.343}$$

and finally

$$F_{312}(2) = -6\mathcal{P}_3(z) - 6\mathcal{P}_3(1-z) + \frac{1}{2}\log(u)\log^2(v) + \frac{1}{2}\log^2(u)\log(v) + 6\zeta_3\,, \tag{4.344}$$

where $u = \frac{q_1^2}{q_3^2}$, $v = \frac{q_2^2}{q_3^2}$ and z is given by

$$\begin{aligned} z &= \frac{1}{2}\left(1+u-v+i\sqrt{-\bar{\lambda}}\right)\,, \\ \bar{\lambda} &= (1+u-v)^2 - 4u\,. \end{aligned} \tag{4.345}$$

The $\mathcal{P}_i(z)$ are real (purely imaginary) functions over the complex plane when i is odd (real). They can be expressed using polylogarithms:

$$\begin{aligned} \mathcal{P}_2(z) &= \mathrm{Li}_2(z) - \mathrm{Li}_2(\bar{z}) + \log|z|(\log(1-z) - \log(1-\bar{z})) \\ \mathcal{P}_3(z) &= \mathrm{Li}_3(z) + \mathrm{Li}_3(\bar{z}) - \log|z|(\mathrm{Li}_2(z) + \mathrm{Li}_2(\bar{z})) - \frac{1}{3}\log^2|z|(\log(1-z) + \log(1-\bar{z})) \\ \mathcal{P}_4(z) &= \mathrm{Li}_4(z) - \mathrm{Li}_4(\bar{z}) - \log|z|(\mathrm{Li}_3(z) - \mathrm{Li}_3(\bar{z})) + \frac{1}{3}\log^2|z|(\mathrm{Li}_2(z) - \mathrm{Li}_2(\bar{z})) \end{aligned} \tag{4.346}$$

The polylogarithms can be defined recursively

$$\mathrm{Li}_n(z) = \int_0^z \frac{dt}{t}\mathrm{Li}_{n-1}(t)\ \text{, and } \mathrm{Li}_1(z) = -\log(1-z)\,. \tag{4.347}$$

The $\mathcal{P}_i$ satisfy a number of relations

$$\begin{aligned} &\mathcal{P}_2(z) = -\mathcal{P}_2(1/z)\,, \\ &\mathcal{P}_3(z) = \mathcal{P}_3(1/z)\,, \\ &\mathcal{P}_4(z) = -\mathcal{P}_4(1/z)\,, \\ &\mathcal{P}_2(z) = \mathcal{P}_2(1-1/z) = -\mathcal{P}_2(1-z) = \mathcal{P}_2(1/(1-z)) = -\mathcal{P}_2(z/(z-1))\,, \\ &\mathcal{P}_3(z) + \mathcal{P}_3(1-z) + \mathcal{P}_3(1-1/z) = \mathcal{P}_3(1) = 2\zeta(3) \end{aligned} \tag{4.348}$$

which can be used to show that the master integrals have the required symmetries under interchange of momenta.

4.2.B Analytical formulae

In this section we present analytical formulae for the scalar functions entering into the calculation of a_μ^{HLbL}. We in particular discuss the momentum expansions of the master integrals needed to make spurious singularities cancel numerically. As an explicit example, we also give the expressions for the $\hat{\Pi}$ at the symmetric point $Q_1 = Q_2 = Q_3$ for the quark loop and gluonic correction in App. 4.2.B.2.

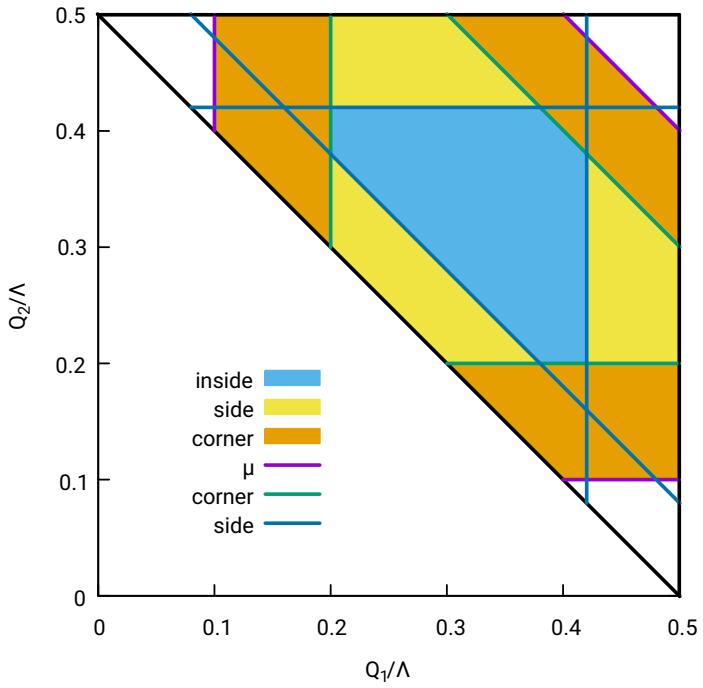

Figure 4.15: Different regions to consider in order to deal with the singularities of the $\hat{\Pi}$ when $\lambda \to 0$. The regions are shown for $Q_1 + Q_2 + Q_3 = \Lambda$.

4.2.B.1 Expansions

In the numerical evaluation of a_μ^{HLbL} there are certain limits of the kinematics requiring particular care. The integration domain can be divided into several regions as in Fig. 4.15. We there see the so-called side, corner and inside regions together with their boundaries. Also the cut-off μ has been indicated. Unless the side and corner regions are properly taken care of, the numerical integration will diverge as one obtains zeros in denominators that numerically do not cancel the zeros in numerators. Below we discuss the two types of problematic regions.

The precise definition of the regions is: $Q_i \geq \mu = Q_{\mathrm{min}}$. The corners are defined by $Q_i/(Q_1 + Q_2 + Q_3) \leq \epsilon_1$ for $i = 1, 2, 3$. The sides are the part of the remaining region that satisfy $(2Q_i/(Q_1 + Q_2 + Q_3) - 1 \leq \epsilon_2$ for $i = 1, 2, 3$. The inside is the remaining allowed region.

Side regions The side regions are defined as the kinematical limit where one Q_i is close to $Q_j + Q_k$, or, in other words when

$$\text{Side Region } S_i: \quad Q_i^2 = (Q_j + Q_k)^2 - \delta \equiv \overline{Q}_i^2 - \delta\,, \tag{4.349}$$

where δ is a small parameter. The inverse powers of the Källén function in the $\hat{\Pi}_i$ diverge in the side regions. These apparent singularities do, however, cancel when all the kinematical factors, the master integrals $C_{123}(0)$, $W_{312}(0)$, $W_{213}(0)$, $W_{123}(0)$, $F_{312}(2)$, $F_{213}(2)$ and $F_{123}(2)$ as well as the Källén function itself are expanded in δ. For a finite result we have to expand the master integrals up to order δ^9. The analytical forms of these expansions are very long and we here therefore only give the first two orders for one case, S_3. In the supplementary file

`sideexpansions.txt`, however, we provide the full expansions needed for all S_i. In region S_{+3} we have

$$\begin{aligned}C_{123}(0) =&\frac{1}{Q_2\overline{Q}_3}\log\left(\frac{Q_1^2}{\overline{Q}_3^2}\right)+\frac{1}{Q_1\overline{Q}_3}\log\left(\frac{Q_2^2}{\overline{Q}_3^2}\right)\\&+\delta\Bigg[\frac{Q_1}{6Q_2^2\overline{Q}_3^3}\log\left(\frac{Q_1^2}{\overline{Q}_3^2}\right)+\frac{Q_2}{6Q_1^2\overline{Q}_3^3}\log\left(\frac{Q_2^2}{\overline{Q}_3^2}\right)+\frac{1}{3Q_2\overline{Q}_3^3}+\frac{1}{2Q_2\overline{Q}_3^3}\log\left(\frac{Q_1^2}{\overline{Q}_3^2}\right)\\&+\frac{1}{3Q_1\overline{Q}_3^3}+\frac{1}{2Q_1\overline{Q}_3^3}\log\left(\frac{Q_2^2}{\overline{Q}_3^2}\right)\Bigg]+\mathcal{O}(\delta^2)\,,\end{aligned}\tag{4.350}$$

$$\begin{aligned}F_{312}(2) =&-6\zeta_3+\frac{1}{2}\log\left(\frac{Q_1^2}{\overline{Q}_3^2}\right)\log^2\left(\frac{Q_2^2}{\overline{Q}_3^2}\right)+\frac{1}{2}\log^2\left(\frac{Q_1^2}{\overline{Q}_3^2}\right)\log\left(\frac{Q_2^2}{\overline{Q}_3^2}\right)+6\mathcal{P}_3\left(-\frac{Q_2}{Q_1}\right)\\&+\delta\Bigg[-\frac{Q_2}{Q_1\overline{Q}_3^2}\log^2\left(\frac{Q_2^2}{\overline{Q}_3^2}\right)-\frac{Q_2}{Q_1\overline{Q}_3^2}\log\left(\frac{Q_1^2}{\overline{Q}_3^2}\right)\log\left(\frac{Q_2^2}{\overline{Q}_3^2}\right)-\frac{Q_2}{Q_1\overline{Q}_3^2}\log^2\left(\frac{Q_1^2}{\overline{Q}_3^2}\right)\\&-\frac{3}{Q_1\overline{Q}_3}\log\left(\frac{Q_2^2}{\overline{Q}_3^2}\right)+\frac{1}{Q_1\overline{Q}_3}\log^2\left(\frac{Q_2^2}{\overline{Q}_3^2}\right)+\frac{3}{Q_1\overline{Q}_3}\log\left(\frac{Q_1^2}{\overline{Q}_3^2}\right)\\&+\frac{1}{Q_1\overline{Q}_3}\log\left(\frac{Q_1^2}{\overline{Q}_3^2}\right)\log\left(\frac{Q_2^2}{\overline{Q}_3^2}\right)+\frac{1}{Q_1\overline{Q}_3}\log^2\left(\frac{Q_1^2}{\overline{Q}_3^2}\right)-\frac{3}{Q_1Q_2}\log\left(\frac{Q_1^2}{\overline{Q}_3^2}\right)\Bigg]\\&+\mathcal{O}(\delta^2)\,,\end{aligned}\tag{4.351}$$

$$\begin{aligned}W_{312}(0) =&\frac{3}{Q_1Q_2}\mathcal{P}_3\left(-\frac{Q_2}{Q_1}\right)\\&+\delta\Bigg[-\frac{1}{12Q_1^2\overline{Q}_3^2}\log^2\left(\frac{Q_2^2}{\overline{Q}_3^2}\right)+\frac{1}{6Q_1^2\overline{Q}_3^2}\log\left(\frac{Q_1^2}{\overline{Q}_3^2}\right)\log\left(\frac{Q_2^2}{\overline{Q}_3^2}\right)-\frac{1}{12Q_1^2\overline{Q}_3^2}\log^2\left(\frac{Q_1^2}{\overline{Q}_3^2}\right)\\&-\frac{1}{2Q_1^2Q_2\overline{Q}_3}\log\left(\frac{Q_2^2}{\overline{Q}_3^2}\right)+\frac{1}{12Q_1^2Q_2\overline{Q}_3}\log^2\left(\frac{Q_2^2}{\overline{Q}_3^2}\right)+\frac{1}{2Q_1^2Q_2\overline{Q}_3}\log\left(\frac{Q_1^2}{\overline{Q}_3^2}\right)\\&-\frac{1}{6Q_1^2Q_2\overline{Q}_3}\log\left(\frac{Q_1^2}{\overline{Q}_3^2}\right)\log\left(\frac{Q_2^2}{\overline{Q}_3^2}\right)+\frac{1}{12Q_1^2Q_2\overline{Q}_3}\log^2\left(\frac{Q_1^2}{\overline{Q}_3^2}\right)-\frac{1}{2Q_1^2Q_2^2}\log\left(\frac{Q_1^2}{\overline{Q}_3^2}\right)\\&+\frac{1}{2Q_1^2Q_2^2}\mathcal{P}_3\left(-\frac{Q_2}{Q_1}\right)\Bigg]+\mathcal{O}(\delta^2)\,,\end{aligned}\tag{4.352}$$

$$
\begin{aligned}
F_{213}(2) =& -6\zeta_3 - \log^3\left(\frac{Q_2^2}{\overline{Q}_3^2}\right) + \frac{3}{2}\log\left(\frac{Q_1^2}{\overline{Q}_3^2}\right)\log^2\left(\frac{Q_2^2}{\overline{Q}_3^2}\right) - \frac{1}{2}\log^2\left(\frac{Q_1^2}{\overline{Q}_3^2}\right)\log\left(\frac{Q_2^2}{\overline{Q}_3^2}\right) \\
&+ 6\mathcal{P}_3\left(1+\frac{Q_2}{Q_1}\right) + \delta\Bigg[3\frac{Q_2}{Q_1\overline{Q}_3^2}\log\left(\frac{Q_2^2}{\overline{Q}_3^2}\right) + \frac{3Q_2}{2Q_1\overline{Q}_3^2}\log^2\left(\frac{Q_2^2}{\overline{Q}_3^2}\right) \\
&- \frac{3Q_2}{Q_1\overline{Q}_3^2}\log\left(\frac{Q_1^2}{\overline{Q}_3^2}\right) - \frac{5Q_2}{2Q_1\overline{Q}_3^2}\log\left(\frac{Q_1^2}{\overline{Q}_3^2}\right)\log\left(\frac{Q_2^2}{\overline{Q}_3^2}\right) + \frac{Q_2}{Q_1\overline{Q}_3^2}\log^2\left(\frac{Q_1^2}{\overline{Q}_3^2}\right) \\
&- \frac{3}{2Q_1\overline{Q}_3}\log^2\left(\frac{Q_2^2}{\overline{Q}_3^2}\right) + \frac{3}{Q_1\overline{Q}_3}\log\left(\frac{Q_1^2}{\overline{Q}_3^2}\right) + \frac{5}{2Q_1\overline{Q}_3}\log\left(\frac{Q_1^2}{\overline{Q}_3^2}\right)\log\left(\frac{Q_2^2}{\overline{Q}_3^2}\right) \\
&- \frac{1}{Q_1\overline{Q}_3}\log^2\left(\frac{Q_1^2}{\overline{Q}_3^2}\right)\Bigg] + \mathcal{O}(\delta^2)\,,
\end{aligned}
\tag{4.353}
$$

$$
\begin{aligned}
W_{213}(0) =& -\frac{3}{Q_1\overline{Q}_3}\mathcal{P}_3\left(1+\frac{Q_2}{Q_1}\right) \\
&+ \delta\Bigg[-\frac{Q_2}{2Q_1^2\overline{Q}_3^3}\log\left(\frac{Q_2^2}{\overline{Q}_3^2}\right) + \frac{Q_2}{2Q_1^2\overline{Q}_3^3}\log\left(\frac{Q_1^2}{\overline{Q}_3^2}\right) + \frac{Q_2}{4Q_1^2\overline{Q}_3^3}\log\left(\frac{Q_1^2}{\overline{Q}_3^2}\right)\log\left(\frac{Q_2^2}{\overline{Q}_3^2}\right) \\
&- \frac{Q_2}{4Q_1^2\overline{Q}_3^3}\log^2\left(\frac{Q_1^2}{\overline{Q}_3^2}\right) + \frac{Q_2}{Q_1^2\overline{Q}_3^3}\mathcal{P}_3\left(1+\frac{Q_2}{Q_1}\right) - \frac{1}{2Q_1^2\overline{Q}_3^2}\log\left(\frac{Q_1^2}{\overline{Q}_3^2}\right) \\
&- \frac{1}{4Q_1^2\overline{Q}_3^2}\log\left(\frac{Q_1^2}{\overline{Q}_3^2}\right)\log\left(\frac{Q_2^2}{\overline{Q}_3^2}\right) + \frac{5}{12Q_1^2\overline{Q}_3^2}\log^2\left(\frac{Q_1^2}{\overline{Q}_3^2}\right) - \frac{3}{2Q_1^2\overline{Q}_3^2}\mathcal{P}_3\left(1+\frac{Q_2}{Q_1}\right) \\
&- \frac{1}{6Q_1^2Q_2\overline{Q}_3}\log^2\left(\frac{Q_1^2}{\overline{Q}_3^2}\right)\Bigg] + \mathcal{O}(\delta^2)\,,
\end{aligned}
\tag{4.354}
$$

$$
\begin{aligned}
F_{123}(2) =& -6\zeta_3 - \frac{1}{2}\log\left(\frac{Q_1^2}{\overline{Q}_3^2}\right)\log^2\left(\frac{Q_2^2}{\overline{Q}_3^2}\right) + \frac{3}{2}\log^2\left(\frac{Q_1^2}{\overline{Q}_3^2}\right)\log\left(\frac{Q_2^2}{\overline{Q}_3^2}\right) - \log^3\left(\frac{Q_1^2}{\overline{Q}_3^2}\right) \\
&+ 6\mathcal{P}_3\left(1+\frac{Q_1}{Q_2}\right) + \delta\Bigg[-\frac{3Q_1}{Q_2\overline{Q}_3^2}\log\left(\frac{Q_2^2}{\overline{Q}_3^2}\right) + \frac{Q_1}{Q_2\overline{Q}_3^2}\log^2\left(\frac{Q_2^2}{\overline{Q}_3^2}\right) \\
&+ \frac{3Q_1}{Q_2\overline{Q}_3^2}\log\left(\frac{Q_1^2}{\overline{Q}_3^2}\right) - \frac{5Q_1}{2Q_2\overline{Q}_3^2}\log\left(\frac{Q_1^2}{\overline{Q}_3^2}\right)\log\left(\frac{Q_2^2}{\overline{Q}_3^2}\right) + \frac{3Q_1}{2Q_2\overline{Q}_3^2}\log^2\left(\frac{Q_1^2}{\overline{Q}_3^2}\right) \\
&+ \frac{3}{Q_2\overline{Q}_3}\log\left(\frac{Q_2^2}{\overline{Q}_3^2}\right) - \frac{1}{Q_2\overline{Q}_3}\log^2\left(\frac{Q_2^2}{\overline{Q}_3^2}\right) + \frac{5}{2Q_2\overline{Q}_3}\log\left(\frac{Q_1^2}{\overline{Q}_3^2}\right)\log\left(\frac{Q_2^2}{\overline{Q}_3^2}\right) \\
&- \frac{3}{2Q_2\overline{Q}_3}\log^2\left(\frac{Q_1^2}{\overline{Q}_3^2}\right)\Bigg] + \mathcal{O}(\delta^2)\,,
\end{aligned}
\tag{4.355}
$$

$$
\begin{aligned}
W_{123}(0) = &-\frac{3}{Q_2\overline{Q}_3}\mathcal{P}_3\left(1+\frac{Q_1}{Q_2}\right)\\
&+\delta\Bigg[\frac{Q_1}{2Q_2^2\overline{Q}_3^3}\log\left(\frac{Q_2^2}{\overline{Q}_3^2}\right)-\frac{Q_1}{4Q_2^2\overline{Q}_3^3}\log^2\left(\frac{Q_2^2}{\overline{Q}_3^2}\right)-\frac{Q_1}{2Q_2^2\overline{Q}_3^3}\log\left(\frac{Q_1^2}{\overline{Q}_3^2}\right)\\
&+\frac{Q_1}{4Q_2^2\overline{Q}_3^3}\log\left(\frac{Q_1^2}{\overline{Q}_3^2}\right)\log\left(\frac{Q_2^2}{\overline{Q}_3^2}\right)+\frac{Q_1}{Q_2^2\overline{Q}_3^3}\mathcal{P}_3\left(1+\frac{Q_1}{Q_2}\right)-\frac{1}{2Q_2^2\overline{Q}_3^2}\log\left(\frac{Q_2^2}{\overline{Q}_3^2}\right)\\
&+\frac{5}{12Q_2^2\overline{Q}_3^2}\log^2\left(\frac{Q_2^2}{\overline{Q}_3^2}\right)-\frac{1}{4Q_2^2\overline{Q}_3^2}\log\left(\frac{Q_1^2}{\overline{Q}_3^2}\right)\log\left(\frac{Q_2^2}{\overline{Q}_3^2}\right)-\frac{3}{2Q_2^2\overline{Q}_3^2}\mathcal{P}_3\left(1+\frac{Q_1}{Q_2}\right)\\
&-\frac{1}{6Q_1Q_2^2\overline{Q}_3}\log^2\left(\frac{Q_2^2}{\overline{Q}_3^2}\right)\Bigg]. \qquad (4.356)
\end{aligned}
$$

To obtain these one has to expand the relevant $\mathcal{P}_i$ functions around a general z. Note that one obtains e.g. $\mathcal{P}_3(1+Q_2/Q1)$, which, from the definition of the function in (4.346) gives rise to $\log(-Q_2/Q_1)$. This lies on the branch-cut of the (poly-)logarithm. However, the $\mathcal{P}_i$ are well-behaved, single-valued functions without branch-cuts and one can safely neglect these issues.

When the $\hat{\Pi}$ are expanded, the negative powers of δ cancel. The expressions are not displayed here due to their length, but they can be found in the supplementary file `resultsgluon.txt`. Equivalent expressions are provided for the quark loop in `resultsquark.txt`.

Corner regions In the corner regions the situation is different. There one has two small parameters instead of one

$$
\text{Corner Region } C_i: \quad Q_i \ll Q_j, Q_k \text{ and } \delta \equiv Q_j - Q_k \ll \overline{Q}_i \equiv Q_j + Q_k\,. \qquad (4.357)
$$

Below, we list the expansions in the region C_3 [21]. The expansions of the master integrals are given by

$$
C_{123}(0) = -\frac{8}{\overline{Q}_3^2}+\frac{8}{\overline{Q}_3^2}\log\left(2\frac{Q_3}{\overline{Q}_3}\right)+Q_3^2\left[-\frac{40}{9\overline{Q}_3^4}+\frac{16}{3\overline{Q}_3^4}\log\left(2\frac{Q_3}{\overline{Q}_3}\right)\right]+\mathcal{O}\left(Q_3^4,\delta^2,\delta Q_3^2\right), \qquad (4.358)
$$

$$
W_{312}(0) = -\frac{24}{\overline{Q}_3^2}\zeta_3+Q_3^2\left[\frac{88}{3\overline{Q}_3^4}-\frac{16}{\overline{Q}_3^4}\zeta_3-\frac{16}{\overline{Q}_3^4}\log\left(2\frac{Q_3}{\overline{Q}_3}\right)\right]+\mathcal{O}\left(Q_3^4,\delta^2,\delta Q_3^2\right), \qquad (4.359)
$$

$$
F_{312}(2) = 6\zeta_3-8\log^3\left(2\frac{Q_3}{\overline{Q}_3}\right)+Q_3^2\left[-\frac{36}{\overline{Q}_3^2}+\frac{24}{\overline{Q}_3^2}\log\left(2\frac{Q_3}{\overline{Q}_3}\right)\right]+\mathcal{O}\left(Q_3^4,\delta^2,\delta Q_3^2\right) \qquad (4.360)
$$

$$
\begin{aligned}
W_{213}(0) = &-\frac{24}{\overline{Q}_3^2}+\frac{24}{\overline{Q}_3^2}\log\left(2\frac{Q_3}{\overline{Q}_3}\right)-\frac{8}{\overline{Q}_3^2}\log^2\left(2\frac{Q_3}{\overline{Q}_3}\right)\\
&+Q_3^2\left[-\frac{130}{27\overline{Q}_3^4}+\frac{76}{9\overline{Q}_3^4}\log\left(2\frac{Q_3}{\overline{Q}_3}\right)-\frac{40}{9\overline{Q}_3^4}\log^2\left(2\frac{Q_3}{\overline{Q}_3}\right)\right]\\
&+\delta\left[\frac{18}{\overline{Q}_3^3}-\frac{20}{\overline{Q}_3^3}\log\left(2\frac{Q_3}{\overline{Q}_3}\right)+\frac{8}{\overline{Q}_3^3}\log^2\left(2\frac{Q_3}{\overline{Q}_3}\right)\right]+\mathcal{O}\left(Q_3^4,\delta^2,\delta Q_3^2\right), \qquad (4.361)
\end{aligned}
$$

[21] In the supplementary file `cornerexpansions.txt`, we provide the full expansions needed for all corner regions.

$$F_{213}(2) = -6\zeta_3 + Q_3^2\left[\frac{18}{\overline{Q}_3^2} - \frac{12}{\overline{Q}_3^2}\log\left(2\frac{Q_3}{\overline{Q}_3}\right)\right] + \delta\left[\frac{24}{\overline{Q}_3} - \frac{24}{\overline{Q}_3}\log\left(2\frac{Q_3}{\overline{Q}_3}\right) + \frac{16}{\overline{Q}_3}\log^2\left(2\frac{Q_3}{\overline{Q}_3}\right)\right] + \mathcal{O}\left(Q_3^4, \delta^2, \delta Q_3^2\right), \tag{4.362}$$

$$W_{123}(0) = -\frac{24}{\overline{Q}_3^2} + \frac{24}{\overline{Q}_3^2}\log\left(2\frac{Q_3}{\overline{Q}_3}\right) - \frac{8}{\overline{Q}_3^2}\log^2\left(2\frac{Q_3}{\overline{Q}_3}\right) + Q_3^2\left[-\frac{130}{27\overline{Q}_3^4} + \frac{76}{9\overline{Q}_3^4}\log\left(2\frac{Q_3}{\overline{Q}_3}\right) - \frac{40}{9\overline{Q}_3^4}\log^2\left(2\frac{Q_3}{\overline{Q}_3}\right)\right] + \delta\left[-\frac{18}{\overline{Q}_3^3} + \frac{20}{\overline{Q}_3^3}\log\left(2\frac{Q_3}{\overline{Q}_3}\right) - \frac{8}{\overline{Q}_3^3}\log^2\left(2\frac{Q_3}{\overline{Q}_3}\right)\right] + \mathcal{O}\left(Q_3^4, \delta^2, \delta Q_3^2\right), \tag{4.363}$$

$$F_{123}(2) = -6\zeta_3 + Q_3^2\left[\frac{18}{\overline{Q}_3^2} - \frac{12}{\overline{Q}_3^2}\log\left(2\frac{Q_3}{\overline{Q}_3}\right)\right], + \delta\left[-\frac{24}{\overline{Q}_3} + \frac{24}{\overline{Q}_3}\log\left(2\frac{Q_3}{\overline{Q}_3}\right) - \frac{16}{\overline{Q}_3}\log^2\left(2\frac{Q_3}{\overline{Q}_3}\right)\right] + \mathcal{O}\left(Q_3^4, \delta^2, \delta Q_3^2\right). \tag{4.364}$$

In the corner regions one has to expand the $\mathcal{P}_i(z)$ for three different z, namely $z = 0, 1, \infty$. However, from the relations in (4.348) one can relate $\mathcal{P}_i(z)$ to $\mathcal{P}_i(1/z)$, so only $z = 0, 1$ are needed in practice.

The $\hat{\Pi}$ in region C_3 are given by

$$\frac{\hat{\Pi}_1}{c_s} = \frac{1}{Q_3^2}\left[\frac{192}{\overline{Q}_3^2}\right] + \frac{3568}{15\overline{Q}_3^4} - \frac{2048}{5\overline{Q}_3^4}\zeta_3 + \frac{3776}{9\overline{Q}_3^4}\log\left(2\frac{Q_3}{\overline{Q}_3}\right) - \frac{256}{\overline{Q}_3^4}\log^2\left(2\frac{Q_3}{\overline{Q}_3}\right) + Q_3^2\left[\frac{39375808}{39375\overline{Q}_3^6} - \frac{36864}{35\overline{Q}_3^6}\zeta_3 + \frac{528896}{1125\overline{Q}_3^6}\log\left(2\frac{Q_3}{\overline{Q}_3}\right) - \frac{12288}{25\overline{Q}_3^6}\log^2\left(2\frac{Q_3}{\overline{Q}_3}\right)\right] + \frac{\delta^2}{Q_3^2}\left[\frac{1280}{9\overline{Q}_3^4} - \frac{2560}{9\overline{Q}_3^4}\log\left(2\frac{Q_3}{\overline{Q}_3}\right)\right] + \mathcal{O}(\delta^2, \delta^4 Q_3^{-2}), \tag{4.365}$$

$$\frac{\hat{\Pi}_4}{c_s} = -\frac{12544}{45\overline{Q}_3^4} + \frac{2048}{5\overline{Q}_3^4}\zeta_3 + \frac{2048}{9\overline{Q}_3^4}\log\left(2\frac{Q_3}{\overline{Q}_3}\right) + Q_3^2\left[-\frac{13533568}{13125\overline{Q}_3^6} + \frac{49152}{35\overline{Q}_3^6}\zeta_3 + \frac{1935872}{1125\overline{Q}_3^6}\log\left(2\frac{Q_3}{\overline{Q}_3}\right) - \frac{14336}{25\overline{Q}_3^6}\log^2\left(2\frac{Q_3}{\overline{Q}_3}\right)\right] + \mathcal{O}(\delta^2, Q_3^2, \delta^2 Q_3^2), \tag{4.366}$$

$$\frac{\hat{\Pi}_7}{c_s} = -\frac{1024}{5\overline{Q}_3^6} + \frac{8192}{5\overline{Q}_3^6}\zeta_3 + \frac{8192}{9\overline{Q}_3^6}\log\left(2\frac{Q_3}{\overline{Q}_3}\right) - \frac{\delta}{Q_3^2}\left[\frac{1024}{9\overline{Q}_3^5}\right] + \delta\left[-\frac{78295808}{13125\overline{Q}_3^7} + \frac{196608}{35\overline{Q}_3^7}\zeta_3 - \frac{17408}{1125\overline{Q}_3^7}\log\left(2\frac{Q_3}{\overline{Q}_3}\right) + \frac{69632}{75\overline{Q}_3^7}\log^2\left(2\frac{Q_3}{\overline{Q}_3}\right)\right] + Q_3^2\left[-\frac{128872192}{39375\overline{Q}_3^8} + \frac{98304}{35\overline{Q}_3^8}\zeta_3 + \frac{13229056}{1125\overline{Q}_3^8}\log\left(2\frac{Q_3}{\overline{Q}_3}\right) - \frac{323584}{75\overline{Q}_3^8}\log^2\left(2\frac{Q_3}{\overline{Q}_3}\right)\right] + \mathcal{O}(\delta^2, \delta Q_3^2, \delta^3 Q_3^{-2}), \tag{4.367}$$

$$\begin{aligned}\frac{\hat{\Pi}_{17}}{c_s} =& \frac{1}{Q_3^2}\left[-\frac{512}{\overline{Q}_3^4}+\frac{1024}{9\overline{Q}_3^4}\log\left(2\frac{Q_3}{\overline{Q}_3}\right)\right]\\ &-\frac{112018624}{118125\overline{Q}_3^6}+\frac{45056}{35\overline{Q}_3^6}\zeta_3-\frac{1769216}{1125\overline{Q}_3^6}\log\left(2\frac{Q_3}{\overline{Q}_3}\right)+\frac{115712}{225\overline{Q}_3^6}\log^2\left(2\frac{Q_3}{\overline{Q}_3}\right)\\ &+Q_3^2\left[-\frac{139984302592}{24310125\overline{Q}_3^8}+\frac{212992}{35\overline{Q}_3^8}\zeta_3-\frac{52059136}{25725\overline{Q}_3^8}\log\left(2\frac{Q_3}{\overline{Q}_3}\right)+\frac{1101824}{735\overline{Q}_3^8}\log^2\left(2\frac{Q_3}{\overline{Q}_3}\right)\right]\\ &+\frac{\delta^2}{Q_3^2}\left[-\frac{336896}{1125\overline{Q}_3^6}+\frac{47104}{225\overline{Q}_3^6}\log\left(2\frac{Q_3}{\overline{Q}_3}\right)\right]+\mathcal{O}(\delta^2,\delta^4Q_3^{-2})\,,\end{aligned}\tag{4.368}$$

$$\begin{aligned}\frac{\hat{\Pi}_{39}}{c_s} =& \frac{1}{Q_3^2}\left[-\frac{1024}{9\overline{Q}_3^4}+\frac{1024}{9\overline{Q}_3^4}\log\left(2\frac{Q_3}{\overline{Q}_3}\right)\right]\\ &-\frac{53725888}{118125\overline{Q}_3^6}-\frac{4096}{35\overline{Q}_3^6}\zeta_3+\frac{725248}{1125\overline{Q}_3^6}\log\left(2\frac{Q_3}{\overline{Q}_3}\right)-\frac{80896}{225\overline{Q}_3^6}\log^2\left(2\frac{Q_3}{\overline{Q}_3}\right)\\ &+Q_3^2\left[-\frac{75027492352}{121550625\overline{Q}_3^8}-\frac{16384}{35\overline{Q}_3^8}\zeta_3-\frac{356996096}{385875\overline{Q}_3^8}\log\left(2\frac{Q_3}{\overline{Q}_3}\right)-\frac{167936}{1225\overline{Q}_3^8}\log^2\left(2\frac{Q_3}{\overline{Q}_3}\right)\right]\\ &+\frac{\delta^2}{Q_3^2}\left[\frac{11264}{1125\overline{Q}_3^6}+\frac{47104}{225\overline{Q}_3^6}\log\left(2\frac{Q_3}{\overline{Q}_3}\right)\right]+\mathcal{O}(\delta^2,\delta^4Q_3^{-2})\,,\end{aligned}\tag{4.369}$$

$$\begin{aligned}\frac{\hat{\Pi}_{54}}{c_s} =& \frac{\delta}{Q_3^2}\left[-\frac{1408}{9\overline{Q}_3^5}-\frac{1024}{3\overline{Q}_3^5}\log\left(2\frac{Q_3}{\overline{Q}_3}\right)\right]\\ &+\delta\left[-\frac{1937408}{1575\overline{Q}_3^7}+\frac{24576}{35\overline{Q}_3^7}\zeta_3-\frac{687104}{225\overline{Q}_3^7}\log\left(2\frac{Q_3}{\overline{Q}_3}\right)+\frac{4096}{5\overline{Q}_3^7}\log^2\left(2\frac{Q_3}{\overline{Q}_3}\right)\right]\\ &+\mathcal{O}(\delta Q_3^2,\delta^3Q_3^{-2},\delta^3)\,,\end{aligned}\tag{4.370}$$

with the overall factor $c_s = \frac{2\pi\alpha_s(N_c^2-1)e_q^4}{(16\pi^2)^2}$. While all these expressions are finite when the small parameter δ tends to zero, some of them diverge when $Q_3^2 \to 0$. However, this divergence has no physical meaning, since that limit lies outside the region of validity of the OPE. The expansion of the $\hat{\Pi}$ in the other corner regions can be found in the supplementary file `resultsgluon.txt`. Equivalent expressions are provided for the quark loop in `resultsquark.txt`.

4.2.B.2 Symmetric Point

In this section, we write the expressions for the $\hat{\Pi}$ at the symmetric point $Q_1 = Q_2 = Q_3 = Q$.[22] For the quark loop these are

$$\begin{aligned}
\frac{16\pi^2\hat{\Pi}_1^{\text{quark}}}{N_c e_q^4} &= -\frac{32}{3\,Q^4}\,,\\
\frac{16\pi^2\hat{\Pi}_4^{\text{quark}}}{N_c e_q^4} &= \frac{2}{Q^4}\left(-\frac{352}{27}+\frac{128}{81}\,\Delta^{(1)}\right),\\
\frac{16\pi^2\hat{\Pi}_7^{\text{quark}}}{N_c e_q^4} &= \frac{1}{Q^6}\left(-\frac{352}{27}+\frac{128}{81}\,\Delta^{(1)}\right),\\
\frac{16\pi^2\hat{\Pi}_{17}^{\text{quark}}}{N_c e_q^4} &= \frac{1}{Q^6}\left(-\frac{384}{27}+\frac{192}{81}\,\Delta^{(1)}\right),\\
\frac{16\pi^2\hat{\Pi}_{39}^{\text{quark}}}{N_c e_q^4} &= \frac{1}{Q^6}\left(\frac{320}{27}-\frac{64}{81}\,\Delta^{(1)}\right),\\
\frac{16\pi^2\hat{\Pi}_{54}^{\text{quark}}}{N_c e_q^4} &= 0\,,
\end{aligned} \tag{4.371}$$

where

$$\Delta^{(n)} \equiv \psi^{(n)}(1/3) - \psi^{(n)}(2/3)\,. \tag{4.372}$$

and $\psi^{(n)}$ is the polygamma function of order n defined by

$$\psi^{(n)}(z) \equiv \frac{d^{n+1}}{dz^{n+1}}\log\Gamma(z)\,. \tag{4.373}$$

One then has

$$\Delta^{(1)} \approx 7.031721716\,, \tag{4.374}$$

$$\Delta^{(3)} \approx 456.8524809\,. \tag{4.375}$$

These expressions agree with those given in Ref. [30]. For the gluonic correction the result is

$$\begin{aligned}
\frac{\hat{\Pi}_1^{\text{gluon}}}{c_s} &= \frac{1}{Q^4}\left(\frac{640\zeta_3}{3}+\frac{400}{9}\,\Delta^{(1)}-\frac{32}{27}\,\Delta^{(3)}\right),\\
\frac{\hat{\Pi}_4^{\text{gluon}}}{c_s} &= \frac{1}{Q^4}\left(-32+\frac{1664\zeta_3}{3}+\frac{1040}{9}\,\Delta^{(1)}-\frac{256}{81}\,\Delta^{(3)}\right),\\
\frac{\hat{\Pi}_7^{\text{gluon}}}{c_s} &= \frac{1}{Q^6}\left(\frac{512\zeta_3}{3}+\frac{320}{9}\,\Delta^{(1)}-\frac{80}{81}\,\Delta^{(3)}\right),\\
\frac{\hat{\Pi}_{17}^{\text{gluon}}}{c_s} &= \frac{1}{Q^6}\left(-32+384\zeta_3+\frac{272}{3}\,\Delta^{(1)}-\frac{64}{27}\,\Delta^{(3)}\right),\\
\frac{\hat{\Pi}_{39}^{\text{gluon}}}{c_s} &= \frac{1}{Q^6}\left(-\frac{32}{3}-128\zeta_3-\frac{272}{9}\,\Delta^{(1)}+\frac{64}{81}\,\Delta^{(3)}\right),\\
\frac{\hat{\Pi}_{54}^{\text{gluon}}}{c_s} &= 0\,,
\end{aligned} \tag{4.376}$$

where $c_s = \frac{2\pi\alpha_s(N_c^2-1)e_q^4}{(16\pi^2)^2}$.

[22] The associated $\tilde{\Pi}$ are also available upon request.

Chapter 5

Satisfying the short-distance contraints for HLbL

Fail, fail again, fail better.

Samuel Beckett

In the following articles, the Melnikov-Vainshtein (MV) constraint is reviewed and translated into the current dispersive framework for HLbL. A large-N_c inspired Regge model for the transition form factors of excited pseudoscalars is then constructed. This model is compatible with the dispersive description of the pion and η, η'-poles and ensures that the short-distance constraints on HLbL are satisfied.

Since the release of these articles, the two-loop perturbative correction of the HLbL OPE when $Q_1^2, Q_2^2, Q_3^2 \gg \Lambda_{\text{QCD}}$ has been calculated (see chapter 4 of this work). It means that, in addition to the two constraints (the MV constraint and the symmetric Q_i limit) used in the above articles, we now have functions of three different scales to compare to. In addition, the 20% estimate for the pQCD error on the quark loop initially used can be improved upon. These points will shortly be addressed in section 5.3.

5.1 Short-distance constraints on hadronic light-by-light scattering in the anomalous magnetic moment of the muon

This section is a copy of Ref. [39], published in Physical Review D on March 5, 2020

Authors: Gilberto Colangelo, Franziska Hagelstein, Martin Hoferichter, Laetitia Laub, and Peter Stoffer

---

Abstract: A key ingredient in the evaluation of hadronic light-by-light (HLbL) scattering in the anomalous magnetic moment of the muon $(g-2)_\mu$ concerns short-distance constraints that follow from QCD by means of the operator product expansion. Here we concentrate on the most important such constraint, in the longitudinal amplitudes, and show that it can be

implemented efficiently in terms of a Regge sum over excited pseudoscalar states, constrained by phenomenological input on masses, two-photon couplings, as well as short-distance constraints on HLbL scattering and the pseudoscalar transition form factors. Our estimate of the effect of the longitudinal short-distance constraints on the HLbL contribution is: $\Delta a_\mu^{\text{LSDC}} = 13(6) \times 10^{-11}$. This is significantly smaller than previous estimates, which mostly relied on an ad-hoc modification of the pseudoscalar poles and led to up to a 40% increase with respect to the nominal pseudoscalar-pole contributions, when evaluated with modern input for the relevant transition form factors. We also comment on the status of the transversal short-distance constraints and, by matching to perturbative QCD, argue that the corresponding correction will be significantly smaller than its longitudinal counterpart.

5.1.1 Introduction

The precision of the Standard-Model (SM) prediction for the anomalous magnetic moment of the muon, $a_\mu = (g-2)_\mu/2$, is limited by hadronic contributions. Already at the level of the current experiment [5]

$$a_\mu^{\text{exp}} = 116\ 592\ 089(63) \times 10^{-11}, \tag{5.1}$$

estimates of the hadronic effects are crucial in evaluating the significance of the tension with the SM value, at the level of $3.5\,\sigma$. With the forthcoming Fermilab E989 experiment [6], promising an improvement by a factor of 4, as well as the E34 experiment at J-PARC [104], the SM model evaluation needs to follow suit.

To this end, the relevant matrix elements need to be calculated either directly from QCD or be constrained by experimental data. The latter approach has traditionally been followed for hadronic vacuum polarization (HVP), which requires the two-point function of two electromagnetic currents and can be reconstructed from the cross subsection of $e^+e^- \to$ hadrons [8,9,11,62, 159]. More recently, evaluations in lattice QCD have made significant progress [15,16,18–21,160], but are not yet at the level of the data-driven, dispersive approach.

Next to HVP, the second-largest contribution to the uncertainty arises from hadronic light-by-light scattering. While also in this case progress in lattice QCD is promising [161–163], another key development in recent years concerns the phenomenological evaluation, i.e., the use of dispersion relations to remove the reliance on hadronic models, either directly for the required four-point function that defines the HLbL tensor [27, 77, 164–167], the Pauli form factor [81], or in terms of sum rules [32, 82, 168–170]. In particular, organizing the calculation in terms of dispersion relations for the HLbL tensor has led to a solid understanding of the contributions related to the lowest-lying singularities—the single-particle poles from $P = \pi^0, \eta, \eta'$ and cuts from two-pion intermediate states—largely because the hadronic quantities determining the strength of these singularities, the $P \to \gamma^*\gamma^*$ transition form factors [26, 28, 29, 171–173] and the helicity amplitudes for $\gamma^*\gamma^* \to \pi\pi$ [174–179], respectively, can be provided as external input quantities, in a similar spirit as the $e^+e^- \to$ hadrons cross section for HVP. Higher-order iterations of HVP [8, 13, 180] and HLbL [63] are already sufficiently under control.

For both HVP and HLbL, data-driven evaluations of the hadronic corrections to $(g-2)_\mu$ are fundamentally limited by the fact that experimental input is only available in a given energy range, so that the tails of the dispersion integrals have to be estimated by other means, most

notably short-distance constraints as derived from perturbative QCD (pQCD). In addition, even for HVP, short-distance constraints have been used for energies as low as 2 GeV as a supplement to (and check of) experiment, with good agreement found between the pQCD prediction and data in between resonances [8, 11]. For HLbL scattering such constraints become even more important given the limited information on the HLbL tensor for intermediate and high energies.

Two kinematic configurations are relevant for the HLbL contribution, one in which all photon virtualities Q_i^2 are large, and a second in which one of the non-vanishing virtualities remains small compared to the others $Q_3^2 \ll Q_1^2 \sim Q_2^2$. Recently, it was shown that the former situation can be addressed in a systematic operator product expansion (OPE), in which the pQCD quark loop emerges as the first term in the expansion [1]. The second configuration is related to so-called mixed regions in the $g-2$ integral, i.e., integration regions in which asymptotic arguments only apply to a subset of the kinematic variables, while hadronic physics may still be relevant for others. A key insight derived in [2] was that such effects can also be constrained with an OPE, by reducing the HLbL tensor to a vector–vector–axial-vector (VVA) three-point function and using known results for the corresponding anomaly and its (non-) renormalization [60, 103, 181–184]. The explicit implementation suggested in [2] relied on the observation that both the OPE constraint and the normalization are satisfied if the momentum dependence of the singly-virtual form factor describing the pseudoscalar-pole contribution is neglected. However, such a modification is not compatible with a description based on dispersion relations for the HLbL tensor.

Here, we suggest to implement the corresponding longitudinal short-distance constraints in terms of excited pseudoscalar states. As we will show, not only can the asymptotic limits be implemented in a fairly economical manner, but the critical mixed regions can be constrained by phenomenological input for the masses and two-photon couplings of the lowest pseudoscalar excitations. The model dependence can be further reduced by matching to the pQCD quark loop, which, in addition, allows one to gain some insights into the scale where hadronic and pQCD-based descriptions should meet.

5.1.2 OPE constraints on HLbL scattering

The HLbL tensor is defined as the four-point function

$$\begin{aligned}\Pi^{\mu\nu\lambda\sigma}(q_1,q_2,q_3) = -i\int d^4x\, d^4y\, d^4z\, e^{-i(q_1\cdot x+q_2\cdot y+q_3\cdot z)} \\ \times \langle 0|T\{j^\mu_{\text{em}}(x)j^\nu_{\text{em}}(y)j^\lambda_{\text{em}}(z)j^\sigma_{\text{em}}(0)\}|0\rangle\end{aligned} \tag{5.2}$$

of four electromagnetic currents

$$j^\mu_{\text{em}} = \bar{q}\mathcal{Q}\gamma^\mu q, \quad \mathcal{Q} = \text{diag}\left(\frac{2}{3},-\frac{1}{3},-\frac{1}{3}\right), \tag{5.3}$$

where q_i denote the photon virtualities, $q_4 = q_1+q_2+q_3$, and $q = (u,d,s)^T$ the quark fields. We work with the decomposition into scalar functions Π_i,

$$\Pi^{\mu\nu\lambda\sigma} = \sum_{i=1}^{54} T_i^{\mu\nu\lambda\sigma}\Pi_i, \tag{5.4}$$

derived in [27, 77] following the general principle established by Bardeen, Tung [78], and Tarrach [79] (BTT). The contribution to $(g-2)_\mu$ then follows via

$$a_\mu^{\text{HLbL}} = \frac{2\alpha^3}{3\pi^2}\int_0^\infty dQ_1 \int_0^\infty dQ_2 \int_{-1}^1 d\tau \sqrt{1-\tau^2}\, Q_1^3 Q_2^3 \times \sum_{i=1}^{12} T_i(Q_1,Q_2,\tau)\bar{\Pi}_i(Q_1,Q_2,Q_3), \tag{5.5}$$

where $Q_i^2 = -q_i^2$ are the Wick-rotated virtualities, $Q_3^2 = Q_1^2 + Q_2^2 + 2Q_1Q_2\tau$, the $\bar{\Pi}_i$ refer to certain linear combinations of Π_i, and the T_i are known kernel functions [27, 77].

In the limit where all Q_i^2 are large, the calculation from [1] proves the earlier statement of [2] that the pQCD quark loop arises as the first term in a systematic OPE. In particular, this implies the constraint

$$\lim_{Q\to\infty} Q^4\, \bar{\Pi}_1(Q,Q,Q) = -\frac{4}{9\pi^2}. \tag{5.6}$$

The second kinematic configuration [2], $Q^2 \equiv Q_1^2 \sim Q_2^2 \gg Q_3^2$, when expressed in BTT basis, leads to the constraint

$$\lim_{Q_3\to\infty}\lim_{Q\to\infty} Q^2 Q_3^2\, \bar{\Pi}_1(Q,Q,Q_3) = -\frac{2}{3\pi^2}. \tag{5.7}$$

The latter result can be derived by considering the VVA triangle anomaly and its non-renormalization theorems [60, 103, 181–184]. Its constraint on $\bar{\Pi}_1$ (and, by crossing symmetry, $\bar{\Pi}_2$) corresponds to the longitudinal amplitudes in the VVA matrix element and we will therefore refer to $\bar{\Pi}_{1,2}$ as the longitudinal amplitudes and, accordingly, their constraints as longitudinal short-distance constraints. Further, the limit (5.7) is intimately related to the pseudoscalar poles

$$\bar{\Pi}_1^{P\text{-pole}} = \frac{F_{P\gamma^*\gamma^*}(q_1^2,q_2^2)F_{P\gamma\gamma^*}(q_3^2)}{q_3^2 - M_P^2}, \tag{5.8}$$

where $P = \pi^0, \eta, \eta'$, and the doubly-virtual $F_{P\gamma^*\gamma^*}(q_1^2,q_2^2)$ and singly-virtual $F_{P\gamma\gamma^*}(q_3^2)$ transition form factors determine the residue of the poles. They are subject to short-distance constraints themselves, for the pion we have the asymptotic constraint [101]

$$\lim_{Q^2\to\infty} Q^2 F_{\pi^0\gamma^*\gamma^*}(-Q^2,-Q^2) = \frac{2F_\pi}{3}, \tag{5.9}$$

as well as the Brodsky–Lepage limit [185–187]

$$\lim_{Q^2\to\infty} Q^2 F_{\pi^0\gamma\gamma^*}(-Q^2) = 2F_\pi. \tag{5.10}$$

Together with the normalization

$$F_{\pi^0\gamma\gamma} = \frac{1}{4\pi^2 F_\pi}, \tag{5.11}$$

the former shows that if $F_{\pi^0\gamma\gamma^*}(q_3^2) \to F_{\pi^0\gamma\gamma}$ in (5.8), the pion decay constant F_π would drop out and the pion would account for $-1/(6\pi^2)$ in (5.7). Similarly, η and η' would provide the remaining $-1/(2\pi^2)$. This is the essence of the model suggested in [2, 83].

However, a constant singly-virtual transition form factor cannot be justified within a dispersive approach for general HLbL scattering. Instead, one would need to consider dispersion relations in the photon virtualities q_i^2 already in reduced $g-2$ kinematics, and even then the

residue would involve $F_{\pi^0\gamma\gamma^*}(M_P^2)$, not the normalization itself. Further, when writing dispersion relations in the q_i^2 for $g-2$ kinematics, there is no clear separation between the singularities of the HLbL amplitude and those generated by hadronic intermediate states directly coupling to individual electromagnetic currents, such as 2π states. In the dispersive approach for general HLbL scattering the latter appear only in the transition form factors, which factor out and can be treated as external input quantities. In this sense, neglecting the momentum dependence of the singly-virtual transition form factor without at the same time accounting for the additional cuts, leads to a distortion of the low-energy properties of the HLbL tensor.

Instead, we propose here a solution based on a remark already made in [2]: while a finite number of pseudoscalar poles, due to (5.11), cannot fulfill the OPE constraint (5.7), an infinite series potentially can. The basic idea can be illustrated for large-N_c Regge models of the transition form factor itself [188, 189], which assume a radial Regge trajectory to describe the masses of excited vector mesons,

$$M_{V(n)}^2 = M_V^2 + n\,\sigma_V^2, \tag{5.12}$$

and rely on the ansatz:

$$\begin{aligned} F_{P\gamma^*\gamma^*}(-Q^2,-Q^2) &\propto \sum_{n=0}^{\infty} \frac{1}{[Q^2+M_{V(n)}^2]^2} \\ &= \frac{1}{\sigma_V^4}\,\psi^{(1)}\left(\frac{M_V^2+Q^2}{\sigma_V^2}\right) \sim \frac{1}{Q^2}, \end{aligned} \tag{5.13}$$

with $\psi^{(1)}$ the trigamma function and the Regge slope σ_V. In this way, the infinite sum produces the correct asymptotic behavior (5.10), even though none of the individual terms do.

One may wonder about the fate of the infinite sum over excited pseudoscalar states in the chiral limit, given that their decay constants are expected to vanish with the quark masses. We show below how the matching to pQCD removes the model dependence regarding which states are used to satisfy the short-distance constraints, so that the implementation in terms of pseudoscalar excitations mainly adds an estimate for the mixed-region contribution, driven by the phenomenology of the lowest excitations as well as the respective short-distance constraints.

5.1.3 Large-N_c Regge model

In the following, we present a large-N_c-inspired Regge model in the pseudoscalar and vector-meson sectors of QCD that allows us to satisfy the short-distance constraints via an infinite sum of pseudoscalar-pole diagrams (see, e.g., [190–192] for the use of large-N_c arguments to simultaneously fulfill low- and high-energy constraints). For brevity, we focus our description on the pion, referring for a complete and more detailed account to [30]. We start from a standard large-N_c ansatz for the pion transition form factors as in (5.13), but differentiate between ρ and ω trajectories, which are assumed to enter with diagonal couplings due to the wave function overlap [188, 189]. In a first step, we seek an extension of this model that satisfies the constraints (5.9)–(5.11) for the transition form factor as well as (5.6) and (5.7) for the HLbL

tensor

$$
\begin{aligned}
&F_{\pi(n)\gamma^*\gamma^*}(-Q_1^2,-Q_2^2)\\
&=\frac{1}{8\pi^2F_\pi}\left\{\left(\frac{M_\rho^2M_\omega^2}{D^1_{\rho(n)}D^2_{\omega(n)}}+\frac{M_\rho^2M_\omega^2}{D^2_{\rho(n)}D^1_{\omega(n)}}\right)\left[c_{\text{anom}}\right.\right.\\
&\left.+\frac{1}{\Lambda^2}\left(c_AM^2_{+,n}+c_BM^2_{-,n}\right)+c_{\text{diag}}\frac{Q_1^2Q_2^2}{\Lambda^2(Q_+^2+M^2_{\text{diag}})}\right]\\
&+\frac{Q_-^2}{Q_+^2}\left[c_{\text{BL}}+\frac{1}{\Lambda^2}\left(c_AM^2_{-,n}+c_BM^2_{+,n}\right)\right]\\
&\left.\times\left(\frac{M_\rho^2M_\omega^2}{D^1_{\rho(n)}D^2_{\omega(n)}}-\frac{M_\rho^2M_\omega^2}{D^2_{\rho(n)}D^1_{\omega(n)}}\right)\right\},
\end{aligned}
\tag{5.14}
$$

where $Q^2_\pm=Q_1^2\pm Q_2^2$, $M^2_{\pm,n}=\frac{1}{2}[M^2_{\omega(n)}\pm M^2_{\rho(n)}]$, $D^i_X=Q_i^2+M_X^2$, and $\Lambda=\mathcal{O}(1\,\text{GeV})$ a typical QCD scale. The five dimensionless parameters c_{anom}, c_A, c_B, c_{diag}, c_{BL} are used to fulfill all the constraints, while the remaining parameter M_{diag} is adjusted to reproduce the ground-state π^0 transition form factor [28, 172]. In the minimal model (5.14), we only allow $\pi(n)$ to couple to $\rho(n)$ and $\omega(n)$, i.e., the couplings are fully diagonal in the excitation numbers, while the effect of the eliminated vector-meson excitations is subsumed into a Q_i^2 dependence of the numerator multiplying the resonance propagators. In addition, we also considered an untruncated large-N_c model, in which both the Regge summation in the transition form factor itself (5.13) and the HLbL tensor are retained, to assess the systematics in the large-N_c ansatz [30]. Using the Regge slopes from [193] and the other input parameters from [100], we find that we can indeed reproduce well the π^0 transition form factor, which also ensures that effective-field-theory constraints on the pion-pole contribution to $(g-2)_\mu$ [194, 195] are fulfilled [28]. Finally, the model predicts a two-photon coupling of the first excited pion, $\pi(1300)$, in line with its phenomenological bound $F_{\pi(1300)\gamma\gamma}<0.0544(71)\,\text{GeV}^{-1}$ [196, 197].

Constructing a large-N_c Regge model for $\eta^{(\prime)}$ proceeds along the same lines, but involves several complications. First, the ρ and ω trajectories do not suffice to incorporate all constraints since due to the $I=0$ nature of $\eta^{(\prime)}$ only equal-mass combinations of vector mesons (2ρ, 2ω, 2ϕ) contribute to (5.14), so that only three model parameters survive. To provide sufficient freedom in satisfying all constraints the consideration of ω–ϕ mixing cannot be avoided. In addition, η–η' mixing needs to be taken into account, both for the flavor decomposition of the short-distance constraints as well as the relative weights of the vector-meson combinations in the transition form factors. The former is directly constrained by data on the transition form factors [26,198], but for the calculation of the weights, which we extract from effective pseudoscalar–vector–vector and photon–vector Lagrangians [199, 200], it is more convenient to work with the phenomenological two-angle mixing scheme from [201, 202]. We therefore use the latter everywhere. All variants are covered by the error analysis.

The resulting η and η' transition form factors are in good agreement with experimental data in the singly-virtual [203–206] and doubly-virtual regions [207], as well as the fit results using Canterbury approximants [26]. Furthermore, there are some phenomenological constraints on the two-photon couplings for $\eta(1295)$ [208, 209], $\eta(1405)$ [208–210], $\eta(1475)$ [210, 211], $\eta(1760)$ [212], and $X(1835)$ [210, 212], where $\eta(1475)$ and $\eta(1760)$ are actually seen in $\gamma\gamma$ collisions, while for the others only limits are available. The detailed comparison depends on the assignment of these

states into η and η' trajectories, but the predictions of our model are compatible with either the assignment from [100, 193] (our main choice) or the one from [213], see [30].

By construction, the ground-state pseudoscalar-pole contributions to $(g-2)_\mu$ reproduce literature values [26, 28, 172, 214] within errors, while the sum over excited-pseudoscalar poles leads to the increase:

$$\begin{aligned} \Delta a_\mu^{\pi\text{-poles}} &= 2.7\,(0.4)_{\text{Model}}\,(1.2)_{\text{syst}} \times 10^{-11}, \\ \Delta a_\mu^{\eta\text{-poles}} &= 3.4\,{}^{+0.9}_{-0.7}\big|_{\text{Model}}\,(0.9)_{\text{syst}} \times 10^{-11}, \\ \Delta a_\mu^{\eta'\text{-poles}} &= 6.5\,(1.1)_{\text{Model}}\,(1.7)_{\text{syst}} \times 10^{-11}, \end{aligned} \tag{5.15}$$

where the first error refers to the uncertainties propagated from the input parameters and the systematic error is estimated by comparison to an alternative untruncated large-N_c Regge model [30]. Combining all pseudoscalars, we find:

$$\begin{aligned} \Delta a_\mu^{\text{PS-poles}} &= \Delta a_\mu^{\pi\text{-poles}} + \Delta a_\mu^{\eta\text{-poles}} + \Delta a_\mu^{\eta'\text{-poles}} \\ &= 12.6\,{}^{+1.6}_{-1.5}\big|_{\text{Model}}\,(3.8)_{\text{syst}} \times 10^{-11} \\ &= 12.6(4.1) \times 10^{-11}. \end{aligned} \tag{5.16}$$

This result should be contrasted with the one suggested in [2] to satisfy the mixed-region short-distance constraint (using transition form factor models from [109]): $\Delta a_\mu^{\text{PS-poles}}\big|_{\text{MV}} = 23.5 \times 10^{-11}$, which would become 38×10^{-11} once updated with modern input for the transition form factors, and thus suggest an increase nearly three times as large as (5.16) or almost 40% of the nominal pseudoscalar-pole contribution. Given that arguments following [2] have been included in previous compilations of HLbL [149], a central result of this work is that such a large increase does not occur if the short-distance constraints are implemented without compromising the low-energy properties of HLbL scattering.

5.1.4 Matching to perturbative QCD

Since, by construction, the sum over the pseudoscalar excitations fulfills the short-distance constraints, it has to match onto the pQCD quark loop for sufficiently large momentum transfers. In the upper plot of Fig. 5.1, the contribution to $(g-2)_\mu$ from the massless pQCD quark loop (black) and the pseudoscalar-pole contributions (sum of ground-state and excited states in orange) are compared after imposing a cutoff $Q_{\text{min}} \leq Q_i$ in the integration: the matching occurs somewhere around 1.5–2 GeV. The lower plot, where the opposite cutoff $Q_{\text{max}} \geq Q_i$ is imposed, shows that the contribution of the excited pseudoscalars (blue) to the low-energy region is very small and entirely saturated by the first few excitations (blue dot-dashed). These observations suggest to evaluate the asymptotic part of the integral $Q_i \geq Q_{\text{min}}$ with pQCD, to make explicit that this part of the result does not depend on the nature of hadronic states used in the implementation. Defining an optimal matching scale would require information on the uncertainty of the pQCD result. Here, we simply use a rough 20% estimate, which is the size of pQCD corrections for inclusive τ decays, a process that has a similar energy scale and has been studied in detail [215–220].

Together with the uncertainties from the Regge model, these considerations lead to a scale $Q_{\text{match}} = 1.7\,\text{GeV}$. Varying this scale within $\pm 0.5\,\text{GeV}$ and adding the systematic uncertainty

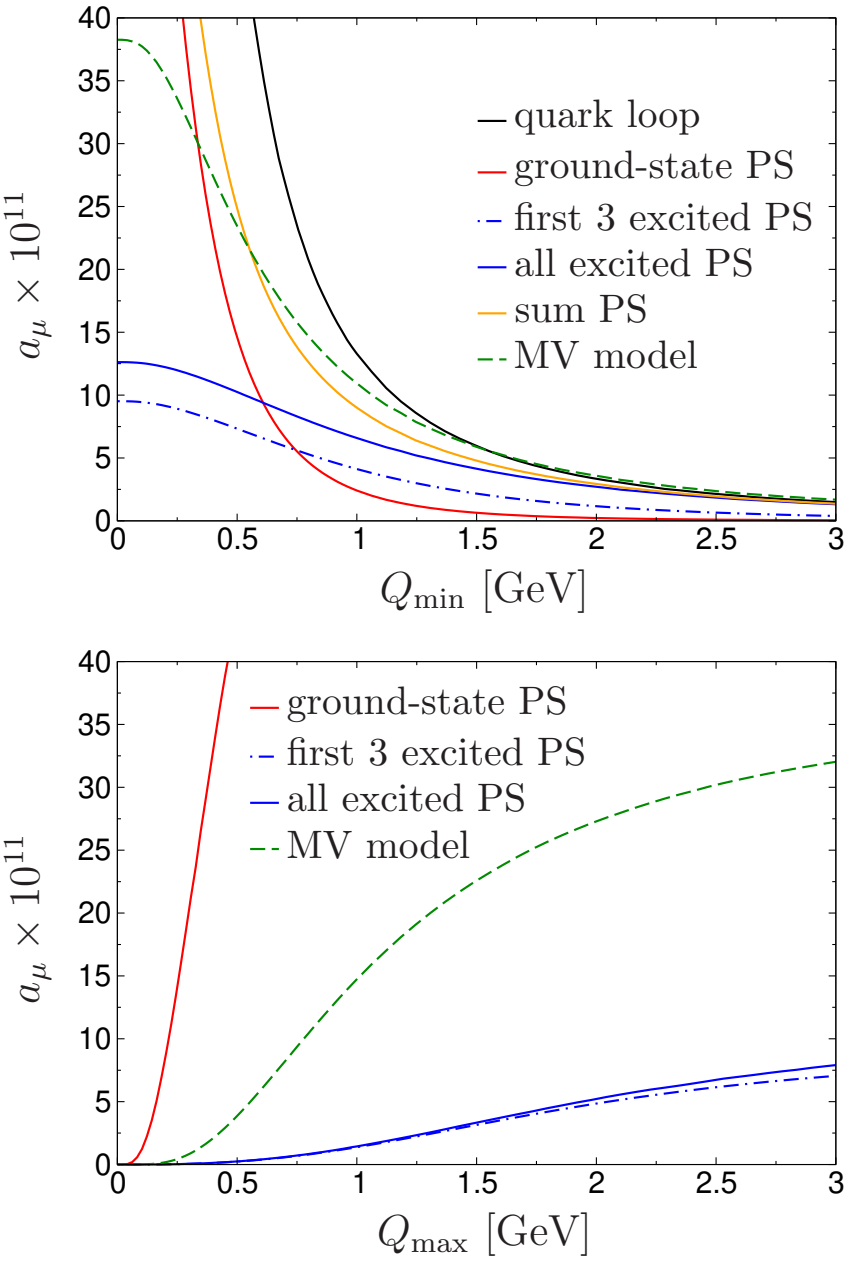

Figure 5.1: The longitudinal part of the massless pQCD quark loop (black), the ground-state pseudoscalars (red), the sum of all excitations from the large-N_c Regge model (blue), the first three excitations (blue dot-dashed), the sum of ground and excited states (orange), and the increase found in the Melnikov–Vainshtein model (green dashed). The upper plot shows the contribution to a_μ for $Q_i \geq Q_{\min}$, the lower for $Q_i \leq Q_{\max}$.

from the comparison to the untruncated Regge model, we obtain as our final result:

$$\begin{aligned} \Delta a_\mu^{\text{LSDC}} &= [8.7(5.5)_{\text{PS-poles}} + 4.6(9)_{\text{pQCD}}] \times 10^{-11} \\ &= 13(6) \times 10^{-11} \end{aligned} \tag{5.17}$$

for the increase of $(g-2)_\mu$ due to longitudinal short-distance constraints. In particular, the lowest three pseudoscalar excitations, whose contribution is at least partly constrained by phenomenological input on masses and two-photon couplings, give 7.8×10^{-11}. Given that the most uncertain contribution, from $n > 3$, thus amounts to only 10% of the total, the uncertainty

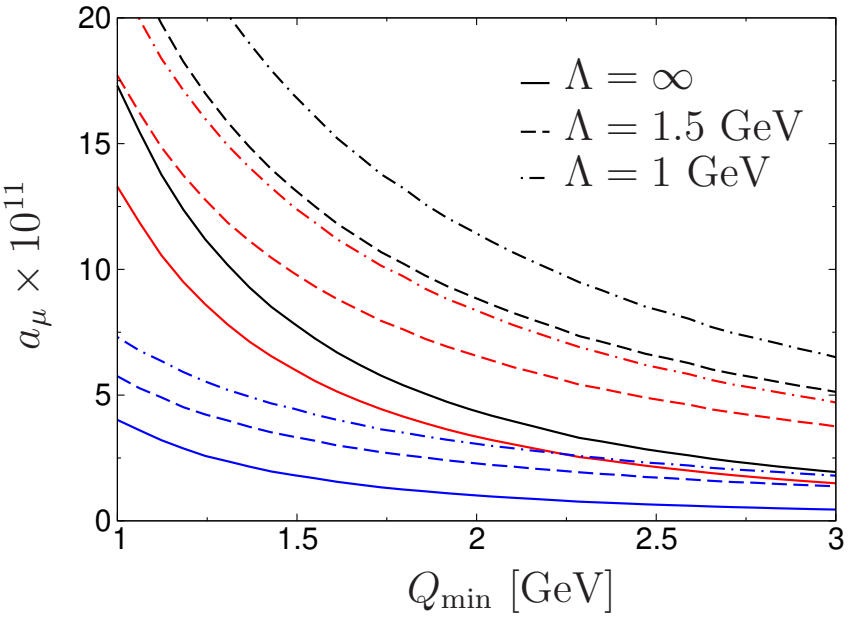

Figure 5.2: Contribution of the massless pQCD quark loop to a_μ from the region $Q_{1,2} \geq Q_{\rm min}$, with the contribution from Q_3 below $Q_{\rm min}$ damped by $Q_3^2/(Q_3^2+\Lambda^2)$ (plus crossed). The total contribution (black) is split into longitudinal (red) and transversal (blue) components. The limit $Q_i \geq Q_{\rm min}$ for all Q_i is reproduced for $\Lambda \to \infty$.

estimate in (5.17) should be conservative enough to cover the remaining model dependence. In particular, the error in (5.17) includes an inflation of the Regge slope uncertainties by a factor three, to allow for systematic effects that might occur if other hadronic states were used to implement the short-distance constraints. More recently, this expectation has been confirmed by models in holographic QCD based on a summation of an infinite tower of axial-vector resonances instead [41, 42], which despite very different assumptions and systematics yield results remarkably close to (5.17).

With the impact of the longitudinal short-distance constraints estimated as in (5.17), it is natural to inquire about the role of the transversal short-distance constraints. A first estimate could again be obtained by matching to pQCD. Fig. 5.2 extends the integration region beyond $Q_i \geq Q_{\rm min}$ into the mixed region, but suppressing this additional contribution by a factor $Q_3^2/(Q_3^2+\Lambda^2)$, because otherwise part of the ground-state pseudoscalar contribution would be double-counted. The longitudinal result is reproduced for scales around $\Lambda \sim Q_{\rm min} \sim 1.4\,\text{GeV}$, for which one would read off $\Delta a_\mu^{\rm TSDC} \sim 4 \times 10^{-11}$. Accordingly, we would expect the impact of the transversal short-distance constraints to be significantly less than that of the longitudinal ones.

We stress that the calculation presented here is complementary to higher-order calculations in pQCD and/or the OPE [1], which would allow one to improve the matching between hadronic implementations and a perturbative description. Similarly, more experimental guidance on the two-photon couplings of hadronic states in the 1–2 GeV region would be beneficial for the phenomenological analysis, not only for the excited pseudoscalars, but for axial-vector resonances as well, which outlines avenues for future work. We conclude that with the present analysis the biggest systematic uncertainty due to short-distance constraints has been reduced significantly,

with the result that the asymptotic part of the HLbL tensor is under sufficient control for the first release from the Fermilab experiment.

Acknowledgments We thank R. Arnaldi, P. Bickert, J. Bijnens, S. Eidelman, A. Gérardin, C. Hanhart, S. Holz, B. Kubis, S. Leupold, J. Lüdtke, A. Manohar, V. Metag, M. Procura, E. Ruiz Arriola, P. Sanchez-Puertas, A. Uras, G. Usai, A. Vainshtein, and E. Weil for useful communication on various aspects of this work. Financial support by the DOE (Grant Nos. DE-FG02-00ER41132 and DE-SC0009919) and the Swiss National Science Foundation is gratefully acknowledged. M.H. is supported by an SNSF Eccellenza Professorial Fellowship (Project No. PCEFP2_181117).

5.2 Longitudinal short-distance constraints for the hadronic light-by-light contributions to $(g-2)_\mu$ with large-N_c Regge models

This section is a copy of Ref. [30], published in the Journal of High-Energy Physics (JHEP) on March 17, 2020

Authors: Gilberto Colangelo, Franziska Hagelstein, Martin Hoferichter, Laetitia Laub, and Peter Stoffer

---

Abstract: While the low-energy part of the hadronic light-by-light (HLbL) tensor can be constrained from data using dispersion relations, for a full evaluation of its contribution to the anomalous magnetic moment of the muon $(g-2)_\mu$ also mixed- and high-energy regions need to be estimated. Both can be addressed within the operator product expansion (OPE), either for configurations where all photon virtualities become large or one of them remains finite. Imposing such short-distance constraints (SDCs) on the HLbL tensor is thus a major aspect of a model-independent approach towards HLbL scattering. Here, we focus on longitudinal SDCs, which concern the amplitudes containing the pseudoscalar-pole contributions from π^0, η, η'. Since these conditions cannot be fulfilled by a finite number of pseudoscalar poles, we consider a tower of excited pseudoscalars, constraining their masses and transition form factors from Regge theory, the OPE, and phenomenology. Implementing a matching of the resulting expressions for the HLbL tensor onto the perturbative QCD quark loop, we are able to further constrain our calculation and significantly reduce its model dependence. We find that especially for the π^0 the corresponding increase of the HLbL contribution is much smaller than previous prescriptions in the literature would imply. Overall, we estimate that longitudinal SDCs increase the HLbL contribution by $\Delta a_\mu^{\text{LSDC}} = 13(6) \times 10^{-11}$. This number does not include the contribution from the charm quark, for which we find $a_\mu^{c\text{-quark}} = 3(1) \times 10^{-11}$.

5.2.1 Introduction

Current Standard Model (SM) evaluations of the anomalous magnetic moment of the muon, $a_\mu = (g-2)_\mu/2$, differ from the value measured at the Brookhaven National Laboratory [5]

$$a_\mu^{\text{exp}} = 116\ 592\ 089(63) \times 10^{-11}, \tag{5.18}$$

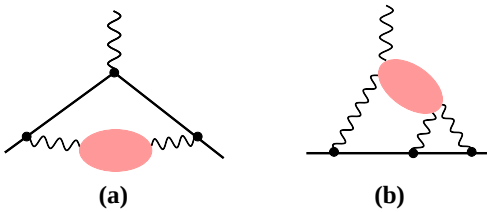

Figure 5.3: Hadronic contributions to $(g-2)_\mu$: (a) HVP, (b) HLbL. The pink blobs symbolize hadronic intermediate states.

by around $3.5\,\sigma$. In the near future, the new Fermilab E989 experiment [6] will be able to reduce the experimental uncertainty by a factor 4, and the E34 experiment at J-PARC [104] will provide an important cross check, see ref. [221] for a comparison of the experimental methods. Therefore, the theoretical calculation of a_μ needs to be improved accordingly.

The uncertainty of the SM prediction mainly stems from hadronic contributions, such as hadronic vacuum polarization (HVP), see figure 5.3 (a), and HLbL scattering, see figure 5.3 (b). Since the HVP contribution can be systematically calculated with a data-driven dispersive approach [8, 9, 11, 62, 159], lattice QCD [15, 16, 18–21, 160], and potentially be accessed independently by the proposed MUonE experiment [222, 223], which aims to measure the space-like fine-structure constant $\alpha(t)$ in elastic electron–muon scattering, the HLbL contribution may end up dominating the theoretical error.[1]

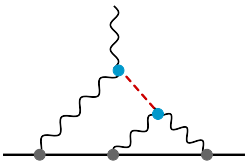

Figure 5.4: Pseudoscalar-pole contribution to $(g-2)_\mu$. The cyan dots indicate the TFF of the pseudoscalar meson.

Apart from lattice QCD [161–163], recent data-driven approaches towards HLbL scattering are again rooted in dispersion theory, either for the HLbL tensor [27, 77, 164–167], the Pauli form factor [81], or in terms of sum rules [32, 82, 168–170]. In all approaches, the most important HLbL contributions are the π^0-pole and other pseudoscalar-meson-pole contributions, see figure 5.4. The strength of these pseudoscalar poles is determined by the transition form factors (TFFs), which in turn can be reconstructed from dispersion theory [28, 171, 172, 227–229], leading to [28, 172]

$$a_\mu^{\pi^0\text{-pole}} = 62.6^{+3.0}_{-2.5} \times 10^{-11}, \tag{5.19}$$

in agreement with determinations from lattice QCD [29], Canterbury approximants (CA) [26], and Dyson–Schwinger equations (DSE) [173]. Since the central value (5.19) is close to earlier model-based calculations, e.g., within lowest-meson-dominance+vector (LMD+V) models [109], the second-most important aspect of the dispersive approach apart from rigorous uncertainty

[1] Note that higher-order insertions of HVP [8, 13, 180] and HLbL [63] are already under sufficient control, as are hadronic corrections in the anomalous magnetic moment of the electron, where recently a $2.5\,\sigma$ tension between the direct measurement [69] and the SM prediction [224] using the fine-structure constant from Cs interferometry [74] emerged [225, 226].

estimates is the clear definition of the pseudoscalar intermediate states in terms of physical, on-shell form factors, in contrast to earlier notions of a pion-exchange contribution, see ref. [230], which involve the model-dependent concept of an off-shell pion. This becomes particularly important when combined with other intermediate states, ensuring that the pseudoscalar poles are consistent with, for instance, the dispersive definition of two-pion intermediate states [27, 167], which in turn are determined by the corresponding on-shell quantities, in this case the helicity amplitudes for $\gamma^*\gamma^* \to \pi\pi$ [174–179].

However, in contrast to HVP there is no closed formula that resums all possible intermediate states (in terms of the cross section for $e^+e^- \to$ hadrons [231, 232]), in such a way that the consideration of exclusive channels will break down eventually, irrespective of the complications when extending the dispersive formalism to higher-multiplicity intermediate states. Therefore, to control the regions in the $(g-2)_\mu$ integral where either two or all three independent photon virtualities become large, additional constraints are required. In close analogy to HVP, where perturbative QCD (pQCD) becomes applicable in the high-energy tail of the dispersive integral, such constraints arise from the OPE and pQCD. In the regime where all three virtualities are large it was shown recently [1] that the pQCD quark loop indeed arises as the first term in a controlled OPE, with the next order suppressed by small quark masses and condensates. For the case in which one virtuality remains small, the leading OPE constraint was derived in ref. [2], by reducing the HLbL tensor in this limit to the triangle anomaly and its known non-renormalization theorems [60, 103, 181, 182].[2]

The latter constraint decomposes into longitudinal and transversal contributions. As noted in ref. [2], the longitudinal part is intimately related to the pseudoscalar poles, but cannot be saturated by π^0, η, η' alone, nor by any finite number of poles. As a remedy it was suggested to drop the momentum dependence of the TFF at the vertex to which the external photon is attached, see figure 5.4, which leads to a substantial increase of the pseudoscalar-pole HLbL contribution. Based on an LMD+V model for the π^0 and vector-meson-dominance (VMD) models for η, η' from ref. [109], this increase was found to be 13.5×10^{-11} for the π^0 and 5×10^{-11} each for η and η'. This shift has been included, in one way or another, in subsequent estimates of the total HLbL value [149, 230]. In fact, as we will show below, with modern input for the TFFs the corresponding increase would become even larger. While there is no doubt that the SDC is important—it is, in fact, one of the few constraints on the mixed-energy regions in which one photon virtuality remains small—modifying the expression for the pseudoscalar poles in this way is not compatible with the dispersive description of the four-point HLbL tensor [27, 77, 165–167] and spoils consistency with other intermediate states in the same framework.

In this work we address the question from a different standpoint: already in ref. [2] it was observed that while a finite number of poles cannot saturate the SDC, an infinite tower of them potentially can—dropping the TFF at the external vertex has in fact been described in ref. [2] as a model for the resummation of the tower of pseudoscalar states. Here we present explicit constructions that implement the Melnikov–Vainshtein (MV) constraint in terms of an infinite tower of excited pseudoscalars, constraining their properties from Regge theory, all available

[2]These non-renormalization theorems strictly apply only in the chiral limit and to the non-singlet components. Instances where additional corrections for the singlet component arise are pointed out throughout the discussion of the various SDCs in sections 5.2.2 and 5.2.3.

SDCs, and phenomenology wherever possible [233]. Given all these constraints the resulting models for the HLbL tensor prove remarkably rigid, without altering the low-energy properties. Since phenomenological information on excited pseudoscalars, especially their TFFs, is scarce, we do not attempt to construct TFF representations that apply for arbitrary kinematics, but concentrate on minimal models that cover the space-like region needed for $(g-2)_\mu$ and at the same time are able to fulfill all SDCs. Systematic uncertainties are estimated by comparing two such representations, either based on a truncated or untruncated Regge sum for the TFFs themselves, as well as the available phenomenological constraints, see appendices 5.2.D and 5.2.E. Moreover, our model is only needed for the low-energy part of the $(g-2)_\mu$ integral: above the energy where the matching occurs, we calculate the integral with the quark loop. This strategy also ensures that the estimate of the asymptotic region still applies in the chiral limit, in which the excited pseudoscalar states decouple, see section 5.2.5.3, while at low energies phenomenological input is needed either way to account for the effect of quark-mass corrections. All this leads to a more reliable estimate for the impact of the OPE constraints on the total HLbL contribution. To this end, we first review the expression for the pQCD quark loop and the known OPE constraints on the HLbL tensor in sections 5.2.2 and 5.2.3, adapting the conventions to the language suitable for the decomposition of the HLbL tensor from refs. [27, 77], in which the expressions for both the pseudoscalar poles and the pQCD quark loop become remarkably simple. Next, we present in section 5.2.4 the explicit construction of large-N_c-inspired Regge models[3] implementing the OPE constraints and derive the consequences for HLbL scattering and $(g-2)_\mu$. In section 5.2.5, we match the resulting expressions for the HLbL tensor to the pQCD loop to obtain a first estimate of the scale where the description of the HLbL tensor in terms of hadronic intermediate states and its asymptotic properties should meet. A more detailed comparison to the results obtained with the MV model is provided in section 5.2.6, before we summarize our main results and discuss future developments in section 5.2.7. Technical details and alternative evaluations that are used to estimate the systematic uncertainty are collected in the appendices.

5.2.2 The hadronic light-by-light tensor

5.2.2.1 Lorentz decomposition and $(g-2)_\mu$ integral

Throughout, we follow the conventions for the decomposition of the HLbL tensor and its contribution to $(g-2)_\mu$ from ref. [27]. Starting point is the HLbL tensor defined as the four-point function

$$\Pi^{\mu\nu\lambda\sigma}(q_1,q_2,q_3) = -i\int d^4x\, d^4y\, d^4z\, e^{-i(q_1\cdot x+q_2\cdot y+q_3\cdot z)}\langle 0|T\{j^\mu(x)j^\nu(y)j^\lambda(z)j^\sigma(0)\}|0\rangle \tag{5.20}$$

of the electromagnetic current

$$j^\mu = \bar\psi\mathcal{Q}\gamma^\mu\psi, \quad \psi=(u,d,s)^T, \quad \mathcal{Q}=\operatorname{diag}\left(\frac{2}{3},-\frac{1}{3},-\frac{1}{3}\right), \tag{5.21}$$

and momenta assigned as $q_1+q_2+q_3=q_4\to 0$. Its Lorentz decomposition in terms of scalar functions Π_i is written following the Bardeen–Tung–Tarrach (BTT) prescription [78, 79]

$$\Pi^{\mu\nu\lambda\sigma} = \sum_{i=1}^{54} T_i^{\mu\nu\lambda\sigma}\Pi_i, \tag{5.22}$$

[3] For brevity we call our large-N_c-inspired Regge models simply large-N_c Regge models.

where the Π_i are free of kinematic singularities and thus amenable to a dispersive treatment. However, this decomposition does not allow for a projection onto independent Lorentz structures, given that there are only 41 independent helicity amplitudes for fully off-shell photon–photon scattering. Moreover, two of these redundancies only occur in four space-time dimensions [234]. A given expression for the HLbL tensor is thus most conveniently projected onto a subset of 43 Lorentz structures

$$\Pi^{\mu\nu\lambda\sigma} = \sum_{i=1}^{43} \mathcal{B}_i^{\mu\nu\lambda\sigma} \tilde{\Pi}_i. \tag{5.23}$$

The functions $\tilde{\Pi}_i$ are no longer free of kinematic singularities, but the form of their singularities follows from the projection of the BTT decomposition. The necessary projectors are provided in ref. [77]. Next, only a subset of the structures $T_i^{\mu\nu\lambda\sigma}$ actually contributes to $(g-2)_\mu$. To make this explicit it is convenient to perform another basis change

$$\Pi^{\mu\nu\lambda\sigma} = \sum_{i=1}^{54} T_i^{\mu\nu\lambda\sigma} \Pi_i = \sum_{i=1}^{54} \hat{T}_i^{\mu\nu\lambda\sigma} \hat{\Pi}_i, \tag{5.24}$$

in such a way that in the limit $q_4 \to 0$ the derivative of 35 structures $\hat{T}_i^{\mu\nu\lambda\sigma}$ vanishes. The 19 structures $\hat{T}_i^{\mu\nu\lambda\sigma}$ that do contribute to $(g-2)_\mu$ can be chosen as [27]

$$\begin{aligned} \hat{T}_i^{\mu\nu\lambda\sigma} &= T_i^{\mu\nu\lambda\sigma}, \quad i = 1, \ldots, 11, 13, 14, 16, 17, 50, 51, 54, \\ \hat{T}_{39}^{\mu\nu\lambda\sigma} &= \frac{1}{3}\left(T_{39}^{\mu\nu\lambda\sigma} + T_{40}^{\mu\nu\lambda\sigma} + T_{46}^{\mu\nu\lambda\sigma}\right). \end{aligned} \tag{5.25}$$

In this way, the 19 relevant linear combinations of scalar functions are

$$\begin{aligned} \hat{\Pi}_1 &= \Pi_1 + q_1 \cdot q_2 \Pi_{47}, \\ \hat{\Pi}_4 &= \Pi_4 - q_1 \cdot q_3 \left(\Pi_{19} - \Pi_{42}\right) - q_2 \cdot q_3 \left(\Pi_{20} - \Pi_{43}\right) + q_1 \cdot q_3 q_2 \cdot q_3 \Pi_{31}, \\ \hat{\Pi}_7 &= \Pi_7 - \Pi_{19} + q_2 \cdot q_3 \Pi_{31}, \\ \hat{\Pi}_{17} &= \Pi_{17} + \Pi_{42} + \Pi_{43} - \Pi_{47}, \\ \hat{\Pi}_{39} &= \Pi_{39} + \Pi_{40} + \Pi_{46}, \\ \hat{\Pi}_{54} &= \Pi_{42} - \Pi_{43} + \Pi_{54}, \end{aligned} \tag{5.26}$$

together with the crossed versions

$$\begin{aligned} &\hat{\Pi}_2 = \mathcal{C}_{23}\big[\hat{\Pi}_1\big], \quad \hat{\Pi}_3 = \mathcal{C}_{13}\big[\hat{\Pi}_1\big], \quad \hat{\Pi}_5 = \mathcal{C}_{23}\big[\hat{\Pi}_4\big], \quad \hat{\Pi}_6 = \mathcal{C}_{13}\big[\hat{\Pi}_4\big], \quad \hat{\Pi}_8 = \mathcal{C}_{12}\big[\hat{\Pi}_7\big], \\ &\hat{\Pi}_9 = \mathcal{C}_{12}\big[\mathcal{C}_{13}\big[\hat{\Pi}_7\big]\big], \quad \hat{\Pi}_{10} = \mathcal{C}_{23}\big[\hat{\Pi}_7\big], \quad \hat{\Pi}_{13} = \mathcal{C}_{13}\big[\hat{\Pi}_7\big], \quad \hat{\Pi}_{14} = \mathcal{C}_{12}\big[\mathcal{C}_{23}\big[\hat{\Pi}_7\big]\big], \\ &\hat{\Pi}_{11} = \mathcal{C}_{13}\big[\hat{\Pi}_{17}\big], \quad \hat{\Pi}_{16} = \mathcal{C}_{23}\big[\hat{\Pi}_{17}\big], \quad \hat{\Pi}_{50} = -\mathcal{C}_{23}\big[\hat{\Pi}_{54}\big], \quad \hat{\Pi}_{51} = \mathcal{C}_{13}\big[\hat{\Pi}_{54}\big], \end{aligned} \tag{5.27}$$

where the crossing operators $\mathcal{C}_{ij}$ exchange momenta and Lorentz indices of the photons i and j

$$\mathcal{C}_{12}[f] := f(\mu \leftrightarrow \nu, q_1 \leftrightarrow q_2), \quad \mathcal{C}_{14}[f] := f(\mu \leftrightarrow \sigma, q_1 \leftrightarrow -q_4), \tag{5.28}$$

and multiple operations are understood to act as in the example $\mathcal{C}_{12}[\mathcal{C}_{23}[f(q_1,q_2,q_3,q_4)]] = \mathcal{C}_{12}[f(q_1,q_3,q_2,q_4)] = f(q_2,q_3,q_1,q_4)$. In addition, the $\hat{\Pi}_i$ preserve the crossing symmetries

$$\begin{aligned} &\hat{\Pi}_1 = \mathcal{C}_{12}\big[\hat{\Pi}_1\big], \quad \hat{\Pi}_4 = \mathcal{C}_{12}\big[\hat{\Pi}_4\big], \quad \hat{\Pi}_{17} = \mathcal{C}_{12}\big[\hat{\Pi}_{17}\big], \\ &\hat{\Pi}_{39} = \mathcal{C}_{12}\big[\hat{\Pi}_{39}\big] = \mathcal{C}_{13}\big[\hat{\Pi}_{39}\big] = \ldots, \quad \hat{\Pi}_{54} = -\mathcal{C}_{12}\big[\hat{\Pi}_{54}\big]. \end{aligned} \tag{5.29}$$

The $\hat{\Pi}_i$ defined in this way display all crossing symmetries that survive in the limit $q_4 \to 0$ and are thus particularly well suited for the HLbL application. In consequence, only the six functions (5.26) need to be specified, with all the rest following from crossing symmetry.

In terms of these functions the HLbL contribution to $(g-2)_\mu$ becomes

$$a_\mu^{\text{HLbL}} = \frac{2\alpha^3}{3\pi^2}\int_0^\infty dQ_1 \int_0^\infty dQ_2 \int_{-1}^1 d\tau \sqrt{1-\tau^2} Q_1^3 Q_2^3 \sum_{i=1}^{12} T_i(Q_1,Q_2,\tau)\bar{\Pi}_i(Q_1,Q_2,\tau), \tag{5.30}$$

where $Q_1 = |Q_1|$ and $Q_2 = |Q_2|$ denote the norm of the Euclidean four-vectors and we have used the symmetry of the kernel functions under $q_1 \leftrightarrow -q_2$ to reduce the sum to only 12 terms. The remaining kernel functions $T_i(Q_1,Q_2,\tau)$ are listed in ref. [27] and the 12 scalar function $\bar{\Pi}_i$ simply correspond to a subset of the $\hat{\Pi}_i$

$$\begin{aligned}
&\bar{\Pi}_1 = \hat{\Pi}_1, && \bar{\Pi}_2 = \hat{\Pi}_2, && \bar{\Pi}_3 = \hat{\Pi}_4, && \bar{\Pi}_4 = \hat{\Pi}_5,\\
&\bar{\Pi}_5 = \hat{\Pi}_7, && \bar{\Pi}_6 = \hat{\Pi}_9, && \bar{\Pi}_7 = \hat{\Pi}_{10}, && \bar{\Pi}_8 = \hat{\Pi}_{11},\\
&\bar{\Pi}_9 = \hat{\Pi}_{17}, && \bar{\Pi}_{10} = \hat{\Pi}_{39}, && \bar{\Pi}_{11} = \hat{\Pi}_{50}, && \bar{\Pi}_{12} = \hat{\Pi}_{54}.
\end{aligned} \tag{5.31}$$

They are evaluated for the kinematics

$$s = q_3^2 = -Q_3^2 = -Q_1^2 - 2Q_1Q_2\tau - Q_2^2, \quad t = q_2^2 = -Q_2^2, \quad u = q_1^2 = -Q_1^2, \quad q_4^2 = 0, \tag{5.32}$$

where s, t, u are the Mandelstam variables of the original HLbL scattering process. Finally, we quote an alternative formulation of (5.30) based on the parameterization [235]

$$\begin{aligned}
Q_1^2 &= \frac{\Sigma}{3}\left(1 - \frac{r}{2}\cos\phi - \frac{r}{2}\sqrt{3}\sin\phi\right),\\
Q_2^2 &= \frac{\Sigma}{3}\left(1 - \frac{r}{2}\cos\phi + \frac{r}{2}\sqrt{3}\sin\phi\right),\\
Q_3^2 &= Q_1^2 + 2Q_1Q_2\tau + Q_2^2 = \frac{\Sigma}{3}\left(1 + r\cos\phi\right).
\end{aligned} \tag{5.33}$$

This variable transformation leads to

$$a_\mu^{\text{HLbL}} = \frac{\alpha^3}{432\pi^2}\int_0^\infty d\Sigma\,\Sigma^3 \int_0^1 dr\, r\sqrt{1-r^2}\int_0^{2\pi} d\phi \sum_{i=1}^{12} T_i(Q_1,Q_2,\tau)\bar{\Pi}_i(Q_1,Q_2,\tau), \tag{5.34}$$

which often facilitates the numerical evaluation.

5.2.2.2 Pseudoscalar poles

The pseudoscalar poles only appear in $\hat{\Pi}_1$ (and by crossing symmetry in $\hat{\Pi}_{2,3}$)

$$\hat{\Pi}_1^{P\text{-pole}} = \frac{F_{P\gamma^*\gamma^*}(q_1^2,q_2^2)F_{P\gamma\gamma^*}(q_3^2)}{q_3^2 - M_P^2}, \tag{5.35}$$

with $F_{P\gamma^*\gamma^*}(q_1^2,q_2^2)$ the doubly-virtual TFF, $F_{P\gamma\gamma^*}(q^2) = F_{P\gamma^*\gamma^*}(q^2,0)$ the singly-virtual TFF, and $P = \pi^0,\eta,\eta'$ (see ref. [77] for the detailed derivation). The TFFs are normalized to the two-photon decays according to

$$\Gamma(P\to\gamma\gamma) = \frac{\pi\alpha^2 M_P^3}{4}F_{P\gamma\gamma}^2, \qquad F_{P\gamma\gamma} = F_{P\gamma^*\gamma^*}(0,0). \tag{5.36}$$

They are defined by the matrix element

$$i\int d^4x\, e^{iq_1\cdot x}\langle 0|T\{j_\mu(x)j_\nu(0)\}|P(q_1+q_2)\rangle = \epsilon_{\mu\nu\alpha\beta}\, q_1^\alpha\, q_2^\beta\, F_{P\gamma^*\gamma^*}(q_1^2,q_2^2). \tag{5.37}$$

In the chiral limit, the non-singlet normalizations are determined by the Adler–Bell–Jackiw anomaly [236–238]

$$\sum_P F_P^a F_{P\gamma\gamma} = \frac{3}{2\pi^2}C_a, \qquad C_a = \frac{1}{2}\mathrm{Tr}(\mathcal{Q}^2\lambda_a), \tag{5.38}$$

with Gell-Mann matrices λ_a, $\lambda_0 = \sqrt{2/3}\,\mathbb{1}$,

$$C_3 = \frac{1}{6}, \qquad C_8 = \frac{1}{6\sqrt{3}}, \qquad C_0 = \frac{2}{3\sqrt{6}}, \tag{5.39}$$

and decay constants defined through F_P^a:

$$\langle 0|A_\mu^a(0)|P(p)\rangle =: ip_\mu F_P^a, \tag{5.40}$$

which is in general a 3×3 matrix. Ignoring for simplicity any possible mixing between the π^0 and the other two states, this takes the form:

$$F_P^a = \begin{pmatrix} F_\pi^3 & 0 & 0 \\ 0 & F_\eta^8 & F_{\eta'}^8 \\ 0 & F_\eta^0 & F_{\eta'}^0 \end{pmatrix} = \begin{pmatrix} F_\pi^3 & 0 & 0 \\ 0 & F^8\cos\theta_8 & F^8\sin\theta_8 \\ 0 & -F^0\sin\theta_0 & F^0\cos\theta_0 \end{pmatrix}, \tag{5.41}$$

where, after the second equality sign, we have already introduced the standard two-angle mixing scheme between η and η'. For the pion $a=3$, the corresponding low-energy theorem

$$F_{\pi^0\gamma\gamma} = \frac{3}{2\pi^2 F_\pi}C_3 = \frac{1}{4\pi^2 F_\pi} \tag{5.42}$$

is very close to phenomenology, while for η, η' chiral corrections and mixing effects need to be taken into account. In particular, we stress that due to the renormalization of the singlet current F_P^0 is not actually an observable quantity, and the corresponding α_s corrections [156,239] need to be considered when relating the normalization, asymptotic constraints, and η–η' mixing parameters [198, 240–243]. In the present work, we will take the η, η' normalizations from experiment, so that the singlet corrections become most relevant when comparing the asymptotic constraints and η–η' mixing parameters in different schemes. As described in section 5.2.4.2, we studied the impact of different such determinations on the numerics, with the result that the corresponding variations were numerically irrelevant in view of the accuracy anticipated for the pseudoscalar TFF models discussed in the following sections.

In addition to the normalizations, the pseudoscalar TFFs are subject to the (leading) asymptotic constraint [185–187]

$$F_{P\gamma^*\gamma^*}(-Q_1^2,-Q_2^2) = 4\sum_a C_a F_P^a \int_0^1 \mathrm{d}x \frac{\phi_P^a(x)}{xQ_1^2+(1-x)Q_2^2}, \tag{5.43}$$

which for the asymptotic wave function $\phi_P^a(x) = 6x(1-x)$, and again ignoring α_s corrections

for the singlet component, produces the limits[4]

$$\lim_{Q^2\to\infty} Q^2 F_{P\gamma\gamma^*}(-Q^2) = 12\sum_a C_a F_P^a,$$
$$\lim_{Q^2\to\infty} Q^2 F_{P\gamma^*\gamma^*}(-Q^2,-Q^2) = 4\sum_a C_a F_P^a. \tag{5.44}$$

In view of (5.38), multiplying these limits by $F_{P\gamma\gamma}$ and summing over P one obtains an expression which depends neither on decay constants nor on mixing angles. Moreover, the block form of the matrix (5.41) leads to two separate combinations with such a property:

$$F_{\pi^0\gamma\gamma}\lim_{Q^2\to\infty} Q^2 F_{\pi^0\gamma^*\gamma^*}(-Q^2,-Q^2) = \frac{6}{\pi^2}C_3^2 = \frac{1}{6\pi^2},$$
$$\sum_{P=\eta,\eta'} F_{P\gamma\gamma}\lim_{Q^2\to\infty} Q^2 F_{P\gamma^*\gamma^*}(-Q^2,-Q^2) = 4\sum_{P,a} F_P^a F_{P\gamma\gamma} C_a = \frac{6}{\pi^2}\sum_{a=0,8} C_a^2 = \frac{1}{2\pi^2}, \tag{5.45}$$

and similarly for the asymptotic limit of the singly-virtual TFF. Beyond the singlet α_s corrections that describe the scale dependence of F_P^0 [240–242], there are genuine pQCD corrections to the TFFs suppressed by α_s at scales related to the photon virtualities [245]. The impact of such next-to-leading-order pQCD corrections was studied in ref. [28] in the context of the pion TFF, with the result that even for the ground-state pion the effect is small and safely covered by the uncertainty estimated from the onset of the asymptotic region.

5.2.2.3 The perturbative QCD quark loop

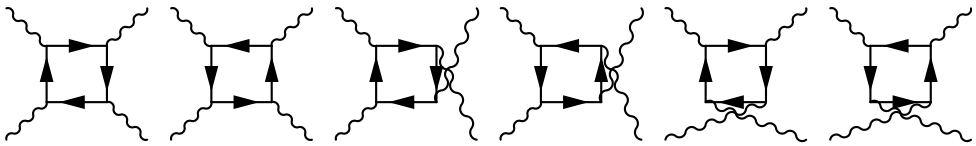

Figure 5.5: Quark-loop contribution to HLbL scattering.

The quark-loop contribution to HLbL scattering is shown in figure 5.5, indicating the different permutations that need to be considered. Compact expressions for the BTT scalar functions can be obtained as follows: we use a Feynman parameterization for the loop integrals and project the result onto the scalar basis functions $\tilde{\Pi}_i$ [27, 77]. We find all necessary BTT functions Π_i in the limit $q_4 \to 0$ by taking this limit in the appropriate order, so that the Tarrach poles drop out. Then we combine the functions Π_i according to (5.26) to obtain the scalar functions $\hat{\Pi}_i$. Due to the limit $q_4 \to 0$, one integral can be carried out and we are left with a two-dimensional Feynman-parameter integral. The result for the integrands contains spurious kinematic singularities, but the residues of these poles vanish when the Feynman integrals are carried out. Therefore, we can subtract these poles and obtain a representation that is manifestly free of kinematic singularities

$$\hat{\Pi}_i^{\text{quark loop}} = \sum_q N_c\, Q_q^4 \frac{1}{16\pi^2}\int_0^1 dx \int_0^{1-x} dy\, I_i(x,y), \tag{5.46}$$

[4] As argued in ref. [244], the first limit goes beyond a strict OPE, but is consistent with the phenomenology of the ground-state TFFs, see, e.g., refs. [26, 28].

where

$$
\begin{aligned}
I_1(x,y) &= -\frac{16x(1-x-y)}{\Delta_{132}^2} - \frac{16xy(1-2x)(1-2y)}{\Delta_{132}\Delta_{32}},\\
I_4(x,y) &= \frac{32xy(1-2x)(x+y)(1-x-y)^2(q_1^2-q_2^2+q_3^2)}{\Delta_{312}^3} - \frac{32(1-x)x(x+y)(1-x-y)}{\Delta_{312}^2}\\
&\quad - \frac{32xy(1-2x)(1-2y)}{\Delta_{312}\Delta_{12}},\\
I_7(x,y) &= -\frac{64xy^2(1-x-y)(1-2x)(1-y)}{\Delta_{132}^3},\\
I_{17}(x,y) &= -\frac{32x^2y^2(1-2x)(1-2y)}{\Delta_{312}^2\Delta_{12}},\\
I_{39}(x,y) &= \frac{64xy(1-x-y)\big((2x-1)y^2+xy(2x-3)+x(1-x)+y\big)}{\Delta_{132}^3},\\
I_{54}(x,y) &= -\frac{16xy(1-x-y)(1-2x)(1-2y)(x-y)}{\Delta_{312}\Delta_{12}}\left(\frac{1}{\Delta_{312}}+\frac{1}{\Delta_{12}}\right),
\end{aligned}
\tag{5.47}
$$

and

$$
\begin{aligned}
\Delta_{ijk} &= m_q^2 - xyq_i^2 - x(1-x-y)q_j^2 - y(1-x-y)q_k^2,\\
\Delta_{ij} &= m_q^2 - x(1-x)q_i^2 - y(1-y)q_j^2.
\end{aligned}
\tag{5.48}
$$

In principle, it is also possible to extract the results by projecting onto the singly-on-shell basis $\check{\Pi}_i$ [27]. However, it turns out that this method is less straightforward, because different spurious kinematic singularities appear, which have to be subtracted again and make the calculation more complicated.

As a cross check of (5.47) we have evaluated light-quark loops for $q = u, d, s$ with (constituent) quark mass m_q, including a factor $N_c \sum_{q=u,d,s} Q_q^4 = 2/3$ as well as the lepton loops. The latter agree well with the known analytic expressions [246], while apart from the electron loop the results are well reproduced from the heavy-mass expansion [116]. Throughout, for the matching to our Regge models in section 5.2.5, we use the pQCD quark loop with $m_q = 0$, given that even in configurations where chiral corrections for the light quarks $q = u, d, s$ can be controlled within pQCD, they only enter at subleading orders.

As a first application, we consider the contribution from the charm quark. Assuming that this contribution is fully perturbative, with mass $m_c = 1.27(2)\,\text{GeV}$ [100], the quark loop evaluates to $a_\mu^{c\text{-loop}} = 3.1(1) \times 10^{-11}$. In analogy to the light quarks, one would expect the most important non-perturbative effect to be related to the pole contribution from the lowest-lying $c\bar{c}$ resonance, the $\eta_c(1S)$ with mass $m_{\eta_c(1S)} = 2.9839(5)\,\text{GeV}$ and two-photon width $\Gamma(\eta_c(1S) \to \gamma\gamma) = 5.0(4)\,\text{keV}$ [100]. Using a VMD-type form factor with scale set by the J/Ψ (as suggested by a significant branching fraction $\text{BR}(J/\Psi \to \eta_c(1S)\gamma) = 1.7(4)\%$ [100]), this leads to the estimate $a_\mu^{\eta_c(1S)} = 0.8 \times 10^{-11}$ (this estimate agrees with the LMD result $a_\mu^{\eta_c(1S)} = 0.9(1) \times 10^{-11}$ from [247]). Given the relatively low scale set by m_c one may also expect α_s corrections in a similar ballpark. Altogether, we estimate

$$
a_\mu^{c\text{-quark}} = 3(1) \times 10^{-11},
\tag{5.49}
$$

while the b-quark contribution is already suppressed to the level of 10^{-13} and the t-quark loop to 10^{-15}.

5.2.3 OPE constraints for the hadronic light-by-light tensor

5.2.3.1 OPE for the asymptotic region

The first term in the OPE for the kinematic configuration in which all three momenta are large coincides with the pQCD quark loop. This has long been suspected in the literature, including ref. [2], but was only demonstrated recently in ref. [1], by working out the next order in the expansion. While at leading order all quark masses can simply be put to zero, this is no longer true at subleading orders. In fact, it is the presence of quark masses and condensates that numerically suppresses the next-to-leading order corrections.

In the limit $q_1^2 = q_2^2 = q_3^2 \equiv q^2$ the expressions for the pQCD quark loop simplify to

$$\begin{aligned}
\hat{\Pi}_1^{\text{pQCD}} &= -\frac{4}{9\pi^2 q^4}, \qquad \hat{\Pi}_{54}^{\text{pQCD}} = 0, \\
\hat{\Pi}_4^{\text{pQCD}} &= -\frac{8}{243\pi^2 q^4}\left[33 - 16\sqrt{3}\,\text{Cl}_2\Big(\frac{\pi}{3}\Big)\right], \\
\hat{\Pi}_7^{\text{pQCD}} &= \frac{4}{243\pi^2 q^6}\left[33 - 16\sqrt{3}\,\text{Cl}_2\Big(\frac{\pi}{3}\Big)\right], \\
\hat{\Pi}_{17}^{\text{pQCD}} &= \frac{16}{81\pi^2 q^6}\left[3 - 2\sqrt{3}\,\text{Cl}_2\Big(\frac{\pi}{3}\Big)\right], \\
\hat{\Pi}_{39}^{\text{pQCD}} &= -\frac{8}{243\pi^2 q^6}\left[15 - 4\sqrt{3}\,\text{Cl}_2\Big(\frac{\pi}{3}\Big)\right],
\end{aligned} \tag{5.50}$$

where the Clausen function is defined as

$$\text{Cl}_2(x) = -\int_0^x dt \log\left|2\sin\frac{t}{2}\right|. \tag{5.51}$$

This result again includes the factor 2/3 due to N_c and quark charges, after summing over $q = u, d, s$.

5.2.3.2 OPE for the mixed regions

The OPE constraint derived in ref. [2] applies to the case where one virtuality remains smaller than the others, $Q_3^2 \ll Q_1^2 \sim Q_2^2$, also referred to as the mixed regions. This constraint traces back to non-renormalization theorems for the VVA correlator [103, 181], which had been used before in the context of the electroweak contributions to $(g-2)_\mu$ [60, 182]. Explicit pQCD calculations at two- and three-loop order exist [183, 184], but the main argument in ref. [2] was that the non-renormalization theorems allow one to address the regions in which both perturbative and non-perturbative aspects might be important. We first review this derivation, while casting the results in a form suitable for the BTT decomposition of the HLbL tensor.

The central object is the OPE for two electromagnetic currents:

$$\Pi^{\mu\nu}(q_1, q_2) = i\int d^4x\, d^4y\, e^{-i(q_1\cdot x + q_2\cdot y)} T\{j^\mu(x) j^\nu(y)\}. \tag{5.52}$$

We consider large momenta $\hat{q} = (q_1 - q_2)/2$ flowing through the currents and expand the operator product into a series of local operators. For $|\hat{q}| \gg \Lambda_{\text{QCD}}$, the coefficients can be calculated in perturbation theory. At leading order in α_s, only two-quark operators are generated, hence the

matching can be easily obtained by inserting the operator (5.52) into external quark states and expanding the diagrams for large momenta $\hat{q}$:

$$\begin{aligned}
&i\langle\psi_q(p_2)|\Pi^{\mu\nu}(q_1,q_2)|\psi_q(p_1)\rangle \\
&\quad= (2\pi)^4\delta^{(4)}(q_1+q_2+p_1-p_2)\bigg[\bar{u}_q(p_2)i^2\mathcal{Q}_q^2\gamma^\nu\frac{i(\not{p}_1+\not{q}_1+m_q)}{(p_1+q_1)^2-m_q^2}\gamma^\mu u_q(p_1) \\
&\qquad\qquad + \bar{u}_q(p_2)i^2\mathcal{Q}_q^2\gamma^\mu\frac{i(\not{p}_2-\not{q}_1+m_q)}{(p_2-q_1)^2-m_q^2}\gamma^\nu u_q(p_1)\bigg] \\
&\quad= (2\pi)^4\delta^{(4)}(q_1+q_2+p_1-p_2)\bar{u}_q(p_2)i\mathcal{Q}_q^2\bigg[-2i\epsilon^{\mu\nu\lambda\sigma}\frac{\hat{q}_\lambda}{\hat{q}^2}\gamma_\sigma\gamma_5-2g^{\mu\nu}\frac{m_q}{\hat{q}^2} \\
&\quad- (\gamma^\mu g^{\nu\sigma}+\gamma^\nu g^{\mu\sigma}-\gamma^\sigma g^{\mu\nu})\bigg(\frac{1}{\hat{q}^2}(p_1+p_2)_\sigma-\frac{2(p_1+p_2)\cdot\hat{q}}{(\hat{q}^2)^2}\hat{q}_\sigma\bigg)+\mathcal{O}(\hat{q}^{-3})\bigg]u_q(p_1),
\end{aligned}\tag{5.53}$$

where we used

$$\gamma^\mu\gamma^\alpha\gamma^\nu = g^{\mu\alpha}\gamma^\nu+g^{\nu\alpha}\gamma^\mu-g^{\mu\nu}\gamma^\alpha-i\epsilon^{\mu\alpha\nu\beta}\gamma_5\gamma_\beta \tag{5.54}$$

with $\epsilon^{0123}=+1$. Introducing the scalar density $S(x)$, the axial vector $j_5^\mu(x)$, and the energy-momentum tensor $\theta^{\mu\nu}(x)$ with flavors weighted by the squared electric charges,

$$S(x)=\bar{\psi}(x)\mathcal{Q}^2\mathcal{M}\psi(x),\quad j_5^\mu(x)=\bar{\psi}(x)\mathcal{Q}^2\gamma^\mu\gamma_5\psi(x),\quad \theta^{\mu\nu}(x)=\frac{i}{2}\bar{\psi}(x)\mathcal{Q}^2\gamma^\mu\partial_-^\nu\psi(x), \tag{5.55}$$

with the quark-mass matrix $\mathcal{M}=\mathrm{diag}(m_u,m_d,m_s)$ as well as the derivative $\partial_-=\overrightarrow{\partial}-\overleftarrow{\partial}$, we read off the matching for the OPE:

$$\begin{aligned}
\Pi_{\mu\nu}(q_1,q_2) = \int d^4z\, e^{-i(q_1+q_2)\cdot z}\bigg[&-\frac{2i}{\hat{q}^2}\epsilon_{\mu\nu\alpha\beta}\hat{q}^\alpha j_5^\beta(z)-\frac{2}{\hat{q}^2}\Big(\theta_{\mu\nu}(z)+\theta_{\nu\mu}(z)-g_{\mu\nu}\theta^\alpha_\alpha(z)\Big) \\
&+\frac{4}{(\hat{q}^2)^2}\Big(\hat{q}_\mu\hat{q}^\alpha\theta_{\nu\alpha}+\hat{q}_\nu\hat{q}^\alpha\theta_{\mu\alpha}-g_{\mu\nu}\hat{q}^\alpha\hat{q}^\beta\theta_{\alpha\beta}\Big)-\frac{2}{\hat{q}^2}g_{\mu\nu}S(z)+\mathcal{O}(\hat{q}^{-3})\bigg].
\end{aligned}\tag{5.56}$$

The first term reproduces the expansion given in ref. [2], but differs in sign just because of different conventions (they use $\epsilon^{0123}=-1$).

Applying the OPE to the HLbL tensor in the limit $Q_1^2\sim Q_2^2\gg Q_3^2,Q_4^2$ we then find at leading order

$$\begin{aligned}
\Pi_{\mu\nu\lambda\sigma}(q_1,q_2,q_3) &= \frac{2i}{\hat{q}^2}\epsilon_{\mu\nu\alpha\beta}\hat{q}^\alpha\int d^4x\,d^4y\,e^{-i(q_1+q_2)\cdot x}e^{-iq_3\cdot y}\langle 0|T\{j_5^\beta(x)j_\lambda(y)j_\sigma(0)\}|0\rangle \\
&= \frac{2i}{\hat{q}^2}\epsilon_{\mu\nu\alpha\beta}\hat{q}^\alpha\int d^4x\,d^4y\,e^{-iq_3\cdot x}e^{iq_4\cdot y}\langle 0|T\{j_\lambda(x)j_\sigma(y)j_5^\beta(0)\}|0\rangle \\
&= \frac{2}{\hat{q}^2}\epsilon_{\mu\nu\alpha\beta}\hat{q}^\alpha W_{\lambda\sigma}{}^\beta(-q_3,q_4),
\end{aligned}\tag{5.57}$$

where the correlator $W_{\mu\nu\rho}$ is defined as

$$W_{\mu\nu\rho}(q_1,q_2)=i\int d^4x\,d^4y\,e^{i(q_1\cdot x+q_2\cdot y)}\langle 0|T\{j_\mu(x)j_\nu(y)j_\rho^5(0)\}|0\rangle. \tag{5.58}$$

Introducing the vector and axial-vector currents

$$V_\mu^a(x)=\bar{\psi}(x)\gamma_\mu\frac{\lambda_a}{2}\psi(x),\quad A_\mu^a(x)=\bar{\psi}(x)\gamma_\mu\gamma_5\frac{\lambda_a}{2}\psi(x), \tag{5.59}$$

where $\{\lambda_a, \lambda_b\} = 4/3\delta_{ab} + 2d_{abc}\lambda_c$, we also define the correlator

$$W^{abc}_{\mu\nu\rho}(q_1, q_2) = i \int d^4x\, d^4y\, e^{i(q_1\cdot x + q_2\cdot y)} \langle 0|T\{V^a_\mu(x) V^b_\nu(y) A^c_\rho(0)\}|0\rangle. \tag{5.60}$$

Performing the flavor decompositions

$$j^5_\mu(x) = \sum_{a=0,3,8} 2C_a A^a_\mu(x), \quad j_\mu(x) = \sum_{a=3,8} 2D_a V^a_\mu(x) \tag{5.61}$$

with C_a defined in (5.38) and $D_a = \frac{1}{2}\mathrm{Tr}(\mathcal{Q}\lambda_a)$, we write the correlator (5.58) as

$$W_{\mu\nu\rho}(q_1, q_2) = 4 \sum_{a=0,3,8} C_a^2\, W^{(a)}_{\mu\nu\rho}(q_1, q_2), \tag{5.62}$$

where

$$W^{(a)}_{\mu\nu\rho}(q_1, q_2) := \frac{2}{C_a} \sum_{b,c=3,8} D_b D_c W^{bca}_{\mu\nu\rho}(q_1, q_2). \tag{5.63}$$

The Lorentz decomposition of the VVA correlator is chosen as [103]

$$\begin{aligned} W^{(a)}_{\mu\nu\rho}(q_1, q_2) = -\frac{1}{8\pi^2}\Big[& - w_L^{(a)}\big(q_1^2, q_2^2, (q_1+q_2)^2\big)\epsilon_{\mu\nu\alpha\beta} q_1^\alpha q_2^\beta (q_1+q_2)_\rho \\ & + w_T^{+(a)}\big(q_1^2, q_2^2, (q_1+q_2)^2\big) t^+_{\mu\nu\rho} + w_T^{-(a)}\big(q_1^2, q_2^2, (q_1+q_2)^2\big) t^-_{\mu\nu\rho} \\ & + \tilde{w}_T^{-(a)}\big(q_1^2, q_2^2, (q_1+q_2)^2\big) \tilde{t}^-_{\mu\nu\rho}\Big], \end{aligned} \tag{5.64}$$

with the following Lorentz structures:

$$\begin{aligned} t^+_{\mu\nu\rho} &= \epsilon_{\mu\rho\alpha\beta} q_{1\nu} q_1^\alpha q_2^\beta - \epsilon_{\nu\rho\alpha\beta} q_{2\mu} q_1^\alpha q_2^\beta - q_1\cdot q_2 \epsilon_{\mu\nu\rho\alpha}(q_1 - q_2)^\alpha \\ &\quad + \frac{q_1^2 + q_2^2 - (q_1+q_2)^2}{(q_1+q_2)^2} \epsilon_{\mu\nu\alpha\beta} q_1^\alpha q_2^\beta (q_1+q_2)_\rho, \\ t^-_{\mu\nu\rho} &= \left((q_1 - q_2)_\rho - \frac{q_1^2 - q_2^2}{(q_1+q_2)^2}(q_1+q_2)_\rho\right)\epsilon_{\mu\nu\alpha\beta} q_1^\alpha q_2^\beta, \\ \tilde{t}^-_{\mu\nu\rho} &= \epsilon_{\mu\rho\alpha\beta} q_{1\nu} q_1^\alpha q_2^\beta + \epsilon_{\nu\rho\alpha\beta} q_{2\mu} q_1^\alpha q_2^\beta - q_1\cdot q_2 \epsilon_{\mu\nu\rho\alpha}(q_1+q_2)^\alpha. \end{aligned} \tag{5.65}$$

In the massless limit, one finds at one loop the contribution of the axial anomaly [236, 237]

$$w_L^{(a)}(q_1^2, q_2^2, (q_1+q_2)^2) = \frac{2N_c}{(q_1+q_2)^2}. \tag{5.66}$$

For the non-singlet contributions $a = 3, 8$, this result is modified neither by higher-order perturbative [102] nor non-perturbative contributions [248], while the singlet contribution is affected by the gluonic $U(1)$ anomaly.

In the chiral limit, the factor C_a^2 in (5.62) arises naturally due to the flavor decomposition. One factor of C_a stems from (5.61), the second factor emerges as follows. We consider singlet and octet parts of the axial current and define

$$W^{bc0}_{\mu\nu\rho}(q_1, q_2) =: \sqrt{\frac{2}{3}}\delta^{bc}\overline{W}_{\mu\nu\rho}(q_1, q_2), \quad W^{bca}_{\mu\nu\rho}(q_1, q_2) =: d^{abc}\overline{\overline{W}}_{\mu\nu\rho}(q_1, q_2), \tag{5.67}$$

which implies

$$W^{(0)}_{\mu\nu\rho} = \frac{2}{C_0}\Big(\sqrt{\frac{2}{3}}\sum_{b=3,8} D_b^2\Big)\overline{W}_{\mu\nu\rho}, \quad W^{(a\neq 0)}_{\mu\nu\rho} = \frac{2}{C_a}\Big(\sum_{b,c=3,8} D_b D_c d^{abc}\Big)\overline{\overline{W}}_{\mu\nu\rho}. \tag{5.68}$$

The coefficients can be simplified to

$$\begin{aligned}
\sqrt{\frac{2}{3}}\sum_{b=3,8} D_b^2 &= \frac{1}{\sqrt{6}}\sum_{b=3,8} D_b \mathrm{Tr}(\mathcal{Q}\lambda_b) = \frac{1}{\sqrt{6}}\mathrm{Tr}(\mathcal{Q}^2) = C_0,\\
\sum_{b,c=3,8} D_b D_c d^{abc} &= \frac{1}{2}\sum_{b,c=3,8} D_b \mathrm{Tr}(\mathcal{Q}\lambda_c) d^{abc} = \frac{1}{4}\sum_{b=3,8} D_b \mathrm{Tr}\Big(\mathcal{Q}\Big(\{\lambda_a,\lambda_b\} - \frac{4}{3}\delta_{ab}\Big)\Big)\\
&= \frac{1}{4}\mathrm{Tr}\Big(\mathcal{Q}\{\lambda_a,\mathcal{Q}\}\Big) = C_a,
\end{aligned} \tag{5.69}$$

hence both singlet and octet components lead to another factor C_a.

In pQCD and in the chiral limit, the following non-renormalization theorems were derived in [103] for the non-singlet part of the axial current:

$$\begin{aligned}
0 &= (w_T^+ + w_T^-)\big(q_1^2, q_2^2, (q_1+q_2)^2\big) - (w_T^+ + w_T^-)\big((q_1+q_2)^2, q_2^2, q_1^2\big),\\
0 &= (\tilde{w}_T^- + w_T^-)\big(q_1^2, q_2^2, (q_1+q_2)^2\big) + (\tilde{w}_T^- + w_T^-)\big((q_1+q_2)^2, q_2^2, q_1^2\big),\\
w_L\big((q_1+q_2)^2, q_2^2, q_1^2\big) &= (w_T^+ + \tilde{w}_T^-)\big(q_1^2, q_2^2, (q_1+q_2)^2\big) + (w_T^+ + \tilde{w}_T^-)\big((q_1+q_2)^2, q_2^2, q_1^2\big)\\
&\quad + \frac{2q_2\cdot(q_1+q_2)}{q_1^2} w_T^+\big((q_1+q_2)^2, q_2^2, q_1^2\big)\\
&\quad - \frac{2q_1\cdot q_2}{q_1^2} w_T^-\big((q_1+q_2)^2, q_2^2, q_1^2\big).
\end{aligned} \tag{5.70}$$

The transversal functions in these relations are subject to non-perturbative corrections.

In the following, we will use the OPE constraints as they arise at leading order and in the chiral limit. Both the anomaly constraint (5.66) and the non-renormalization theorems (5.70) receive quark-mass corrections [249].

5.2.3.3 Projection onto BTT

In this section, we derive the asymptotic constraints that the leading-order expression (5.57) of the OPE imposes on the scalar BTT functions $\hat{\Pi}_i$ (5.26) entering the master formula for a_μ. One might be tempted to simply project the OPE expression (5.57) onto the BTT scalar functions. However, there are several problems with such an approach. First of all, the leading-order expression of the OPE is not manifestly gauge invariant: the contraction with $(q_1-q_2)^\mu$ vanishes, but the one with $(q_1+q_2)^\mu$ does not. Due to $q_1 = -q_2 + \mathcal{O}(1)$ this does ensure gauge invariance at $\mathcal{O}(1/\hat{q})$, while for the subleading orders relations with the matrix elements of the energy-momentum tensor are needed to restore gauge invariance. At leading order, gauge invariance could be restored by applying a gauge projector

$$\epsilon_{\mu\nu\alpha\beta}(q_1^\alpha - q_2^\alpha) \to \epsilon_{\mu\nu'\alpha\beta} q_1^\alpha \left(g_\nu^{\nu'} - \frac{q_{2\nu}q_2^{\nu'}}{q_2^2}\right) - \epsilon_{\mu'\nu\alpha\beta} q_2^\alpha \left(g_\mu^{\mu'} - \frac{q_{1\mu}q_1^{\mu'}}{q_1^2}\right), \tag{5.71}$$

which does not alter the $\mathcal{O}(\hat{q}^{-1})$ terms of the OPE expression. The subsequent projection onto BTT and extraction of the scalar functions $\hat{\Pi}_i$ could then be performed immediately. However,

this procedure is not uniquely defined: the BTT structures themselves become degenerate depending on the order of the expansion for large $\hat{q}$. This implies that the leading-order OPE only constrains certain linear combinations of scalar functions $\hat{\Pi}_i$. In an assignment of these constraints to individual scalar functions ambiguities are introduced. For the longitudinal amplitudes the linear combination of scalar functions that is uniquely constrained happens to coincide with $\hat{\Pi}_{1\text{–}3}$, but for the transversal amplitudes the situation becomes more complicated. We proceed as follows in order to determine this ambiguity explicitly and to work out the exact form of the OPE constraint at the level of BTT functions.

First, we remember that the HLbL tensor is linear in the external momentum q_4. Due to the relation

$$\Pi_{\mu\nu\lambda\rho} = -q_4^\sigma \frac{\partial}{\partial q_4^\rho} \Pi_{\mu\nu\lambda\sigma} \tag{5.72}$$

following from gauge invariance, it is enough to consider the derivative with respect to q_4^ρ and then take the limit $q_4 \to 0$, as required for $(g-2)_\mu$ kinematics. The BTT functions $\hat{\Pi}_i$ in this limit are unambiguously defined, hence they have their own proper expansion in $1/\hat{q}$, which we would like to constrain using the OPE. The derivatives of the Lorentz structures $\hat{T}_i$ multiplying the functions $\hat{\Pi}_i$ in the tensor decomposition (5.24) however contain several terms with different scaling for large $\hat{q}$. For instance, for the tensor structure $\hat{T}_5^{\mu\nu\lambda\sigma}$, one finds

$$\begin{aligned}
\frac{\partial}{\partial q_4^\rho} \hat{T}_5^{\mu\nu\lambda\sigma} \bigg|_{q_4=0} &= \frac{1}{4}\Big(q_3^\mu q_3^\lambda - g^{\mu\lambda} q_3^2\Big)\Big(q_3^\sigma g^{\nu\rho} - q_3^\rho g^{\nu\sigma}\Big) + \frac{1}{2}\Big(q_3^\mu q_3^\lambda - g^{\mu\lambda} q_3^2\Big)\Big(\hat{q}^\sigma g^{\nu\rho} - \hat{q}^\rho g^{\nu\sigma}\Big) \\
&\quad - \frac{1}{2}\Big(q_3^\mu \hat{q}^\lambda - g^{\mu\lambda} q_3 \cdot \hat{q}\Big)\Big(q_3^\sigma g^{\nu\rho} - q_3^\rho g^{\nu\sigma}\Big) \\
&\quad - \Big(q_3^\mu \hat{q}^\lambda - g^{\mu\lambda} q_3 \cdot \hat{q}\Big)\Big(\hat{q}^\sigma g^{\nu\rho} - \hat{q}^\rho g^{\nu\sigma}\Big),
\end{aligned} \tag{5.73}$$

where the first term scales as $\mathcal{O}(\hat{q}^0)$, the second and third terms are of $\mathcal{O}(\hat{q})$, and the last term is of $\mathcal{O}(\hat{q}^2)$. This illustrates that a certain coefficient of the expansion in $1/\hat{q}$ of a scalar function $\hat{\Pi}_i$ can contribute to different orders in the expansion in $1/\hat{q}$ of the full HLbL tensor, i.e., to different orders of the OPE. Vice versa, in order to determine the leading-order OPE constraint on the BTT functions, we e.g. have to consider terms up to and including $\mathcal{O}(\hat{q}^{-3})$ in $\hat{\Pi}_5$. We now write the scalar functions $\hat{\Pi}_i$ as a generic expansion in $1/\hat{q}$ and sum up the scalar functions times (derivatives of) tensor structures. Collecting in the resulting tensor terms according to the scaling with $\hat{q}$ and requiring equality with the leading-order OPE limit (5.57) determines the

expansion coefficients of the 19 BTT functions relevant in the $(g-2)_\mu$ limit as

$$
\begin{aligned}
\hat{\Pi}_1 &= 2w_L(q_3^2,0,q_3^2)f(\hat{q}^2) + \mathcal{O}(\hat{q}^{-3}),\\
\hat{\Pi}_5 &= \frac{4}{3}\big(w_T^+ + \tilde{w}_T^-\big)(q_3^2,0,q_3^2)f(\hat{q}^2) + c_5^{(2)} + c_5^{(3)} + \mathcal{O}(\hat{q}^{-4}),\\
\hat{\Pi}_6 &= \frac{4}{3}\big(w_T^+ + \tilde{w}_T^-\big)(q_3^2,0,q_3^2)f(\hat{q}^2) + c_6^{(2)} + c_6^{(3)} + \mathcal{O}(\hat{q}^{-4}),\\
\hat{\Pi}_7 &= c_7^{(5)} + \mathcal{O}(\hat{q}^{-6}),\\
\hat{\Pi}_8 &= -c_7^{(5)} + \mathcal{O}(\hat{q}^{-6}),\\
\hat{\Pi}_9 &= c_9^{(3)} + \mathcal{O}(\hat{q}^{-4}),\\
\hat{\Pi}_{10} &= -\frac{4}{3\hat{q}^2}\big(w_T^+ + \tilde{w}_T^-\big)(q_3^2,0,q_3^2)f(\hat{q}^2) - \frac{1}{\hat{q}^2}\Big(c_5^{(2)} + c_5^{(3)}\Big) - c_{16}^{(5)} - c_{54}^{(5)} + \mathcal{O}(\hat{q}^{-6}),\\
\hat{\Pi}_{11} &= \frac{1}{2\hat{q}^2}\Big(c_5^{(2)} - c_6^{(2)} - 2c_6^{(3)}\Big) - c_{14}^{(5)} + c_{54}^{(5)} + \mathcal{O}(\hat{q}^{-6}),\\
\hat{\Pi}_{13} &= -c_9^{(3)} + \mathcal{O}(\hat{q}^{-4}),\\
\hat{\Pi}_{14} &= -\frac{4}{3\hat{q}^2}\big(w_T^+ + \tilde{w}_T^-\big)(q_3^2,0,q_3^2)f(\hat{q}^2) - \frac{1}{\hat{q}^2}c_6^{(2)} + c_{14}^{(5)} + \mathcal{O}(\hat{q}^{-6}),\\
\hat{\Pi}_{16} &= -\frac{1}{2\hat{q}^2}\Big(c_5^{(2)} - c_6^{(2)}\Big) + c_{16}^{(5)} + \mathcal{O}(\hat{q}^{-6}),\\
\hat{\Pi}_{39} &= \frac{4}{3\hat{q}^2}\big(w_T^+ + \tilde{w}_T^-\big)(q_3^2,0,q_3^2)f(\hat{q}^2) + \frac{1}{2\hat{q}^2}\Big(c_5^{(2)} + c_6^{(2)}\Big) + \mathcal{O}(\hat{q}^{-5}),\\
\hat{\Pi}_{50} = \hat{\Pi}_{51} &= \frac{2}{3\hat{q}^2}\big(w_T^+ + \tilde{w}_T^-\big)(q_3^2,0,q_3^2)f(\hat{q}^2) - \frac{1}{2\hat{q}^2}\Big(c_5^{(2)} + c_6^{(2)} - (q_1^2 - q_2^2)c_9^{(3)}\Big) + \mathcal{O}(\hat{q}^{-5}),\\
\hat{\Pi}_{54} &= \frac{1}{2\hat{q}^2}\Big(c_5^{(2)} - c_6^{(2)}\Big) + c_{54}^{(5)} + \mathcal{O}(\hat{q}^{-4}),\\
\hat{\Pi}_i &= \mathcal{O}(\hat{q}^{-4}), \qquad i \in \{2,3,4,17\},
\end{aligned}
\tag{5.74}
$$

where

$$
f(\hat{q}^2) = -\frac{1}{2\pi^2\hat{q}^2}\sum_a C_a^2 = -\frac{1}{18\pi^2\hat{q}^2} \tag{5.75}
$$

and the remaining ambiguities are parameterized by functions $c_i^{(n)}$ behaving as $c_i^{(n)} \sim 1/\hat{q}^n$, which are subject to certain crossing-symmetry relations following from (5.27) and (5.29). Note that the small dimensional quantity that makes the expansion parameter dimensionless can be any of the small scales, e.g., the small momentum or matrix elements of the operators in (5.56). Due to the scaling of the tensor structures, the neglected terms in (5.74) affect the HLbL tensor first at $\mathcal{O}(1/\hat{q}^2)$ and therefore cannot interfere with the leading-order OPE. This result specifies the configuration $Q_1^2 \sim Q_2^2 \equiv -q^2 = -\hat{q}^2 \gg Q_3^2$. The related limits for small q_1^2 or q_2^2 follow directly from crossing symmetry.

Since the longitudinal amplitude w_L only contributes to $\hat{\Pi}_{1\text{–}3}$, we will refer to these scalar functions as the longitudinal ones, and accordingly to the remaining $\hat{\Pi}_i$ as the transversal contribution. The non-trivial constraint on the non-singlet part of the latter emerges from the corresponding limit of (5.70)

$$
w_L(q_3^2,0,q_3^2) = 2\big(w_T^+ + \tilde{w}_T^-\big)(q_3^2,0,q_3^2), \tag{5.76}
$$

but in contrast to the anomaly condition (5.66), which is exact in the chiral limit, this relation does receive non-perturbative corrections. As noted above, the projection (5.74) shows that only

the OPE constraints on the longitudinal amplitudes are free from ambiguities, whereas all those on the transversal ones are affected by them. The presence of these ambiguities is not a problem per se: it simply means that at leading order the OPE only constrains certain linear combinations of BTT functions. We also note that the ambiguities would be moved to higher orders if the next terms in the OPE were included.

For asymptotic values of q_3^2, the OPE constraints can be compared with the pQCD quark loop evaluated in the chiral limit and for $q_1^2 = q_2^2 \equiv q^2$, $q_3^2/q^2 \to 0$,

$$\begin{aligned}
\hat{\Pi}_1^{\text{pQCD}} &= -\frac{2}{3\pi^2 q^2 q_3^2}, \\
\hat{\Pi}_5^{\text{pQCD}} &= \hat{\Pi}_6^{\text{pQCD}} = -\frac{2}{9\pi^2 q^2 q_3^2}, \\
\hat{\Pi}_{10}^{\text{pQCD}} &= \hat{\Pi}_{14}^{\text{pQCD}} = -\hat{\Pi}_{17}^{\text{pQCD}} = -\hat{\Pi}_{39}^{\text{pQCD}} = -2\hat{\Pi}_{50}^{\text{pQCD}} = -2\hat{\Pi}_{51}^{\text{pQCD}} = \frac{2}{9\pi^2 q^4 q_3^2}.
\end{aligned} \tag{5.77}$$

These expressions perfectly agree with (5.74) if we use the non-renormalization theorem in the form (5.76) and set the ambiguities $c_i^{(n)}$ to zero, which demonstrates that the OPE constraint and the pQCD quark loop coincide in the appropriate kinematic limit [250] (neither chiral effects nor α_s corrections related to the gluon anomaly in the singlet channel matter in this limit). We stress that one could impose the OPE constraints on the transversal functions without having to deal with these ambiguities by first building linear combinations of the BTT functions that are free from them. In principle, one could even use the freedom in the projection at a given order to simplify expressions, e.g., at leading order one could choose the $c_i^{(n)}$ in such a way that the only non-vanishing contribution arises in $\hat{\Pi}_{50} = \hat{\Pi}_{51} = 2/\hat{q}^2\big(w_T^+ + \tilde{w}_T^-\big)(q_3^2, 0, q_3^2) f(\hat{q}^2)$. However, such a simplification would no longer hold at subleading orders, therefore, we keep here the general form (5.74) that shows directly how the OPE limit corresponds to the pQCD quark loop (5.77) evaluated in the same kinematics. In the following we will focus on the OPE constraint on the longitudinal contribution, which can be unambiguously assigned to the BTT functions $\hat{\Pi}_{1-3}$ already at leading order.

5.2.3.4 Relation to pseudoscalar poles

Separating the longitudinal OPE constraint into flavor components one finds

$$\hat{\Pi}_1^3 = -\frac{6}{\pi^2 q^2 q_3^2} C_3^2 = -\frac{1}{6\pi^2 q^2 q_3^2}, \tag{5.78}$$

$$\hat{\Pi}_1^{0,8} = -\frac{6}{\pi^2 q^2 q_3^2}\big(C_8^2 + C_0^2\big) = -\frac{1}{2\pi^2 q^2 q_3^2}, \tag{5.79}$$

which due to (5.45) matches precisely onto (5.35) when the meson masses and, crucially, the momentum dependence of the singly-virtual form factor are neglected. This is the basic premise of the model suggested in ref. [2]. We stress that for the non-singlet component these relations are exact in the chiral limit, see section 5.2.5.3 for an extensive discussion of this point. For non-vanishing quark masses and, in the case of the singlet, due to the gluon anomaly they do receive corrections. However, at low energies, where such corrections matter most, we always use the full dispersive result that automatically corresponds to physical quantities, while (5.78) and (5.79) are only implemented for asymptotic values of the virtualities q_i^2.

The OPE constraint becomes potentially valuable in the context of the mixed-energy regions, where both a description in terms of hadronic intermediate states and pQCD have limited applicability. In practice, the constraint is rigorous once all momenta are large compared to Λ_{QCD} to ensure that quark-mass corrections can be neglected. The Regge approach in the next section is our proposal for an explicit implementation of the OPE constraint, following a remark made in ref. [2]: while the $1/q_3^2$ behavior in (5.78) and (5.79) cannot be obtained with any finite number of pseudoscalar poles, an infinite sum over excited states can produce the required asymptotics.

5.2.4 Regge models for the pseudoscalar-pole contribution

Assuming confinement, in the large-N_c limit of QCD [133] the spectrum of the theory in any sector (set of quantum numbers) reduces to an infinite number of narrow resonances. One should not expect the spectral functions in this limit to be close to those of QCD with $N_c = 3$ locally: a series of δ-functions does not look like the continuum observed in nature for any spectral function. On the other hand, one expects the large-N_c limit to provide a good approximation to QCD *on average*, and in particular to reproduce to a reasonable accuracy its global properties such as asymptotic limits. There is a vast literature on the subject that shows that these theoretical considerations can be used with good success to build large-N_c models that simultaneously satisfy low- and high-energy constraints [190–192, 251–253].

The aim of the present section is to construct a large-N_c Regge model in the pseudoscalar and vector-meson sectors of QCD that allows us to satisfy the SDCs discussed above via an infinite tower of pseudoscalar-pole contributions. The logic we follow in the construction of the model is very simple: we seek minimal models, in terms of algebraic form and number of free parameters, that are able to satisfy all known constraints, both of experimental as well as of theoretical nature, i.e., phenomenological constraints wherever available and all known high- and low-energy limits. Accordingly, we construct these large-N_c Regge models with the application to HLbL scattering in mind and thus work with physical quark masses. We will comment on the chiral limit and the potential role of axial-vector resonances in section 5.2.5.3.

5.2.4.1 Large-N_c Regge model for the pion transition form factor

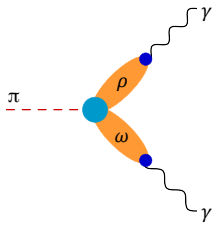

Figure 5.6: Pion TFF in the large-N_c limit.

The pion TFF describes the transition of a pion into two photons. VMD, LMD, and LMD+V models for the pseudoscalar TFFs are widely used [109, 254], cf. figures 5.6 and 5.10. In this work, we use an untruncated large-N_c model for the TFF, in which the pion couples to the photons through a tower of isovector, $I^G = 1^+$, and a tower of isoscalar, $I^G = 0^-$, vector mesons, $J^{PC} = 1^{--}$, e.g., the ρ and ω, respectively. Here, a tower of ρ (ω) mesons means an infinite sum

over radially-excited ρ (ω) mesons. The contributions from a ϕ instead of an ω are subdominant, see appendix 5.2.A, and thus will be neglected for the pion.

The standard large-N_c ansatz for the pion TFF (see refs. [188, 189]) reads:

$$F_{\pi^0\gamma^*\gamma^*}(-Q_1^2,-Q_2^2) = \sum_{V_\rho,V_\omega} G_{\pi V_\rho V_\omega}\, F_{V_\rho}\, F_{V_\omega} \left[\frac{1}{D^1_{V_\rho} D^2_{V_\omega}} + \frac{1}{D^1_{V_\omega} D^2_{V_\rho}}\right], \tag{5.80}$$

where

$$D^i_X := Q_i^2 + M_X^2, \tag{5.81}$$

F_{V_ρ} and F_{V_ω}, represented by blue dots in figure 5.6, are the current–vector-meson couplings and $G_{\pi V_\rho V_\omega}$, the cyan dot in figure 5.6, is the coupling of two vector mesons to the neutral pion. We stress that the couplings in (5.80) are Q^2 independent as required by the large-N_c approach (combined with analyticity): the contribution of a given intermediate state is fixed by its imaginary part, which for narrow resonances is a δ-function, which freezes any Q^2 dependence. Indeed the latter could be interpreted as coming from the continuum between resonances, which is suppressed in the large-N_c limit. Another potential source of Q^2-dependent corrections to (5.80) is related to subtraction terms: while (5.80) follows from an unsubtracted double-spectral representation for the TFF, introducing subtractions would produce single-propagator terms and, eventually, a polynomial. However, for a δ-function subtractions are not necessary, and even before taking the large-N_c limit the pQCD behavior of the TFF implies that an unsubtracted representation holds. As argued in ref. [28], the advantage of using an unsubtracted dispersion relation, in favor of a subtracted variant that could suppress some of the high-energy input, is precisely that it allows one to manifestly incorporate the correct pQCD asymptotics. The large-N_c ansatz (5.80) corresponds to this scenario. In the following, the vector-meson spectra are assumed to obey a radial Regge model, see figure 5.7:

$$\begin{aligned} M^2_{V_\rho} &= M^2_{\rho(n_\rho)} = M_\rho^2 + n_\rho\, \sigma_\rho^2, \\ M^2_{V_\omega} &= M^2_{\omega(n_\omega)} = M_\omega^2 + n_\omega\, \sigma_\omega^2, \end{aligned} \tag{5.82}$$

where σ_ρ and σ_ω are the slope parameters of the Regge trajectories, n_ρ and n_ω are radial excitation numbers, and the ground-state masses are $M_\rho = M_{\rho(770)} = 775.26(25)\,\text{MeV}$ and $M_\omega = M_{\omega(782)} = 782.65(12)\,\text{MeV}$ [100].

Having fixed the masses of the towers of vector resonances, our model for the pion TFF still has an infinite number of parameters, namely the couplings $G_{\pi V_\rho V_\omega}$, F_{V_ρ}, and F_{V_ω}. One could in principle reduce the number of free parameters to a finite one by imposing a certain algebraic dependence of these couplings on the excitation numbers n_ρ and n_ω, as has been done for the masses. In doing so one would have to be able to satisfy low- and high-energy constraints for the pion TFF, which we recollect here from (5.42) and (5.44):

$$\text{chiral anomaly [236–238]:} \qquad F_{\pi^0\gamma\gamma} = \frac{1}{4\pi^2 F_\pi}; \tag{5.83}$$

$$\text{BL limit [186, 187]:} \qquad \lim_{Q^2\to\infty} Q^2 F_{\pi^0\gamma\gamma^*}(-Q^2) = 2F_\pi; \tag{5.84}$$

$$\text{symmetric pQCD limit [101]:} \qquad \lim_{Q^2\to\infty} Q^2 F_{\pi^0\gamma^*\gamma^*}(-Q^2,-Q^2) = \frac{2F_\pi}{3}. \tag{5.85}$$

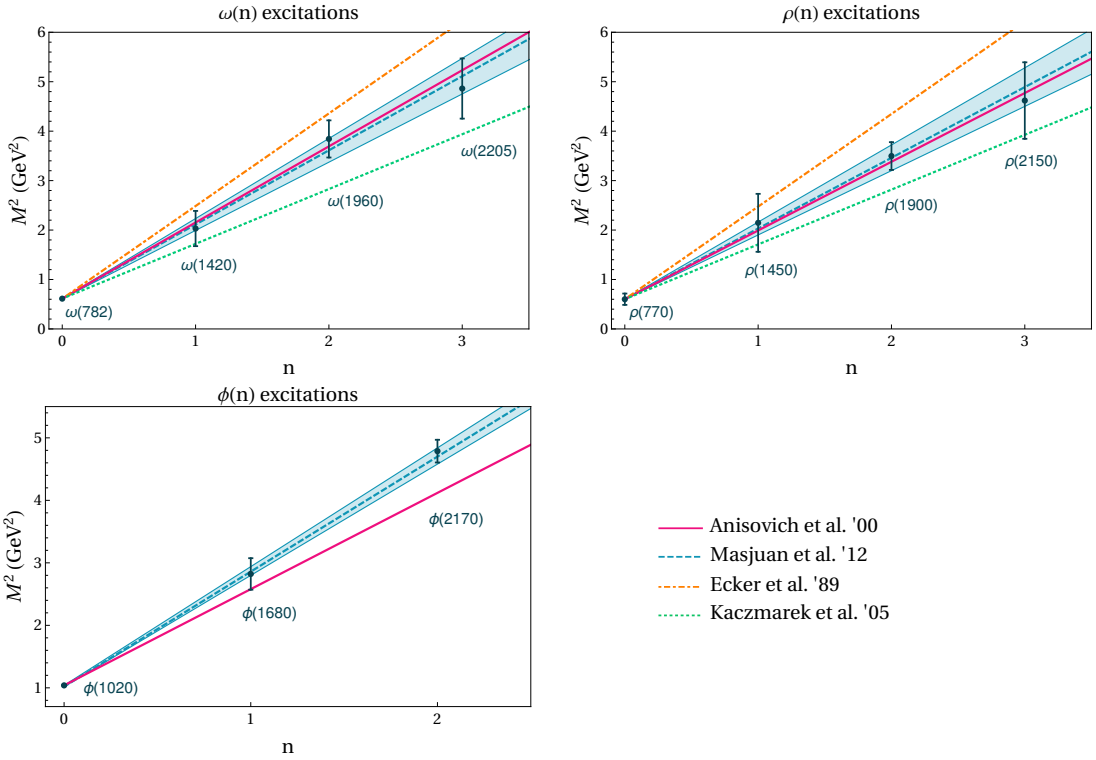

Figure 5.7: Radial Regge trajectories of the isovector ρ and isoscalar ω and ϕ vector mesons. The states $\omega(782)$, $\omega(1420)$, $\rho(770)$, $\rho(1450)$, $\phi(1020)$, $\phi(1680)$, and $\phi(2170)$ are from PDG [100]. The states $\omega(1960)$, $\omega(2205)$, $\rho(1900)$, and $\rho(2150)$ are extracted from ref. [193]. The errors are defined as $\Delta M^2 = \Gamma M$ [193]. The solid magenta lines are from ref. [255] with $\sigma_\omega^2 = 1.54$, $\sigma_\rho^2 = 1.39$ GeV^2, and $\sigma_\phi^2 = 1.54$ GeV^2. The turquoise bands are from ref. [193] with $\sigma_\omega^2 = 1.50(12)$ GeV^2, $\sigma_\rho^2 = 1.43(13)$ GeV^2, and $\sigma_\phi^2 = 1.84(6)$ GeV^2. The green dotted lines with slope $\sigma^2 = 1.11$ GeV^2 are based on the lattice calculation of ref. [256]. The orange dot-dashed lines with slope $\sigma^2 = 1.87$ GeV^2 are based on the $\rho \to 2\pi$ decay [137, 188].

One immediately notices that while the Q^2 dependence of each individual term in (5.80) is compatible with the Brodsky–Lepage (BL) limit, the symmetric pQCD limit can only be satisfied after resumming the series of vector resonances. To this end, the coupling constants must be arranged in such a way that the Q^{-4} behavior of the individual terms becomes a Q^{-2} behavior after resummation. That this is possible was shown in refs. [188, 189].

In addition, the pion TFF has been measured quite well in the singly-virtual case [204, 205, 258, 259], and our model for the TFF would have to describe the data. For the doubly-virtual case a recent dispersive analysis has shown that data for related processes and theoretical arguments constrain the behavior of the TFF in that kinematical region [28, 171, 172]—a constraint we will also take into account.

Imposing all these constraints on the model (5.80) by adjusting its free parameters is technically cumbersome, especially if we consider that we must still add a third sum over the tower of pseudoscalar mesons, $J^{PC} = 0^{-+}$, cf. figure 5.4, with which we aim to change the large-Q^2 behavior of the whole HLbL tensor. In particular, we will implement the SDCs on $\hat{\Pi}_1$ introduced

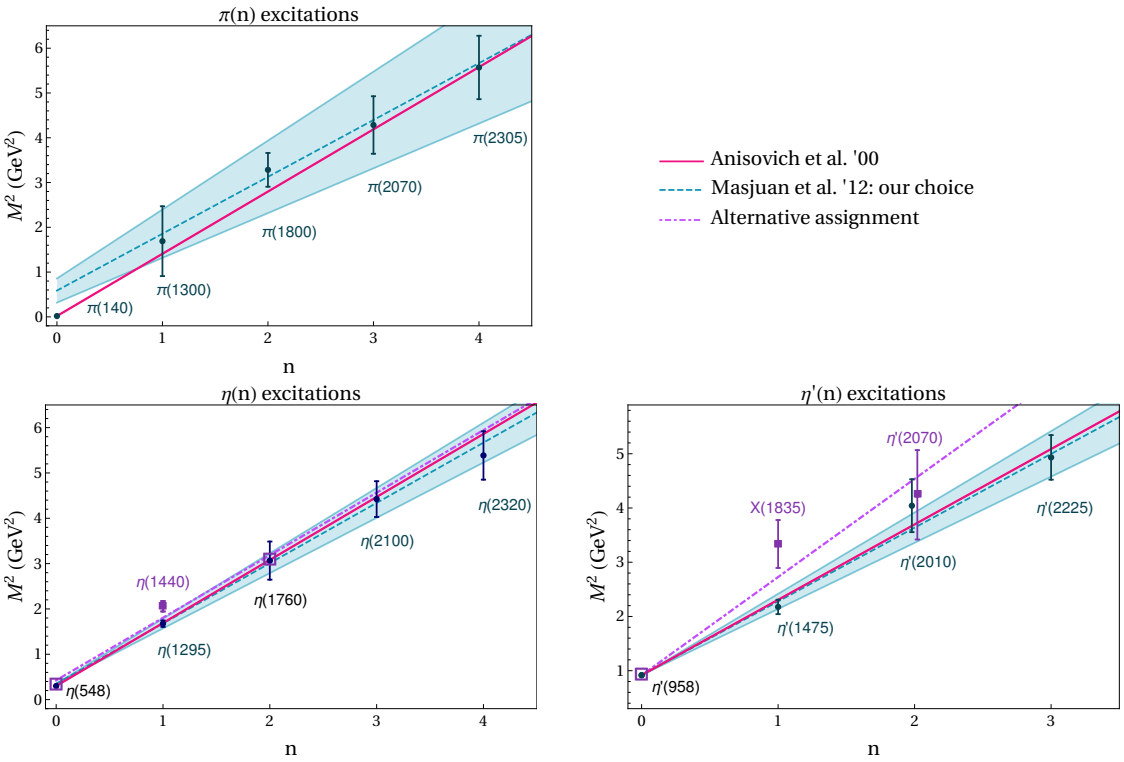

Figure 5.8: Radial Regge trajectories of the π, η, and η' pseudoscalar mesons. The states $\pi(140)$, $\pi(1300)$, $\pi(1800)$, $\eta(548)$, $\eta(1295)$, $\eta(1760)$, $\eta'(958)$, $\eta'(1475)$, $X(1835)$, and $\eta'(2225)$ are from PDG [100]. Note that the states $\eta(1760)$, $X(1835)$, and $\eta'(2225)$ are omitted from the PDG summary tables. The state $\eta(1440)$ is from PDG '00 [257]. The states $\pi(2070)$, $\pi(2305)$, $\eta(2100)$, $\eta(2320)$, and $\eta'(2010)$ are extracted from ref. [193]. The state $\eta'(2070)$ is taken from [213, Table 26]. The errors are defined as $\Delta M^2 = \Gamma M$ [193]. The solid magenta lines are fits from ref. [255]: $\sigma_\pi^2 = \sigma_\eta^2 = \sigma_{\eta'}^2 = 1.39\,\text{GeV}^2$. The turquoise bands are fits from ref. [193] which exclude the ground states of the pion and the η: $\sigma_\pi^2 = 1.27(27)\ \text{GeV}^2$ and $\hat{M}_\pi = 766$ MeV as in (5.89), $\sigma_\eta^2 = 1.33(11)$ GeV^2 and $\hat{M}_\eta = 591$ MeV as in (5.118), and $\sigma_{\eta'}^2 = 1.36(14)$ GeV^2. The $\eta(1440)$, $X(1835)$, and $\eta'(2070)$ states (purple squares) correspond to a different assignment of $\eta^{(\prime)}$ excitations suggested in ref. [213, Table 27]. The dot-dashed purple lines correspond to our fits of these alternative trajectories: $\sigma_\eta^2 = 1.38\,\text{GeV}^2$ with $\hat{M}_\eta = 0.652$ GeV, and $\sigma_{\eta'}^2 = 1.81\,\text{GeV}^2$.

in (5.50) and (5.78):[5]

$$\text{SDC for the mixed region [2]:}\quad \lim_{Q_3^2\to\infty}\lim_{Q^2\to\infty}\sum_{n=0}^{\infty}\hat{\Pi}_1^{\pi(n)\text{-pole}}(-Q^2,-Q^2,-Q_3^2)$$
$$= -\lim_{Q_3^2\to\infty}\lim_{Q^2\to\infty}\sum_{n=0}^{\infty}\frac{F_{\pi(n)\gamma^*\gamma^*}(-Q^2,-Q^2)\,F_{\pi(n)\gamma\gamma^*}(-Q_3^2)}{Q_3^2+M_{\pi(n)}^2}$$
$$= -\frac{1}{6\pi^2}\frac{1}{Q^2}\frac{1}{Q_3^2}; \tag{5.86}$$

(5.87)

[5]Note that while for the MV SDC, which is derived based on the VVA triangle, the flavor decomposition into pion, η, and η' is unambiguously given by C_a^2, see (5.78), the decomposition presented here for the SDC in the asymptotic region (5.50) is not unique. We choose to adopt the same separation as for the MV constraint.

$$\text{SDC for the asymptotic region:} \quad \lim_{Q^2\to\infty}\sum_{n=0}^{\infty}\hat{\Pi}_1^{\pi(n)\text{-pole}}(-Q^2,-Q^2,-Q^2)$$
$$= -\lim_{Q^2\to\infty}\sum_{n=0}^{\infty}\frac{F_{\pi(n)\gamma^*\gamma^*}(-Q^2,-Q^2)\,F_{\pi(n)\gamma\gamma^*}(-Q^2)}{Q^2+M_{\pi(n)}^2}$$
$$= -\frac{4}{9\pi^2}\frac{C_3^2}{\sum_{a=0,3,8}C_a^2}\frac{1}{Q^4}. \tag{5.88}$$

Here, $F_{\pi(n)\gamma^*\gamma^*}$ is the TFF of the n-th radially-excited pion and a radial Regge model is assumed for the pion masses starting from the first excitation, see figure 5.8:

$$M_{\pi(n)}^2 = \begin{cases} M_\pi^2 & n=0, \\ \hat{M}_\pi^2 + n\,\sigma_\pi^2 & n\geq 1, \end{cases} \tag{5.89}$$

where $M_\pi = 134.9770(5)$ MeV is the π^0 mass [100].[6] Given the complexity of implementing all these constraints simultaneously in terms of the general couplings of the Regge model, we therefore adopted a different approach:

1. we allow the ground-state pion to couple only to the ground-state ρ and ω mesons, and the n-th pion excitation to couple only to the n-th ρ and ω excitations;

2. we subsume the effect of the vector-meson excitations that we have just eliminated into a Q_i^2 dependence of the numerator multiplying the resonance propagators;

3. the latter Q_i^2 dependence will be parameterized in simple terms with as few free parameters as necessary to satisfy the constraints listed above.

The first step is motivated by the fact that non-diagonal couplings are suppressed by the reduced overlap of radial wave functions with different numbers of nodes [188]. For the same reason we are only considering the leading S-wave vector-meson trajectories and neglecting the D-wave daughter trajectories. In appendix 5.2.B we will consider an alternative model that already for the pQCD limit of the TFF itself, cf. (5.85), uses the Regge resummation from ref. [188], but for the main text we restrict the presentation to the most economical form sufficient to fulfill all constraints simultaneously. This strategy leads us to

$$F_{\pi(n)\gamma^*\gamma^*}(-Q_1^2,-Q_2^2) = \frac{1}{8\pi^2 F_\pi}\left\{\left(\frac{M_\rho^2 M_\omega^2}{D_{\rho(n)}^1 D_{\omega(n)}^2}+\frac{M_\rho^2 M_\omega^2}{D_{\rho(n)}^2 D_{\omega(n)}^1}\right)\right. \tag{5.90}$$
$$\times\left[c_{\text{anom}}+c_A\frac{M_{+,n}^2}{\Lambda^2}+c_B\frac{M_{-,n}^2}{\Lambda^2}+c_{\text{diag}}\frac{Q_1^2Q_2^2}{\Lambda^2(Q_+^2+M_{\text{diag}}^2)}\right]$$
$$\left.+\frac{Q_-^2}{Q_+^2}\left(\frac{M_\rho^2M_\omega^2}{D_{\rho(n)}^1D_{\omega(n)}^2}-\frac{M_\rho^2M_\omega^2}{D_{\rho(n)}^2D_{\omega(n)}^1}\right)\left[c_{\text{BL}}+c_A\frac{M_{-,n}^2}{\Lambda^2}+c_B\frac{M_{+,n}^2}{\Lambda^2}\right]\right\},$$

where

$$M_{\pm,n}^2 = \frac{1}{2}\left(M_{\omega(n)}^2 \pm M_{\rho(n)}^2\right), \quad Q_\pm^2 = Q_1^2 \pm Q_2^2, \tag{5.91}$$

[6] Note that the ground-state is treated separately because for the Goldstone bosons a strong non-linearity of the Regge trajectory is expected [260].

and $\Lambda = \mathcal{O}(1\,\text{GeV})$ is a typical QCD scale introduced to make all model parameters (c_anom, c_A, c_B, c_diag, c_BL) dimensionless. The second mass scale M_diag is determined by fitting the experimental data, it parameterizes the doubly-virtual behavior of the TFF.

With this parameterization, the three conditions for the TFF of the ground-state pion from (5.83)–(5.85) can be expressed as follows:

$$\text{anomaly:} \qquad 1 = c_\text{anom} + \frac{1}{\Lambda^2}\left(c_A M_{+,0}^2 + c_B M_{-,0}^2\right); \tag{5.92}$$

$$\text{BL limit:} \qquad 1 = \frac{1}{8\pi^2 F_\pi^2}\left(c_\text{anom} M_{+,0}^2 - c_\text{BL} M_{-,0}^2 + c_A \frac{M_\omega^2 M_\rho^2}{\Lambda^2}\right); \tag{5.93}$$

$$\text{symmetric pQCD limit:} \qquad 1 = \frac{3 M_\omega^2 M_\rho^2}{16\pi^2 F_\pi^2 \Lambda^2}\, c_\text{diag}. \tag{5.94}$$

Since the mass scales M_ρ, M_ω, $M_{+,0}$, and Λ as well as $\pi^2 F_\pi$ are of about the same order, all coupling constants that appear in the constraint equations (5.92)–(5.94) multiplied by ratios of these mass scales are expected to be of $\mathcal{O}(1)$. $M_{-,0}$, on the other hand, is much smaller, so that the coupling constants multiplied by it (c_BL and c_B) are expected to be of $\mathcal{O}(\Lambda^2/M_{-,0}^2) \sim 100$, otherwise their role in the equations would become irrelevant.

Of course these three conditions are not sufficient to determine all five model parameters. Two more constraints follow from resumming the contributions of all excited pseudoscalars to the HLbL amplitude, see (5.86) and (5.88). Details on the evaluation of infinite sums over rational functions can be found in appendix 5.2.C. The MV SDC for the mixed region translates into:

$$1 = \frac{M_\omega^2 M_\rho^2}{2\Lambda^2}\left[(c_A + c_B)\frac{L_{\rho\pi}}{\Delta_{\rho\pi}} + (c_A - c_B)\frac{L_{\omega\pi}}{\Delta_{\omega\pi}}\right], \tag{5.95}$$

where c_diag from (5.94) has been used and

$$L_{ij} = \log\frac{\sigma_i^2}{\sigma_j^2}, \quad \Delta_{ij} \coloneqq \sigma_i^2 - \sigma_j^2. \tag{5.96}$$

The second SDC concerns the limit $Q_i^2 = Q^2 \to \infty$, for all $i = 1, 2, 3$. It also involves c_A and c_B, but now in a different combination together with c_diag:

$$\begin{aligned}
1 = \frac{9}{64\pi^2 F_\pi^2 \Lambda^4}\frac{M_\rho^4 M_\omega^4}{\Omega_{\rho\omega\pi}^2}\Bigg\{ & c_A^2\,\Delta_{\rho\omega}\Sigma_{\rho\omega}\Big[\sigma_\pi^2\left(\Delta_{\omega\pi}^2 L_{\rho\pi} - \Delta_{\rho\pi}^2 L_{\omega\pi}\right) + \Omega_{\rho\omega\pi}\Big] \\
& + c_B^2\,\Delta_{\rho\omega}\Big[\left(\Sigma_{\rho\omega}\sigma_\pi^2 - 2\sigma_\rho^4\right)\Delta_{\omega\pi}^2 L_{\rho\pi} - \left(\Sigma_{\rho\omega}\sigma_\pi^2 - 2\sigma_\omega^4\right)\Delta_{\rho\pi}^2 L_{\omega\pi} + \left(\Delta_{\rho\pi} + \Delta_{\omega\pi}\right)\Omega_{\rho\omega\pi}\Big] \\
& - 2c_A c_B\Big[\sigma_\pi^2\left(\sigma_\rho^4 + \sigma_\omega^4\right)\left(\Delta_{\omega\pi}^2 L_{\rho\pi} - \Delta_{\rho\pi}^2 L_{\omega\pi}\right) + \Sigma_{\rho\omega}\left(\sigma_\omega^4\Delta_{\rho\pi}^2 L_{\omega\pi} - \sigma_\rho^4\Delta_{\omega\pi}^2 L_{\rho\pi}\right) \\
& - \Omega_{\rho\omega\pi}\left(\sigma_\pi^2\Sigma_{\rho\omega} - \sigma_\rho^4 - \sigma_\omega^4\right)\Big] - c_\text{diag}c_B\Big[\sigma_\rho^2\left\{\sigma_\rho^4 + \sigma_\omega^2(\sigma_\rho^2 - 2\sigma_\pi^2)\right\}\Delta_{\omega\pi}^2 L_{\rho\pi} \\
& - \sigma_\omega^2\left\{\sigma_\omega^4 + \sigma_\rho^2(\sigma_\omega^2 - 2\sigma_\pi^2)\right\}\Delta_{\rho\pi}^2 L_{\omega\pi} + \left(\sigma_\pi^2\Sigma_{\rho\omega} - 2\sigma_\rho^2\sigma_\omega^2\right)\Omega_{\rho\omega\pi}\Big] \\
& + c_\text{diag}c_A\,\Delta_{\rho\omega}\Big[\sigma_\rho^2(\sigma_\rho^2 - 2\sigma_\pi^2)\Delta_{\omega\pi}^2 L_{\rho\pi} - \sigma_\omega^2(\sigma_\omega^2 - 2\sigma_\pi^2)\Delta_{\rho\pi}^2 L_{\omega\pi} - \sigma_\pi^2\,\Omega_{\rho\omega\pi}\Big]\Bigg\},
\end{aligned} \tag{5.97}$$

with

$$\Omega_{ijk} \coloneqq (\sigma_i^2 - \sigma_j^2)(\sigma_k^2 - \sigma_i^2)(\sigma_k^2 - \sigma_j^2), \quad \Sigma_{ij} \coloneqq \sigma_i^2 + \sigma_j^2. \tag{5.98}$$

	π	η	η'
c_{anom}	-1.670	—	—
c_A	6.794	2.542	2.635
c_B	-252.346	-23.535	-23.706
c_{diag}	1.218	0.401	0.502
c_{BL}	141.688	18.721	18.877
M_{diag}	1.519	0.898	0.898

Table 5.1: "Natural" model parameters of the large-N_c Regge models for the pion, η, and η' TFFs. Note that here we rescaled the $\eta^{(\prime)}$ parameters c_A, c_B, and c_{BL} with a factor of $C_{\phi\omega}^{\eta^{(\prime)}}/\mathcal{N}$.

In appendix 5.2.F.1, this system of equations is solved analytically. Here, we discuss numerical values for all parameters, also summarized in table 5.1, based on the following choice of Regge slopes [193]:[7]

$$\sigma_\pi^2 = 1.27(27)\,\text{GeV}^2, \quad \sigma_\rho^2 = 1.43(13)\,\text{GeV}^2, \quad \sigma_\omega^2 = 1.50(12)\,\text{GeV}^2. \tag{5.99}$$

Furthermore, we use $F_\pi = 92.28$ MeV, $\Lambda = 1$ GeV, and other input from the PDG [100].

The constant c_{diag} is independent of all the others and is directly determined by (5.94):

$$c_{\text{diag}} = 1.218. \tag{5.100}$$

Once this is fixed, equations (5.95) and (5.97) determine c_A and c_B. Since the second equation is quadratic it has two solutions, but one can be readily discarded because the two-photon couplings of the excited pions become unreasonably large, and so do the values of the constants c_A and c_B. The physical solution gives:

$$c_A = 6.794, \qquad c_B = -252.346. \tag{5.101}$$

Having determined c_A and c_B, (5.92) determines c_{anom} to the value:

$$c_{\text{anom}} = -1.670, \tag{5.102}$$

and finally (5.93) fixes the remaining parameter:

$$c_{\text{BL}} = 141.688. \tag{5.103}$$

As expected, all constants are of $\mathcal{O}(1)$, with the exception of c_{BL}, $c_B \sim \mathcal{O}(100)$.

Since there is no direct empirical information on the doubly-virtual π^0 TFF available, we fit our model parameter M_{diag} to the dispersive description of the π^0 TFF from refs. [28, 172]. To find the best fit, we minimize the estimated variance:

$$\chi^2 = \frac{1}{j_{\max} - p} \sum_{j=1}^{j_{\max}} \left(\frac{f(-Q_{1,j}^2, -Q_{2,j}^2) - f^{\text{data}}(-Q_{1,j}^2, -Q_{2,j}^2)}{\Delta f^{\text{data}}(-Q_{1,j}^2, -Q_{2,j}^2)} \right)^2, \tag{5.104}$$

[7] From figure 5 of ref. [193] we extracted $\hat{M}_\pi = 766\,\text{MeV}$.

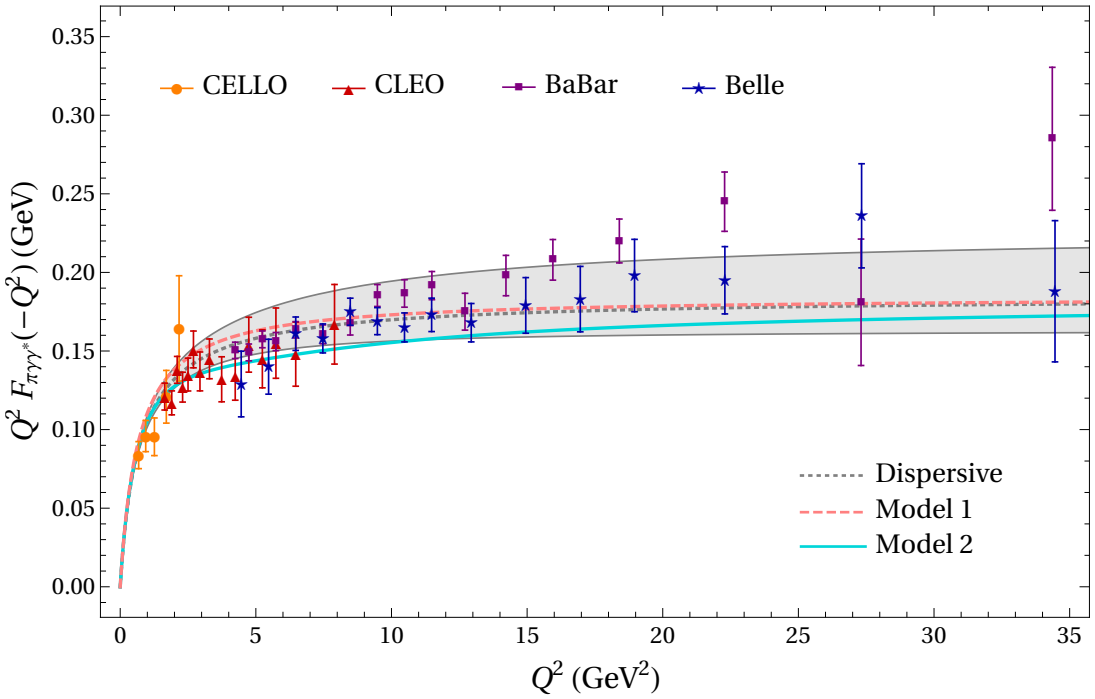

Figure 5.9: Singly-virtual π^0 TFF. The large-N_c Regge model, "Model 1" (5.90), is indicated by the dashed pink curve. Our alternative TFF model, "Model 2" (5.161), is indicated by the solid cyan curve. The gray band with the dotted curve is the dispersive result from refs. [28,172]. The data are from CELLO [204], CLEO [205], BaBar [258], and Belle [259].

where $j_{\max}$ is the length of the data set and p is the number of fit parameters. Here, f is our model and f^{data} is the dispersive TFF.[8] The sum is over $j_{\max} = \mathcal{O}(2{\times}10^4)$ selected points in the region of $0 < Q_1 \leq Q_2$, where $Q_2^2 \in [0, 40]\,\text{GeV}^2$. As a result, we obtain $M_{\text{diag}} = 1.519\,\text{GeV}$ with $\chi^2 \sim 0.37$.

The singly-virtual TFF of the ground-state pion is shown in figure 5.9. The large-N_c Regge model presented above is labeled as "Model 1." In appendix 5.2.B, an alternative TFF model, to which we refer as "Model 2," is introduced, based on a Regge resummation for the TFF itself. Both models give a reasonable description of the experimental data, while Model 1 shows better agreement with the dispersive TFF in the intermediate-Q region. In appendix 5.2.F.2, both models are shown also in the doubly-virtual region and further compared to the dispersive TFF [28, 171, 172], a prediction from lattice QCD [29], and a result from DSE [173]. We stress that neither model should be evaluated for other than purely space-like virtualities, both are constructed in such a way as to provide an efficient implementation of all constraints relevant for the space-like region, but do not properly incorporate the analytic structure required to continue to time-like virtualities. In addition to our fits to the dispersive π^0 TFF, we also checked that the π^0 contribution to $(g-2)_\mu$ is reproduced correctly

$$\begin{aligned} a_\mu^{\pi^0\text{-pole}}\big|_{\text{Model 1}} &= 64.3 \times 10^{-11}, \qquad a_\mu^{\pi^0\text{-pole}}\big|_{\text{Model 2}} = 64.5 \times 10^{-11}, \\ a_\mu^{\pi^0\text{-pole}}\big|_{[28,172]} &= 62.6\,^{+3.0}_{-2.5} \times 10^{-11}. \end{aligned} \tag{5.105}$$

[8] Since the error band of the dispersive TFF is asymmetric, for each kinematic point its smallest value was extracted to obtain $\Delta f^{\text{data}}(-Q_{1,j}^2, -Q_{2,j}^2)$.

Finally, as detailed in ref. [28], effective-field-theory constraints on the pseudoscalar-pole contributions [194, 195] are automatically encoded in the TFF phenomenology, for the leading constraint in its normalization, for the subleading one in the momentum dependence.

5.2.4.2 Large-N_c Regge model for the η and η' transition form factors

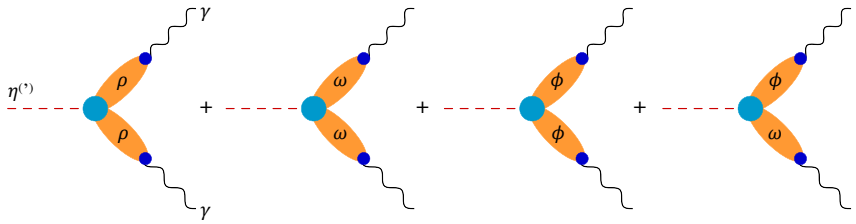

Figure 5.10: η and η' TFFs in the large-N_c limit.

Analogously to the pion case, our large-N_c Regge model for the η and η' TFFs shall satisfy the following five low- and high-energy constraints, cf. (5.36), (5.44), (5.50), and (5.78):

$$\text{normalization:} \qquad F^{\text{exp}}_{\eta\gamma\gamma} = 0.2739(48)\,\text{GeV}^{-1} \;\; [100],$$
$$F^{\text{exp}}_{\eta'\gamma\gamma} = 0.3413(76)\,\text{GeV}^{-1} \;\; [100]; \tag{5.106}$$

$$\text{BL limit [186, 187]:} \qquad \lim_{Q^2\to\infty} Q^2 F_{\eta\gamma\gamma^*}(-Q^2) = 12\,C_8 F_\eta,$$
$$\lim_{Q^2\to\infty} Q^2 F_{\eta'\gamma\gamma^*}(-Q^2) = 12\,C_0 F_{\eta'}; \tag{5.107}$$

$$\text{symmetric pQCD limit [101]:} \qquad \lim_{Q^2\to\infty} Q^2 F_{\eta\gamma^*\gamma^*}(-Q^2,-Q^2) = 4\,C_8 F_\eta,$$
$$\lim_{Q^2\to\infty} Q^2 F_{\eta'\gamma^*\gamma^*}(-Q^2,-Q^2) = 4\,C_0 F_{\eta'}; \tag{5.108}$$

$$\begin{aligned}\text{SDC for the mixed region [2]:} \qquad & \lim_{Q_3^2\to\infty}\lim_{Q^2\to\infty}\sum_{n=0}^{\infty}\hat{\Pi}_1^{\eta^{(\prime)}(n)\text{-pole}}(-Q^2,-Q^2,-Q_3^2)\\ &= -\lim_{Q_3^2\to\infty}\lim_{Q^2\to\infty}\sum_{n=0}^{\infty}\frac{F_{\eta^{(\prime)}(n)\gamma^*\gamma^*}(-Q^2,-Q^2)\,F_{\eta^{(\prime)}(n)\gamma\gamma^*}(-Q_3^2)}{Q_3^2+M^2_{\eta^{(\prime)}(n)}}\\ &= -\frac{6\,C^2_{\eta^{(\prime)}}}{\pi^2}\frac{1}{Q^2}\frac{1}{Q_3^2};\end{aligned} \tag{5.109}$$

$$\begin{aligned}\text{SDC for the asymptotic region:} \qquad & \lim_{Q^2\to\infty}\sum_{n=0}^{\infty}\hat{\Pi}_1^{\eta^{(\prime)}(n)\text{-pole}}(-Q^2,-Q^2,-Q^2)\\ &= -\lim_{Q^2\to\infty}\sum_{n=0}^{\infty}\frac{F_{\eta^{(\prime)}(n)\gamma^*\gamma^*}(-Q^2,-Q^2)\,F_{\eta^{(\prime)}(n)\gamma\gamma^*}(-Q^2)}{Q^2+M^2_{\eta^{(\prime)}(n)}}\\ &= -\frac{4}{9\pi^2}\frac{C^2_{\eta^{(\prime)}}}{\sum_{a=0,3,8}C_a^2}\frac{1}{Q^4}.\end{aligned} \tag{5.110}$$

Here, as compared to (5.44), we now use the notation

$$F_\eta = \frac{1}{C_8}\sum_a C_a F^a_\eta, \qquad F_{\eta'} = \frac{1}{C_0}\sum_a C_a F^a_{\eta'}. \tag{5.111}$$

	π	η	η'
$\rho\omega$	1.154	—	—
$\rho\phi$	0.032	—	—
$\rho\rho$	—	1.248	1.022
$\omega\omega$	—	0.139	0.114
$\phi\phi$	—	−0.256	0.314
$\phi\omega$	—	0.015	−0.002

Table 5.2: Pseudoscalar–vector–vector couplings derived in appendix 5.2.A: $C^P_{V_1V_2}$ with $P = \pi, \eta, \eta'$ and $V_i = \rho, \omega, \phi$ as defined in (5.159) and (5.160).

Furthermore, we introduced:

$$C_\eta^2 = \frac{\left(F^8\cos\theta_8 - 2\sqrt{2}F^0\sin\theta_0\right)\left(F^0\cos\theta_0 - 2\sqrt{2}F^8\sin\theta_8\right)}{108F^0F^8\cos\left(\theta_0-\theta_8\right)},$$
$$C_{\eta'}^2 = \frac{\left(2\sqrt{2}F^8\cos\theta_8 + F^0\sin\theta_0\right)\left(2\sqrt{2}F^0\cos\theta_0 + F^8\sin\theta_8\right)}{108F^0F^8\cos\left(\theta_0-\theta_8\right)}, \tag{5.112}$$

as follow by separating the η and η' contributions to (5.45) according to (5.41). These coefficients fulfill $C_\eta^2 + C_{\eta'}^2 = C_0^2 + C_8^2 = 1/12$.

Switching to the η and η' we face the problem that, since these are $I = 0$ mesons, they couple to isovector–isovector and isoscalar–isoscalar vector mesons, so to same-mass vector mesons only (ignoring ϕ–ω mixing), see figure 5.10. Taking the limit $M_{\omega(n)} = M_{\rho(n)} = M_{V(n)}$ in our parameterization of the pion TFF (5.90), we obtain a significant simplification:

$$F_{\pi(n)\gamma^*\gamma^*(-Q_1^2,-Q_2^2)} \propto \frac{M_V^4}{D^1_{V(n)}D^2_{V(n)}}\left[c_{\text{anom}} + c_A\frac{M^2_{V(n)}}{\Lambda^2} + c_{\text{diag}}\frac{Q_1^2Q_2^2}{\Lambda^2(Q_+^2+M^2_{\text{diag}})}\right]. \tag{5.113}$$

Since two free parameters dropped out, this parameterization cannot satisfy all relevant low- and high-energy constraints.

Fortunately, via vector-meson mixing in the isoscalar sector, there is a possible contribution of a mixed ϕ–ω term to the TFFs of the $\eta^{(\prime)}$, which would be absent in the case of ideal mixing. The ϕ–ω coupling to $\eta^{(\prime)}$ will certainly be small when compared to the same-mass vector-meson couplings, see table 5.2, but since it contributes where the others cannot, it is important to retain.

In summary, our large-N_c Regge model for the $\eta^{(\prime)}$ TFFs reads:

$$F_{\eta^{(\prime)}(n)\gamma^*\gamma^*}(-Q_1^2,-Q_2^2) = \frac{F_{\eta^{(\prime)}\gamma\gamma}}{\mathcal{N}}\left[F^{(a)}_{\eta^{(\prime)}(n)\gamma^*\gamma^*}(-Q_1^2,-Q_2^2) + F^{(b)}_{\eta^{(\prime)}(n)\gamma^*\gamma^*}(-Q_1^2,-Q_2^2)\right], \tag{5.114}$$

where the two parts parameterize the same-mass and mixed vector-meson contributions, respec-

tively:

$$F^{(a)}_{\eta^{(\prime)}(n)\gamma^*\gamma^*}(-Q_1^2,-Q_2^2) = \sum_{V=\rho,\omega,\phi} C_{VV}^{\eta^{(\prime)}} \left[1 + c_{\text{diag}} \frac{\Lambda^2}{M_V^4} \frac{Q_1^2 Q_2^2}{(Q_+^2 + M_{\text{diag}}^2)}\right] \frac{M_V^4}{D^1_{V(n)} D^2_{V(n)}}, \tag{5.115}$$

$$\begin{aligned} F^{(b)}_{\eta^{(\prime)}(n)\gamma^*\gamma^*}(-Q_1^2,-Q_2^2) = C_{\phi\omega}^{\eta^{(\prime)}} \Bigg\{ &\left[1 + c_A \frac{M^2_{+,n} - M^2_{+,0}}{\Lambda^2} + c_B \frac{M^2_{-,n} - M^2_{-,0}}{\Lambda^2}\right] \\ &\times \left(\frac{M_\phi^2 M_\omega^2}{D^1_{\omega(n)} D^2_{\phi(n)}} + \frac{M_\phi^2 M_\omega^2}{D^2_{\omega(n)} D^1_{\phi(n)}}\right) + \left[c_{\text{BL}} + c_A \frac{M^2_{-,n}}{\Lambda^2} + c_B \frac{M^2_{+,n}}{\Lambda^2}\right] \\ &\times \frac{Q_-^2}{Q_+^2} \left(\frac{M_\phi^2 M_\omega^2}{D^1_{\omega(n)} D^2_{\phi(n)}} - \frac{M_\phi^2 M_\omega^2}{D^2_{\omega(n)} D^1_{\phi(n)}}\right) \Bigg\}. \end{aligned} \tag{5.116}$$

Here we again use the short-hand notations from (5.91), with the modification that

$$M^2_{\pm,n} = \frac{1}{2}\left(M^2_{\phi(n)} \pm M^2_{\omega(n)}\right). \tag{5.117}$$

All meson spectra are assumed to follow a radial Regge model. For the ϕ meson, we use the analog of (5.82). For the η and η' mesons, we distinguish:

$$M^2_{\eta(n)} = \begin{cases} M_\eta^2 & n = 0, \\ \hat{M}_\eta^2 + n\,\sigma_\eta^2 & n \geq 1, \end{cases} \tag{5.118}$$

and

$$M^2_{\eta'(n)} = M^2_{\eta'} + n\,\sigma^2_{\eta'} \tag{5.119}$$

with the ground-state masses $M_\eta = 547.862(17)$ MeV and $M_{\eta'} = 957.78(6)$ MeV [100].

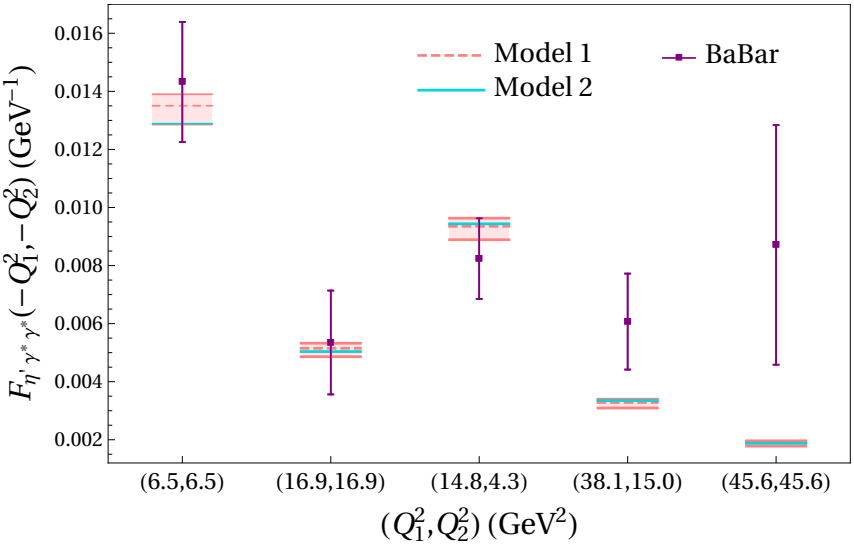

Figure 5.11: Comparison to the doubly-virtual η' TFF data from BaBar [207]. The large-N_c Regge model, "Model 1" (5.114), is indicated by the pink bands with the dashed lines. Our alternative TFF model, "Model 2" (5.161), is indicated by the solid cyan lines.

The normalization coefficient is defined as:

$$\mathcal{N} = C^{\eta}_{\rho\rho} + C^{\eta}_{\omega\omega} + C^{\eta}_{\phi\phi} + 2C^{\eta}_{\phi\omega}, \tag{5.120}$$

where $C^{P}_{V_1V_2}$ are the pseudoscalar–vector–vector couplings derived in appendix 5.2.A, and $C^{\eta}_{\phi\omega}$ is the parameter that measures the deviation from ideal mixing. By construction, each vector-meson pair contributes (up to normalization) exactly $C^{P}_{V_1V_2}$ to $F_{\eta^{(\prime)}\gamma\gamma}$.

To simplify the parameterization, equation (5.116) only contains terms which are unique to the ϕ–ω contribution, and the n-dependence has been removed from the numerator of (5.115). In this way, (5.116) is used to satisfy the BL limit for the ground-state $\eta^{(\prime)}$ TFF as well as the two SDCs on the HLbL tensor.

The constraint equations following from (5.107) and (5.108) read:

$$\begin{aligned} \text{BL limit:} \qquad 1 = \frac{1}{\mathcal{N}}\frac{F_{\eta\gamma\gamma}}{12C_8F_\eta}\Bigg[& C^{\eta}_{\rho\rho}M^2_\rho + C^{\eta}_{\omega\omega}M^2_\omega + C^{\eta}_{\phi\phi}M^2_\phi \\ & + 2C^{\eta}_{\phi\omega}\left(M^2_{+,0} - c_{\text{BL}}M^2_{-,0} - c_A\frac{M^4_{-,0}}{\Lambda^2} - c_B\frac{M^2_{+,0}M^2_{-,0}}{\Lambda^2}\right)\Bigg]; \end{aligned} \tag{5.121}$$

$$\text{symmetric pQCD limit:} \qquad 1 = \frac{C^{\eta}_{\rho\rho} + C^{\eta}_{\omega\omega} + C^{\eta}_{\phi\phi}}{\mathcal{N}}\frac{\Lambda^2 F_{\eta\gamma\gamma}}{8C_8F_\eta}\,c_{\text{diag}}; \tag{5.122}$$

where the same equations hold for the η' with the obvious replacements (including $C_8 \to C_0$). The MV SDC for the HLbL tensor in the mixed region translates to:

$$1 = \frac{C^{\eta}_{\phi\omega}}{\mathcal{N}}\frac{2\pi^2 C_8F_\eta F_{\eta\gamma\gamma}M^2_\phi M^2_\omega}{3C^2_\eta\Lambda^2}\left[(c_A + c_B)\frac{L_{\omega\eta}}{\Delta_{\omega\eta}} + (c_A - c_B)\frac{L_{\phi\eta}}{\Delta_{\phi\eta}}\right], \tag{5.123}$$

where c_{diag} has already been inserted. The SDC for the HLbL tensor in the asymptotic region

becomes more complicated due to the presence of additional mass scales:

$$
\begin{aligned}
1 = \frac{C^\eta_{\phi\omega}}{\mathcal{N}^2}\frac{\pi^2 F^2_{\eta\gamma\gamma} M^2_\phi M^2_\omega}{16 C^2_\eta \Lambda^4}\Bigg[\frac{4C^\eta_{\phi\omega}M^2_\phi M^2_\omega}{\Omega^2_{\phi\omega\eta}}\Bigg\{ c_A^2 \Delta_{\phi\omega}\Sigma_{\phi\omega}\Big[\Omega_{\phi\omega\eta} + \sigma^2_\eta\left(\Delta^2_{\omega\eta}L_{\phi\eta} - \Delta^2_{\phi\eta}L_{\omega\eta}\right)\Big] \\
+ c_B^2\Delta_{\phi\omega}\Big[\left(\Sigma_{\phi\omega}\sigma^2_\eta - 2\sigma^4_\phi\right)\Delta^2_{\omega\eta}L_{\phi\eta} - \left(\Sigma_{\phi\omega}\sigma^2_\eta - 2\sigma^4_\omega\right)\Delta^2_{\phi\eta}L_{\omega\eta} + \left(\Delta_{\phi\eta}+\Delta_{\omega\eta}\right)\Omega_{\phi\omega\eta}\Big] \\
+ 2c_A c_B\Big[\sigma^2_\eta\left(\sigma^4_\phi + \sigma^4_\omega\right)\left(\Delta^2_{\omega\eta}L_{\phi\eta} - \Delta^2_{\phi\eta}L_{\omega\eta}\right) + \Sigma_{\phi\omega}\left(\sigma^4_\omega\Delta^2_{\phi\eta}L_{\omega\eta} - \sigma^4_\phi\Delta^2_{\omega\eta}L_{\phi\eta}\right) \\
- \Omega_{\phi\omega\eta}\left(\sigma^2_\eta\Sigma_{\phi\omega} - \sigma^4_\phi - \sigma^4_\omega\right)\Big]\Bigg\} + c_{\text{diag}}c_A\,\Lambda^4\Bigg(\frac{2C^\eta_{\rho\rho}}{\Delta_{\rho\phi}\Delta_{\rho\omega}}\Bigg\{\frac{\sigma^2_\rho\left(\Delta_{\rho\phi}+\Delta_{\rho\omega}\right)}{\Delta_{\rho\eta}} \\
+ \frac{1}{\Omega_{\rho\phi\eta}\Omega_{\rho\omega\eta}\Omega_{\phi\omega\eta}}\Big[\Omega_{\phi\omega\eta}\sigma^4_\eta\Delta^2_{\rho\phi}\Delta^2_{\rho\omega}\left(\Delta_{\phi\eta}+\Delta_{\omega\eta}\right)L_{\rho\eta} - \Delta_{\phi\omega}\left(\Omega^2_{\rho\omega\eta}\sigma^4_\phi\Delta_{\phi\eta}L_{\rho\phi}\right. \\
\left.+\Omega^2_{\rho\phi\eta}\sigma^4_\omega\Delta_{\omega\eta}L_{\rho\omega}\right)\Big]\Bigg\} + \frac{C^\eta_{\phi\phi}\Delta_{\omega\eta}}{\Omega^2_{\phi\omega\eta}\Delta_{\phi\eta}}\Big[2\sigma^4_\eta\Delta^2_{\phi\omega}\left(\Delta_{\phi\eta}+\Delta_{\omega\eta}\right)L_{\phi\eta} - 2\sigma^4_\omega\Delta^3_{\phi\eta}L_{\phi\omega} \\
+ \Omega_{\phi\omega\eta}\left(3\sigma^4_\phi - \sigma^2_\phi\sigma^2_\omega - 5\sigma^2_\phi\sigma^2_\eta + 3\sigma^2_\omega\sigma^2_\eta\right)\Big] + \frac{C^\eta_{\omega\omega}\Delta_{\phi\eta}}{\Omega^2_{\phi\omega\eta}\Delta_{\omega\eta}}\Big[2\sigma^4_\phi\Delta^3_{\omega\eta}L_{\phi\omega} \\
+ 2\sigma^4_\eta\Delta^2_{\phi\omega}\left(\Delta_{\phi\eta}+\Delta_{\omega\eta}\right)L_{\omega\eta} + \Omega_{\phi\omega\eta}\left(\sigma^2_\phi\sigma^2_\omega - 3\sigma^4_\omega - 3\sigma^2_\phi\sigma^2_\eta + 5\sigma^2_\omega\sigma^2_\eta\right)\Big]\Bigg) \\
- c_{\text{diag}}c_B\,\Lambda^4\Bigg(\frac{2C^\eta_{\rho\rho}}{\Delta_{\rho\phi}\Delta_{\rho\omega}}\Bigg\{\frac{\sigma^2_\rho\Delta_{\phi\omega}}{\Delta_{\rho\eta}} - \frac{1}{\Omega_{\rho\phi\eta}\Omega_{\rho\omega\eta}\Omega_{\phi\omega\eta}}\Big[\Omega^2_{\rho\omega\eta}\sigma^4_\phi\Delta_{\phi\omega}\Delta_{\phi\eta}L_{\rho\phi} \\
- \Omega^2_{\rho\phi\eta}\sigma^4_\omega\Delta_{\phi\omega}\Delta_{\omega\eta}L_{\rho\omega} + \Omega^2_{\rho\phi\omega}\sigma^4_\eta\Delta_{\phi\eta}\Delta_{\omega\eta}L_{\rho\eta}\Big]\Bigg\} - \frac{C^\eta_{\omega\omega}\Delta_{\phi\eta}}{\Omega^2_{\phi\omega\eta}\Delta_{\omega\eta}}\Big[2\left(\sigma^4_\phi\Delta^3_{\omega\eta} + \sigma^4_\eta\Delta^3_{\phi\omega}\right)L_{\omega\eta} \\
- 2\sigma^4_\phi\Delta^3_{\omega\eta}L_{\phi\eta} + \Omega_{\phi\omega\eta}\left(\sigma^2_\phi\sigma^2_\omega + \sigma^4_\omega - 3\sigma^2_\phi\sigma^2_\eta + \sigma^2_\omega\sigma^2_\eta\right)\Big] - \frac{C^\eta_{\phi\phi}\Delta_{\omega\eta}}{\Omega^2_{\phi\omega\eta}\Delta_{\phi\eta}}\Big[2\sigma^4_\omega\Delta^3_{\phi\eta}L_{\omega\eta} \\
- 2\left(\sigma^4_\omega\Delta^3_{\phi\eta} - \sigma^4_\eta\Delta^3_{\phi\omega}\right)L_{\phi\eta} + \Omega_{\phi\omega\eta}\left(\sigma^4_\phi + \sigma^2_\phi\sigma^2_\omega + \sigma^2_\phi\sigma^2_\eta - 3\sigma^2_\omega\sigma^2_\eta\right)\Big]\Bigg)\Bigg].
\end{aligned}
\tag{5.124}
$$

In appendix 5.2.G.1, the above system of equations is solved analytically. In the following, we discuss numerical values for all input parameters. The couplings $C^{\eta^{(\prime)}}_{V_1V_2}$ are collected in table 5.2. They are calculated based on (5.159) with the phenomenological η–η' mixing parameters [201, 202]:

$$
F^8 = 1.26(4)F_\pi, \quad F^0 = 1.17(3)F_\pi, \quad \theta_8 = -21.2(1.6)^\circ, \quad \theta_0 = -9.2(1.7)^\circ, \tag{5.125}
$$

and the ϕ–ω mixing angle $\theta_V = 36.4^\circ$ [100]. The parameters $C^2_{\eta^{(\prime)}}$, which describe our choice for the splitting of the SDCs on the HLbL tensor into η and η' contributions, evaluate to:

$$
C^2_\eta \sim 0.027 \qquad C^2_{\eta'} \sim 0.057, \tag{5.126}
$$

as follows from (5.112) with the η–η' mixing parameters in (5.125). The decay constants $F_{\eta^{(\prime)}}$, on the other hand, are not deduced from the η–η' mixing parameters, but fit to experimental data for the singly-virtual $\eta^{(\prime)}$ TFFs:

$$
\begin{aligned}
F_\eta &= 139^{+27}_{-2}\,\text{MeV}, \\
F_{\eta'} &= 79^{+3}_{-5}\,\text{MeV},
\end{aligned}
\tag{5.127}
$$

with an estimated variance of $\chi^2 \sim 1.1$ and $\chi^2 \sim 0.9$, respectively. The errors are increased in order to cover the Padé approximant predictions from refs. [26] and [198] for η and η', respectively. The large error on F_η may be partly due to the fact that it is not clear when the asymptotic BL limit sets in, accordingly, we will keep the full range in the error analysis. M_{diag} is fit to the recent BaBar data for the doubly-virtual η' TFF [207], see figure 5.11. The resulting value $M_{\text{diag}} = 898$ MeV (with $\chi^2 \sim 1.6$) is used for both the η and η' large-N_c Regge model. Furthermore, we use the Regge slopes collected in (5.99) as well as [193]:[9]

$$\sigma_\eta^2 = 1.33(11)\,\text{GeV}^2, \quad \sigma_{\eta'}^2 = 1.36(14)\,\text{GeV}^2, \quad \sigma_\phi^2 = 1.84(6)\,\text{GeV}^2. \tag{5.128}$$

The final model parameters (c_A, c_B, c_{diag}, c_{BL}) are summarized in table 5.1, where we rescaled the numerical values with $C^\eta_{\phi\omega}/\mathcal{N} \sim 0.0129$ and $C^{\eta'}_{\phi\omega}/\mathcal{N} \sim -0.0017$, respectively, to show that all parameters are of "natural" size.

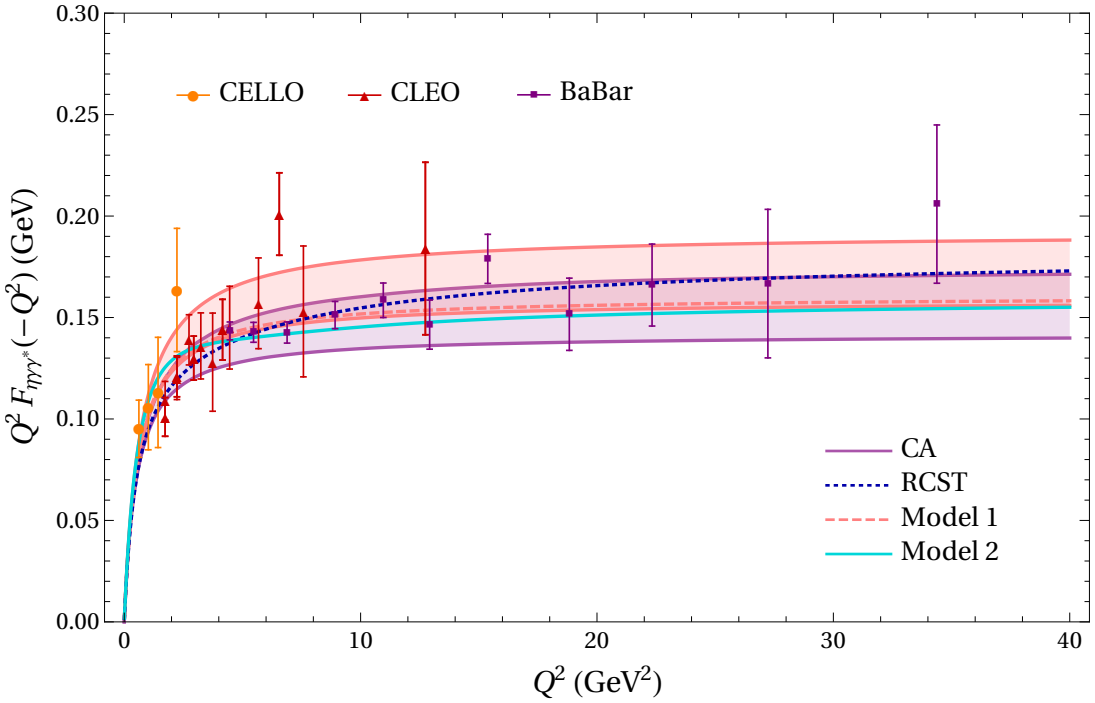

Figure 5.12: Singly-virtual η TFF. The large-N_c Regge model, "Model 1" (5.114), is indicated by the pink band with the dashed curve. Our alternative TFF model, "Model 2" (5.161), is indicated by the solid cyan curve. The purple band is the CA result from ref. [26]. The dark blue dotted curve is the RCST result from ref. [261]. The data are from CELLO [204], CLEO [205], and BaBar [206].

The singly-virtual TFFs of the ground-state η and η' are shown in figures 5.12 and 5.13. The large-N_c Regge model presented above is labeled as "Model 1." The alternative TFF model, introduced in appendix 5.2.B, is referred to as "Model 2." The model error of the large-N_c Regge TFFs is propagated from the errors of the input parameters σ_P, σ_V, $F_{P\gamma\gamma}$, F_P, as well as the η–η' mixing parameters, see (5.99), (5.106), (5.128), (5.125), and (5.127). While Model 2, for which we do not provide an error estimate, runs outside the error band of the Model 1 η' (η) TFF for some low (intermediate) values of Q^2, both models give a good description of the experimental

[9] From figure 3 of ref. [193] we extracted $\hat{M}_\eta = 591\,\text{MeV}$.

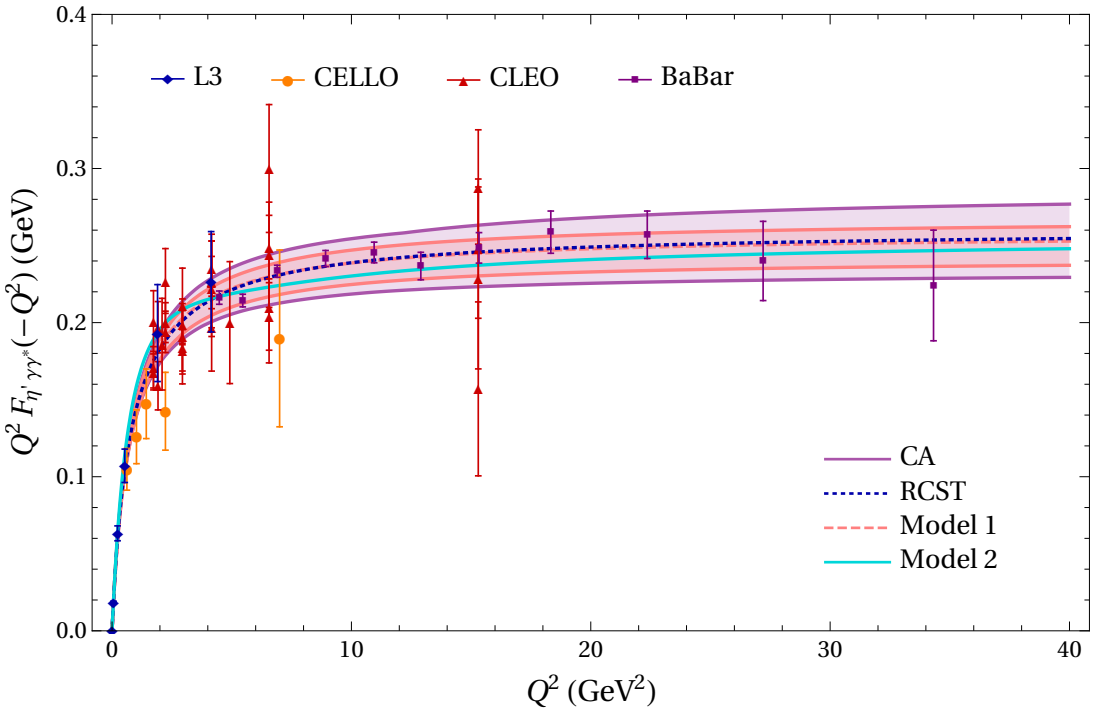

Figure 5.13: Singly-virtual η' TFF. The large-N_c Regge model, "Model 1" (5.114), is indicated by the pink band with the dashed curve. Our alternative TFF model, "Model 2" (5.161), is indicated by the solid cyan curve. The purple band is the CA result from ref. [26]. The dark blue dotted curve is the RCST result from ref. [261]. The data are from L3 [203], CELLO [204], CLEO [205], and BaBar [206].

data and, thus, come out close to the results from CAs [26] and fits within resonance chiral symmetric theory (RCST) [261].[10] In appendices 5.2.G.2 and 5.2.G.3, both models are further compared to CA, RCST, and DSE [173], and the decomposition of Model 1 into 2ρ, 2ϕ, 2ω, and $\phi\omega$ contributions is illustrated. We stress again that neither model should be evaluated for other than purely space-like virtualities.

Both the ground-state η contribution to $(g-2)_\mu$,

$$\begin{aligned} a_\mu^{\eta\text{-pole}}\big|_{\text{Model 1}} &= 16.4\,^{+1.3}_{-0.5} \times 10^{-11}, \qquad a_\mu^{\eta\text{-pole}}\big|_{\text{Model 2}} = 17.8 \times 10^{-11}, \\ a_\mu^{\eta\text{-pole}}\big|_{[26,214]} &= 16.3(1.4) \times 10^{-11}, \end{aligned} \tag{5.129}$$

and the ground-state η' contribution to $(g-2)_\mu$

$$\begin{aligned} a_\mu^{\eta'\text{-pole}}\big|_{\text{Model 1}} &= 14.8\,^{+0.6}_{-0.7} \times 10^{-11}, \qquad a_\mu^{\eta'\text{-pole}}\big|_{\text{Model 2}} = 16.1 \times 10^{-11}, \\ a_\mu^{\eta'\text{-pole}}\big|_{[26,214]} &= 14.5(1.9) \times 10^{-11}, \end{aligned} \tag{5.130}$$

are reproduced correctly with our $\eta^{(\prime)}$ TFF models.

n	η				η'			
	Assignment 1		Assignment 2		Assignment 1		Assignment 2	
1	$\eta(1295)$	0.0354	$\eta(1440)$	0.0351	$\eta'(1475)$	0.0594	$X(1835)$	0.0561
2	$\eta(1760)$	0.0171	$\eta(1760)$	0.0169	$\eta'(2010)$	0.0305	$\eta'(2070)$	0.0281
3	$\eta(2100)$	0.0111		0.0110	$\eta'(2225)$	0.0203		0.0185
4	$\eta(2320)$	0.0082		0.0081		0.0151		0.0137

Table 5.3: Two-photon couplings, $F_{P\gamma\gamma}$, of excited $\eta^{(\prime)}$ states from the large-N_c Regge model (5.114), in units of GeV^{-1}. "Assignment 1" and "Assignment 2" refer to the assignments of $\eta^{(\prime)}$ excitations shown in figure 5.8 and suggested in refs. [100, 193] and [213, Table 27], respectively.

5.2.4.3 Comparison of two-photon couplings

Apart from the Regge slopes for the trajectories of pion, η, η', as well the vector mesons, phenomenological input for the excited-pseudoscalar contributions could in principle be provided by their TFFs. Even though the normalizations are poorly known, it is still important to verify that the two-photon couplings implied by our Regge models compare reasonably to the available phenomenological constraints. For the first excited state in the pion trajectory, there is a limit

$$F_{\pi(1300)\gamma\gamma} < 0.0544(71)\,\mathrm{GeV}^{-1}, \tag{5.131}$$

see appendix 5.2.D, which is indeed satisfied by $F_{\pi(1300)\gamma\gamma} = 0.050\,\mathrm{GeV}^{-1}$ from our Regge model. Nothing is known about the two-photon coupling of the $\pi(1800)$ and even heavier excited pions.

The situation is more involved in the $\eta^{(\prime)}$ sector. As alluded to in the caption of figure 5.8, the spectroscopy of excited $\eta^{(\prime)}$ states is contentious, especially regarding the role of the states below 1500 MeV. Table 5.3 collects two possible assignments of states to Regge trajectories. The first interpretation, favored by ref. [100], considers the $\eta(1295)$ the lowest η excitation and differentiates between $\eta(1405)$ and $\eta(1475)$ states. The latter is considered as the first η' excitation, while the $\eta(1405)$ is described as a glueball candidate. In contrast, ref. [213] argues that there is only a single state below 1500 MeV, the $\eta(1440)$, which should be interpreted as the first η excitation. The $X(1835)$ is identified as suitable candidate for the first η' excitation, although its quantum numbers are not yet established. In both cases, the $\eta(1760)$ emerges as the second η excitation.

The available constraints on the two-photon couplings of $\eta^{(\prime)}$ are collected in table 5.4, see appendix 5.2.D for details. The results from the second column are valid under the assumption that the branching fractions listed in the PDG are accurate, while the third column assumes, in addition, dominance by some decay channels (given in the last column). For the $\eta(1295)$ only an indirect limit is available, in the first assignment the two-photon coupling of the $\eta(1295)$ comes out slightly larger. Note, however, that the very existence of the $\eta(1295)$ is called into question in ref. [213], with the fact that in contrast to the $\eta(1475)$ this resonance has not been seen in

[10] The RCST result is reproduced from fit 2 in ref. [261] and PDG input for the masses of $\rho(770)$, $\rho(1450)$, $\rho(1700)$, $\omega(782)$, $\omega(1420)$, $\omega(1650)$, $\phi(1020)$, $\phi(1680)$, and $\phi(2170)$ [100].

	$F_{P\gamma\gamma}[\,\mathrm{GeV}^{-1}]$		
P	direct	indirect	assuming dominance of
$\eta(1295)$	—	< 0.030	$\eta\pi\pi$, $K\bar{K}\pi$
$\eta(1405)$	< 0.122	< 0.033	$\eta\pi\pi$, $K\bar{K}\pi$
$\eta(1475)$	< 0.195, $> 0.041(6)$	$= 0.041(6)$	$K\bar{K}\pi$
$\eta(1760)$	$> 0.014(2)$	$= 0.014(2)$	$\eta'\pi\pi$
$X(1835)$	< 0.235	< 0.022	$\eta'\pi\pi$

Table 5.4: Constraints on the two-photon couplings of excited $\eta^{(\prime)}$ states, as collected in appendix 5.2.D. The column labeled "direct" includes constraints that follow directly from branching fractions listed in the PDG, while the column labeled "indirect" lists results obtained when assuming that the channels from the last column are dominant.

the $\gamma\gamma$ reaction as one of the arguments. The $\eta(1405)$ is discarded in either assignment of Regge trajectories. However, in the second assignment the $\eta(1440)$ would be interpreted as a single state instead of $\eta(1405)$ and $\eta(1475)$, see also ref. [262], in such a way that for the comparison the two-photon couplings of both states should be considered. Remarkably, the measured value for the $\eta(1475)$, $F_{\eta(1475)\gamma\gamma} = 0.041(6)\,\mathrm{GeV}^{-1}$, agrees perfectly with $F_{\eta(1440)\gamma\gamma} = 0.035\,\mathrm{GeV}^{-1}$ from Assignment 2. In Assignment 1, where the $\eta(1475)$ is considered the first η' excitation, there is still reasonable agreement. Next, the experimental result for the $\eta(1760)$ nicely confirms the two-photon coupling implied by both assignments, since a tiny correction beyond the dominant $\eta'\pi\pi$ channel would suffice to bring the numbers into complete agreement. Finally, the two-photon coupling of the $X(1835)$ in Assignment 2 fulfills the direct limit but not the one assuming dominance of $\eta'\pi\pi$, which may indicate that in case this assignment is correct, other channels besides $\eta'\pi\pi$ may play a role (as indeed suggested by other decay channels listed in the PDG). Moreover, the significance of the two-resonance fit from ref. [212] used to obtain the much stricter limit is only quoted at $2.8\,\sigma$. Taken together with the fact that not even the quantum numbers of the $X(1835)$ are firmly established, it thus seems difficult to draw meaningful conclusions on its two-photon coupling at this point.

Altogether, we conclude that the two-photon couplings implied by our large-N_c Regge models are well compatible with the phenomenological constraints. In particular, for the cases where measurements and not just limits exist, the $\eta(1475)$ and the $\eta(1760)$, the resulting couplings are close to the ones that our large-N_c Regge models would imply. The same is true for our alternative TFF model (5.161), see figure 5.21, whose couplings are similar to the ones of the large-N_c Regge models. We stress that the detailed comparison depends on the assignment of observed states to Regge trajectories, but in both variants considered there is reasonable agreement with the two-photon phenomenology of excited $\eta^{(\prime)}$ states.

5.2.4.4 Excited-pseudoscalar contributions to $(g-2)_\mu$

The ground-state pseudoscalar-pole contributions to $(g-2)_\mu$, calculated based on our TFF models, are given in (5.105), (5.129), and (5.130). The uncertainty on the predictions from

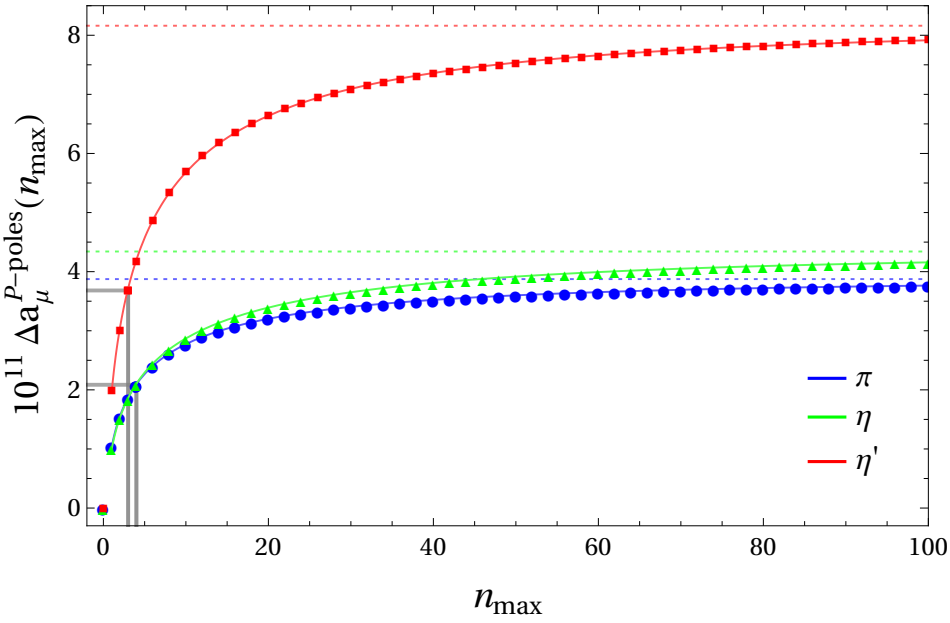

Figure 5.14: Sum over radially-excited pion, η, and η' contributions to $(g-2)_\mu$, as defined in (5.133). The dotted curves are the extrapolated values $\Delta a_\mu^{P\text{-poles}}$ corresponding to the limit $n_{\max} \to \infty$. The gray lines indicate the contributions from the lowest (observed) pseudoscalar excitations shown in figure 5.8. All results are calculated with the Model 2 TFFs (5.161).

Model 1 is the propagated error from the input parameters σ_P, σ_V, $F_{P\gamma\gamma}$, F_P, and the η–η' mixing parameters. In all cases we observe good agreement with the literature [26, 28, 172, 214], which demonstrates that in addition to fulfilling the various SDCs, our Regge models capture the properties of the TFFs most relevant for the $g-2$ integral.

In the following, we derive the contribution to $(g-2)_\mu$ originating from radially-excited pseudoscalar mesons. The large-N_c Regge models introduced in the preceding sections and the alternative model discussed in appendix 5.2.B are constructed in such a way as to describe not only the ground-state pseudoscalar TFFs, but also the TFFs of excited pseudoscalar mesons. Phenomenological input on these excited states enters mainly in terms of their masses as contained in the Regge parameters, while the infinite sum restores the correct asymptotic properties of the HLbL tensor, which cannot be achieved with a finite number of pseudoscalar-pole contributions. Moreover, for some of the excited states limits on their two-photon couplings are available, see appendix 5.2.D as well as the discussion in the previous subsection, which shows that the couplings implied by our Regge model are consistent with the available constraints from phenomenology.

With the large-N_c Regge model, we can calculate the pseudoscalar-meson tower exactly, i.e., we can perform the infinite sum over pseudoscalar-pole diagrams with excited pseudoscalars. For Model 2, we sum over the lowest $n = 100$ radially-excited pseudoscalars ($P = \pi, \eta, \eta'$) and then fit a saturation curve,

$$\Delta a_\mu^{P\text{-poles}}(n_{\max}) = \Delta a^{P\text{-poles}} - (\Delta a^{P\text{-poles}} - a_0)\, e^{-b\,(n_{\max})^c}, \tag{5.132}$$

in order to extrapolate to infinity. Here, we defined:

$$\Delta a_\mu^{P\text{-poles}}(n_{\max}) = \sum_{n=1}^{n_{\max}} a_\mu^{P(n)\text{-pole}}, \tag{5.133}$$

with the infinite-summation result denoted as:

$$\Delta a_\mu^{P\text{-poles}} \coloneqq \Delta a_\mu^{P\text{-poles}}(\infty). \tag{5.134}$$

The saturation curve procedure is illustrated in figure 5.14, where for reasons of clarity only every other data point is plotted above $n = 4$. The fits start from $n_{\max} = 1$ and describe the data perfectly. The dotted lines indicate the extrapolated values for $\Delta a_\mu^{P\text{-poles}}$ and illustrate the good convergence of the summation already at $n_{\max} = 100$. This procedure has been verified with the large-N_c Regge model, for which the sum is already saturated at $n_{\max} = 100$.

For the full pseudoscalar-pole contributions to $(g-2)_\mu$, we obtain:

$$\begin{aligned}
&\sum_{n=0}^{\infty} a_\mu^{\pi(n)\text{-pole}}\big|_{\text{Model 1}} = 67.1(0.4) \times 10^{-11}, \qquad \sum_{n=0}^{\infty} a_\mu^{\pi(n)\text{-pole}}\big|_{\text{Model 2}} = 68.4 \times 10^{-11},\\
&\sum_{n=0}^{\infty} a_\mu^{\eta(n)\text{-pole}}\big|_{\text{Model 1}} = 19.9\,^{+1.1}_{-0.9} \times 10^{-11}, \qquad \sum_{n=0}^{\infty} a_\mu^{\eta(n)\text{-pole}}\big|_{\text{Model 2}} = 22.1 \times 10^{-11},\\
&\sum_{n=0}^{\infty} a_\mu^{\eta'(n)\text{-pole}}\big|_{\text{Model 1}} = 21.3(1.2) \times 10^{-11}, \qquad \sum_{n=0}^{\infty} a_\mu^{\eta'(n)\text{-pole}}\big|_{\text{Model 2}} = 24.2 \times 10^{-11},\\
&\sum_{n=0}^{\infty} a_\mu^{\pi(n)\text{-pole}} + a_\mu^{\eta(n)\text{-pole}} + a_\mu^{\eta'(n)\text{-pole}}\big|_{\text{Model 1}} = 108.3\,^{+1.8}_{-1.7} \times 10^{-11},
\end{aligned} \tag{5.135}$$

where the uncertainty of the Model 1 prediction is solely estimated based on the error propagated from the input parameters on $\sum_{n=0}^{100} a_\mu^{P(n)\text{-pole}}$. Isolating the contribution from excited pseudoscalars, one finds:

$$\begin{aligned}
\Delta a_\mu^{\pi\text{-poles}}\big|_{\text{Model 1}} &= 2.7(0.4) \times 10^{-11}, & \Delta a_\mu^{\pi\text{-poles}}\big|_{\text{Model 2}} &= 3.9 \times 10^{-11},\\
\Delta a_\mu^{\eta\text{-poles}}\big|_{\text{Model 1}} &= 3.4\,^{+0.9}_{-0.7} \times 10^{-11}, & \Delta a_\mu^{\eta\text{-poles}}\big|_{\text{Model 2}} &= 4.3 \times 10^{-11},\\
\Delta a_\mu^{\eta'\text{-poles}}\big|_{\text{Model 1}} &= 6.5(1.1) \times 10^{-11}, & \Delta a_\mu^{\eta'\text{-poles}}\big|_{\text{Model 2}} &= 8.2 \times 10^{-11}.
\end{aligned} \tag{5.136}$$

The difference between the $\Delta a_\mu^{P\text{-poles}}$ results from Model 1 and Model 2 can be used to quantify the systematic uncertainty of our prediction:

$$\begin{aligned}
\Delta a_\mu^{\pi\text{-poles}} &= 2.7\,(0.4)_{\text{Model 1}}\,(1.2)_{\text{syst}} \times 10^{-11} = 2.7\,(1.3) \times 10^{-11},\\
\Delta a_\mu^{\eta\text{-poles}} &= 3.4\,^{+0.9}_{-0.7}\big|_{\text{Model 1}}\,(0.9)_{\text{syst}} \times 10^{-11} = 3.4\,^{+1.3}_{-1.1} \times 10^{-11},\\
\Delta a_\mu^{\eta'\text{-poles}} &= 6.5\,(1.1)_{\text{Model 1}}\,(1.7)_{\text{syst}} \times 10^{-11} = 6.5\,(2.0) \times 10^{-11}.
\end{aligned} \tag{5.137}$$

With the alternative assignment of $\eta^{(\prime)}$ excitations in the radial Regge trajectories [213], see dot-dashed purple lines in figure 5.8, we obtain:

$$\Delta a_\mu^{\eta\text{-poles}} = 3.4 \times 10^{-11}, \qquad \Delta a_\mu^{\eta'\text{-poles}} = 6.4 \times 10^{-11}, \tag{5.138}$$

indicating that the net effect is remarkably insensitive to the assignment of the η, η' Regge trajectories. Expressing $C^2_{\eta^{(\prime)}}$ through the experimental $F_{\eta^{(\prime)}\gamma\gamma}$ and $F_{\eta^{(\prime)}}$, see left-hand side of (5.45),

instead of the η–η' mixing parameters, leads to a decrease of $a_\mu^{\eta^{(\prime)}\text{-poles}}$ that is well within the uncertainty quoted in (5.137). Our final result for the sum of pion, η, and η' states is:

$$\begin{aligned}\Delta a_\mu^{\text{PS-poles}} &= \Delta a_\mu^{\pi\text{-poles}} + \Delta a_\mu^{\eta\text{-poles}} + \Delta a_\mu^{\eta'\text{-poles}} \\ &= 12.6\,{}^{+1.6}_{-1.5}\big|_{\text{Model 1}}\,(3.8)_{\text{syst}} \times 10^{-11} \\ &= 12.6(4.1) \times 10^{-11}. \end{aligned} \tag{5.139}$$

For Model 2 (Model 1) roughly 50 % (80 %) of $\Delta a_\mu^{\text{PS-poles}}$ is generated by the lowest (observed) pseudoscalar excitations listed in figure 5.8. This can be seen in figure 5.14 where $\Delta a_\mu^{P\text{-poles}}(n_{\max})$ is shown for Model 2.

5.2.5 Matching quark loop and Regge model

5.2.5.1 Matching at the level of $(g-2)_\mu$

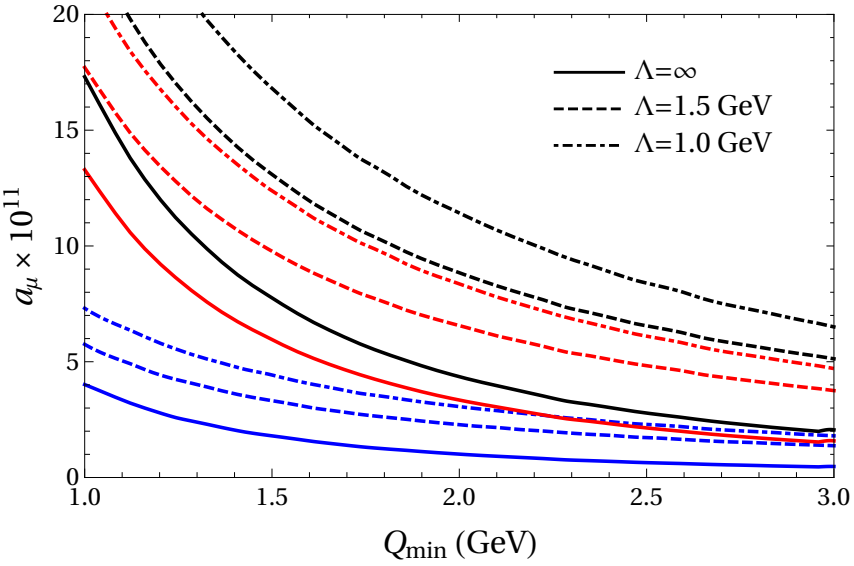

Figure 5.15: Contribution of the pQCD quark loop (with vanishing quark mass) to a_μ from the region $Q_{1,2} \geq Q_{\min}$ with the contribution from Q_3 below $Q_{\min}$ damped by $Q_3^2/(Q_3^2+\Lambda^2)$ (plus crossed). The total contribution from $\bar{\Pi}_{1\text{–}12}$ is shown in black, together with the partial ones from $\bar{\Pi}_{1\text{–}2}$ (red) and $\bar{\Pi}_{3\text{–}12}$ (blue). The pQCD contribution with common lower cutoff in all Q_i is reproduced in the limit $\Lambda \to \infty$.

The simplest and most instructive matching to the massless pQCD quark loop proceeds at the level of the $(g-2)_\mu$ integral. The asymptotic pQCD region where all Q_i are large can be captured by imposing the condition that all Q_i be larger than $Q_{\min}$. To be able to add the mixed regions, where one virtuality is smaller than $Q_{\min}$, in the quark-loop integration, one needs to dampen the contribution in the additional integration region, since it is already partly covered by the ground-state pseudoscalar poles. To this end, we introduce the suppression factor $Q^2/(Q^2+\Lambda^2)$ for the virtuality $Q < Q_{\min}$, while retaining the cut that at least two $Q_i \geq Q_{\min}$. In this way, the limit $\Lambda \to \infty$ reproduces a common lower cutoff on all Q_i. The results are shown in figure 5.15 for the total ($\bar{\Pi}_{1\text{–}12}$) as well as for longitudinal ($\bar{\Pi}_{1\text{–}2}$) and transversal ($\bar{\Pi}_{3\text{–}12}$) contributions separately.

The Regge models in the preceding section predict a ratio $\Delta a_\mu^{\eta,\eta'}/\Delta a_\mu^{\pi^0}$ near the expectation $(C_0^2 + C_8^2)/C_3^2 = 3$. Similarly, we obtain $\Delta a_\mu^{\eta'}/\Delta a_\mu^{\eta}$ close to 2, as suggested by the scaling with $C_{\eta'}^2/C_\eta^2$ (5.112). To first approximation, the implementation of the various asymptotic constraints on the HLbL tensor thus reproduces the simple scaling that originates from the weight factors (5.39) appearing in the VVA triangle. For the mixed regions this behavior is exact due to (5.86) and (5.109), as long as the low-energy properties of the HLbL tensor are not disturbed, while for the asymptotic region it is a consequence of the flavor decomposition chosen in (5.88) and (5.110). The fact that the results from the summation of excited pseudoscalars confirm these expectations indicates that the pQCD quark loop dictates, if not the overall size of the effect, at least its decomposition in the various isospin channels. This is an encouraging sign that the model dependence which is intrinsic in the approach we are following here is mitigated by the QCD constraints. To understand even better the extent to which this mitigation occurs we analyze here in detail the matching between the Regge models and the quark loop integral, after introducing appropriate cutoffs.

For $\Delta a_\mu^{\text{PS-poles}} \sim 13\times10^{-11}$ figure 5.15 suggests scales Λ and Q_{min} around 1.4 GeV. In addition, the pQCD quark loop would predict an additional increase from the transversal amplitudes around 4×10^{-11}, but for these scales the interplay with axial-vector resonance contributions needs to be studied in more detail. In the following, we will instead focus on the comparison of our Regge model and the pQCD quark loop in the longitudinal amplitudes.

5.2.5.2 Matching of short-distance contributions

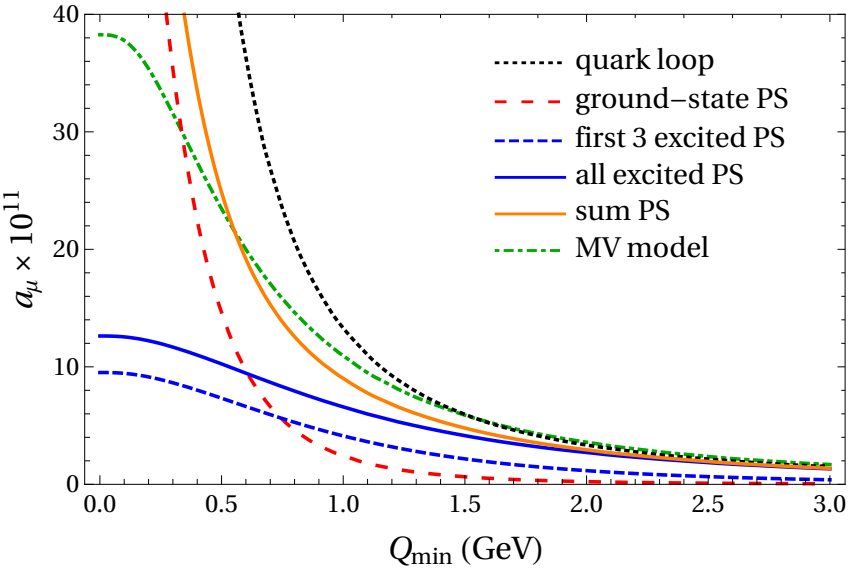

Figure 5.16: Contribution to a_μ for $Q_i \geq Q_{\text{min}}$: the longitudinal part of the massless pQCD quark loop (dotted black), the ground-state pseudoscalars (long-dashed red), their excitations from the large-N_c Regge model (blue), the sum of both (orange), and the short-distance implementation from the MV model (dot-dashed green). The blue dot-dashed curve refers the sum of the first three excited pseudoscalars in each trajectory.

Beyond the matching at the level of $(g-2)_\mu$, it could be instructive to also compare the specific contributions to the BTT functions in the various kinematic domains. However, once

the respective scaling with the virtualities is factored out, we find that the coefficient converges relatively slowly to its asymptotic value. We conclude that it is rather the convolution with the kernel functions T_i that becomes important to assess the relevant scales of the SDCs for the HLbL contribution.

This is illustrated in figure 5.16, which shows various contributions to a_μ as a function of a lower cutoff on all three virtualities Q_i, as well as in figure 5.17, which shows the opposite case of an upper cutoff on all three virtualities Q_i. The ground-state pseudoscalars are saturated by 90% for $Q_{\text{max}} = 1.5\,\text{GeV}$, while for the excited pseudoscalars only about 25% of the total contribution comes from this energy region. By construction, their contribution asymptotically matches onto the one from the pQCD quark loop, and figure 5.16 shows how fast that asymptotic limit is reached after convolution with the $(g-2)_\mu$ integral kernels: at 1.5 GeV it is saturated by 70%, or about 80% if the tail of the ground-state pseudoscalars is included.

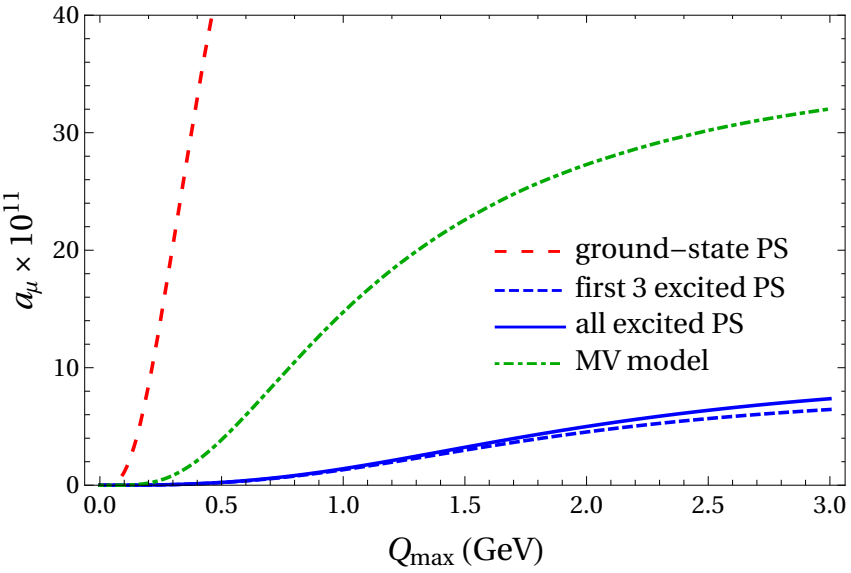

Figure 5.17: Same as figure 5.16, but for $Q_i \leq Q_{\text{max}}$.

The mixed region is more difficult to illustrate, especially for the corresponding OPE constraint, because in addition to the hierarchy $Q_3^2 \ll Q_1^2 \sim Q_2^2$ the small virtuality still needs to be large compared to Λ_{QCD}, otherwise chiral corrections will become important. For that reason, the low-energy part of the integration region was suppressed by the second cutoff Λ in figure 5.15. To obtain some measure of the size of the mixed-region contribution, figure 5.18 shows the remainder if for a given cutoff Q_{cut} both the regions where all $Q_i \leq Q_{\text{cut}}$ and all $Q_i \geq Q_{\text{cut}}$ are subtracted. For the ground-state pseudoscalars at $Q_{\text{cut}} = 1.5\,\text{GeV}$, this produces the remaining 10% beyond the low-energy region, while the asymptotic region $Q_i \geq Q_{\text{cut}}$ is already largely negligible. For the sum of excited pseudoscalars, it is instructive to further scrutinize the decomposition at this scale into low-energy (25%), mixed (40%), and asymptotic (35%) regions. As concerns the contribution from the lowest excitations, in Model 1, the low-energy region is entirely saturated by the sum of the first three excitations, the mixed region by 80%, but for the asymptotic part of the integral the higher excitations make up about 50%. This pattern suggests the interpretation that indeed the lowest excitations are most important for the low-energy and mixed regions, while the infinite tower of resonances restores the correct asymptotic behavior.

In fact, we find that the numerical impact of the integration regions where the OPE constraint strictly applies, i.e., where both $Q_3 \ll Q_{1,2}$ and $Q_i \gg \Lambda_{\text{QCD}}$, is already very small, so that in practice its main effect lies in constraining the TFF Regge models.

Altogether, this discussion indicates that at some point around 1.5 GeV the description of the HLbL tensor in terms of hadronic intermediate states should be matched onto the one from pQCD. In particular, the implementation of the SDCs in terms of excited pseudoscalars gives an indication how big an impact the intermediate regime may have (in the longitudinal amplitudes): while from pQCD alone one may have guessed a contribution around 5×10^{-11} from the asymptotic region, for a value of Q_{min} chosen at 1.5 GeV, the excited pseudoscalars with masses in the same region will add a contribution of similar size, covering also the mixed regions of the $(g-2)_\mu$ integral.

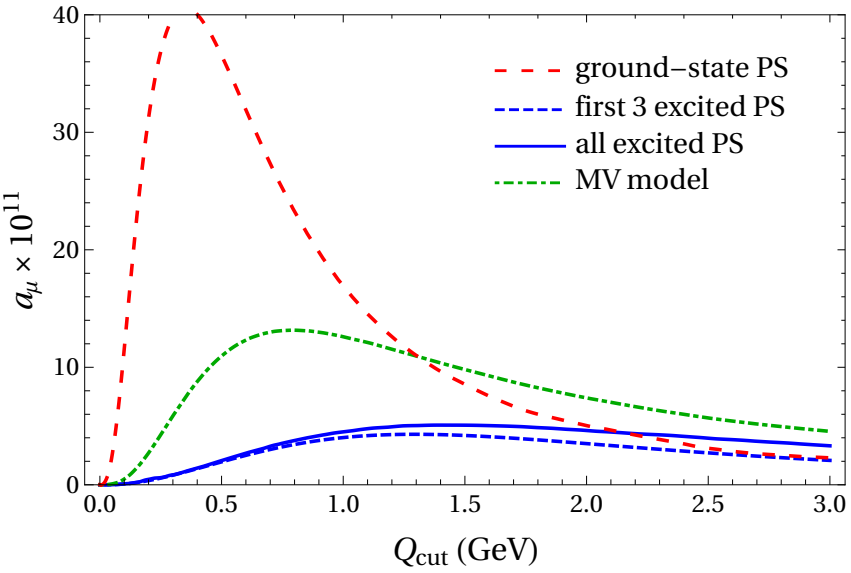

Figure 5.18: Mixed-region contribution to a_μ, defined as the full integral minus the contributions from the low-energy (all $Q_i \leq Q_{\text{cut}}$) and high-energy (all $Q_i \geq Q_{\text{cut}}$) regions.

To quantify the matching between the quark loop and the description in terms of hadronic states, one would need to define a concrete criterion for the matching scale. One way to define an optimal scale could be to consider the difference between Regge model and quark loop as a function of Q_{min} in combination with the uncertainties of each description for a particular cutoff. For the Regge model, we can estimate this uncertainty as before, but for the quark loop one would need to know the α_s corrections and/or higher orders in the OPE, which when compared to the leading-order quark loop would already entail information about the scale where pQCD becomes an efficient description of the HLbL tensor. Absent such calculations, we may obtain a first estimate by comparison to similar pQCD uncertainties in inclusive τ decays [215–220], given that we expect a matching scale not too far off the τ mass, which would suggest an uncertainty around 20%. Based on the combined uncertainties of the Regge model and the pQCD quark loop, we then find a preference for a matching scale around $Q_{\text{match}} = 1.7\,\text{GeV}$, leading to the

decomposition

$$\begin{aligned} \Delta a_\mu^{\text{PS-poles}} - a_\mu^{\text{PS-poles}}\big|_{Q_{\min}=Q_{\text{match}}} &= 8.7(3.6)\times 10^{-11}, \\ a_\mu^{q\text{-loop}}\big|_{Q_{\min}=Q_{\text{match}}} &= 4.6(9)\times 10^{-11}, \end{aligned} \tag{5.140}$$

Note that, in the first line, we also subtracted the very small contribution from the ground-state pseudoscalars from the integration region $Q_i \geq Q_{\text{match}}$ to avoid any double counting. As expected, the comparison to (5.139) confirms that for the asymptotic part of the integral it does not matter whether a description based on hadronic intermediate states or pQCD is employed: this means that about one third (i.e., the second line) of (5.140) is a model-independent part of the effect we have calculated. But how model dependent is the rest and can we adequately cover this model dependence with our uncertainty estimate? There are different uncertainties which need to be considered and we summarize all of them here:

- 3.6 units coming from the uncertainties in the parameters of Model 1, as given in (5.140), obtained by stretching the uncertainties in the Regge slopes by a factor three;[11]
- 1.7 units are obtained by varying the matching point by 0.5 GeV (the main effect comes from the lowest Q_{match}, which we vary to as low as 1.2 GeV);
- 3.8 estimated from the difference between Model 1 and 2, cf. (5.139).

All these uncertainties concern essentially the contribution below the matching point of $Q_{\text{match}} = 1.7\,\text{GeV}$, as estimated in the previous section. The outcome of our analysis for this part therefore reads:

$$\begin{aligned} \Delta a_\mu^{\text{PS-poles}} - a_\mu^{\text{PS-poles}}\big|_{Q_{\min}=Q_{\text{match}}} &= 8.7(3.6)_{\text{excited PS}}\,{}^{+1.7}_{-0.4}\big|_{Q_{\text{match}}}(3.8)_{\text{syst}}\times 10^{-11} \\ &= 8.7(5.5)\times 10^{-11}, \end{aligned} \tag{5.141}$$

with a 65% uncertainty, which we consider as sufficiently conservative and, in addition, covers the systematic effects related to the asymptotic behavior of the excited-state TFFs as discussed in appendix 5.2.E. Another observation corroborating this conclusion is that the contribution to the central value due to the first three pseudoscalar excitations (whose masses and, in part, two-photon couplings are constrained by phenomenology) amounts to 7.8 units out of 8.7. On the basis of these considerations we give as our final estimate

$$\Delta a_\mu^{\text{LSDC}} = [8.7(5.5)_{\text{PS-poles}} + 4.6(9)_{q\text{-loop}}]\times 10^{-11} = 13(6)\times 10^{-11}, \tag{5.142}$$

and stress that the contribution of the higher excitations ($n > 3$), which has been calculated with our Regge model and is the most uncertain and model-dependent part of our calculation, amounts to only less than 10% of the total. We conclude that our final result (5.142) has a generously estimated uncertainty that we expect to cover the remaining model dependence.

[11] We thereby aim to cover scenarios in which other hadronic states could be used to implement the SDCs, in which case the Regge slopes would differ; e.g., according to ref. [193], the Regge slopes of the axial-vector a_1 and f_1 trajectories are $\sigma_{a_1}^2 = 1.36(49)\,\text{GeV}^2$ and $\sigma_{f_1}^2 = 1.27(64)\,\text{GeV}^2$.

5.2.5.3 Chiral limit and role of axial-vector mesons

One may ask whether the implementation of the longitudinal SDCs adopted here would work in the chiral limit: in this limit, excited pseudoscalars have a vanishing coupling to the axial current and therefore would not be able to contribute to the fulfillment of the OPE constraint.[12] However, there are known cases in which the chiral and the large-N_c limits do not commute, most notably in the context of baryon chiral perturbation theory. For instance, if one first takes $N_c \to \infty$ and then $m_q \to 0$, the entire tower of excited baryons contributes to the first non-analytic term in the quark-mass expansion of the nucleon mass, while in the opposite order only nucleon intermediate states appear [263, 264], and similar subtleties arise elsewhere due to mass splittings of order $1/N_c$ [265]. Further subtleties in the order of the chiral limit have been pointed out before even for the VVA anomaly itself: the discontinuity of the fermion triangle loop function in the axial-vector virtuality vanishes with the fermion mass, but in a dispersion relation the mass dependence is canceled and produces the anomaly that survives in the chiral limit [266, 267]. While these examples show that care is required when exchanging the limits, at least the implementation of the large-N_c Regge models described here does not allow any such subtleties to occur and is meant to be used only away from the chiral limit.

If the excited pseudoscalar poles were to decouple in the chiral limit, an alternative solution could be provided by axial-vector intermediate states, which do contribute in the chiral and large-N_c limits. For these mesons, however, only model-dependent calculations are available in the literature so far,[13] whereas a calculation based on a dispersive framework is still lacking. Such a framework would allow one to express the contribution to HLbL scattering in the most general way in terms of all TFFs of the axial vectors (which admit three), as is the case for the pseudoscalars (which admit only one). Another significant difference is that while for pseudoscalars the sum rules that guarantee the absence of ambiguities in the evaluation of the HLbL contribution [27] are automatically satisfied, this is not the case for axial-vector mesons. We believe that at present it is fair to say that even the ground-state contributions of the latter are poorly understood.

Besides these theoretical reasons, there are also phenomenological ones that favor a discussion in terms of pseudoscalars: while for the most relevant excited pseudoscalar resonances, those in the energy range between 1–2 GeV, there is at least some information on the phenomenology relevant for HLbL, the situation is even worse for the known axial-vector resonances in the same mass range. This is related to the fact that for axial vectors a decay into two real photons is forbidden by the Landau–Yang theorem [268, 269]: hadronic channels such as three pions are dominant with respect to suppressed decays to virtual photons, which have been observed only for two ground-state axial-vector resonances [211, 270].

If a viable implementation of the longitudinal SDCs in terms of axial-vector resonances were possible, it would have to look quite different from ours in terms of pseudoscalars excitations. Besides the fact that different TFFs contribute, we observe that the axial-vector contribution to $\hat{\Pi}_{1\text{–}3}$ does not resemble the pseudoscalar-pole contribution (5.35), in fact, both in a Lagrangian-

[12] We thank Arkady Vainshtein for calling our attention to this point.

[13] They are either based on the relation to transversal SDCs [2,33] or proceed in terms of Lagrangian models [31, 36].

based approach and in dispersion theory the pole in $q_3^2 - m_A^2$ cancels in the longitudinal BTT amplitudes. Based on what is known about the axial-vector TFFs, we cannot preclude the possibility that a finite number of axial vectors could be used to construct such a solution. If that were possible while being consistent with phenomenology and the SDCs on the axial-vector TFFs, this would be an appealing solution, but the necessary theoretical framework for carrying out such an analysis is not yet available. For the moment we took the pragmatic point of view that we implement the longitudinal SDCs in terms of the hadronic intermediate states that we can control best, both theoretically as well as phenomenologically. Having adopted this strategy, we need to address the question of whether our estimate of the systematic uncertainty is large enough to cover the possibility of implementing the SDCs in terms of other hadronic intermediate states.

We believe that we can answer positively this question under the reasonable assumption that even in an alternative scenario the matching to pQCD will occur in the range we have considered. In this case the contribution from the quark loop will remain unchanged and all we need to discuss is the excited-pseudoscalar-pole contribution estimated as $8.7(5.5) \times 10^{-11}$. About one unit out of nine comes from excited states with $n > 3$: if these were not needed to satisfy the SDCs, this contribution would have to be dropped, a possibility amply covered by our uncertainties. The bulk of the contribution comes from excited states with $n \leq 3$, and as we have discussed in section 5.2.4.3 and in appendix 5.2.D, the estimate of their two-photon couplings we have obtained by requiring that the longitudinal SDCs be satisfied is compatible with what is know from phenomenology. Our uncertainty estimate covers the present phenomenological uncertainties on these couplings and could be reduced if the phenomenological information on them were improved. In the end, even if the SDCs were to be implemented using axial-vector states, the first few pseudoscalar excitations would need to be included regardless, it is just that the pseudoscalar TFFs would not be constrained by the HLbL SDCs.

In conclusion, we believe that the uncertainty related to the nature of the hadronic states used in the implementation of the SDCs should be covered by the error assigned in (5.141), an expectation that has been supported more recently by models in holographic QCD [41, 42], in which the SDCs are implemented by summation of an infinite tower of axial-vector resonances instead. Beyond the model context, assessing the role of axial-vector resonances in fulfilling the SDCs, especially the transversal ones, will first of all require an improved understanding of their ground-state contributions.

5.2.6 Comparison to the Melnikov–Vainshtein model

In this section, we compare our implementation of the longitudinal SDCs to the one from ref. [2], which is based on the observation that the modification

$$\hat{\Pi}_1^{P\text{-pole}} = \frac{F_{P\gamma^*\gamma^*}(q_1^2, q_2^2) F_{P\gamma\gamma^*}(q_3^2)}{q_3^2 - M_P^2} \to \hat{\Pi}_1\big|_{\text{MV}} = \frac{F_{P\gamma^*\gamma^*}(q_1^2, q_2^2) F_{P\gamma\gamma}}{q_3^2 - M_P^2} \tag{5.143}$$

of (5.35) ensures that both the normalization and the mixed-region OPE constraint (5.79) are fulfilled.[14] Since the form (5.35) of the pseudoscalar poles is a direct consequence of the dispersion relation for the HLbL tensor, which we suggested in refs. [27, 77, 165–167] for the case of

[14] A reply to the preprint [83], which appeared in response to our paper, is provided in appendix 5.2.H.

general four-point kinematics, this modification is not compatible with the description of other intermediate states in the same framework. However, the replacement (5.143) could be justified by a dispersion relation for the HLbL amplitudes directly in the kinematic limit relevant for $(g-2)_\mu$, i.e., for $q_4 = 0$. In this limit it is not possible to work with a dispersion relation in the Mandelstam variables s, t, and u at fixed q_i^2, because they cease to be independent: $s = q_3^2$, $t = q_2^2$, and $u = q_1^2$. This means that when writing dispersion relations in the q_i^2 for $g-2$ kinematics, there is no clear separation between the singularities of the HLbL amplitude and those generated by hadronic intermediate states directly coupling to individual electromagnetic currents, e.g., two-pion states as in figure 5.19: in this framework the pseudoscalar TFFs can no longer be treated as external input quantities. The same holds for higher intermediate states, so that in general the factorization of form factors and scattering amplitudes of the intermediate state in question would cease to apply.

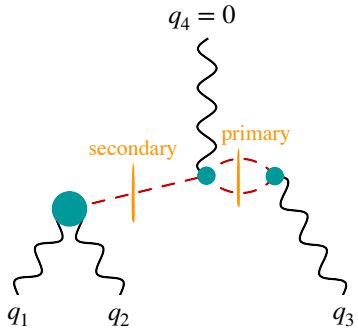

Figure 5.19: Dispersion relation for the HLbL tensor in the $(g-2)_\mu$ kinematic limit with singularities from primary and secondary channels (2π state and pseudoscalar pole).

Nevertheless, we observe that, in principle, both forms of dispersion relations are perfectly legitimate—the transition from the dispersion relation for the four-point function [27,77,165–167] to a dispersion relation in the photon virtualities in the $(g-2)_\mu$ kinematic limit amounts to a relabeling of contributions from different principal cuts. This is illustrated by writing the pseudoscalar pole (5.35) in our framework as

$$\hat{\Pi}_1^{P\text{-pole}} = \frac{F_{P\gamma^*\gamma^*}(q_1^2, q_2^2) F_{P\gamma\gamma^*}(M_P^2)}{q_3^2 - M_P^2} + \frac{F_{P\gamma^*\gamma^*}(q_1^2, q_2^2)\big(F_{P\gamma\gamma^*}(q_3^2) - F_{P\gamma\gamma^*}(M_P^2)\big)}{q_3^2 - M_P^2}, \tag{5.144}$$

where the first term reproduces the pole in the alternative dispersive framework for $(g-2)_\mu$ kinematics, while the second term does not contain a pole at $q_3^2 = M_P^2$. More precisely, the second term is the contribution due to intermediate states X in a cut through the TFF, with the discontinuity determined by the sub-processes $\gamma^*(q_3) \to X$ and a pseudoscalar-pole contribution to $\gamma^*(q_1)\gamma^*(q_2) \to \gamma X$, as illustrated in figure 5.19. This piece is present even in the alternative dispersive framework, which demonstrates that changing the dispersive framework simply amounts to a reshuffling of contributions between different principal cuts. Due to the mixed-region SDC, for large $q_1^2 \sim q_2^2$ the second piece in (5.144) has to cancel against the contribution from the infinite tower of higher intermediate states up to chiral corrections. Since this is a key point in ref. [2], and the basis for the construction of the MV model, it is worthwhile discussing in detail how this cancellation has to work. For simplicity we concentrate on the pion contribution only (isospin-triplet component) and include all other contributions other than the

pion pole to $\hat{\Pi}_1^3$ into a single function G:

$$\hat{\Pi}_1^3 = \hat{\Pi}_1^{\pi\text{-pole}}(q_1^2, q_2^2, q_3^2) + G(q_1^2, q_2^2, q_3^2). \tag{5.145}$$

From the requirement that (5.78) provide the leading term for asymptotic $q_1^2 \sim q_2^2$, but that it be exact (in the chiral limit) as far as the q_3^2 dependence is concerned, it follows that the function G must have the following asymptotic behavior:

$$\lim_{\hat{q}^2\to\infty} \hat{q}^2 G(\hat{q}^2, \hat{q}^2, q_3^2)\Big|_{m_q=0} = \frac{2F_\pi}{3}\frac{F_{\pi\gamma\gamma^*}(q_3^2) - F_{\pi\gamma\gamma}}{q_3^2}\Big|_{m_q=0}. \tag{5.146}$$

We stress that (5.146) is exact in the chiral limit, a property inherited from (5.78), which is a remarkable and interesting result. The MV model (5.143) consists of taking the pion pole as the only contribution to $\hat{\Pi}_1^3$. This effectively amounts to promoting (5.146) to an equation valid for any value of q_1^2 and q_2^2:

$$G(q_1^2, q_2^2, q_3^2)\Big|_{m_q=0} = -F_{\pi\gamma^*\gamma^*}(q_1^2, q_2^2)\frac{F_{\pi\gamma\gamma^*}(q_3^2) - F_{\pi\gamma\gamma}}{q_3^2}\Big|_{m_q=0}. \tag{5.147}$$

While this provides a simple way to exactly satisfy (5.146), there is no physical justification in support of such a very strong assumption. It is therefore not surprising that this leads to uncontrolled numerical effects, which we have been able to quantify here. In addition, we note that away from the chiral limit the residue in (5.144) contains $F_{P\gamma\gamma^*}(M_P^2)$ instead of $F_{P\gamma\gamma}$, which at least for $\eta^{(\prime)}$ entails significant chiral corrections.

Numerically, ref. [2] concluded an increase of 13.5×10^{-11} for the pion and 5×10^{-11} each for $\eta^{(\prime)}$, based on the modification in (5.143) and the TFFs from ref. [109] (LMD+V for the pion and VMD for $\eta^{(\prime)}$):

$$\Delta a_\mu^{\text{PS-poles}}\big|_{\text{MV}} = 23.5 \times 10^{-11}. \tag{5.148}$$

However, we note that with modern input for the TFFs this number would increase substantially: for the pion, our Model 1 implies an increase of 16.2×10^{-11}, which would increase to 17.3×10^{-11} if one used the dispersive TFF instead. Here, the change to the original MV number mainly reflects the differences between the LMD+V model from ref. [109] and the dispersive result for the π^0 TFF [28,172]. For $\eta^{(\prime)}$, the differences are more severe because the incorrect asymptotic behavior of the VMD form factors in the pQCD limit suppresses the impact of taking the singly-virtual form factor to a constant. We find 10.0×10^{-11} and 12.1×10^{-11} for η and η', respectively, which in total produces an increase of 38×10^{-11} beyond the pseudoscalar ground-state contributions, nearly three times the result given in (5.139).

Apart from the overall size, another key difference in our implementation concerns the hierarchy $\Delta a_\mu^{\pi\text{-poles}} < \Delta a_\mu^{\eta\text{-poles}} < \Delta a_\mu^{\eta'\text{-poles}}$ found with the excited pseudoscalars, see (5.137), while in ref. [2] the largest effect was found for the pion. The fact that $\Delta a_\mu^{\eta\text{-poles}}$ comes out much smaller than $\Delta a_\mu^{\eta'\text{-poles}}$ can be partly explained by the two-photon couplings, $F_{\eta(n)\gamma\gamma} < F_{\eta'(n)\gamma\gamma}$, and also through the scaling of the excited state TFFs in the BL limit, see figure 5.21.

This observation also has consequences for the matching to the quark loop. While in our case the scaling of the flavor components follows essentially the expectation from the weights C_a^2, this is not the case for the MV model, and therefore it is less clear how the matching to

pQCD should proceed. In fact, as shown in figure 5.16, despite not being implemented explicitly, the MV model also comes close to the pQCD asymptotics: the main difference to our Regge model occurs in the low-energy region below 1 GeV. This matching onto pQCD asymptotics is coincidental, however: by construction, the model saturates the MV constraint also in the limit in which all virtualities are large and therefore exceeds the proper pQCD limit by a factor of 3/2. Since the asymptotic value is approached rather slowly, the resulting curve happens to be close to the pQCD quark loop for the range of Q_{min} displayed in figure 5.16.

Figures 5.16–5.18 also illustrate the origin of the difference between our implementations. For the reference scale of 1.5 GeV, the low-, mixed-, and high-energy regions contribute 75%, 20%, and 5%, respectively, which demonstrates that indeed the approximations of the MV model manifest themselves primarily in the low-energy region, where the dispersive framework provides the best constraints and the contribution of higher states only leads to a moderate uncertainty.

5.2.7 Summary and outlook

In this work, we studied short-distance constraints (SDCs) for the hadronic light-by-light (HLbL) contribution to $(g-2)_\mu$. We concentrated on the longitudinal constraints that are intimately related to pseudoscalar-pole contributions. Since the HLbL tensor can only be constrained from data in the low-energy region, but not in the mixed- and high-energy regions, SDCs are important for a model-independent approach towards HLbL scattering. In sections 5.2.2 and 5.2.3, the Lorentz decomposition of the HLbL tensor from refs. [27, 77] was used to formulate the known expressions for the perturbative QCD (pQCD) quark loop and the operator-product-expansion (OPE) constraints on the HLbL tensor, respectively. The OPE constraint in the symmetric region with $Q_1^2 = Q_2^2 = Q_3^2 \equiv Q^2$ is given in (5.50), the Melnikov–Vainshtein constraint [2] for the mixed region with $Q_3^2 \ll Q_1^2 \sim Q_2^2$ in (5.74). Both are implemented including the singlet component, for which in addition to chiral corrections also perturbative corrections arise.

Subsequently, we focused on the longitudinal SDCs, related to the pseudoscalar-pole diagrams (5.35) by means of (5.79). While a finite number of poles cannot saturate the SDCs, an infinite tower of them can [2]. To that end, we have constructed two models for the transition form factors (TFFs) of ground-state and radially-excited pseudoscalar mesons: our large-N_c Regge model for pion, η, and η' is described in sections 5.2.4.1 and 5.2.4.2, and an alternative model using the Regge resummation from ref. [188] is introduced in appendix 5.2.B to estimate the systematic uncertainty (see also appendix 5.2.E). While applicable only in the space-like region as relevant for $(g-2)_\mu$, both models satisfy all relevant low- and high-energy constraints for the TFFs—the chiral anomaly (normalization), the Brodsky–Lepage limit, and the symmetric pQCD limit, see (5.92)–(5.94) and (5.106)–(5.108)—give a good description of the experimental data, and reproduce the established results for the ground-state contributions to $(g-2)_\mu$. In addition, with an infinite tower of excited pseudoscalars, they restore the correct asymptotic Q^2-behavior of the HLbL tensor in the mixed- and high-energy regions, see (5.86) and (5.88), as well as (5.109) and (5.110).

Thus, it has been shown that the SDCs on the HLbL tensor, and in particular the MV constraint, can indeed be satisfied with an infinite sum over excited pseudoscalar-pole diagrams,

while maintaining the correct low-energy behavior. Our result (5.139)

$$\Delta a_\mu^{\text{PS-poles}} = \Delta a_\mu^{\pi\text{-poles}} + \Delta a_\mu^{\eta\text{-poles}} + \Delta a_\mu^{\eta'\text{-poles}} = 12.6(4.1) \times 10^{-11}, \tag{5.149}$$

derived from the large-N_c Regge models alone, is significantly smaller than the original estimate $\Delta a_\mu|_{\text{MV}} = 23.5 \times 10^{-11}$ from ref. [2], which was obtained by removing the momentum dependence of the TFF at the external photon vertex. In fact, with modern input for the pseudoscalar TFFs this effect would increase further to $\Delta a_\mu|_{\text{MV}} \sim 38 \times 10^{-11}$, demonstrating the dangers of ad-hoc modifications of the low-energy properties of the HLbL tensor. Indeed, we observe that by far the main part of the difference to our implementation originates from the low-energy part of the $g-2$ integral.

Furthermore, in contrast to ref. [2], we find $\Delta a_\mu^{\pi\text{-poles}} < \Delta a_\mu^{\eta\text{-poles}} < \Delta a_\mu^{\eta'\text{-poles}}$. Accordingly, the flavor decomposition into excited π^0, η, η' states follows roughly the expectation from the coefficients determining the SDCs, motivating a matching of our hadronic implementation onto a description in terms of the pQCD quark loop. This matching, illustrated in figures 5.15–5.18, shows that, as expected, the ground-state pseudoscalars are relevant only at low energies, but about half the excited-state contribution comes from the integration region of $Q_i \geq 1\,\text{GeV}$, while the other half could be interpreted as an estimate of the mixed regions. Since, by construction, the excited-state contribution asymptotically matches onto the one from pQCD, we then replaced the hadronic formulation in favor of the quark loop in the asymptotic part of the integral, at a matching scale of $Q_{\text{match}} = 1.7\,\text{GeV}$ obtained from our best estimates of the uncertainties in the Regge models and pQCD corrections. Due to the assumed pQCD uncertainties and variation of the matching scale, as well as the inflated errors for the Regge slopes in Model 1, see discussion between (5.140) and (5.141), the uncertainty of our final result (5.142)

$$\Delta a_\mu^{\text{LSDC}} = [8.7(5.5)_{\text{PS-poles}} + 4.6(9)_{q\text{-loop}}] \times 10^{-11} = 13(6) \times 10^{-11}, \tag{5.150}$$

slightly increases with respect to (5.149), the advantage being that the asymptotic part of the result is manifestly independent of the nature of the hadronic states in terms of which the correct asymptotic behavior was restored. In this way, our final result mainly relies on the Regge models for an estimate of potential contributions for which the asymptotic constraints do not yet apply, and, while data is scarce, this is the energy region where at least some phenomenological guidance for the excited pseudoscalar states is available. In particular, this strategy ensures that since the excited pseudoscalars decouple in the chiral limit, see section 5.2.5.3, our implementation of the asymptotic part of the integral remains valid for vanishing quark masses, while for the low-energy phenomenology chiral corrections are essential.

In the future, the matching to pQCD could be improved if explicit calculations of pQCD corrections became available, a first step in this direction was already taken in ref. [1]. Moreover, the phenomenological analysis would profit from further experimental information on the two-photon physics of hadronic resonances in the 1–2 GeV region, which holds true not only for the longitudinal amplitudes but in general. In fact, to address the transversal amplitudes, the effects of axial-vector resonances need to be understood in the context of dispersion relations, especially given that their masses are much closer to the typical matching scale found for the longitudinal SDCs in this paper. Work along these lines is in progress.

Acknowledgements: We thank P. Bickert, J. Bijnens, S. Eidelman, S. Holz, B. Kubis, S. Leupold, J. Lüdtke, A. Manohar, M. Procura, E. Ruiz Arriola, P. Sanchez-Puertas, and

A. Vainshtein for useful discussions; A. Gérardin, C. Hanhart, S. Holz, P. Sanchez-Puertas, and E. Weil for providing us with their results; R. Arnaldi, A. Uras, G. Usai, and V. Metag for helping us with the experimental data sets. Financial support by the DOE (Grant Nos. DE-FG02-00ER41132 and DE-SC0009919) and the Swiss National Science Foundation is gratefully acknowledged. M.H. is supported by an SNSF Eccellenza Professorial Fellowship (Project No. PCEFP2_181117).

5.2.A Anomalous Pseudoscalar–Vector–Vector Coupling

For the pion TFF, we only considered the coupling of the pion to a $\rho\omega$ pair, see figure 5.6, and neglected the contribution given by a $\rho\phi$ pair. In the following, we motivate why the $\rho\phi$ pair can be neglected for the pion, and derive the relative strength of 2ρ, 2ω, 2ϕ, and $\phi\omega$ contributions to the TFFs of the η and η', see figure 5.10.

In ref. [200], we find the Lagrangians for the anomalous pseudoscalar–vector–vector coupling,

$$\mathcal{L}_{\mathrm{VV}\Phi} = -g_{\mathrm{VV}\Phi}\,\epsilon^{\mu\nu\alpha\beta}\,\mathrm{Tr}\left(\partial_\mu V_\nu \partial_\alpha V_\beta \Phi\right), \tag{5.151}$$

with $g_{\mathrm{VV}\Phi} = 3g^2/32\pi^2 F_\pi^2$, and the electromagnetic photon–vector interaction,

$$\mathcal{L}_{\mathrm{em}} = \frac{\sqrt{2}\,e}{g} A^\mu \left(m_\rho^2 \rho_\mu + \frac{1}{3} m_\omega^2 \omega_\mu - \frac{\sqrt{2}}{3} m_\phi^2 \phi_\mu \right) = A^\mu (g_{\rho\gamma}\,\rho_\mu + g_{\omega\gamma}\,\omega_\mu + g_{\phi\gamma}\,\phi_\mu), \tag{5.152}$$

with $g_{V\gamma}$ the individual coupling strengths. Φ stands for the neutral ground-state pseudoscalar mesons, denoted by π^0, $\eta^{(8)}$ and $\eta^{(0)}$:

$$\Phi = \frac{1}{\sqrt{2}} \begin{pmatrix} \pi^0 + \frac{1}{\sqrt{3}}\,\eta^{(8)} + \sqrt{\frac{2}{3}}\,\eta^{(0)} & 0 & 0 \\ 0 & -\pi^0 + \frac{1}{\sqrt{3}}\,\eta^{(8)} + \sqrt{\frac{2}{3}}\,\eta^{(0)} & 0 \\ 0 & 0 & -\frac{2}{\sqrt{3}}\,\eta^{(8)} + \sqrt{\frac{2}{3}}\,\eta^{(0)} \end{pmatrix}, \tag{5.153}$$

and V_μ stands for the neutral ground-state vector mesons, denoted by ρ_μ, $\phi_\mu^{(8)}$, and $\phi_\mu^{(0)}$:

$$V_\mu = \frac{1}{\sqrt{2}} \begin{pmatrix} \rho_\mu + \frac{1}{\sqrt{3}}\,\phi_\mu^{(8)} + \sqrt{\frac{2}{3}}\,\phi_\mu^{(0)} & 0 & 0 \\ 0 & -\rho_\mu + \frac{1}{\sqrt{3}}\,\phi_\mu^{(8)} + \sqrt{\frac{2}{3}}\,\phi_\mu^{(0)} & 0 \\ 0 & 0 & -\frac{2}{\sqrt{3}}\,\phi_\mu^{(8)} + \sqrt{\frac{2}{3}}\,\phi_\mu^{(0)} \end{pmatrix}. \tag{5.154}$$

Note that the latter Lagrangian (5.152) for the neutral vector mesons is given in the ideal mixing situation: $\rho \sim 1/\sqrt{2}\left(u\bar{u} - d\bar{d}\right)$, $\omega \sim 1/\sqrt{2}\left(u\bar{u} + d\bar{d}\right)$ and $\phi \sim -s\bar{s}$. In general, we use a ϕ–ω mixing:

$$\begin{pmatrix} \phi_8 \\ \phi_0 \end{pmatrix} = \begin{pmatrix} \cos\theta_V & \sin\theta_V \\ -\sin\theta_V & \cos\theta_V \end{pmatrix} \begin{pmatrix} \phi \\ \omega \end{pmatrix}, \tag{5.155}$$

with $\theta_V = 36.4°$ [100] which, however, almost corresponds to the ideal case ($\theta_V^{\mathrm{ideal}} = \arctan 1/\sqrt{2} \sim 35.3°$). For the η–η' mixing, we use the short-hand notation:

$$\begin{pmatrix} \eta_8 \\ \eta_1 \end{pmatrix} = T \begin{pmatrix} \eta \\ \eta' \end{pmatrix} = \begin{pmatrix} T_{11} & T_{12} \\ T_{21} & T_{22} \end{pmatrix} \begin{pmatrix} \eta \\ \eta' \end{pmatrix}, \tag{5.156}$$

where the mixing matrix in the standard two-angle mixing scheme is given by:

$$T \coloneqq F_\pi \begin{pmatrix} F^8 \cos\theta_8 & -F^0 \sin\theta_0 \\ F^8 \sin\theta_8 & F^0 \cos\theta_0 \end{pmatrix}^{-1}, \tag{5.157}$$

with the mixing parameters introduced in (5.41).

The coupling strengths of the pseudoscalar meson to two-photon interactions in the VMD picture, see figures 5.6 and 5.10, can be reconstructed from the above Lagrangians, taking into account the ϕ–ω and η–η' mixings:

$$\begin{aligned}
\Gamma_{\Phi\gamma\gamma} \propto \frac{3\alpha}{4\pi F_\pi^2}\,\epsilon^{\mu\nu\alpha\beta} \Bigg\{ & \frac{\sqrt{2}}{3\sqrt{3}}\,\pi^0 \Big[\partial_\mu\rho_\nu\,\partial_\alpha\omega_\beta \left(\sqrt{2}\cos\theta_V + \sin\theta_V\right) \\
& - \sqrt{2}\partial_\mu\rho_\nu\,\partial_\alpha\phi_\beta \left(\cos\theta_V - \sqrt{2}\sin\theta_V\right) \Big] \\
& + \frac{1}{2\sqrt{6}}\,\eta \Big[2\,\partial_\mu\rho_\nu\,\partial_\alpha\rho_\beta \left(T_{11} + \sqrt{2}\,T_{21}\right) \\
& + \frac{1}{9}\left(2\sqrt{2}\,T_{21} - T_{11}\right)\left(\partial_\mu\omega_\nu\,\partial_\alpha\omega_\beta + 2\partial_\mu\phi_\nu\,\partial_\alpha\phi_\beta\right) \\
& + \frac{1}{9}\,T_{11}\left(\cos 2\theta_V + 2\sqrt{2}\sin 2\theta_V\right)\left(\partial_\mu\omega_\nu\,\partial_\alpha\omega_\beta - 2\partial_\mu\phi_\nu\,\partial_\alpha\phi_\beta\right) \\
& - \frac{2\sqrt{2}}{9}\,T_{11}\left(2\sqrt{2}\cos 2\theta_V - \sin 2\theta_V\right)\partial_\mu\omega_\nu\,\partial_\alpha\phi_\beta \Big] \\
& + \frac{1}{2\sqrt{6}}\,\eta' \Big[2\,\partial_\mu\rho_\nu\,\partial_\alpha\rho_\beta \left(T_{12} + \sqrt{2}\,T_{22}\right) \\
& + \frac{1}{9}\left(2\sqrt{2}\,T_{22} - T_{12}\right)\left(\partial_\mu\omega_\nu\,\partial_\alpha\omega_\beta + 2\partial_\mu\phi_\nu\,\partial_\alpha\phi_\beta\right) \\
& + \frac{1}{9}\,T_{12}\left(\cos 2\theta_V + 2\sqrt{2}\sin 2\theta_V\right)\left(\partial_\mu\omega_\nu\,\partial_\alpha\omega_\beta - 2\partial_\mu\phi_\nu\,\partial_\alpha\phi_\beta\right) \\
& - \frac{2\sqrt{2}}{9}\,T_{12}\left(2\sqrt{2}\cos 2\theta_V - \sin 2\theta_V\right)\partial_\mu\omega_\nu\,\partial_\alpha\phi_\beta \Big] \Bigg\}.
\end{aligned} \tag{5.158}$$

A similar approach is chosen in ref. [199], where the contributions to the singly-virtual TFFs are analyzed through the combination of pseudoscalar–photon–vector and photon–vector interactions. The dependence of the electromagnetic photon–vector interactions (5.152) on the vector-meson masses are canceled out by the vector-meson propagators. Our final couplings read, for $P = \eta, \eta'$:

$$\begin{aligned}
C^P_{\rho\rho} &= T_{1I_P} + \sqrt{2}T_{2I_P}, \\
C^P_{\omega\omega} &= \frac{1}{18}\left[(\cos 2\theta_V + 2\sqrt{2}\sin 2\theta_V - 1)T_{1I_P} + 2\sqrt{2}T_{2I_P}\right], \\
C^P_{\phi\phi} &= -\frac{1}{9}\left[(\cos 2\theta_V + 2\sqrt{2}\sin 2\theta_V + 1)T_{1I_P} - 2\sqrt{2}T_{2I_P}\right], \\
C^P_{\omega\phi} &= \frac{\sqrt{2}}{9}(\sin 2\theta_V - 2\sqrt{2}\cos 2\theta_V)T_{1I_P},
\end{aligned} \tag{5.159}$$

with $I_\eta = 1$, $I_{\eta'} = 2$, and T_{IJ} given in (5.157). Similarly, we define for the pion:

$$\begin{aligned}
C^\pi_{\rho\omega} &= \frac{2}{3}\left(\sqrt{2}\cos\theta_V + \sin\theta_V\right), \\
C^\pi_{\rho\phi} &= -\frac{2\sqrt{2}}{3}\left(\cos\theta_V - \sqrt{2}\sin\theta_V\right).
\end{aligned} \tag{5.160}$$

	π	η	η'
M_{V_1} [MeV]	779	774	859
M_{V_2} [MeV]	585	404	452
$\sigma^2_{V_1}$ [GeV^2]	1.252	1.593	1.577
$\sigma^2_{V_2}$ [GeV^2]	0.076	0.034	0.060
Λ [GeV]	1.318	1.318	1.318

Table 5.5: Parameters of the alternative model for pion, η, and η' TFFs.

Note that in (5.159) and (5.160) we divided all couplings by a common factor: $\sqrt{3}\alpha/(4\sqrt{2}\pi F_\pi^2)$. This is allowed because the relative strength of the different couplings does not change. The large-N_c Regge model for the $\eta^{(\prime)}$ TFFs is then constructed such that each vector-meson pair contributes exactly $C^P_{V_1V_2}/\mathcal{N}$ to $F_{\eta^{(\prime)}\gamma\gamma}$, where $\mathcal{N}$ is the normalization (5.120).

Numerical values for $C^P_{V_1V_2}$ can be found in table 5.2. One can clearly see that $C^\pi_{\rho\omega} \gg C^\pi_{\rho\phi}$, which is why we neglected the $\rho\phi$ contribution to the pion TFF. Furthermore, one can see that the ground-state $\eta^{(\prime)}$ TFFs are dominated by the 2ρ, while the contribution from ϕ–ω mixing is small. This is also illustrated in figures 5.32 and 5.35, where we show the 2ρ, 2ω, 2ϕ, and $\phi\omega$ contributions to the singly-virtual and doubly-virtual $\eta^{(\prime)}$ TFFs.

5.2.B Alternative model for pion, η, and η' transition form factors

In this appendix, we present an alternative model for the pseudoscalar TFFs, which will help us to study the systematic uncertainty of our $g-2$ result. This alternative model uses the Regge resummation from ref. [188] to satisfy the pQCD limit of the TFF, cf. (5.44). It reads:

$$F_{P(n)\gamma^*\gamma^*}(-Q_1^2,-Q_2^2) = \sum_{i=0}^{\infty}\int_0^1 dx\,\left\{\frac{c_1\, e^{-(Q_1^2+Q_2^2)/\Lambda^2}}{\left[M^2_{V_1(n+i)} + Q_1^2\,x + Q_2^2\,(1-x)\right]^2}\right.$$
$$\left. + \frac{c_2\left[1-e^{-(Q_1^2+Q_2^2)/\Lambda^2}\right]x(1-x)}{\left[M^2_{V_2(n+i)} + Q_1^2\,x + Q_2^2\,(1-x)\right]^2}\right\}, \tag{5.161}$$

where $P=\pi,\eta,\eta'$ and the introduced mass spectra again follow a radial Regge ansatz:

$$M^2_{V_1(i)} = M^2_{V_1} + i\,\sigma^2_{V_1},$$
$$M^2_{V_2(i)} = M^2_{V_2} + i\,\sigma^2_{V_2}. \tag{5.162}$$

The first term in (5.161), proportional to c_1, corresponds to a variant of a large-N_c Regge TFF model with equal mass spectra for all vector mesons. The second term in (5.161), proportional to c_2, has an additional factor of $x(1-x)$ in the numerator, originating from the asymptotic wave function, cf. (5.43). This term is crucial for the model to satisfy the BL limit (5.44):

$$\lim_{Q^2\to\infty} Q^2 F_{P\gamma\gamma^*}(-Q^2) = \frac{c_2}{2\sigma^2_{V_2}}, \tag{5.163}$$

with

$$c_2 = \begin{cases} 4F_\pi\,\sigma_{V_2}^2 & \text{for } \pi, \\ 24\,C_8 F_\eta\,\sigma_{V_2}^2 & \text{for } \eta, \\ 24\,C_0 F_{\eta'}\,\sigma_{V_2}^2 & \text{for } \eta', \end{cases} \tag{5.164}$$

and the fit F_η, $F_{\eta'}$ from (5.127). The exponential functions in the numerator, $e^{-(Q_1^2+Q_2^2)/\Lambda^2}$, shall support the VMD in the region of small momentum transfers, and suppress the $x(1-x)$ correction which is only needed in the asymptotic region. Therefore, the real-photon limit (5.36) is proportional to c_1:

$$F_{P\gamma\gamma} = \frac{c_1}{\sigma_{V_1}^4}\,\psi^{(1)}\left(\frac{M_{V_1}^2}{\sigma_{V_1}^2}\right), \tag{5.165}$$

with $\psi^{(1)}$ the trigamma function and

$$c_1 = \begin{cases} \sigma_{V_1}^4 F_{\pi\gamma\gamma}\left[\psi^{(1)}\left(\frac{M_{V_1}^2}{\sigma_{V_1}^2}\right)\right]^{-1} & \text{for } \pi, \\ \sigma_{V_1}^4 F_{\eta\gamma\gamma}\left[\psi^{(1)}\left(\frac{M_{V_1}^2}{\sigma_{V_1}^2}\right)\right]^{-1} & \text{for } \eta, \\ \sigma_{V_1}^4 F_{\eta'\gamma\gamma}\left[\psi^{(1)}\left(\frac{M_{V_1}^2}{\sigma_{V_1}^2}\right)\right]^{-1} & \text{for } \eta', \end{cases} \tag{5.166}$$

whereas the symmetric pQCD limit (5.44), to leading order in Q^2, is proportional to c_2:

$$\lim_{Q^2\to\infty} Q^2 F_{P\gamma^*\gamma^*}(-Q^2,-Q^2) = \frac{c_2}{6\sigma_{V_2}^2}. \tag{5.167}$$

In this way, c_1 and c_2 are fixed and the TFF model reproduces the chiral anomaly, the BL limit, and the symmetric pQCD limit exactly.

Evaluating the SDCs of the HLbL tensor, cf. (5.50) and (5.78), we obtain for the mixed region:

$$\begin{aligned} &-\lim_{Q_3^2\to\infty}\lim_{Q^2\to\infty}\sum_{n=0}^{\infty}\frac{F_{P(n)\gamma^*\gamma^*}(-Q^2,-Q^2)F_{P(n)\gamma\gamma^*}(-Q_3^2)}{Q_3^2+M_{P(n)}^2} \\ &= \frac{1}{Q^2Q_3^2}\frac{c_2^2}{24\sigma_P^6\sigma_{V_2}^4}\Big\{2\sigma_P^2\left(2\sigma_{V_2}^2-\sigma_P^2\right)L_{PV_2} - \sigma_P^2\left(4\sigma_{V_2}^2-3\sigma_P^2\right) \\ &- 4\sigma_{V_2}^2\Delta_{PV_2}\left[\frac{\pi^2}{6}-\mathrm{Li}_2\left(1-\frac{\sigma_P^2}{\sigma_{V_2}^2}\right)\right]\Big\}, \end{aligned} \tag{5.168}$$

with Li_2 the dilogarithm, and for the asymptotic region:

$$\begin{aligned} &-\lim_{Q^2\to\infty}\sum_{n=0}^{\infty}\frac{F_{P(n)\gamma^*\gamma^*}(-Q^2,-Q^2)F_{P(n)\gamma\gamma^*}(-Q^2)}{Q^2+M_{P(n)}^2} \\ &= \frac{1}{Q^4}\frac{c_2^2}{12\sigma_P^4\sigma_{V_2}^4\Delta_{PV_2}}\Big\{\sigma_P^2\left(2\sigma_{V_2}^2-\sigma_P^2\right)L_{PV_2} + 2\sigma_P^2\Delta_{PV_2} \\ &- 2\sigma_{V_2}^2\Delta_{PV_2}\left[\frac{\pi^2}{6}-\mathrm{Li}_2\left(1-\frac{\sigma_P^2}{\sigma_{V_2}^2}\right)\right]\Big\}. \end{aligned} \tag{5.169}$$

Thus, both the mixed region and the asymptotic region acquire the correct Q^2 behavior, as is discussed in detail in appendix 5.2.C.

The model parameters M_{V_i}, σ_{V_i}, and Λ are determined as follows, see table 5.5:

- For the pion TFF we use $M_{V_1} = \frac{1}{2}\left[M_{\rho(770)} + M_{\omega(782)}\right] = 0.779$ GeV; for the η and η' TFFs we use for M_{V_1} the pole-mass parameters of a VMD ansatz fit to the CLEO data [205].

- For reasons of comparison, σ_{V_1} is chosen to reproduce the values of the two-photon couplings to the first excited pseudoscalars obtain with our large-N_c Regge model:

$$F_{\pi(1)\gamma\gamma} \sim 0.0500\,\text{GeV}^{-1}, \quad F_{\eta(1)\gamma\gamma} \sim 0.0354\,\text{GeV}^{-1}, \quad F_{\eta'(1)\gamma\gamma} \sim 0.0594\,\text{GeV}^{-1}.$$

  Alternatively, one could use the phenomenological constraints on the two-photon couplings listed in table 5.4;

- σ_{V_2} is chosen to satisfy the MV SDC;

- For the pion TFF Λ and M_{V_2} are adjusted to bring the model in line with the dispersive description of the π^0 TFF [28, 171, 172];[15] for the η and η' TFFs the same Λ as in the pion case is used, while M_{V_2} is fit to the available experimental data.

With the parameters in table 5.5, the MV SDC is satisfied to about $\sim 2 \times 10^{-3}$ relative accuracy or better, and the two-photon couplings of our large-N_c Regge model are reproduced to about $\sim 3 \times 10^{-4}$ relative accuracy or better. The SDC for the asymptotic region, cf. (5.88) and (5.110), is not implemented in our alternative TFF model, however, even without further adjustments it is reproduced to 117 % for the pion, 124 % for the η, and 120 % for the η'. Of course, one could also choose the model parameters differently and implement the SDC for the asymptotic region precisely and the MV limit approximately. Note that the parameters M_{V_1} and σ_{V_1} are close to the physical values for the masses of the lightest vector mesons and the slopes of their radial Regge trajectories, cf. figure 5.7. These physical values assure that the first term in (5.161) indeed resembles a large-N_c Regge model.

In figure 5.20, the TFF presented in this appendix (Model 2) is compared to the large-N_c Regge model (Model 1) from section 5.2.4 for the lowest radial excitations of pion, η, and η'. A comparison to experimental data for the ground-state pseudoscalars is postponed to appendices 5.2.F.2, 5.2.G.2, and 5.2.G.3. The two-photon couplings $F_{P(n)\gamma\gamma}$ of the excited states come out in close agreement between both models, see also figure 5.21. For Model 2, we observe an enhancement of the excited-state TFFs in the low-Q region, especially for the doubly-virtual kinematics. This enhancement becomes weaker with increasing Λ, since it is an artefact of the interplay between the two terms in (5.161). Fitting both M_{V_2} and Λ to data for the ground-state η and η' TFFs would lead to $\Lambda < 1$ GeV, and thus, exacerbate the enhancement of the excited-state TFFs at low Q. Therefore, we decided to use $\Lambda = 1.318\,\text{GeV}$, as obtained for the pion, also for η and η'.

Note that for Model 1 the derivatives of the TFFs in the limit of zero momentum transfer are not unique but depend on the direction, a consequence of the construction in terms of Q_-^2/Q_+^2 in (5.90) as a minimal way to implement the different asymptotic limits. This can be seen when comparing the slopes of the singly-virtual and symmetric doubly-virtual TFFs in the left and right panels of figure 5.20. The modifications of Model 1 described in (5.216) and (5.217) reduce the direction-dependence of the derivative at the origin. However, the derivative of the TFFs is

[15] We find $\Lambda = 1.318$ GeV and $M_{V_2} = 585$ MeV with estimated variance $\chi^2 \sim 0.33$ for a fit of $\mathcal{O}(2{\times}10^4)$ selected points in the region of $Q_1 \leq Q_2$ and $Q_2^2 \in [0, 40]\,\text{GeV}^2$.

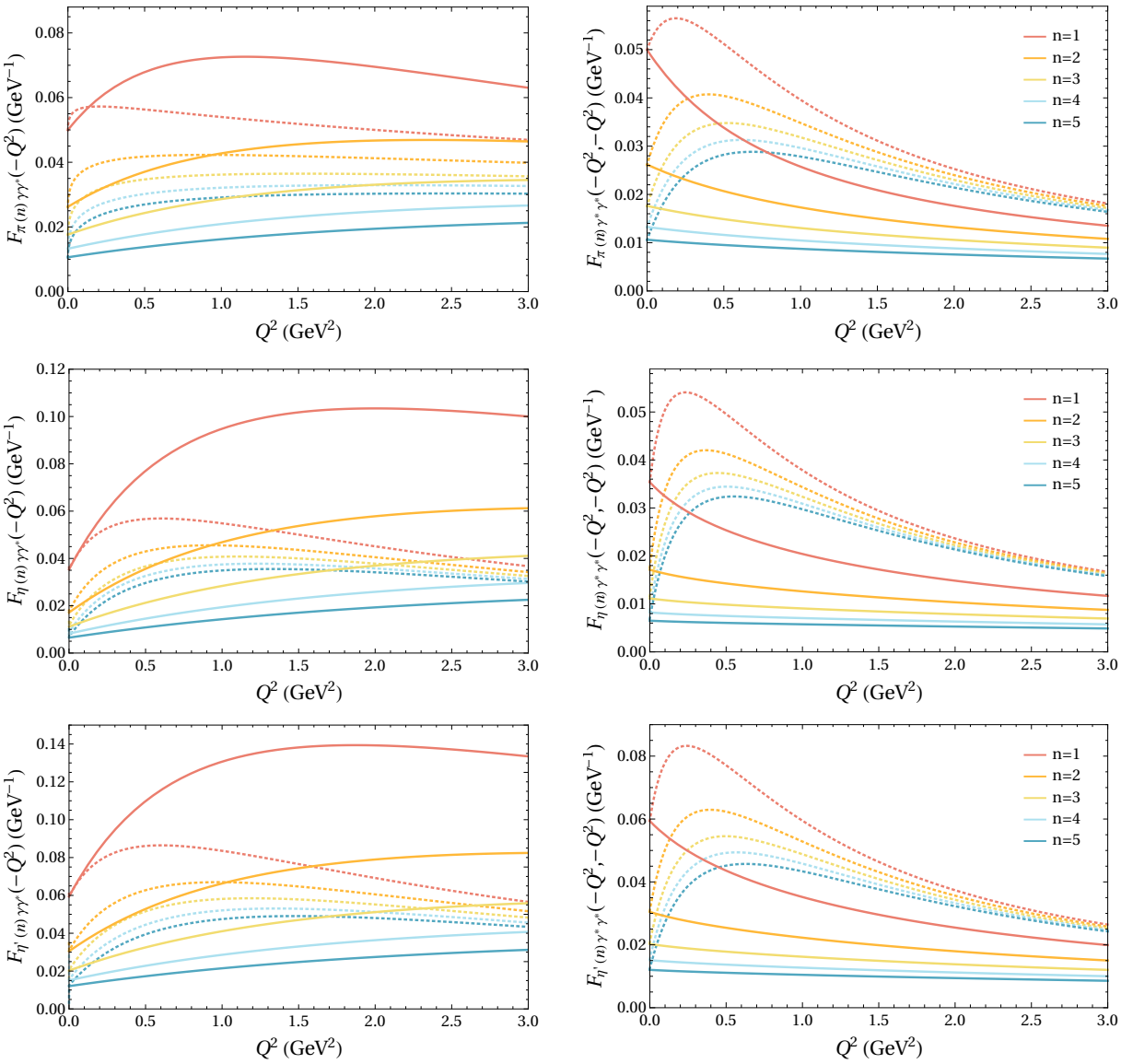

Figure 5.20: TFFs of the first $n = 1, \ldots 5$ radially excited pion, η, and η' states. Comparison of the large-N_c Regge models from section 5.2.4, indicated by the solid curves, and our alternative TFF model (5.161), indicated by the dotted curves. The left panel shows the TFFs in the singly-virtual limit, the right panel shows the doubly-virtual region with $Q_1^2 = Q_2^2 = Q^2$.

not needed for the evaluation of $(g-2)_\mu$ and the alternative implementation in Model 2 does not exhibit this issue: in figure 5.20, the slopes for Model 2 are always positive, but for Model 1 they change sign between the left and right panels. Accordingly, this will be another systematic effect estimated by the comparison of the two models. We stress again that neither model has the required good analytic properties to remain valid outside the space-like region relevant for $(g-2)_\mu$, of which the zero-momentum-transfer limit of the derivatives in Model 1 is one particular manifestation.

In the right panel of figure 5.21, the BL limits of the excited-state TFFs are shown. For Model 1 this limit increases with the excitation number n until it reaches an asymptotic value, but for Model 2 it remains constant. Since the true asymptotic behavior for radially-excited pseudoscalar TFFs in the BL limit is unknown, the two models with different asymptotics will allow us to

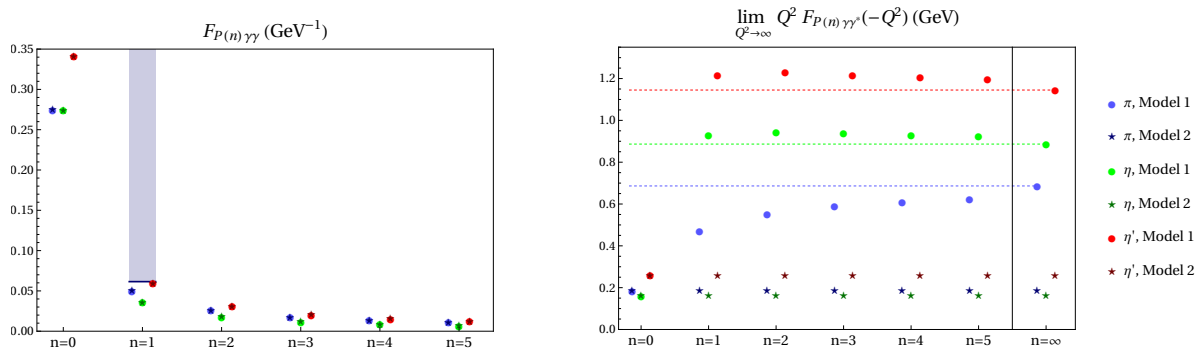

Figure 5.21: Two-photon couplings and BL limits of the excited-state pion, η, and η' TFFs. The blue, green, and red points (stars) are from the large-N_c Regge model (alternative model) for pion, η, and η', respectively. The blue bar indicates values excluded for $F_{\pi(1)\gamma\gamma}$ by the empirical estimate (5.200).

understand the systematic uncertainty of our prediction for the excited-state contributions to $(g-2)_\mu$. The symmetric pQCD limit of the TFFs, on the other hand, is independent of the excitation number n for both models. The two-photon couplings, which enter dominantly into the $(g-2)_\mu$ integral, agree by default for $n=0$ and $n=1$, and also match perfectly for $n>2$.

5.2.C Verifying short-distance constraints for the HLbL tensor

In this appendix, the mathematical formalism used to derive the behavior of the HLbL tensor in the mixed-energy region, cf. (5.95), (5.123), and (5.168), and the high-energy region, cf. (5.97), (5.124), and (5.169), is presented.

5.2.C.1 Polygamma functions and infinite sums over rational functions

The gamma function is defined on $\mathbb{R}_+^*$ as [271]:

$$\Gamma(z) = \int_0^\infty dt\, t^{z-1} e^{-t}. \tag{5.170}$$

It can be analytically continued to a meromorphic function in the complex plane, with poles at non-positive integers. In order to deal with the infinite sums over pseudoscalar and vector-meson poles, we use the polygamma functions, which are defined on $\mathbb{C}$ as derivatives of the logarithm of the gamma function:

$$\psi^{(m)}(z) := \frac{d^{m+1}}{dz^{m+1}} \log\Gamma(z). \tag{5.171}$$

They are meromorphic in the complex plane and admit the following series representation [271]:

$$\psi^{(n)}(z) = \begin{cases} -\gamma + \sum_{k=0}^\infty \left(\frac{1}{k+1} - \frac{1}{k+z}\right) & n=0, \\ (-1)^{n+1}\, n! \sum_{k=0}^\infty \frac{1}{(z+k)^{n+1}} & n>0, \end{cases} \tag{5.172}$$

which is converging for any $z\in\mathbb{C}$ except negative integers. With this, we can express an infinite sum over rational functions. Let $\{f_n\}_{n\in\mathbb{N}}$ be a sequence of the form $f_n = \frac{p(n)}{q(n)}$ where $p(n)$ and

$q(n)$ are polynomials in n with $\deg(p(n)) < \deg(q(n))$. Let α_k be the roots of the denominator $q(n)$. If all the roots are simple, the fraction f_n can be written as (partial fraction decomposition):

$$f_n = \sum_{k=1}^{m} \frac{A_k}{n - \alpha_k}, \tag{5.173}$$

where $m = \deg(q(n))$. In general, if one or more roots α_k have multiplicity $m_k \geq 2$, the formula becomes:

$$f_n = \sum_{k=1}^{\tilde{m}} \sum_{r_k=1}^{m_k} \frac{A_{k,r_k}}{(n - \alpha_k)^{r_k}}, \tag{5.174}$$

where $\tilde{m} \leq \deg(q(n))$ is the number of distinct roots. It follows that:

$$\sum_{n=0}^{\infty} f_n = \sum_{n=0}^{\infty} \sum_{k=1}^{\tilde{m}} \sum_{r_k=1}^{m_k} \frac{A_{k,r_k}}{(n - \alpha_k)^{r_k}} = \sum_{k=1}^{\tilde{m}} \sum_{r_k=1}^{m_k} \frac{(-1)^{r_k}}{(r_k - 1)!} A_{k,r_k}\, \psi^{(r_k-1)}(-\alpha_k), \tag{5.175}$$

provided that the series based on the sequence $\{f_n\}_{n\in\mathbb{N}}$ is converging. This can be used to compute the infinite sum over pseudoscalar poles, $\sum_{n=0}^{\infty} \hat{\Pi}_1^{P(n)\text{-pole}}(-Q_1^2, -Q_2^2, -Q_3^2)$, within our large-$N_c$ Regge model for the TFFs.

5.2.C.2 Euler–Maclaurin summation formula

A key ingredient in the discussion of the SDCs for the HLbL tensor is the Euler–Maclaurin summation formula, which describes the difference between an integral and a related sum, see for instance ref. [272, chapter 8]. Notably, it can be used to derive asymptotic expansions.

Let $a < b$ and $m > 0$ be integers, and f be a function whose derivatives $f^{(2m)}(x)$ are absolutely integrable over the interval (a, b). Then the **Euler–Maclaurin formula** reads:

$$\sum_{k=a}^{b} f(k) = \int_a^b dx\, f(x) + \frac{1}{2}\left[f(a) + f(b)\right] + \sum_{s=1}^{m-1} \frac{B_{2s}}{(2s)!}\left[f^{(2s-1)}(b) - f^{(2s-1)}(a)\right] + R_m(b), \tag{5.176}$$

where the remainder is given by:

$$R_m(n) = \int_a^b dx\, \frac{B_{2m} - B_{2m}(x - \lfloor x \rfloor)}{(2m)!}\, f^{(2m)}(x), \tag{5.177}$$

where $\lfloor x \rfloor$ is the greatest integer smaller or equal to x, B_s are the Bernoulli numbers, and $B_s(x)$ are the Bernoulli polynomials.[16] Using (5.180), we can find a bound for the remainder:

$$|R_m(b)| \leq \left(2 - 2^{1-2m}\right) \frac{|B_{2m}|}{(2m)!} \int_a^b dx\, |f^{(2m)}(x)|. \tag{5.181}$$

[16] The Bernoulli numbers can be generated through:

$$B_s = \begin{cases} 1 & s = 0, \\ -\frac{1}{s+1} \sum_{j=0}^{s-1} \binom{s+1}{j} B_j & s \geq 1, \end{cases} \tag{5.178}$$

and the Bernoulli polynomials can be constructed according to:

$$B_s(x) = \sum_{j=0}^{\infty} \binom{s}{j} B_{s-j} x^j. \tag{5.179}$$

For $0 \leq x \leq 1$, they satisfy [272]:

$$|B_{2s}(x) - B_{2s}| \leq (2 - 2^{1-2s})|B_{2s}|. \tag{5.180}$$

In particular, if $f^{(2m)}(x)$ does not change sign in the considered interval, the remainder is bounded by $\left(2-2^{1-2m}\right)$ times the first neglected term in (5.176).

The Euler–Maclaurin formula can be used to derive the asymptotic expansion of the polygamma functions (5.171) at large $z \in \mathbb{R}$. To illustrate, consider the trigamma function $\psi^{(1)}(z) = \sum_{k=0}^{\infty} \frac{1}{(z+k)^2}$. Inserting $f(x) = \frac{1}{(z+x)^2}$, $a = 0$, $b = \infty$, and $m = 1$ into (5.176) leads to the asymptotic expansion:

$$\psi^{(1)}(z) = \int_0^\infty dx\, \frac{1}{(z+x)^2} + \frac{1}{2z^2} + R_1(\infty, z) = \frac{1}{z} + \frac{1}{2z^2} + R_1(\infty, z), \tag{5.182}$$

where the notation of the remainder has been slightly modified compared to (5.176) in order to highlight the additional z-dependence. The derivatives $f^{(2m)}(x) = \frac{(2m+1)!}{(x+z)^{2m+2}}$ do not change sign and the first neglected term in (5.182) is given by $\frac{B_2}{2!}(0 + \frac{2}{z^3}) = \frac{1}{6z^3}$. This implies that $|R_1(\infty, z)| \leq (2 - 2^{1-2})\frac{1}{6z^3} = \frac{1}{4z^3}$. In the next subsection, we will be interested in the remainder generated by truncating the asymptotic expansion in (5.182) after the first term:

$$\psi^{(1)}(z) =: \frac{1}{z} + R_0(\infty, z). \tag{5.183}$$

It follows from (5.182) that:

$$\begin{aligned} |R_0(\infty, z)| &= \left|\frac{1}{2z^2} + R_1(\infty, z)\right| \leq \left|\frac{1}{2z^2}\right| + |R_1(\infty, z)| \\ &\leq \frac{1}{2z^2} + \frac{1}{4z^3} \leq \frac{1}{2z^2} + \frac{1}{4z^2} = \frac{3}{4z^2}, \end{aligned} \tag{5.184}$$

where the last inequality holds when $z \geq 1$. For a general $n \in \mathbb{N}$, a similar procedure leads to [271]:

$$\psi^{(n)}(z) \sim \begin{cases} \log(z) - \frac{1}{2z} - \sum_{k=2}^{\infty} \frac{B_k}{k z^k} & n = 0, \\ (-1)^{n+1} \left(\frac{(n-1)!}{z^n} + \frac{n!}{2z^{n+1}} + \sum_{k=2}^{\infty} \frac{(k+n-1)!}{k!} \frac{B_k}{z^{k+n}} \right) & n > 0. \end{cases} \tag{5.185}$$

The asymptotic expansion (5.185) in combination with (5.172) is sufficient to derive (5.95), (5.97), (5.123), and (5.124), and thereby fix the parameters of the large-N_c Regge models to satisfy the required SDCs on the HLbL tensor.

5.2.C.3 Short-distance constraints for the alternative transition form factor model

For the alternative TFF model, introduced in appendix 5.2.B, the situation is more complicated, because the summation over the pseudoscalar-pole diagrams involves three infinite sums—one additional sum over vector-meson towers per TFF (5.161)—and only two of them can be performed analytically. Therefore, one needs to use the Euler–Maclaurin formula to extract the asymptotic behavior.

We first consider the mixed-energy region $Q_1^2 \approx Q_2^2 \gg Q_3^2$. The terms in our TFF model (5.161)

with exponential weights in the numerator are suppressed and do not contribute to the MV limit:

$$\begin{aligned}
&\sum_{n=0}^{\infty} \hat{\Pi}_1^{P(n)\text{-pole}}(-Q^2,-Q^2,-Q_3^2) \\
&\sim c_2^2 \sum_{n=0}^{\infty}\sum_{i=0}^{\infty}\sum_{j=0}^{\infty} \int_0^1 dy \int_0^1 dx \frac{y(1-y)\,x(1-x)}{\left[Q_3^2+M_{P(n)}^2\right]\left[M_{V_2(n+i)}^2+Q^2\right]^2\left[M_{V_2(n+j)}^2+Q_3^2\,y\right]^2} \\
&= \frac{c_2^2}{6}\int_0^1 dy \sum_{n=0}^{\infty}\sum_{i=0}^{\infty}\sum_{j=0}^{\infty} \underbrace{\frac{y(1-y)\,x(1-x)}{\left[Q_3^2+M_{P(n)}^2\right]\left[M_{V_2(n+i)}^2+Q^2\right]^2\left[M_{V_2(n+j)}^2+Q_3^2\,y\right]^2}}_{:=f_{nij}(y)}\,. \qquad (5.186)
\end{aligned}$$

The integration over the Feynman parameter x is trivial. Since the $f_{nij}(y)$ in (5.186) do not contain any singularities in the space-like region and the integration domains are bounded, the convergence is uniform and the commutation of integrations and summations is justified.[17] Using (5.172), we can express the sums over i and j in (5.186) with trigamma functions:

$$\begin{aligned}
&\sum_{n=0}^{\infty} \hat{\Pi}_1^{P(n)\text{-pole}}(-Q^2,-Q^2,-Q_3^2) \\
&\sim \frac{c_2^2}{6\sigma_{V_2}^8}\int_0^1 dy \sum_{n=0}^{\infty} \frac{y(1-y)}{Q_3^2+M_{P(n)}^2}\,\psi^{(1)}\left(\frac{M_{V_2(n)}^2+Q^2}{\sigma_{V_2}^2}\right)\psi^{(1)}\left(\frac{M_{V_2(n)}^2+Q_3^2\,y}{\sigma_{V_2}^2}\right), \qquad (5.187)
\end{aligned}$$

where we use the notations from (5.89), (5.118), (5.119), and (5.162), assuming for simplicity that $\hat{M}_P = M_P$. The remaining sum over n cannot be performed analytically. We can, however, rewrite the trigamma function as the first term in its asymptotic expansion and a remainder, see (5.183):

$$\begin{aligned}
&\sum_{n=0}^{\infty} \hat{\Pi}_1^{P(n)-\text{pole}}(-Q^2,-Q^2,-Q_3^2) \\
&= \frac{c_2^2}{6\sigma_{V_2}^8}\int_0^1 dy \sum_{n=0}^{\infty} \frac{y(1-y)}{Q_3^2+M_{P(n)}^2}\left\{\frac{\sigma_{V_2}^2}{M_{V_2(n)}^2+Q^2}+R_0\left(\infty,\frac{M_{V_2(n)}^2+Q^2}{\sigma_{V_2}^2}\right)\right\} \\
&\times\left\{\frac{\sigma_{V_2}^2}{M_{V_2(n)}^2+Q_3^2\,y}+R_0\left(\infty,\frac{M_{V_2(n)}^2+Q_3^2\,y}{\sigma_{V_2}^2}\right)\right\} \\
&=: H_{\text{MV}}^P(Q^2,Q_3^2)+\delta H_{\text{MV}}^P(Q^2,Q_3^2). \qquad (5.188)
\end{aligned}$$

Here, we defined:

$$H_{\text{MV}}^P(Q^2,Q_3^2) = \frac{c_2^2}{6\sigma_{V_2}^4}\int_0^1 dy \sum_{n=0}^{\infty} \frac{y(1-y)}{\left[M_{V_2(n)}^2+Q^2\right]\left[Q_3^2+M_{P(n)}^2\right]\left[M_{V_2(n)}^2+Q_3^2\,y\right]}, \qquad (5.189)$$

and included the remaining terms of (5.188) in δH_{MV}^P. The sum over n in (5.189) can now be expressed in terms of polygamma functions, but the integral over the Feynman parameter y is

[17] Formally, we use the **dominated convergence theorem** (in the setting of Riemann integrals) [272, p. 54]: Let $(a,b) \subset \mathbb{R}$ be an open, finite or infinite interval. Let $\{f_n\}_{n\in\mathbb{N}}$ be a sequence of real or complex functions which are continuous on (a,b) and satisfy:

1. The series $\sum_{n=1}^{\infty} f_n(x)$ converges uniformly in any compact interval in (a,b)
2. Either $\int_a^b dx \sum_{n=1}^{\infty} |f_n(x)| < \infty$ or $\sum_{n=1}^{\infty} \int_a^b dx\, |f_n(x)| < \infty$

Then $\int_a^b dx \sum_{n=1}^{\infty} f_n(x) = \sum_{n=1}^{\infty} \int_a^b dx\, f_n(x)$.

difficult to perform analytically. Therefore, we expand in Q^2 and Q_3^2 before integrating over y. The assumption that the two operations commute will be checked a posteriori. We find $(Q^2 \gg Q_3^2)$:

$$H^P_{\rm MV}(Q^2,Q_3^2) = \int_0^1 dy \left\{ \frac{f^P_{\rm MV}(y)}{Q^2Q_3^2} + \mathcal{O}\left(\frac{1}{Q^2Q_3^4}\right)\right\} = \frac{a^P_{\rm MV}}{Q^2Q_3^2} + \mathcal{O}\left(\frac{1}{Q^2Q_3^4}\right), \tag{5.190}$$

with

$$\begin{aligned} a^P_{\rm MV} = \frac{c_2^2}{24\sigma_P^6\sigma_{V_2}^4}\Bigg\{ & 2\sigma_P^2\left(2\sigma_{V_2}^2-\sigma_P^2\right)L_{PV_2} - \sigma_P^2\left(4\sigma_{V_2}^2-3\sigma_P^2\right) \\ & - 4\sigma_{V_2}^2\Delta_{PV_2}\left[\frac{\pi^2}{6} - {\rm Li}_2\left(1-\frac{\sigma_P^2}{\sigma_{V_2}^2}\right)\right]\Bigg\}. \end{aligned} \tag{5.191}$$

An appropriate choice of σ_{V_2} in $a^P_{\rm MV}$ therefore reproduces the MV limit.

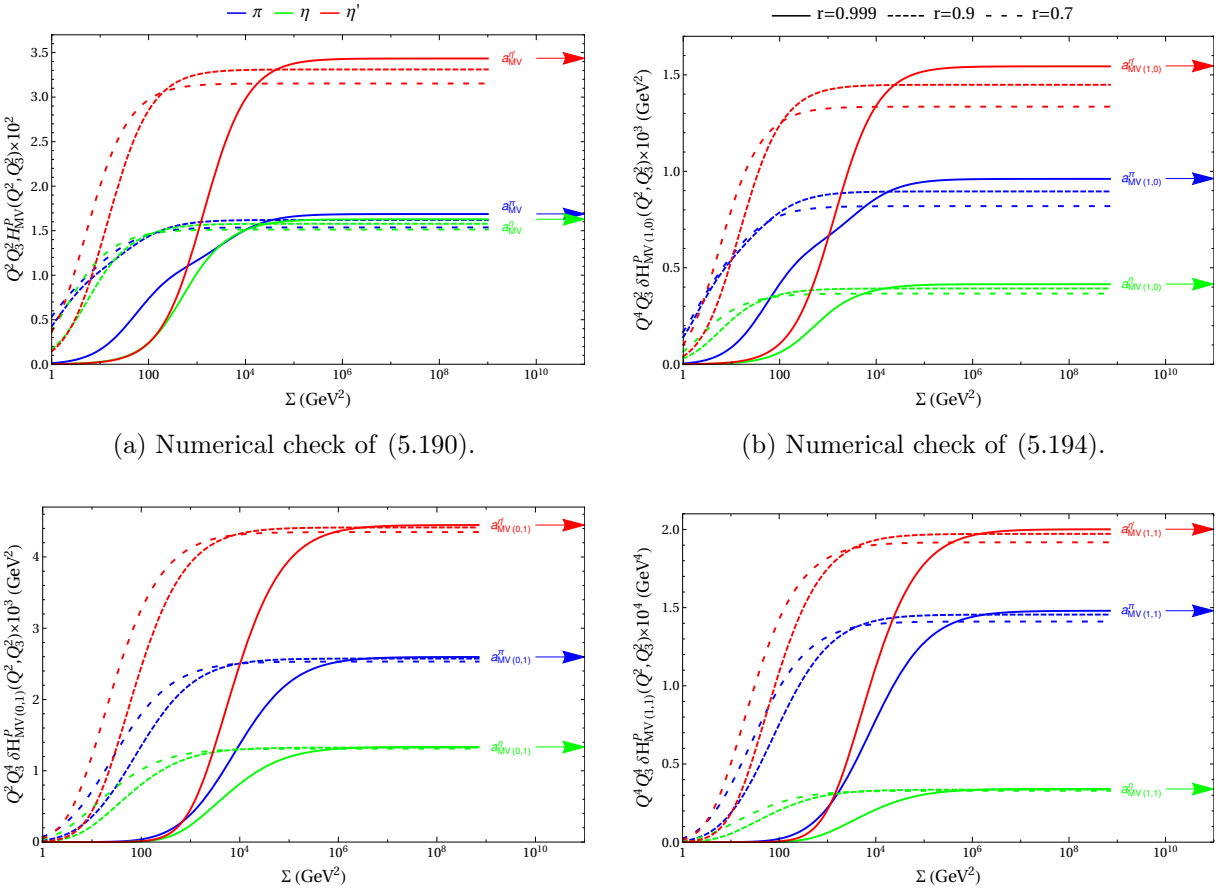

(a) Numerical check of (5.190).

(b) Numerical check of (5.194).

(c) Numerical check of (5.195).

(d) Numerical check of (5.196).

Figure 5.22: Numerical checks for the validity of commuting the expansion in Q^2 and Q_3^2, and the integration over y in (5.188). In all cases, we can see that when $r \to 1$ (MV kinematics), the curves tend to the coefficients obtained by expanding in the virtualities first and then integrating over the Feynman parameter y. Note that the scales on the y-axis vary between the plots.

Let us now verify that expanding before integrating in (5.190) was justified and that $\delta H^P_{\rm MV}(Q^2,Q_3^2)$ is subleading. The first issue can be addressed numerically. We use the coordinates defined

in (5.33). The kinematics corresponding to the MV limit can be expressed in those coordinates by setting $\phi = \pi$,

$$Q_1^2 = Q_2^2 = Q^2 = \frac{\Sigma}{3}\left(1 + \frac{r}{2}\right), \qquad Q_3^2 = \frac{\Sigma}{3}(1 - r), \tag{5.192}$$

then considering r close to 1, and finally taking the limit $\Sigma \to \infty$. In figure 5.22a, we study the function $Q^2 Q_3^2 H^P_{\mathrm{MV}}(Q^2, Q_3^2)$ in (5.189) for different values of r using a numerical integration over y. One can see that with r getting closer to 1 the curves tend to a^P_{MV} and this justifies the commutation of expansion and integration in this case.

We are left to study the error made by considering only H^P_{MV} and not the remainder δH^P_{MV}, which can be decomposed into three terms:

$$\delta H^P_{\mathrm{MV}}(Q^2, Q_3^2) = \delta H^P_{\mathrm{MV}(0,1)}(Q^2, Q_3^2) + \delta H^P_{\mathrm{MV}(1,0)}(Q^2, Q_3^2) + \delta H^P_{\mathrm{MV}(1,1)}(Q^2, Q_3^2). \tag{5.193}$$

The notation can be understood as follows. From (5.187) to (5.188), two trigamma functions, which stem from the doubly-virtual TFF $F_{P\gamma^*\gamma^*}(Q^2, Q^2)$ (first index) and the singly-virtual TFF $F_{P\gamma\gamma^*}(Q_3^2)$ (second index), were expanded in a leading piece (0) and a remainder (1). In other words, $\delta H^P_{\mathrm{MV}(1,0)}$ combines the remainder of the trigamma function in Q^2 with the leading term in the expansion of the trigamma function in Q_3^2:

$$\begin{aligned}
&\delta H^P_{\mathrm{MV}(1,0)}(Q^2, Q_3^2) \\
&= \frac{c_2^2}{6\sigma_{V_2}^6} \int_0^1 dy \sum_{n=0}^{\infty} R_0\left(\infty, \frac{M_{V_2(n)}^2 + Q^2}{\sigma_{V_2}^2}\right) \frac{y(1-y)}{\left[Q_3^2 + M_{P(n)}^2\right]\left[M_{V_2(n)}^2 + Q_3^2\, y\right]} \\
&\leq \frac{c_2^2}{8\sigma_{V_2}^6} \int_0^1 dy \sum_{n=0}^{\infty} \frac{\sigma_{V_2}^4}{\left[M_{V_2(n)}^2 + Q^2\right]^2} \frac{y(1-y)}{\left[Q_3^2 + M_{P(n)}^2\right]\left[M_{V_2(n)}^2 + Q_3^2\, y\right]} \\
&= \int_0^1 dy \left\{ \frac{f^P_{\mathrm{MV}(0,1)}(y)}{Q^4 Q_3^2} + \mathcal{O}\left(\frac{1}{Q^4 Q_3^4}\right)\right\} = \frac{a^P_{MV(0,1)}}{Q^4 Q_3^2} + \mathcal{O}\left(\frac{1}{Q^4 Q_3^4}\right).
\end{aligned} \tag{5.194}$$

Here, we used (5.181) to show that the term is bounded from above, as can be done for each term in (5.193). As before, it can be checked numerically that $H^P_{\mathrm{MV}(0,1)}$ indeed tends to the result obtained by expanding first and integrating second, see figure 5.22b. We proceed analogously for the two remaining terms:

$$\begin{aligned}
&\delta H^P_{\mathrm{MV}(0,1)}(Q^2, Q_3^2) \\
&= \frac{c_2^2}{6\sigma_{V_2}^6} \int_0^1 dy \sum_{n=0}^{\infty} \frac{y(1-y)}{\left[M_{V_2(n)}^2 + Q^2\right]\left[Q_3^2 + M_{P(n)}^2\right]} R_0\left(\infty, \frac{M_{V_2(n)}^2 + Q_3^2\, y}{\sigma_{V_2}^2}\right) \\
&\leq \frac{c_2^2}{8\sigma_{V_2}^6} \int_0^1 dy \sum_{n=0}^{\infty} \frac{y(1-y)}{\left[M_{V_2(n)}^2 + Q^2\right]\left[Q_3^2 + M_{P(n)}^2\right]} \frac{\sigma_{V_2}^4}{\left[M_{V_2(n)}^2 + Q_3^2\, y\right]^2} \\
&= \int_0^1 dy \left\{ \frac{f^P_{\mathrm{MV}(1,0)}(y)}{Q^2 Q_3^4} + \mathcal{O}\left(\frac{1}{Q^2 Q_3^6}\right)\right\} = \frac{a^P_{\mathrm{MV}(1,0)}}{Q^2 Q_3^4} + \mathcal{O}\left(\frac{1}{Q^2 Q_3^6}\right),
\end{aligned} \tag{5.195}$$

which is checked numerically in figure 5.22c and:

$$\begin{aligned}
&\delta H^P_{\mathrm{MV}(1,1)}(Q^2,Q_3^2)\\
&= \frac{c_2^2}{6\sigma_{V_2}^8}\int_0^1 dy \sum_{n=0}^{\infty} R_0\left(\infty, \frac{M_{V_2(n)}^2+Q^2}{\sigma_{V_2}^2}\right)\frac{y(1-y)}{Q_3^2+M_{P(n)}^2} R_0\left(\infty, \frac{M_{V_2(n)}^2+Q_3^2\,y}{\sigma_{V_2}^2}\right)\\
&\leq \frac{3c_2^2}{32\sigma_{V_2}^8}\int_0^1 dy \sum_{n=0}^{\infty} \frac{y(1-y)}{Q_3^2+M_{P(n)}^2}\frac{\sigma_{V_2}^8}{\left[M_{V_2(n)}^2+Q^2\right]^2\left[M_{V_2(n)}^2+Q_3^2\,y\right]^2}\\
&= \int_0^1 dy\left\{\frac{f^P_{\mathrm{MV}(1,1)}(y)}{Q^4Q_3^4}+\mathcal{O}\left(\frac{1}{Q^4Q_3^6}\right)\right\} = \frac{a^P_{\mathrm{MV}(1,1)}}{Q^4Q_3^4}+\mathcal{O}\left(\frac{1}{Q^4Q_3^6}\right),
\end{aligned} \tag{5.196}$$

see figure 5.22d. The above considerations add up to:

$$\delta H^P_{\mathrm{MV}}(Q^2,Q_3^2) = \mathcal{O}\left(\frac{1}{Q^2Q_3^4}\right), \tag{5.197}$$

i.e., the error we make by keeping only the leading term in the expansion of the $\psi^{(1)}$ in (5.188) is subdominant.

When considering the high-energy region $Q_1^2 \approx Q_2^2 \approx Q_3^2 = Q^2$, the same technique can be applied, but the situation simplifies slightly, since there is only one large scale. The pQCD constraint on the HLbL tensor reads:

$$\begin{aligned}
&\sum_{n=0}^{\infty}\hat{\Pi}_1^{P(n)\text{-pole}}(-Q^2,-Q^2,-Q^2)\\
&\sim \frac{c_2^2}{6\sigma_{V_2}^8}\int_0^1 dy\sum_{n=0}^{\infty}\frac{y(1-y)}{Q^2+M_{P(n)}^2}\,\psi^{(1)}\left(\frac{M_{V_2(n)}^2+Q^2}{\sigma_{V_2}^2}\right)\psi^{(1)}\left(\frac{M_{V_2(n)}^2+Q^2\,y}{\sigma_{V_2}^2}\right).
\end{aligned} \tag{5.198}$$

Similarly to the previous case, since the sum over n cannot be performed analytically, we rewrite the polygamma function as the first term in its asymptotic expansion and a remainder. This leads to:

$$\begin{aligned}
H^P_{\mathrm{pQCD}}(Q^2) &:= \frac{c_2^2}{6\sigma_{V_2}^4}\int_0^1 dy\sum_{n=0}^{\infty}\frac{y(1-y)}{\left[Q^2+M_{P(n)}^2\right]\left[M_{V_2(n)}^2+Q^2\right]\left[M_{V_2(n)}^2+Q^2\,y\right]},\\
\delta H^P_{\mathrm{pQCD}(1,0)}(Q^2) &:= \frac{c_2^2}{6\sigma_{V_2}^6}\int_0^1 dy\sum_{n=0}^{\infty} R_0\left(\infty,\frac{M_{V_2(n)}^2+Q^2}{\sigma_{V_2}^2}\right)\frac{y(1-y)}{\left[Q^2+M_{P(n)}^2\right]\left[M_{V_2(n)}^2+Q^2\,y\right]},\\
\delta H^P_{\mathrm{pQCD}(0,1)}(Q^2) &:= \frac{c_2^2}{6\sigma_{V_2}^6}\int_0^1 dy\sum_{n=0}^{\infty}\frac{y(1-y)}{\left[Q^2+M_{P(n)}^2\right]\left[M_{V_2(n)}^2+Q^2\right]} R_0\left(\infty,\frac{M_{V_2(n)}^2+Q^2\,y}{\sigma_{V_2}^2}\right),\\
\delta H^P_{\mathrm{pQCD}(1,1)}(Q^2) &:= \frac{c_2^2}{6\sigma_{V_2}^8}\int_0^1 dy\sum_{n=0}^{\infty}\frac{y(1-y)}{Q^2+M_{P(n)}^2} R_0\left(\infty,\frac{M_{V_2(n)}^2+Q^2}{\sigma_{V_2}^2}\right)\\
&\qquad\times R_0\left(\infty,\frac{M_{V_2(n)}^2+Q^2\,y}{\sigma_{V_2}^2}\right).
\end{aligned} \tag{5.199}$$

Analogously to H^P_{MV}, the term H^P_{pQCD} is treated as follows: the sum over n is performed, the expression is expanded in Q^2, and the integration over y is carried out. The commutation of the expansion and integration is checked numerically in figure 5.23. For the other terms, $\delta H^P_{\mathrm{pQCD}(i,j)}$, we use (5.184) and then proceed analogously to the leading term, see figure 5.23 for the numerical checks.

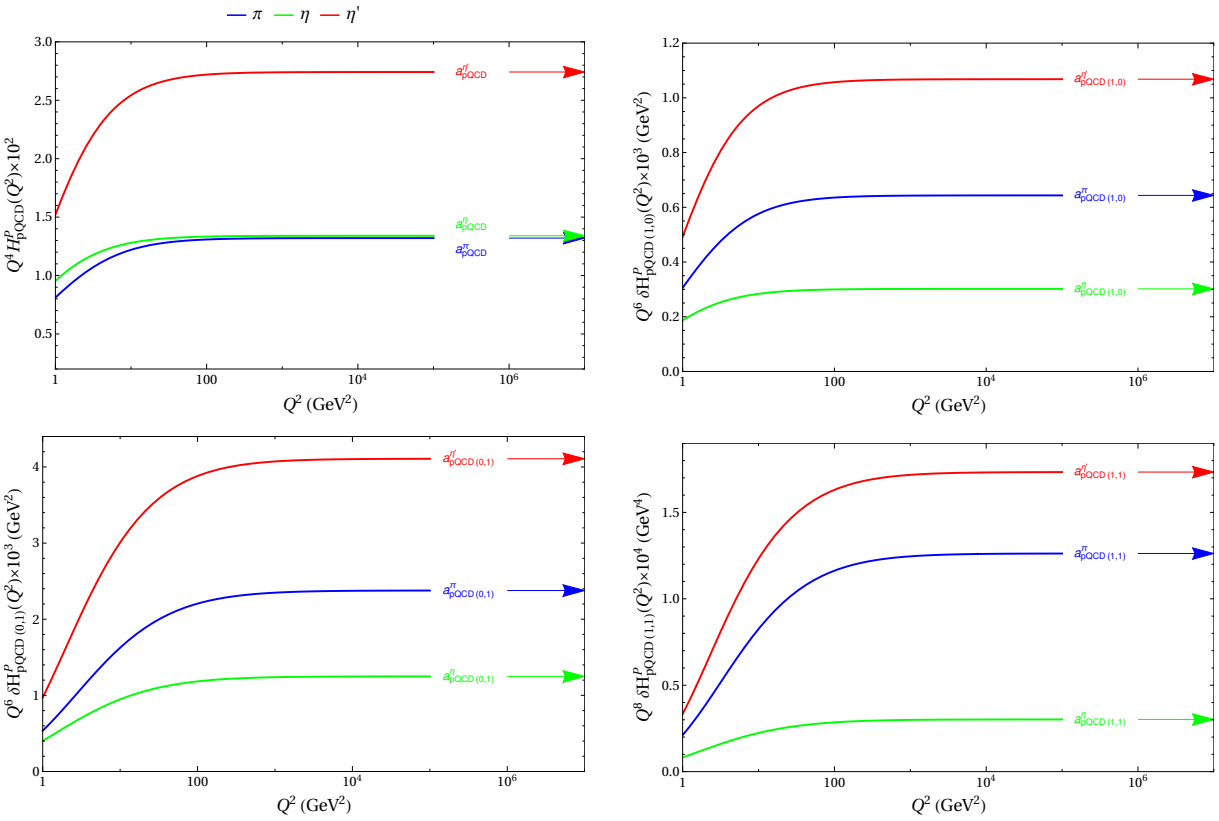

Figure 5.23: Numerical checks for the validity of commuting the expansion in Q^2 and the integration over y in (5.199). In all cases, we can see that the curves tend to the coefficients obtained by expanding in the virtualities first and then integrating over the Feynman parameter y. Note that the scales on the y-axis vary between the plots.

5.2.D Two-photon couplings of excited pseudoscalars

In this appendix we collect the phenomenological information that is available on the two-photon couplings of the excited pseudoscalars listed in the PDG [100], in comparison to the two-photon couplings of the first radially-excited pion, η, and η' states as shown in figure 5.21 for both the large-N_c Regge and the alternative TFF model.

Phenomenologically, the two-photon couplings of the excited pseudoscalars are unknown, but for many states some information on these couplings can be extracted either from direct limits on the two-photon channel or from measurements of particular branching fractions. For the excited pion states, the only available information concerns the $\pi(1300)$. The blue bar in the left panel of figure 5.21 indicates values excluded by the limit

$$F_{\pi(1300)\gamma\gamma} < 0.0544(71)\,\text{GeV}^{-1}. \tag{5.200}$$

Since at present there is no measurement of the $\pi(1300)$ width and the two-photon branching ratio, the above bound is an estimate based on the available empirical information. The $\pi(1300)$

decays predominantly into 3π, e.g., into $\rho\pi$:[18]

$$\frac{\Gamma(\gamma\gamma)\Gamma(\rho\pi)}{\Gamma_{\text{total}}} < 85\,\text{eV} \;\; [196], \qquad \frac{\Gamma(\pi(\pi\pi)_{S\text{-wave}})}{\Gamma(\rho\pi)} = 2.2(4) \;\; [197], \tag{5.201}$$

whereas the $\pi f_0(1300)$ and $\gamma\gamma$ decays are suppressed [275]. Assuming

$$\Gamma_{\text{total}} \sim \Gamma(\rho\pi) + \Gamma(\pi(\pi\pi)_{S\text{-wave}}), \tag{5.202}$$

this leads to:

$$\Gamma(\pi(1300) \to \gamma\gamma) < 272(34)\,\text{eV}, \tag{5.203}$$

where the error is propagated from (5.201). The bound in (5.200) follows from (5.36) with (5.203) and $M_{\pi(1300)} = 1300(100)\,\text{MeV}$. As one can see from figure 5.21, the large-N_c Regge model indeed satisfies the bound (5.200), it has $F_{\pi(1300)\gamma\gamma} = 0.0500\,\text{GeV}^{-1}$. Thus, even though it is not possible to generate a suppression by inverse powers of the pseudoscalar mass in our models, as seen in (5.36), the two-photon couplings of the excited pseudoscalars are sufficiently suppressed by inverse powers of the excited vector-meson masses.

Similar constraints exist for several excited η, η' states. As discussed in the main text, the assignment of Regge trajectories is not settled, so here we simply reproduce the listing according to the PDG, see section 5.2.4.3 for a discussion of the phenomenological implications. We stress that given that even the identification of states is contentious, the experimental limits should be treated with caution and mainly serve as guidance that our Regge models do not assume implausible values for the two-photon couplings. For the $\eta(1295)$, $M_{\eta(1295)} = 1294(4)\,\text{MeV}$, we have

$$\frac{\Gamma(\gamma\gamma)\Gamma(\eta\pi\pi)}{\Gamma_{\text{total}}} < 66\,\text{eV} \;\; [208], \qquad \frac{\Gamma(\gamma\gamma)\Gamma(K\bar{K}\pi)}{\Gamma_{\text{total}}} < 14\,\text{eV} \;\; [209]. \tag{5.204}$$

Assuming that the branching fraction into other channels can be neglected,[19] we would conclude $\Gamma(\gamma\gamma) < 80\,\text{eV}$ and thus

$$F_{\eta(1295)\gamma\gamma} < 0.030\,\text{GeV}^{-1}. \tag{5.205}$$

For the $\eta(1405)$, $M_{\eta(1405)} = 1408.8(2.0)\,\text{MeV}$, we have

$$\begin{aligned} &\frac{\Gamma(\gamma\gamma)\Gamma(K\bar{K}\pi)}{\Gamma_{\text{total}}} < 35\,\text{eV} \;\; [209], \qquad \frac{\Gamma(\gamma\gamma)\Gamma(\eta\pi\pi)}{\Gamma_{\text{total}}} < 95\,\text{eV} \;\; [208], \\ &\frac{\Gamma(\gamma\gamma)}{\Gamma(K\bar{K}\pi)} < 1.78 \times 10^{-3} \;\; [210]. \end{aligned} \tag{5.206}$$

Using the total width $\Gamma_{\eta(1405)} = 48(4)\,\text{MeV}$ as measured in the $K\bar{K}\pi$ channel, the two limits involving this channel imply $\Gamma(\gamma\gamma) < 1.73\,\text{keV}$, while assuming that $K\bar{K}\pi$ and $\eta\pi\pi$ constitute the dominant decay channels would lead to a much stronger constraint $\Gamma(\gamma\gamma) < 130\,\text{eV}$. The two limits on the two-photon coupling are

$$F_{\eta(1405)\gamma\gamma} < 0.122\,\text{GeV}^{-1}, \qquad F_{\eta(1405)\gamma\gamma} < 0.033\,\text{GeV}^{-1}, \tag{5.207}$$

[18] Note that the role of the S-wave component is not settled: while $\Gamma(\pi(\pi\pi)_{S\text{-wave}}/\Gamma(\rho\pi) = 2.12$ from ref. [273] agrees with ref. [197], ref. [274] found a negligible S-wave component $\Gamma(\pi(\pi\pi)_{S\text{-wave}}/\Gamma(\rho\pi) < 0.15$. In the latter case the limit on the two-photon decay width $F_{\pi(1300)\gamma\gamma}$ would become stricter by a factor $\sqrt{3.2} \sim 1.8$, in which case there would be some mild tension with $F_{\pi(1300)\gamma\gamma}$ implied by our Regge models.

[19] The limit from ref. [208] already includes the conversion factor $\Gamma(\eta\pi^+\pi^-)/(\Gamma(\eta\pi^+\pi^-) + \Gamma(\eta\pi^0\pi^0)) = 2/3$, which emerges from the combination of isospin and symmetry factors in $\Gamma(\eta\pi^0\pi^0)/\Gamma(\eta\pi^+\pi^-) = 1/2$.

respectively. Similarly, for the $\eta(1475)$, $M_{\eta(1475)} = 1475(4)\,\text{MeV}$, the PDG lists

$$\frac{\Gamma(\gamma\gamma)\Gamma(K\bar{K}\pi)}{\Gamma_{\text{total}}} = 230(71)\,\text{eV}\ \ [211], \qquad \frac{\Gamma(\gamma\gamma)}{\Gamma(K\bar{K}\pi)} < 1.27\times 10^{-3}\ \ [210], \tag{5.208}$$

which together with $\Gamma_{\eta(1475)} = 90(9)\,\text{MeV}$ implies the limit $\Gamma(\gamma\gamma) < 5.13\,\text{keV}$ or, assuming the $K\bar{K}\pi$ channel to be dominant, $\Gamma(\gamma\gamma) = 230(71)\,\text{eV}$, leading to

$$F_{\eta(1475)\gamma\gamma} < 0.195\,\text{GeV}^{-1}, \qquad F_{\eta(1475)\gamma\gamma} = 0.041(6)\,\text{GeV}^{-1}. \tag{5.209}$$

Next, for the $\eta(1760)$, $M_{\eta(1760)} = 1751(15)\,\text{MeV}$, we have

$$\frac{\Gamma(\gamma\gamma)\Gamma(\eta'\pi^+\pi^-)}{\Gamma_{\text{total}}} = 28.2(8.7)\,\text{eV}\ \ [212], \tag{5.210}$$

which, assuming dominance of $\eta'\pi\pi$ and including the neutral channel by means of the relation $\Gamma(\eta'\pi^0\pi^0)/\Gamma(\eta'\pi^+\pi^-) = 1/2$, translates into

$$F_{\eta(1760)\gamma\gamma} = 0.014(2)\,\text{GeV}^{-1}. \tag{5.211}$$

In case other channels do contribute, this number would have to be considered a lower limit.

Finally, there is some information available on the two-photon couplings of the $X(1835)$,

$$\frac{\Gamma(\gamma\gamma)\Gamma(\eta'\pi^+\pi^-)}{\Gamma_{\text{total}}} < 83\,\text{eV}\ \ [212], \qquad \frac{\Gamma(\gamma\gamma)}{\Gamma(\eta'\pi^+\pi^-)} < 9.80\times 10^{-3}\ \ [210], \tag{5.212}$$

where the two-resonance fit from ref. [212] only quotes a significance of $2.8\,\sigma$. The combination of the two produces the limit $\Gamma(\gamma\gamma) < 14.0\,\text{keV}$, again a lot weaker than the limit $\Gamma(\gamma\gamma) < 124.5\,\text{eV}$ obtained when assuming dominance of the $\eta'\pi\pi$ channel. The resulting two-photon couplings are

$$F_{X(1835)\gamma\gamma} < 0.235\,\text{GeV}^{-1}, \qquad F_{X(1835)\gamma\gamma} < 0.022\,\text{GeV}^{-1}. \tag{5.213}$$

The above phenomenological constraints on the two-photon couplings are collected in table 5.4, while the couplings from our large-N_c Regge models with different Regge trajectory assignments are listed in table 5.3.

5.2.E Systematic uncertainties and decay constants of excited pseudoscalars

The systematic errors quoted for Δa_μ in section 5.2.5.2 are based on comparing results from two different models for the pseudoscalar TFFs introduced in section 5.2.4 and appendix 5.2.B, respectively. This has then been added to a conservatively estimated uncertainty coming directly from the parameters of our models. By construction, our models link the TFFs of the different pion, η, or η' states such that a resummation is at all possible, but it is clear that the details of the TFFs so obtained may turn out not to be realistic, at least for the lowest lying excited pseudoscalars. Here, we explore this specific question in particular for the first excited pseudoscalars, on which some information from the phenomenology is indeed available. As we will show, if we adapt the parameters of our models presented in sections 5.2.4.1 and 5.2.4.2 to be in agreement with phenomenology, or theoretical expectations, we obtain shifts in our results which are well covered by the present error budget.

In section 5.2.4.3 and appendix 5.2.D, we confirmed that our TFF models are well compatible with phenomenological constraints for the two-photon couplings of $\eta(1295)$, $\eta(1405)$, $\eta(1475)$, $\eta(1760)$, and $X(1835)$. In the following, we will be interested in the leptonic decay constants, $F_{P(n)}$, of the excited pseudoscalars, limiting our analysis to $n \leq 3$ states. Since all pseudoscalar mesons, except for the Goldstone mode, decouple from the axial-vector current in the chiral limit, the corresponding decay constants, defined in (5.40), are suppressed. Note that contrary to the decay constants, the two-photon couplings are non-vanishing in the chiral limit. At low Q^2 it is the latter that are most relevant.

There are several theoretical studies of the leptonic decay constants of excited pions, e.g., based on lattice QCD [276, 277], QCD sum rules [278], quark models [279, 280], or finite-energy sum rules [281, 282]. Experimentally, $F_{\pi(1300)}$ can be measured in τ decays. Presently, there is only an upper bound $|F_{\pi(1300)}| < 8.4$ MeV [283], deduced from the branching fraction $\mathrm{Br}(\tau \to \pi(1300)\nu_\tau) < 10^{-4}$ [257]. The predictions in refs. [278–282] are all in agreement with this bound. In the following, we will work with $F_{\pi(1300)} = 2.20(46)\,\mathrm{MeV}$ [281], which implies $F_{\pi(1300)}/F_\pi \approx 2\%$. For the $\eta^{(\prime)}$, the suppression is expected to be weaker as it is given by the $SU(3)$ chiral limit, thus, we assume $F_{\eta^{(\prime)}(1)}/F_{\eta^{(\prime)}} \approx 20\%$. Furthermore, it is expected that the decay constants of the excited states, $F_{P(n)}$, are inversely proportional to the excited-state masses, $M_{P(n)}$, or the masses squared [278, 282], which generates an additionally suppression for the decay constants of the higher excitations.

We start by considering the symmetric pQCD limit of the TFFs, which for the ground-state pseudoscalars is given in (5.85) and (5.108). The same relations also hold for the excited pseudoscalars, replacing only the ground-state decay constants, i.e., $F_P \to F_{P(n)}$. To change the asymptotic limit of $F_{P(n)\gamma^*\gamma^*}(-Q^2,-Q^2)$ for $n = 1, 2, 3$, we modify c_{diag} by replacing (5.220) with

$$c_{\mathrm{diag}} \to c_{\mathrm{diag}} + \frac{16\Lambda^2\pi^2 F_\pi}{3M_\rho^2 M_\omega^2}\left[F_{\pi(1300)} - F_\pi\right], \tag{5.214}$$

and (5.226) with

$$c_{\mathrm{diag}} \to c_{\mathrm{diag}} + \frac{\mathcal{N}}{C^\eta_{\rho\rho} + C^\eta_{\omega\omega} + C^\eta_{\phi\phi}} \frac{8C_8}{\Lambda^2 F_{\eta\gamma\gamma}}\left[F_{\eta(1)} - F_\eta\right], \tag{5.215}$$

and analogously for η', while keeping all other model parameters the same, cf. table 5.1. Varying only the TFFs of the lowest excitations $n \leq 3$, it is ensured that the SDCs remain intact. Applying this modification for $n = 1$ decreases Δa_μ by $(0.22 + 0.27 + 0.45) \times 10^{-11} = 0.94 \times 10^{-11}$, where the individual numbers are the pion, η, and η' contributions, respectively. Note that we are removing the contribution from $Q_i \geq Q_{\mathrm{match}}$, as this region is described by the pQCD quark loop, cf. section 5.2.5.2.

The BL limit of the pseudoscalar TFFs is not known for general n. Presently, this limit is therefore not fine-tuned in our large-N_c Regge models, as can be seen in the right panel of figure 5.21. Here, we want to assume a BL limit constant in n, $\lim_{Q^2\to\infty} F_{P(n)\gamma\gamma^*} = \lim_{Q^2\to\infty} F_{P\gamma\gamma^*}$, which is also found for the alternative TFF model introduced in appendix 5.2.B. Replacing (5.222) with

$$c_{\mathrm{BL}} = \frac{1}{M^2_{-,n}}\left[c_{\mathrm{anom}} M^2_{+,n} + M^2_{\rho(n)} M^2_{\omega(n)}\left(\frac{c_A}{\Lambda^2} - \frac{8\pi^2 F_\pi^2}{M_\rho^2 M_\omega^2}\right)\right], \tag{5.216}$$

and (5.227) with

$$c_{\mathrm{BL}} = \left(\frac{1}{M^2_{\phi(n)}} - \frac{1}{M^2_{\omega(n)}}\right)^{-1} \left\{ \frac{1}{C^\eta_{\phi\omega} M^2_\phi M^2_\omega} \left[\frac{12 C_8 F_\eta \mathcal{N}}{F_{\eta\gamma\gamma}} - \frac{C^\eta_{\rho\rho} M^4_\rho}{M^2_{\rho(n)}} - \frac{C^\eta_{\omega\omega} M^4_\omega}{M^2_{\omega(n)}} - \frac{C^\eta_{\phi\phi} M^4_\phi}{M^2_{\phi(n)}} \right] \right.$$
$$\left. - \frac{2c_A}{\Lambda^2} - \left(\frac{1}{M^2_{\phi(n)}} + \frac{1}{M^2_{\omega(n)}}\right) \left(1 + \frac{c_B}{2\Lambda^2}(M^2_\omega - M^2_\phi) - \frac{c_A}{2\Lambda^2}(M^2_\phi + M^2_\omega)\right) \right\}, \tag{5.217}$$

while keeping all other model parameters the same, this is achieved without changing the two-photon couplings or other SDCs. Looking at the $n = 1$ case, Δa_μ decreases by $(0.49 + 1.18 + 1.92) \times 10^{-11} = 3.59 \times 10^{-11}$. This shift predominantly comes from a change of the low-Q^2 shape of the TFFs and not from the different asymptotic limits.

Combining the changes in (5.214) and (5.216), as well as (5.215) and (5.217), the total decrease of Δa_μ amounts to $(0.62{+}1.27{+}2.10){\times}10^{-11} = 3.99{\times}10^{-11}$ if only $n = 1$ is modified, $5.26{\times}10^{-11}$ if also $n = 2$ is modified, and 5.82×10^{-11} if $n = 1, 2, 3$ are modified.

As a last point, we study the effect of non-diagonal couplings. To be more precise, in our large-N_c Regge models from section 5.2.4, we allowed the n-th pion, η, or η' excitation to couple only to the n-th ρ, ω, and ϕ excitations, whereas now we allow the first excited pseudoscalars to couple to the ground-state vector mesons. For the $\pi(1300)$, we modify

$$F_{\pi(1)\gamma^*\gamma^*}(-Q_1^2, -Q_2^2) \to F_{\pi(1)\gamma^*\gamma^*}(-Q_1^2, -Q_2^2) - \frac{F_{\pi(1)\gamma\gamma}}{2} \left[M^2_\rho M^2_\omega \left(\frac{1}{D^1_\rho D^2_\omega} + \frac{1}{D^1_\omega D^2_\rho} \right) \right.$$
$$\left. - M^2_{\rho(1)} M^2_{\omega(1)} \left(\frac{1}{D^1_{\rho(1)} D^2_{\omega(1)}} + \frac{1}{D^1_{\omega(1)} D^2_{\rho(1)}} \right) \right], \tag{5.218}$$

and generate the two-photon coupling through $\rho(770)$ and $\omega(782)$. For the first excited $\eta^{(\prime)}$, we only express the dominant isovector–isovector part of the two-photon coupling through $\rho(770)$:

$$F_{\eta^{(\prime)}(1)\gamma^*\gamma^*}(-Q_1^2, -Q_2^2) \to F_{\eta^{(\prime)}(1)\gamma^*\gamma^*}(-Q_1^2, -Q_2^2)$$
$$- \frac{F_{\eta^{(\prime)}(1)\gamma\gamma} C^{\eta^{(\prime)}}_{\rho\rho}}{\mathcal{N}} \left[\frac{M^4_\rho}{D^1_\rho D^2_\rho} - \frac{M^4_{\rho(1)}}{D^1_{\rho(1)} D^2_{\rho(1)}} \right]. \tag{5.219}$$

These modifications lead to a decrease of $(0.53 + 0.54 + 0.72) \times 10^{-11} = 1.79 \times 10^{-11}$. Such non-diagonal couplings are also present in the alternative TFF model introduced in appendix 5.2.B.

All these modifications affect in one way or another the low-Q^2 behavior of the excited-state TFFs, which could be constrained more rigorously if data were available. At present, we observe that the corresponding changes, which tend to lower Δa_μ, are well covered by our final uncertainty estimate in (5.141). Since, on the other hand, the consideration of Model 2 suggests systematic effects in the opposite direction, we leave the central value as derived from Model 1, with uncertainties as assigned in (5.141).

5.2.F Pion transition form factors $F_{\pi(n)\gamma^*\gamma^*}$

5.2.F.1 Large-N_c Regge model

In this appendix, we describe the large-N_c Regge model for the pion TFF, given in (5.90), in more details. A comparison to experimental data and other parameterizations available from the

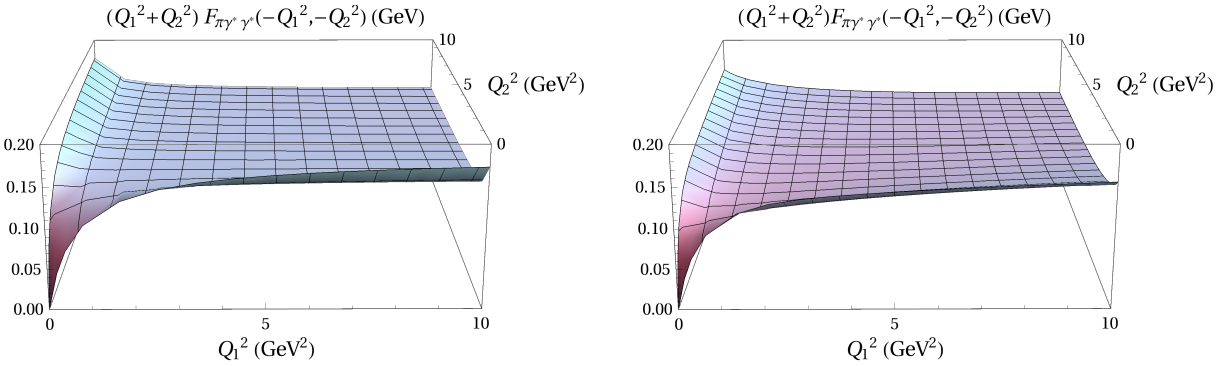

Figure 5.24: π^0 TFF in the full space-like region for $Q_1^2, Q_2^2 < 10$ GeV^2. The large-N_c Regge model, (5.90), is shown in the left panel, and our alternative model, (5.161), is shown in the right panel.

literature is postponed to section 5.2.F.2. Based on the constraint equations in (5.94), (5.95), and (5.97), the model parameters should be replaced by:

$$c_{\text{diag}} = \frac{16\pi^2 F_\pi^2 \Lambda^2}{3 M_\omega^2 M_\rho^2}, \tag{5.220}$$

$$c_{\text{anom}} = 1 - \frac{1}{\Lambda^2}\left(c_A M_{+,0}^2 + c_B M_{-,0}^2\right), \tag{5.221}$$

$$c_{\text{BL}} = -\frac{8\pi^2 F_\pi^2}{M_{-,0}^2} + \frac{M_{+,0}^2}{M_{-,0}^2} - \frac{1}{\Lambda^2}\left(c_A M_{-,0}^2 + c_B M_{+,0}^2\right), \tag{5.222}$$

where the parameters related to the asymptotic limits of the HLbL tensor simplify to:

$$c_{\substack{A\\B}} = \frac{\Lambda^2}{M_\omega^2 M_\rho^2}\left[\frac{\Delta_{\pi\rho}}{L_{\pi\rho}} - 4\pi^2 F_\pi\left(\frac{\Delta_{\pi\rho}L_{\pi\omega}}{\Delta_{\pi\omega}L_{\pi\rho}} \mp 1\right)\left(\frac{b}{2a} + \sqrt{\left(\frac{b}{2a}\right)^2 - \frac{1}{a}\left(c - \frac{1}{9\pi^2}\right)}\right)\right], \tag{5.223}$$

with

$$\begin{aligned}
a &= \frac{\Delta_{\pi\rho}}{\Omega_{\rho\omega\pi}^2}\left[f_2(\sigma_\pi,\sigma_\rho,\sigma_\omega) - \frac{L_{\pi\omega}}{L_{\pi\rho}} f_2(\sigma_\pi,\sigma_\omega,\sigma_\rho)\right]\left(\sigma_\rho^2 - \sigma_\omega^2\,\frac{\Delta_{\pi\rho}L_{\pi\omega}}{\Delta_{\pi\omega}L_{\pi\rho}}\right),\\
b &= \frac{\Delta_{\pi\rho}}{\Omega_{\rho\omega\pi}^2}\Bigg\{-\frac{2F_\pi}{3}\left[f_1(\sigma_\pi,\sigma_\omega,\sigma_\rho) - \frac{L_{\pi\omega}}{L_{\pi\rho}} f_1(\sigma_\pi,\sigma_\rho,\sigma_\omega)\right]\\
&\quad - \frac{1}{4\pi^2 F_\pi}\frac{\Delta_{\pi\omega}}{L_{\pi\rho}}\left[\sigma_\rho^2\, f_2(\sigma_\pi,\sigma_\omega,\sigma_\rho) + \frac{\Delta_{\pi\rho}}{\Delta_{\pi\omega}}\sigma_\omega^2\left(f_2(\sigma_\pi,\sigma_\rho,\sigma_\omega) - \frac{2L_{\pi\omega}}{L_{\pi\rho}} f_2(\sigma_\pi,\sigma_\omega,\sigma_\rho)\right)\right]\Bigg\},\\
c &= \frac{\Delta_{\pi\rho}}{\Omega_{\rho\omega\pi}^2}\frac{\Delta_{\pi\omega}}{L_{\pi\rho}}\left[\frac{1}{(4\pi^2 F_\pi)^2}\frac{\Delta_{\pi\rho}\sigma_\omega^2}{L_{\pi\rho}} f_2(\sigma_\pi,\sigma_\omega,\sigma_\rho) + \frac{f_1(\sigma_\pi,\sigma_\rho,\sigma_\omega)}{6\pi^2}\right],
\end{aligned} \tag{5.224}$$

and the auxiliary functions

$$\begin{aligned}
g_1(\sigma_P,\sigma_{V_1},\sigma_{V_2}) &\coloneqq \sigma_P^2\left(\sigma_{V_1}^4 - \sigma_{V_2}^4\right) - \Delta_{V_1V_2}\left(\sigma_P^4 + \sigma_{V_1}^2\sigma_{V_2}^2\right) + \sigma_{V_2}^4\sigma_{V_1}^2 L_{V_1V_2}, \qquad (5.225)\\
g_2(\sigma_P,\sigma_{V_1},\sigma_{V_2}) &\coloneqq \sigma_P^2\Delta_{V_1V_2}^2 L_{PV_1},\\
f_1(\sigma_P,\sigma_{V_1},\sigma_{V_2}) &\coloneqq \sigma_{V_1}^2\, g_1(\sigma_P,\sigma_{V_1},\sigma_{V_2}) + \sigma_P^2\, g_2(\sigma_P,\sigma_{V_1},\sigma_{V_2}) + \left(\sigma_P^2 - 2\sigma_{V_1}^2\right)\sigma_{V_2}^4\sigma_P^2\, L_{V_1V_2},\\
f_2(\sigma_P,\sigma_{V_1},\sigma_{V_2}) &\coloneqq g_1(\sigma_P,\sigma_{V_1},\sigma_{V_2}) - g_2(\sigma_P,\sigma_{V_1},\sigma_{V_2}) + \left(\sigma_P^2\sigma_{V_1}^2 - \sigma_{V_1}^4 - \sigma_{V_2}^4\right)\sigma_P^2\, L_{V_1V_2}.
\end{aligned}$$

Here, the definitions from (5.96) and (5.98) are used.

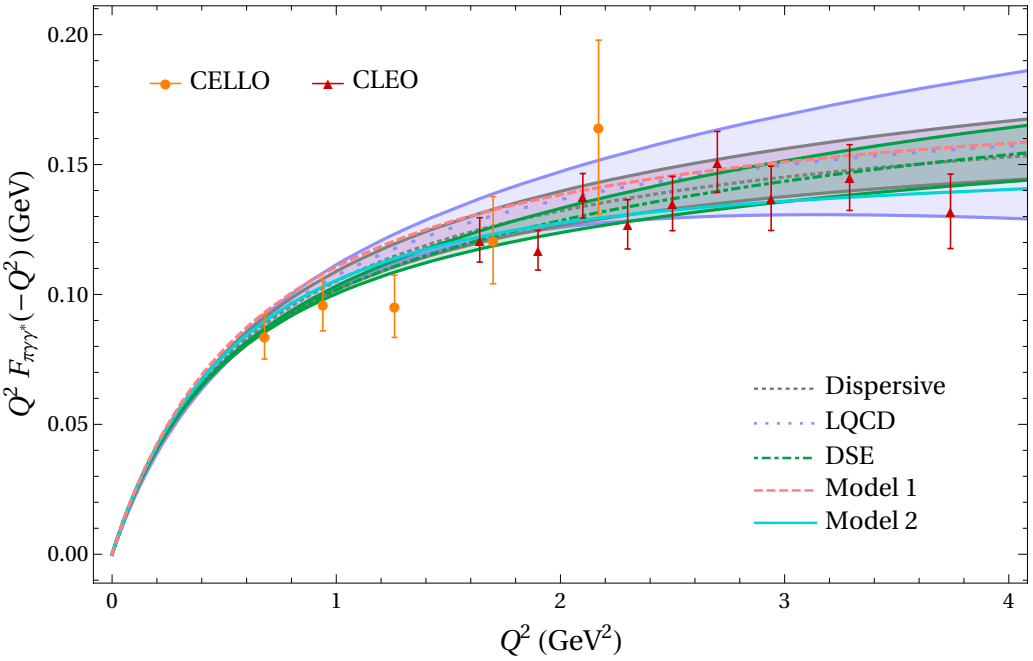

Figure 5.25: Singly-virtual π^0 TFF in the low-Q region. The large-N_c Regge model, "Model 1" (5.90), is indicated by the dashed pink curve. Our alternative TFF model, "Model 2" (5.161), is indicated by the solid cyan curve. The gray band with the dotted curve is the dispersive result from refs. [28, 172]. The blue band with the long-dotted curve is the lattice QCD result from ref. [29]. The green band with the dot-dashed curve is the DSE result from ref. [173]. The data are from CELLO [204] and CLEO [205].

5.2.F.2 Comparison of data and literature: $F_{\pi(n)\gamma^*\gamma^*}$

In this appendix, we compare our large-N_c Regge model, "Model 1" (5.90), and our alternative model, "Model 2" (5.161), for $F_{\pi(n)\gamma^*\gamma^*}$ to data and other parameterizations available from the literature.

In figure 5.9, the singly-virtual π^0 TFF is shown for $Q^2 \in [0, 35]\,\text{GeV}^2$. In figure 5.25, we focus on the low-Q region and include a comparison to the recent lattice QCD [29] and DSE [173] results. Our π^0 TFF models, for which we do not display error estimates, are in good agreement with the dispersive and lattice QCD TFFs, while we observe some deviation of our Model 1 from the DSE prediction. However, the error quoted for the DSE result in ref. [173], as pointed out therein, is only a rough estimate based on the variation of their one model parameter and does not account for the total truncation error. Therefore, we conclude that our π^0 TFF models also agree with the DSE prediction in the singly-virtual region.

In figure 5.26, we show the doubly-virtual π^0 TFF in the low-Q region. Both lattice QCD and DSE are able to give much more accurate predictions of the (pseudoscalar) TFFs for doubly-virtual than for singly-virtual kinematics, as is obvious by comparing the error bands in figures 5.25 and 5.26. In the symmetric region, $Q_1^2 = Q_2^2 = Q^2$, starting from $\sim 1\ \text{GeV}^2$, the DSE predict a slightly larger π^0 TFF than lattice QCD, see left panel in figure 5.26. Our models for the π^0 TFF run just between these DSE and lattice QCD predictions. Note, however, that the discrepancy in figure 5.26 is visually enhanced by showing $Q^2 F_{\pi^0\gamma^*\gamma^*}(-Q^2, -Q^2)$ instead

of $F_{\pi^0\gamma^*\gamma^*}(-Q^2,-Q^2)$. For doubly-virtual kinematics away from the symmetric limit, see for instance $Q_1^2 = Q^2$ and $Q_2^2 = 2Q^2$ in the right panel of figure 5.26, our π^0 TFF models are in closer agreement with the lattice QCD prediction.

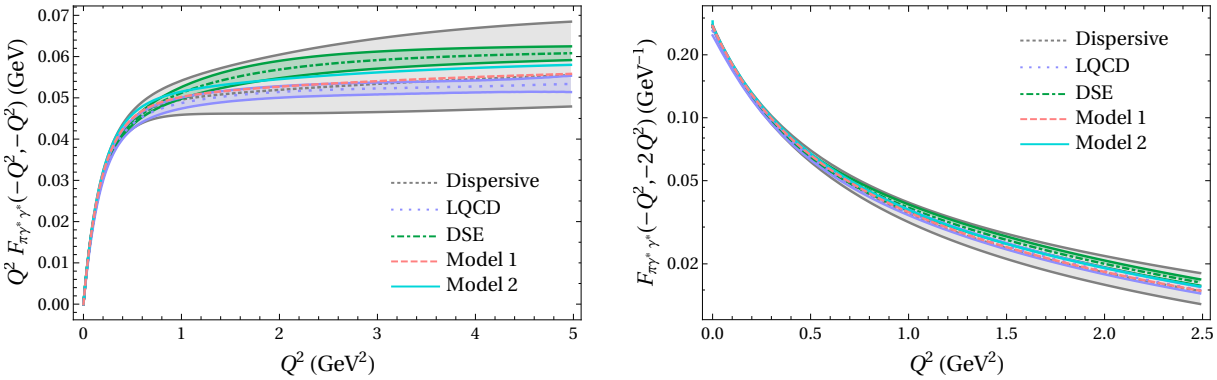

Figure 5.26: Doubly-virtual π^0 TFF in the symmetric region $Q_1^2 = Q_2^2 = Q^2$ (left) and in the region where $Q_1^2 = Q^2$ and $Q_2^2 = 2Q^2$ (right). Legend is the same as in figure 5.25.

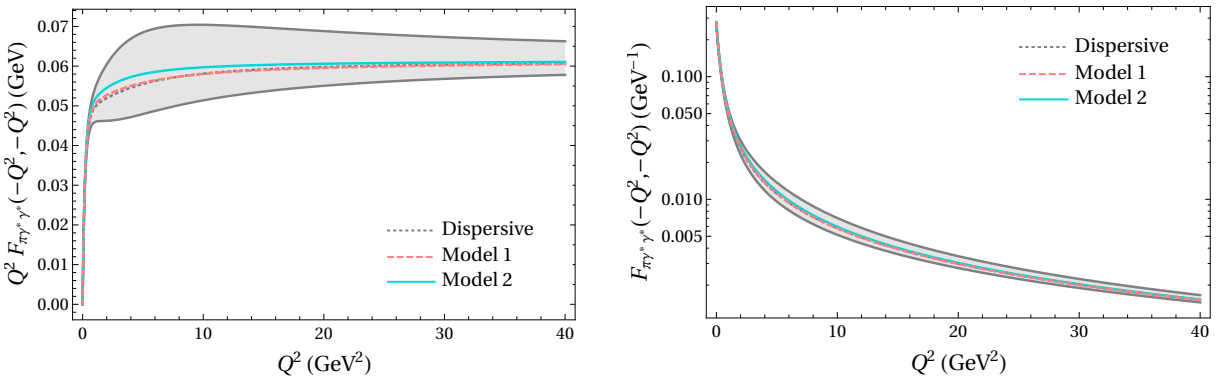

Figure 5.27: Doubly-virtual π^0 TFF in the symmetric region $Q_1^2 = Q_2^2 = Q^2$ for $Q^2 \in [0, 40]$ GeV^2. Legend is the same as in figure 5.25.

In figure 5.27, we show the doubly-virtual π^0 TFF in the symmetric region for $Q^2 \in [0, 40]$ GeV^2. Both models, but in particular Model 1, are in perfect agreement with the dispersive description [28,172]. In figure 5.24, Model 1 and 2 are shown in the full space-like region for $Q_1^2, Q_2^2 < 10$ GeV^2. One can see that their main difference is in the regions where at least one of the photon virtualities is small.

5.2.G η and η' transition form factors $F_{\eta^{(\prime)}(n)\gamma^*\gamma^*}$

5.2.G.1 Large-N_c Regge model

In this appendix, we describe the large-N_c Regge model for the η and η' TFFs, introduced in section 5.2.4.2, in more details. A comparison to experimental data and other parameterizations available from the literature is postponed to appendices 5.2.G.2 and 5.2.G.3.

All expressions are given for the η, but hold as well for the η' after obvious replacements (including $C_8 \to C_0$). Based on the constraint equations in (5.122), (5.123), and (5.124) the

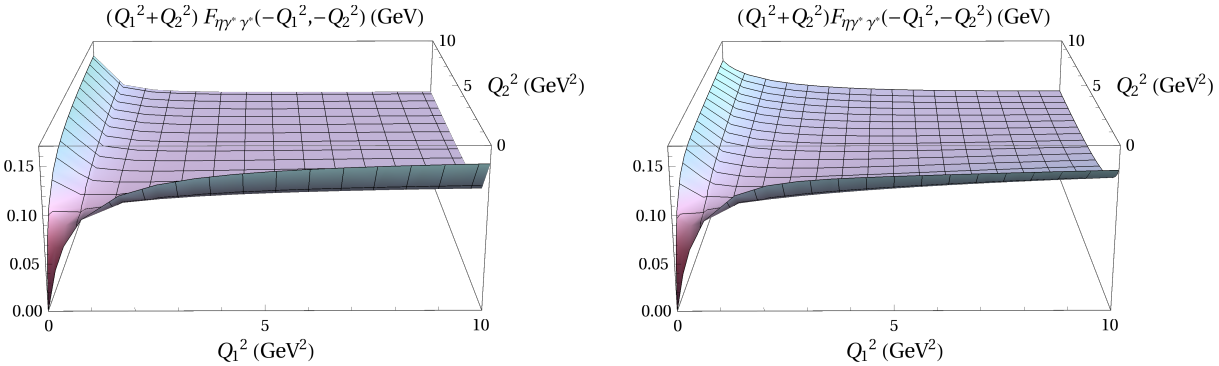

Figure 5.28: η TFF in the full space-like region for $Q_1^2, Q_2^2 < 10$ GeV^2. The large-N_c Regge model, (5.114), is shown in the left panel, and our alternative model, (5.161), is shown in the right panel.

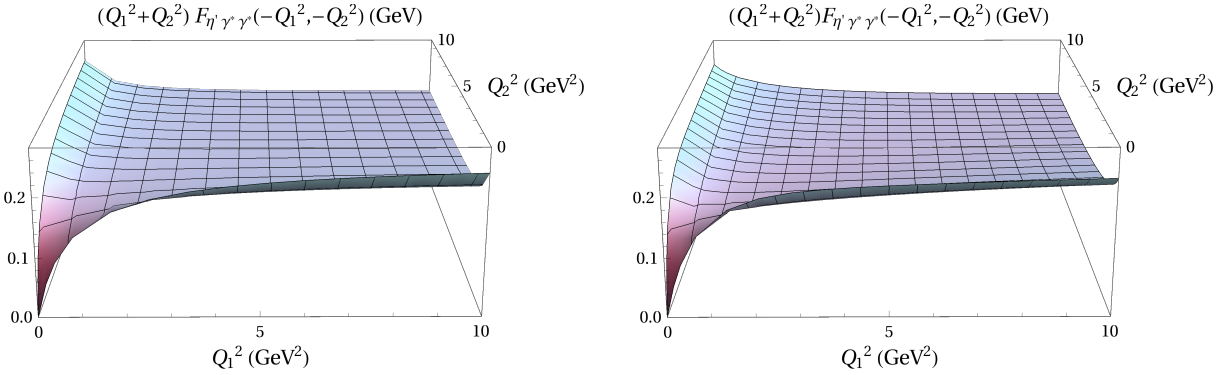

Figure 5.29: η' TFF in the full space-like region for $Q_1^2, Q_2^2 < 10$ GeV^2. The large-N_c Regge model, (5.114), is shown in the left panel, and our alternative model, (5.161), is shown in the right panel.

model parameters should be replaced by:

$$c_{\rm diag} = \frac{\mathcal{N}}{C^\eta_{\rho\rho}+C^\eta_{\omega\omega}+C^\eta_{\phi\phi}}\frac{8C_8F_\eta}{\Lambda^2 F_{\eta\gamma\gamma}}, \tag{5.226}$$

$$c_{\rm BL} = \frac{1}{M^2_{-,0}}\left[\frac{C^\eta_{\rho\rho}M_\rho^2+C^\eta_{\omega\omega}M_\omega^2+C^\eta_{\phi\phi}M_\phi^2}{2C^\eta_{\phi\omega}} - \frac{\mathcal{N}}{C^\eta_{\phi\omega}}\frac{6C_8F_\eta}{F_{\eta\gamma\gamma}} + M^2_{+,0} - c_A\frac{M^4_{-,0}}{\Lambda^2}\right.$$
$$\left. - c_B\frac{M^2_{+,0}M^2_{-,0}}{\Lambda^2}\right], \tag{5.227}$$

where the parameters related to the asymptotic limits of the HLbL tensor simplify to:

$$c_{\substack{A\\B}} = \frac{\Lambda^2}{2}\left[\frac{\Delta_{\omega\eta}}{L_{\omega\eta}}\frac{\mathcal{N}}{C^\eta_{\phi\omega}}\frac{3C_\eta^2}{2\pi^2 C_8F_\eta F_{\eta\gamma\gamma}M_\phi^2M_\omega^2}\right.$$
$$\left. + \left(\frac{\Delta_{\omega\eta}L_{\phi\eta}}{\Delta_{\phi\eta}L_{\omega\eta}}\mp 1\right)\left(\frac{b}{2a} - \sqrt{\left(\frac{b}{2a}\right)^2 - \frac{1}{a}\left(c-\frac{4C_\eta^2}{\pi^2}\right)}\right)\right], \tag{5.228}$$

with

$$
\begin{aligned}
a &= \left(\frac{C^\eta_{\phi\omega} F_{\eta\gamma\gamma} M_\phi^2 M_\omega^2}{\mathcal{N}}\right)^2 \frac{\Delta_{\omega\eta}}{\Omega^2_{\phi\omega\eta}} \left[f_2(\sigma_\eta,\sigma_\omega,\sigma_\phi) - \frac{L_{\phi\eta}}{L_{\omega\eta}} f_2(\sigma_\eta,\sigma_\phi,\sigma_\omega)\right] \left(\sigma_\phi^2 \frac{\Delta_{\omega\eta} L_{\phi\eta}}{\Delta_{\phi\eta} L_{\omega\eta}} - \sigma_\omega^2\right), \\
b &= -\frac{C^\eta_{\phi\omega} F_{\eta\gamma\gamma} M_\phi^2 M_\omega^2}{\mathcal{N} \Delta_{\phi\eta} L_{\omega\eta}} \Bigg\{ \frac{-4 C_8 F_\eta}{C^\eta_{\rho\rho} + C^\eta_{\phi\phi} + C^\eta_{\omega\omega}} \left[\frac{C^\eta_{\rho\rho}}{\Delta^2_{\rho\eta}} \left(\frac{L_{\phi\eta}}{\Delta^2_{\rho\omega}} f_1(\sigma_\eta,\sigma_\rho,\sigma_\omega) - \frac{L_{\omega\eta}}{\Delta^2_{\rho\phi}} f_1(\sigma_\eta,\sigma_\rho,\sigma_\phi) \right) \right. \\
&\quad + \frac{C^\eta_{\phi\phi}}{\Delta^2_{\phi\eta}} \left(\frac{L_{\phi\eta}}{\Delta^2_{\phi\omega}} f_1(\sigma_\eta,\sigma_\phi,\sigma_\omega) + \frac{L_{\omega\eta}}{2} f_3(\sigma_\eta,\sigma_\phi) \right) - \frac{C^\eta_{\omega\omega}}{\Delta^2_{\omega\eta}} \left(\frac{L_{\omega\eta}}{\Delta^2_{\phi\omega}} f_1(\sigma_\eta,\sigma_\omega,\sigma_\phi) \right. \\
&\quad \left. \left. + \frac{L_{\phi\eta}}{2} f_3(\sigma_\eta,\sigma_\omega) \right) \right] - \frac{3 C_\eta^2}{2\pi^2 C_8 F_\eta \Omega_{\phi\omega\eta} \Delta_{\phi\omega}} \left[\left(2\sigma_\phi^2 \Delta_{\omega\eta} \frac{L_{\phi\eta}}{L_{\omega\eta}} - \sigma_\omega^2 \Delta_{\phi\eta} \right) f_2(\sigma_\eta,\sigma_\phi,\sigma_\omega) \right. \\
&\quad \left. - \sigma_\phi^2 \Delta_{\omega\eta} f_2(\sigma_\eta,\sigma_\omega,\sigma_\phi) \right] \Bigg\}, \\
c &= -\frac{3 C_\eta^2}{2\pi^2 C_8 F_\eta \Delta_{\phi\eta} L_{\omega\eta}} \left[\frac{3 C_\eta^2}{2\pi^2 C_8 F_\eta} \frac{\sigma_\phi^2}{\Delta^2_{\phi\omega} L_{\omega\eta}} f_2(\sigma_\eta,\sigma_\phi,\sigma_\omega) - \frac{4 C_8 F_\eta \Delta_{\phi\eta}}{C^\eta_{\rho\rho} + C^\eta_{\phi\phi} + C^\eta_{\omega\omega}} \right. \\
&\quad \left. \times \left(\frac{C^\eta_{\omega\omega}}{2\Delta^2_{\omega\eta}} f_3(\sigma_\eta,\sigma_\omega) - \frac{C^\eta_{\rho\rho}}{\Delta^2_{\rho\omega}\Delta^2_{\rho\eta}} f_1(\sigma_\eta,\sigma_\rho,\sigma_\omega) - \frac{C^\eta_{\phi\phi}}{\Delta^2_{\phi\omega}\Delta^2_{\phi\eta}} f_1(\sigma_\eta,\sigma_\phi,\sigma_\omega) \right) \right].
\end{aligned} \tag{5.229}
$$

Here, the definitions from (5.96) and (5.98), the auxiliary functions from (5.225), as well as

$$
f_3(\sigma_P,\sigma_V) \coloneqq 3\sigma_P^4 - 4\sigma_P^2\sigma_V^2 + \sigma_V^4 - 2\sigma_P^4 L_{PV}, \tag{5.230}
$$

are used. Note that for the η' one has to instead choose:

$$
\begin{aligned}
c^{\ A}_{\ B} &= \frac{\Lambda^2}{2} \left[\frac{\Delta_{\omega\eta'}}{L_{\omega\eta'}} \frac{\mathcal{N}}{C^{\eta'}_{\phi\omega}} \frac{3 C^2_{\eta'}}{2\pi^2 C_0 F_{\eta'} F_{\eta'\gamma\gamma} M_\phi^2 M_\omega^2} \right. \\
&\quad \left. + \left(\frac{\Delta_{\omega\eta'} L_{\phi\eta'}}{\Delta_{\phi\eta'} L_{\omega\eta'}} \mp 1 \right) \left(\frac{b}{2a} + \sqrt{\left(\frac{b}{2a}\right)^2 - \frac{1}{a}\left(c - \frac{4C^2_{\eta'}}{\pi^2}\right)} \right) \right],
\end{aligned} \tag{5.231}
$$

as the physical solution for the quadratic equation (5.124).

5.2.G.2 Comparison of data and literature: $F_{\eta(n)\gamma^*\gamma^*}$

In this appendix, we compare our large-N_c Regge model, "Model 1" (5.114), and our alternative model, "Model 2" (5.161), for $F_{\eta(n)\gamma^*\gamma^*}$ to data and other parameterizations available from the literature. The error band shown for Model 1 is generated by propagating the errors of the input parameters σ_P, σ_V, $F_{\eta\gamma\gamma}$, F_η, F^8, F^0, θ_8, θ_0.

In figure 5.12, the singly-virtual TFF of the ground-state η is shown for $Q^2 \in [0, 40]\,\text{GeV}^2$. In figure 5.30, we focus on the low-Q region and include a comparison to the DSE result [173]. One can see that our models agree with the experimental data from CELLO [204] and CLEO [205], but tend to a larger η TFF than CA [26] and DSE. In addition, Model 2 is larger than Model 1 for $Q^2 < 2.4\ \text{GeV}^2$. This low-Q enhancement explains why $a_\mu^{\eta\text{-pole}}|_{\text{Model 2}} > a_\mu^{\eta\text{-pole}}|_{\text{Model 1}}$, see (5.129).

In figure 5.31, the doubly-virtual η TFF is shown for two kinematic situations: symmetric momenta, and $Q_1^2 = Q^2$ and $Q_2^2 = 2Q^2$. Considering Model 1, we observe a slight tension with

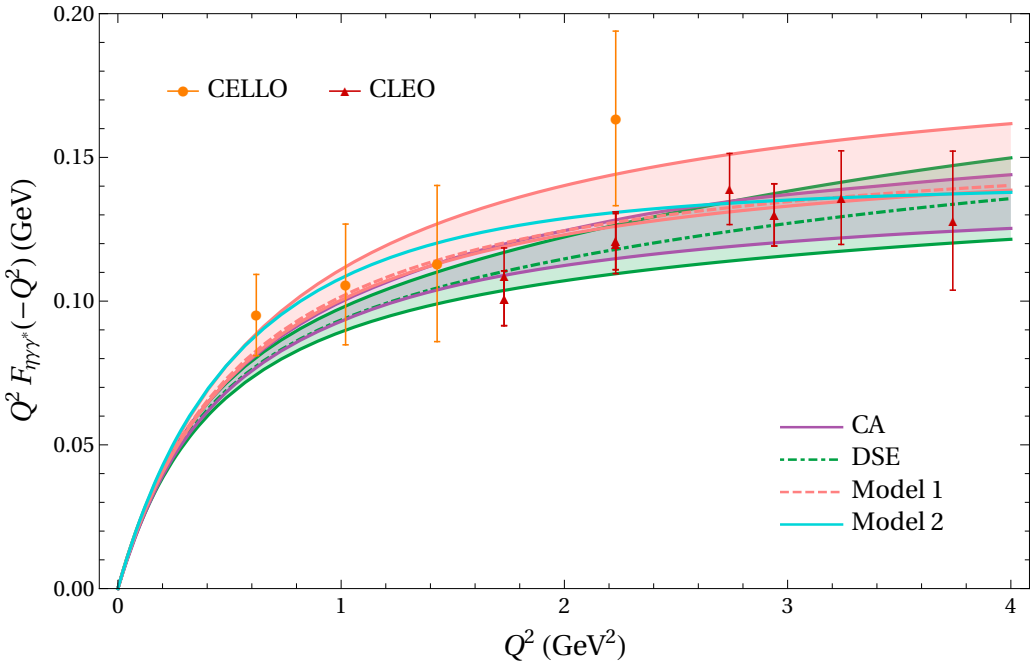

Figure 5.30: Singly-virtual η TFF in the low-Q region. The large-N_c Regge model, "Model 1" (5.114), is indicated by the pink band with the dashed curve. Our alternative TFF model, "Model 2" (5.161), is indicated by the solid cyan curve. The purple band is the CA result from ref. [26]. The green band with the dot-dashed curve is the DSE result from ref. [173]. The data are from CELLO [204] and CLEO [205].

the DSE prediction in the region of $Q^2 \in [0.2, 0.8]\,\text{GeV}^2$. This tension should, however, not be taken too serious, because both the DSE and our error band are only based on the variation of input parameters and do not take into account all possible error sources.

In figure 5.28, Model 1 and 2 are shown in the full space-like region for $Q_1^2, Q_2^2 < 10$ GeV^2. One can see that their main difference lies, similarly as for the π^0 TFF, in the regions where at least one of the photon virtualities is small.

In the left panel of figure 5.32, the ground-state η TFF is decomposed into the contributions from 2ρ, 2ω, 2ϕ, and $\phi\omega$ vector mesons. As expected, the TFF is dominated by the isovector–isovector 2ρ contribution, followed by the isoscalar–isoscalar 2ϕ contribution. The $\phi\omega$ contribution (5.116), which was needed to generate enough freedom in our large-N_c Regge model to satisfy the BL limit of the TFF and the two SDCs on the HLbL tensor, is small.

In the right panel of figure 5.32, we show the TFF of the first ($n = 1$) radially-excited η state. In the doubly-virtual region, the relative strength of vector-meson pairs is comparable to what one finds for the ground-state η. The 2ρ contribution is now slightly smaller than the total TFF, and the $\phi\omega$ contribution is now larger than the 2ω contribution. In contrast, the singly-virtual TFFs of the radially-excited η states will be dominated by the $\phi\omega$ contribution. This enhancement is generated by the n-dependence in the numerator of (5.116) through terms proportional to $M_{+,n}$. The two-photon couplings and BL limits of the excited-state η TFFs are shown in figure 5.21.

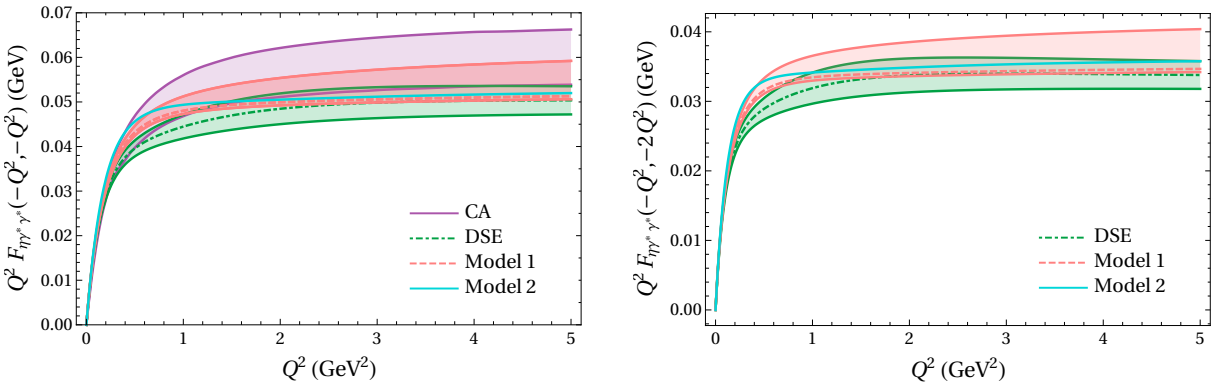

Figure 5.31: Doubly-virtual η TFF in the symmetric region $Q_1^2 = Q_2^2 = Q^2$ (left) and in the region where $Q_1^2 = Q^2$ and $Q_2^2 = 2Q^2$ (right). Legend is the same as in figure 5.30.

5.2.G.3 Comparison of data and literature: $F_{\eta'(n)\gamma^*\gamma^*}$

In this appendix, we compare our large-N_c Regge model, "Model 1" (5.114), and our alternative model, "Model 2" (5.161), for $F_{\eta(n)\gamma^*\gamma^*}$ to data and other parameterizations available from the literature. The error band shown for Model 1 is generated by propagating the errors of the input parameters σ_P, σ_V, $F_{\eta'\gamma\gamma}$, $F_{\eta'}$, F^8, F^0, θ_8, θ_0.

In figure 5.13, the singly-virtual TFF of the ground-state η' is shown for $Q^2 \in [0, 40]\,\text{GeV}^2$. In figure 5.33, we focus on the low-Q region and include a comparison to the DSE result [173]. One can see that Model 1 agrees with the experimental data from L3 [203], CELLO [204], and CLEO [205], as well as the CA [26] and DSE results. Model 2 tends to a larger η TFF for $Q^2 < 2$ GeV^2. This low-Q enhancement explains why $a_\mu^{\eta'\text{-pole}}|_{\text{Model 2}} > a_\mu^{\eta'\text{-pole}}|_{\text{Model 1}}$, see (5.130).

In figure 5.34, the doubly-virtual η' TFF is shown for two kinematic situations: symmetric momenta, and $Q_1^2 = Q^2$ and $Q_2^2 = 2Q^2$. Model 1 is in slight tension with the DSE prediction for $Q^2 \in [0.2, 1.6]\,\text{GeV}^2$. This tension should, however, not be taken too serious. A comparison of our models with the CA result shows perfect agreement for symmetric momenta. For large photon virtualities, both models agree with each other and give a reasonably good description of the recent doubly-virtual η' TFF data from BaBar [207], see figure 5.11.

In figure 5.29, Model 1 and 2 are shown in the full space-like region for $Q_1^2, Q_2^2 < 10$ GeV^2. One can see that their main difference is, similar as for the η TFF, in the regions where at least one of the photon virtualities is small.

In the left panel of figure 5.35, the ground-state η' TFF is decomposed into the contributions from 2ρ, 2ω, 2ϕ, and $\phi\omega$ vector mesons. As expected, the largest contribution to the TFF is coming from the isovector–isovector 2ρ mesons, followed by the isoscalar–isoscalar 2ϕ mesons. Unlike in the case of the η TFF, the 2ϕ mesons gives a positive contribution to the η' TFF, just like the 2ρ, 2ω, and $\phi\omega$ mesons. Thus, since the 2ρ contribution does not need to cancel out a negative 2ϕ contribution as it does in the η TFF, it appears to be smaller than the total η' TFF. The $\phi\omega$ contribution (5.116), generated through ϕ–ω mixing, is small.

In the right panel of figure 5.35, we show the TFF of the first ($n = 1$) radially-excited η' state. In the doubly-virtual region, the relative strength of vector-meson pairs is similar to what one finds for the ground-state η'. The $\phi\omega$ contribution is now larger than the 2ω contribution,

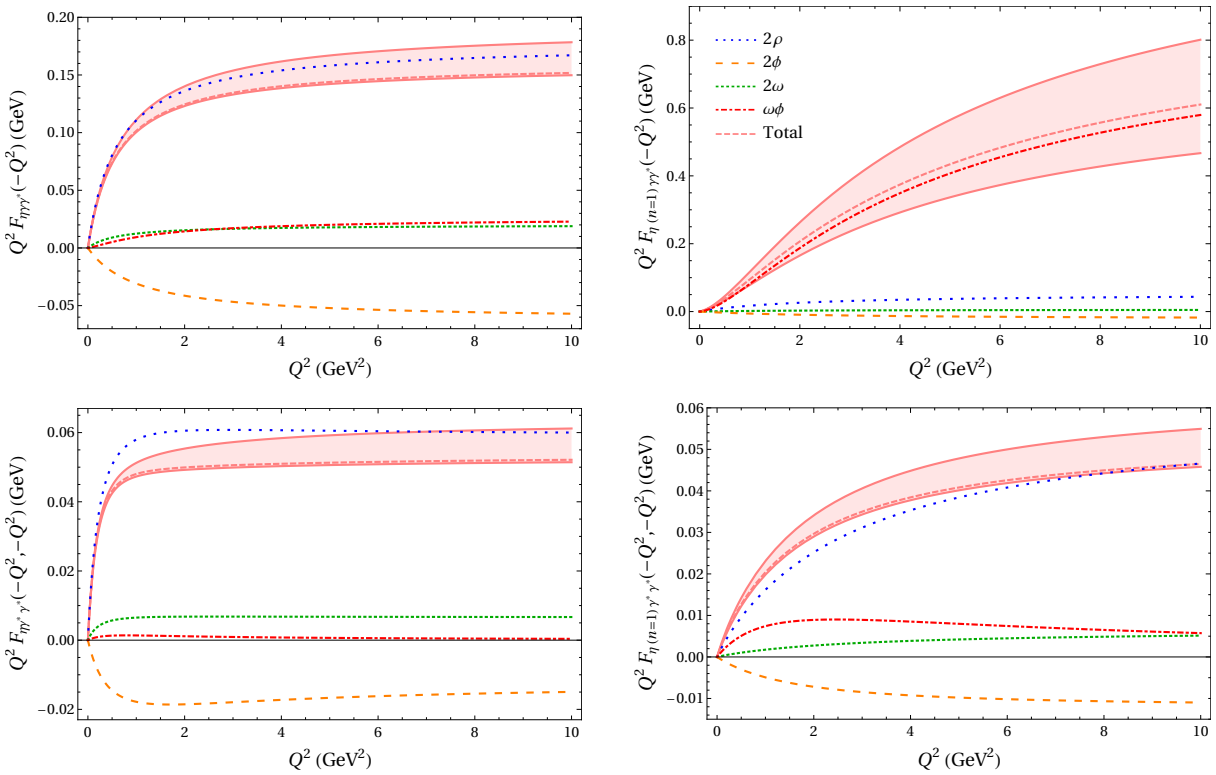

Figure 5.32: 2ρ, 2ω, 2ϕ, and $\phi\omega$ contributions to the singly-virtual (top) and doubly-virtual (bottom) η ground state (left) and first excited state (bottom).

and the 2ϕ contribution at low Q. In contrast, the singly-virtual TFFs of the radially-excited η' states will be dominated by the $\phi\omega$ contribution, while all other contributions are of negligible size. This enhancement is generated by the n-dependence in the numerator of (5.116) through terms proportional to $M_{+,n}$. The two-photon couplings and BL limits of the excited-state η' TFFs are shown in figure 5.21.

5.2.H Reply to `arXiv:1911.05874`

The analysis presented here has been criticized in a preprint by MV [83], which appeared during the review process of this manuscript. In this appendix we refute the main objections raised therein:

1. We disagree with the claim that in the pion-pole contribution to HLbL the second form factor has to be taken at $q_3^2 = M_\pi^2$, see discussion in the paragraphs from (3) to (5). The claim is a consequence of the statement in the paragraph after (5) in ref. [83]: "with obvious constraints on $q_{1,\dots,4}$ in the form factors $s = (q_1+q_2)^2 = (q_3+q_4)^2 = M_\pi^2$." This statement is incorrect. We recall that in the definition of the TFF (5.37), translation invariance has already been applied and the resulting overall delta function is not part of the TFF. In the unitarity relation for HLbL, the single-pion intermediate state generates an imaginary part proportional to $\delta(s - M_\pi^2)$, which however disappears when it is put into the dispersion integral to generate the pion pole, i.e., no constraint on s is left. The independent variables in the HLbL process are q_1^2, q_2^2, q_3^2, q_4^2, s, and t and the residue of the pion pole, i.e., the

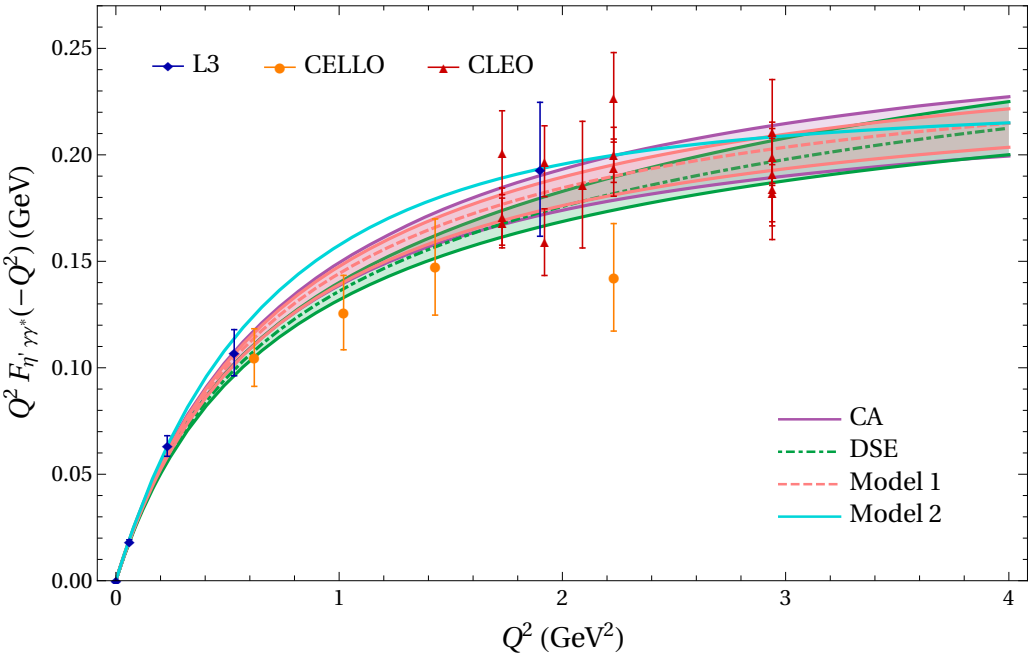

Figure 5.33: Singly-virtual η' TFF in the low-Q region. The large-N_c Regge model, "Model 1" (5.114), is indicated by the pink band with the dashed curve. Our alternative TFF model, "Model 2" (5.161), is indicated by the solid cyan curve. The purple band is the CA result from ref. [26]. The green band with the dot-dashed curve is the DSE result from ref. [173]. The data are from L3 [203], CELLO [204], and CLEO [205].

product of two pion TFFs, can only depend on the first four. If one takes the limit $q_4 \to 0$ this implies $s = q_3^2$ and $t = q_2^2$, but by no means does it imply $q_3^2 = M_\pi^2$. Of course one is free at that point to separate the pure pole in q_3^2 (with only its residue in the numerator) from non-pole terms. Between the two different dispersive representations, a simple reshuffling takes place, see (5.144) and the whole discussion in section 5.2.6.

2. As discussed in section 5.2.6, the MV model is based on an unjustified extrapolation to low $q_{1,2}^2$ of the constraint at high $q_{1,2}^2$. We have called this a "distortion" of the low-energy behavior of the HLbL tensor in ref. [233], a description considered unjustified in ref. [83]. Figures 5.16 and 5.17 very clearly illustrate this distortion. An alternative solution to the SDCs based on a tower of axial-vector mesons in holographic QCD has been presented in two papers [41, 42], which appeared after ref. [83]. These alternative solutions to the SDCs have a very similar behavior as the curves corresponding to our model in figures 5.16 and 5.17, and confirm that the MV model [2] leads to a low-q^2 behavior of the HLbL amplitude that cannot be explained in terms of any other physical states—in other words, a "distortion."

3. After (18) in ref. [83] it is stated that: the model in the present manuscript "violates the above equation and claims, effectively, that $c_L^\rho \sim 1$ also in the chiral limit." This statement is incorrect: in our model we are not able to take the chiral limit simply because it is formulated in terms of effective parameters that are fit to data or theoretical constraints. It is not the point of the model to make any claim about the behavior in the chiral limit. The underlying philosophy is to fulfill the SDCs only for large q_3^2, where the chiral limit becomes

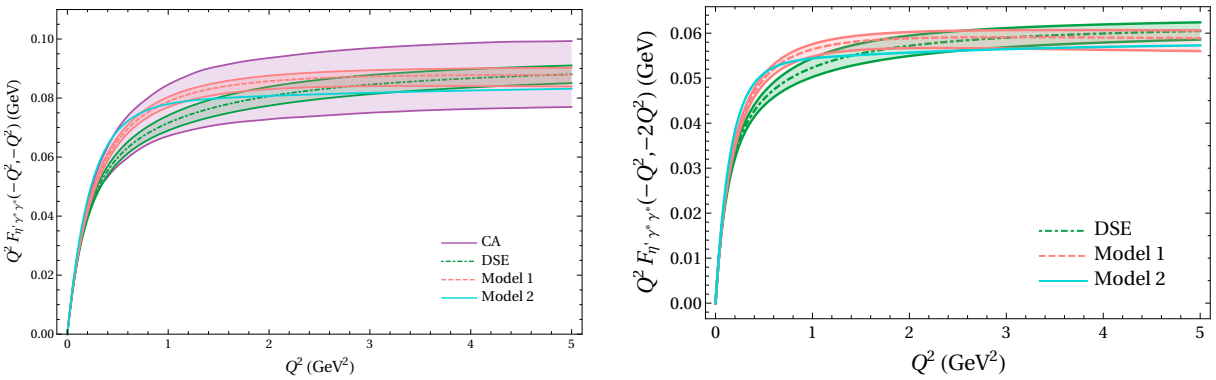

Figure 5.34: Doubly-virtual η' TFF in the symmetric region $Q_1^2 = Q_2^2 = Q^2$ (left) and in the region where $Q_1^2 = Q^2$ and $Q_2^2 = 2Q^2$ (right). Legend is the same as in figure 5.33.

irrelevant, and not to rely on it at low q_3^2, because it would be a bad approximation and we can instead use known phenomenological constraints. Such a strategy is best carried out with excited pseudoscalars because, unlike for axial-vector resonances, there are no ambiguities regarding their dispersive definition and because at least some information from phenomenology is available. Section 5.2.5.3 explicitly discusses the issue of the chiral limit in our model.

4. The conclusion of ref. [83] contains the following three statements: "there is no doubt that: (a) this region ($Q_{1,2}^2 \gg Q_3^2$) provides the largest contribution to a_μ^{HLbL}; (b) it allows for an exact non-perturbative analysis of the longitudinal structure function in the chiral limit and (c) it supplies strong evidence that corrections to the chiral limit are small." The first statement is plainly wrong, in particular for the model by MV, which actually receives most of its corrections from the region $Q_{1,2,3}^2 < Q_{\mathrm{match}}^2$, as can be clearly seen from figure 5.16. It is precisely this observation that leads to the conclusion that the modifications in the low-q^2 region are unphysical. Point (b) is correct, by construction, but the question is whether the chiral limit is a useful approximation at low q^2, which is the most important region for a_μ. This is claim (c), which, unfortunately, is also not correct: the difference between the original MV model (5.143) and the first term in (5.144) is such a quark-mass correction. In the case of the pion the two expressions give contributions to a_μ^{HLbL} that indeed differ by a small amount (about 10%), but in the case of η and η' the difference is much larger, about 100%, as anticipated in section 5.2.6.

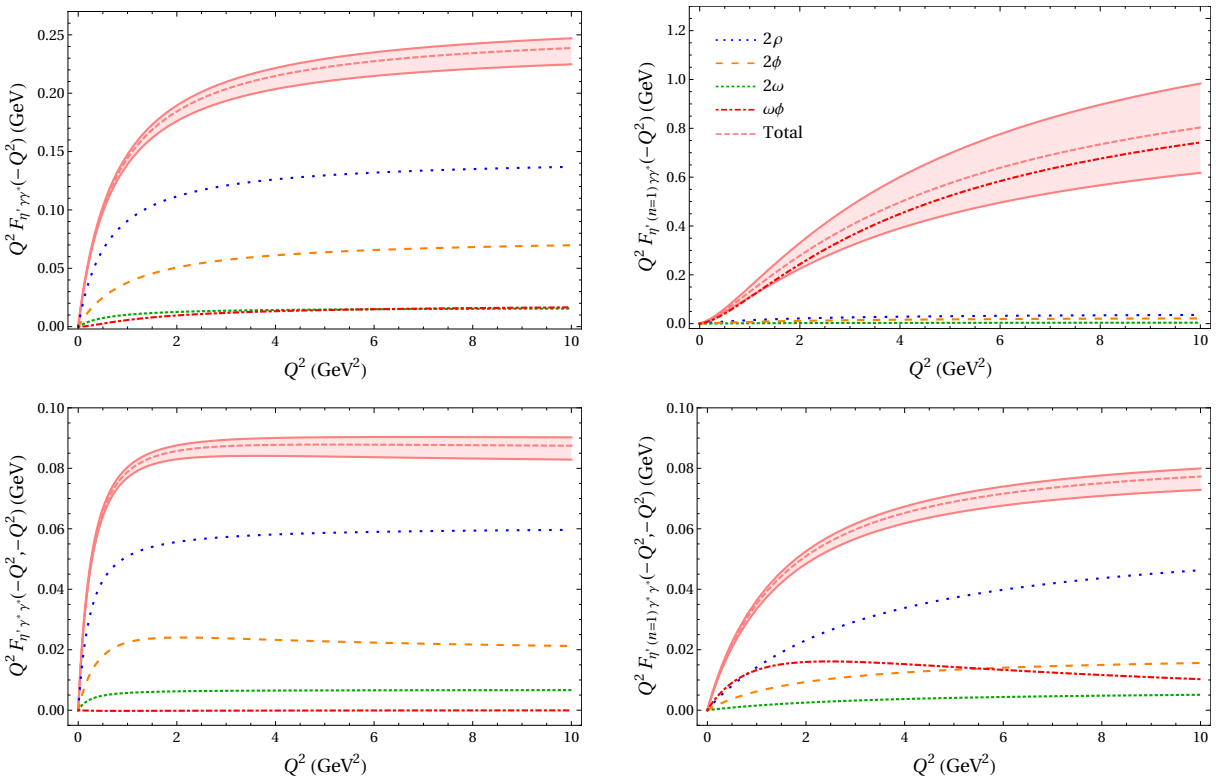

Figure 5.35: 2ρ, 2ω, 2ϕ, and $\phi\omega$ contributions to the singly-virtual (top) and doubly-virtual (bottom) η' ground state (left) and first excited state (bottom).

5.3 Updated results

At the time of the publication of the papers reproduced in this chapter (Refs. [30, 39]), the computation of the gluonic corrections presented in section 4.2 (corresponding to Ref. [38]) was not yet available. Here, the discussion of section 5.2.5.2 is updated: we study the implications of this new result for the matching of the large-N_c inspired Regge Model 1 for the pseudoscalars to the HLbL OPE result valid when all three virtualities are large [20].

Fig. 5.36 is the updated version of Fig. 5.16 and shows the various contributions to a_μ when all the three photon virtualities are larger than a cutoff Q_{min}. After inclusion of the α_s-correction[21], the OPE result is lowered: see purple band. By construction, the dotted black curve (quark loop corresponding to the LO of the OPE), the purple dotted curve and the orange curve (i.e. the contribution of the sum of all the pseudoscalars from Model 1) have the same asymptotic behavior when $Q_{\text{min}} \to \infty$, but including the α_s corrections to the quark loop improves the agreement between our model and the OPE result at lower energies. In addition, the uncertainty on the OPE, coming from higher-order terms, can be estimated by varying the scale at which α_s is estimated [22], which is more precise than the previous 20% error estimate.

The estimation of the matching scale obtained by minimizing the combined error of the

[20] Previously, only the quark loop was used, which corresponds to the LO contribution to that OPE, as discussed first in Ref. [1] but also in sections 3.4 and 4.1.4.1 of this work.

[21] As discussed in section 4.1 (Ref. [37]) and explained in section 4.2 (Ref. [38]), the non-perturbative corrections are numerically negligeable.

[22] Refer to the discussion in section 4.2.4 for a more detailed description of the uncertainty estimate.

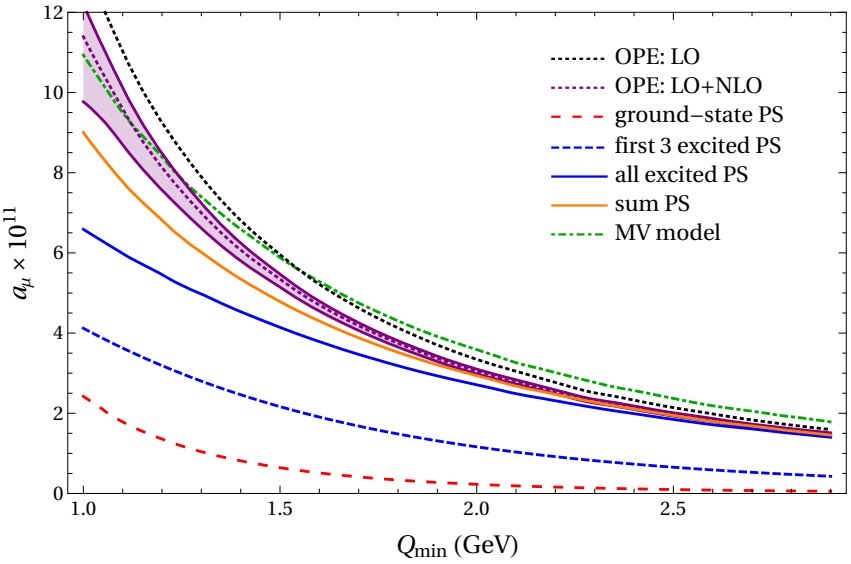

Figure 5.36: Updated contribution to a_μ for $Q_i \geq Q_{\rm min}$: the longitudinal part of the massless pQCD quark loop (dotted black), the longitudinal part of the NLO result for the HLbL OPE (purple band), the ground-state pseudoscalars (long-dashed red), their excitations from the large-N_c Regge model (blue), the sum of both (orange), and the short-distance implementation from the MV model (dot-dashed green). The blue dot-dashed curve refers the sum of the first three excited pseudoscalars in each trajectory.

Regge model and of the quark loop previously used would lead to a lower matching scale. This is because the perturbative error is significantly smaller and does not weigh as much. However, the matching between the orange and purple curves becomes worse at low energy. Taking that into account, the choice $Q_{\rm match} = 1.7$ GeV remains reasonable[23].

Equation (5.140) therefore becomes

$$\begin{aligned} \Delta a_\mu^{\text{PS-poles}} - a_\mu^{\text{PS-poles}}\big|_{Q_{\rm min}=Q_{\rm match}} &= 8.7(3.6) \times 10^{-11} \text{ (unchanged)}, \\ a_\mu^{\text{OPE}}\big|_{Q_{\rm min}=Q_{\rm match}} &= 4.2(1) \times 10^{-11}, \end{aligned} \tag{5.232}$$

The estimation of the uncertainties from the parameters of Model 1 is unchanged and equal to 3.6. The systematic uncertainty based on the difference between Models 1 and 2 also remains the same. The only part that is affected is the effect of varying the matching scale $Q_{\rm match}$ by 0.5 GeV. Compared to (5.141), this uncertainty is reduced and we find

$$\begin{aligned} \Delta a_\mu^{\text{PS-poles}} - a_\mu^{\text{PS-poles}}\big|_{Q_{\rm min}=Q_{\rm match}} &= 8.7(3.6)_{\text{excited PS}}\, {}^{+1.0}_{-0.2}\big|_{Q_{\rm match}} (3.8)_{\text{syst}} \times 10^{-11} \\ &= 8.7(5.3) \times 10^{-11}\,. \end{aligned} \tag{5.233}$$

The final result is therefore updated from

$$\Delta a_\mu^{\text{LSDC}} = [8.7(5.5)_{\text{PS-poles}} + 4.6(9)_{q\text{-loop}}] \times 10^{-11} = 13(6) \times 10^{-11}\,. \tag{5.234}$$

to

$$\Delta a_\mu^{\text{LSDC}} = [8.7(5.3)_{\text{PS-poles}} + 4.2(1)_{q\text{-loop}}] \times 10^{-11} = 13(5) \times 10^{-11}\,, \tag{5.235}$$

[23]The effect of varying the matching scale between $[1.2, 2.2]$ GeV is taken into account: see below.

The effect of the gluonic corrections to the OPE is smaller than the rounding effect and the central value therefore remains the same. The uncertainty is slightly reduced.

Chapter 6

Conclusion and outlook

> Great things are done by a series of small things brought together.
>
> Vincent Van Gogh

In this thesis, the proof that the massless quark loop is an accurate description of the HLbL tensor in the $g-2$ kinematics was presented. [1, 37, 38] In addition, the description was also improved by including the gluonic corrections and the error made from truncating the series in α_s was estimated. [38] A model for the TFF of radially excited pseudoscalars was also presented which reconciled the dispersive description and the high-energy description for the HLbL tensor from pQCD. [30, 39] The short-distance contribution was then evaluated through a matching of the model to the OPE description of the HLbL when all the virtualities are large. [30, 39] It was also shown that the inclusion of the gluonic corrections in the OPE improves the matching, without changing the central result:

$$\Delta a_\mu = 13(5) \times 10^{-11} \,. \tag{6.1}$$

Since the release of the results presented in this thesis, other works have analyzed the question of the implementation of the short-distances constraints in the HLbL description. [40–42]

In Refs. [41, 42], holographic QCD models are considered, where an infinite tower of axial-vector states are used as an alternative to pseudoscalars to fulfil the SDCs. In Ref. [41], two different sets of parameters are used. One of the set focuses on reproducing the correct behaviour for the pion TFF form factor at low energy, while the second focuses on its asymptotic behavior instead. Both choices lead to the following longitudinal[1] short-distance contribution to a_μ [41]

$$\Delta a_\mu = 14 \times 10^{-11} \,. \tag{6.2}$$

In Ref. [42], two different models are presented, which are referred to as hard-wall models 1 and 2 (HW1 and HW2) and differ in the boundary conditions used for the five-dimensional axial wave-function [2]. [42] The model HW2 corresponds to the model used in Ref. [41], but different

[1] The holographic QCD models can also be used to evaluate the transversal short-distance contributions, but we here focus on the longitudinal part for comparison with the Regge Model presented in this work.

[2] More details on the holographic models can be found in Refs. [41, 42].

choices are made for the parameters. This leads to [42]

$$\Delta a_\mu = 23 \times 10^{-11} \qquad \text{(HW1)}\,, \tag{6.3}$$

$$\Delta a_\mu = 17 \times 10^{-11} \qquad \text{(HW2)}\,. \tag{6.4}$$

where only the longitudinal contributions are considered.

Ref. [40] takes a completely different approach, which does not depend on the heavy intermediate states used to saturate the short-distance constraints. The idea is to consider interpolation functions which have the correct asymptotic behavior at high energy and which are compatible with the dispersive low-energy description of the pseudoscalar poles. This leads to

$$\Delta a_\mu = 9.1(5.0) \times 10^{-11}\,. \tag{6.5}$$

All the results presented above agree with our estimation of the short-distance contributions within uncertainties, with the exception of the HW1 model of Ref. [42], reproduced in (6.3). However, as pointed out in Ref. [42], the HW1 model overestimates the two-photon rate of the axial $f_1(1285)$, which might indicate that (6.3) is also too large. But even this result is way smaller than what is obtained using the Melnikov-Vainshtein prescription of dropping the singly virtual form factor:

$$\Delta a_\mu = 38 \times 10^{-11}\,, \tag{6.6}$$

where the result from Ref. [2] has been updated using modern inputs for the form factor. These considerations indicate that the nature of the intermediate states used to saturate the short-distance constraints has little impact on the a_μ contribution, as long as the low-energy behavior of the scalar functions respects the constraints imposed by unitarity and analyticity.

More experimental information on intermediate states such as the two-photon coupling of excited pseudoscalars or on the axials, as well as a full dispersive treatment of the latter could shed more light on these considerations in the future. This combined with other theoretical improvements (for example on the lattice) and a statistical reduction of the error on the experimental determination point toward a bright future for the muon $g-2$ physics!

Bibliography

[1] J. Bijnens, N. Hermansson-Truedsson, and A. Rodríguez-Sánchez, Phys. Lett. B **798**, 134994 (2019), 1908.03331.

[2] K. Melnikov and A. Vainshtein, Phys. Rev. D **70**, 113006 (2004), hep-ph/0312226.

[3] Muon g-2, B. Abi *et al.*, Phys. Rev. Lett. **126**, 141801 (2021), 2104.03281.

[4] T. Aoyama *et al.*, Phys. Rept. **887**, 1 (2020), 2006.04822.

[5] Muon g-2, G. W. Bennett *et al.*, Phys. Rev. D **73**, 072003 (2006), hep-ex/0602035.

[6] Muon g-2, J. Grange *et al.*, (2015), 1501.06858.

[7] M. Davier, A. Hoecker, B. Malaescu, and Z. Zhang, Eur. Phys. J. C **77**, 827 (2017), 1706.09436.

[8] A. Keshavarzi, D. Nomura, and T. Teubner, Phys. Rev. D **97**, 114025 (2018), 1802.02995.

[9] G. Colangelo, M. Hoferichter, and P. Stoffer, JHEP **02**, 006 (2019), 1810.00007.

[10] M. Hoferichter, B.-L. Hoid, and B. Kubis, JHEP **08**, 137 (2019), 1907.01556.

[11] M. Davier, A. Hoecker, B. Malaescu, and Z. Zhang, Eur. Phys. J. C **80**, 241 (2020), 1908.00921, [Erratum: Eur.Phys.J.C 80, 410 (2020)].

[12] A. Keshavarzi, D. Nomura, and T. Teubner, Phys. Rev. D **101**, 014029 (2020), 1911.00367.

[13] A. Kurz, T. Liu, P. Marquard, and M. Steinhauser, Phys. Lett. B **734**, 144 (2014), 1403.6400.

[14] Fermilab Lattice, LATTICE-HPQCD, MILC, B. Chakraborty *et al.*, Phys. Rev. Lett. **120**, 152001 (2018), 1710.11212.

[15] Budapest-Marseille-Wuppertal, S. Borsanyi *et al.*, Phys. Rev. Lett. **121**, 022002 (2018), 1711.04980.

[16] RBC, UKQCD, T. Blum *et al.*, Phys. Rev. Lett. **121**, 022003 (2018), 1801.07224.

[17] ETM, D. Giusti, V. Lubicz, G. Martinelli, F. Sanfilippo, and S. Simula, Phys. Rev. **D99**, 114502 (2019), 1901.10462.

[18] PACS, E. Shintani and Y. Kuramashi, Phys. Rev. **D 100**, 034517 (2019), 1902.00885.

[19] Fermilab Lattice, LATTICE-HPQCD, MILC, C. T. H. Davies *et al.*, Phys. Rev. **D101**, 034512 (2020), 1902.04223.

[20] A. Gérardin *et al.*, Phys. Rev. **D 100**, 014510 (2019), 1904.03120.

[21] C. Aubin *et al.*, Phys. Rev. **D101**, 014503 (2020), 1905.09307.

[22] D. Giusti and S. Simula, PoS **LATTICE2019**, 104 (2019), 1910.03874.

[23] S. Borsanyi *et al.*, (2020), 2002.12347.

[24] T. Blum *et al.*, Phys. Rev. Lett. **124**, 132002 (2020), 1911.08123.

[25] E.-H. Chao *et al.*, (2021), 2104.02632.

[26] P. Masjuan and P. Sanchez-Puertas, Phys. Rev. D **95**, 054026 (2017), 1701.05829.

[27] G. Colangelo, M. Hoferichter, M. Procura, and P. Stoffer, JHEP **04**, 161 (2017), 1702.07347.

[28] M. Hoferichter, B.-L. Hoid, B. Kubis, S. Leupold, and S. P. Schneider, JHEP **10**, 141 (2018), 1808.04823.

[29] A. Gérardin, H. B. Meyer, and A. Nyffeler, Phys. Rev. D **100**, 034520 (2019), 1903.09471.

[30] G. Colangelo, F. Hagelstein, M. Hoferichter, L. Laub, and P. Stoffer, JHEP **03**, 101 (2020), 1910.13432.

[31] V. Pauk and M. Vanderhaeghen, Eur. Phys. J. **C 74**, 3008 (2014), 1401.0832.

[32] I. Danilkin and M. Vanderhaeghen, Phys. Rev. **D 95**, 014019 (2017), 1611.04646.

[33] F. Jegerlehner, Springer Tracts Mod. Phys. **274**, pp.1 (2017).

[34] M. Knecht, S. Narison, A. Rabemananjara, and D. Rabetiarivony, Phys. Lett. **B787**, 111 (2018), 1808.03848.

[35] G. Eichmann, C. S. Fischer, and R. Williams, Phys. Rev. **D101**, 054015 (2020), 1910.06795.

[36] P. Roig and P. Sanchez-Puertas, (2019), 1910.02881.

[37] J. Bijnens, N. Hermansson-Truedsson, L. Laub, and A. Rodríguez-Sánchez, JHEP **10**, 203 (2020), 2008.13487.

[38] J. Bijnens, N. Hermansson-Truedsson, L. Laub, and A. Rodríguez-Sánchez, JHEP **04**, 240 (2021), 2101.09169.

[39] G. Colangelo, F. Hagelstein, M. Hoferichter, L. Laub, and P. Stoffer, Phys. Rev. D **101**, 051501 (2020), 1910.11881.

[40] J. Lüdtke and M. Procura, (2020), 2006.00007.

[41] L. Cappiello, O. Catà, G. D'Ambrosio, D. Greynat, and A. Iyer, Phys. Rev. D **102**, 016009 (2020), 1912.02779.

[42] J. Leutgeb and A. Rebhan, Phys. Rev. D **101**, 114015 (2020), 1912.01596.

[43] M. Knecht, JHEP **08**, 056 (2020), 2005.09929.

[44] S. I. Tomonaga, *The story of spin* (the University of Chicago Press, 1997).

[45] S. Schweber, *QED and the men who made it: Dyson, Feynman, Schwinger, and Tomonaga* (Princeton, USA: Univ. Pr., 1994).

[46] S. Weinberg, *The Quantum theory of fields. Vol. 1: Foundations* (Cambridge University Press, 2005).

[47] W. Pauli, ZS. f. Phys. **31**, 765 (1925).

[48] E. D. Commins, Ann. Rev. Nucl. Part. Sci. **62**, 133 (2012).

[49] S. Goudsmit, ZS. f. Phys. **32**, 794 (1925).

[50] G. Eaton, S. Eaton, and K. Salikhov, *Foundations of Modern EPR* (World Scientific, 1998).

[51] H. M. Foley and P. Kusch, Phys. Rev. **73**, 412 (1948).

[52] H. M. Foley and P. Kusch, Phys. Rev. **72**, 1256 (1947).

[53] P. Kusch and H. M. Foley, Phys. Rev. **74**, 250 (1948).

[54] J. S. Schwinger, Phys. Rev. **73**, 416 (1948).

[55] J. S. Schwinger, Phys. Rev. **74**, 1439 (1948).

[56] J. S. Schwinger, Phys. Rev. **75**, 651 (1948).

[57] T. Aoyama, T. Kinoshita, and M. Nio, Atoms **7**, 28 (2019).

[58] L. Morel, Z. Yao, P. Cladé, and S. Guellati-Khélifa, Nature **588**, 61 (2020).

[59] T. Aoyama, M. Hayakawa, T. Kinoshita, and M. Nio, Phys. Rev. Lett. **109**, 111808 (2012), 1205.5370.

[60] A. Czarnecki, W. J. Marciano, and A. Vainshtein, Phys. Rev. **D67**, 073006 (2003), hep-ph/0212229, [Erratum: Phys. Rev.D73,119901(2006)].

[61] C. Gnendiger, D. Stöckinger, and H. Stöckinger-Kim, Phys. Rev. D **88**, 053005 (2013), 1306.5546.

[62] M. Hoferichter, B.-L. Hoid, and B. Kubis, JHEP **08**, 137 (2019), 1907.01556.

[63] G. Colangelo, M. Hoferichter, A. Nyffeler, M. Passera, and P. Stoffer, Phys. Lett. B **735**, 90 (2014), 1403.7512.

[64] Particle Data Group, P. A. Zyla *et al.*, PTEP **2020**, 083C01 (2020).

[65] A. T. Fienberg, *Measuring the Precession Frequency in the E989 Muon $g-2$ Experiment*, PhD thesis, Washington U., Seattle, 2019.

[66] A. Fienberg, The muon $g-2$ experiment at fermilab, in 54^{th} *Rencontre de Moriond session*, 2019.

[67] Muon g-2, A. Keshavarzi, EPJ Web Conf. **212**, 05003 (2019), 1905.00497.

[68] N. Froemming *et al.*, Commissioning the Superconducting Magnetic Inflector System for the Muon g-2 Experiment, in *9th International Particle Accelerator Conference*, p. WEPAF014, 2018.

[69] D. Hanneke, S. Fogwell, and G. Gabrielse, Phys. Rev. Lett. **100**, 120801 (2008), 0801.1134.

[70] P. J. Mohr, D. B. Newell, and B. N. Taylor, Rev. Mod. Phys. **88**, 035009 (2016), 1507.07956.

[71] W. Liu *et al.*, Phys. Rev. Lett. **82**, 711 (1999).

[72] D. W. Hertzog, EPJ Web Conf. **118**, 01015 (2016), 1512.00928.

[73] M. E. Peskin and D. V. Schroeder, *An Introduction to quantum field theory* (Addison-Wesley, Reading, USA, 1995).

[74] R. H. Parker, C. Yu, W. Zhong, B. Estey, and H. Müller, Science **360**, 191 (2018), 1812.04130.

[75] M. Passera, Graduate course at the University of Bern: Precision electroweak physics, 2018.

[76] C. Bouchiat and L. Michel, J. Phys. Radium **22**, 121 (1961).

[77] G. Colangelo, M. Hoferichter, M. Procura, and P. Stoffer, JHEP **09**, 074 (2015), 1506.01386.

[78] W. A. Bardeen and W. K. Tung, Phys. Rev. **173**, 1423 (1968), [Erratum: Phys. Rev. **D 4**, 3229 (1971)].

[79] R. Tarrach, Nuovo Cim. **A 28**, 409 (1975).

[80] V. Pauk and M. Vanderhaeghen, (2014), 1403.7503.

[81] V. Pauk and M. Vanderhaeghen, Phys. Rev. D **90**, 113012 (2014), 1409.0819.

[82] F. Hagelstein and V. Pascalutsa, Phys. Rev. Lett. **120**, 072002 (2018), 1710.04571.

[83] K. Melnikov and A. Vainshtein, (2019), 1911.05874.

[84] M. Neubert, (2019), 1901.06573.

[85] P. Pascual and R. Tarrach, Lect. Notes Phys. **194**, 1 (1984).

[86] K. G. Wilson, Phys. Rev. **179**, 1499 (1969).

[87] G. Buchalla, A. J. Buras, and M. E. Lautenbacher, Rev. Mod. Phys. **68**, 1125 (1996), hep-ph/9512380.

[88] N. Hermansson-Truedsson, Graduate course at the university of Bern: Introduction to the operator product expansion, 2021.

[89] P. Gubler and D. Satow, Prog. Part. Nucl. Phys. **106**, 1 (2019), 1812.00385.

[90] S. Bodenstein, C. A. Dominguez, S. I. Eidelman, H. Spiesberger, and K. Schilcher, JHEP **01**, 039 (2012), 1110.2026.

[91] M. A. Shifman, A. I. Vainshtein, and V. I. Zakharov, Nucl. Phys. **B147**, 385 (1979).

[92] J. Gasser and H. Leutwyler, Phys. Rept. **87**, 77 (1982).

[93] C. McNeile *et al.*, Phys. Rev. D **87**, 034503 (2013), 1211.6577.

[94] Flavour Lattice Averaging Group, S. Aoki *et al.*, Eur. Phys. J. C **80**, 113 (2020), 1902.08191.

[95] M. A. Shifman, A. I. Vainshtein, and V. I. Zakharov, Nucl. Phys. B **147**, 448 (1979).

[96] S. Vandoren and P. van Nieuwenhuizen, (2008), 0802.1862.

[97] H. Forkel, (2000), hep-ph/0009136.

[98] G. M. Shore, Nucl. Phys. B **362**, 85 (1991).

[99] S. Eidelman, F. Jegerlehner, A. L. Kataev, and O. Veretin, Phys. Lett. B **454**, 369 (1999), hep-ph/9812521.

[100] Particle Data Group, M. Tanabashi *et al.*, Phys. Rev. **D98**, 030001 (2018).

[101] V. A. Novikov, M. A. Shifman, A. I. Vainshtein, M. B. Voloshin, and V. I. Zakharov, Nucl. Phys. B **237**, 525 (1984).

[102] S. L. Adler and W. A. Bardeen, Phys. Rev. **182**, 1517 (1969).

[103] M. Knecht, S. Peris, M. Perrottet, and E. de Rafael, JHEP **03**, 035 (2004), hep-ph/0311100.

[104] M. Abe *et al.*, PTEP **2019**, 053C02 (2019), 1901.03047.

[105] P. Masjuan, P. Roig, and P. Sanchez-Puertas, (2020), 2005.11761.

[106] J. Bijnens, E. Pallante, and J. Prades, Phys. Rev. Lett. **75**, 1447 (1995), hep-ph/9505251, [Erratum: Phys.Rev.Lett. 75, 3781 (1995)].

[107] J. Bijnens, E. Pallante, and J. Prades, Nucl. Phys. B **474**, 379 (1996), hep-ph/9511388.

[108] M. Hayakawa and T. Kinoshita, Phys. Rev. D **57**, 465 (1998), hep-ph/9708227, [Erratum: Phys.Rev.D 66, 019902 (2002)].

[109] M. Knecht and A. Nyffeler, Phys. Rev. D **65**, 073034 (2002), hep-ph/0111058.

[110] T. Kinoshita, B. Nizic, and Y. Okamoto, Phys. Rev. D **31**, 2108 (1985).

[111] T. Goecke, C. S. Fischer, and R. Williams, Phys. Rev. D **83**, 094006 (2011), 1012.3886, [Erratum: Phys.Rev.D 86, 099901 (2012)].

[112] R. Boughezal and K. Melnikov, Phys. Lett. B **704**, 193 (2011), 1104.4510.

[113] D. Greynat and E. de Rafael, JHEP **07**, 020 (2012), 1204.3029.

[114] P. Masjuan and M. Vanderhaeghen, J. Phys. G **42**, 125004 (2015), 1212.0357.

[115] A. Dorokhov, A. Radzhabov, and A. Zhevlakov, Eur. Phys. J. C **75**, 417 (2015), 1502.04487.

[116] J. H. Kuhn, A. Onishchenko, A. Pivovarov, and O. Veretin, Phys. Rev. D **68**, 033018 (2003), hep-ph/0301151.

[117] B. L. Ioffe and A. V. Smilga, Nucl. Phys. **B232**, 109 (1984).

[118] I. I. Balitsky and A. V. Yung, Phys. Lett. **129B**, 328 (1983).

[119] J. Aldins, T. Kinoshita, S. J. Brodsky, and A. J. Dufner, Phys. Rev. **D1**, 2378 (1970).

[120] W. Zimmermann, Annals Phys. **77**, 570 (1973), [Lect. Notes Phys.558,278(2000)].

[121] A. Pich, Effective field theory: Course, in *Probing the standard model of particle interactions. Proceedings, Summer School in Theoretical Physics, NATO Advanced Study Institute, 68th session, Les Houches, France, July 28-September 5, 1997. Pt. 1, 2*, pp. 949–1049, 1998, hep-ph/9806303.

[122] A. V. Manohar, Introduction to Effective Field Theories, in *Les Houches summer school: EFT in Particle Physics and Cosmology Les Houches, Chamonix Valley, France, July 3-28, 2017*, 2018, 1804.05863.

[123] M. Jamin and M. Munz, Z. Phys. **C60**, 569 (1993), hep-ph/9208201.

[124] V. A. Novikov, M. A. Shifman, A. I. Vainshtein, and V. I. Zakharov, Fortsch. Phys. **32**, 585 (1984).

[125] S. C. Generalis and D. J. Broadhurst, Phys. Lett. **139B**, 85 (1984).

[126] D. J. Broadhurst and S. C. Generalis, Phys. Lett. **142B**, 75 (1984).

[127] E. Braaten, S. Narison, and A. Pich, Nucl. Phys. **B373**, 581 (1992).

[128] O. Cata and V. Mateu, JHEP **09**, 078 (2007), 0705.2948.

[129] N. Craigie and J. Stern, Phys. Rev. D **26**, 2430 (1982).

[130] I. Balitsky, A. Kolesnichenko, and A. Yung, Sov. J. Nucl. Phys. **41**, 178 (1985).

[131] M. Knecht and A. Nyffeler, Eur. Phys. J. C **21**, 659 (2001), hep-ph/0106034.

[132] V. Mateu and J. Portoles, Eur. Phys. J. **C52**, 325 (2007), 0706.1039.

[133] G. 't Hooft, Nucl. Phys. **B72**, 461 (1974).

[134] E. Witten, Nucl. Phys. **B160**, 57 (1979).

[135] A. Pich, Colorless mesons in a polychromatic world, in *Phenomenology of large N(c) QCD. Proceedings, Tempe, USA, January 9-11, 2002*, pp. 239–258, 2002, hep-ph/0205030.

[136] O. Cata and V. Mateu, Phys. Rev. **D77**, 116009 (2008), 0801.4374.

[137] G. Ecker, J. Gasser, A. Pich, and E. de Rafael, Nucl. Phys. **B321**, 311 (1989).

[138] G. S. Bali *et al.*, JHEP **02**, 044 (2012), 1111.4956.

[139] G. S. Bali, G. Endrődi, and S. Piemonte, JHEP **07**, 183 (2020), 2004.08778.

[140] V. Belyaev and B. Ioffe, Sov. Phys. JETP **56**, 493 (1982).

[141] J. Vermaseren, (2000), math-ph/0010025.

[142] J. Kuipers, T. Ueda, J. Vermaseren, and J. Vollinga, Comput. Phys. Commun. **184**, 1453 (2013), 1203.6543.

[143] A. von Manteuffel and C. Studerus, (2012), 1201.4330.

[144] P. Maierhöfer, J. Usovitsch, and P. Uwer, Comput. Phys. Commun. **230**, 99 (2018), 1705.05610.

[145] H. J. Lu and C. A. Perez, Massless one loop scalar three point integral and associated Clausen, Glaisher and L functions, SLAC-PUB-5809, 1992.

[146] T. Hahn, Computer Physics Communications **168**, 78 (2005).

[147] J. Bijnens, E. Pallante, and J. Prades, Nucl. Phys. B **626**, 410 (2002), hep-ph/0112255.

[148] M. Hayakawa and T. Kinoshita, (2001), hep-ph/0112102.

[149] J. Prades, E. de Rafael, and A. Vainshtein, Adv. Ser. Direct. High Energy Phys. **20**, 303 (2009), 0901.0306.

[150] M. Hoferichter and P. Stoffer, JHEP **05**, 159 (2020), 2004.06127.

[151] J. Bijnens, N. Hermansson-Truedsson, L. Laub, and A. Rodríguez-Sánchez, Supplementary material from arXiv:2101.09169 [hep-ph]: files `pitildes.txt, resultsgluon.txt, resultsquark.txt, cornerexpansions.txt, sideexpansions.txt` .

[152] T. Birthwright, E. Glover, and P. Marquard, JHEP **09**, 042 (2004), hep-ph/0407343.

[153] F. Chavez and C. Duhr, JHEP **11**, 114 (2012), 1209.2722.

[154] J. Kodaira, S. Matsuda, T. Muta, K. Sasaki, and T. Uematsu, Phys. Rev. D **20**, 627 (1979).

[155] J. Kodaira, S. Matsuda, K. Sasaki, and T. Uematsu, Nucl. Phys. B **159**, 99 (1979).

[156] J. Kodaira, Nucl. Phys. **B 165**, 129 (1980).

[157] F. Herren and M. Steinhauser, Comput. Phys. Commun. **224**, 333 (2018), 1703.03751.

[158] N. I. Usyukina and A. I. Davydychev, Phys. Lett. B **332**, 159 (1994), hep-ph/9402223.

[159] F. Jegerlehner, EPJ Web Conf. **199**, 01010 (2019), 1809.07413.

[160] D. Giusti, F. Sanfilippo, and S. Simula, Phys. Rev. **D 98**, 114504 (2018), 1808.00887.

[161] T. Blum *et al.*, Phys. Rev. Lett. **118**, 022005 (2017), 1610.04603.

[162] T. Blum *et al.*, Phys. Rev. **D 96**, 034515 (2017), 1705.01067.

[163] N. Asmussen, A. Gérardin, A. Nyffeler, and H. B. Meyer, SciPost Phys. Proc. **1**, 031 (2019), 1811.08320.

[164] M. Hoferichter, G. Colangelo, M. Procura, and P. Stoffer, Int. J. Mod. Phys. Conf. Ser. **35**, 1460400 (2014), 1309.6877.

[165] G. Colangelo, M. Hoferichter, M. Procura, and P. Stoffer, JHEP **09**, 091 (2014), 1402.7081.

[166] G. Colangelo, M. Hoferichter, B. Kubis, M. Procura, and P. Stoffer, Phys. Lett. **B 738**, 6 (2014), 1408.2517.

[167] G. Colangelo, M. Hoferichter, M. Procura, and P. Stoffer, Phys. Rev. Lett. **118**, 232001 (2017), 1701.06554.

[168] V. Pascalutsa, V. Pauk, and M. Vanderhaeghen, Phys. Rev. **D 85**, 116001 (2012), 1204.0740.

[169] J. Green, O. Gryniuk, G. von Hippel, H. B. Meyer, and V. Pascalutsa, Phys. Rev. Lett. **115**, 222003 (2015), 1507.01577.

[170] F. Hagelstein and V. Pascalutsa, (2019), 1907.06927.

[171] M. Hoferichter, B. Kubis, S. Leupold, F. Niecknig, and S. P. Schneider, Eur. Phys. J. **C 74**, 3180 (2014), 1410.4691.

[172] M. Hoferichter, B.-L. Hoid, B. Kubis, S. Leupold, and S. P. Schneider, Phys. Rev. Lett. **121**, 112002 (2018), 1805.01471.

[173] G. Eichmann, C. S. Fischer, E. Weil, and R. Williams, Phys. Lett. **B 797**, 134855 (2019), 1903.10844.

[174] R. García-Martín and B. Moussallam, Eur. Phys. J. **C 70**, 155 (2010), 1006.5373.

[175] M. Hoferichter, D. R. Phillips, and C. Schat, Eur. Phys. J. **C 71**, 1743 (2011), 1106.4147.

[176] B. Moussallam, Eur. Phys. J. **C 73**, 2539 (2013), 1305.3143.

[177] I. Danilkin and M. Vanderhaeghen, Phys. Lett. **B 789**, 366 (2019), 1810.03669.

[178] M. Hoferichter and P. Stoffer, JHEP **07**, 073 (2019), 1905.13198.

[179] I. Danilkin, O. Deineka, and M. Vanderhaeghen, Phys. Rev. **D101**, 054008 (2020), 1909.04158.

[180] J. Calmet, S. Narison, M. Perrottet, and E. de Rafael, Phys. Lett. **61B**, 283 (1976).

[181] A. Vainshtein, Phys. Lett. **B 569**, 187 (2003), hep-ph/0212231.

[182] M. Knecht, S. Peris, M. Perrottet, and E. de Rafael, JHEP **11**, 003 (2002), hep-ph/0205102.

[183] F. Jegerlehner and O. V. Tarasov, Phys. Lett. **B 639**, 299 (2006), hep-ph/0510308.

[184] J. Mondejar and K. Melnikov, Phys. Lett. **B 718**, 1364 (2013), 1210.0812.

[185] G. P. Lepage and S. J. Brodsky, Phys. Lett. **87B**, 359 (1979).

[186] G. P. Lepage and S. J. Brodsky, Phys. Rev. **D 22**, 2157 (1980).

[187] S. J. Brodsky and G. P. Lepage, Phys. Rev. **D 24**, 1808 (1981).

[188] E. Ruiz Arriola and W. Broniowski, Phys. Rev. **D 74**, 034008 (2006), hep-ph/0605318.

[189] E. Ruiz Arriola and W. Broniowski, Phys. Rev. **D 81**, 094021 (2010), 1004.0837.

[190] S. Peris, M. Perrottet, and E. de Rafael, JHEP **05**, 011 (1998), hep-ph/9805442.

[191] M. Knecht, S. Peris, and E. de Rafael, Phys. Lett. **B 443**, 255 (1998), hep-ph/9809594.

[192] J. Bijnens, E. Gámiz, E. Lipartia, and J. Prades, JHEP **04**, 055 (2003), hep-ph/0304222.

[193] P. Masjuan, E. Ruiz Arriola, and W. Broniowski, Phys. Rev. **D 85**, 094006 (2012), 1203.4782.

[194] M. Knecht, A. Nyffeler, M. Perrottet, and E. de Rafael, Phys. Rev. Lett. **88**, 071802 (2002), hep-ph/0111059.

[195] M. J. Ramsey-Musolf and M. B. Wise, Phys. Rev. Lett. **89**, 041601 (2002), hep-ph/0201297.

[196] L3, M. Acciarri *et al.*, Phys. Lett. **B 413**, 147 (1997).

[197] OBELIX, P. Salvini *et al.*, Eur. Phys. J. **C 35**, 21 (2004).

[198] R. Escribano, S. Gonzàlez-Solís, P. Masjuan, and P. Sanchez-Puertas, Phys. Rev. **D 94**, 054033 (2016), 1512.07520.

[199] L. G. Landsberg, Phys. Rept. **128**, 301 (1985).

[200] U.-G. Meißner, Phys. Rept. **161**, 213 (1988).

[201] T. Feldmann, P. Kroll, and B. Stech, Phys. Rev. **D 58**, 114006 (1998), hep-ph/9802409.

[202] T. Feldmann, Int. J. Mod. Phys. **A 15**, 159 (2000), hep-ph/9907491.

[203] L3, M. Acciarri *et al.*, Phys. Lett. **B 418**, 399 (1998).

[204] CELLO, H. J. Behrend *et al.*, Z. Phys. **C 49**, 401 (1991).

[205] CLEO, J. Gronberg *et al.*, Phys. Rev. **D 57**, 33 (1998), hep-ex/9707031.

[206] BaBar, P. del Amo Sanchez *et al.*, Phys. Rev. **D 84**, 052001 (2011), 1101.1142.

[207] BaBar, J. P. Lees *et al.*, Phys. Rev. **D 98**, 112002 (2018), 1808.08038.

[208] L3, M. Acciarri *et al.*, Phys. Lett. **B 501**, 1 (2001), hep-ex/0011035.

[209] CLEO, R. Ahohe *et al.*, Phys. Rev. **D 71**, 072001 (2005), hep-ex/0501026.

[210] BESIII, M. Ablikim *et al.*, Phys. Rev. **D 97**, 072014 (2018), 1802.09854.

[211] L3, P. Achard *et al.*, JHEP **03**, 018 (2007).

[212] Belle, C. C. Zhang *et al.*, Phys. Rev. **D 86**, 052002 (2012), 1206.5087.

[213] E. Klempt and A. Zaitsev, Phys. Rept. **454**, 1 (2007), 0708.4016.

[214] P. Sanchez-Puertas, private communications (2019).

[215] M. Davier, S. Descotes-Genon, A. Hocker, B. Malaescu, and Z. Zhang, Eur. Phys. J. **C 56**, 305 (2008), 0803.0979.

[216] M. Beneke and M. Jamin, JHEP **09**, 044 (2008), 0806.3156.

[217] K. Maltman and T. Yavin, Phys. Rev. **D 78**, 094020 (2008), 0807.0650.

[218] S. Narison, Phys. Lett. **B 673**, 30 (2009), 0901.3823.

[219] I. Caprini and J. Fischer, Eur. Phys. J. **C 64**, 35 (2009), 0906.5211.

[220] A. Pich, Prog. Part. Nucl. Phys. **75**, 41 (2014), 1310.7922.

[221] T. P. Gorringe and D. W. Hertzog, Prog. Part. Nucl. Phys. **84**, 73 (2015), 1506.01465.

[222] C. M. Carloni Calame, M. Passera, L. Trentadue, and G. Venanzoni, Phys. Lett. **B 746**, 325 (2015), 1504.02228.

[223] G. Abbiendi *et al.*, Eur. Phys. J. **C 77**, 139 (2017), 1609.08987.

[224] T. Aoyama, T. Kinoshita, and M. Nio, Phys. Rev. **D 97**, 036001 (2018), 1712.06060.

[225] H. Davoudiasl and W. J. Marciano, Phys. Rev. **D 98**, 075011 (2018), 1806.10252.

[226] A. Crivellin, M. Hoferichter, and P. Schmidt-Wellenburg, Phys. Rev. **D 98**, 113002 (2018), 1807.11484.

[227] S. P. Schneider, B. Kubis, and F. Niecknig, Phys. Rev. **D 86**, 054013 (2012), 1206.3098.

[228] M. Hoferichter, B. Kubis, and D. Sakkas, Phys. Rev. **D 86**, 116009 (2012), 1210.6793.

[229] M. Hoferichter, B. Kubis, and M. Zanke, Phys. Rev. **D 96**, 114016 (2017), 1710.00824.

[230] F. Jegerlehner and A. Nyffeler, Phys. Rept. **477**, 1 (2009), 0902.3360.

[231] C. Bouchiat and L. Michel, J. Phys. Radium **22**, 121 (1961).

[232] S. J. Brodsky and E. de Rafael, Phys. Rev. **168**, 1620 (1968).

[233] G. Colangelo, F. Hagelstein, M. Hoferichter, L. Laub, and P. Stoffer, Phys. Rev. **D 101**, 051501 (2020), 1910.11881.

[234] G. Eichmann, C. S. Fischer, W. Heupel, and R. Williams, AIP Conf. Proc. **1701**, 040004 (2016), 1411.7876.

[235] G. Eichmann, C. S. Fischer, and W. Heupel, Phys. Rev. **D 92**, 056006 (2015), 1505.06336.

[236] S. L. Adler, Phys. Rev. **177**, 2426 (1969).

[237] J. S. Bell and R. Jackiw, Nuovo Cim. **A 60**, 47 (1969).

[238] W. A. Bardeen, Phys. Rev. **184**, 1848 (1969).

[239] D. Espriu and R. Tarrach, Z. Phys. **C 16**, 77 (1982).

[240] H. Leutwyler, Nucl. Phys. Proc. Suppl. **64**, 223 (1998), hep-ph/9709408.

[241] R. Kaiser and H. Leutwyler, (1998), hep-ph/9806336.

[242] R. Kaiser and H. Leutwyler, Eur. Phys. J. **C 17**, 623 (2000), hep-ph/0007101.

[243] R. Escribano, P. Masjuan, and P. Sanchez-Puertas, Eur. Phys. J. **C 75**, 414 (2015), 1504.07742.

[244] A. V. Manohar, Phys. Lett. **B 244**, 101 (1990).

[245] E. Braaten, Phys. Rev. **D 28**, 524 (1983).

[246] S. Laporta and E. Remiddi, Phys. Lett. **B 301**, 440 (1993).

[247] K. Raya, A. Bashir, and P. Roig, (2019), 1910.05960.

[248] G. 't Hooft, NATO Sci. Ser. B **59**, 135 (1980).

[249] K. Melnikov, Phys. Lett. **B 639**, 294 (2006), hep-ph/0604205.

[250] R. J. Crewther, Phys. Rev. Lett. **28**, 1421 (1972).

[251] M. Golterman, S. Peris, B. Phily, and E. de Rafael, JHEP **01**, 024 (2002), hep-ph/0112042.

[252] M. Golterman and S. Peris, JHEP **01**, 028 (2001), hep-ph/0101098.

[253] G. D'Ambrosio, D. Greynat, and M. Knecht, Phys. Lett. **B 797**, 134891 (2019), 1906.03046.

[254] A. Nyffeler, Phys. Rev. **D 79**, 073012 (2009), 0901.1172.

[255] A. V. Anisovich, V. V. Anisovich, and A. V. Sarantsev, Phys. Rev. **D 62**, 051502 (2000), hep-ph/0003113.

[256] O. Kaczmarek and F. Zantow, Phys. Rev. **D 71**, 114510 (2005), hep-lat/0503017.

[257] Particle Data Group, D. E. Groom *et al.*, Eur. Phys. J. **C 15**, 1 (2000).

[258] BaBar, B. Aubert *et al.*, Phys. Rev. **D 80**, 052002 (2009), 0905.4778.

[259] Belle, S. Uehara *et al.*, Phys. Rev. **D 86**, 092007 (2012), 1205.3249.

[260] E. Ruiz Arriola and W. Broniowski, (2011), 1110.2863.

[261] H. Czyż, P. Kisza, and S. Tracz, Phys. Rev. **D 97**, 016006 (2018), 1711.00820.

[262] J.-J. Wu, X.-H. Liu, Q. Zhao, and B.-S. Zou, Phys. Rev. Lett. **108**, 081803 (2012), 1108.3772.

[263] J. Gasser, Annals Phys. **136**, 62 (1981).

[264] R. F. Dashen, E. E. Jenkins, and A. V. Manohar, Phys. Rev. **D 49**, 4713 (1994), hep-ph/9310379, [Erratum: Phys. Rev. **D 51**, 2489(1995)].

[265] T. D. Cohen, Rev. Mod. Phys. **68**, 599 (1996).

[266] A. D. Dolgov and V. I. Zakharov, Nucl. Phys. **B 27**, 525 (1971).

[267] V. I. Zakharov, Phys. Rev. **D 42**, 1208 (1990).

[268] L. D. Landau, Dokl. Akad. Nauk Ser. Fiz. **60**, 207 (1948).

[269] C.-N. Yang, Phys. Rev. **77**, 242 (1950).

[270] L3, P. Achard *et al.*, Phys. Lett. **B 526**, 269 (2002), hep-ex/0110073.

[271] M. Abramowitz and I. Stegun, *Handbook of mathematical functions* (Dover Publications, 1972).

[272] F. W. J. Olver, *Asymptotics and Special Functions* (Academic Press, 1974).

[273] R. Aaron and R. S. Longacre, Phys. Rev. **D 24**, 1207 (1981).

[274] Crystal Barrel, A. Abele *et al.*, Eur. Phys. J. **C 19**, 667 (2001).

[275] T. Barnes, F. E. Close, P. R. Page, and E. S. Swanson, Phys. Rev. **D 55**, 4157 (1997), hep-ph/9609339.

[276] UKQCD, C. McNeile and C. Michael, Phys. Lett. **B 642**, 244 (2006), hep-lat/0607032.

[277] Hadron Spectrum, E. V. Mastropas and D. G. Richards, Phys. Rev. **D 90**, 014511 (2014), 1403.5575.

[278] V. Elias, A. Fariborz, M. A. Samuel, F. Shi, and T. G. Steele, Phys. Lett. **B 412**, 131 (1997), hep-ph/9706472.

[279] M. K. Volkov and C. Weiss, Phys. Rev. **D56**, 221 (1997), hep-ph/9608347.

[280] A. A. Andrianov, D. Espriu, and R. Tarrach, Nucl. Phys. **B533**, 429 (1998), hep-ph/9803232.

[281] K. Maltman and J. Kambor, Phys. Rev. **D 65**, 074013 (2002), hep-ph/0108227.

[282] A. L. Kataev, N. V. Krasnikov, and A. A. Pivovarov, Phys. Lett. **B 123**, 242 (1983).

[283] M. Diehl and G. Hiller, JHEP **06**, 067 (2001), hep-ph/0105194.

Declaration of consent

on the basis of Article 18 of the PromR Phil.-nat. 19

Name/First Name: Laub Laetitia

Registration Number: 12-825-527

Study program: PhD in Physics

Bachelor ☐ Master ☐ Dissertation ☑

Title of the thesis: Short-distance constraints on the hadronic light-by-light contribution to the muon g-2

Supervisor: Prof. Dr. Gilberto Colangelo

I declare herewith that this thesis is my own work and that I have not used any sources other than those stated. I have indicated the adoption of quotations as well as thoughts taken from other authors as such in the thesis. I am aware that the Senate pursuant to Article 36 paragraph 1 litera r of the University Act of September 5th, 1996 and Article 69 of the University Statute of June 7th, 2011 is authorized to revoke the doctoral degree awarded on the basis of this thesis.
For the purposes of evaluation and verification of compliance with the declaration of originality and the regulations governing plagiarism, I hereby grant the University of Bern the right to process my personal data and to perform the acts of use this requires, in particular, to reproduce the written thesis and to store it permanently in a database, and to use said database, or to make said database available, to enable comparison with theses submitted by others.

Place/Date

Signature